

City Research Online

City St George's, University of London

Citation: Forrester, E. (2024). Investigating the effect of sodium coupled glucose transporters (SLC5) and their inhibitors on arterial function. (Unpublished Doctoral thesis, St George's, University of London)

This is the accepted version of the paper.

This version of the publication may differ from the final published version. To cite this item please consult the publisher's version.

Permanent repository link: https://openaccess.city.ac.uk/id/eprint/36947/

Copyright and Reuse: Copyright and Moral Rights remain with the author(s) and/or copyright holders. Copies of full items can be used for personal research or study, educational, or not-for-profit purposes without prior permission or charge, unless otherwise indicated, provided that the authors, title and full bibliographic details are credited, a hyperlink and/or URL is given for the original metadata page and the content is not changed in any way. For full details of reuse please refer to City Research Online policy.

City Research Online: http://openaccess.city.ac.uk/ publications@citystgeorges.ac.uk

Investigating the effect of sodium-coupled glucose transporters (SLC5) and their inhibitors on arterial function

Elizabeth Forrester BSc (Hons)

A thesis presented for the degree of Doctor of Philosophy (PhD)

Supervised by:

Prof. Iain A Greenwood

Prof. Anthony P Albert

Dr Vincenzo Barrese

St George's University, London

October 2024

‘In Loving Memory of Auntie Julie, Nannie and Grandad’

General Abstract

Introduction: The sodium myo-inositol transporter SMIT1 (Slc5a3) and sodium-glucose transporter SGLT2 (Slc5a2) are part of the SLC5 family. Their roles in the vasculature are not well understood. SMIT1 interacts with Kv7 channels to regulate vascular contractility. Meanwhile, SGLT2 inhibitors that lower blood glucose have recently been found to treat heart failure, reduce blood pressure, and relax arteries ex vivo. However, the mechanisms behind SGLT2-inhibitor-induced relaxation and SMIT1's vascular role remain unclear. This project investigates SGLT1 and SGLT2-inhibitor-induced relaxations and explores SMIT1's role in regulating arterial tone in male and female vascular beds.

Methods: RT-qPCR, immunocytochemistry, immunohistochemistry, western blot and PLA determined Slc5a protein expression and interactions. Vascular responses were recorded using wire myography and ex vivo morpholino oligonucleotide transfection, determined SMIT1's role in vascular tone and NHE1's role in SGLT2-induced relaxations.

Key Results: SMIT1 and SGLT2 proteins were expressed in mesenteric, renal, and coronary arteries of male and female rats, with minimal Slc5a1 and Slc5a11 mRNA transcripts. Hyperosmotic 150 mM raffinose increased SMIT1 membrane expression, reduced vascular contractility, and enhanced vasorelaxation, coinciding with increased interaction of SMIT1 with Kv7.4/5, Gβγ, and SGK1 proteins. Downregulation of SMIT1 increased arterial contractility and reduced relaxant responses to ML213, isoprenaline, and CGRP. SGLT2 inhibitors (1μM-100μM) and cariporide relaxed mesenteric arteries but had little effect on renal and septal arteries. Immunohistochemistry showed dense sensory nerve innervation in mesenteric arteries but not in renal and septal arteries. SGLT2 inhibitor-induced relaxations in mesenteric arteries were reduced by CGRP receptor antagonist BIBN-4096, TRPV1 antagonist AMG-517, and NHE1 knockdown.

Conclusions: This thesis reveals an oestrus cycle difference in SMIT1 expression in vascular smooth muscle cells and a novel role of SMIT1 in regulating vascular contractility through interactions with Kv7.4/5, Gβγ, and SGK. Additionally, SGLT2 inhibitors relax mesenteric arteries by promoting CGRP release from sensory neurons via NHE1 inhibition.

Declaration by the Candidate

I, Elizabeth Forrester, hereby declare that this thesis is my own work and that it has not been submitted elsewhere for any award.

Where other sources of work have been used, they have been acknowledged,

Signature:



Date: 29.10.2024

Acknowledgements

Throughout my PhD, many individuals have given me unwavering support and guidance. First and foremost, I would like to thank Professor Iain Greenwood. Throughout my education, I have struggled with my confidence and doubted my capabilities. However, Iain has shown me that with dedication and the right guidance, I can overcome these challenges and achieve more than I ever thought possible. I do become 'floppy' occasionally, but his belief in me has been a constant source of motivation, helping me grow into a confident and capable researcher. He creates such a welcoming and productive environment, making it easy for any student to thrive. His enthusiasm and deep knowledge of pharmacology are incredibly inspiring, and it has sparked my own passion for the field. He has opened up so many opportunities for me, broadening my horizons in ways I never imagined. I am not the same student I once was, and that is entirely because of his exceptional support and guidance. I deeply value our friendship and am excited about potential collaborations in the future.

A special thank you must also go to my co-supervisors, Dr Vincenzo Barrese and Professor Anthony Albert. Vincenzo, I am incredibly grateful for your warm welcome into your lab and the countless hours you and Camilla dedicated to teaching me Immunocytochemistry and PLA. Your encouragement, patience, and invaluable advice have profoundly helped me, and I want to thank you for showing me around Naples and introducing me to the best food. Celebrating your birthday with you and all your lab in Naples made my experience exceptionally memorable. Anthony, you have always been willing to help, giving insightful feedback and friendly guidance. Thank you both for believing in me and making this journey a truly uplifting experience.

Throughout my PhD, I have enjoyed working alongside Dr Isabelle Salles-Crawley, Dr Jennifer Stott, Dr Sam Baldwin, Ms Zena Wehbe, Ms Brianna Watson and Ms Skye Lau, and for a short time, Mr Ugo Ejiegbu. Each of them have played a pivotal role in shaping me into a confident and skilled scientific researcher. I want to thank them for being so patient with me and creating a fun and productive working environment. Our lunches at Simply and Tooting Market and evenings in the SU bar have been a central part of my experience, and I will deeply miss them. I also wish Brianna, Skye, and Ugo good luck with their projects.

To my close friends Skye and Vanessa, I will never forget the amazing fun we have had over the last 3 years, from long cheerleading competitions to our weekend in Naples, where Vanessa tried to cheer Skye and me up after we were both sick during the week and, of course, the infamous vodka pineapple. You have supported me, celebrating all the highs, empathising with the lows, embracing my goofiness, and listening to me frequently rant. I can truly say it's like I have gained another two sisters, and I want to thank you for your continued and generous friendship.

To Nack, you have made these last three years a fleeting adventure, always keeping me on my toes. Ziplining in Singapore, running away from monkeys in Malaysia, biking to the tallest mountain in Langkawi, and scuba diving in Cyprus have been some of the best highlights over the last three years. Thank you for always surprising me with great food, spontaneous days out in central London, and endless loving hugs when stressed with work. I am so lucky to have had you by my side, and without you, this PhD would have been a lot harder.

Lastly, to my whole family. A thank you is insufficient for the unconditional love, time, and endless guidance my mum and dad have always given me. You have both worked so hard as a team to ensure that my siblings Amy, Matthew, Philip, and I have had the best loving upbringing and education possible. No matter the time, day or night, you're always just a phone call away to listen to our struggles, offer advice, or lend a shoulder to cry on when times are tough. To Amy, Matt, and Phil, you are the best siblings anyone could wish for. Amy, you have been my anchor, supporting me through my lowest points over the past 3 years. Our holiday in Ibiza with your friends remains one of my favourite highlights, and I'll make sure to be the best auntie ever to baby Forrester-Smith. Matt, you have been my biggest cheerleader, always the first to express pride in my achievements. Thank you for travelling home on weekends, making me laugh, and cheering me up with your goofy personality and immense generosity. Phil, my university experience wouldn't have been the same without you. I cherish our daily car journeys to St. George's, studying together for exams, and every night out—from Toga and Tequila to WW8. Thank you for always looking after me and for introducing me to Iain; none of this would have been possible without you. Thank you, Auntie Wendy, Uncle David, and Amelia, for all the fun evenings around Woodmere Riviera. These times brought the family together to destress through good food and drink with Auntie

Faith and Julie, Uncle George, and Nannie. These times were so special and created fond memories that will last a lifetime. You all have lit a fire in me to persevere, even when times have been tough and hard to carry on. Finally, to Auntie Julie and Nannie, you have both been my biggest supporters and were proud of all my achievements, no matter how small. Though I wish you could see the final product, I’m so grateful you helped me to get this far, and I know you are here in spirit, cheering me on. I love you all to the moon and back again, all the world and tuppence ha'penny.

Publications and Communications:

- **Forrester EA**, Benítez-Angeles M, Redford KE, Rosenbaum T, Abbott GW, Barrese V, Dora K, Albert AP, Dannesboe J, Salles-Crawley I, Jepps TA, and Greenwood IA (2024). Crucial role for sensory nerves and Na/H exchanger inhibition in dapagliflozin and empagliflozin-induced arterial relaxation, Cardiovascular Research. doi:10.1093/cvr/cvae156.
- Barrese, V., Wehbe, Z., Linden, A., McDowell, SE., **Forrester, EA**., Oleksander Povstyan, McCloskey, K., & Greenwood, IA. (2023). Key role for Kv11.1 (ether-a-go-go related gene) channels in rat bladder contractility. Physiological Reports, 11(3). https://doi.org/10.14814/phy2.15583.
- Baldwin, SN., **Forrester, EA**., Homer, NZ., et al. (2022) 'Marked oestrous cycle-dependent regulation of rat arterial Kv7.4 channels driven by GPER1', British Journal of Pharmacology, 180(2), pp. 174–193. doi:10.1111/bph.15947.
- Baldwin, SN., **Forrester, EA**., McEwan, L and Greenwood, IA (2022) 'Sexual dimorphism in prostacyclin-mimetic responses within rat mesenteric arteries: A novel role for Kv7.1 in shaping IP receptor-mediated relaxation', British Journal of Pharmacology, 179(7), pp. 1338–1352. doi:10.1111/bph.15722.

Conference presentations:

Oral communications:

- 2024 - International Symposium on Mechanisms of Vasodilation, Oxford, UK: Crucial role for Na/H exchanger inhibition on sensory nerves in dapagliflozin and empagliflozin-induced arterial relaxation – Awarded Best Oral Presentation Prize
- 2023 - St George's Post Graduate Symposium, London, UK: Identification of a role for sodium hydrogen exchangers in SGLT2 inhibitor-induced relaxations
- 2022 - British Pharmacological Society's annual Pharmacology meeting, Liverpool, UK: SGLT2 Inhibitors induce vasorelaxation via a Kv7-dependent mechanism.

Poster presentations:

- 2023 - 2nd International Kv7 Channel Symposium, Naples, Italy: Sodium Myo-Inositol transporters: A New Kv7 modulator regulating arterial tone.

- 2023 - Sophion Bioscience Ion Channel Modulation Symposium, Cambridge, UK: Sodium Myo-Inositol transporters: A new Kv7 channel modulator regulating arterial tone - Awarded Best Poster Presentation prize.
- 2022 - St George’s Research Day, London, UK: SGLT2 Inhibitors induce vasorelaxation via a Kv7-dependent mechanism.
- 2021 - British Pharmacological Society's annual Pharmacology meeting: Sexual dimorphism in prostacyclin-mimetic responses of rat mesenteric artery.

Table of Contents

General Abstract 2

Declaration by the Candidate 4

Acknowledgements 5

Publications and Communications: 8

List of Figures 18

List of Tables 26

List of Abbreviations 27

Chapter 1: Introduction 34

1.1 | The circulatory System 34

1.2 | Smooth muscle 34

1.2.1 | Smooth muscle contraction 34

1.2.2 | Ion channel activation resulting in an increase in intracellular calcium concentration 36

1.3 | Regulating cell membrane potential 38

1.3.1 | TRP channels 38

1.3.2 | Chloride channels 39

1.4 | Vasorelaxation in vascular smooth muscle cells 41

1.5 | Potassium channels 43

1.5.1 | Calcium-activated potassium channels (K_{Ca}) 44

1.5.2 | Inward rectifier potassium channels (K_{IR}) 45

1.5.3 | ATP-sensitive potassium channels (K_{ATP}) 46

1.5.4 | Voltage-gated potassium channels 47

1.5.5 | Kv7 channels in vascular smooth muscle 49

1.5.6 | Kv7 channel function 51

1.5.7 | Kv7 channel regulation 54

1.6 | Smooth muscle solute transporters 56

1.6.1 | SLC2 transporters 57
1.6.2 | SLC5 transporters 57
1.6.3 | Sex Differences in Vascular Physiology 72
1.7 | Thesis Aims 74
Chapter 2: Methods and Materials 75
2.1 | Animals and Dissection 75
2.2 | Solutions: 77
2.3 | Rat Oestrus cycle staging 78
2.4 | Myography 80
2.4.1 | Outline and preparation 80
2.4.2 | Normalisation protocol 81
2.4.3 | Vitality testing protocol. 83
2.4.4 | Drugs 84
2.4.5 | Experimental protocols 86
2.5 | Ex Vivo morpholino Knockdown in whole arteries 87
2.6 | Gene Expression 88
2.6.1 | RNA extraction and purification 88
2.6.2 | RNA Quantification 89
2.6.3 | Reverse transcription polymerase chain reaction (RT-PCR) 90
2.6.4 | Quantitative polymerase chain reaction (qPCR) 91
2.6.5 | Melt Curve analysis. 94
2.6.6 | QPCR analysis 95
2.7 | Cell Isolation 95
2.8 | Fluorescence microscopy 96
2.8.1 | Immunocytochemistry (ICC) 96
2.8.2 | Immunohistochemistry (IHC) 97
2.8.3 | Proximity ligation assay 100

2.9 | Western Blot....102
2.9.1 | Tissue lysis....102
2.9.2 | Lysis of HEK293 cells....102
2.9.3 | Total Protein quantification....102
2.9.4 | Gel electrophoresis and membrane transfer. 103
2.9.5 | Probing and detection....104
2.9.6 | Stripping and re-probing....105
2.10 | Cell Culture....105
2.10.1 | Plasmid extraction and purification....105
2.11 | Data Analysis....106
Chapter 3: Characterising the expression of SLC5 proteins in the vasculature 108
3.1 | Introduction....108
3.2 | Methods....111
3.3 | Results....112
3.3.1 | Relative expression of Slc5a genes in the vasculature....112
3.3.2 | Comparing the relative transcript abundance of Slc5a genes in male and female arteries....116
3.3.3 | Immunocytochemistry staining in isolated vascular smooth muscle cells 118
3.3.4 | The expression of SMIT1 in vascular smooth muscle cells from male mesenteric, renal and coronary arteries. 119
3.3.5 | Classifying the expression of SGLT2 in mesenteric renal and coronary arteries....122
3.3.6 | Immunohistochemistry staining in whole mesenteric and renal arteries 126
3.3.7 | The expression of SMIT in endothelial cells of whole mesenteric and coronary arteries....127

3.3.8 | The expression of SGLT2 in endothelial cells of whole mesenteric and coronary arteries 129

3.3.9 | Expression of SMIT in mesenteric and coronary VSMCs from female rats 131

3.3.10 | Expression of SGLT2 in female mesenteric, renal and coronary arteries 135

3.4 | Discussion 139

3.4.1 | Expression of SGLT2 and SMIT1 in different vascular beds 139

3.4.2 | Sex differences in the arterial expression of SGLT2 and SMIT1 ..141

3.4.3 | Limitations 142

3.4.4 | Conclusion 143

Chapter 4: Investigating the role of sensory nerves in SGLT2 inhibitor-induced relaxation. 144

4.1 | Introduction 144

4.2 | Methods 146

4.2.1 | Cell Cultures 146

4.2.2 | Electrophysiology 146

4.2.3 | Two-electrode voltage clamp (TEVC) 147

4.2.4 | Transient cell transfection and patch-clamp 147

4.3 | Results 149

4.3.1 | Characteristics of vasoconstrictor-induced contractions in mesenteric, renal and coronary arteries. 149

4.3.2 | Effect of methoxamine and U46619 in coronary arteries. 151

4.3.3 | The vasoconstrictor responses in mesenteric, renal, septal and LAD arteries. 152

4.3.4 | SGLT2 inhibitors relax mesenteric arteries in an endothelium-independent manner. 155

4.3.5 | Effect of SGLT2 inhibitors in renal and septal arteries. 157

4.3.6 | Comparing the effect of dapagliflozin and empagliflozin in mesenteric, renal and septal arteries 158

4.3.7 | Characterising the expression of Kv7 ion channels in mesenteric and renal arteries 159

4.3.8 | Characterising Kv7 channel blockers in mesenteric and renal arteries 160

4.3.9 | The role of Kv7 channels in SGLT2 inhibitor induced relaxations. 163

4.3.10 | Responses to SGLT inhibitors with different spasmogens. 166

4.3.11 | SGLT2 inhibitors do not activate Kv7 channels 169

4.3.12 | Sensory nerve contribution in mesenteric arteries compared to renal and septal arteries. 171

4.3.13 | Mesenteric arteries are more sensitive to capsaicin and CGRP-induced relaxations than renal and septal arteries. 173

4.3.14 | Comparing the CGRP and TRPV1 expression in the adventitial layer of whole arteries 175

4.3.15 | SGLT1 and SGLT2 inhibitor-induced relaxations are sensitive to CGRP blockade. 177

4.3.16 | SGLT1 and SGLT2 evoked relaxations are sensitive to TRPV1 blockade. 178

4.3.17 | Dapagliflozin-induced relaxations are not sensitive to TRPA1 blockade. 181

4.3.18 | Effect of SGLT2 inhibitors on heterologously expressed TRPV1 currents. 182

4.3.19 | NHE1 co-localises with TRPV1 in the adventitial layer 185

4.3.20 | The effect of the NHE1 inhibitor cariporide in arteries. 188

4.3.21 | Cariporide prevents SGLT2 inhibitor-induced responses in mesenteric arteries. 189

4.3.22 | Knock-down of NHE1 impairs the relaxation to dapagliflozin and empagliflozin. 191

4.4 | Discussion 194
4.4.1 | SGLT inhibitors induce arterial relaxations. 195
4.4.2 | The role of CGRP release in SGLT1 and SGLT2 inhibitor-induced arterial relaxation 196
4.4.3 | NHE1 in arterial relaxation 197
4.4.4 | Limitations 199
4.4.5 | Conclusion 199
Chapter 5: Characterising the functional role of sodium myo-inositol transporters in arteries 201
5.1 | Introduction 201
5.2 | Methods 204
5.3 | Results 205
5.3.1 | The effect of SMIT1-specific morpholino oligonucleotide on vascular smooth muscle cell vasocontractile and relaxant responses 205
5.3.2 | SMIT1 knock-down impaired the relaxation responses of CGRP and isoprenaline 208
5.3.3 | Raffinose incubation increased SMIT1 expression in isolated vascular smooth muscle cells 211
5.3.4 | Augmenting membrane expression of SMIT1 attenuated the vasoconstrictor responses to methoxamine, U46619 and KCl 215
5.3.5 | SMIT1 knock-down prevented the pro-relaxant effects of raffinose 219
5.3.6 | The effect of augmented SMIT1 expression on Adenosine-induced relaxations in mesenteric arteries 222
5.3.7 | Expression of Kv7.4 in male mesenteric and coronary arteries post incubating in 150mM raffinose PSS 224
5.3.8 | SMIT physically interacts with Kv7.4 and Kv7.5 ion channels in mesenteric and coronary arteries 227
5.3.9 | Augmenting SMIT1 membrane expression increased ML213 relaxations in mesenteric and coronary arteries 230

5.3.10 | SMIT1-Gβγ protein interactions in mesenteric and coronary arteries 233

5.3.11 | Inhibitors of the Kv7 channel and βγ subunits prevent the reduction of methoxamine-induced contractions in raffinose incubated vessels. 236

5.3.12 | SGK1 regulates SMIT1 membrane expression 239

5.3.13 | Change in SMIT expression in female mesenteric and coronary arteries when incubated in 150 mM raffinose 244

5.3.14 | The effect of increasing membrane SMIT1 expression on methoxamine-induced contractions in DM and PE female mesenteric arteries. 249

5.3.15 | Kv7.4 expression in males and females 251

5.3.16 | Change in Kv7.4 expression in female mesenteric and coronary arteries when incubated in 150 mM raffinose 253

5.3.17 | SMIT1 physically interacts with Kv7.4 and Kv7.5 ion channel proteins in mesenteric and coronary arteries from female rats.....255

5.3.18 | The effect of incubating mesenteric and coronary arteries in hyperglycaemic PSS 260

5.4 | Discussion.....266

5.4.1 | SMIT1 induces vasorelaxation through activating Kv7.4/5 ion channels mediated by the Gβγ Subunit.....266

5.4.2 | Oestrus cycle differences in SMIT1-induced relaxations.....270

5.4.3 | SGK1 regulates SMIT1 expression and functional effect 271

5.4.4 | Limitations.....273

5.4.5 | Conclusion: 274

Summary figure: 275

Chapter 6: Discussion 276

6.1 | Overview 276

6.2 | Oestrus cycle differences in vascular physiology 279

6.3 | Conclusion 280

Chapter 7: Bibliography 281

Chapter 8: Appendices 336

List of Figures

Chapter 1:

Figure 1.1 : Schematic of calcium sensitisation 37
Figure 1.2: $G_{q/11}$ - GPCR mediated vasoconstriction 40
Figure 1.3: Function and classification of potassium channels 44
Figure 1.4: Summary overview of VSMC relaxation: 56
Figure 1.5: Function of SGLT1 and SGLT2 within the proximal tubule. 64
Figure 1.6: Diagram of SMIT1 and 2 production: 68
Figure 1.7: Interaction of Kv7 channels with SMIT1 in VSM cells 71

Chapter 2:

Figure 2.1: Mesenteric, renal and coronary artery dissection 76
Figure 2.2: Vaginal cytology and uterine characteristics in each rat oestrus stage 79
Figure 2.3: Representation of a mounted artery segment on a wire and pin myograph (Source: Author) 81
Figure 2.4: Normalisation settings 82
Figure 2.5: Normalisation protocol 82
Figure 2.6: Representative trace of the vitality testing protocol 83
Figure 2.7: Schematic of the two experimental protocols 1 and 2. 87
Figure 2.8: Absorbance spectrum of a purified RNA sample using NanoDrop 3300 Fluorospectrometer 90
Figure 2.9: Representative Amplification curve: 92
Figure 2.10: Melt curve analysis: 94
Figure 2.11: Schematic of RT-qPCR methodology (Source: Author using Biorender.com). 95
Figure 2.12: Diagram of Immunocytochemistry methodology (Source: Author using Biorender.com). 97
Figure 2.13: Primary and Secondary Antibody detection in ICC and IHC (Source: Author): 98
Figure 2.14: Schematic of BCA assay protocol (Source: Author using Biorender.com). 103

Chapter 3:

Figure 3.1: Expression of Slc5 genes in heart myocardium, brain and kidney tissue from male rats. 113
Figure 3.2: The relative transcript abundance of Slc5a genes in mesenteric, renal, coronary and cerebral arteries from male rats. 113
Figure 3.3: The relative transcript abundance of Slc5a genes in mesenteric, renal and coronary arteries from DM and PE female rats. 115
Figure 3.4: Comparison of Slc5a expression in male, DM female and PE female mesenteric and renal arteries. 117
Figure 3.5: Expression of alpha-smooth muscle actin (αSMA) in mesenteric, renal and coronary vascular smooth muscle cells 118
Figure 3.6: The protein expression of SMIT in mesenteric, renal and coronary arteries from male rats. 120
Figure 3.7: The membrane abundance of SMIT1 in mesenteric, renal and coronary arteries from male rats. 121
Figure 3.8: Western blot quantification of SGLT2. 122
Figure 3.9: Expression of SGLT2 protein in mesenteric, renal and coronary arteries. 124
Figure 3.10: The distribution of SGLT2 in various vascular smooth muscle beds. 125
Figure 3.11: Markers for smooth muscle cells and endothelial cells. 126
Figure 3.12: Expression of SMIT1 in the smooth muscle layer of whole mesenteric, renal and coronary arteries. 127
Figure 3.13: Expression of SMIT1 in the endothelial layer of whole mesenteric, renal and coronary arteries. 128
Figure 3.14: Expression of SGLT2 in the smooth muscle layer of whole mesenteric, renal and coronary arteries. 129
Figure 3.15: Expression of SGLT2 in the endothelial layer of whole mesenteric, renal and coronary arteries 130
Figure 3.16: The protein expression of SMIT in mesenteric, renal and coronary arteries from DM and PE Female rats. 132
Figure 3.17: The membrane abundance and distribution of SMIT1 in the mesenteric, renal, and coronary arteries of DM and PE female rats. 133
Figure 3.18: Comparison of the total expression of SMIT1 in mesenteric and coronary arteries from male, DM female and PE female rats. 134

Figure 3.19: Shows the protein expression of SGLT2 in the mesenteric, renal, and coronary arteries of DM and PE Female rats. 136
Figure 3.20: The membrane abundance and distribution of SGLT2 in the mesenteric, renal, and coronary arteries of DM and PE Female rats. 137
Figure 3.21: Comparison of the total expression of SGLT2 in mesenteric and coronary arteries from male, DM female and PE female rats. 138

Chapter 4:

Figure 4.1: Representative traces of U46619 and methoxamine curves in the presence and absence of their respective blockers. 150
Figure 4.2: Mean effect of prazosin and ICI192605 on vasocontractile agents: 151
Figure 4.3: Effect of methoxamine and U46619 on coronary arteries. 152
Figure 4.4: Comparison of the resting basal tone of mesenteric, renal, septal and left anterior descending artery. 153
Figure 4.5: Comparison of mesenteric, renal, septal and LAD arterial contractions (mN). 154
Figure 4.6: The effect of dapagliflozin on pre-contracted mesenteric arteries. 155
Figure 4.7: The effect of 2 structurally different SGLT2 inhibitors and one SGLT1 inhibitor on mesenteric arteries pre-contracted with 10 μM methoxamine. 156
Figure 4.8: Lack of correlation between SGLT2 inhibitor and carbachol response in mesenteric arteries. 157
Figure 4.9: The effect of dapagliflozin and empagliflozin on renal and septal arteries. 158
Figure 4.10: Comparison of the relaxation to dapagliflozin and empagliflozin in mesenteric and renal arteries pre-contracted with 10μM methoxamine. 159
Figure 4.11: Expression of Kcnq1-5 in mesenteric and renal arteries. 160
Figure 4.12: The relaxation to Pan Kv7 channel activator ML213. 161
Figure 4.13: Effect of linopirdine on the relaxant action of Kv7 activator ML213. 162
Figure 4.14: The effect of a pan Kv7 channel blocker linopirdine on SGLT2 inhibitor-induced relaxation: 164
Figure 4.15: SGLT2 inhibitor-induced relaxation in renal arteries is not linopirdine sensitive. 165

Figure 4.16: The effect of non-selective Kv blockers on the relaxation produced by dapagliflozin and empagliflozin in mesenteric arteries. 165
Figure 4.17: The effect of SGLT1 inhibitor, mizagliflozin on pre-contracted mesenteric arteries are spasmogen specific but SGLT2 inhibitors are not. 167
Figure 4.18: The effect of mizagliflozin is spasmogen dependent and linopirdine sensitive. 168
Figure 4.19: SGLT2 inhibitors do not activate Kv7.4/5 channels directly. 170
Figure 4.20: The effect of CGRP on mesenteric and renal arteries 172
Figure 4.21: The effect of CGRP in mesenteric and renal arteries in the presence and absence of BIBN-4096 and linopirdine. 173
Figure 4.22: The effect of capsaicin on pre-contracted mesenteric arteries 174
Figure 4.23: Mesenteric arteries produce greater relaxations to capsaicin compared to renal and septal arteries. 174
Figure 4.24: Expression of TRPV1 and CGRP in the adventitial layer of whole mesenteric arteries. 175
Figure 4.25: Expression of TRPV1 and CGRP in the adventitial layer of whole renal and septal arteries. 176
Figure 4.26: Lack of TRPV1 and CGRP expression in mesenteric and renal smooth muscle cells (SMC) and endothelial cell (EC) layers. 177
Figure 4.27: Dapagliflozin, empagliflozin and mizagliflozin relaxations are sensitive to CGRP blocker, BIBN-4096. 178
Figure 4.28: Effect of sensory nerve depletion and TRPV1 blockade on capsaicin-induced relaxations. 179
Figure 4.29: Dapagliflozin and empagliflozin-induced relaxations are impaired by sensory nerve depletion and TRPV1 blockade. 180
Figure 4.30: Mean amplitude of methoxamine evoked contractions. 181
Figure 4.31: Effect of TRPA1 blocker AM0902 on dapagliflozin induced-relaxations. 182
Figure 4.32: Dapagliflozin does not activate TRPV1 directly. 183
Figure 4.33: Empagliflozin does not activate TRPV1 directly 184
Figure 4.34: NHE1 expression is found in smooth muscle and adventitial cell layers but not endothelial cell layers of mesenteric arteries 186
Figure 4.35: SGLT2 expression in the adventitial, smooth muscle, and endothelial cell layers of mesenteric arteries. 187

Figure 4.36: Expression of SGLT2 and NHE1 in renal artery adventitial, smooth muscle and endothelial cell layers. 187
Figure 4.37: Comparison in the relaxation to cariporide in mesenteric and renal arteries pre-contracted with 10μM methoxamine. 188
Figure 4.38: Cariporide induced relaxations are impaired by the CGRP blocker, BIBN and TRPV1 blocker, AMG-517. 189
Figure 4.39: Effect of cariporide on SGLT2 inhibitor-induced relaxations. 190
Figure 4.40: Knock-down of NHE1 impairs the relaxation to dapagliflozin and empagliflozin in mesenteric arteries. 192
Figure 4.41: Representative labelling for TRPV1 (green) and NHE1 (magenta) in the adventitia of whole mesenteric arteries transfected with scrambled morpholino and NHE1 targeted morpholino. 193
Figure 4.42: Pathway of SGLT2 induced relaxation in mesenteric arteries. 200

Chapter 5:

Figure 5.1: SMIT protein expression in control and knockdown smooth muscle cell and endothelial cell layers of whole mesenteric arteries 206
Figure 5.2: The contractile response to methoxamine and 60mM KCl in mesenteric arteries incubated with a scrambled control morpholino or SMIT1 knock-down morpholino 207
Figure 5.3: The contractile response to methoxamineU46619 in mesenteric arteries incubated with a scrambled control morpholino or SMIT1 knock-down morpholino 208
Figure 5.4: The relaxation response to the beta-adrenergic receptor agonist, isoprenaline in control and SMIT1 targeted morpholino vessels. 209
Figure 5.5: The relaxation response to CGRP receptor agonist in control and SMIT1 targeted morpholino vessels. 210
Figure 5.6- The expression of SMIT1 in VSMCs from mesenteric and coronary arteries isolated from male rats with and without incubating in raffinose for 4 hours: 212
Figure 5.7: The change in membrane abundance of SMIT1 in male mesenteric and coronary arteries after incubating in 150 mM raffinose for 4-hours. 214
Figure 5.8: The concentration dependent contraction to methoxamine in mesenteric arteries after overnight incubation (~16h) in 150 mM raffinose. 216

Figure 5.9: The concentration-dependent contraction to methoxamine after different timed interval incubations with 150 mM raffinose PSS. 217
Figure 5.10: The concentration-dependent contraction to U46619 after 4 hours of raffinose incubation in mesenteric arteries with either positive endothelium or denuded. 218
Figure 5.11: The contractile response to U46619 in coronary arteries from male rats when incubated in 150mM raffinose for 4-hours. 219
Figure 5.12: The effect of raffinose incubation on the contractile response to methoxamine in control and SMIT1 targeted morpholino vessels. 220
Figure 5.13: The effect of augmenting SMIT expression on KCL-induced contractions. 221
Figure 5.14: Adenosine-mediated relaxation is sensitive to Kv7 channel blockade. 223
Figure 5.15: Adenosine-induced relaxations are enhanced in mesenteric arteries incubated in 150mM raffinose for 2-hours. 224
Figure 5.16 :Expression of Kv7.4 in male mesenteric and coronary arteries when incubated with either control PSS or 150 mM raffinose PSS for 4-hours. 226
Figure 5.17: The interaction of SMIT with Kv7.4 and Kv7.5 in mesenteric and coronary arteries from male rats for 4-hours. 227
Figure 5.18: The interaction of SMIT with Kv7.4 and Kv7.5 in mesenteric and coronary VSMCs from male rats following 4-hour incubation in raffinose. 229
Figure 5.19: The relaxation to ML213 in mesenteric arteries when incubated in 150 mM raffinose for 10 minutes, 30 minutes and 1 hour. 231
Figure 5.20: The relaxation to ML213 in coronary arteries when incubated in 150 mM raffinose for 2-hours. 232
Figure 5.21: The relaxation response to Pan Kv7 channel activator ML213 in control and SMIT1 targeted morpholino vessels. 233
Figure 5.22: Kv7.4 and Gβγ interaction in mesenteric and coronary arteries incubated in either control PSS or 4-hours 150 mM raffinose PSS. 234
Figure 5.23: The interaction of SMIT1 with Gβγ in mesenteric and coronary arteries incubated in 150mM raffinose for 4-hours. 235
Figure 5.24: The effect of the concentration-dependent contraction to methoxamine in mesenteric arteries in raffinose (4-hours) when in the presence of a pan Kv7 channel, beta-gamma and SGK blocker. 237

Figure 5.25: The concentration-dependent contraction to U46619 in coronary arteries in raffinose (4-hours) in the presence of either a pan Kv7 channel, beta-gamma or SGK blocker. 238
Figure 5.26: The expression of SMIT1 in mesenteric arteries incubated in raffinose for 4-hours with and without an SGK inhibitor. 240
Figure 5.27:The interaction of SMIT1 with SGK in mesenteric and coronary arteries following 4-hour raffinose incubation. 242
Figure 5.28: The effect of the concentration-dependent contraction to methoxamine in mesenteric and coronary arteries in raffinose (4-hours) when in the presence of the SGK inhibitor EMD638683. 243
Figure 5.29: The expression of SMIT1 in mesenteric and coronary arteries from DM and PE female rats with and without incubating in raffinose for 4 hours: 245
Figure 5.30: Expression of SMIT1 in mesenteric and coronary arteries from males, DM females and PE females in the presence and absence of 4-hour 150 mM raffinose incubation. 246
Figure 5.31: Membrane abundance of SMIT1 in female mesenteric and coronary arteries after a 4-hour raffinose incubation. 247
Figure 5.32: The membrane abundance of SMIT1 in mesenteric and coronary arteries from male, DM female and PE female rats. 248
Figure 5.33: Effect of methoxamine-induced contractions on female mesenteric arteries when incubated overnight in raffinose PSS. 250
Figure 5.34: The concentration-dependent contraction to methoxamine in female mesenteric arteries incubated in either 20mM or 150mM raffinose for 4-hours. 250
Figure 5.35: Expression of Kv7.4 in mesenteric and coronary arteries from male and female rats 252
Figure 5.36: Expression of Kv7.4 in female mesenteric and coronary arteries when incubated in raffinose for 4-hours. 254
Figure 5.37: Membrane expression Kv7.4 in female mesenteric and coronary arteries when incubated in raffinose for 4-hours. 255
Figure 5.38: The interaction of SMIT with Kv7.4 and Kv7.5 in mesenteric and coronary VSMCs from male, DM female and PE female rats. 256
Figure 5.39: The interactions of SMIT1 with Kv7.4 and Kv7.5 in mesenteric and coronary VSMCs from DM female and PE female rats. 257

Figure 5.40: Interaction of SMIT1 with Gβγ in mesenteric and coronary arteries from male, DM female and PE female rats. 259
Figure 5.41: The interaction of SMIT with Gβγ in raffinose-incubated mesenteric and coronary arteries in DM and PE females. 260
Figure 5.42: The change in the expression of SMIT1 in mesenteric and coronary arteries incubated in control or 4 hours of glucose PSS. 261
Figure 5.43: The change in the expression of SGLT2 in mesenteric and coronary arteries incubated in either control or 4 hours of 20 mM glucose PSS. 262
Figure 5.44: The concentration-dependent contraction to methoxamine in male mesenteric arteries incubated overnight in glucose PSS. 263
Figure 5.45: The contraction to methoxamine following overnight incubation in hyperglycaemic 20mM glucose PSS in female DM and PE mesenteric arteries. 264
Figure 5.46: The contraction to methoxamine in female mesenteric arteries incubated in 20mM raffinose and 20mM glucose for 4-hours. 265
Figure 5.47 –Overview of SMIT1 activity in VSMCs 275

Chapter 8: Appendix

Figure 8.1: Representative labelling for TRPV1 (Green) and CGRP (magenta) in mesenteric arteries, showing all three representative repeats. 336
Figure 8.2: Representative labelling for TRPV1 (Green) and CGRP (magenta) in renal arteries, showing all three representative repeats. 337
Figure 8.3: Representative labelling for TRPV1 (Green) and NHE1 (magenta) in mesenteric arteries, showing all three representative repeats. 338
Figure 8.4: Representative labelling for TRPV1 (Green) and NHE1 (magenta) in renal arteries, showing all three representative repeats. 339
Figure 8.5: Representative labelling for TRPV1 (Green) and SGLT2 (magenta) in mesenteric arteries, showing all three representative repeats. 340
Figure 8.6: Representative labelling for TRPV1 (Green) and SGLT2 (magenta) in renal arteries, showing all three representative repeats. 341
Figure 8.7: Representative labelling for TRPV1 (green) and NHE1 (magenta) in the adventitia of whole mesenteric arteries transfected with scrambled morpholino (Top) and NHE1 targeted morpholino (Bottom), showing all three representative repeats. 342

List of Tables

Chapter 1:

Table 1.1: Summary of K_V7 channel expression and their channelopathies. 48
Table 1.2: Kv7 channel and KCNE auxiliary subunit distribution in the vasculature 50
Table 1.3: Table of Kv7 channel activators and their selectivity 53
Table 1.4: Table of Kv7 channel blockers and their selectivity to Kv7 isomers 54
Table 1.5: A summary of the expression and transport of all 12 SLC5 proteins 58

Chapter 2:

Table 2.1: The composition of every solution used in this study. 77
Table 2.2: Cervical cell populations in female Wistar rats 80
Table 2.3: A list of all reagents used: 84
Table 2.4: Table of morpholino oligonucleotides used: 88
Table 2.5: Table of primers used for RT-qPCR with their respective amplicon and accession numbers 92
Table 2.6 - List of primary antibodies used (Source: Author): 99
Table 2.7 - List of secondary antibodies for Immunocytochemistry (Source: Author): 100

Chapter 4:

Table 4.1 - Summary of vasoconstrictor responses in all arteries tested in myograph experiments. 154

List of Abbreviations

IP_3	1,4,5-inositol triphosphate
E2	17-β Oestradiol
DAPI	4’,6-diamidino-2-phenylindole
α-MG	α-Mangostin
AKAP	A-kinase anchoring proteins
ADP	Adenosine diphosphate
ATP	Adenosine triphosphate
N	Amino
AT_{II}	Angiotensin II
AT_1	Angiotensin II receptor
A.U.	Arbitrary units
K_{ATP}	ATP-sensitive potassium channel
ANP	Atrial natriuretic peptide
BP	Blood pressure
CGRP	Calcitonin gene-related peptide
Ca^{2+}	Calcium
CaCC	Calcium-activated chloride channel
$I_{Cl(Ca)}$	Calcium-activated chloride currents
K_{Ca}	Calcium-activated potassium currents
Ca/CaM	calcium calmodulin complexes
CaM	Calmodulin
CanX	Calnexin
CCh	Carbachol

C	Carboxy
CO	Cardiac output
CD	Cardiovascular Disease
CVS	Cardiovascular System
CHO	Chinese hamster ovarian
Cl^-	Chloride
CHT	Choline transporter
V_{cmd}	Command voltage
CEC	Concentration effect curve
G	Conductance
CTCF	Corrected total cell florescence
I	Current
IV	Current-voltage
cAMP	Cyclin adenosine monophosphate
cGMP	Cyclin guanine monophosphate
COX	Cyclooxygenase
Cyc1	Cytochrome C1
CFTR	Cystic fibrosis transmembrane conductance regulator
I_{Ks}	Delayed rectifier potassium current
DAG	Diacylglycerol
DM	Diabetes Mellitus
DPP-4	Dipeptidyl peptidase-4
dsDNA	Double-stranded DNA
ECs	Endothelial cells
EDH	Endothelial-derived hyperpolarisation

EGF	Endothelial growth factor
eNOS	Endothelial nitric oxide synthase
ENaC	Epithelial sodium channel
E_{Cl}	Equilibrium potential for Cl^-
E_K	Equilibrium potential for K^+
E_{ion}	Equilibrium potential of an ion
EPAC	Exchange protein directly activated by cAMP
ERK	Extracellular signal-regulated kinase
DM	Females in Met-Oestrus and Di-Oestrus
PE	Females in Pro-Oestrus and Oestrus
GPER1	G-protein coupled oestrogen receptor
GPCR	G-protein kinase receptor
GIP	Gastric inhibitory polypeptide
GLUT	Glucose transporter
GLP	Glucagon-like peptide
Gapdh	Glyceraldehyde 3-phosphate dehydrogenase
GDP	Guanosine diphosphate
GTP	Guanosine triphosphate
HSP70	Heat shock protein 70
HSP90	Heat shock protein 90
KPSS	High K+ physiological salt solution
HEK	Human embryonic kidney 293B
HMIT	Hydrogen myo-inositol transporter
IK_{Ca}	Intermediate conductance K_{Ca} channels
$[Ca^{2+}]_i$	Intracellular calcium concentration

K_{ir}	Inwardly rectifying potassium channels
L-NAME	L- Nitroarginine methyl ester
BK_{Ca}	Large conductance K_{Ca} channels
LAD	Left anterior descending
CaATPase	Membrane calcium ATPase pumps
MAPK	Mitogen-activated protein kinase
MEGJ	Myoendothelial gap junction
MLCK	Myosin light chain kinase
MLCP	Myosin light chain phosphatase
MYPT-1	Myosin phosphatase targeting subunit-1
NCX	Na^+/Ca^{2+} exchangers
NO	Nitric oxide
NRT	No reverse transcription
NTC	No template control
PBS	Phosphate buffered serum
PIP_2	Phosphatidylinositol 4,5-bisphosphate
PIP4K	Phosphatidylinositol 5-phosphate 4-kinase
PI3K	Phosphoinositide 3-kinases
PLC	Phospholipase-C
PSS	Physiological salt solution
PMCA	Plasma membrane Ca^{2+} ATPase
PD	Pore domain
PET	Positron emission tomography
PGI_2	Prostacyclin
PKA	Protein Kinase A

PKC	Protein Kinase C
PKG	Protein Kinase G
PLA	Proximity ligation assay
Cq	Quantification cycle
ROC	Receptor-operated channel
R	Resistance
RMP	Resting membrane potential
qPCR	Quantitative polymerase chain reaction
RT-qPCR	Reverse transcription-quantitative polymerase chain reaction
RhoK	Rho-Kinase
RhoGEF	Rho-guanine exchange factor
RT	Room temperature
SR	Sarcoplasmic reticulum
SERCA	sarcoplasmic/endoplasmic reticulum Ca^{2+}ATPase
STIM1	Sensor-stromal interaction molecule 1
SNP	Single nucleotide polymorphism
SK_{Ca}	Small conductance K_{ca} channels
Na^{+}	Sodium
SMCT	Sodium-coupled monocarboxylate transporters
SGLT	Sodium-dependent glucose transporter
SMVT	Sodium-dependent multivitamin transporter
NHE	Sodium hydrogen exchanger
SMIT	Sodium myo-inositol transporter
NIS	Sodium/ Iodide symporter
SLC	solute carrier family

SOC	Store-operated channel
SOCE	Store-operated calcium entry
SVR	Systemic vascular resistance
TWIK-1	Tanderm of P domains in a week Inwardly rectifying K+ channel
TRIK	Tandem pore domain K^+ channel
TXA	Thromboxane
TonE	Tonicity response element
TonEBP	Tonicity-responsive enhancer-binding protein
TPR	Total peripheral resistance
TMD	Transmembrane domain
TGFβ	Transforming growth factor beta
TRP	Transient Receptor Potential
TRPA	Transient receptor potential ankyrin
TRPC	Transient receptor potential canonical
TRPM	Transient receptor potential melastatin
TRPML	Transient receptor potential mucolipin
TRPP	Transient receptor potential polycystin
V_m	Transmembrane potential
TASK	TWIK-related acid-sensitive K^+ channel
TREK	TWIK-related K^+ channels of the TWIK type
TALK	TWIK-related acid-sensitive K^+ channels
K_{2P}	Two pore domain channels
T2DM	Type 2 Diabetes
VSMC	Vascular smooth muscle cell
$Vsmc_m$	Vascular smooth muscle cell membrane potential

VRCC	Volume regulated Cl^- channels
VSD	Voltage sensing domain
VGCC	Voltage-gated calcium channels
ClCs	Voltage-gated Cl^- channels
K_v	Voltage-gated potassium channels
V	Volts
WGA	Wheat germ agglutinin

Chapter 1: Introduction

1.1 | The circulatory System

The circulatory system enables adequate perfusion of oxygen and nutrients to all the organs in the body, allowing sufficient metabolic and cellular function. Deoxygenated blood enters the right side of the heart through the vena cava and is pumped through the pulmonary circulation to be re-oxygenated in the lungs. Blood returns to the left side of the heart via the pulmonary veins and is then pumped through the aorta into the systemic circulation to deliver oxygen and nutrients to surrounding tissues. The pressure of blood within the artery and against the blood vessel walls is termed blood pressure, which is determined by the product of cardiac output (CO) and systemic vascular resistance (SVR). Hence, an increase in either CO or SVR will elevate blood pressure. Vascular tone determines SVR, therefore, when vasoconstriction occurs, there is an increase in SVR (Anderson, 1996). A myriad of stimuli affect vascular contractility, from hormonal to neuronal output. Hence, a change in stimuli can cause an imbalance in the signalling molecules involved in vascular tone, which can lead to elevated blood pressure and hypertension.

1.2 | Smooth muscle

Smooth muscle lines the walls of hollow organs such as blood vessels, GI tract, bladder, and airways. Its contractile state is controlled upon receiving neuronal innervation via the autonomic nervous system as well as autocrine and paracrine signalling cascades. Some types of smooth muscle exhibit spontaneous phasic contractions, for example the GI tract, bladder detrusor and uterine myometrium. Whereas, vascular smooth muscle is quiescent, until provoked by external stimuli (Horowitz et al., 1996; Kuo & Ehrlich, 2015).

1.2.1 | Smooth muscle contraction

An interaction of myosin with actin is needed for smooth muscle contraction to occur. The myosin filament is made up of 2 heavy chains coiled around each other. These chains diverge and fold, forming a globular structure that makes the myosin

heads, which bind to actin during a contractile state. 2 light polypeptide chains are between each head and are bound at 20-kDa and 17-kDa at rest, preventing it from interacting with actin. A rise in the concentration of intracellular calcium ([Ca2+]i) results in the binding and formation of calcium calmodulin complexes (Ca/CaM), that activate myosin light chain kinase (MLCK)(Webb, 2003). MLCK phosphorylates the myosin light chain at 20-kDa Ser19, resulting in increased ATPase activation (1000 x) and improved structural rigidity. ATPase hydrolyses ATP, leading to actin myosin crosslinking, and the myosin head tilts, causing the actin to be moved across the myosin filament (Cole & Welsh, 2011). Myosin light chain phosphatase dephosphorylates (MLCP) Ser19, reducing actin myosin cross bridging, which can be inhibited by calcium-independent contractile pathways, for example, ROCK-induced contraction (Solaro, 2000). This involves G12/13 activation, resulting in RhoA release from a guanine nucleotide dissociation inhibitor (GDI). Inactive RhoA is bound to guanosine diphosphate (GDP), which is exchanged for guanosine triphosphate (GTP) by GEFs, activating the RhoA-ROCK pathway (Rattan et al., 2010). Thus resulting in phosphorylation of MLCK and contraction. Activation of ROCK can also occur via phosphatidylinositol-4, 5-bisphosphate 3-kinase (PI3K)-dependent pathways (Yu et al., 2017). Smooth muscle contraction can be initiated independently from MLCK. Caldesmon is an actin-binding protein responsible for directly inhibiting ATPase activity on the myosin filament. Experimental studies demonstrate that serine kinases like ERK can phosphorylate caldesmon on Ser789, resulting in the reversal of caldesmon-mediated inhibition of ATPase and actin-myosin cross-linking to occur (Brozovich et al., 2016). This phenomenon can be simultaneous to the Rho-Kinase pathway (Foster et al., 2000). Moreover, the enzyme protein kinase C (PKC), involved in the signalling during Gαq/11 coupled receptor-induced contractions, can be activated by the differentiation marker calponin. Studies investigating this show acute knockdown of calponin levels in ferrets inhibits PKC-dependent vascular smooth muscle (VSM) contractions (Je et al., 2001; Kim & Nimigean, 2016). This demonstrates calponin is required to mediate VSM contractions. Therefore, smooth muscle contraction is modulated specifically by direct downstream activation of MLCK or via molecule activation of actin.

1.2.2 | Ion channel activation resulting in an increase in intracellular calcium concentration

The initiation of increased $[Ca^{2+}]_i$ occurs due to various stimuli. This triggers calcium release from the sarcoplasmic reticulum or influx of extracellular calcium via voltage-activated ion channels. Voltage-gated calcium channels (VGCC) form calcium-permeable pores, allowing calcium influx through the cell membrane. The channels are formed from several subunits which control the gating kinetics and the voltage sensing; the α1 subunit forms the ion-conducting pore and voltage sensor. This voltage-gated calcium channel (VGCC) subfamily can be divided based on their voltage activation. L type (Cav1.1, Cav1.2, Cav1.3, Cav1.4), P/Q-type (Cav2.1) and N-type (Cav2.2) are high voltage Calcium channels. R-type calcium channels (Cav2.3) are intermediate voltage, whereas T-type calcium channels (Cav3.1, Cav3.2, Cav3.3) are transient low voltage-activated channels (Ghosh et al., 2017). The L-type channels have long been known to be the primary route of calcium transport in vascular smooth muscle cells (VSMC), with T-type calcium channels controlling myogenic tone. In vitro and in vivo studies have demonstrated that inhibiting the α1 subunit activity by either dihydropyridine antagonists (Knot & Nelson, 1998) or knockout (Moosmang et al., 2003) in VGCCs abolished the increase in $[Ca^{2+}]_i$ preventing VSM contraction. Meanwhile, dihydropyridine agonists (e.g., Bay K8644) increased the L-type calcium channel activity and hence elevated myogenic tone (Hwa & Bevan, 1986).

Several G protein-coupled receptors (GPCR) are expressed on the surface of VSM cell membranes. Some are linked to phospholipase C (PLC) via Gαq/11 subunit proteins that respond to stimuli such as noradrenaline, vasopressin, angiotensin 2 and thromboxane A2. Upon ligand binding, a conformational change in the alpha subunit causes the exchange of guanosine diphosphate (GDP) with guanosine triphosphate (GTP). The Gα/GTP complex dissociates from the βγ subunit and activates PLC in the plasma membrane. PLC hydrolyses phosphatidylinositol bisphosphate (PIP_2) to inositol 1,4,5-triphosphate (IP3) and diacylglycerol (DAG). IP3 directly binds to its receptor on the sarcoplasmic reticulum (SR), opening Ca^{2+} channels and increasing cytosolic $[Ca^{2+}]$ levels. Ryanodine receptors (RyR) on the SR detect Ca_{2+} elevation and initiate calcium-induced calcium release.

As smooth muscle cells actively accumulate chloride ions, the opening of Cl channels in vascular smooth muscle cells (VSMCs) results in Cl efflux and membrane depolarisation. Activation of these channels in response to IP3 and ryanodine receptor-modulated calcium elevation produces depolarisation, stimulating further calcium efflux through VGCCs and promoting VSMC contractions (Askew-Page et al., 2019). The [Ca2+]i elevation coupled with PKC activates transient receptor potential channels (TRPC) (Ghosh et al., 2017). There are several TRPC channels, TRPC1 channels form heteromers with TRPC4/TRPC5, which are regulated by Gαq GPCR signalling (Kwan et al., 2009). Whereas TRPC3 is active once coupled to IP3 receptors, resulting in calcium and sodium influx and the eventual opening of L-type calcium channels, evoking depolarisation (Xi et al., 2008). A schematic of calcium sensitisation leading to inhibition of MLCP and activation of MLCK resulting in vasoconstriction is shown in figure 1.1.

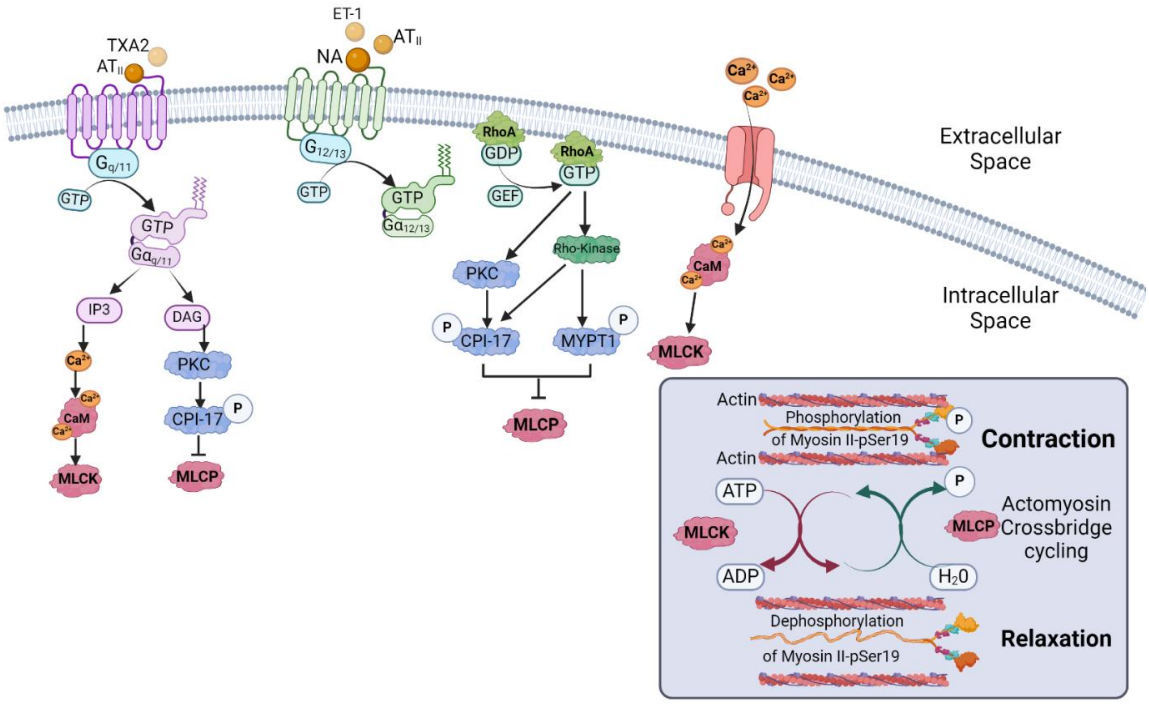


Figure 1.1 : Schematic of calcium sensitisation
$G_{q/11}$ and $G_{12/13}$- GPCR signalling activates MLCK and inhibits MLCP by PKC phosphorylating CPI-17 and rho-kinase-mediated inhibition of MYPT-1. Inhibiting MLCP promotes myosin light chain phosphorylation of Ser19, causing actin-myosin cross bridging and vasoconstriction. (Source: Author using Biorender.com).

1.3 | Regulating cell membrane potential

The resting membrane potential of VSMCs is between -60mV and -70mV, which measures the electrical potential across the plasma membrane of VSMCs when it is in an unstimulated state. Several ion channels and transporters set the resting membrane potential by establishing electrochemical gradients and aiding the movement of potassium (K^+), sodium (Na^+), and chloride (Cl^-) ions through the plasma membrane (Aaronson & Smirnov, 1996). The cell's permeability to these ions refers to their ability to cross the cell membrane. At resting tone potassium leak channels as well as the Na+/K+ ATPase pump that creates the concentration gradient to potassium by transferring two K^+ ions into the cell for three Na^+ ions are open. This results in potassium having the highest membrane permeability at rest, with the potassium equilibrium potential (Ek) at -90mV being a major contributor to the resting potential of VSMCs (Clay, 2009; Enyedi & Czirják, 2010; Morth et al., 2007). The sodium equilibrium potential of +60mV also contributes to the cell membrane potential regulation alongside potassium (Wright et al., 2004; Aaronson & Smirnov, 1996). The initial activation of voltage-gated sodium channels occurs when the membrane potential becomes less negative. Depolarisation of the cell membrane occurs when the membrane potential is around -40mV to -55mV this threshold enables the opening of voltage-gated calcium channels and eventual VSMC contraction. The efflux of potassium or influx of chloride through several types of ion channels causes the membrane potential to become more negative (roughly ≤ -80mV) and results in hyperpolarisation (Clay, 2009; Wright et al., 2004; Aaronson & Smirnov, 1996). Therefore, the activity of these ion channels and transporters is vital to regulating vascular contractility.

1.3.1 | TRP channels

The transient receptor potential (TRP) superfamily is a group of 28 cation channels divided into six subfamilies based on their sequence similarity: ankyrin (TRPA), vanilloid (TRPV), canonical (TRPC), mucolipin (TRPML), polycystin (TRPP) and melastatin (TRPM) (Samanta et al., 2018; Zhang et al., 2023). Four TRP subunits are needed to form a TRP ion channel arranged around a central pore. Each TRP subunit contains six transmembrane domains (TMD), a pore-forming loop between the S5 and S6 domains and an N and C terminus located intracellularly

(Moiseenkova-Bell et al., 2008). These channels are calcium and sodium permeable cation channels regulated by various exogenous and endogenous activators, including receptor stimulation, temperature, pressure, osmolarity, pH, fatty acids and intracellular calcium (Bradshaw et al., 2013). In vascular smooth muscle, TRPC, TRPV, TRPM and TRPP channels are the most expressed where they help regulate vascular tone (Alonso-Carbajo et al., 2017; Thakore & Earley, 2019).

The TRPC subfamily was the first to be discovered by cloning the mutated Drosophila TRP gene. It has seven members, all of which activate following Gq/11 GPCR stimulation and all are expressed in various arterial beds (Gonzalez-Cobos & Trebak, 2010). TRPC1 contributes to store-operated calcium entry (SOCE) when activated by STIM1 and Orai1 (Ng et al., 2009; Yuan et al., 2007). SOCE occurs when there is a depletion in intracellular calcium stores following PIP_2-coupled receptor-induced contractions. Similarly, TRPC4 and TRPC5 channels have also been linked to SOCE and interact with STIM1, however, their role in SOCE remains unknown (Worley et al., 2007). TRPC1, TRPC4, and TRPC5 channels can be activated directly by PLC (Myeong et al., 2018), whereas TRPC3, TRPC6, and TRPC7 channels are classed as receptor-operated channels (ROC) activated by DAG independent of PKC and changes in calcium store depletion (Harteneck & Gollasch, 2011). These channels sustain calcium entry during Gq/11 GPCR-induced contractions and promote membrane depolarisation in coronary, mesenteric, renal, cerebral and aortic arteries (Inoue et al., 2001; Reading et al., 2005; Saleh et al., 2008; Walker et al., 2001).

1.3.2 | Chloride channels

Chloride (Cl^-) is a vital anion regulating smooth muscle membrane potential and vascular contractility. In smooth muscle cells, chloride is accumulated intracellularly by $Cl^-/HCO3^-$ exchangers and sodium, potassium and chloride cotransport, resulting in a high intracellular concentration (30-50 mM) and a chloride equilibrium potential between -6mV to -26 mV (Aickin & Vermuë, 1983; Claire & Brading, 1982; Kitamura & Yamazaki, 2001). This potential is more positive than the smooth muscle membrane potential; hence, the open probability of L-type calcium channels is greater and activation of chloride channels leads to chloride efflux, VGCC activation, an increase in [Ca2+] I and depolarization.

Chloride channels are grouped into 5 families based on their structure and function: Voltage-gated Cl^- channels (ClCs), cystic fibrosis transmembrane conductance regulator (CFTR), ligand-gated Cl^- channels, calcium-activated chloride channels (CACC) and volume regulated Cl^- channels (VRCC). These channels allow the passive diffusion of Cl^- ions down their electrochemical gradients, regulating membrane potential, cell volume and intracellular pH. VSMCs are known to express three main chloride channel families:

1) CACC encoded by TMEM16A (Byrne & Large, 1987; Leblanc et al., 2015; Thomas-Gatewood et al., 2011)
2) VRCC, also known as volume sensitive Cl^- currents ($I_{Cl,vol}$) (Ellershaw et al., 2000; Greenwood & Large, 1998; Yamazaki et al., 1998; Zhou et al., 2005)
3) CFTR (Robert et al., 2005; Robert et al., 2004; Zhang et al., 2021)

Comparatively, the evidence for voltage-gated chloride channels (ClC) encode by *CLCN1-9* (Guan et al., 2006) in vascular smooth muscle cells is negligible, with only VGCC (ClC-3) identified in VSMC, involved in regulating vascular tone. A summary of GPCR-mediated vasoconstriction is shown in figure 1.2.

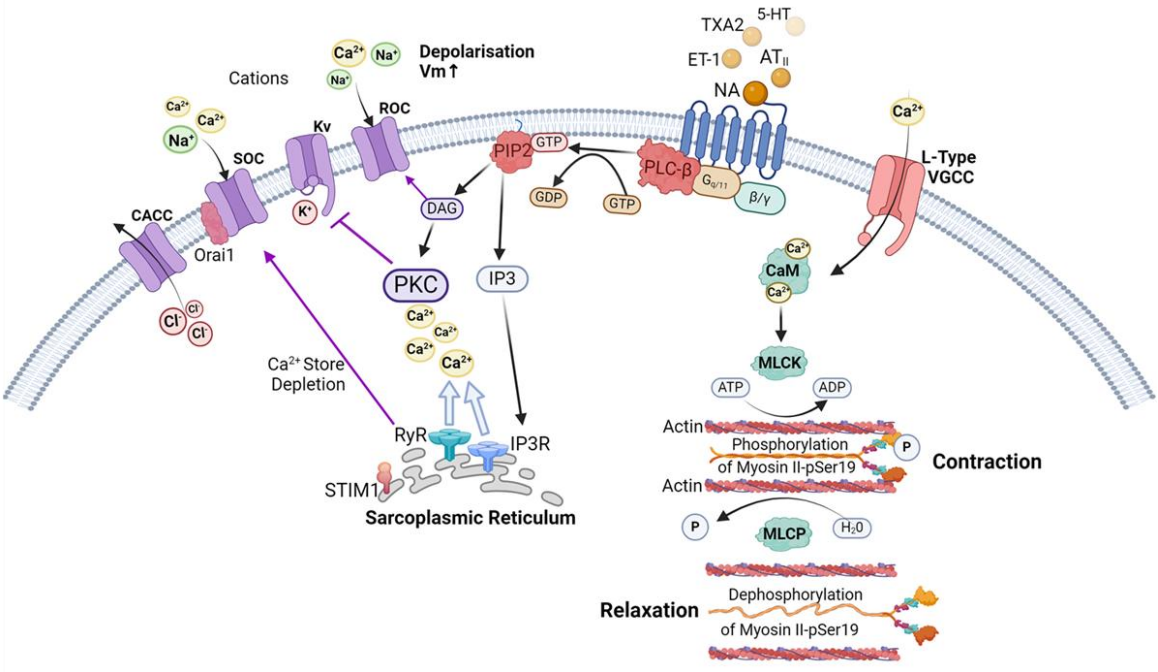


Figure 1.2: $G_{q/11}$ - GPCR mediated vasoconstriction
Activation of $G_{q/11}$-GPCR mediated signalling evokes VSMC contraction by the opening of receptor-operated channels (ROC), store-operated channels (SOC) and calcium-activated chloride channels (CACC) and the inactivation of potassium channels. Calcium influx through L-type VGCC results in depolarisation. An

increase in intracellular calcium levels activates MLCK, which phosphorylates the myosin light chain at Ser19, causing actomyosin cross-bridge cycling and vasoconstriction. (Source: Author using Biorender.com).

1.4 | Vasorelaxation in vascular smooth muscle cells

For relaxation to occur, a decrease in intracellular calcium concentration and a reduction in myosin light chain (MLC) phosphorylation need to be initiated (Touyz et al., 2018). This can either result from a vasodilator inhibiting the contractile pathway or the removal of the contractile stimulus. Several mechanisms are utilised to decrease intracellular calcium concentration:

1. The sarcoplasmic/endoplasmic reticulum Ca^{2+}ATPase (SERCA) pump reduces cytosolic calcium levels by actively transporting and sequestering calcium ions into the sarcoplasmic reticulum (SR) (Floyd & Wray, 2007).
2. The plasma membrane Ca^{2+} ATPase (PMCA) pump actively transports calcium from the cytosol of smooth muscle cells to the extracellular space, directly decreasing intracellular calcium levels (Oceandy et al., 2007).
3. Na^{+}/Ca^{2+} exchangers (NCX) expel calcium ions from the smooth muscle cell powered by the electrochemical gradient of sodium ions (Ottolia et al., 2021).

The SR stores calcium, controlling its cytosolic concentration in VSMCs. The SERCA pump transports calcium into the SR. Mg^{2+} binds to the catalytic site of the ATPase, mediating the hydrolysis of ATP and transferring two Ca^{2+} ions from the cytosol to the luminal of the SR (Floyd & Wray, 2007). The regulatory proteins phospholamban and sarcolipin control the SERCA pump's rate of transferring calcium into the SR (Koller et al., 2003). At the same time, Calsequestrin is a protein located inside the SR that binds to free calcium, resulting in a greater concentration gradient for the SERCA to allow more calcium to enter and be stored in the SR (Wang & Michalak, 2020). Calmodulin in the smooth muscle cell cytosol will combine with calcium and bind to the PMCA pump autoinhibitory domain activating it and causing the transfer calcium ions out of the smooth muscle cell, further lowering intracellular calcium (Gong et al., 2018). Comparatively, Na^{+}/Ca^{2+} exchangers also on the plasma membrane utilise the sodium electrochemical gradient to transfer one calcium ion for three sodium ions. This, in turn, lowers intercellular calcium levels aiding in calcium sequestration (Ottolia et al., 2021).

These processes coincide with the inhibition of VGCCs and ROC, thus preventing further calcium influx and evoking vasodilation.

VSM relaxation is fundamentally regulated by MLCP activation. Without MLCP the interaction between actin and myosin filaments would be sustained and perpetuate the contraction. MLCP dephosphorylates the MLC reverting it back to its original conformation and inhibits its interaction with actin. MLCP was initially thought to be constitutively active, however it is now known that protein kinase A (PKA) and PKG are involved in activating MLCP by phosphorylating its regulatory subunit MYPT-1 at Ser 695. This directly prevents the kinase MYPT1K phosphorylating MLCP at Thr-696 by MYPT1K, which would otherwise render MLCP inactive (Chang et al., 2016; Morgado et al., 2011; Qiao et al., 2014; Wooldridge et al., 2004). There are two key vasodilatory pathways that control vascular tone and lead to MLCP activation:

1. Release of the main endothelial derived relaxing factor, nitric oxide. Nitric oxide is produced by endothelial nitric oxide synthase (eNOS) synthesising NO gas from the amino acid L-arginine. eNOS is mainly inactive at resting levels of intracellular calcium and bound to caveolin in the plasma membrane (Gheibi et al., 2018). eNOS activity and its interaction with other proteins is regulated by post-translational phosphorylation and acetylation. Certain stimuli such as sheer stress can phosphorylate eNOS within the reductase domain at Ser1177, this will enhance the enzymes calcium sensitivity and reductase activity (Fleming, 2010). A raise in intracellular calcium, bradykinin, histamine, or Ca^{2+} ionophores can also activate eNOS via dephosphorylation of the CaM binding domain threonine residue (Thr 495), this results in the dissociation of caveolin from eNOS and allows calmodulin to bind elevating eNOS activity (Fleming, 2010). NO diffuses from endothelial cells into surrounding VSMCs to activate guanylyl cyclase that converts GTP to cyclic GMP (cGMP). cGMP activates the SERCA pump and PKG resulting in decreased calcium sensitivity. PKG phosphorylates Rho and the myosin binding subunit of MLCP, resulting in inhibition of the Rho/ROCK pathway and activation of MLCP. PKG mediates vasorelaxation further by phosphorylating several other intracellular targets, lowering intracellular calcium.

2. Activation of Gs GPCRs such as the adenosine receptor, β-adrenergic receptor and calcitonin gene-related peptide (CGRP) receptor, evoking vasorelaxation. GαS will dissociate from GTP and activate adenylate cyclase (AC), which mediates the conversion of adenosine triphosphate (ATP) to cyclic adenosine monophosphate (cAMP). This results in activation of protein kinase A (PKA) and EPACs (exchange proteins activated by cAMP) (Morgado et al., 2011). PKA relaxes VSMC through promoting membrane hyperpolarisation, enhancing SERCA pumps and membrane calcium ATPase pumps (CaATPase), which decreases intracellular calcium (Rogue et al., 1998; Yang et al., 2008) and phosphorylating of MLCK. Moreover, PKA and EPAC both increase endothelial NO release and inhibit the RhoA pathway (García-Morales et al., 2014; Wehbe et al., 2020; Yu et al., 2017), further lowering intracellular calcium and promoting vasorelaxation.

1.5 | Potassium channels

Potassium channels are expressed in a myriad of cell types, controlling their membrane potential by selectively allowing potassium movement down its concentration gradient, out of the cell (Kuang et al., 2015). Said channels have a tetrameric structure formed from subunits encoded by over 75 genes and are categorised into four major classes, these are: tandem pore domain (TASK, TKIK, TWIK, TREK, TALK), inwardly rectifying (Kir1-7), calcium activated (Kca) and voltage activated (Kv). Each class has 2-6 transmembrane domains (TMD) spanning the lipid-bilayer of the membrane. A summary of the types of potassium channels is shown in figure 1.3. Irrespective of the class these TMDs create a pore forming domain, responsible for ion permeation and a regulatory domain, responsible for sensing stimuli and initiating the conformational change and opening of the channel pore (Islas, 2016). The high selectivity of potassium ions is due to the selectivity filter within the central pore of the channel. Hydrated potassium ions enter the channel pore, dehydrated in the selectivity filter and rehydrated upon exiting into the extracellular space. This stabilises the conductivity of the selectivity filter causing rapid selective movement of potassium ions (Kuang et al., 2015; MacKinnon Ã et al., 2003).

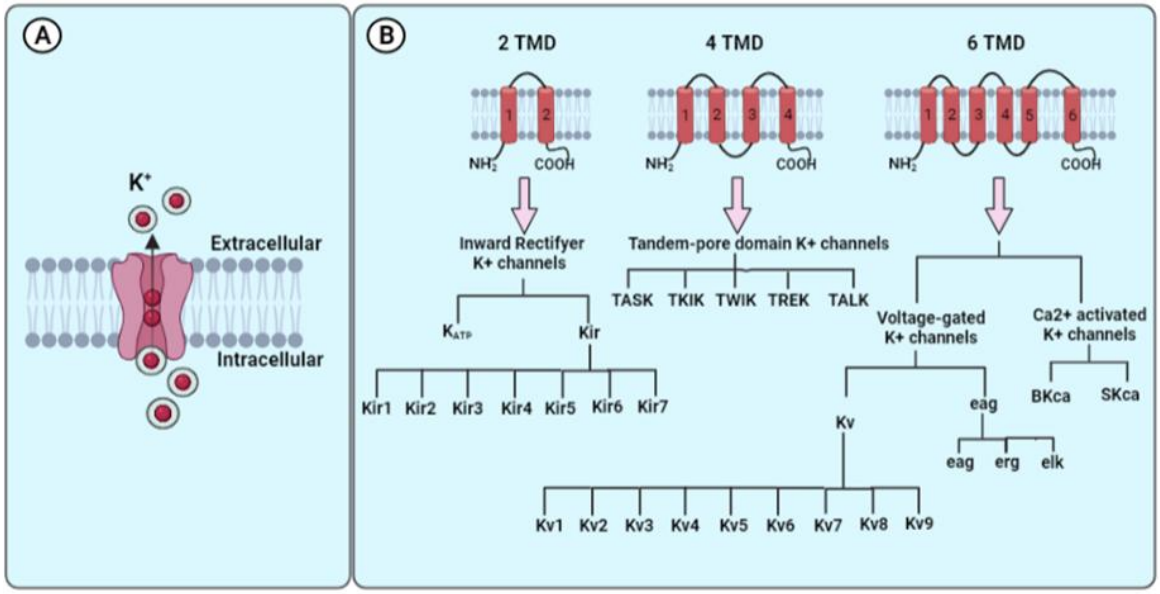


Figure 1.3: Function and classification of potassium channels
A- The selective movement of potassium ions through potassium channels. B- the classification of Potassium channels by structure and function, adapted from Zhong et al.,2013. (Source: Author using Biorender.com).

1.5.1 | Calcium-activated potassium channels (K_{Ca})

Calcium-activated potassium channels are divided into 2 group subtypes. This is based on the functionality of the channels and sequence similarity of the calmodulin calcium-sensing domain in the pore region and C-terminals:

1. The large conductance calcium-activated potassium channels (BK_{Ca}), mainly the $K_{Ca}1.1$ subunit encoded by Kcnm1.
2. The small conductance calcium-activated potassium channels (SK_{Ca}), including the KCa2.1, KCa2.2, and $K_{Ca}2.3$ subunits encoded by Kcnn1, KCNN2, KCNN3 and intermediate conductance calcium-activated potassium channels (IK_{Ca}), mainly the $K_{Ca}3.1$ subunit encoded by Kcnn4.

BK_{Ca} channels are both voltage-gated and calcium-regulated potassium channels predominantly expressed in VSMCs, where they regulate vascular tone and activate upon smooth muscle relaxation. Accessory β-subunits (β1 – β4) and leucine-rich repeat-containing proteins (LRRC26, LRRC38, LRRC52, and LRRC55), also known as γ-subunits, interact with BK_{Ca} channels, modifying their

gating kinetics and voltage-gated calcium sensitivity (Jackson, 2017; Yan & Aldrich, 2012). Activation of these channels occurs mainly via calcium sparks sensed by the C-terminal calcium binding domain that is produced by the opening of ryanodine receptors in the sarcoplasmic reticulum and membrane depolarization through VGCCs (Gollasch et al., 2000; Jaggar et al., 1998; Wellman et al., 2002). The accessory β1 subunit can increase the BK_{Ca} channel coupling by enhancing sensitivity to calcium sparks (Brenner et al., 2000). Upon activation, the BK_{Ca} channels cause potassium efflux and deactivation of VGCCs ($Ca_v1.2$ L-type calcium channels), leading to hyperpolarisation and promoting vasorelaxation (Sausbier et al., 2005; Tano & Gollasch, 2014; Yang et al., 2012) . Vasodilators inducing relaxation through Gαs GPCR pathways are also associated with activating BK_{Ca} channels via PIP_2, PKA and cAMP (Tano & Gollasch, 2014; Tian et al., 2004; Yang et al., 2012). Phosphorylation of BKca channels by PKA and the negatively charged inositol head of PIP_2 binding to the α-subunit cytoplasmic domain directly activates BK_{Ca} channels (Sancho & Kyle, 2021; Vaithianathan et al., 2008). Endothelial-derived NO vasodilators also stimulate BK_{Ca} activation by phosphorylation from PKG. A left shift in the voltage activation and an increase in BK_{Ca} channel open probability occur upon phosphorylation with either PKA or PKG (Robertson et al., 1993), whereas phosphorylation of BK_{Ca} by PKC leads to a significant attenuation in BK_{Ca} channel currents (Taguchi et al., 2000).

Comparatively, SK_{Ca} and IK_{Ca} channels are voltage-independent and predominantly expressed in endothelial cells. SK_{Ca} channels are predominantly expressed in endothelial gap junctions, whereas IK_{Ca} channels are mainly expressed in endothelial projections (Dora et al., 2008; Ledoux et al., 2008). Upon an increase in intracellular calcium, SK_{Ca} and IK_{Ca} channels open, producing hyperpolarisation of endothelial cells, resulting in endothelial-derived hyperpolarisation of VSMCs (Garcia et al., 2023; Sheng et al., 2009).

1.5.2 | Inward rectifier potassium channels (K_{IR})

The inward rectifier potassium channel (K_{IR}) is characterised by a large influx of potassium ions when the cell membrane potential is below the equilibrium potential for potassium (E_K) but less current flow of potassium out of the cell at positive membrane potentials compared to E_K (Hibino et al., 2010; Li & Yang, 2023; Sakmann & Trube, 1984). These K_{IR} currents were first discovered in skeletal

muscle (Katz, 1949), and subsequently, seven families of K_{IR} channels have been identified (K_{IR}1.0- K_{IR}7.0), with strong rectifier K_{IR}2 and weak rectifier K_{IR}6 families being found to have a role in regulating vascular smooth muscle tone (Bradley et al., 1999; Cole & Clément-Chomienne, 2003). K_{IR} channels comprise four α-subunits, each with two membrane-spanning domains (M1 and M2) arranged in a tetramer forming a central pore. The M1 and M2 are linked by P-loops forming the central pore and selectivity filter for potassium ions. The selectivity filter prevents the outward potassium currents by intracellular magnesium and polyamines interacting with the membrane-spanning domains negatively charged amino acids and carboxy-terminal region (Lopatin et al., 1994; Matsuda et al., 1987). K_{IR}2.1 currents have been recorded in cerebral (Johnson et al., 1998; Knot et al., 1996), coronary (Park et al., 2007; Robertson et al., 1996), mesenteric (Goto et al., 2004; Kim et al., 2005) and pulmonary (Tennant et al., 2006) arteries where they are most expressed. They activate upon hyperpolarisation facilitated by two potassium binding sights in the P-loop of the channel, increasing their selectivity to potassium (Lopatin et al., 1994). Ba^{2+} and Cs^{+} can inhibit K_{IR} currents in a voltage-dependent manner, increasing their effect as the membrane hyperpolarises (Knot et al., 1996; Blair et al. et al., 1996). However, other pharmaceutical inhibitors, such as 4-aminopyridine (4-AP) or tetraethylammonium (TEA), did not affect K_{IR} channel activity. Also, a small increase in extracellular potassium concentration from 6mM to 15mM can shift the membrane potential to -60mV, increasing the outward current of K_{IR} and closing VGCCs leading to hyperpolarisation and vasodilation (Knot et al., 1996; Knot & Nelson, 1998). Therefore, K_{IR} channels do play a vital role in potassium mediated vasorelaxation.

1.5.3 | ATP-sensitive potassium channels (K_{ATP})

The K_{ATP} channel was first identified in cardiac myocytes, whereby the channel's potassium currents increase as intracellular ATP decreases (Noma, 1983). The K_{ATP} channel expressed in VSMCs comprises of four pore-forming K_{IR}6.1 α-subunits and four accessory sulphonylurea receptors (SUR). Pharmacological inhibitors glibenclamide and pinacidil inhibit K_{ATP} function by acting on the SUR2B subunit, whereas the sensitivity to ATP is predominantly governed by the K_{IR}6.1 α-subunit (Foster & Coetzee, 2016). Vasoconstrictors that signal through PKC (norepinephrine, endothelin and 5-HT etc) lead to the closure of K_{ATP} channels by

altering the voltage gating and increasing the duration of closure (Chrissobolis & Sobey, 2002; Cole et al., 2000; Sampson et al., 2007) or by internalising the channels by PKC coupling with caveolin (Jiao et al., 2008). Several vasoconstrictors like angiotensin two that signal through Gαi/o GPCRs lower adenylate cyclase, leading to the inhibition of K_{ATP} channels. The increase in intracellular calcium can also activate calcineurin, which dephosphorylates and closes K_{ATP} channels (Wilson et al., 2000). Whereas vasodilators that signal through the cAMP pathway activate K_{ATP} channels by PKA phosphorylating both the $K_{IR}6.1$ α-subunits and SUR subunits to open the channel. Similarly, NO and cGMP-mediated vasodilation pathways have been shown to increase K_{ATP} current activity using patch-clamp electrophysiology on coronary arteries and cultured aortic VSMCs. However, Endothelium-derived NO was found to not activate K_{ATP} channels in mesenteric (Mustafa et al., 2011; Quayle et al., 1994) and coronary (Jackson et al., 1993) arteries. Hence, K_{ATP} activity is predominantly derived from VSMC-evoked relaxations.

1.5.4 | Voltage-gated potassium channels

There are 40 genes encoding Kv channels, divided into 12 subfamilies (Kv1-12). Kv channels are vital for all cellular functions; this includes cardiac and VSMC activity, regulation of cell turnover, release of neurotransmitters and hormones and much more. Within this family, Kv1.2, Kv1.3, Kv1.5, Kv2.1, Kv7.1, Kv7.4 and Kv7.5 have the greatest abundance within VSM and contribute to regulating vascular tone (Jepps et al., 2015; Lu et al., 2002; Xu et al., 1999). Each of these channels can be formed from different subunits known as a heteromeric assembly; for example, Kv7.4 and Kv7.5 form heteromeric ion channels in VSMCs (Cox, 2005). Electrophysiological recordings have demonstrated Kv1.2 and Kv1.5 are sensitive to the potassium channel inhibitor 4-Aminopyridine (4-AP), whereas Kv2 channels are more sensitive to inhibition from Tetraethylammonium (TEA) (Ko et al., 2010). K_v7 proteins have been implicated in smooth muscle disorders, hence, understanding K_v7 channel function is crucial in determining its disease contribution. The K_v7 subfamily is encoded by Kcnq1-5 genes that express five Kv7 isoforms, $K_v7.1$-Kv7.5. The opening of Kv7 channels maintains membrane potential by generating potassium efflux, preventing cell depolarisation and limiting

the open probability of VGCCs (Soldovieri et al., 2011). Each isoform possesses a diverse expression within the body as shown in table 1.

Table 1.1: Summary of K_V7 channel expression and their channelopathies. Information is taken from (Soldovieri et al., 2011; Tian et al., 2014, Nappi et al.,2020).

Kv7 isotype	***Locus***	***Expression***	***Channelopathy***
KCNQ1	11p15.5	Heart, inner ear marginal cells, smooth and skeletal muscle, brain stem nuclei, forebrain, small intestine, gastrointestinal tract, lung ovaries, pancreas	Long QT syndrome (LQTS), Short QT syndrome (SQTS), Jervell and Lange-Nielsen syndrome (JLNS1), familial atrial fibrillation (FAF)
KCNQ2	20q13.3	Hippocampus, striatum, neocortex, cerebellum, PNS	Benign familial Neonatal seizures (BFNS), Neonatal-onset developmental and epileptic encephalopathy (DEE)
KCNQ3	8q24	Hippocampus, striatum, neocortex, cerebellum, amygdala, thalamus, PNS	Benign familial Neonatal seizures (BFNS), Neonatal-onset developmental and epileptic encephalopathy (DEE), Autism spectrum disorder
KCNQ4	1p34	Smooth and skeletal muscle, central auditory pathway	Nonsyndromic hearing loss (DFNA2)
KCNQ5	6q14	Smooth and skeletal muscle, hippocampus caudate putamen, auditory system, PNS, piriform and entorhinal cortex	Autism spectrum disorder

Kv7 channels form as tetramers of identical or compatible α subunits arranged to form a central pore. Kv7.1 channels are homomeric, whereas Kv7.2-Kv7.5 isoforms can co-assemble to form heteromeric channels. Each α subunit contains 6 transmembrane domains (S1-6) and an intracellular NH2 and COOH termini. S1-4 makes up the voltage sensing domain and between S5-6 there is a membrane P-loop which forms the central pore (Greenwood & Ohya, 2009). The COOH-terminal region of Kv7 isoforms is the site of tetrameric assembly, as well as accessory protein (KCNE) and regulatory protein interactions (i.e., Ankyrin-G, Nedd4 –2, PIP_2 and calmodulin), which modulate Kv7 activity (Stott et al., 2018).

1.5.5 | Kv7 channels in vascular smooth muscle

Kv7 channels are widely expressed in smooth muscle and activate at negative thresholds, remaining open at resting membrane potential. Said channels maintain hyperpolarisation and reduce the open probability of VGCCs, opposing smooth muscle contraction, hence are vital to regulating smooth muscle tone. The first evidence of KCNQ expression in vascular smooth muscle was discovered by Ohya et al in 2003, where qPCR and immunocytochemistry identified Kcnq1 splice variants in mouse portal veins (Ohya et al., 2003). Years later, Kcnq4 and Kcnq5 expression was also found within the cell membrane of the mouse portal vein (Yeung et al., 2007; Yeung et al., 2008). Brueggemann et al supported these findings, demonstrating rat aortic smooth muscle cells expressed KCNQ1, KCNQ4 and KCNQ5, however, cultured rat embryonic aorta (A7r5) only expressed KCNQ5 (Brueggemann et al., 2007). A turning point in the overall understanding of KCNQ expression arose from Yeung et al (2007), who identified that KCNQ1, 4 and 5 were found to be the most abundant transcripts within mouse femoral, thoracic and carotid arteries (Yeung et al., 2007). This expression profile was consistent within most rodent arterial beds. In contrast, the expression of KCNE genes that encode for proteins known to modulate Kv7 trafficking, and function was artery-specific (Yeung et al., 2007). Moreover, human arterial studies replicated these expression profiles, with KCNQ4 expression having the greatest abundance and KCNQ2 being absent in all samples (Ng et al., 2011). Previously, Kv7 channels were thought only to be expressed in vascular smooth muscle however more recently, cell isolation and expression analysis has discovered Kv7.4 and Kv7.5 are expressed in endothelial cells within mesenteric arteries (Baldwin et al.,2020) coronary arteries

(Chen et al., 2016) and brain capillaries (Celentano et al.,2024). A summary of KCNQ and KCNE expression in the vasculature is shown in table 1.2.

Table 1.2: Kv7 channel and KCNE auxiliary subunit distribution in the vasculature
The expression of KCNQ and KCNE isomers in the vasculature and the respective studies that identified their expression.

	KCNQ expression	***KCNE expression***	***References and Model***
Portal vein	KCNQ4 > KCNQ5 > KCNQ1	KCNE3	Mouse: (Ohya et al., 2003)
Aorta	KCNQ4 > KCNQ5 > KCNQ1	KCNE1-5	Rat: (Jepps et al., 2015) Mouse: (Yeung et al.,2007)
Coronary artery	KCNQ4 > KCNQ5 > KCNQ1	KCNE2-5	Rat: (Khanamiri et al., 2013; Morales-Cano et al., 2015)
Mesenteric artery	KCNQ4 > KCNQ5 > KCNQ1	KCNE2-4	Mouse: (Yeung et al.,2007) Rat: (Baldwin et al., 2020;. Jepps et al., 2015; Mackie et al., 2008) Human: (Ng et al., 2011)
Pulmonary artery	KCNQ4 > KCNQ5 > KCNQ1		Rat: (Joshi et al., 2006; Mondéjar-Parreño et al., 2020)
Cerebral arteries	KCNQ4 > KCNQ5 > KCNQ1	KCNE1-4	Rat: (de Jong & Jepps,

			2018; Lee et al., 2015)
Carotid artery	KCNQ4 > KCNQ5 > KCNQ1	KCNE1-5	Mouse: (S. Y.M. Yeung et al., 2007)
Renal artery	KCNQ4 > KCNQ5 > KCNQ1	KCNE2-4	Rat: (Chadha et al., 2012a; Jepps et al., 2015)
Femoral artery	KCNQ4 > KCNQ5 > KCNQ1	KCNE1, KCNE4, KCNE5	Mouse: (Yeung et al., 2007)
Gracilis artery	KCNQ4 > KCNQ5 > KCNQ1		Rat: (Ma et al., 2020a)
Penile artery	KCNQ4 > KCNQ5		Rat: (Jepps et al., 2016)
Saphenous Artery	KCNQ4 > KCNQ5 > KCNQ1		Rat: (Ma et al., 2020b)

1.5.6 | Kv7 channel function

For decades, linopirdine and XE991 have been routinely used to characterise Kv7 channels due to their ability to selectively block all 5 K_V7 isotypes. linopirdine was initially shown by Wang et al (1998) to block Kv7.2/Kv7.3 channels and the M current in sympathetic neurones via a direct interaction (Wang et al., 1998). Electrophysiological patch-clamp recordings carried out by Yeung and Greenwood (2005) demonstrated that Pan Kv7 blockers linopirdine and XE991 concentration-dependently depolarised the resting membrane of mouse portal veins and increased the spontaneous contractility of VSMCs (Yeung & Greenwood., 2005). This was the first to demonstrate that Kv7 channels regulate vascular resting membrane potential and that their activation is voltage dependent. These contractions were also reversed by VGCC blockers, which is indicative of enhanced calcium influx. (Jepps et al., 2015; Mackie et al., 2008; Yeung et al., 2005). Later, Søgaard et al showed in patch clamp recordings Kv7.4 channels were blocked in a voltage-independent manner by direct interaction with linopirdine and

XE991 (Søgaard et al., 2001). By using Cryoelectron microscopy (cryo-EM) of human Kv7.4, the direct binding sight of linopirdine to the channel has been identified within the VSD and underneath the inner gate respectively (Li et al., 2021). Moreover, using other Kv channel inhibitors (glibenclamide, iberiotoxin, 4-AP and TEA) Kv7 currents were proved to be separate from other potassium channel currents (Mackie et al., 2008). This confirmed the function of Kv7 channels at resting membrane potential.

Kv7 activators such as retigabine, flupirtine, S1, ML213 and NS15370 act on the tryptophan residual at the S5 pore domain. While other Kv7 activators can act via the voltage sensing domain either at the S2-3 linker (27243, ICA-069673 and ICA-110381) or via the S4 segment (diclofenac, meclofenac, and NH29) to elicit their effects (Boehlen et al., 2013; Brueggemann et al., 2014b; Rogawski, 2006). These drugs negatively shift the activation curves, increasing conductance and slowing current deactivation kinetics through Kv7.4 and Kv7.5 homomers or heteromeric Kv7.4/5 channels (Brueggemann et al., 2014). This subsequently hyperpolarises VSMCs causing vasorelaxation. Kv7.1 is pharmacologically distinct from the other Kv7 isoforms due to it not containing the tryptophan residue (Lange et al., 2009; Schenzer et al., 2005; Wuttke et al., 2005), thus ML277, R-L3 and mefenamic acid were produced as Kv7.1 specific activators. However, their role in vascular function is highly ill defined, with many findings postulating Kv7.1 channels are not likely contributors to regulating vascular tone. The Kv7.1 selective blocker HMR1556 or chromanol 293B does not produce contractions in rodent or human arteries whereas the pan-Kv7 blockers linopirdine or XE991 elicit contraction (Chadha et al., 2012; Yeung et al., 2007). Nevertheless, recent studies using myography showed pharmacological and molecular inhibition of Kv7.1 in mesenteric arteries attenuated the selective IP-mediated relaxant MRE-269 (Baldwin et al., 2022). This indicates Kv7.1 channels could have a novel role in IP-mediated relaxation and suggests Kv7.1 may function in VSMCs under certain conditions. A summary of all the Kv7 activators and inhibitors with their selectivity can be seen in table 1.3 and 1.4 respectively with information taken from (Barrese et al., 2018).

Table 1.3: Table of Kv7 channel activators and their selectivity
Information taken from (Barrese et al., 2018)

Compound	***Selectivity***
Retigabine	Kv7.2–7.5 Enhancer but inhibits at positive potentials Blocks Kv7.1 at 100 μM
Flupirtine	Kv7.2–7.5
ML213	Kv7.2 = Kv7.4 ≫ Kv7.3 and Kv7.5
BMS-204352 (Maxipost)	Kv7.2–Kv7.5
ICA-27243	Kv7.2/7.3 > Kv7.4 and Kv7.5
ICA-069673	Kv7.2 > Kv7.3; Kv7.4 > Kv7.5
NH29	Kv7.2 and Kv7.2/7.3 > Kv7.4 > Kv7.3
Zinc pyrithione	Kv7.1–7.5 No effect on heterologous Kv7.1 + KCNE1/KCNE3 and native IKs
NS15370	
Acrylamide S-1/S-2	Kv7.4 > Kv7.2, Kv7.3, and Kv7.5
Meclofenac	Kv7.2/7.3
Diclofenac	Kv7.2–7.5
Kv7.1 specific	
ML277	Kv7.1
R-L3	Kv7.1
Mefenamic acid	Kv7.1 + KCNE1

Table 1.4: Table of Kv7 channel blockers and their selectivity to Kv7 isomers Information taken from (Barrese et al., 2018).

Compound	***Selectivity***
Linopirdine	Kv7.1-Kv7.5
XE991	Kv7.1-Kv7.5
Kv7.1 Specific	
Chromanol 293B	Kv7.1 + KCNE1/E3 > Kv7.1
HMR1556	Kv7.1 + KCNE1 > Kv7.1
JNJ303	Kv7.1 + KCNE1 > Kv7.1

1.5.7 | Kv7 channel regulation

Receptor-evoked relaxation and contraction pathways can alter Kv7 channel function. Beta adrenoreceptor agonists like Isoprenaline and CGRP induce smooth muscle relaxation in various arteries by activating PIP_2, cAMP and PKA, decreasing intracellular calcium. PIP_2, cAMP, PKA and AKAP can all interact with the C-terminal region of the Kv7 channel, enhancing its activity (Barrese et al., 2018; Haitin & Attali, 2008; Hernandez et al., 2008). Chadha et al 2012 demonstrated that isoprenaline- and CGRP-mediated relaxations of renal arteries were attenuated by Kv7 channel inhibitors linopirdine and XE991 and, more specifically, knockdown of Kv7.4 with siRNA or morpholinos also inhibited isoprenaline and CGRP induced relaxations. Beta-adrenoreceptor activation in rat aortic A7r5 cell lines and isolated renal arteries (Chadha et al., 2012; Stott et al., 2015, 2018) also elevated Kv7.5 and Kv7.4/Kv7.5 currents but not homomeric Kv7.4 currents (Mani et al., 2016). Hence, Kv7.4 as well as Kv7.5 activation is imperative for VSM cell relaxation. PIP_2 enhances the function of all Kv7 channel subtypes by mediating the coupling of the Kv7 channel voltage sensing domain to the pore-forming domain, increasing the channel open probability (Li et al., 2005; Zaydman & Cui, 2014). PIP_2 can also interact with the S2-S3 and S4-S5 linkers of

Kv7.3 and Kv7.5 channel proteins, promoting pore opening. Calmodulin also alters Kv7 channel activity with its binding domain overlapping with the PIP_2 binding sight on the C-terminus of Kv7 channels; this results in calmodulin inhibiting Kv7.2.3, Kv7.4, and Kv7.5, but stabilising Kv7.1 proteins. EPAC enhances Kv7 channel activity by targeting PKA or AKAP shown in mesenteric and renal arteries with isoprenaline (Stott et al., 2016; Chadha et al., 2012). cerebral arteries with CGRP (Chadha et al., 2014) and coronary arteries with adenosine (Khanamiri et al., 2013). Comparatively, during $G_{q/11}$ coupled receptor evoked contraction, the calcium sensor calmodulin (CaM) forms a complex with calcium that binds to the Kv7 C-terminal domain, impairing Kv7.4/5 channel open probability (Xu et al., 2013).

It is now known that the βγ subunit also modulates Kv7s. The modulation of Kv7 channels through βγ subunits was first identified by Stott et al (2015) from patch clamp recordings, showing that stimulation of GPCRs enhanced Kv7 channel open probability and augmented its activity. This effect was prevented by pre-incubation of the Gβγ subunit inhibitor, gallein. Moreover, proximity ligation assays detected a co-localisation of Gβγ subunits and Kv7.4 isomers within renal and mesenteric arteries (Stott et al., 2015). This demonstrated both Gβγ subunits and Kv7 channels work together to regulate arterial tone. These findings were expanded by Povstyan et al (2016) who revealed Gβγ activity was prevented by depletion of PIP2 levels and elevated levels of both PIP_2 and Gβγ significantly increased Kv7 channel open probability (Povstyan et al., 2017). This suggests that PIP_2 and Gβγ are required to function synergistically to positively regulate Kv7 channels. A summary of VSMC relaxation is shown in figure 1.4.

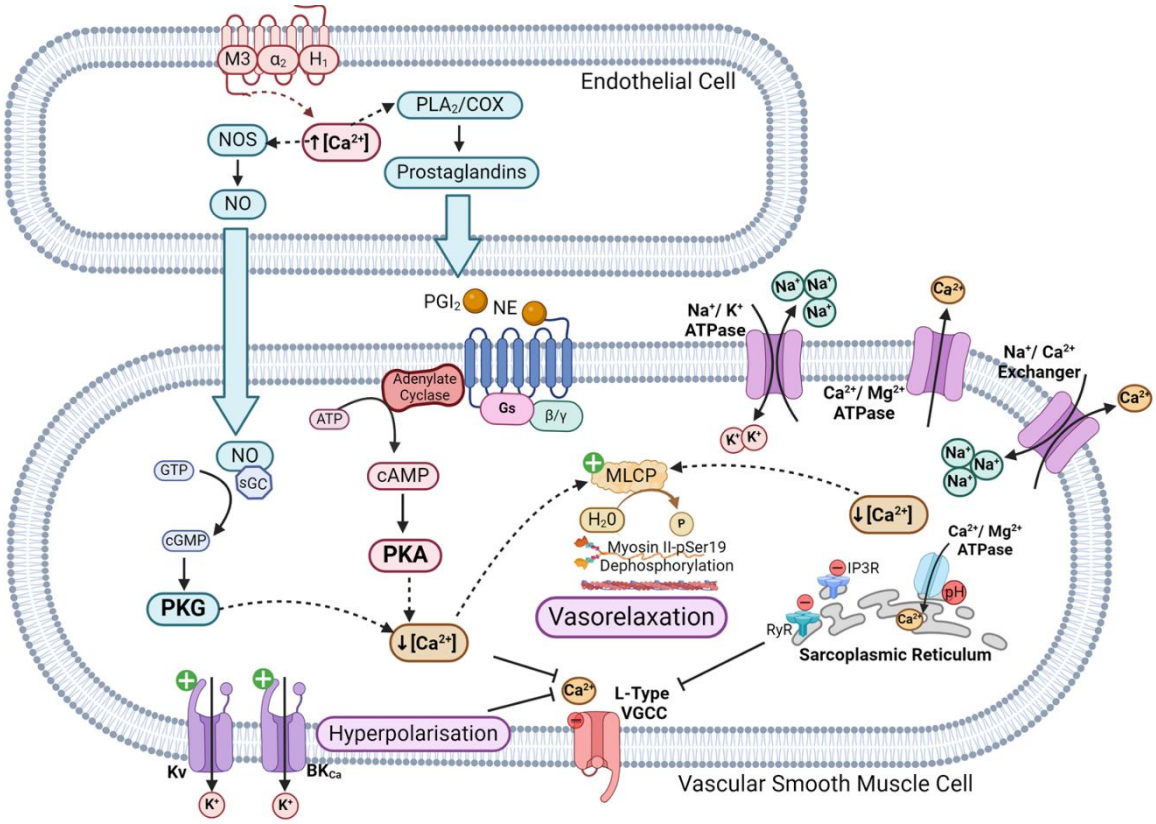


Figure 1.4: Summary overview of VSMC relaxation:
Sheer stress and endothelium-dependent vasorelaxants such as acetylcholine and bradykinin activate their receptors on endothelial cells, leading to a localised increase in intracellular calcium and activating nitric oxide synthase (eNOS) and phospholipase A_2 (PLA_2). Newly synthesised nitric oxide (NO) and prostacyclin (PGI_2) readily diffuse into vascular smooth muscle cells. NO activates soluble guanylate cyclase (sGC), and with guanosine 3',5'-cyclic monophosphate (cGMP) forms active PKG. Competitively, prostacyclin and other receptor-dependent vasodilators activate Gs-GPCR signalling, forming active PKA. Both PKA and PKG lower intracellular calcium by activating potassium channels and inhibiting MLCP, resulting in vasodilation (Source: Author using Biorender.com).

1.6 | Smooth muscle solute transporters

The solute carrier family (SLC) comprises 456 transporters, which the HUGO Gene Nomenclature Committee (HGNC) has classified into 65 families, with each family of transporters having >20% sequence similarity. Other classification systems, such as TCDB and phylogenic analysis, can also be used to define these transporters (Fredriksson et al., 2008; Perland & Fredriksson, 2017). The SLC proteins allow the movement of several molecules, including amino acids, sugars, ions and nucleotides, across the plasma membrane and are either passive

facilitative or secondary active transporters. Facilitative transporters allow one molecule to passively move down its concentration gradient. In contrast, secondary active transporters use electrochemical potential from the passive movement of ions down their concentration gradient to provide the energy needed for another substance to move across the membrane against its concentration gradient, which can either be in the same direction (symporter) or the opposite direction (antiporter). The main families that transport sugars are the SLC2 and SLC5 families, containing 12 and 14 transmembrane domains, respectively. For many of these transporters, the speed of transport is proportional to the electrochemical gradient of the coupled ion. Moreover, the specificity of each transporter to the substrate is determined by the interaction of their binding sites.

1.6.1 | SLC2 transporters

The SLC2 family transports a wide range of carbon compounds, including monosaccharides and polyols, and is a member of the major facilitator superfamily (MFS). The SLC2 proteins have 12 TMD, a large cytoplasmic linker domain, and cytoplasmic N and C termini. The family is divided into 3 classes based on sequence similarity: Class 1 comprises Slc2A1-4 and Slc2A14, which encode the GLUT1-4 and GLUT14 proteins, respectively. Class 2 consists of Slc2A5, Slc2A7, Slc2A9, and Slc2A11 encoding for GLUT5, 7, 9, and 11, respectively and class 3 comprises of Slc2A6, Slc2A8, Slc2A10, Slc2A12, and Slc2A13 encoding for GLUT6, 8, 10, 12, and HMIT proteins, respectively (Mueckler & Thorens, 2013). GLUT proteins are ubiquitously expressed across all tissue types and primarily function as facilitative glucose transporters. However, they also exhibit affinities for other monosaccharides, including fructose, galactose, and mannose. On the other hand, HMIT is the only H+/myo-inositol secondary active symporter in the family and is mainly expressed in the brain and adipose tissue (Holman, 2020).

1.6.2 | SLC5 transporters

The SLC5 family are all sodium-dependent substrate transporters utilising the sodium electrochemical gradient to co-transport various sugars, anions, short-chain fatty acids and vitamins. Twelve genes encompass this family that encodes 12 proteins with 14 transmembrane domains. A summary of these transporters is shown in Table 1.5. These transporters contain an N and C terminal domain with a leucine transporter (LeuT)-like fold producing two large extracellular loops

between segments 6-7 and 8-9, allowing binding of two sodium ions and a large intracellular loop between segments 13-14 to facilitate solute transport. In general, extracellular sodium binds to the Na^{+}_{1} and Na^{+}_{2} binding sites, opening the outer gate and enabling glucose to bind to the substrate binding site located adjacent to the TMD1 and TMD6 unwound regions (Wright et al., 2017). The outer gate closes following glucose binding, forming an occluded state and allowing the internal gate to open, releasing the sodium and glucose molecules into the cytoplasm (Abramson & Wright, 2009).

The SGLT1-5 and SMIT1-2 transporters are more closely related in the SLC5 family due to their ability to transport monosaccharides, such as glucose, galactose, mannose, and fructose. Comparably, the non-sugar transporters (NIS, SMVT, CHT1, SMCT1-2) are more distant relatives.

Table 1.5: A summary of the expression and transport of all 12 SLC5 proteins

	Localisation	***Transports***	***Km***	***Reference***
SGLT1 ***(Slc5a1)***	Kidney, intestine, heart, trachea, colon	1 glucose / 2 Na^+ 1 Galactose / 2 Na^+ α-methyl-d-glucoside (αMG) / 2 Na^+	0.5 mM 1mM	(Carbó & Rodríguez, 2023; Wright et al., 2011)
SGLT2 ***(Slc5a2)***	Heart and Kidney	1 glucose / 1 Na^+ α-MG / 1 Na^+	5mM 1.6 mM	(Carbó & Rodríguez, 2023)
SMIT1 ***(Slc5a3)***	Present in all tissue types but predominantly: Heart, Brain, Kidney	Myo-inositol / 2 Na^+ 1 glucose / 2 Na^+ 1 Galactose / 2 Na^+	0.05mM 20 mM	(Carbó & Rodríguez, 2023; Van Steenbergen et al., 2017)
SGLT3 ***(Slc5a4)***	Is a glucose sensor in kidney, intestine, brain, lung, testes,	1 glucose: 2 Na^+	20mM	(Chen et al., 2010; Gyimesi et al., 2020)

	uterus and skeletal muscle			
NIS ***(Slc5a5)***	thyroid gland	1 iodide / 2 Na^+ Thiocyanate (SCN^-) / 2 Na^+	10–30 µM	(Ravera et al., 2017)
SMVT ***(Slc5a6)***	placenta, intestine, brain, liver, lung, kidney, Heart	1 vitamin molecule / 2 Na^+	4 µM – 18 µM	(Ghosal et al., 2011; Vadlapudi et al., 2012)
CHT1 ***(Slc5a7)***	Tissues containing cholinergic neurons	1 choline / 2 Na^+	2 µM	*(Gyimesi et al., 2020)*
SMCT1 ***(Slc5a8)***	Intestinal colon, kidneys and brain	1 short-chain fatty acid (SCFA) / 2 Na^+		(Gyimesi et al., 2020)
SGLT4 ***(Slc5a9)***	Small intestine, brain and Kidney	Mannose, fructose and α-MG / Na^+	2 mM 2.6 mM	(Gyimesi et al., 2020)
SGLT5 ***(Slc5a10)***	Kidney cortex	Mannose and fructose/ Na^+	0.45 mM 0.62 mM	(Gyimesi et al., 2020)
SMIT2 ***(Slc5a11)***	Present in all tissue types but predominantly: Heart, Brain, Kidney	Myo-inositol / 2 Na^+ D-chiro-inositol (DCI)	120 µM 6.1 mM	(Coady et al., 2002; Sasseville et al., 2014)
SMCT2 ***(Slc5a12)***	Intestinal colon, kidneys and brain	1 SCFA / 1 Na^+		(Gyimesi et al., 2020)

1.6.2.1 | SGLT1

SGLT1 was the first member of the SLC5 family to be sequenced and cloned (Hediger et al., 1987a). SGLT1 is primarily expressed on the intestinal brush-border membrane of enterocytes that secrete glucose-dependent insulinotropic peptide (GIP) and enteroendocrine K and L cells that release glucagon-like peptide 1/2 (GLP-1/GLP-2), where it enables the absorption of glucose and galactose. Non-invasive positron emission tomography (PET) imaging studies of $Slc5a1^{-/-}$ mice identified this using 18F-labeled glucose analogues, demonstrating that SGLT1 was needed for fast glucose absorption, which was prevented by SGLT1 blocker phlorizin (Sala-Rabanal et al., 2016, 2018). Mutations in the Slc5a1 gene or absence of SGLT1 in knock-out $Slc5a1^{-/-}$ mice results in glucose-galactose malabsorption (GGM) syndrome, where patients develop severe diarrhoea leading to severe dehydration, acidosis and fatal outcomes within weeks. These symptoms can subside by having a glucose and galactose-free diet. SGLT1 helps protect the small intestine from pathogens and inflammation caused by activated lymphocytes. This protection was demonstrated when glucose-activated SGLT1 prevented the activation of CD34 and inflammation-related cell death (apoptosis) in the small intestine after lymphocytes were applied orally (Koepsell, 2017; Linda. Yu et al., 2005, 2006).

In the kidney, glucose and galactose that may have escaped reabsorption from SGLT2 in the S1 and S2 segments of the proximal tubule will be reabsorbed by SGLT1 in the brush-border membrane of segments 2 and 3 in the renal proximal tubule. Once glucose entered the tubule cell, the basolateral GLUT1 in the S1 segment and GLUT2 in the S3 segments enabled the passive diffusion of glucose back into the blood (Mueckler & Thorens, 2013). The function of SGLT1 was confirmed in SGLT1 knockout mice, where 98% of filtered glucose was reabsorbed; however, in SGLT2 knockout mice, only 67% of filtered glucose load was reabsorbed (Powell et al., 2013; You et al., 1995). Thus, SGLT2 reabsorbs the majority of glucose in the kidney, with the high-affinity low-capacity SGLT1 transporter absorbing the remaining 2-3%. However, upon SGLT2 knockdown or inactivity, there is an increase in SGLT1-induced glucose reabsorption (You et al., 1995). This indicates why only 67% of glucose was reabsorbed in SGLT2 knock-down mice. SGLT1 mRNA expression has also been identified in the heart, brain,

lung, liver, pancreas, skeletal muscle, uterus and blood vessels (Chen et al., 2010a, 2010b; Poppe et al., 1997; Saponaro et al., 2020a). Immunohistochemical and functional studies using cultured cardiac myocytes found SGLT1 expression in the heart's myocyte sarcolemma and small blood vessels (Kashiwagi et al., 2015; Koepsell, 2017; Zhou et al., 2003). The role of SGLT1 in cardiac myocytes is still not fully understood; however, several papers have found that glucose uptake via SGLT1 increases glycolysis and ATP levels in ischemic and hyperglycaemic hearts (Kashiwagi et al., 2015). SGLT1 can also cause ischemic heart damage and cardiac hypertrophy by increasing the activity of PKC and TGF-β1 and the production of ROS when interacting with epidermal growth factor (EGF) and phosphorylating proliferation factors p38 MAPK and ERK1/2 (Carvajal et al., 2007; Li et al., 2019; Lin et al., 2021; Saadat et al., 2021). Comparatively, *in situ* hybridisation and immunohistochemistry studies have identified SGLT1 expression in brain microvessel endothelial cells, cortical neurones, purkinje cells of the cerebellum and hippocampal pyramidal cells from rabbit pig and rat brains (Balen et al., 2008; Elfeber et al., 2004; Poppe et al., 1997; Yu et al., 2013). Generally, SGLT1 in endothelial cells increases energy and glucose supply to neurones during hypoglycaemia, stabilising their function (Harada et al., 2009; Poppe et al., 1997). However, SGLT1 in these cells can also adjust glucose concentrations linked to the development of ischemic stroke, whereby glucose uptake from SGLT1 under hyperglycaemic conditions is related to neurotoxicity and inhibition of SGLT1 using phlorizin or SGLT1 knockout mouse models had a reduction in ischemic neuronal damage (Yamazaki et al., 2012; Yamazaki et al., 2016; Yamazaki et al., 2015). Interestingly, SGLT1 does possess the ability to function as a Na^+ uniporter by producing a Na^+ leak current in the absence of glucose and experiments using oocytes overexpressed with human SGLT1 showed that SGLT1 can transport water and urea passively independent of the glucose and sodium concentration gradients (Zeuthen et al., 2016).

1.6.2.2 | SGLT2

SGLT2 is predominantly located in the kidney (Chen et al., 2010; Nagai et al., 2014a; Sabolić et al., 2012) with smaller protein expression and transcript found in the brain (Chiba et al., 2020), thyroid (Wang et al., 2022), lungs (Iwai et al., 2024) and pancreas (Bonner et al., 2015; Saponaro et al., 2020; Wang et al., 2022).

SGLT2 transporters on the apical membrane of the S1 and S2 segments in the proximal kidney tubules will reabsorb ~98% of filtered glucose into tubular epithelial cells. GLUT2 transports this glucose across the basolateral membrane back into the blood circulation, and any glucose not taken up by SGLT2 is reabsorbed by SGLT1 in the S3 segment of the proximal tubule. The importance of SGLT2 was shown by loss of function mutations in Slc5a2, resulting in familial renal glycosuria (Van Den Heuvel et al., 2002) and by SGLT2 knockout mice studies whereby micro-puncture of the tubular fluid showed no glucose reabsorption in knockout mice, but 90% of filtered glucose was reabsorbed in wildtype mice (Vallon et al., 2011).

1.6.2.2.1 | SGLT2 regulation

SGLT2 expressed in Xenopus laevis oocytes or mammalian cultured cells did not produce high levels of glucose uptake, and the transporter activity was 10 times lower than that of SGLT1 overexpression systems (Fei et al., 1994; Hediger et al., 1987; Kanai et al., 1994; You et al., 1995). Hence, several papers have proposed that transcriptional and post-transcriptional regulators are required to enable the full function of SGLT2. Transcription factors SP-1, HNF1α and HNF4A regulate the expression of SGLT2, with 5 binding sites found for SP-1 on the promotor region of the Slc5a2 gene and one binding sight for HNF1α above the transcription site (Zhao et al., 2016). The binding affinity of SP-1 and HNF1α was significantly reduced following treatment with adiponectin. Hence, adiponectin reduces SGLT2 activity by preventing its transcription. Chromatin immunoprecipitation and immunofluorescence studies show HNF4A co-localises with SGLT2 and glucagon proteins in human α-pancreatic cells and identified 19 HNF4A binding sites and 2 binding sites in human and mouse Slc5a2 promotor regions respectively (Bonner et al., 2015). The levels of HNF4A and SGLT2 similarly increased in obese and diabetic patients, indicating a role of HNF4A in elevating Slc5a2 transcriptional expression.

Following the cloning of Slc5a2 in Xenopus oocytes, an important post-transcriptional activator of SGLT2 was identified called MAP17. This integral membrane protein was found to significantly increase SGLT2 activity without altering the membrane expression of SGLT2 protein (Sędzikowska & Szablewski,

2021). This was first identified when Slc5a2 was co-expressed with MAP17 in RNA-injected Xenopus oocytes, increasing SGLT2 uptake of α-MG (Coady et al., 2017). MAP17 is predominantly expressed in the apical membrane of the renal proximal tubule. It strongly interacts with the Na/H exchange regulatory cofactor NHE-RF3, also known as PDZK1, which acts as a scaffolding protein with four domains interacting with several transporters, including the sodium hydrogen exchanger 3 (NHE3) that interacts with the PDZ class 1 binding domain (Cha & Donowitz, 2008; Sarma et al., 2015). SGLT2 and NHE3 co-localise in the proximal renal tubule; hence, recent studies suggest MAP17/SGLT2 binding to NHE3 is held together in a complex by the scaffold protein PDZK1, which upregulates one another. For example, upon adding 5mM glucose to rat renal proximal tubules, SGLT2 activation subsequently upregulated the NHE3-mediated Na/HCO3 transport. Also, when applying phlorizin in the absence of glucose, there was a significant inhibition in both SGLT2 and NHE3 activity (Gisler et al., 2003; Hu et al., 2009; Pessoa et al., 2014). The structurally related integral protein MARDI (also known as small integral membrane protein 24, SMIM24) also significantly augments glucose uptake via SGLT2 when co-expressed in oocytes (Coady et al., 2017) and binds to PDZK1 at its C-termini. However, the interaction of MAP17 to PDZK1 is not essential to increasing SGLT2 activity, as deleting the fourth PDZ binding domain for MAP17 did not affect MAP17's ability to enhance SGLT2 activity (Coady et al., 2017). Therefore, it is postulated that MAP17 directly augments SGLT2 activity by altering the protein conformation, but this mechanism is still not understood. A schematic of the function of SGLT1 and SGLT2 in the kidney nephron is shown in figure 1.5.

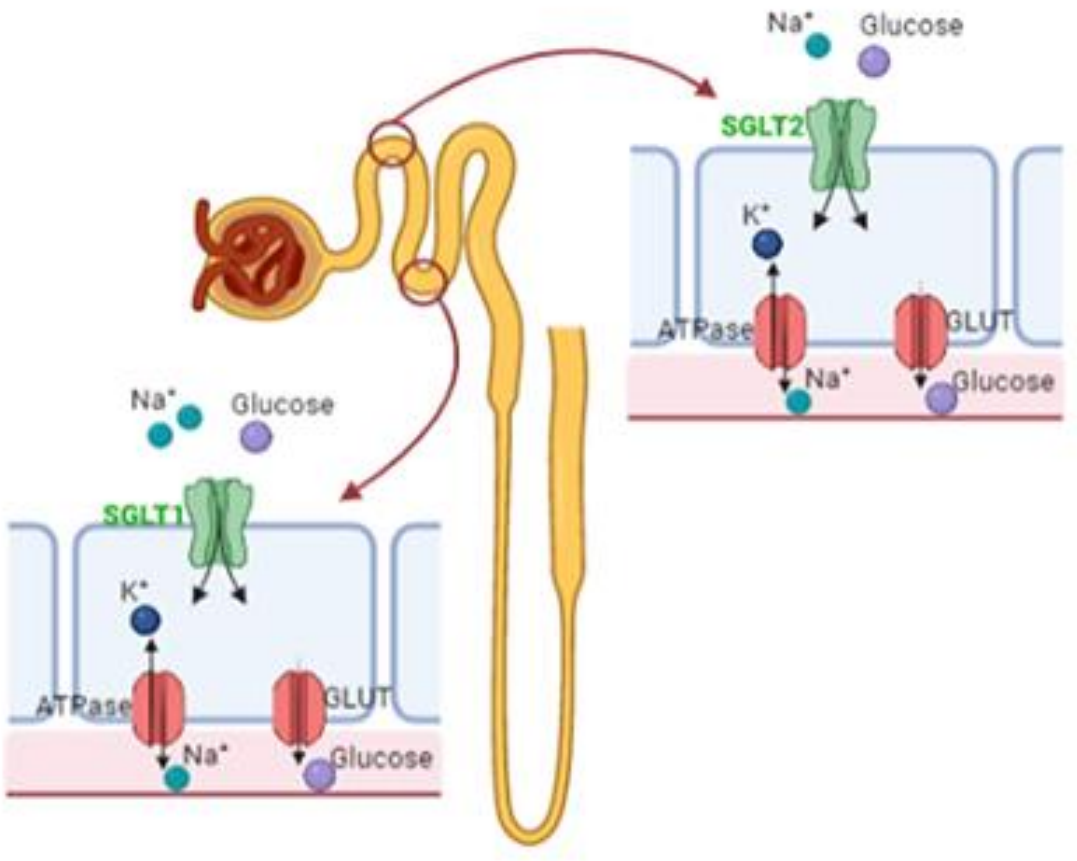


Figure 1.5: Function of SGLT1 and SGLT2 within the proximal tubule.
GLUT (glucose transporter), ATPase (charge transferring complex using energy from hydrolysed ATP), K^+ (potassium), Na^+ (Sodium) (Source: Author using Biorender.com).

1.6.2.2.2 | SGLT2 treatment for patients with type 2 diabetes mellitus (T2DM)

Diabetes mellitus is a metabolic disorder characterised by elevated blood glucose levels and broken down into 2 main types. Type 1 diabetes is an autoimmune associated disease where insulin producing pancreatic beta cells are destroyed. The hormone insulin cannot be produced, and glucose cannot be taken up into cells so accumulates within the blood. Comparatively, type 2 diabetes (T2DM) typically results from obesity, poor diet and exercise and dysfunction in beta pancreatic cells. It is characterised by insulin resistance and in some patients a reduction in insulin production occurs (Tan et al., 2019). The main treatment of T2DM involves glucose lowering drugs including metformin, sulfonylureas, thiazolidinediones, GLP-1 receptor agonists, Dipeptidyl Peptidase-4 inhibitors (DPP-4) and SGLT2 inhibitors (Artasensi et al., 2020).

SGLT inhibitors currently approved by the FDA and EMA include, canagliflozin, dapagliflozin, empagliflozin and ertugliflozin. By inhibiting SGLT2, glucose reuptake from the glomerular filtrate is prevented and is excreted out in the urine, lowering blood glucose levels. SGLT2 is also found in pancreatic α cells and when SGLT2 is inhibited stimulation of glucagon secretion from the alpha cells occurs, increasing gluconeogenesis and opposing the glucose lowering effect of SGLT2 inhibitors (Gronda et al., 2020). This is important to reduce the incidence of hypoglycaemia in patients treated with SGLT2 inhibitors. SGLT1 inhibitors can be beneficial for patients with impaired renal function where they respond less to SGLT2 inhibitors. For example, Mizagliflozin is a potent selective SGLT1 inhibitor, which is not FDA approved but phase 1 clinical trials demonstrate it is a potential treatment for chronic constipation (Inoue et al., 2017).

1.6.2.2.3 | SGLT2 inhibitors and heart failure

Type 2 diabetics (T2DM) have a higher risk of cardiovascular disease and severe cardiac events. As a result, the FDA and EMA looked at the cardiovascular safety outcomes of several clinical trials of glucose lowering drugs to gain assurance that they didn't elevate cardiovascular risk in the patients. The empagliflozin outcome trial in 2015 was the first to demonstrate that SGLT2 inhibitors decrease the rate of adverse cardiovascular events and cardiac death in T2DM by ~3% (Zinman et al., 2015). The DECLARE-TIMI 58 trial was carried out to include a primary outcome of heart failure hospitalisations. Reports showed that dapagliflozin treated patients had a significant 27% reduction in heart failure hospitalisations and a reduction in myocardial infarction (MI) and stroke outcomes (Wiviott et al., 2018). This was linked to a decrease in the incidence of atrial fibrillation/ flutter in patients (Zelniker et al., 2020). These findings highlighted a clear benefit of SGLT2 inhibitors for heart failure outcomes, hence further trials were carried out to see if these cardiovascular benefits also occurred in non-diabetics. The DAPA-HF trial was the first to identify dapagliflozin improved the symptoms and biomarkers of heart failure patients with reduced ejection fraction and lowered the need for high medical therapy, irrespective if the patient had T2DM or not (Martinez et al., 2020; McMurray et al., 2019; Nassif et al., 2019). These results were supported by the EMPERIAL-Reduced trial and DETERMINE-Preserved trials, suggesting SGLT2 inhibitors should be considered for heart failure treatment.

Currently, dapagliflozin is the only SGLT2 inhibitor FDA approved for managing heart failure (class II, III, IV) in patients (Lusk et al., 2022), however, the mechanism of action the SGLT2 inhibitors have in treating heart failure is not understood. Some studies highlight that SGLT2 inhibitors reduce cardiac remodelling by supressing fibroblast activation and inhibiting AMPKα and TGFβ/Smad signalling, overall decreasing cardiac disfunction (Tian et al., 2021). Other studies expand on this showing dapagliflozin prevented myocardial hypertrophy and improved left ventricular disfunction in angiotensin-2 infused rats, without affecting serum glucose levels. These outcomes were associated with dapagliflozin significantly inhibiting angiotensin induced upregulation of TGFβ/Smad, MMP-9 (Zhang et al., 2021) and chemokine 2 and 5 levels (Ortega et al., 2019). These signalling pathways initiate fibroblast transition and extracellular matrix formation, which are known to be involved in the development of aortic aneurysms and cardiac hypertrophy. By preventing these events the development of heart failure is subdued.

Diabetic hearts are known to have an elevated late sodium (Na^+) current and Na^+/ Hydrogen exchanger activity. This results in impaired excitation-contraction coupling and increased risk of arrhythmia due to high [Na^+]i and calcium overload, which leads to production of reactive oxygen species (ROS) (Lambert et al., 2015). Studies carried out by Lee et al (2019) and Hegyi et al (2022) showed via patch clamp recordings that treatment with (1μM) empagliflozin reduced the Na^+/ Hydrogen exchanger currents, late Na^+ currents and ROS in ventricular myocytes (Hegyi et al., 2022; Lee et al., 2019). This results in a reduction of calcium sparks and further calcium leakage from the sarcoplasmic reticulum, preventing myocardial disfunction and lowering blood pressure. Overall, this demonstrates that SGLT inhibitors may also have anti-arrhythmic potential, improve myocardial contractility and reduce blood pressure.

1.6.2.2.4 | Effects of SGLT2 inhibitors on the vasculature

SGLT2 inhibitors are known to lower blood pressure, however the underlying mechanisms are ill-defined. Previous studies demonstrate that other anti-diabetic drugs, including alogliptin (Jung et al., 2021), repaglinide (Kim et al., 2016) and metformin (Agard et al., 2009) can induce relaxation via elevated activation of either PKA/PKG or nitric oxide synthase. Literature demonstrates that the ability

for SGLT2 inhibitors to lower blood pressure is not due to glycosuria alone and rather that SGLT2 inhibitors can act directly on arteries to cause relaxation. One of the first studies to show this applied dapagliflozin to phenylephrine pre-contracted rat aortic segments. The relaxation produced by dapagliflozin was attenuated by Kv channel inhibitor 4-AP and PKG inhibitor KT5823, however PKA, adenylate cyclase and other Kv channel inhibitors did not affect dapagliflozin-induced relaxations (Li et al., 2018). Seo et al., (2020) replicated this study using empagliflozin and supported these findings, demonstrating empagliflozin and dapagliflozin both evoke arterial relaxation via activation of PKG and Kv channels (Seo et al., 2020). This conclusion was later contradicted by Hasan & Hasan, 2021 whereby PKG and guanylate cyclase inhibitors were not able to attenuate empagliflozin induced relaxations in rat mesenteric arteries. Alternatively, Inhibition of Kv7 and Kv1.5 channels attenuated empagliflozin-induced relaxations demonstrating these channels play a major role in this phenomenon. These findings were expanded when western blot experiments found the SGLT2 protein are expressed in mesenteric arteries, but non-selective SGLT inhibition did not evoke relaxation (Hasan et al., 2022). Therefore, it is inferred SGLT2 inhibitors relax resistance arteries by activation of Kv7 channels which is independent of SGLT2.

1.6.2.3 | SMIT1

The rapid equilibration of osmotic gradients is vital for regulating cell volume consistency and controls cytosolic ion homeostasis needed for adequate cellular function. Uncharged osmolytes including myo-inositol and sugars passively diffuse in and out of cells via non-selective ion channels or co-transporters, to regulate osmotic homeostasis without effecting inorganic ion levels (Lang et al., 1998). One co-transporter responsible for this is SMIT.

Slc5a3 and Slc5a11 encode for SMIT1 and SMIT2, respectively, in a myriad of tissue types, including brain, renal, small intestine and lungs. This broad protein expression coincides with SMIT's role in maintaining cellular osmolarity. SMIT transports two sodium ions down their concentration gradient accompanied by either myo-inositol with a Km of 55uM or various other sugars including D or L glucose, L-fucose, L-xylose and scyllo-inositol with a Km > 50 mM. Expression of

SMIT is upregulated by a transcription factor, tonicity-responsive enhancer binding protein (TonEBP), upon extracellular hypertonicity, resulting in elevated intracellular myo-inositol. TonEBP binds to tonicity-responsive enhancers (TonE) on the SMIT gene promotor region, initiating protein transcription (figure 1.6).

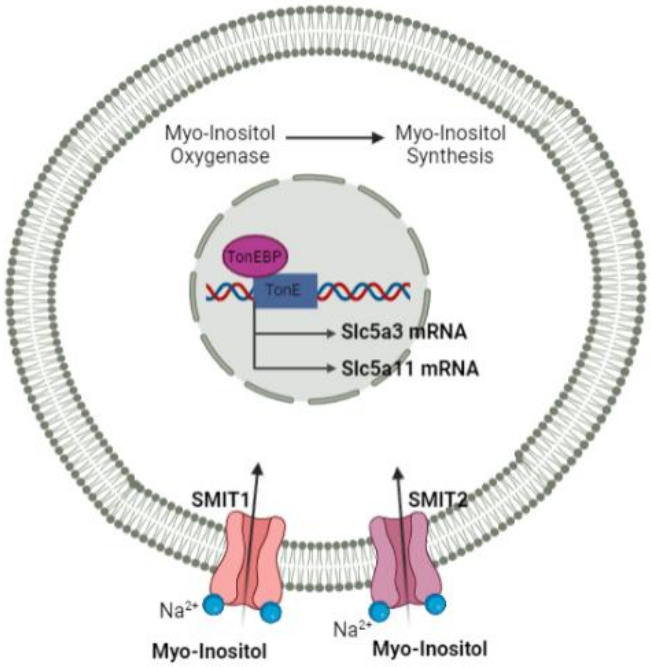


Figure 1.6: Diagram of SMIT1 and 2 production:
TonEBP interacts with a regulatory sequence element, the tonicity responsive enhancer, located in the promotor region of several genes. Said interaction results in transcription and translation of SMIT to the membrane (Source: Author using Biorender.com).

Little is known about the post-translational regulation of the SMIT carrier protein, however serine/threonine-protein kinases (SGK) are known to be co expressed with SMIT1 in several tissues including brain (Moo Kwon et al., 1992; Wärntges et al., 2001) and kidneys (Hou et al., 2002). Moreover, a recent study identified SMIT1 is upregulated by active SGK1 and similar SMIT1 activity was seen when SMIT1 was co-expressed with SGK2, SGK3 and PKB (Klaus et al., 2008). The elevated SMIT1 activity was postulated to be a consequence of increased carrier protein cell surface expression, whereby SGK stabilised the transporter within the cell membrane. The ubiquitin ligase Nedd4-2 is endogenously expressed and removed target proteins from the cell membrane. Nedd4-2 is phosphorylated and inactivated by SGK1. The same study demonstrated that co-expression of active Nedd4-2 decreased SMIT1 activity, which was reversed by further SGK1 co-expression

(Klaus et al., 2008). This regulation of SMIT1 is also seen in studies for glucose transporter SGLT1 (Dieter et al., 2004), demonstrating the similarity in the regulation of these 2 transporter proteins.

Myo-inositol is a vital organic osmolyte catabolised to produce various secondary signalling molecules crucial to many channels and GPCR pathways. PIP_2 is formed from myo-inositol by phosphatidylinositol 4-kinase (PIP4K) and phosphatidylinositol 5-kinase (PIP5K) and plays a pivotal role, whereby if absent, cellular processes, including Kv7 channels, inwardly rectifying potassium channels (Kir), transient receptor potential channels (TRP) and epithelial sodium channels (ENaC) will not function. As such, SMIT has a profound influence on the regulation of ion channel activity.

SMIT expression and function is ill defined within the vasculature. Expression of SMIT in coronary, choroid plexus, renal and mesenteric arteries have been identified (Barrese et al., 2020; Chen et al., 2010b), but their functional role has only been explored recently. Genetic studies show a correlation between coronary heart disease and the SNP near the chromosomal location of Slc5a3-MRPS6-KCNE2, whereby the presence of this SNP had an increased incidence of myocardial infarction and coronary heart disease (Kathiresan et al., 2009; Ripatti et al., 2010). The underlying mechanisms behind this are unknown but is thought to be associated with mutations in KCNE2 giving rise to long-QT syndrome (Beaney et al., 2017) in addition to SMIT1 overexpression which increases the production of reactive oxygen species in the heart (Van Steenbergen et al., 2017b). Both pathways increase the hearts susceptibility to cardiac disfunction.

1.6.2.3.1 | SMIT and ion channel interactions within the brain

Kv7 channels have an obligatory requirement for PIP_2. Co-localisation of the channels with SMIT1 would provide an efficient signal complex for effective cell physiology. Co-localisation of SMIT1 and Kv7s has been reported in neurones and choroid plexus (Abbott et al., 2014; Manville et al., 2017; Roepke et al., 2011) but a greater level of complexity has been revealed.

Manville et al (2017) identified that SMIT1 bound to the KCNQ2 pore (S4-6) and increased the activity of Kv7.1 and Kv7.1/KCNE2 currents by shifting their voltage dependent activation. Comparatively, Kv7.1 alone doubled the SMIT1 uptake of

myo-inositol, however with the addition of bound KCNE2 this effect was reversed and SMIT1 activity is inhibited (Manville et al., 2017). These findings were supported by knockout studies demonstrating that Kcne2 deletion increased mice susceptibility to seizures, underpinned by a reduction in SMIT1 activity perturbing myo-inositol levels within the cerebrospinal fluid (CSF) (Abbott et al., 2014). Furthermore, SMIT1 function is inhibited by Pan Kv7 blocker XE-991 when co-expressed with KCNQ1. Providing further evidence that 'chansporters' regulate one another's activity (Neverisky & Abbott, 2015).

Kv7.2/3 channels also form complexes with SMIT1 and SMIT2 in the nodes of Ranvier. SMIT1 and SMIT2 enhance Kv7.2 and Kv7.2/3 currents without needing myo-inositol by physically interacting with the channel pore and negatively shifting the voltage dependence and speed of channel activation (Manville et al., 2017; Neverisky & Abbott, 2017). Further demonstrating that transporter activity can be targeted via the used of pharmacological ion channel blockers.

1.6.2.3.2 | SMIT and Kv7 channel interactions within the vasculature

Within renal and mesenteric VSMC, expression of SMIT1 but not SMIT2 was detected via Q-PCR and immunocytochemistry. Similarly, proximity ligation assays identified an interaction between SMIT1 and Kv7.4/Kv7.5 heteromers in isolated renal and mesenteric arteries. Hence, SMIT1 is expressed in VSM cells and associates with Kv7.4/Kv7.5 channel proteins (Barrese et al., 2020).

Raffinose is a sucrose derivative that makes solutions hypertonic. When arteries were incubated in a hypertonic solution, SMIT1 expression in the SMC membrane was elevated. Furthermore, incubation of renal arteries with 150mM raffinose reduced the concentration-dependent contractions to alpha 1 adrenoreceptor agonist methoxamine. This contractile inhibition was greater when vessels were incubated with and 150mmol/L raffinose and 1mmol/L myo-inositol. The Kv7 blocker linopirdine or knockout of Kv7.4/Kv7.5 both prevented the attenuation of methoxamine-induced contractions. Interestingly, when SMIT1 was knocked down, there was an impairment in the renal artery response to the Kv7 activator ML213 and an increase in arterial contractility. Finally, incubation of renal artery VSMCs with raffinose increased markedly the linopirdine-sensitive Kv7 channel

currents (Barrese et al., 2020). These data provide evidence that SMIT-Kv7 complexes regulate arterial contractility as shown in figure 1.7.

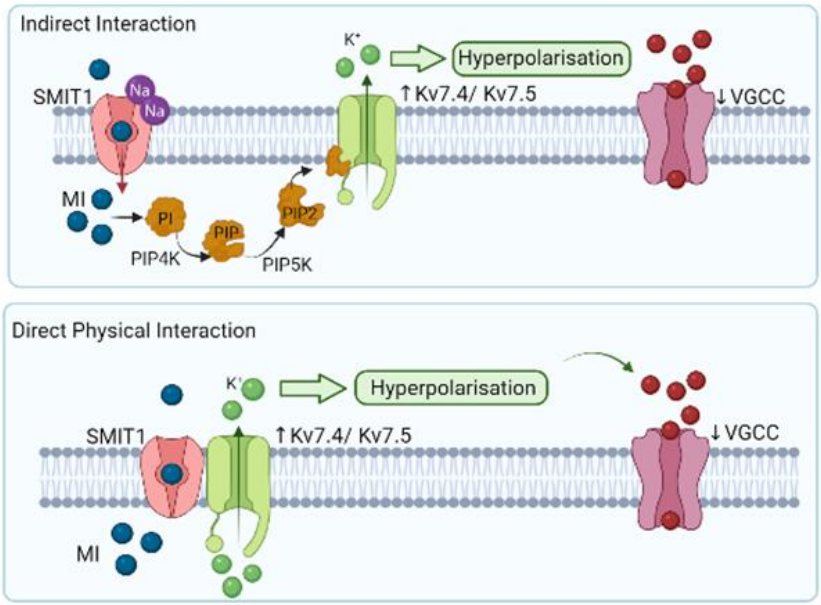


Figure 1.7: Interaction of Kv7 channels with SMIT1 in VSM cells
Top- Indirect interaction of SMIT1 channels with Kv7 channels via PIP_2 signalling. Bottom – Direct interaction of SMIT1 channels with Kv7 channels stimulates potassium efflux and hyperpolarisation (Source: Author using Biorender.com).

1.6.2.4 | SMIT2

The SMIT2 transporter was first characterised in human HepG2 liver cells for its low affinity myo-inositol uptake (Ostlund et al., 1996) and later cloned (Coady et al., 2002) to identify its expression in many other tissues, including the kidney, brain, heart, lungs and liver. SMIT2 was found to have a pre-steady state current inhibited by phlorizin (K_i of 76 μm) and a substrate-independent sodium leak current. The SMIT2 sodium leak current is phlorizin-sensitive and active within the −155 to −5 mV range, where phlorizin is effective in the absence of myo-inositol. This current is fairly large in the presence of external sodium, but as the external sodium concentration decreases due to progressively replacing sodium with NMDG-Cl, the leak current amplitude increases up to 5 fold greater at -155mV (Sasseville et al., 2014). SMIT2, along with SMIT1, regulates myo-inositol levels in the brain, whereby they are expressed in a variety of cells in the cortex, hippocampus, cerebellum, amygdala, caudate, dorsal raphe nucleus, hypothalamus, locus coreuleus, medulla oblongata, nucleus accumbens and

substantia nigra (Chen et al., 2010; Coady et al., 2002). SMIT2 is also highly expressed in the apical membrane of renal proximal tubules, where it reabsorbs nearly all of myo-inositol, which is essential for cellular osmoregulation and function (Bissonnette et al., 2004; Lahjouji et al., 2007). More recently, mice knockdown studies have shown SMIT2 is involved in osteogenesis and regulation of bone formation and mineral density (Dai et al., 2011),, however, presently, there is no role for SMIT2 in vascular smooth muscle.

1.6.3 | Sex Differences in Vascular Physiology

It is well documented that the incidence of hypertension and cardiovascular disease is lower in pre-menopausal women compared to aged-matched males and post-menopausal females, indicating sex hormones are the primary factor driving sex-dependent differences in vascular physiology. Throughout the oestrus (rodent) and menstrual (human) reproductive cycle, cyclical changes in sex hormone levels, including androgens, oestrogen and progesterone, alter vascular function (Baldwin et al., 2023; Pabbidi et al., 2018).

17-β oestradiol (E2) exerts its effects by acting on its cytoplasmic nuclear receptors ERα and ERβ, ubiquitously expressed throughout the vasculature (Pabbidi et al., 2018). Activation of ERα/β enhances nitric oxide and beta-adrenergic coupling, reduces alpha-adrenergic coupling and increases eNOS synthesis, resulting in vasorelaxation (Aryan et al., 2020; Marino et al., 2006; Nuedling et al., 2001). Conversely, testosterone activates nuclear, membrane-bound and G protein-coupled androgen receptors. This process leads to the activation of various secondary signalling molecules, including PKC, PKA, PKG, ERK and mitogen-activated protein kinase (MAPK) (Connelly et al., 2021; Lucas-Herald et al., 2017), or it can modulate the expression of angiotensin-converting enzyme (ACE) and endothelin-1, which can induce both vasodilation and vasoconstriction (Mishra et al., 2019; Pearson et al., 2008). Sex-dependent differences in the expression of SGLT1-2 have also been documented and reviewed comprehensively by Sabolić et al., 2012 demonstrating the importance of characterising these transporters in both male and female arteries. However, the effect of sex hormones and the vascular differences between pre-menopausal and post-menopausal women has only recently been explored. The oestrus cycle lasts 4-5 days and is split into 4

stages (Pro-oestrus, oestrus, Met-oestrus and Di-oestrus), with pro-oestrus and oestrus (PE) stages having high oestrogen levels and di-oestrus and met-oestrus (DM) stages having low oestrogen levels (Cora et al., 2015; Nilsson et al., 2015). In contrast, the menstrual cycle lasts 28 days with 4 stages (follicular, ovulation, luteal and menstruation) (Carlson & Shaw, 2019). Both cycles follow similar rises and falls in sex hormones, making female rodent studies valuable for understanding vascular function in pre- and post-menopausal women. Recently, Baldwin et al. 2022 demonstrated the Kv7.1 channel activator HMR-1556 significantly impaired IP receptor-mediated relaxation in mesenteric arteries from DM female rats but not in PE females (Baldwin et al., 2022). This paper was the first to show an oestrus-cycle-dependent difference in arterial Kv7 channel function. Following this, Baldwin et al 2023 demonstrated that arteries from PE female rats (high E2) were pro-contractile and produced impaired relaxations to pan Kv7 channel and β-adrenoreceptor agonists compared to arteries from DM female rats with significantly lower E2 levels (Baldwin et al., 2023). The pro-contractile vascular responses in PE female arteries were associated with reduced VSMC membrane expression of Kv7.4 compared to DM females due to oestrogen activating GPER1, resulting in reduced interaction of Kv7.4 with the trafficking chaperone HSP90 (Baldwin, Forrester, et al., 2023). Comparatively, oestrogen has also been found to upregulate BK_{Ca} channels through GPER1 signalling and PKC in human uterine and coronary arteries (Hu et al., 2011; Nagar et al., 2005; White et al., 2002; Yu et al., 2011). This further highlights the importance of considering sex hormones and the female oestrous cycle when studying ion channel and transporter activity.

1.7 | Thesis Aims

This research project investigated the roles of sodium-dependent glucose transporter (SGLT) and sodium/myo-inositol transporter (SMIT) within the vasculature. The primary research questions addressed in this thesis were:

1. What are the expression patterns of SGLT1, SGLT2, SMIT1, and SMIT2 across various arterial segments from male and female rats, are there any oestrus cycle differences and what is their specific localization within vascular smooth muscle cells?
2. What is the functional role of SGLT2 within the vascular system, and through which mechanisms do SGLT2 inhibitors induce vasorelaxation?
3. How does SMIT1 regulate vascular tone, and what are the expression patterns and functional roles of SMIT-Kv7 complexes within the vasculature of male and female rats?

Each of these questions forms a chapter in this thesis to thoroughly investigate the role of these transporters in vascular physiology. The expression of Slc5 transporters in arteries is ill-defined, with only a handful of studies (Barrese et al., 2020; Chen et al., 2010; Hasan, Menon, et al., 2022) investigating their role in the vasculature. Hence, the vascular expression of Slc5 transporters was initially investigated using several molecular techniques. The second question was explored due to several clinical trials (Bosch et al., 2019; Wheeler et al., 2021; Williams & Evans, 2020; Wiviott et al., 2018; Zannad et al., 2020) followed by the UK National Institute for Health and Care Excellence (NICE) approving SGLT2 inhibitor treatment for heart failure independent of raised glucose. SGLT2 inhibitors have been demonstrated to lower blood pressure and directly induce relaxation in mesenteric arteries (Hasan, Menon, et al., 2022; Hasan, Zerin, et al., 2022; Hasan & Hasan, 2021) leading to this chapter investigating the underlying mechanisms of SGLT2 inhibitor-induced relaxations. The final chapter builds upon the findings of Barrese et al. (2020) to understand the novel role of SMIT1 transporters in regulating vascular tone in both male and female arteries. The work produced in this thesis focused on mesenteric, renal, and coronary arteries, enabling a comparison of different arterial beds.

Chapter 2: Methods and Materials

2.1 | Animals and Dissection

Experiments were performed on arteries from male and female Wistar rats aged 11-14 weeks and weighing 175-300g, housed within the Institute of Cancer Research facility (Sutton, UK). Rats were housed in cages with LSB Aspen woodchip bedding and a 12-hour light/dark cycle, maintained at constant temperature (21±1°C) and humidity (50%±10%), with free access to water and food in accordance with the Animal Scientific Procedures Act 1986 (ASPA). The tissues were transported daily to St George's University of London, bathed and preserved in a physiological salt solution A (PSS-A, composition shown in solutions table 2.1). Animals were sacrificed by cervical dislocation, and death was confirmed via severing the femoral artery circulation in accordance with Schedule 1 of the ASPA 1986.

Second-order mesenteric arteries, the left and right main renal arteries and left anterior descending (LAD) coronary and septal coronary artery were dissected, cleaned of fat and adjacent tissue and stored on ice in physiological salt solution-B (PSS-B, composition shown in solutions table 2.1) to preserve them, said dissections can be seen in figure 2.1.

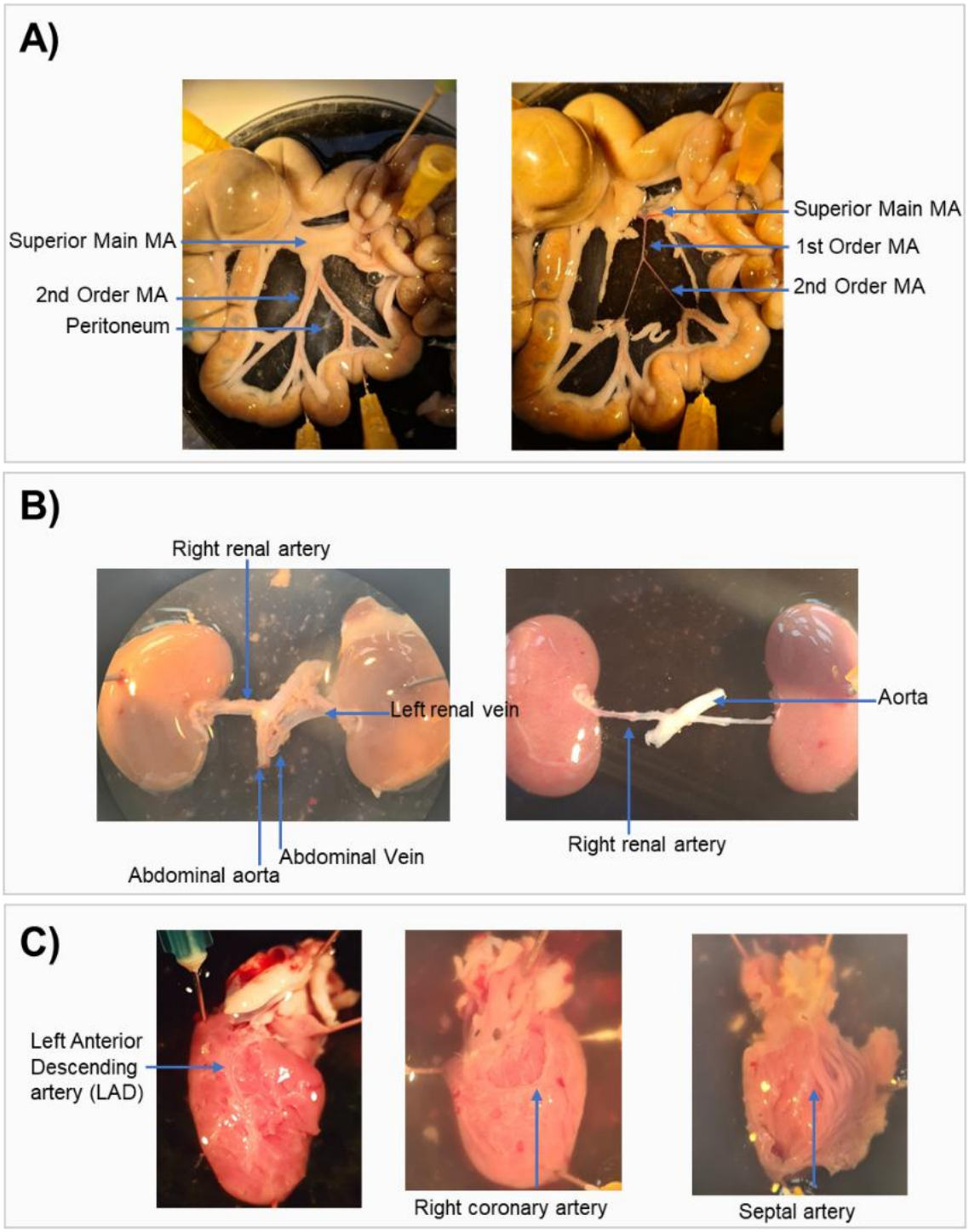


Figure 2.1: Mesenteric, renal and coronary artery dissection
Panel A shows the rat mesentery pinned out on a petri dish to display the arterial plexus, undissected with adherent tissue (left) and cleaned of tissue (right). Panel B shows the rat kidneys with the connecting renal arteries undissected (left) and dissected (right). Panel C shows the dissection of the left anterior descending coronary artery (LAD, left), the right coronary artery (middle) and septal artery (right) (Source: Author).

2.2 | Solutions:

Table 2.1: The composition of every solution used in this study.

Solution	Composition	Technique used
PSS-A	(mmol·L-1): 126 NaCl, 6 KCl, 10 glucose, 11 HEPEs, 1.2 MgCl2 and set to pH7.4 with NaOH	For transporting tissues from Sutton Cancer Research to St George's University
PSS-B	(mmol·L-1): 119 NaCl, 4.5 KCl, 1.17 MgSO4.7H20, 1.18 NaH2PO4, 25 NaHCO3, 5 glucose, 1.25 CaCl2.	Dissecting tissues Functional myography
High glucose PSS	(mmol·L-1): 119 NaCl, 4.5 KCl, 1.17 MgSO4.7H20, 1.18 NaH2PO4, 25 NaHCO3**, 20 glucose**, 1.25 CaCl2.	For chapter 6 investigating the effect of hyperglycaemia on arterial function
Raffinose PSS	(mmol·L-1): 119 NaCl, 4.5 KCl, 1.17 MgSO4.7H20, 1.18 NaH2PO4, 25 NaHCO3, 5 glucose, 1.25 CaCl2 and **150 D-+- raffinose pentahydrate**	For Chapter 6 investigating the effect of hypertonicity on arterial tone.
Smooth muscle dissociation solution (SMDS)	(mmol·L−1); 120 NaCl, 6 KCl, 12 glucose, 10 HEPES and 1.2 MgCl2 and set to pH7.4 with NaOH	Immunocytochemistry (ICC) Proximity ligation assay (PLA)
Phosphate buffered saline-T (PBS-T)	Phosphate buffered saline (PBS) in 0.1% tween 20	Western Blot
Transfer buffer	700mL distilled water, 200mL methanol and 100mL X10 transfer buffer stock	Western Blot
10x transfer buffer	1.92M Glycine and 250mM Tris base in 500mL distilled water	Western Blot

2.3 | Rat Oestrus cycle staging

A rat's oestrus cycle averages 5 days and is divided into 4 stages, which can be identified by changes in cervical cell histology. The 4 stages are: 1) Pro-oestrus – 14 hours; 2) Oestrus – 24-48 hours; 3) Met-Oestrus – 6-8 hours; 4) Di-Oestrus – 48-72 hours. The cyclical levels of progesterone and oestrogen alter the physical features of the uterus and vaginal cytology, which enables us to distinguish between each stage (figure 2.2). A vaginal smear was taken following euthanasia, whereby 50µL of PSS was flushed 4-6 times into the vaginal canal using a 20-200µL pipette tip to liberate cells from the cervix.

The cell suspension was placed onto a glass cover slide and viewed under a light microscope (Olympus CK40). To obtain representative images of each oestrus cycle stage, the cells on the glass slide were left to adhere for 1 hour at RT. The slide was then flooded with 1mL toluidine blue O (0.1% in H2O, passed through a 0.2-µm syringe filter) for 1 minute before being placed in distilled water on a rotating plate (20 RPM) for 45 seconds. The slide was left to dry and then imaged using a Nikon Eclipse Ni.

The variation and abundance of 4 principal cell types were used to identify each stage additional to the shape of the uterus (Ajayi & Akhigbe, 2020; Cora et al., 2015). The differences between each stage can be seen in figure 2.2. Proestrus was identified by the presence of nucleated epithelial cells that form clusters and markedly large ovaries compared to any other stage. Oestrus has a high cell count consisting of mainly anucleated epithelial cells, with the uterine lumen dilated and appearing rugged. When neutrophils are present, the cycle shifts to metestrus, which is characterised by a combination of nucleated epithelial cells and cornified anucleated epithelial cells mixed with neutrophils. As the cycle transitions to di-oestrus, the number of cells (cellularity) diminishes, and neutrophil numbers increase with the uterus lumen becoming small and avascular. The Oestrus stage differences are summarised in Table 2.1.

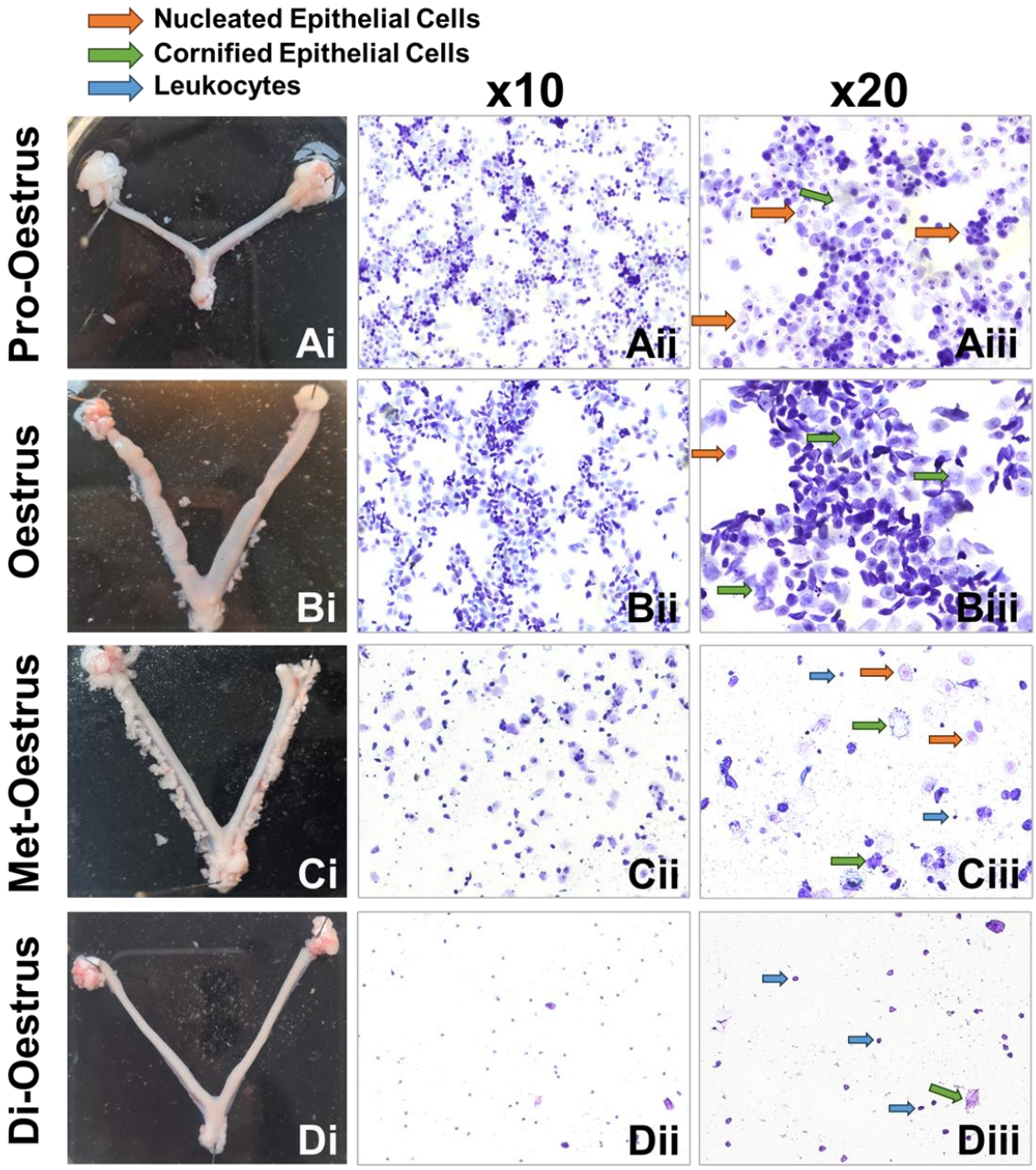


Figure 2.2: Vaginal cytology and uterine characteristics in each rat oestrus stage
The uterus and vaginal cytology at x10 magnification of proestrus (Ai-ii), oestrus (Bi-ii), metestrus (Ci-ii) and diestrus (Di-ii) stages, (Source: Author).

Table 2.2: Cervical cell populations in female Wistar rats (Modified from Cora et al., 2015). *The abundance of each cell type is noted down from very high (+++) to absent (0).*

Oestrus Stage	***Cell Density***	***Neutrophils***	***Nucleated epithelial cells***	***Small nucleated epithelial cells***	***Anucleated cornified epithelial cells***
Proestrus	Low to Moderate	0 - +	0 - +	+++	0 - +
Oestrus	Moderate to High	0 - +	0 - ++	0 - ++	+++
Metestrus	Moderate to High	+ - ++	+ - ++	+ - ++	++ - +++
Diestrus	Low to Moderate	+ - +++	+ - ++	+ - ++	0 - +

2.4 | Myography

2.4.1 | Outline and preparation

2nd order mesenteric arteries (MA), main left and right renal arteries (RA), LAD and septal coronary arteries were cut into ~2mm segments and mounted for isometric tension recordings in a myograph (DMT, Aarhus, Denmark). A wire myograph was used for all mesenteric and LAD coronary artery experiments. The chamber contains two arms with jaws where two 40um wires are threaded through the artery and fixed down by screws onto either jaw. A pin myograph was used for all renal artery experiments, whereby the chamber contains 2 arms, with 100um pins on one side positioned in the artery lumen (schematic is shown in figure 2.3).

For both myographs, one arm is attached to a micrometre to separate the arms and cause the vessel to stretch to the desired circumference, and the other arm is attached to a force transducer. The signal from the transducer located in the myograph chamber was boosted by a PowerLab (ADInstruments, Oxford, UK). The computer program LabChart Pro (ADInstruments, Oxford, UK) records the amplified force and converts this value to a Kilopascal (kPa) reading. Each myograph chamber is filled with 5mL PSS and bubbled with 95% oxygen and 5%

carbon dioxide at 37°C. Once mounted, the vessels were left to equilibrate for 15-30 minutes before normalisation.

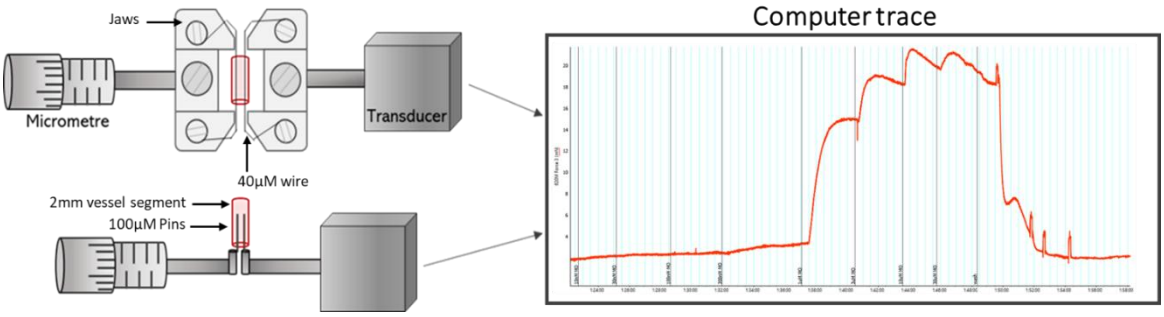


Figure 2.3: Representation of a mounted artery segment on a wire and pin myograph (Source: Author)
Schematic of a mounted artery on 40µM wires and 100µM pins connected to a micrometre on one side and a PowerLab transducer on the other. The PowerLab amplifies the force, and LabChart Pro software forms a computer trace (Source: Author).

2.4.2 | Normalisation protocol

All vessels were subject to a normalisation procedure pioneered by Mulvany and Halpern (1977) to standardise the experimental conditions and ensure the vessels had reliable physiological responsiveness. Mesenteric, renal and let coronary arteries were set to an internal luminal circumference of 90% of the diameter at an in-vivo transmural pressure of 100mmHg (13.3 kPa), as shown in figure 2.4. Comparably, septal arteries were set to a target pressure of 10.7kPa. Using the micrometre, vessels were incrementally stretched, and the force was recorded on Lab Chart Pro (ADInstruments, Oxford, UK) to calculate the internal circumference of the vessel needed to obtain a maximal active response of the vessel mimicked in-vivo (figure 2.5).

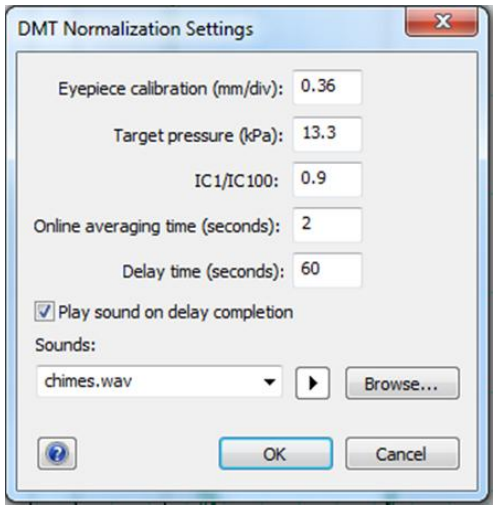


Figure 2.4: Normalisation settings

Mesenteric, renal and left coronary vessels were normalised to achieve an internal circumference at 100mmHg transmural pressure (13.3kPa) and then set to 90% of this pressure (IC1/IC100 of 0.9) (Source: Author).

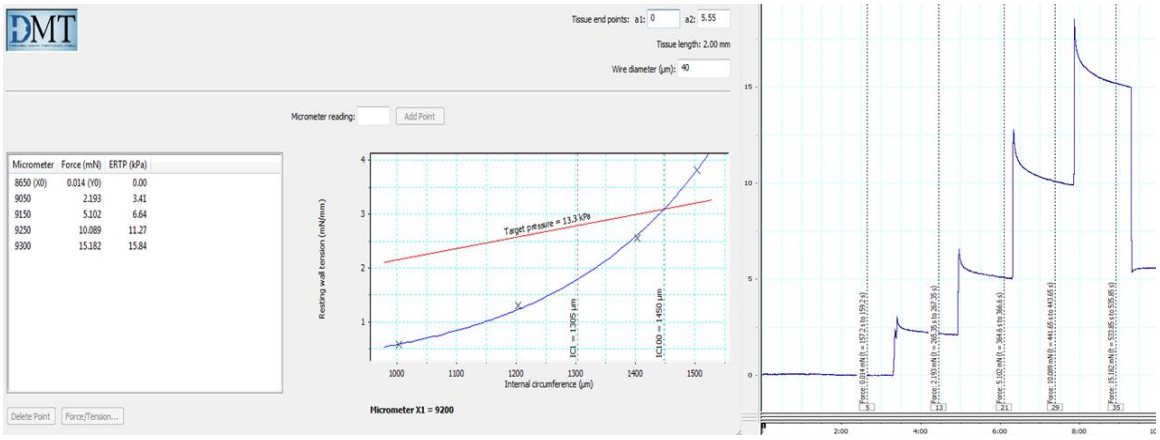


Figure 2.5: Normalisation protocol

When the two wires impose no stretch on the vessel, a zero force (mN) reading is recorded, with a transluminal pressure (kPa) reading and the recorded micrometre value. The vessel is incrementally stretched by rotating the micrometre, increasing the force (mN) applied to the vessel, which is recorded with the equivalent kPa value. Mesenteric arteries are initially stretched to 2mN, whereas renal arteries are stretched to 5mN. The DMT program calculates the targeted amount of stretch to produce a transluminal pressure of 13.33kPa with an internal circumference of 100mmHg, shown by the appropriate micrometre setting value indicated by the red circle (Source: Author).

2.4.3 | Vitality testing protocol.

Once the vessels had established basal tone, the viability of the vascular smooth muscle cells (VSMCs) was determined by replacing the chambers with PSS containing 60mM KCl with a concomitant reduction in NaCl until a sustained contraction was seen. Once the vessels reached a maximal contraction, the solution was washed out, and a period of 10 minutes was given for the vessels to return back to resting tone. A contraction of >1mN was taken as viable based on previous data generated by our laboratory and because recording percentage relaxation on arteries with >1mN becomes inaccurate.

Vessels were then constricted with 10µM of the α1-adrenoreceptor agonist, methoxamine and allowed to plateau before recording the percentage vasorelaxation to 10µM carbachol to determine the endothelial cell integrity. Vessels that relaxed ≥90% of the initial contraction qualified as an endothelial-positive vessel and a vessel that relaxed ≤10% was defined as a vessel with negative endothelium (Wenceslau et al., 2021). Both tests can be seen in figure 2.6.

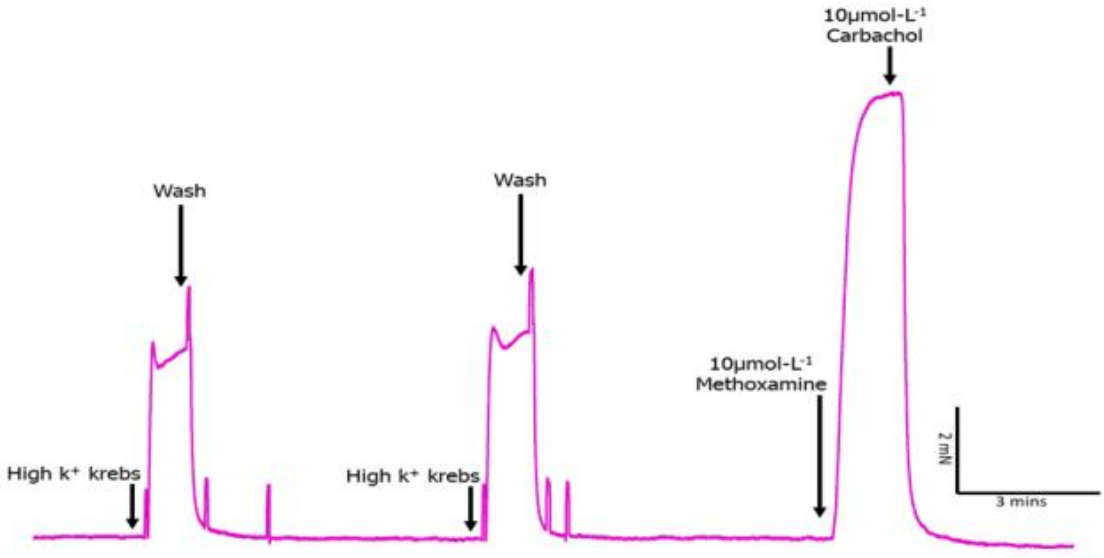


Figure 2.6: Representative trace of the vitality testing protocol
The protocol entails 2 challenges of High potassium PSS determining the arterial response to constrictors and one endothelial challenge. The percentage endothelium was calculated by adding10µmol-L-1 methoxamine followed by 10µmol-L-1 carbachol and the relaxation is recorded (Source: Author)

2.4.4 | Drugs

Table 2.3: A list of all reagents used:
A list of all drugs, their target and concentrations used throughout this study. Drugs were applied at concentrations selective for the target highlighted based on previous literature.

Drug	Target	Concentration used	Supplier #Catalog
4-aminopyridine (4-AP)	Voltage-gated potassium channel Kv1.1 and 1.2 blocker	1mM	Merck (A78403)
AM0902	Transient receptor potential cation channel A1 (TRPA1) blocker	1µM-30µM	Bio-Techne (5914)
AMG-517	TRPV1 inhibitor	1µM	Bio-Techne (5995)
BIBN-4096	Calcitonin gene-related peptide (CGRP) blocker	1µM	Bio-techne (4561)
Capsaicin	TRPV agonist	1-10µM	
Cariporide	Selective Sodium hydrogen exchanger 1 (NHE1) inhibitor	1µM-30µM	Cayman Chemical (CAY16935)
CGRP	endogenous neuropeptide for CGRP	10pM-10nM	Bio-Techne (1161)
Dapagliflozin	Sodium dependant glucose transporter 2 (SGLT2) inhibitor	1µM-100µM	Merck (SML2804)
EMD638683	Serum/Glucocorticoid Regulated Kinase 1 (SGK1) inhibitor	1µM	MedChemExpress (HY-15193)
Empagliflozin	SGLT2 inhibitor	1µM-100µM	SelleckChem (S8022)
Ertugliflozin	SGLT2 inhibitor	1µM-100µM	

Glibenclamide	Classic ATP-sensitive potassium channel (K_{ATP}) channel blocker	1µM	Merck (G0639)
Glucose		20mM	
Gallein	Inhibitor of G protein βγ subunit		Bio-Techne (3090)
HMR-1556	Specific Kv7.1 channel inhibitor	10µM	Merck (SML2354)
Iberiotoxin	large-conductance Ca2+-activated K+ channel (BK_{Ca}) channel blocker	100nM	Bio-Techne (1086)
ICI192605	Thromboxane A2 antagonist	1µM	Cayman Chemical (CAY10135)
Linopirdine	Pan Kv7.1-Kv7.5 channel blocker	10µM	Bio-techne (1999)
Methoxamine	Alpha 1 adrenergic receptor agonist	1nM-30µM	Merck (M6524)
Mizagliflozin	SGLT1 inhibitor	1µM-100µM	SelleckChem (S8939)
Myo-Inositol		1mM	Merck (I5125)
ML213	Pan Kv7.2-Kv7.5 activator	10nM-10µM	Bio-techne (4519)
Phlorizin	Nonselective SGLT inhibitor		Cayman Chemical (CAY11576)
Paxilline	Blocker of high-conductance Ca2+-activated K+ (BK_{Ca}, KCa1.1) channels.		Bio-Techne (2006)
Prazosin	Alpha 1 adrenoreceptor antagonist	100nM	Cayman Chemical

			(CAY15023)
Raffinose		150mM	Merck (R0250)
Tetraethylammonium (TEA)	Non-selective K+ channel blocker	1mM	
U46619	Stable thromboxane mimetic	1nM-10μM	Bio-Techne (1932)
XE-991	Pan Kv7 channel Kv7.2-Kv7.5 blocker	10μM	Bio-Techne (2000)

2.4.5 | Experimental protocols

Two main experimental protocols were used for isometric tension experiments depending on whether the effect of a vasorelaxant (protocol 1) or a vasocontractile (protocol 2) agent was being investigated.

Protocol 1

After the warm-up protocol, the vessels were left for 10 minutes to return to resting basal tone and then the effect of a pharmacological agent on the contractile ability of a vasoconstrictor was investigated. Increasing cumulative concentrations of methoxamine or U46619 were applied to the arteries, and the increase in tone was allowed to plateau before a new concentration was applied. Once the full range of concentrations had been applied, the chamber was washed out, returning the vessel back to resting tone. Several pharmacological modulators were then incubated for 10 minutes in the chosen chambers, and the concentration-effect curve was repeated in the presence of this drug.

Protocol 2

When investigating the effect of a vasorelaxant, the vessel segments were pre-contracted with either methoxamine or U46619 at EC80 concentrations of 10uM and 300nM, respectively. Once the maximal contraction plateaued, increasing cumulative concentrations of the vasorelaxant were applied, and the % relaxation was recorded. The schematic of each protocol can be seen in figure 2.7.

Other protocols specific to certain studies are outlined in their individual results chapters.

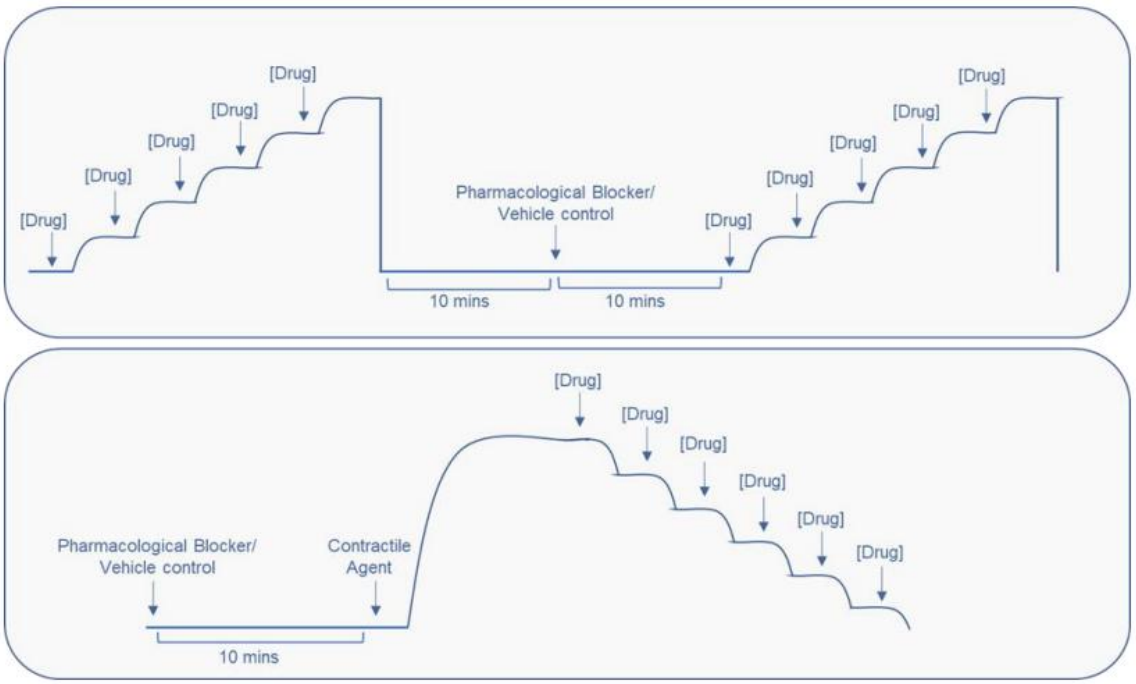


Figure 2.7: Schematic of the two experimental protocols 1 and 2.
Protocol 1 (Top) entails contracting the artery with cumulative application of a vasoconstrictor. The chamber is washed to allow the artery to relax back to basal tone. The testing drug is added, incubated and then the concentration effect curve is repeated. Protocol 2 (Bottom) involves pre-incubating the test drug for 10 minutes then a cumulative concentration effect curve to increasing concentrations of a vasorelaxant is produced on the artery pre-contracted with a vasoconstrictor (Source: Author).

2.5 | Ex Vivo morpholino Knockdown in whole arteries

Knockdown of NHE1, SMIT1, Kv7.4 and Kv7.5 in mesenteric and renal arteries was performed using specific morpholino oligonucleotides targeting mRNA from 5' cap of the untranslated region (UTR) and the following 25 bases of the amino acid coding sequence. The morpholino will bind and inhibit the translation of mRNA into protein and block the splicing of pre-mRNA.

All morpholinos were obtained from Gene Tools Inc., Philomath, OR, USA and came lyophilised at a concentration of 300nM for target Knockdown morpholinos and 100nM for control scrambled morpholinos. All morpholinos used are shown in table 2.4. All stocks are made to a final concentration of 1mM using distilled autoclaved water. Opti-MEM reduced serum medium (Thermo Fisher Scientific, 31985062) was combined with Lipofectamine RNAiMAX Transfection Reagent (Thermo Fisher Scientific, 13778075) in an Eppendorf and left for 5 minutes at RT.

In a separate Eppendorf, the Morpholino oligonucleotide was combined with Opti-MEM and left for 5 minutes at room temperature. The lipofectamine solution was then added to the morpholino solution and incubated at room temperature for 2 hours. 900µL of Dulbecco's Modified Eagle's Medium/Nutrient Mixture F-12 Ham (Sigma, D6421) was added to a 24-well plate, and the morpholino-lipofectamine mixture was subsequently added to the well to give a final morpholino concentration of 10µM. Arteries were then added to the mixture in the 24-well plate and incubated at 37°C in 5% CO2 for 48 hours. Knockdown morpholino samples were run in parallel with a scrambled oligo control with no target or activity. Knockdown of protein was assessed by Western blotting and ICC, and knockdown samples were compared to the controls.

Table 2.4: Table of morpholino oligonucleotides used:

MORPHOLINO	TARGET SEQUENCE
Scrambled Control	5' CCTCTTACCTCAGTTACAATTTATA 3'
Slc9a1	5' AGCATCATACTGATCCCCCAGCCTA 3'
Slc5a3	5' GTCTCCAGCACAGCCCTCATCTG 3'

2.6 | Gene Expression

RT-qPCR determined relative transcript abundance of Slc5 and Kcnq genes in mesenteric, renal, cerebral and coronary arteries. In addition to positive controls in the whole nephron, heart and brain tissue samples.

2.6.1 | RNA extraction and purification

Whole tissues were dissected, cleaned of fat, and then stored in RNAse in preparation for RNA extraction. The 'Monarch Total RNA Miniprep Kit' (New England Biolabs, Ipswich, Massachusetts, USA) was used to extract and purify mRNA from whole cell lysates. Tissue samples were taken and submerged in 300µL 1x DNA/RNA protection reagent, then mechanically homogenised via scissors, followed by a bullet blender with 0.9-2mm beads for 5 minutes. 60µL proteinase K diluted with 30µL proteinase K reaction buffer was added to the homogenised tissue sample and incubated at 55°C for 15-30 minutes. Samples were then centrifuged for 2 minutes at 14,000 x g, and the supernatant was

transferred to a sterile aliquot and vortexed with 300µL of RNA lysis buffer to remove heavy proteins and cell structures from the sample. A gDNA removal column fitted with a collection tube separated gDNA from the sample by centrifugation at 14,000 x g for 30 seconds. Afterwards, an equal volume (700µL) of 100% ethanol was added to the sample, mixed via pipetting, transferred to an RNA purification column and centrifuged for 30 seconds at 14,000 x g. The elution was discarded, and DNase 1 diluted in DNase 1 reaction buffer was applied to the column and incubated at room temperature for 15 minutes, allowing leftover gDNA to be enzymatically removed. RNA purification involved adding 500uL RNA priming buffer to the column, centrifuging for 30 seconds at 14,000 x g, and discarding the follow-through. 500uL of RNA wash buffer was centrifuged through the RNA purification column at 14,000 x g for 2 minutes. The sample was eluted by transferring the purification column to a nuclease-free microfuge tube; 30ul of nuclease-free water was directly pipetted onto the column's filter and centrifuged at 14,00 x g for 30 seconds to extract the pure RNA sample.

2.6.2 | RNA Quantification

The concentration and purity of RNA were calculated using a NanoDrop 3300 Fluorospectrometer with absorbance set to 260nm and 280nm (figure 2.8). This is based on the principle that RNA absorbs UV light at 260nm wavelength because of the conjugated double bonds present in the purine and pyrimidine rings, and proteins absorb at 280nM due to the tyrosine, phenylalanine and tryptophan rings.

1.5uL of the RNA sample is added to the NanoDrop, which records the sample's absorbance at 260nM. A high-purity RNA sample was indicated by an A260/A280 ratio ≥1.8, and the concentration of RNA in the sample (ng/uL) was calculated using the absorbance reading.

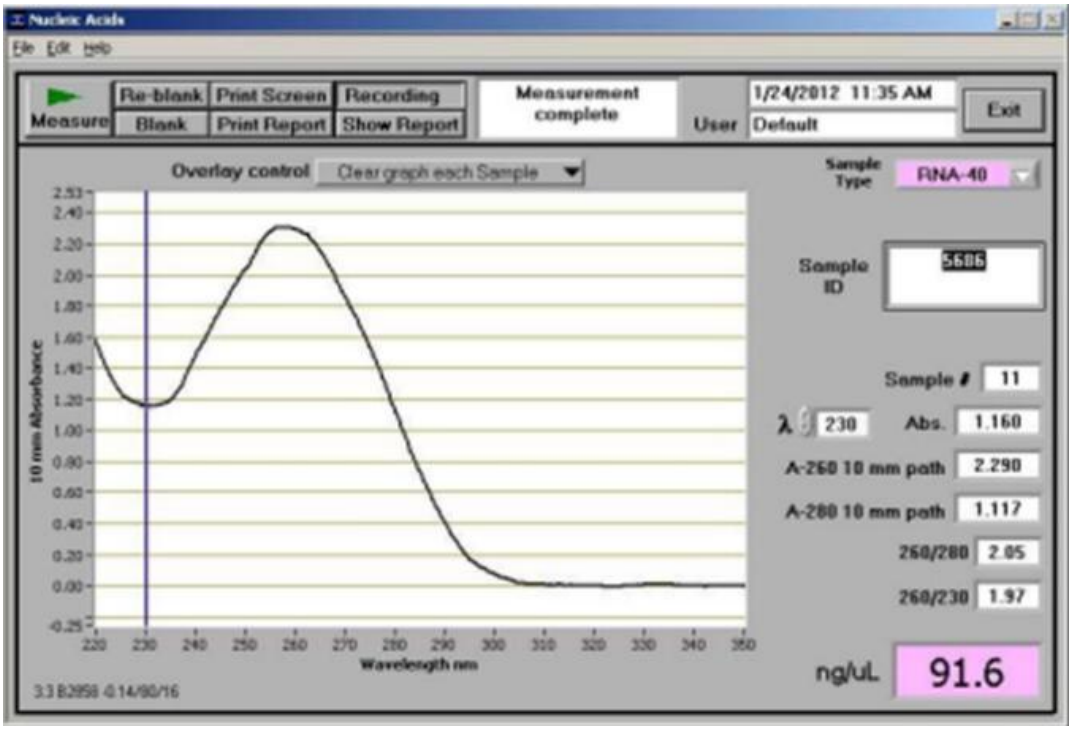


Figure 2.8: Absorbance spectrum of a purified RNA sample using NanoDrop 3300 Fluorospectrometer
There is one absorbance peek which enables the calculation of the concentration of RNA being 91.6ng/μL. The 260/280 ratio is greater than 1.8, indicating a high purity sample (Image taken from: (Edinburgh CRF Genetics Core, 2022).

2.6.3 | Reverse transcription polymerase chain reaction (RT-PCR)

Each RNA sample was reversed transcribed to a more stable complementary DNA (cDNA) sample using LunaScript RT Supermix (New England Biolabs, Ipswich, Massachusetts, USA) and a PCR thermocycler. As per the manufacturer's instructions, up to 1μg of RNA was placed in a PCR tube with 4μL of LunaScript RT Supermix and made up to a total of 20μL using nuclease-free water. The PCR tube is placed in a thermocycler (multigene gradient, Labnet) and run using the following stages; 1) Primer annealing (2 min - 25°C), cDNA synthesis (10 min -

55°C), Heat inactivation (1 min - 95°C). A no-reverse transcription (NRT) control sample was also run alongside RT samples under the same conditions. These samples had up to 1µg of sample RNA, and 4uL of LunaScript no-RT control SuperMix made up to a total of 20µL using nuclease-free water, as per manufacturer's instructions.

2.6.4 | Quantitative polymerase chain reaction (qPCR)

Single-stranded cDNA obtained from RT-PCR was used as a template for the gene-specific primer to amplify. Samples were run in duplicate in a BrightWhite 96 well qPCR plate (primerdesign, Camberley, UK) to account for the interpolate variation. Each well contained 10ng of cDNA, 300nmol/L of a gene-specific target primer (Thermo fisher scientific, USA) and 10µL of SYBR green qPCR master (New England Biolabs, Ipswich, Massachusetts, USA), each used as per manufacturer's instructions and 6.5uL water to make a total volume of 20µL.

qPCR was run using a Bio-Rad CFX96 thermocycler, and the relative gene expression was quantified using a CFX-96 Real-Time PCR Detection System (RRID: SCR_018064, BioRad, Hertfordshire). The qPCR amplification protocol consisted of 4 steps; firstly, the plate was heated to 95°C for 10 minutes (Initiation), then 45 cycles of 15 seconds at 94°C to denature the DNA, followed by 30 seconds at 55°C and 30 seconds at 70°C for the annealing and primer extension steps. The SYBR green dye will non-selectively bind to the major groove of double-stranded DNA (dsDNA) and fluoresces. This fluorescence is recorded at the end of each amplification cycle to determine the quantity of DNA amplified.

The amplification of each target is recorded after each cycle, as shown in figure 2.9, and after the protocol finishes, a melt curve is conducted and measured for each amplicon; this determines the purity of the PCR products. A no template control (NTC) and NRT sample were run for each gene to detect contamination and primer dimers. The number of quantification cycles to reach the fluorescence threshold measures the targeted sequence abundance. The quantification cycle (Cq) for each sequence-specific primer was determined by Bio-rad CFX96 Manager 3.0 software and normalised relative to the housekeeper genes glyceraldehyde-3-phosphate dehydrogenase (Gapdh) and Cytochrome C1 (CYC1)

to produce a value of the relative transcript abundance of a target gene, which is then presented on a bar graph. This method of analysis uses the equation:

$$Relative\ Gene\ Expression = 2^{-\Delta Cq}$$

This equation allows the comparison of different gene expression levels within and between tissues by presuming that all the primers are 100% efficient and that their product fluorescence doubles with each qPCR cycle. All primers used are shown in Table 2.5.

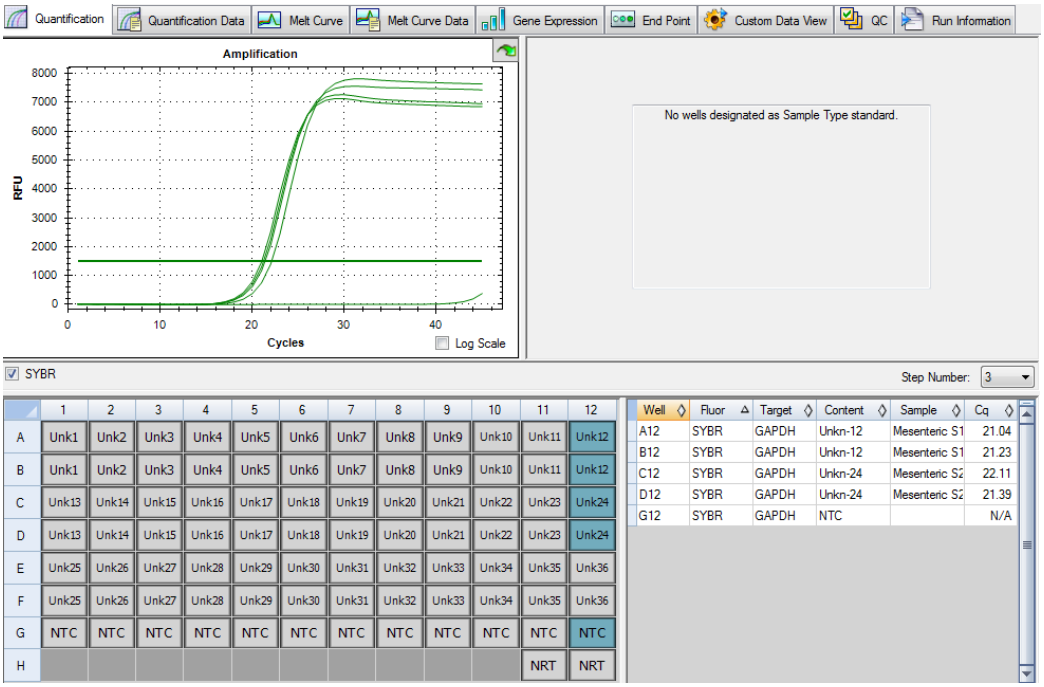


Figure 2.9: Representative Amplification curve:
Amplification curve for gene-specific primer Gapdh with a line showing the threshold where the abundance of each target sequence is measured.

Table 2.5: Table of primers used for RT-qPCR with their respective amplicon and accession numbers

Primer	***Forward sequence (5' to 3')*** ***Reverse sequence (5' to 3')***	***Amplicon (BP)***	***Accession number***
Slc5a1	TAACAGCACAGAAGAGCGCA CAGCCCACAGAACAGGTCAT	148	NM_013033.2
Slc5a2	TCTGGTCATTGCCGCGTATT GTCCTGCCAAGAAGTAGCCA	101	NM_022590.2
Slc5a3	GCATTAAGGGGCTCCAACCT	136	NM_053715.2

	ATGAGAGCTGCTTGCCCATT		
Slc5a11	TCCCTGGTATGGTGAGCAGA CTGTGGGCAAAAGTTCCAGC	141	XM_039101532.1
Slc5a2 v1	GAGAGCTGGCCTGCAACATA AGCGTATCTCTCTGTCCCACT		XM_006721072.5
Slc5a2 v2	AGCGGGGATCTGTGGTTCTA AGCTGGGTACCTGACCTTACA		XM_024450402.2
Kcnq1	TGGGTCTCATCTTCTCCTCC GTAGCCAATGGTGGTGACTG	124	NM_032073
Kcnq2	AAGAGCAGCATCGGCAAAAA GGTGCGTGAGAGGTTAGTAGC A	101	NM_133322
Kcnq3	CAGCAAAGAACTCATCACCG ATGGTGGCCAGTGTGATCAG	161	AF091247
Kcnq4	Primer Design Ltd –Proprietary information of primer sequence not stated - Same primer is used in Baldwin et al 2021 and 2022 publications		
Kcnq5	AACTGATGAGGAGGTCGGTG GATGACCGTGACCTTCCAGT	120	XM_001071249.3
Ramp1	GCTGCTGGCTCATCATCTCT CCTCTTTGAAGCGGCTGAGA	95	NM_031645.1
Calcrl	TAACACTAAGTGCAGGCGGG GCCGGTCCTAAAGCAGAAGT	149	NM_012717.3
Kcne4	AGAGTTCCACACTTGGGACA TGTGCTATTCAGAGGCTCCAT C	91	NM_212526.1
Gapdh	TGTTCTAGAGACAGCCGCAT AAATCCGTTCACACCGACCT	83	NM_017008.4
Cyc1	TGTTTTCCTTGCTCACTGGC TGGCAACATCCTTGGCTACT	183	NM_001277194.1

2.6.5 | Melt Curve analysis.

The melt temperature is when 50% of dsDNA is denatured during heating, which differs for each amplicon. It is presented as the rate of change in fluorescence against temperature, creating a curve. One peak on a melt curve indicates the melting event of one amplicon, but 2 or more peaks suggest several separate amplicons, which can imply genomic DNA contamination or the formation of primer dimers has occurred. Melt curves of amplicons during qPCR can be shown in figure 2.10.

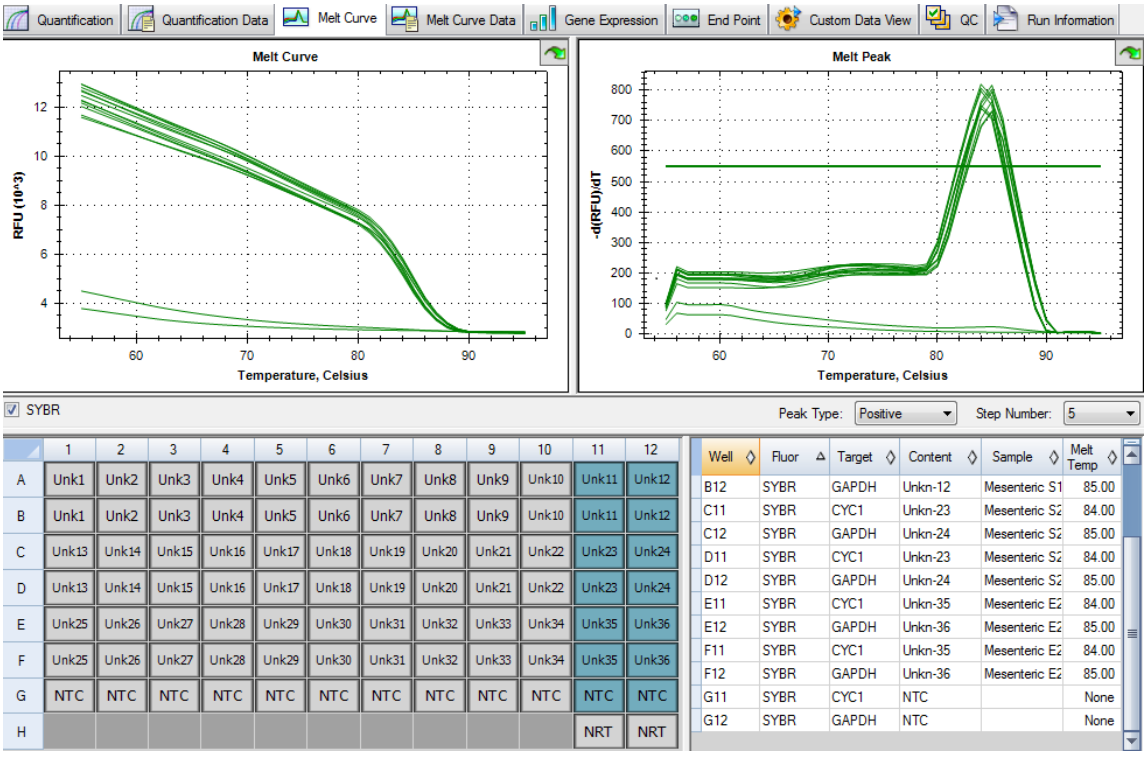


Figure 2.10: Melt curve analysis:
Melt curve and melt peak graphs for several target amplicons (Source: Author).

2.6.6 | QPCR analysis

The transcript abundance of the genes of interest was normalised to the mean transcript abundance of two housekeeper reference genes. Primers were chosen to target the housekeeper genes glyceraldehyde-3-phosphate dehydrogenase (Gapdh) and cytochrome C1 (CYC1). All data values were expressed and plotted as mean 2–ΔCq ±SEM. A summary of qPCR methodology is shown in figure 2.11.

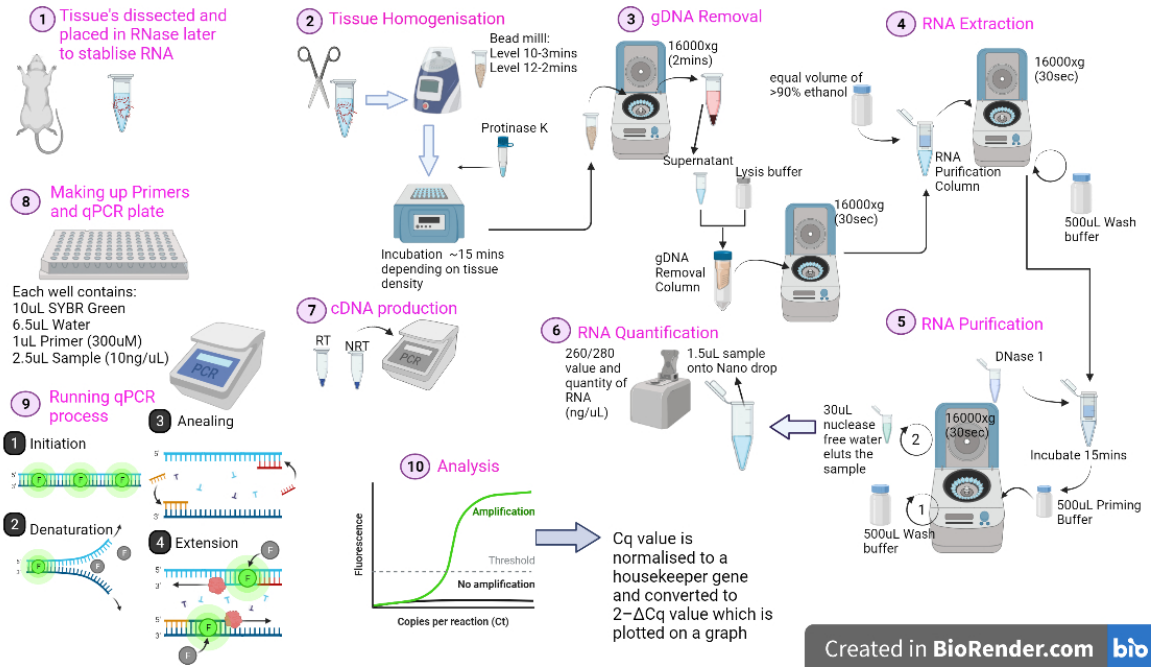


Figure 2.11: Schematic of RT-qPCR methodology (Source: Author using Biorender.com).

2.7 | Cell Isolation

Vascular smooth muscle cells were isolated from whole mesenteric, renal and coronary arteries. Whole arteries were dissected, cleaned of fat and placed in a smooth muscle dissociation solution (SMDS, composition shown in solutions table 1.1) supplemented with 1.75 $mg \cdot ml^{-1}$ Collagenase Type IA, 0.9 $mg \cdot ml^{-1}$ protease, 1 $mg \cdot ml^{-1}$ trypsin inhibitor and 1 $mg \cdot ml^{-1}$ bovine serum albumin (Sigma, UK). Coronary, mesenteric and renal arteries were incubated at 37°C for either 12 minutes, 18 minutes and 30 minutes, respectively. Vessels were washed in SMDS and underwent mechanical trituration using a glass Pasteur pipette to liberate vascular smooth muscle cells.

2.8 | Fluorescence microscopy

2.8.1 | Immunocytochemistry (ICC)

The VSMC suspension was placed onto 13mm coverslips and left at room temperature (RT, 20-22°C) for 45 minutes to adhere. Once the VSMCs had adhered to the coverslips, they were fixed with 4% paraformaldehyde (PFA) solution diluted in filtered phosphate-buffered saline (PBS) for 15 minutes. This PFA solution is then removed, and the coverslips are washed with PBS three times. These cells were either stored at 4°C to undergo ICC at a later date, or the protocol was continued. The PBS was removed from the wells, and a 0.1M Glycine solution diluted in PBS flooded the coverslips and was left on a shaker for 5 minutes at room temperature. The coverslips were then washed three times, followed by a 0.1% Triton X100 + 0.5% Bovine Serum Albumin (BSA) and PBS blocking solution being added to wells and left for 45 minutes at room temperature on a shaker. This blocking buffer permeabilises the cells and prevents non-specific antibody binding. The coverslips are washed 3 times before then being transferred to a humidified chamber and incubated overnight. The chosen primary antibodies were diluted in a blocking solution, and for each coverslip, 35uL was pipetted onto parafilm located inside the chamber. The coverslips were inverted so that the cells were exposed to the antibody. The following morning, the coverslips were transferred back to a 24-well plate and washed thrice with PBS for 5 minutes. The correct secondary antibody conjugated to a fluorophore was diluted in a blocking solution, and the coverslips were transferred back to the humidified chamber for 45 minutes. The coverslips were washed in PBS before being mounted onto a microscope slide with 4',6-diamidino-2-phenylindole (DAPI) (Vectashield, Vector Laboratories, Burlingame, CA) mounting medium, allowing nucleus staining. Coverslips were then sealed with nail varnish and stored at +4°C until imaged using a Nikon A1R plus scanning Confocal Ti2 microscope (Nikon Instruments Europe BV, Amsterdam, Netherlands). Excitation of the fluorophores was achieved with 405, 488, 536 and 635 nm lasers and images were acquired through a 60x oil immersion objective and analysed using Image J software. The primary and secondary antibodies used are shown in Tables 2.6 and 2.7, and a summary of ICC is shown in figure 2.12.

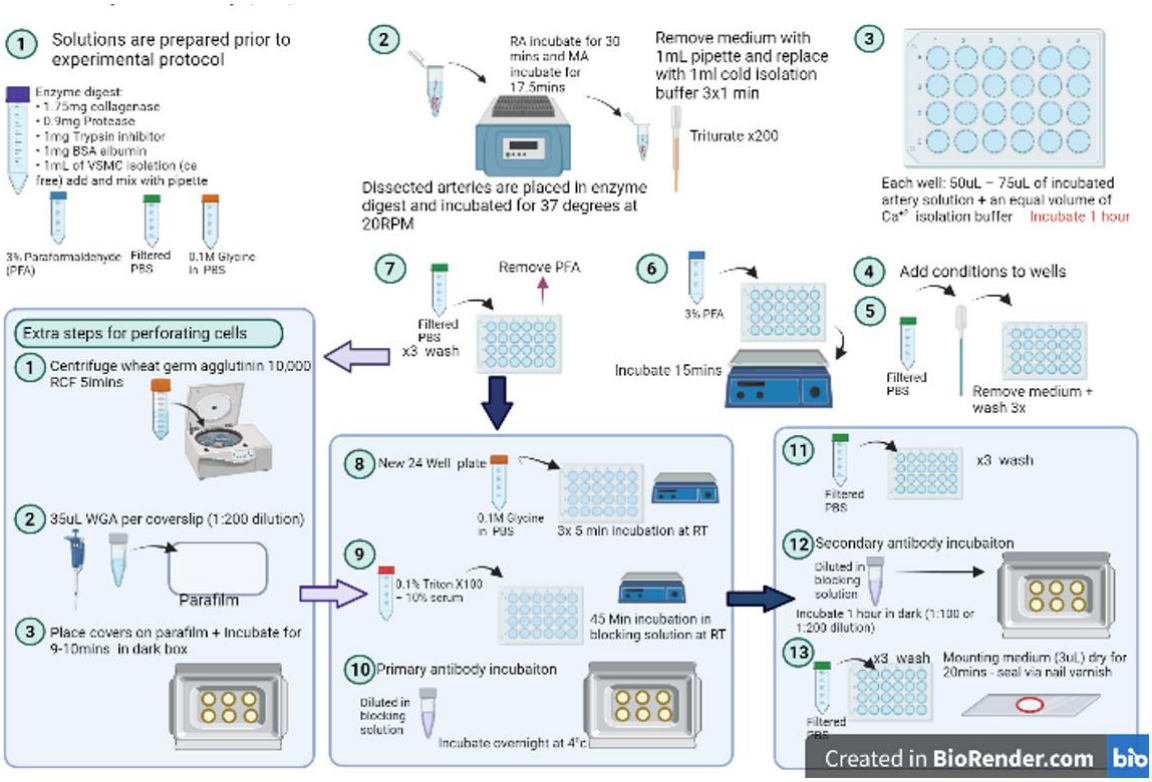


Figure 2.12: Diagram of Immunocytochemistry methodology (Source: Author using Biorender.com).

2.8.2 | Immunohistochemistry (IHC)

After completion of functional myography experiments, mesenteric, coronary and renal arterial segments were fixed *in situ* in myograph chambers with 4% paraformaldehyde (J61899, Thermo Scientific) for 1 hour at room temperature following protocol provided by Professor Kim Dora, University of Oxford (Lin et al., 2023). Fixed arteries were washed three times with PBS, removed from the wire myograph chambers by cutting open laterally, and then separated into 2 fixed segments. These segments were stored in PBS in a 24-well plate until ready to be used.

Arteries were immersed in a blocking buffer comprised of 1% BSA, 0.5% Triton X-100, and 0.05% Tween 20 in PBS for 90 minutes at room temperature. After permeabilising the artery segments, the blocking buffer was removed and replaced with 1mL of chosen primary antibodies, diluted in the blocking buffer, and incubated overnight at 4°C. The primary antibody solution was removed the following day, and artery segments were washed in PBS three times before incubating in specific

secondary antibodies in a blocking buffer for 90 minutes at room temperature. A 4',6-diamidino-2-phenylindole (DAPI) nuclear stain was added to the arteries 15 minutes before the end of the secondary antibody incubation. Arteries were then washed three more times with PBS and ready for mounting. Each arterial segment was placed in a mounting medium (Vectasheild plus Antifade, Vector Laboratories) and laid flat between 2 glass coverslips sealed together using Covergrip sealant (Biotium, 23005).

Arteries were excited at 405, 488, 536, and 635 nm, and fluorescence was acquired through a water immersion objective (1.15, NAI, 1024 x 1024 pixels, x40 lens objective, Olympus) using an Fv1000 laser scanning confocal microscope (Olympus, Southend-on-Sea, UK). Z stacks were taken through every arterial segment starting from the outer arterial wall in 1µm increments using Fluaview version 4.1 and Imaris version 8.0.2 Bitplane software. The primary and secondary antibodies used are shown in Tables 2.6 and 2.7, and a schematic of primary and secondary antibody detection is shown in figure 2.13.

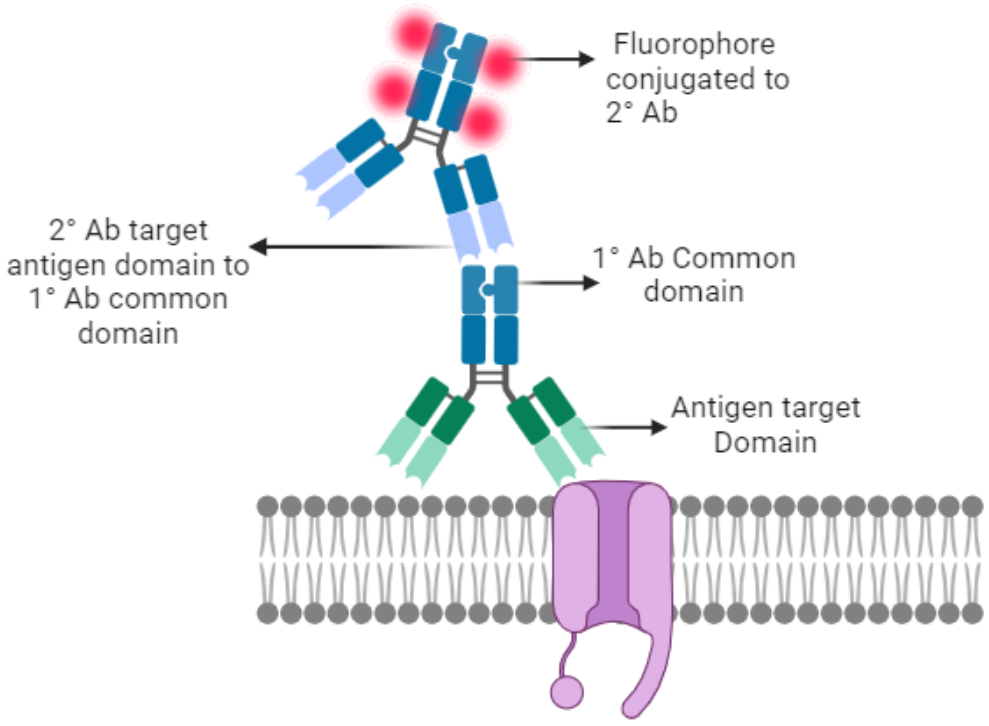


Figure 2.13: Primary and Secondary Antibody detection in ICC and IHC (Source: Author):
Diagrammatic representation of primary antibody (1°) binding to the target protein and secondary antibody (2° Ab) with a conjugated fluorophore binding to the common domain of the primary antibody.

Table 2.6 - List of primary antibodies used (Source: Author):

Antibody	***#CATALOG***	***Raised in***	***Antigenic Sequence***	***Concentration used***	***Supplier***
Anti-alpha smooth muscle actin antibody	ab5694	Rabbit polyclonal	N-terminal	1:200	Abcam
Anti-SGLT2 antibody (D-6)	sc-393350	Mouse monoclonal	Extracellular domain of SGLT-2 against amino acids 226-268	1:200	Santa Cruz
Anti-SMIT antibody (3A6): (SC-293330)	sc-293330	Mouse monoclonal	Raised against amino acids 533-641 of SMIT of human origin	1:200	Santa Cruz
Anti-Kv7.4 antibody	APC-164	Rabbit polyclonal	Intracellular, C-terminus of KCNQ4 against amino acid residues 594-607	1:200	Alomone Labs
Anti-TRPV1 antibody	Ab10295	Guinea pig polyclonal	C-terminus of rat TRPV1	1:1000	Abcam
Anti-CGRP antibody	Ab36001	Goat polyclonal	CGRP whole molecule (1-37) and 23-37 fragment on C terminus	1:1000	Abcam
Anti-NHE1 antibody	PA5115917	Rabbit polyclonal	SLC9A1 corresponding to amino acid residues Q525-N554.	1:1000	Invitrogen
Anti-smooth muscle myosin heavy chain 11 antibody	ab125884	Rabbit polyclonal	Synthetic peptide corresponding to Human smooth muscle Myosin heavy chain 11 aa 1-100 conjugated to keyhole limpet haemocyanin	1:500	Abcam

mouse/rat cd31/pecam-1 alexa fluor® 488-conjugated antibody	AF3628-SP	Goat polyclonal	1:150	R&D Systems

Table 2.7 - List of secondary antibodies for Immunocytochemistry (Source: Author):

Antibody	#CATALOG	Wavelength	Dilution	Supplier
Donkey Anti-Rabbit	A10042	Alexa Fluor ® 568	1:200	Invitrogen
Donkey Anti-Rabbit	A21206	Alexa Fluor ® 488	1:200	Invitrogen
Donkey Anti-Mouse	A21203	Alexa Fluor ® 594	1:200	Invitrogen
Donkey Anti-Mouse	A21202	Alexa Fluor ® 488	1:200	Invitrogen
Donkey Anti-Goat	A21082	Alexa Fluor ® 633	1:1000	Life Technologies
Goat Anti-Guinea pig	A11073	Alexa Fluor ® 488	1:1000	Life Technologies

2.8.3 | Proximity ligation assay

The interaction of SMIT with various ion channel proteins was determined by proximity ligation assay (PLA). This technique detects and quantifies protein-protein interactions ≤30nm within cells *in situ* (S. Fredriksson et al., 2002).

Whole mesenteric and coronary arteries were incubated in either PSS, 150 mM raffinose or 20 mM glucose (diluted in PSS) for 4 hours or overnight, then isolated and fixed as stated above. The cells were permeabilised by washing with 0.1% triton X-100 for 5 minutes at room temperature and then washed three times. The cells were blocked by adding 2 drops of Duolink PLA blocking buffer (DUO82007, Sigma Aldrich, St Louis, MO, USA) to each coverslip and incubating for 30 minutes at 37°C.

An anti-mouse antibody targeting SMIT and an anti-rabbit antibody targeting an ion channel protein (shown in table 1.5) were diluted in antibody dilutant (DUO82008, Sigma Aldrich, St Louis, MO, USA), and for each coverslip, 30µL was pipetted onto

parafilm located inside a humidified chamber. The coverslips were transferred to the chamber and incubated overnight with the chosen primary antibodies. The following morning, the coverslips were transferred back to a 24-well plate and washed three times with wash buffer A (comprising of 1L distilled water, 8.8g NaCl, 1.2g Tris base, 500uL Tween set to pH 7.4) for 5 minutes. The cells were placed in a humidified chamber and incubated for 1 hour at 37°C. During this incubation period, the cells were exposed to a mixture of Duolink In situ oligonucleotide-labelled probes. These probes included mouse minus (DOU92004, Sigma Aldrich, St Louis, MO, USA) and rabbit plus (DUO92002, Sigma Aldrich, St Louis, MO, USA), diluted in an antibody dilutant at a ratio of 1:5, following the manufacturer's guidelines. After incubation, the coverslips containing the cells were carefully moved back to a 24-well plate and washed three times using wash buffer A, lasting 5 minutes.

Following the washing step, the cells underwent a ligation process, which involved incubating them for 30 minutes at 37°C in a solution comprising a ligation buffer (DUO82009, Sigma Aldrich, St Louis, MO, USA) and ligase (1 unit/µL, DUO82027, Sigma Aldrich, St Louis, MO, USA). These components were diluted in distilled water at dilutions of 5x and 40x, respectively. The anti-sense single-stranded DNA sequence on the plus and minus probes bind to one another if the two proteins are within proximity of ≤30nm. Free oligonucleotides and ligase hybridise with the probes during ligation, forming a closed-circle conformation. The coverslips were incubated for 100 minutes at 37°C in an amplification buffer (DUO82011, 5 x, Sigma Aldrich, St Louis, MO, USA) containing red fluorophore oligonucleotide probes (568nm) and polymerase (10 units/µL, 80 x, DUO82030) both diluted in water. The polymerase initiates rolling circle amplification of the newly formed dsDNA, and the red fluorophore binds to the amplified product expressing the interaction as red puncta within the cell. The cells were then mounted on cover slides with a DAPI-containing mounting medium (Vectashield, Vector Laboratories, Burlingame, CA) and then imaged via a Nikon A1R confocal microscope (inverted) on Ti2 chassis (image resource facility, St George's University of London).

2.9 | Western Blot

2.9.1 | Tissue lysis

Whole tissues were dissected, cleaned of fat and then submerged in Triton lysis buffer comprising of 1% Triton x100 (Fisher Scientific, 22040058) supplemented with protease and phosphatase inhibitors (cOmplete mini, 4693159001 and PhosSTOP 4906845001 from Roche). The tissues were homogenised mechanically, followed by a bullet blender with 0.9-2mm beads for 5 minutes and then centrifuged at 1000 RPM for 10 mins at 3°C. The supernatant was transferred to a new sterile aliquot and then stored in a -20 freezer.

2.9.2 | Lysis of HEK293 cells

Transfected HEK293 cells grown on a 6-well plate had their media removed and were washed in sterile PBS. 300µL of NP40 triton lysis buffer (2%NP40; 300mM NaCl;20mM Tris;10mM EDTA pH7.4, Triton x100) supplemented with 1x protease and phosphatase inhibitor (Roche tablets; #4693159001; #4906845001) was added to each well and left at 4°C for 5 minutes to let the cells detach. The cells were further homogenised in lysis buffer using a pipette and transferred to an Eppendorf to be centrifuged at 10,000 RPM for 5 minutes. The supernatant was transferred to a new sterile aliquot and then stored in a -20 freezer.

2.9.3 | Total Protein quantification

Protein concentrations were determined via the Pierce™ Bicinchoninic acid (BCA) Protein Assay Kit (Thermo Fisher Scientific, Loughborough, UK). 25µL of the triton standard was added to each well in a 96-well plate. BSA diluting agent (2mg/mL) was used to produce a series of sequential dilutions of the triton standard across 12 wells. This formed the standard curve to calculate our samples' protein concentration. When plating the unknown tissue samples, 6.25 µL of sample was pipetted into each well with 18.75 µL triton x100 for a 1:4 dilution. The BCA working solution is generated by diluting Reagent B (Comprised of copper sulphate) into Reagent A (Comprised of bicinchoninic acid, sodium carbonate, sodium tartrate, sodium hydroxide and sodium bicarbonate) of a 1:50 dilution. 200 µL of the BCA working solution was pipetted into each well and mixed before being covered with

foil and incubated on a hot plate at 37°C for 30 minutes, as per manufacturer's instruction.

The absorbance of each sample was calculated using a BioTek EL808 plate reader (North Star Scientific) at a wavelength of 562nm (purple wavelength) due to the absorbance being directly proportional to the protein concentration of the sample. A standard curve was produced by plotting the average-blank corrected 562nm absorbance measurement of each triton standard against its known concentration (µg/mL). See the schematic in figure 2.14 for the protocol layout.

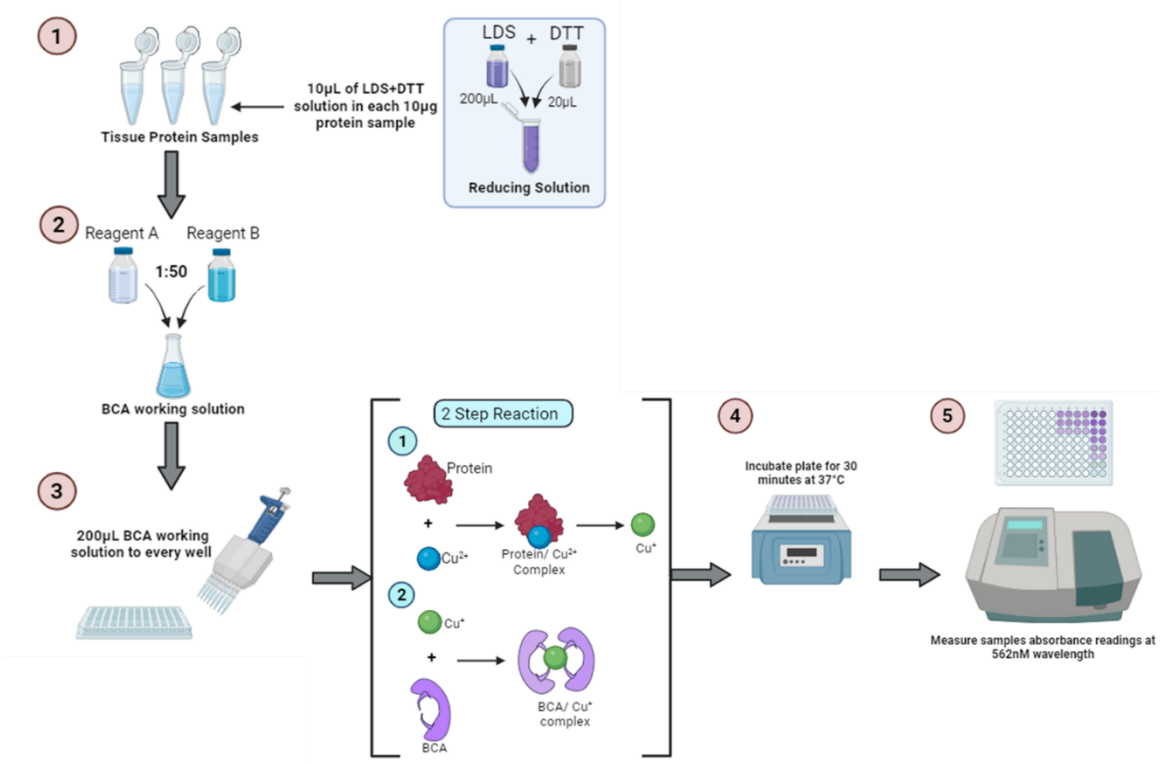


Figure 2.14: Schematic of BCA assay protocol (Source: Author using Biorender.com).

2.9.4 | Gel electrophoresis and membrane transfer.

For gel electrophoresis, the samples were run under reducing conditions with 4-12% Bolt™ Bis-Tris Plus pre-cast gels (NW04120BOX, Invitrogen). A stock of reducing agents was prepared with 200µL NuPAGE™ LDS Sample Buffer (X4, NP0007, Thermo Fisher Scientific) diluted in 20µL dithiothreitol (DTT, Thermo Fisher Scientific). These reducing agents helped to completely denature the protein samples by cleaving the disulphide bonds between cysteine residues. 10µL of this

reducing stock is added to 10µg of protein lysate and then made up to a total volume of 40µL using triton x100 standard solution. The individual sample mixtures are placed onto a hotplate at 70°C for 10 minutes to denature the proteins.

While the samples were heating, the Bis-Tris Plus pre-cast gels were loaded into the mini gel tank (A25977, Invitrogen) filled with Bolt™ MES SDS run buffer (B0002, Thermo Fisher Scientific). The samples were individually pipetted into the gel's wells, and a constant 200v current was applied across the gel for 30 minutes.

The gel was taken and placed in a mini-blot module sandwich (B1000, Thermo Fisher Scientific). The order of assembly of the electro-transfer sandwich encompassed the anode core, sponge pad, filter paper, gel, membrane, filter paper sponge pad and cathode core, which were all soaked in transfer buffer (composition shown in solutions table 1.1). The enclosed mini blot module was vertically placed in the gel tank between the electrodes and ran at 15 volts for 1 hour to allow the proteins to be transferred to the nitrocellulose membrane (Amersham Protran Premium 0.2uM nitrocellulose, GE10600001) via wet electroblotting.

2.9.5 | Probing and detection

The nitrocellulose membrane was washed three times for seven minutes with PBST (PBS in 0.1% tween 20) and then immersed in a 3% BSA-PBS blocking solution for one hour. Membranes were then incubated overnight at 4°C with either the primary SGLT2 mouse monoclonal antibody or the primary SMIT mouse monoclonal antibody, both diluted in blocking solution (details of primary antibodies shown in Table 1.4).

The next day the membranes were washed in PBST 3 times for 7 minutes and then incubated with highly adsorbed horseradish peroxidase-conjugated goat anti-mouse IgG (A16078, Fisher Scientific) secondary antibody diluted in non-fat dried milk powder for 1 hour at RT and developed by adding Immobilon™ Western Chemiluminescent HRP Substrate (WBKLS0500, Millipore). Detection and quantification of chemiluminescence intensities were quantified by using ChemidocTM imaging system and Image Lab 5.2.1 software (BioRad).

2.9.6 | Stripping and re-probing

Blots were stripped by immersing the membrane in 20mL of Restore western blot stripping buffer (21059, Fisher Scientific) according to the manufacturer's instructions. The membrane was then re-probed with primary rabbit-anti-actin antibody (#4970, Cell Signalling Technology) diluted in a blocking buffer for 1 hour at RT. The membrane was washed in PBST 3 times for 7 minutes and then incubated with highly adsorbed horseradish peroxidase-conjugated donkey-anti rabbit IgG secondary antibody (AP182P, Merks). The Membrane was then washed another 3 times and developed by adding Immobilon™ Western Chemiluminescent HRP Substrate (WBKLS0500, Millipore). Detection and quantification of chemiluminescence intensities were again quantified using ChemidocTM imaging system and Image Lab 5.2.1 software (BioRad).

2.10 | Cell Culture

Human Embryonic kidney 239 (HEK293) cells were grown in Minimum Essential Medium Eagle (Sigma-Aldrich, M2279) supplemented with 1% penicillin/ streptomycin and stored in an incubator with 5% CO_2 at 37°C. These cells were transiently transfected with a total of 4µg of either pcDNA3.1(+)-Slc5a2 plasmid (addgene, #132241) or pcDNA3.1-slc5a3 plasmid. Plasmids were diluted in Lipofectamine RNAiMAX Transfection Reagent (Thermo Fisher Scientific, 13778075) suspended in Opti-MEM reduced serum medium (Thermo Fisher Scientific, 31985062) and left to incubate for 20 minutes at RT. HEK293 cells were either growing on a 6-well plate and left to reach >70% confluency, or cells were mounted onto glass coverslips and left to attach for 1h at RT. The cells were washed with sterile 1x PBS and submerged in either 2mL Opti-MEM (6 well plates) or 500mL Opti-MEM (coverslips). The plasmid/ lipofectamine mixture was added in a dropwise motion, and the cells were left for 3 days to allow optimal transfection.

2.10.1 | Plasmid extraction and purification

Transformation of pcDNA3.1-slc5a3 into competent TOP10 bacteria is required to produce large cultures containing slc5a3 gene and extract to make more plasmid. It consists of combining 1ug DNA with competent top 10 bacteria and incubating for 20 minutes on ice. The competent cell mixture is heat shocked to 42°C for 1 minute using a hotplate and then transferred back on ice for 1 minute. 1mL of LB broth (Sigma) was added to the transformed cells and incubated at 37°C for 30

minutes. The mixture was then plated onto an ampicillin-resistant agar plate and incubated overnight at 37°C to form colonies. A single colony was selected and inoculated with 5mL LB broth supplemented with 100ug/ml ampicillin and left overnight at 37°C. This bacterial mixture was then added to 200mL ampicillin containing LB broth and agitated overnight at 37°C.

Plasmid DNA was extracted and purified using the EndoFree plasmid maxi kit (QIAGEN, 12362). Bacterial cells were harvested by centrifugation at 6000 xg for 15 minutes at 4°C. The bacterial pellet formed was resuspended in 10mL buffer P1 supplemented with RNase A and then 10mL of buffer P2 was mixed in the solution and incubated at RT for 5 minutes to allow the lysis reaction to take place. 10mL of buffer P3 was added to the lysate before then being added to the QIfilter cartridge and left for 10 minutes at RT to prime the cartridge and allow the genomic DNA and proteins to form a layer on the top of the mixture. The lysate was filtered into a 50mL tube and 2.5mL of buffer ER was added to the filtrate and placed on ice for 30 minutes. 10mL of buffer QT was added to the Qiagen-tip 500 to equilibrate it and then filtered lysate was added and allowed to follow through. The Qiagen-tip 500 was then washed 2 times with Buffer QC and then DNA was eluted into a 50mL sterile tube by adding 15mLs of buffer QN to the tip. 10.5mL of 2-propanol (RT) was added to the eluted DNA and the DNA was pelleted by centrifuging at 16,000 x g for 30 minutes at 4°C. The supernatant was removed, and the DNA pellet was washed with 5mL 70% ethanol and centrifuged again at 16,000 x g for 10 minutes. The DNA pellet was airdried for 10 minutes before adding 1mL of endotoxin free buffer TE and stored at -20°C ready to use to transfect into HEK293 cells.

2.11 | Data Analysis

All values from functional experiments were expressed as mean ± standard error of the mean (SEM) with no less than 5 individual data points, each representing a biological repeat. Measurements of total cell fluorescence during immunocytochemistry involved five biological repeats with a minimum of five cells recorded per sample. For quantification of SGLT2 and SMIT protein via western blot, a minimum of 3 biological repeats were obtained.

For functional experiments, cumulative concentration effect curves were produced, whereby the contraction produced by 10μM methoxamine at stable tone was taken

as the maximal contraction of 100%. The tone of the artery was recorded after each subsequent addition of a given pharmacological agent and the values were formulated as a percentage of the maximum contraction. Using GraphPad Prism (RRID:SCR_002798, Version 10.0.0) a transformed data set of mean values was generated using X = Log(X), to reduce representative skew. A four parametric linear regression analysis was then performed to produce a concentration effect curve on a log(x) graph with the standard error of mean (SEM).

When comparing multiple groups, a two-way ANOVA was performed followed by a post-hoc Bonferonni for concentration effect curves or Sidak test for one shot experiments. For data comparing 2-3 individual groups, a normality test under column analysis was performed to determine whether the data followed a Gaussian distribution. This involved performing a total of 4 normal distribution tests (D'Agostino and Pearson test, Anderson-Darling test, Shapiro-Wilk test and Kolmogorov-Smirnov test) that calculate a P value. If the P value was greater than 0.05 it confirmed the data followed a Gaussian distribution and an ordinary One-Way ANOVA was performed for 3 individual groups with a 2-sample t-test performed for 2 individual groups. If the P value was less than or equal to 0.05 the data did not follow a Gaussian distribution and a kruskal-Wallis test was performed for data with 3 individual groups with a Mann Whitney test performed for data with 2 individual groups.

Significance values were represented as * = $P<0.05$, ** = $P<0.01$, *** = $P<0.001$ and **** = $P<0.0001$. All data sets subject to statistical analysis contained at least 5 animals per group, where N = number of independent values.

Chapter 3: Characterising the expression of SLC5 proteins in the vasculature

3.1 | Introduction

The sodium-glucose-dependent transporters SGLT1 and SGLT2 (Slc5a1-2) and the sodium myo-inositol transporters SMIT1 and SMIT2 (Slc5a3 and Slc5a11) are close relatives in the solute carrier transporter family (SLC5). These proteins co-transport small solutes such as glucose, myo-inositol and galactose with two Na+ ions per each transported sugar molecule (Gyimesi et al., 2020). The expression of SGLT and SMIT has been excessively studied throughout the literature.

SGLT2 is mainly expressed in the kidney cortex of humans, with rats and mice also expressing SGLT2 in the apical membrane of the kidney proximal convoluted tubule (Kanai et al., 1994). This aligns with SGLT2 being a low-affinity, high-capacity transporter of glucose mediating its absorption from the kidney's glomerular filtrate. However, other studies have found low levels of SGLT2 expression in the small intestine and brain (Chen et al., 2010; Chiba et al., 2020). Zhou et al., 2003 showed ubiquitous expression of SGLT2 in most human tissues by q-PCR, but these findings have since been disproven. SGLT2 reabsorbs 95% of filtered glucose, whereas SGLT1 only reabsorbs around 3%, and, unlike SGLT2, is widely expressed in many tissues. SGLT1 is predominantly expressed in the small intestine, heart and kidney tissue (Vrhovac et al., 2015; L. Zhou et al., 2003). However, other papers have found SGLT1 expression in skeletal muscle, lung, liver and brain of rats (Lee et al., 1994), rabbits, pigs (Poppe et al., 1997) and humans (Bonner et al., 2015; Chen et al., 2010; Vrhovac et al., 2015). The role of SGLT1 in these tissues is still unknown but can be linked to its role in glucose

absorption. SMIT1 transports myo-inositol as well as d-glucose with lower affinity, regulates the osmotic balance of cells, and is expressed in many tissues throughout the body, with the highest expression in the kidney medulla, thyroid gland and choroid plexus (Chen et al., 2010; Nordio & Pajalich, 2013). Like SMIT1, SMIT2 is expressed in various tissues such as the brain, small intestine and kidneys. However, it does not have the affinity to transport d-glucose (Lin et al., 2009).

Over the years, SGLT1 and SGLT2 expression and mutations have become essential in disease development. For example, SGLT1 and SGLT2 polymorphisms lead to overexpression in several pancreatic, prostate (Du et al., 2022), lung (Iwai et al., 2024), and liver (Scafoglio et al., 2015) adenocarcinoma tumour cells. SGLT2 inhibitors attenuate the cancer growth of SGLT2-expressing tumour cells, indicating the importance of its protein expression (Dutka et al., 2022; Jojima et al., 2019; Kaji et al., 2018). SGLT2 inhibitors have also been recently approved for the treatment of heart failure independent of raised glucose levels, with several clinical studies showing these patients experience a decrease in cardiac fluid retention and blood pressure (Beal et al., 2023; Lusk et al., 2022). On the other hand, changes in SMIT1 expression and myo-inositol levels have been associated with heart failure (Alice Marino et al., 2023; Pouleur et al., 2024) and several neurodegenerative disorders such as Alzheimer's (Forlenza et al., 2014; Huang et al., 1999), Parkinson's and epilepsy (Lepore et al., 2021; Pesch et al., 2019).

The expression of these transporters can also be altered by sex hormones, as shown by Sabolić et al., 2012 where SGLT1 and SGLT2 expression was significantly greater in renal proximal tubules of females compared to male rats. This expression of both SGLT1 and SGL2 was enhanced by incubating in oestradiol and was attenuated when incubated in testosterone (Sabolić et al., 2012). These findings were corroborated in mice tissues where SGLT2 and the GLUT transporters had higher expression in female than male mice (Nagai et al., 2014). Recent studies have identified oestrus cycle-dependent variations in vascular smooth muscle cell (VSMC) function, independent of the previously documented sex-dependent differences in arterial function. The rat oestrus cycle has four stages: Pro-oestrus, Oestrus, Met-oestrus, and Di-oestrus, lasting five days. Pro-oestrus and oestrus female rats have high levels of oestrogen (PE rats),

whereas met-oestrus and Di-oestrus females have low oestrogen levels (DM rats). Baldwin et al. 2022 and 2023 have shown that arteries from PE rats are pro-contractile with reduced Kv7.4 channel membrane expression. Meanwhile, DM rats are pro-relaxant and have high Kv7.4 membrane expression. Hence, the oestrus cycle differences should be considered when exploring the expression of proteins in different arteries in male and female rats.

In contrast to expression in other tissues, the expression of SGLT2 and SMIT1 has only been partially examined in the vasculature (mesenteric and renal arteries Barrese et al., 2020; Hasan et al., 2022), and their expression throughout the rest of the vasculature, as well as between sexes, is unknown. We hypothesise that SMIT1 and SGLT2 are expressed in mesenteric, renal, coronary, and cerebral arteries in male, PE female and DM female rats, with PE females having a lower expression of SMIT1 and SGLT2 compared to male and PE female counterparts. Therefore, this chapter sought to understand the expression and distribution of SLC5 solute transporters within the vasculature of male and female rats. The study aims were to:

1. To identify the relative transcript abundance of Slc5a1, Slc5a2, Slc5a3 and SLC5a11 in different arteries from male and female rats.
2. To investigate the protein expression of SMIT1 and SGLT2 in different arteries from male and female rats
3. To determine any sex differences in the expression of SMIT and SGLT2

3.2 | Methods

All aspects of the experiments carried out in this chapter are described in detail in Chapter 2.

3.3 | Results

3.3.1 | Relative expression of Slc5a genes in the vasculature

The expression and distribution of solute carrier transporters (SLC5) in the vasculature are ill-defined; hence the relative transcript abundance of Slc5a1, Slc5a2, Slc5a3 and Slc5a11 was investigated in mesenteric, renal, coronary and cerebral arteries from male and female rats. Initial RT-qPCR experiments were carried out in whole brain, heart and nephron cell lysates to be a positive primer control, where the expression profile of these genes is well established (Chen et al., 2010; Sabolić et al., 2012; Vrhovac et al., 2015). The kidney nephron expressed all four Slc5 genes, with Slc5a3 having the highest transcript abundance. The Slc5a1 and Slc5a3 transcripts were expressed in all three heart, kidney, and brain samples, with Slc5a2 only expressed in the kidney and Slc5a11 expressed in brain and kidney tissue (figure 3.1).

The expression of Slc5 genes in mesenteric, renal, coronary and cerebral arteries was then investigated. Slc5a3 had the greatest expression in all four arterial beds from male rats, with little to no expression of Slc5a1, Slc5a2 or Slc5a11 (figure 3.2A). The relative transcript abundance of Slc5a3 in mesenteric and renal arteries was significantly greater compared to coronary and cerebral arteries. SGLT2 encoded by Slc5a2 is 672 amino acids long, containing 14 exons, four disulphide bonds and has two main isoforms (Slc5a2 variant X1 and X2) (Barata et al., 2023; Calado et al., 2004; Katzmann et al., 2021; Xu et al., 2023; Zimdahl et al., 2017). The isoforms Slc5a2 variant X1 and X2 are 674 and 458 amino acids long, respectively, with 13 and 10 exons. QPCR for these variants using isoform-specific primers revealed considerably greater expression of Slc5a2 X1 and Slc5a2 X2 than the full-length form of Slc5a2 in mesenteric and renal arteries of male rats (figure 3.2B), with slightly higher levels of these isoforms in mesenteric arteries compared to renal. These findings show that Slc5a3 as well as splice variants of Slc5a2 was well expressed in rat arteries.

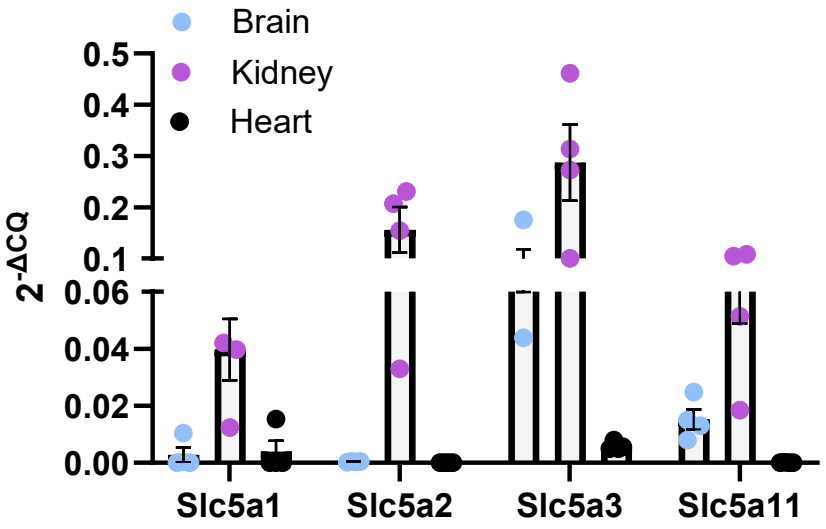


Figure 3.1: Expression of Slc5 genes in heart myocardium, brain and kidney tissue from male rats.

The relative transcript abundance of Slc5a1 (SGLT1), Slc5a2 (SGLT2), Slc5a3 (SMIT1) and Slc5a11 (SMIT2) in the brain (blue), kidney (purple) and heart (black) tissue from male rats. All values are expressed as mean ± SEM denoted by error bars, with N=4 and a two-way ANOVA with post-hoc Bonferroni test was used to calculate significance (N= number of animals used).

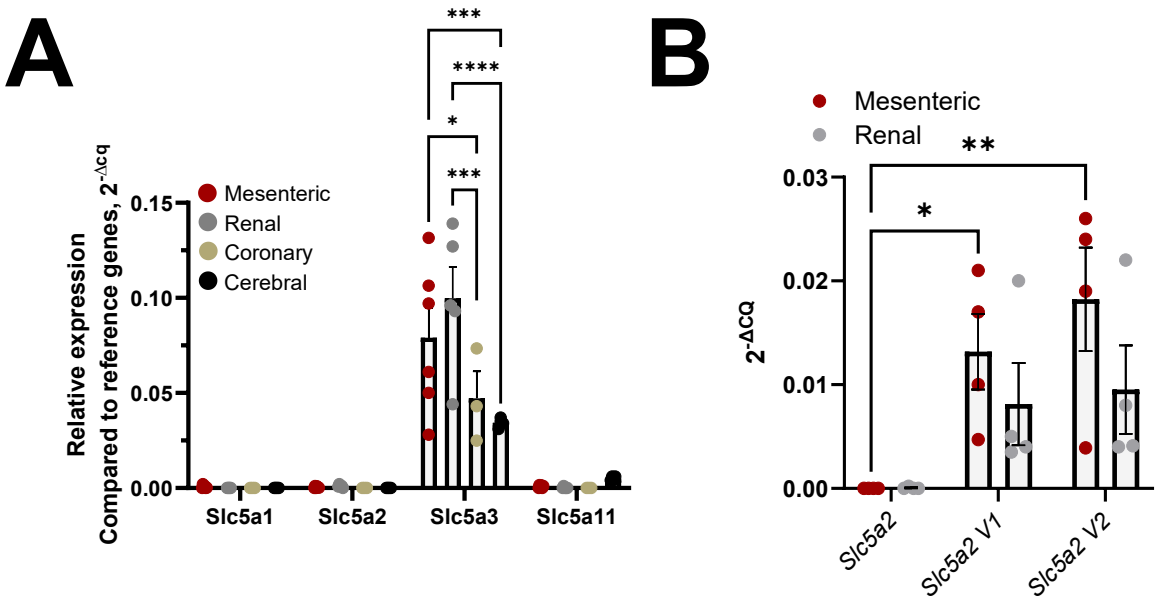


Figure 3.2: The relative transcript abundance of Slc5a genes in mesenteric, renal, coronary and cerebral arteries from male rats.

The relative transcript abundance of Slc5a1 (SGLT1), Slc5a2 (SGLT2), Slc5a3 (SMIT1) and Slc5a11 (SMIT2) in mesenteric (red), renal (grey), coronary (beige) and cerebral (black) arteries from male rats (A, N=5-6). The relative transcript abundance of Slc5a2 variants in mesenteric (red) and renal (grey) arteries (B, N=4). All values are expressed as mean ± SEM denoted by error bars, and a two-way ANOVA with post-hoc Bonferroni test was used to calculate significance (N= number of animals used).

The expression of Slc5a1, Slc5a2, Slc5a3 and Slc5a11 in mesenteric and renal arteries from PE and DM female rats mirrored that in male rats. In both PE and DM females, Slc5a3 had the greatest transcript abundance with minimal expression of Slc5a1, Slc5a2 and Slc5a11 (figure 3.3A-B). Similar levels of Slc5a3 were seen in both mesenteric and renal arteries from DM and PE female rats. The two isoforms of Slc5a2 had significantly greater transcript abundance in mesenteric and renal arteries (figure 3.3C-D). In contrast, in PE female arteries, the expression was greater in mesenteric arteries, like in males (figure 3.3D). Overall, SMIT1 encoded by Slc5a3 and splice variants of Slc5a2 were the most expressed in both male and female arteries.

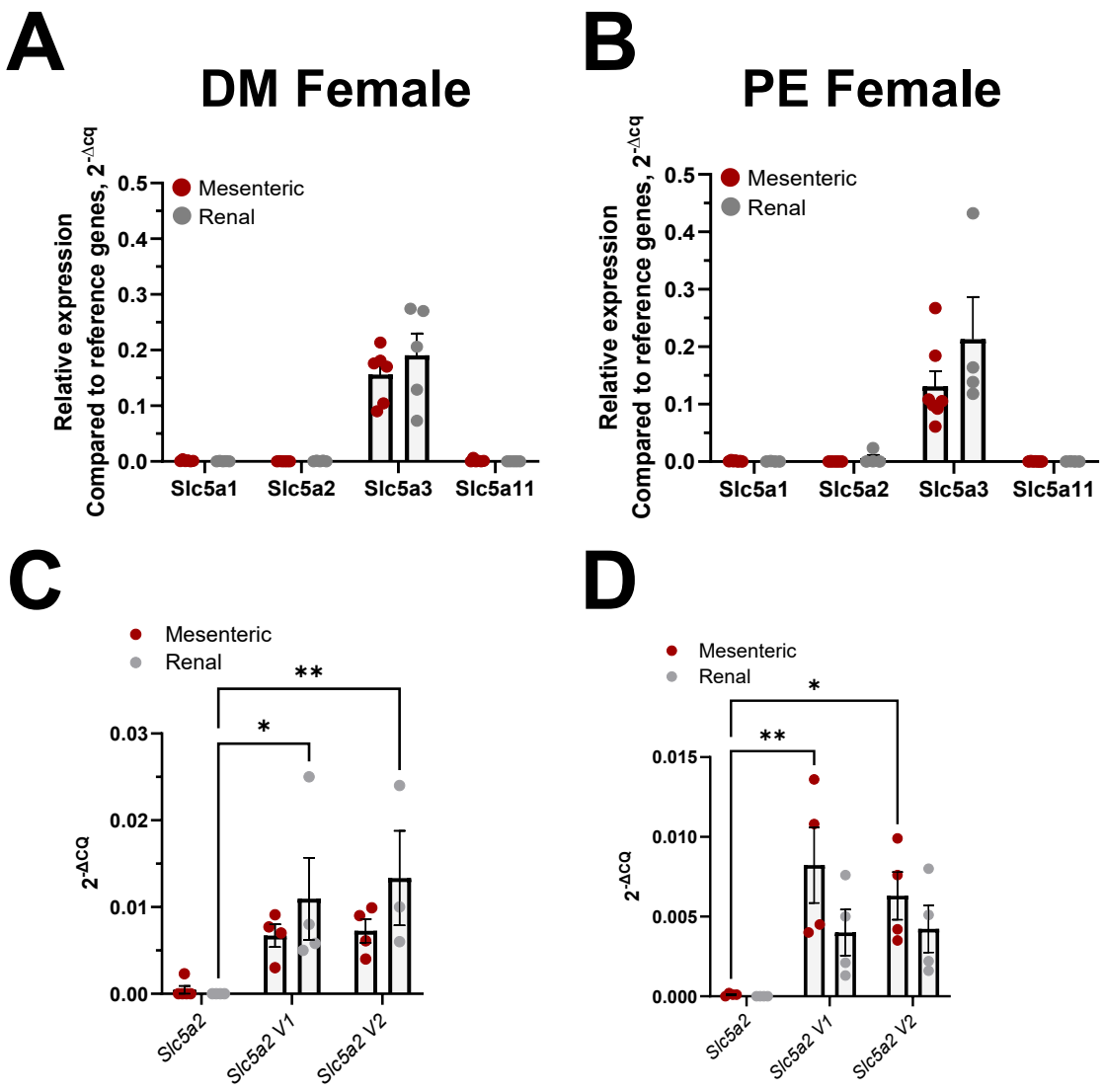


Figure 3.3: The relative transcript abundance of Slc5a genes in mesenteric, renal and coronary arteries from DM and PE female rats.

The relative transcript abundance of Slc5a1 (SGLT1), Slc5a2 (SGLT2), Slc5a3 (SMIT1) and Slc5a11 (SMIT2) in mesenteric (red) and renal (grey) arteries from DM female (A, N=5) and PE female (B, N=5) rats. The relative transcript abundance of Slc5a2 variants in mesenteric (red) and renal (grey) arteries from DM female (C, N=4) and PE female (D, N=4) rats. All values are expressed as mean ± SEM denoted by error bars, and a two-way ANOVA with post-hoc Bonferroni test was used to calculate significance (N= number of animals used).

3.3.2 | Comparing the relative transcript abundance of Slc5a genes in male and female arteries

The expression of solute carrier transporters was compared in mesenteric and renal arteries in male, DM female, and PE female rats. The expression of Slc5a1 and Slc5a11 was similar in all arterial beds. The expression of Slc5a3 was the greatest in both mesenteric and renal arteries in both males and females, with DM females having the highest transcript abundance of Slc5a3 in both arterial beds compared to males and PE females (figure 3.4A-B). Interestingly, the overall transcript abundance of Slc5a2 isoforms was greater in renal arteries compared to mesenteric arteries. DM females also exhibited a higher mRNA expression of all three isoforms compared to PE females and males. However, this did not reach significance (figure 3.4C-D). These findings suggest that the solute transporter SMIT1 has the highest expression abundance in mesenteric, renal and coronary arteries from male and female rats, followed by the Slc5a2 splice variants with minimal expression of their close relatives Slc5a1 and Slc5a11.

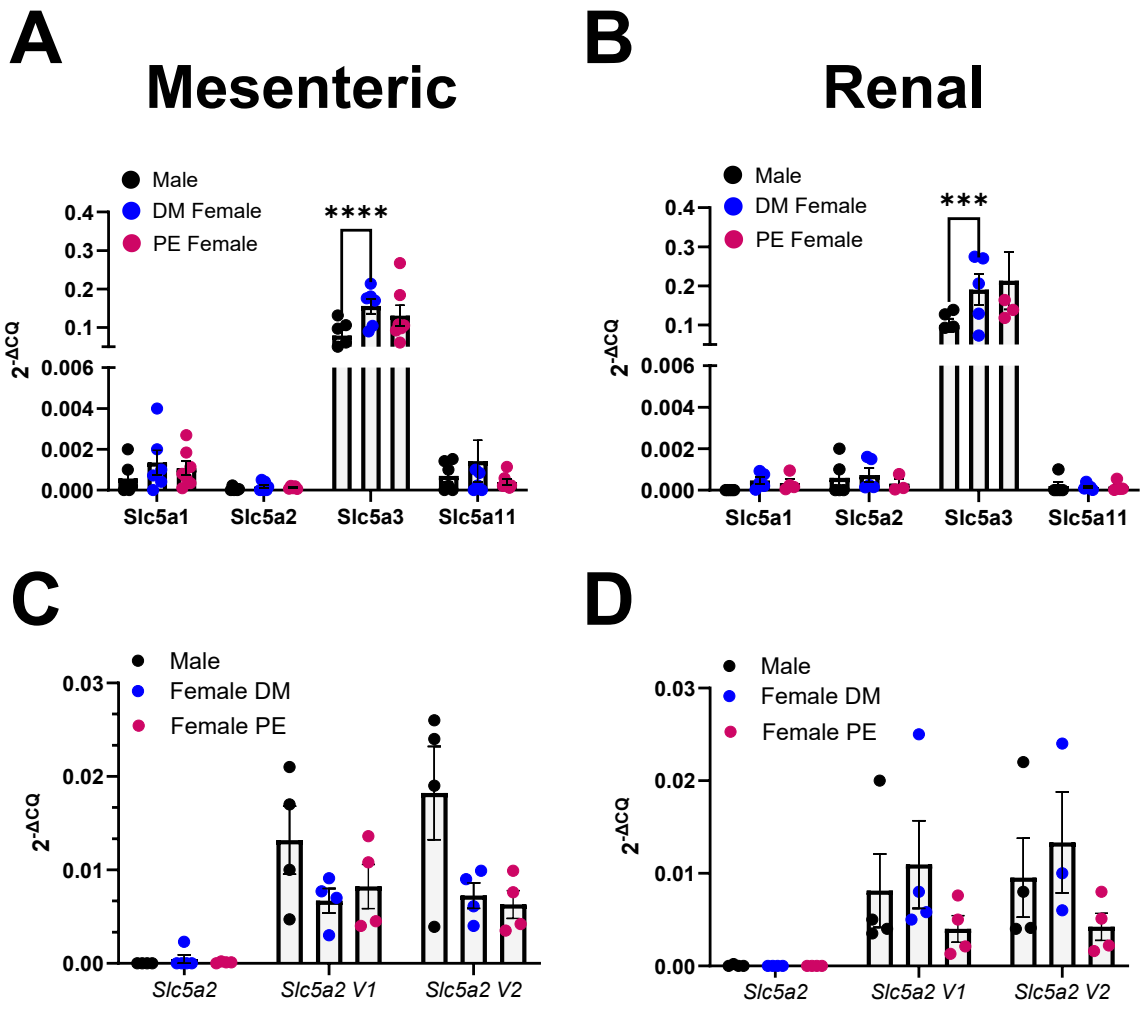


Figure 3.4: Comparison of Slc5a expression in male, DM female and PE female mesenteric and renal arteries.
The relative transcript abundance of Slc5a1 (SGLT1), Slc5a2 (SGLT2), Slc5a3 (SMIT1) and Slc5a11 (SMIT2) in mesenteric (A, N=5-6) and renal (B, N=4-5) arteries from male (black), DM Female (Blue) and PE female (pink) rats. The relative transcript abundance of Slc5a2 variants in mesenteric (C, N=4) and renal (D, N=3) arteries from male (black), DM Female (Blue) and PE female (pink) rats. All values are expressed as mean ± SEM denoted by error bars, and a two-way ANOVA with post-hoc Bonferroni test was used to calculate significance (N= number of animals used).

3.3.3 | Immunocytochemistry staining in isolated vascular smooth muscle cells

Immunocytochemistry was used to investigate protein expression and membrane localisation in vascular smooth muscle cells (VSMCs). VSMCs from mesenteric and renal arteries were identified by staining with alpha-smooth muscle actin (ab5694). In all immunocytochemistry experiments, three separate artery isolations from 3 different animals were used, and up to 5 cells were imaged from each coverslip over the three days. The alpha-smooth muscle stain in red can be seen in figure 3.5, with the DAPI (4′,6-diamidino-2-phenylindole) nuclear stain in blue.

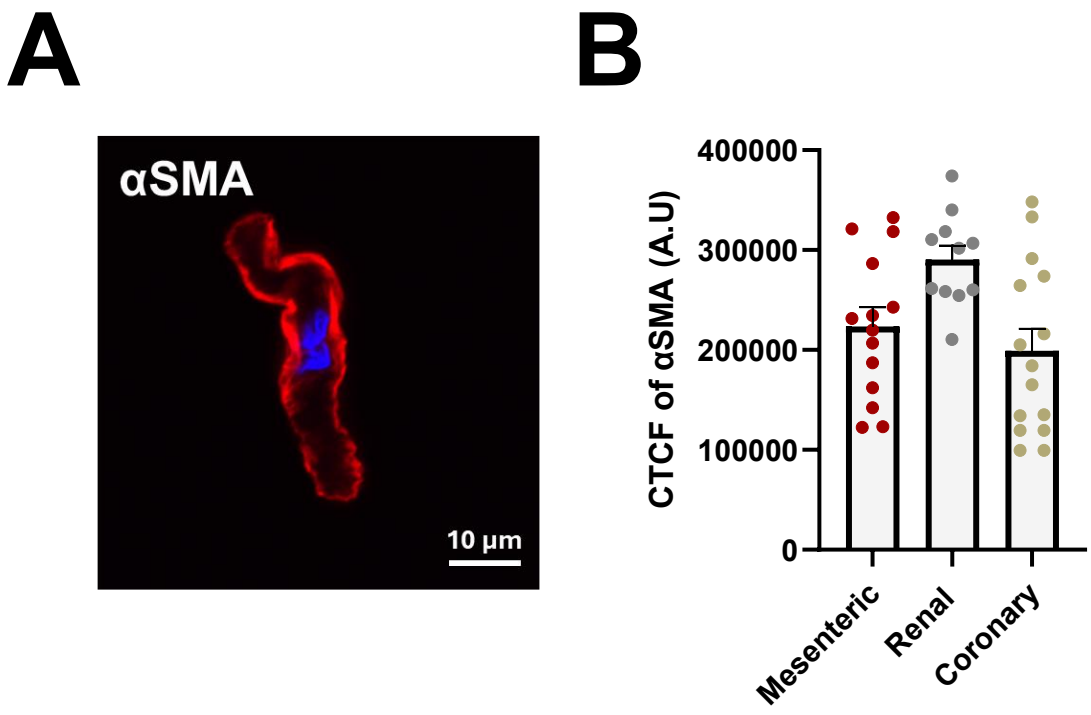


Figure 3.5: Expression of alpha-smooth muscle actin (αSMA) in mesenteric, renal and coronary vascular smooth muscle cells
Representative staining of alpha-smooth muscle actin in VSMCs from coronary arteries (A). The mean corrected total cell fluorescence intensity (CTCF) of αSMA in VSMCs from mesenteric (red), renal (grey) and coronary (beige) arteries (B, N=3, n=15). All data is shown as mean ± SEM denoted by error bars.

3.3.4 | The expression of SMIT1 in vascular smooth muscle cells from male mesenteric, renal and coronary arteries.

Using immunocytochemistry, the protein expression of SMIT1 was investigated in isolated vascular smooth muscle cells (VSMCs) from mesenteric, renal and coronary arteries. SMIT1 was expressed in all three arterial beds of male rats, as shown in figure 3.6A-C, with renal arteries exhibiting the greatest corrected total cell fluorescence intensity (CTCF) compared to mesenteric and coronary arteries (figure 3.6). To identify whether SMIT1 protein expression resided in the membrane of smooth muscle cells, the plasma membrane marker wheat germ agglutinin (WGA) was used to calculate the membrane: cytosol ratio of SMIT1 staining. The staining of SMIT1 was predominantly localised to the membrane in all three VSMC types of male rats, with renal arteries having the greatest membrane abundance (figure 3.7); however, in coronary arteries, small clusters of staining are seen throughout the VSMC (figure 3.6C and figure 3.7C).

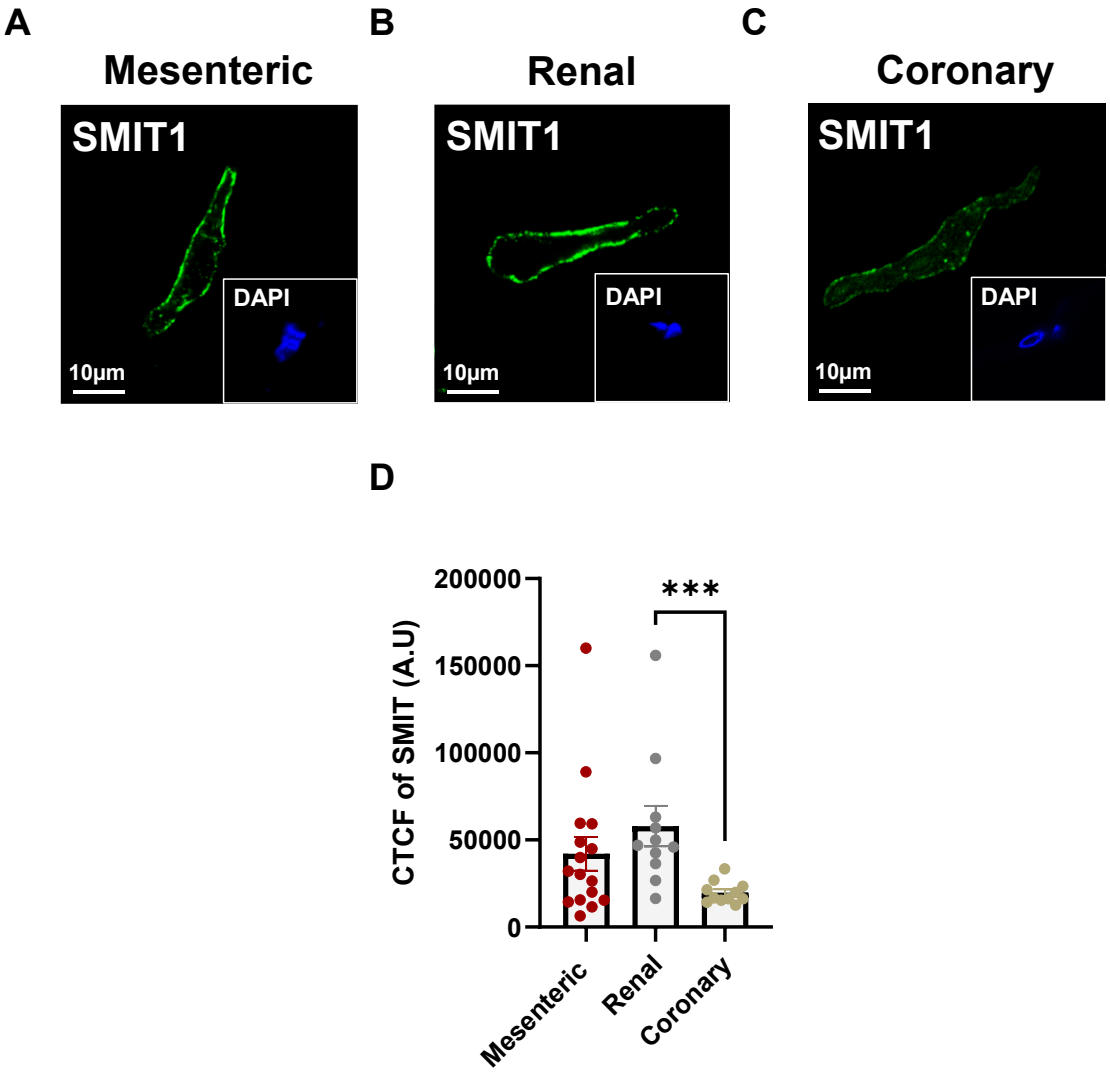


Figure 3.6: The protein expression of SMIT in mesenteric, renal and coronary arteries from male rats.

*Staining of SMIT1 in mesenteric (A, N=3 n=15), renal (B, N=3 n=12) and coronary (C, N=3 n=13) arteries with a nucleus DAPI marker. The total fluorescence intensity of SMIT1 in mesenteric (red), renal (grey), and coronary (beige) arteries is shown in panel D. All values are expressed as mean ± SEM denoted by error bars, and a one-way ANOVA was used to calculate significance where ***=P<0.001 (N= number of animals used, n= number of technical repeats).*

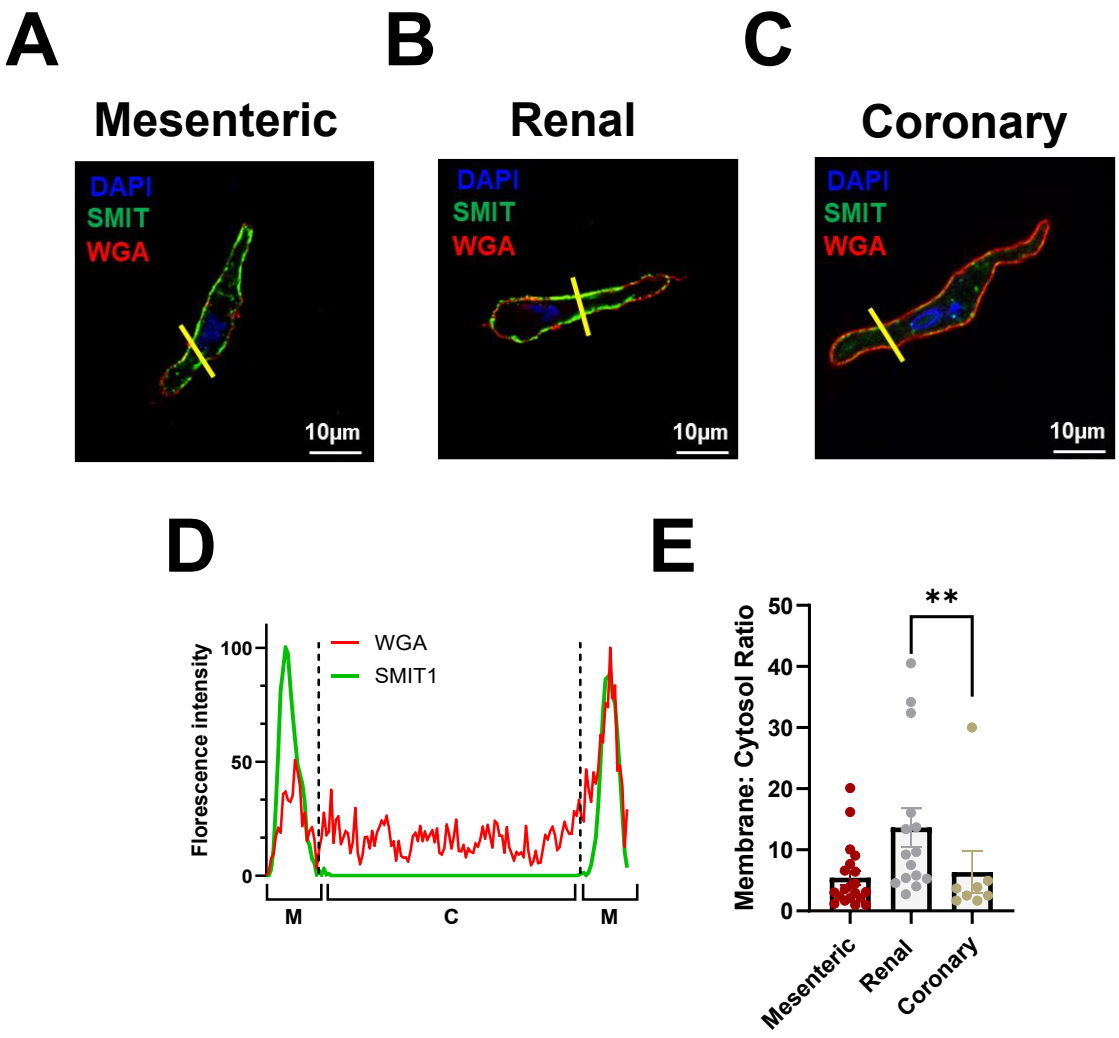


Figure 3.7: The membrane abundance of SMIT1 in mesenteric, renal and coronary arteries from male rats.

*Representative staining of SMIT1 (green), DAPI (nuclear stain, blue) and membrane marker wheat germ agglutinin (WGA, red) in mesenteric (A, N=3 n=15), renal (B, N=3, n=15), and coronary (C, N=3 n=10) arteries from male rats. The line scan of SMIT1 expression and WGA staining across a cell can be seen in panel D, with M representing the cell's membrane and C representing the cell's cytosol. The mean membrane cytosol ratio of SMIT1 in mesenteric (red), renal (grey) and coronary (beige) arteries is in panel E. All values are expressed as mean ± SEM denoted by error bars, and a one-way ANOVA was used to calculate significance where **=P<0.01 (N= number of animals used, n= number of technical repeats).*

3.3.5 | Classifying the expression of SGLT2 in mesenteric renal and coronary arteries

The expression of SGLT2 within the vasculature is ill-defined; hence, we wanted to confirm its expression and distribution in several vascular beds. Western Blot analysis in protein lysates from whole kidney (positive control) and whole mesenteric, renal and septal arteries detected a band at ~75kDa, which is the expected weight for SGLT2 (fig 3.8). Interestingly, two secondary bands were seen in all samples at ~50kDa and ~30kDa. These bands could represent cleavage products in these samples, as previously shown in (Saponaro et al., 2020) or correspond to the translated SGLT2 products shown in Zhao et al., 2005 or could indicate the SGLT2 splice variants. Quantification analysis showed that mesenteric arteries expressed the highest amount of SGLT2 protein compared to renal and coronary arteries (Fig 3.8B). However, the actin band in coronary arterial samples is thinner than in mesenteric and renal samples. Hence, the signal intensity of the western blot bands may not linearly correlate with protein quantity, and it is difficult to accurately compare the SGLT2 protein expression of coronary arteries to that of mesenteric and renal arteries.

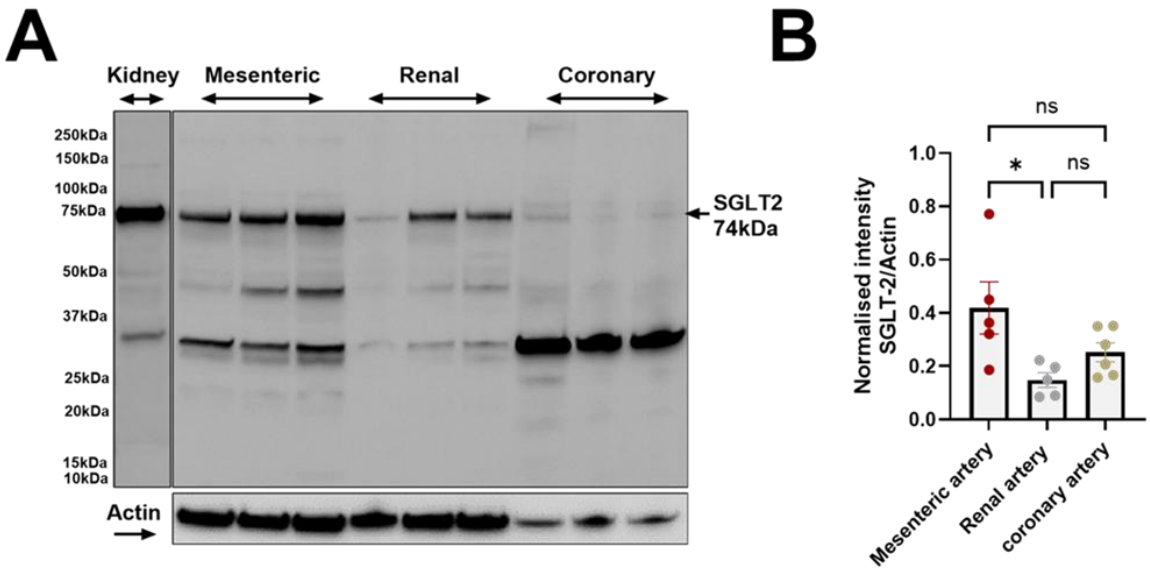


Figure 3.8: Western blot quantification of SGLT2.
*Expression of SGLT2 protein in mesenteric, renal and coronary arteries with whole kidney as positive control (A). The mean quantification of the western blot is shown in panel B (N=3). All values are expressed as mean ± SEM denoted by error bars and a one-way ANOVA was used to calculate significance where *=P<0.05, (N= number of animals used).*

Immunocytochemistry (figure 3.9; N=5) studies confirmed that SGLT2 was expressed in isolated smooth muscle cells from whole mesenteric, renal and septal arteries from male Wistar rats (figure 3.9), with mesenteric and renal arteries having significantly greater total fluorescence of SGLT2 compared to coronary arteries (figure 3.9D). There was a clear co-localisation of SGLT2 with the membrane marker Wheat germ agglutinin in mesenteric (figure 3.10A) and renal (figure 3.10B) VSMCs from male rats, suggesting SGLT2 expression was localised mainly in the plasma membrane. In contrast, in septal arteries, SGLT2 was predominantly in the cytosol of the smooth muscle cells (figure 3.10C-D). The total fluorescence intensity of SGLT2 in these vascular beds contradicted western blot analysis, with mesenteric and renal arteries having greater SGLT2 expression than septal arteries, which could be underpinned by whole artery staining occurring in only septal arteries. However, western blot required the septal, left anterior descending and right coronary arteries to undergo the experiment.

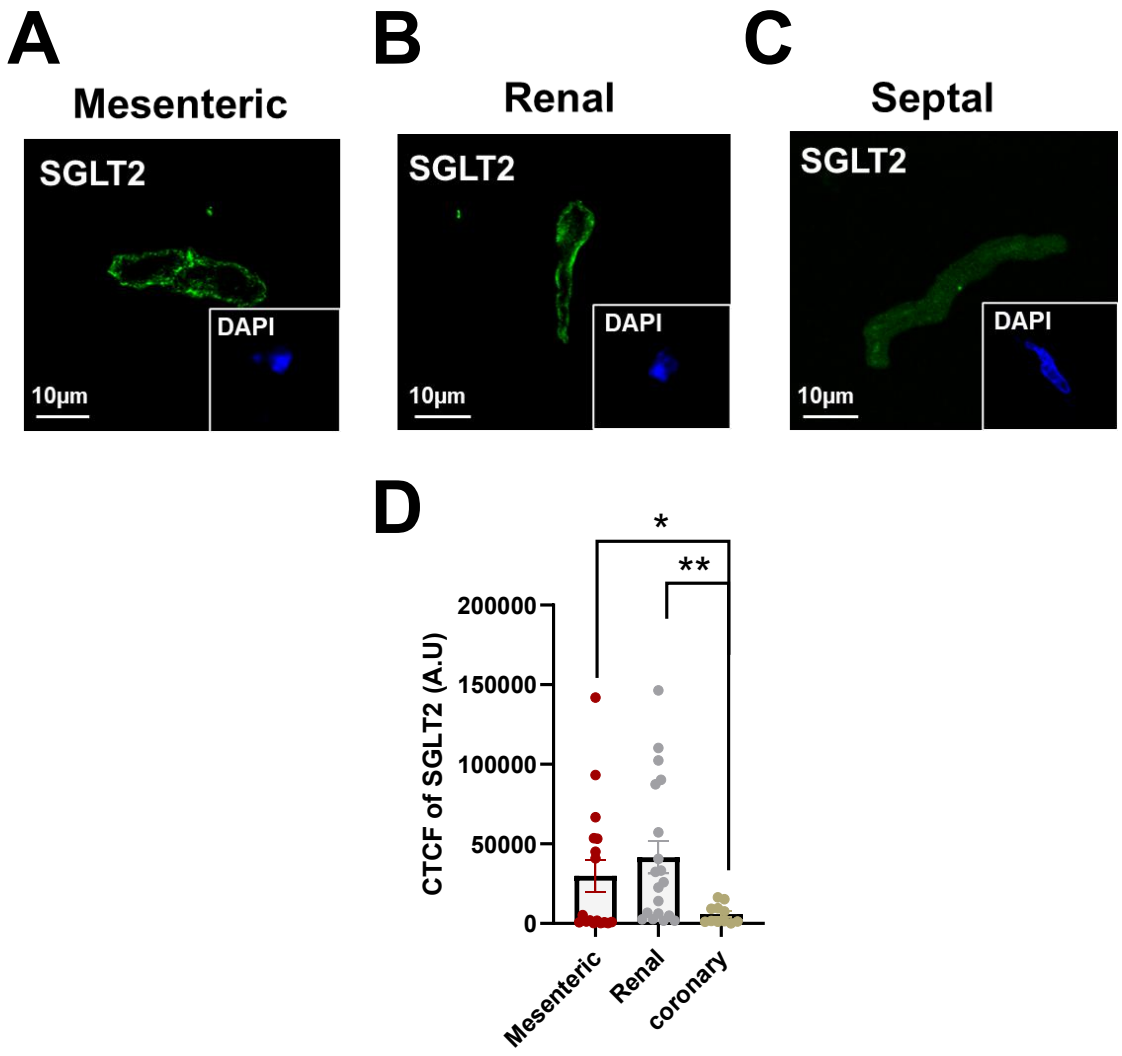


Figure 3.9: Expression of SGLT2 protein in mesenteric, renal and coronary arteries.

*Representative staining of SGLT2 (Green) in isolated mesenteric (A), renal (B) and coronary (C) vascular smooth muscle cells. Total cell fluorescence of mesenteric (red), renal (grey) and coronary (beige) is shown in panel D (N=5, n=20). All values are expressed as mean ± SEM denoted by error bars, and a one-way ANOVA was used to calculate significance where *=P<0.05, **=P<0.01), (N= number of animals used, n= number of technical repeats).*

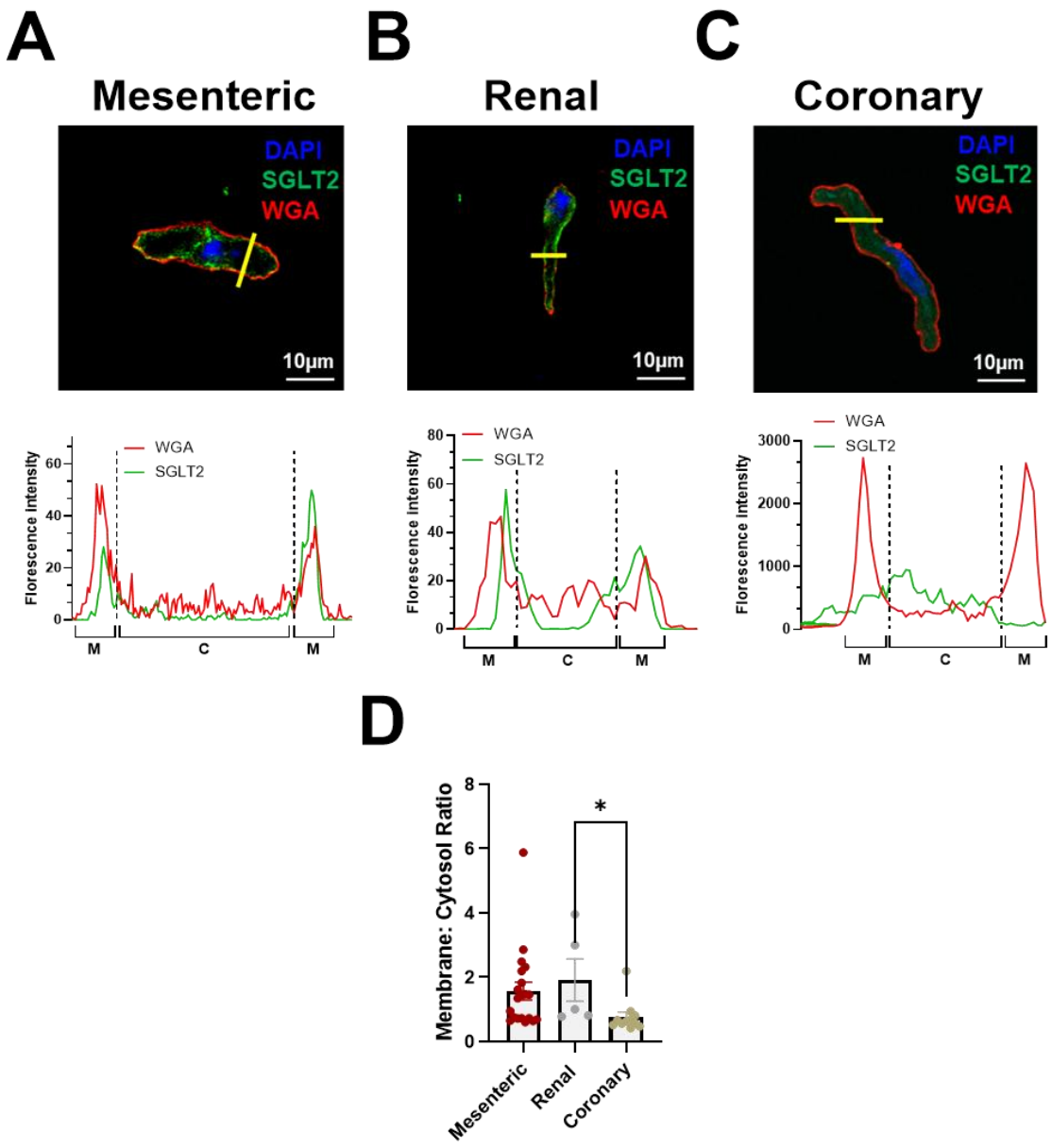


Figure 3.10: The distribution of SGLT2 in various vascular smooth muscle beds. *Representative staining and line scan of SGLT2 (green) and wheat germ agglutinin (WGA, red) in mesenteric (A), renal (B) and septal (C) arteries. Quantification of the membrane cytosol ratio and total fluorescence intensity in mesenteric (red), renal (grey) and coronary (beige) arteries is shown in panels D (N=3 n=9). All values are expressed as mean ± SEM and a one-way ANOVA was used to calculate significance where *=P<0.05, **=P<0.01, (N= number of animals used).*

3.3.6 | Immunohistochemistry staining in whole mesenteric and renal arteries

Immunohistochemistry was used to investigate the expression of SMIT and SGLT2 in whole mesenteric, renal and coronary arteries. The artery's smooth muscle and endothelial layers were identified using myosin heavy chain (MHC) and CD31 antibodies that have been well-validated (Fang et al., 2022; Timraz et al., 2016; Wen et al., 2022). The endothelial antibody CD31 produced membranous cellular staining with circular DAPI nuclei staining appearing in the centre of each endothelial cell (figure 3.11A). The smooth muscle antibody myosin heavy chain (MHC) predominantly displayed cytosolic staining of smooth muscle cells in a longitudinal orientation. The DAPI nuclei staining in the smooth muscle cell layer formed elongated ovals that followed the length of the smooth muscle cells orientated 90 degrees to the circular nuclei located in the endothelial cell layer (figure 3.11B). These differences in nuclei enable the identification of the artery layer, hence enabling the precise localisation of protein expression within the arterial structure.

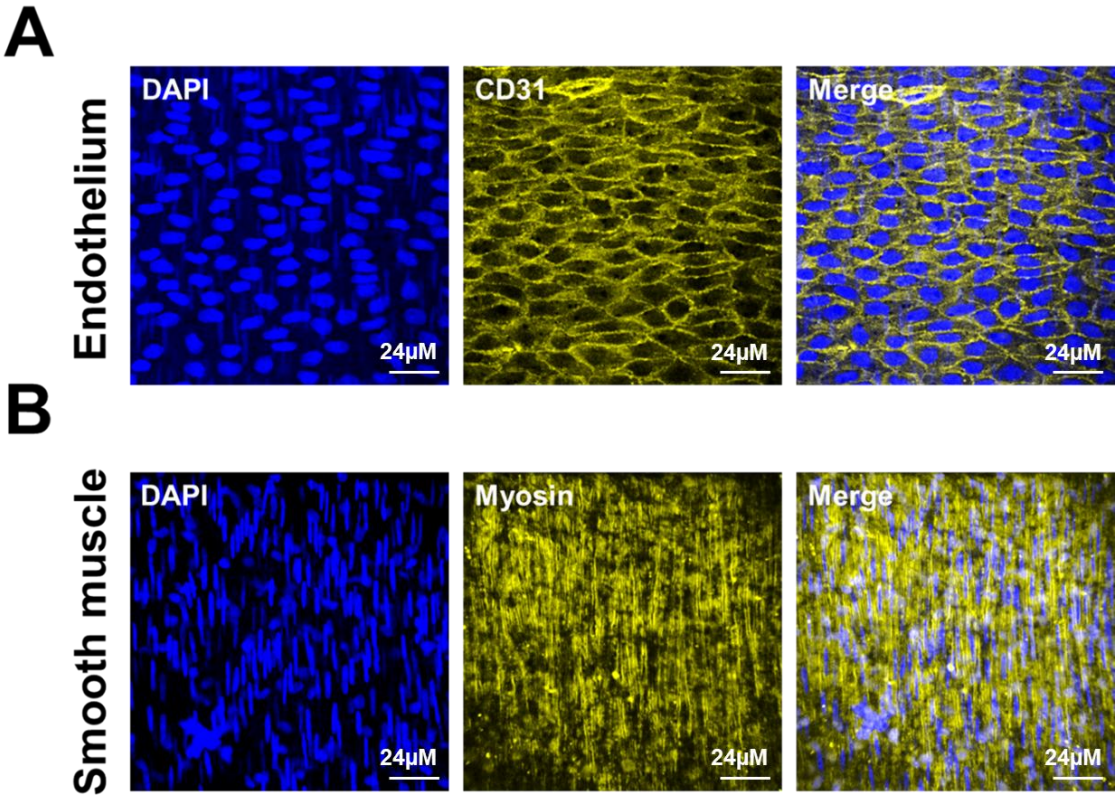


Figure 3.11: Markers for smooth muscle cells and endothelial cells.
Representative staining for the myosin heavy chain (smooth muscle marker) and CD31 (endothelial cell marker) in yellow in endothelial cells (EC, A) and smooth muscle cells (SMC, B) of mesenteric arteries. Nuclei were labelled in blue (representative of N=3-4).

3.3.7 | The expression of SMIT in endothelial cells of whole mesenteric and coronary arteries

The expression of SMIT1 was investigated in whole arteries from male rats. SMIT1 staining was found in the endothelial and smooth muscle cell layers of whole coronary, mesenteric and renal arteries (figures 3.12 and 3.13).

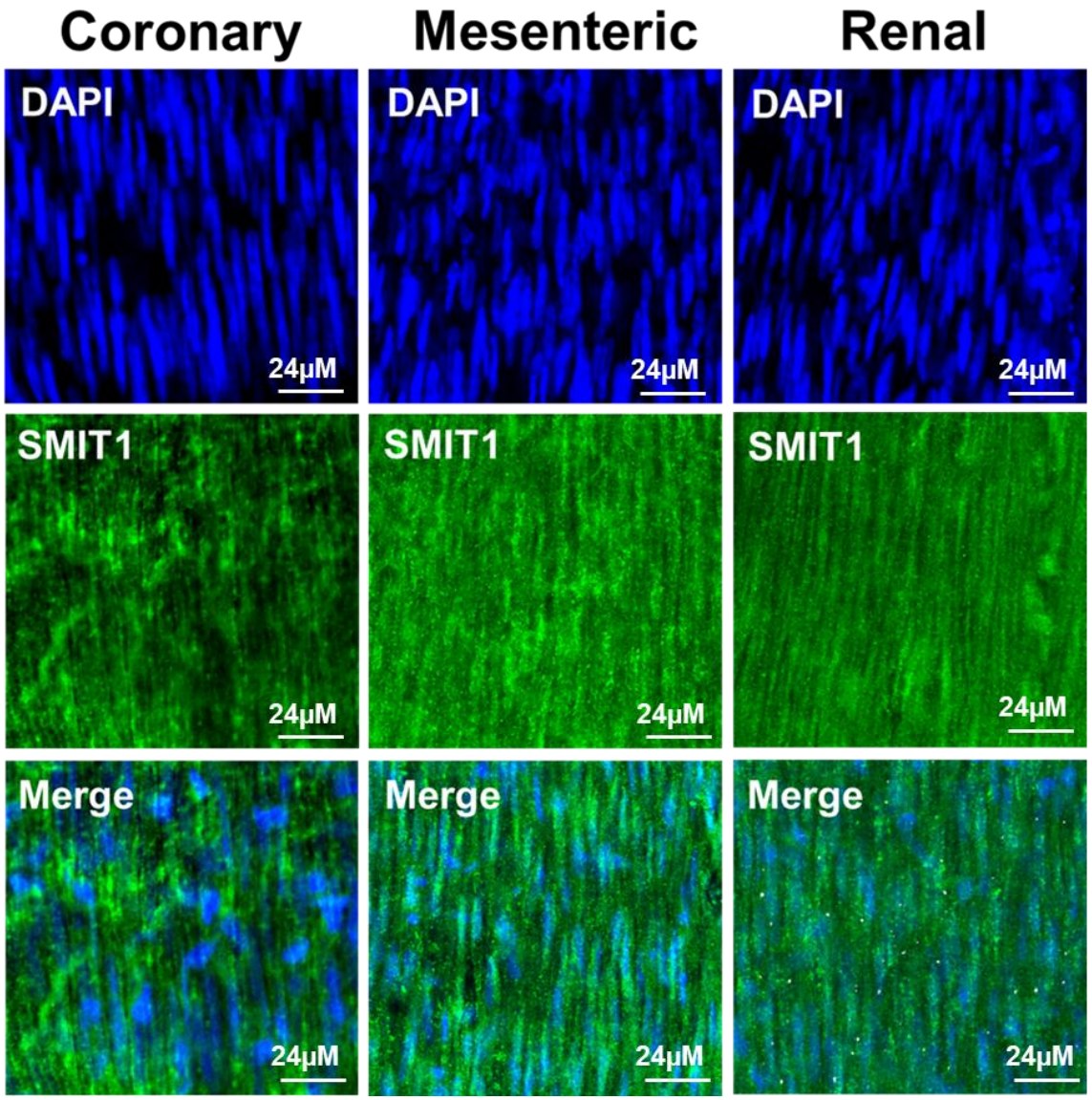


Figure 3.12: Expression of SMIT1 in the smooth muscle layer of whole mesenteric, renal and coronary arteries.
The expression of SMIT1 (green) in the smooth muscle layer of whole coronary, mesenteric and renal arteries with a DAPI nuclear stain (blue). (representative of N=3).

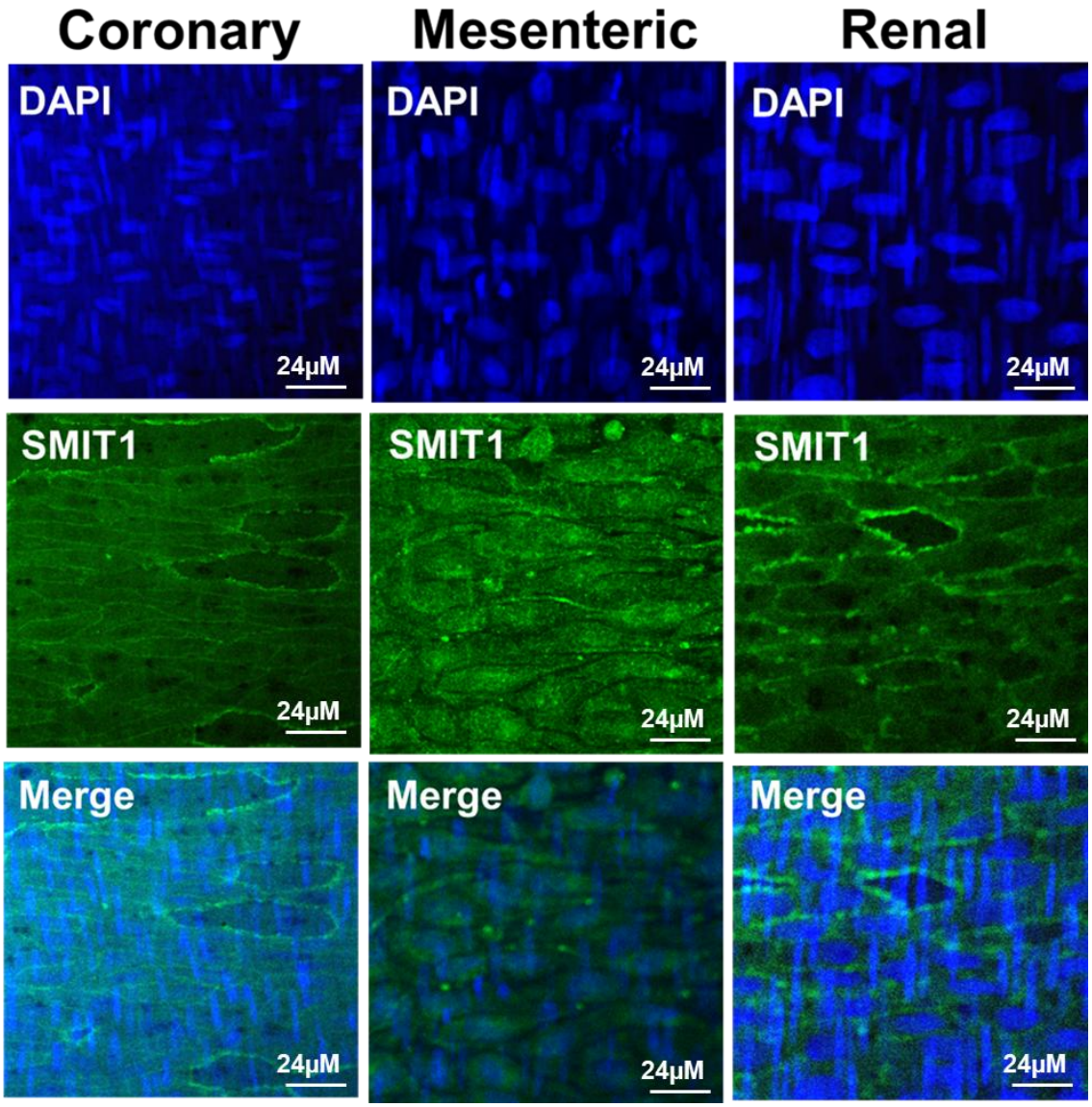


Figure 3.13: Expression of SMIT1 in the endothelial layer of whole mesenteric, renal and coronary arteries.
The expression of SMIT1 (green) in the endothelial layer of whole coronary, mesenteric and renal arteries with a DAPI nuclear stain (blue). (representative of N=3).

3.3.8 | The expression of SGLT2 in endothelial cells of whole mesenteric and coronary arteries

The expression of SGLT2 was investigated in whole arteries from male rats. SGLT2 staining was found in the smooth muscle layer of the whole coronary, mesenteric, and renal arteries. The staining of SGLT2 in the smooth muscle of all three artery types was mainly cytosolic and formed small clusters throughout the tissue (figure 3.14). However, little to no SGLT2 staining was seen in any of the arterial endothelial layers, as shown in figure 3.15.

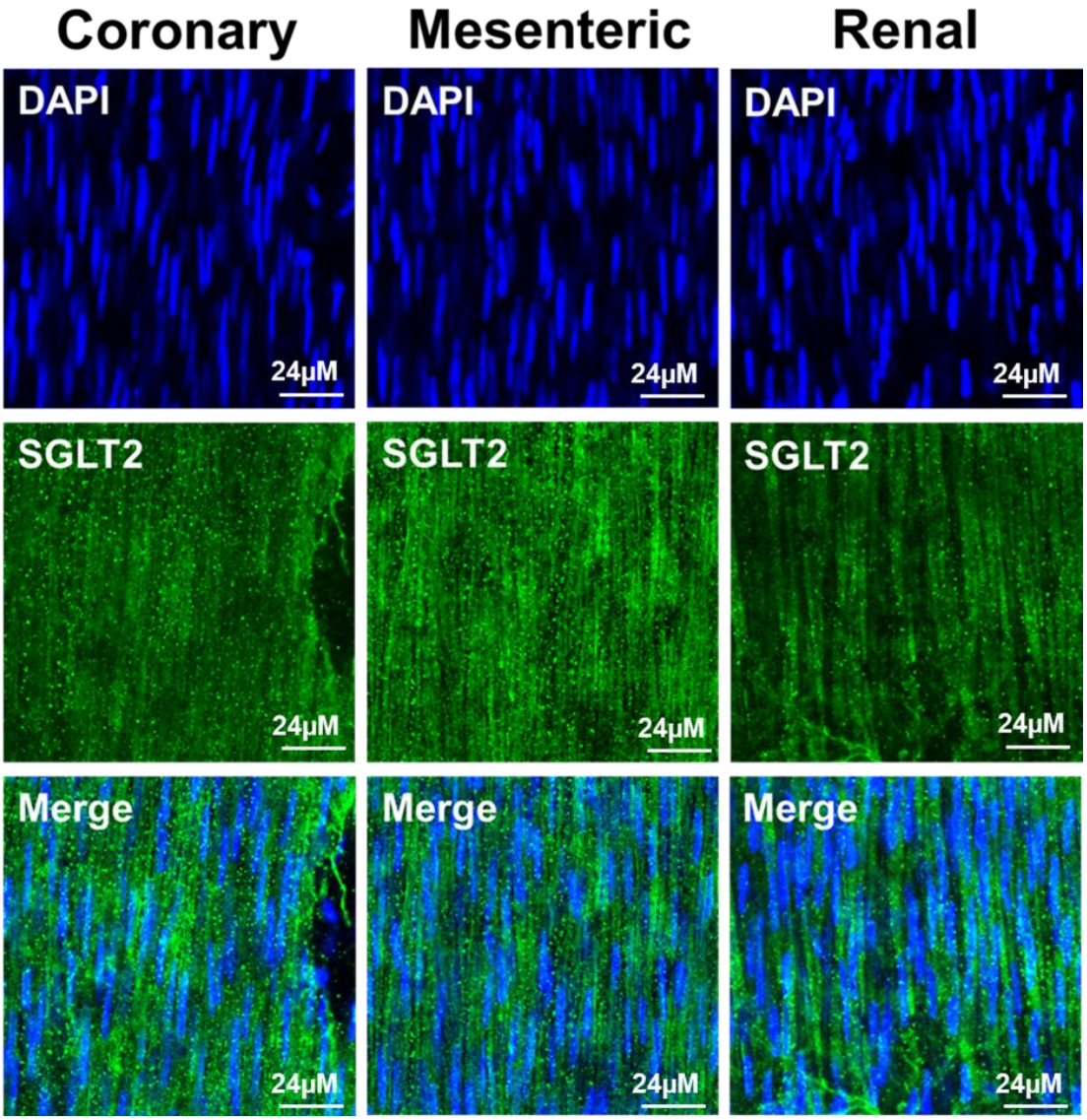


Figure 3.14: Expression of SGLT2 in the smooth muscle layer of whole mesenteric, renal and coronary arteries.
The expression of SGLT2 (green) in the smooth muscle layer of whole coronary, mesenteric and renal arteries with a DAPI nuclear stain (blue). (representative of N=3).

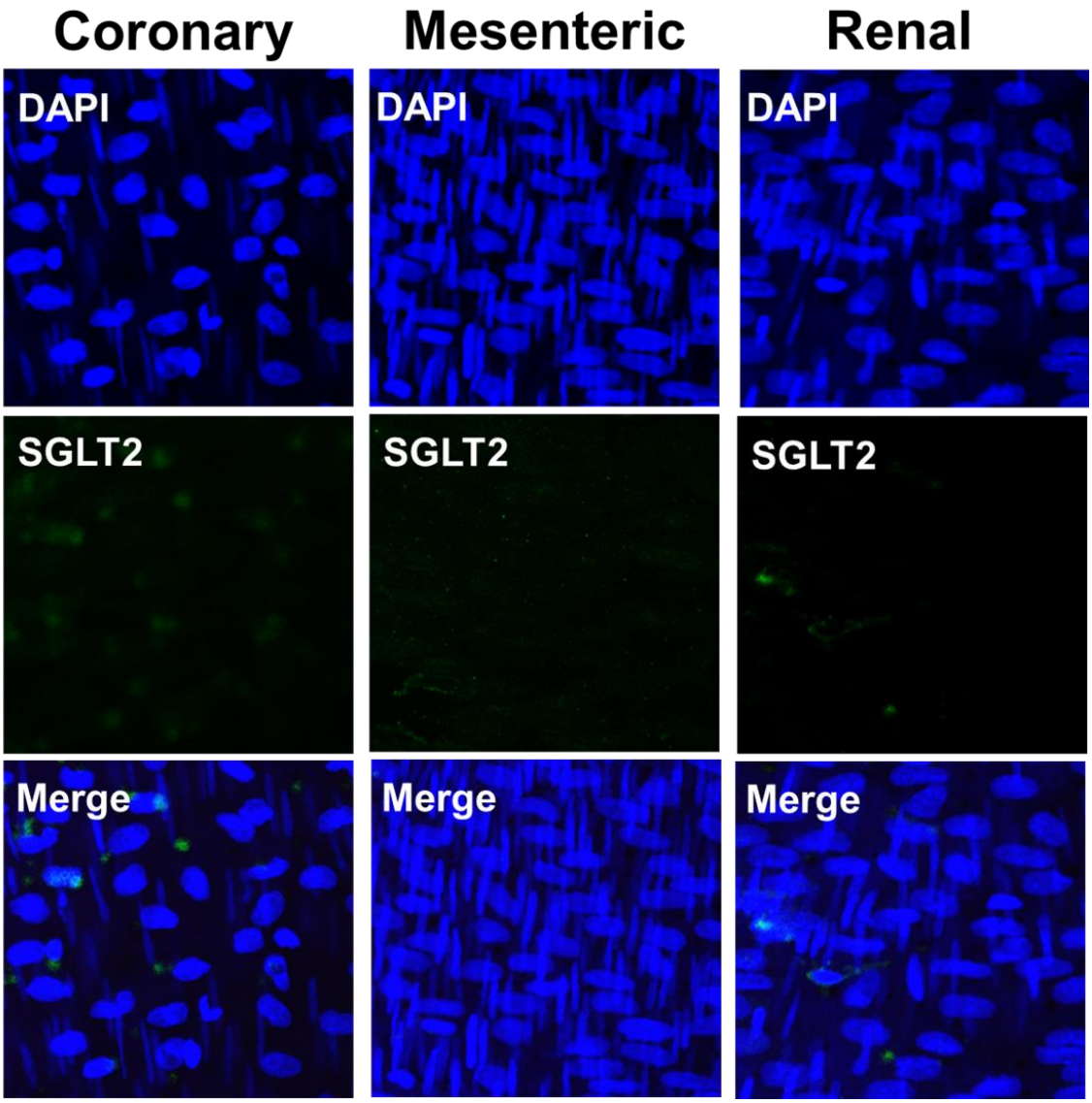


Figure 3.15: Expression of SGLT2 in the endothelial layer of whole mesenteric, renal and coronary arteries

The expression of SGLT2 (green) in the endothelial layer of whole coronary, mesenteric and renal arteries with a DAPI nuclear stain (blue). (representative of N=3).

3.3.9 | Expression of SMIT in mesenteric and coronary VSMCs from female rats

There was clear SMIT1 staining in both mesenteric and coronary arteries from DM and PE female rats, as shown in figure 3.16A. DM females had significantly greater CTCF (figure 3.16) and membrane abundance (figure 3.17) of SMIT1 compared to PE females. Interestingly, the staining of SMIT1 had many clusters in both mesenteric and coronary VSMCs from DM female rats, whereas fewer clusters were seen in VSMCs from PE females (figures 3.16A and 3.17A). These findings suggest that SMIT1 protein was expressed in mesenteric, renal and coronary arteries from male and female rats, with this staining predominantly residing in the membrane of VSMCs from male and DM female arteries. The CTCF of SMIT1 was found to be significantly greater in both mesenteric and coronary arteries from DM female rats compared to males and PE females, with PE females having a greater fluorescence staining of SMIT1 in coronary arteries compared to males (figure 3.18).

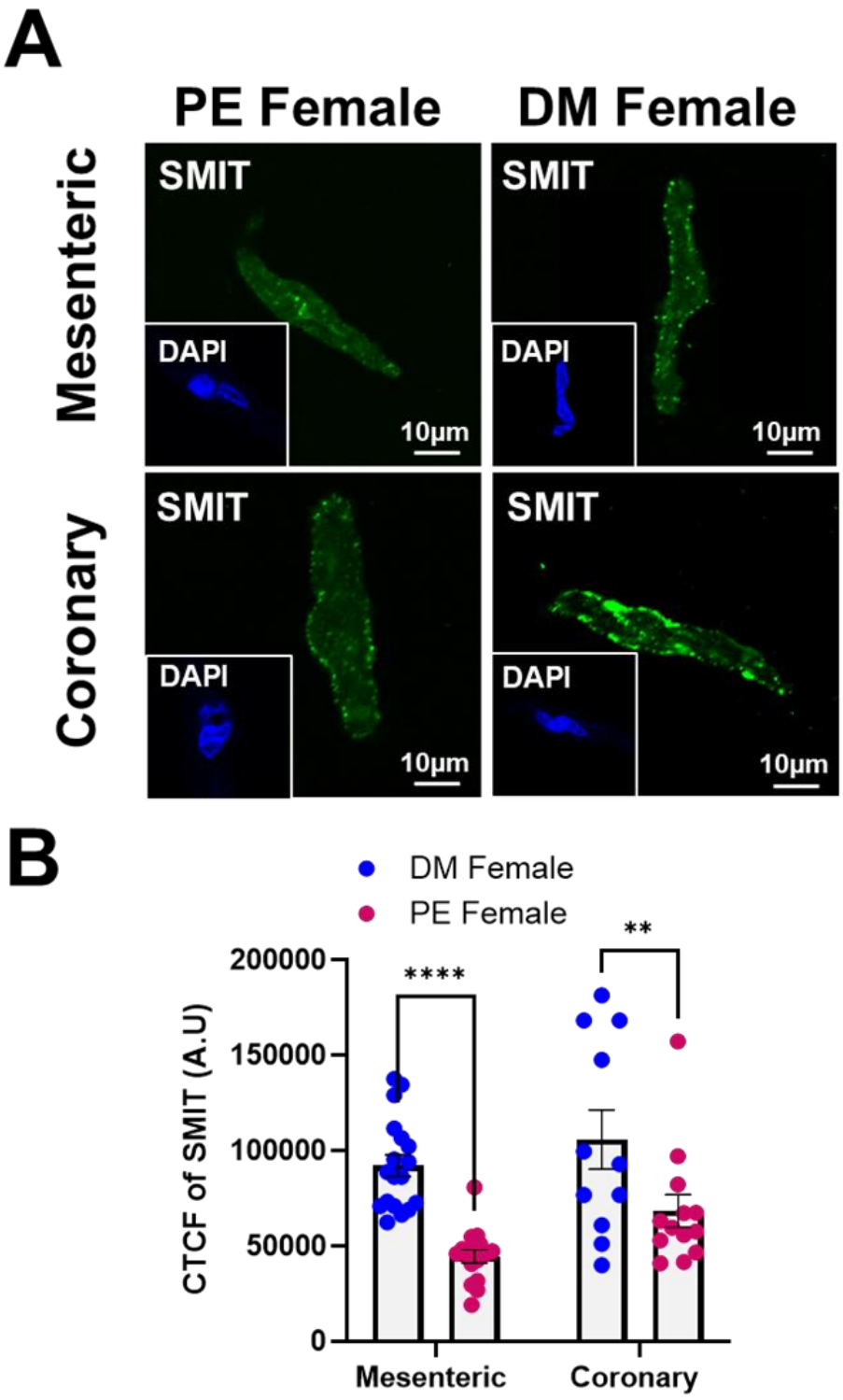


Figure 3.16: The protein expression of SMIT in mesenteric, renal and coronary arteries from DM and PE Female rats.

Staining of SMIT1 in mesenteric and coronary arteries from PE female (left) and DM Female (right) with a nucleus DAPI marker (A). The total fluorescence intensity of SMIT1 in mesenteric and coronary arteries from DM Female (blue, N=3 n=15) and PE female (pink, N=3 n=12) rats is shown in panel B. All values are expressed as mean ± SEM denoted by error bars, and a two-way ANOVA with post-hoc Bonferroni test was used to calculate significance (N= number of animals used, n=number of technical repeats).

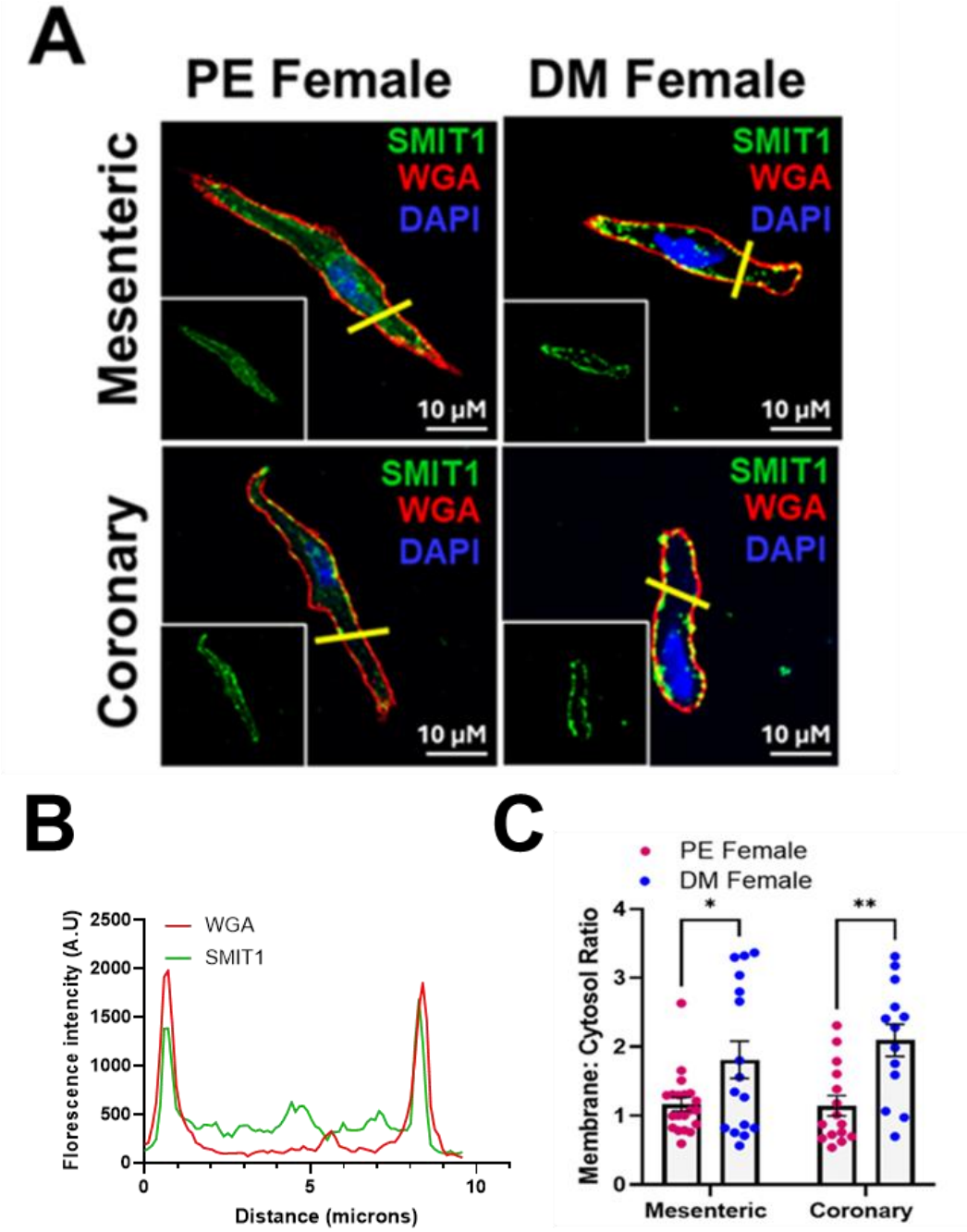


Figure 3.17: The membrane abundance and distribution of SMIT1 in the mesenteric, renal, and coronary arteries of DM and PE female rats.
Representative staining of SMIT1 (green), DAPI (nuclear stain, blue) and membrane marker wheat germ agglutinin (WGA, red) in mesenteric and coronary arteries from DM and PE female rats (A). The line scan of SMIT1 expression and WGA staining across an isolated mesenteric VSMC from DM females can be seen in panel B. The mean membrane cytosol ratio of SMIT1 in mesenteric and coronary arteries from DM female (blue, N=3 n=15) and PE female (pink, N=3 n=15) rats is in panel C. All values are expressed as mean ± SEM denoted by error bars, and a two-way ANOVA with post-hoc Bonferroni test was used to calculate significance (N= number of animals used, n=number of technical repeats).

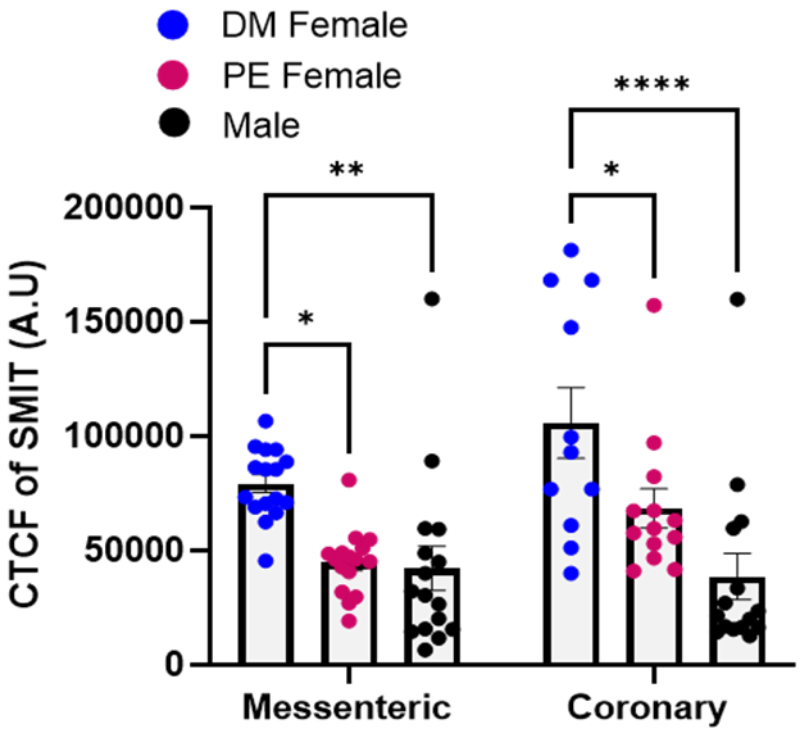


Figure 3.18: Comparison of the total expression of SMIT1 in mesenteric and coronary arteries from male, DM female and PE female rats.
The corrected total cell fluorescence intensity (CTCF) of SMIT1 in mesenteric and coronary arteries from the male (black, N=3 n=15), DM female (blue, N=3 n=11-14) and PE female (pink, N=3 n=15) rats. All values are expressed as mean ± SEM denoted by error bars, and a two-way ANOVA with post-hoc Bonferroni test was used to calculate significance (N= number of animals used, n=number of technical repeats).

3.3.10 | Expression of SGLT2 in female mesenteric, renal and coronary arteries

Both PE and DM females expressed SGTL2 protein in mesenteric and coronary arteries. DM females had greater total cell fluorescence of SGLT2 in mesenteric and coronary arteries compared to PE females (figure 3.19). However, the SGLT2 staining in both DM and PE females was more cytosolic, with little staining localised in the membrane (figure 3.20). Overall, the protein expression of SGLT2 was greater in coronary arteries from male, DM female and PE female arteries compared to mesenteric arteries, and DM females had slightly higher total cell fluorescence of SGLT2 in both arteries compared to male and PE female rats (figure 3.21).

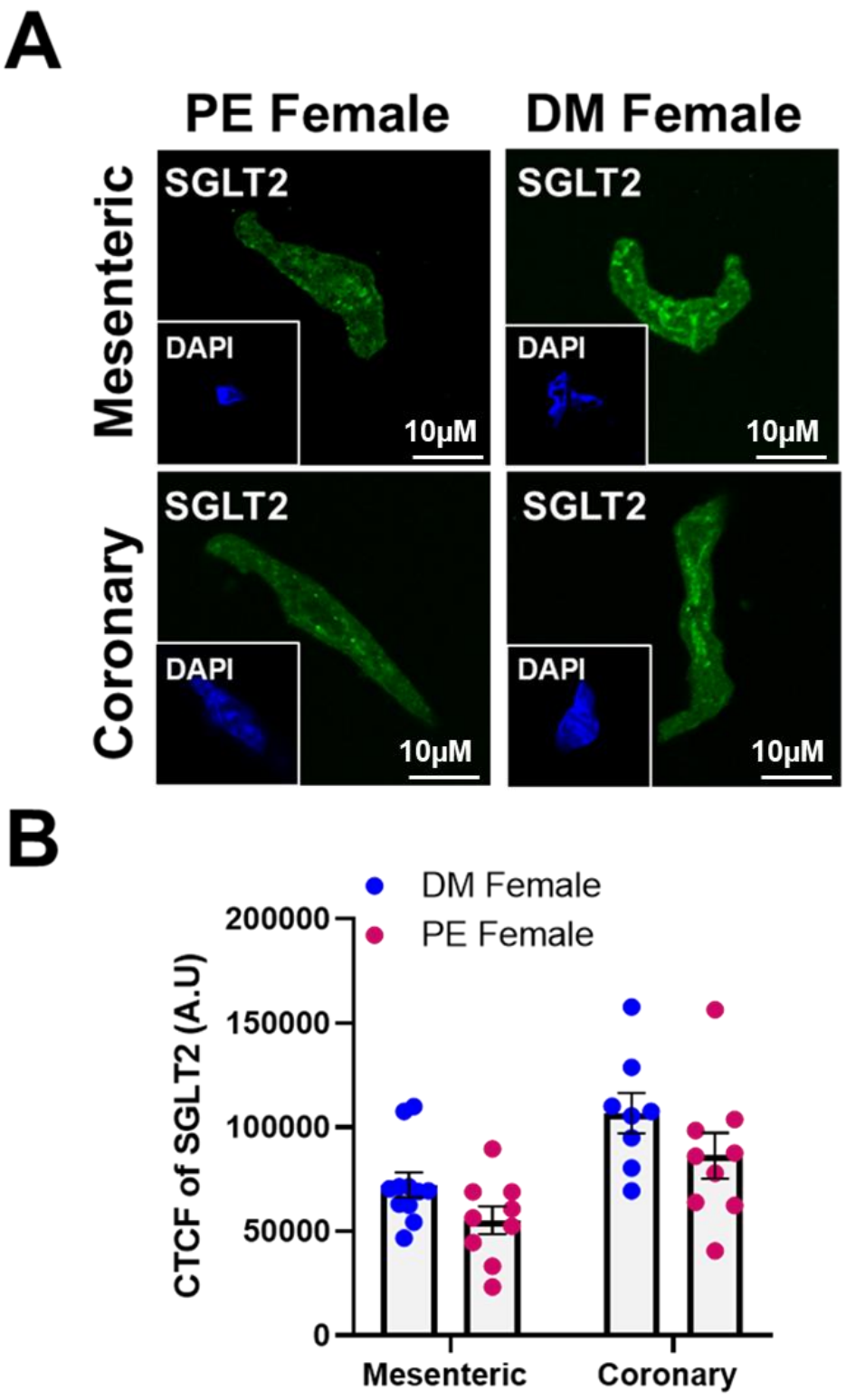


Figure 3.19: Shows the protein expression of SGLT2 in the mesenteric, renal, and coronary arteries of DM and PE Female rats.

Staining of SGLT2 in mesenteric and coronary arteries from PE female (left) and DM Female (right) with a nucleus DAPI marker (A). The total fluorescence intensity of SGLT2 in mesenteric and coronary arteries from PE Female (blue, N=3 n=9) and DM female (pink, N=3 n=9) rats is shown in panel B. All values are expressed as mean ± SEM denoted by error bars, and a one-way ANOVA was used to

calculate significance (N= number of animals used, n=number of technical repeats).

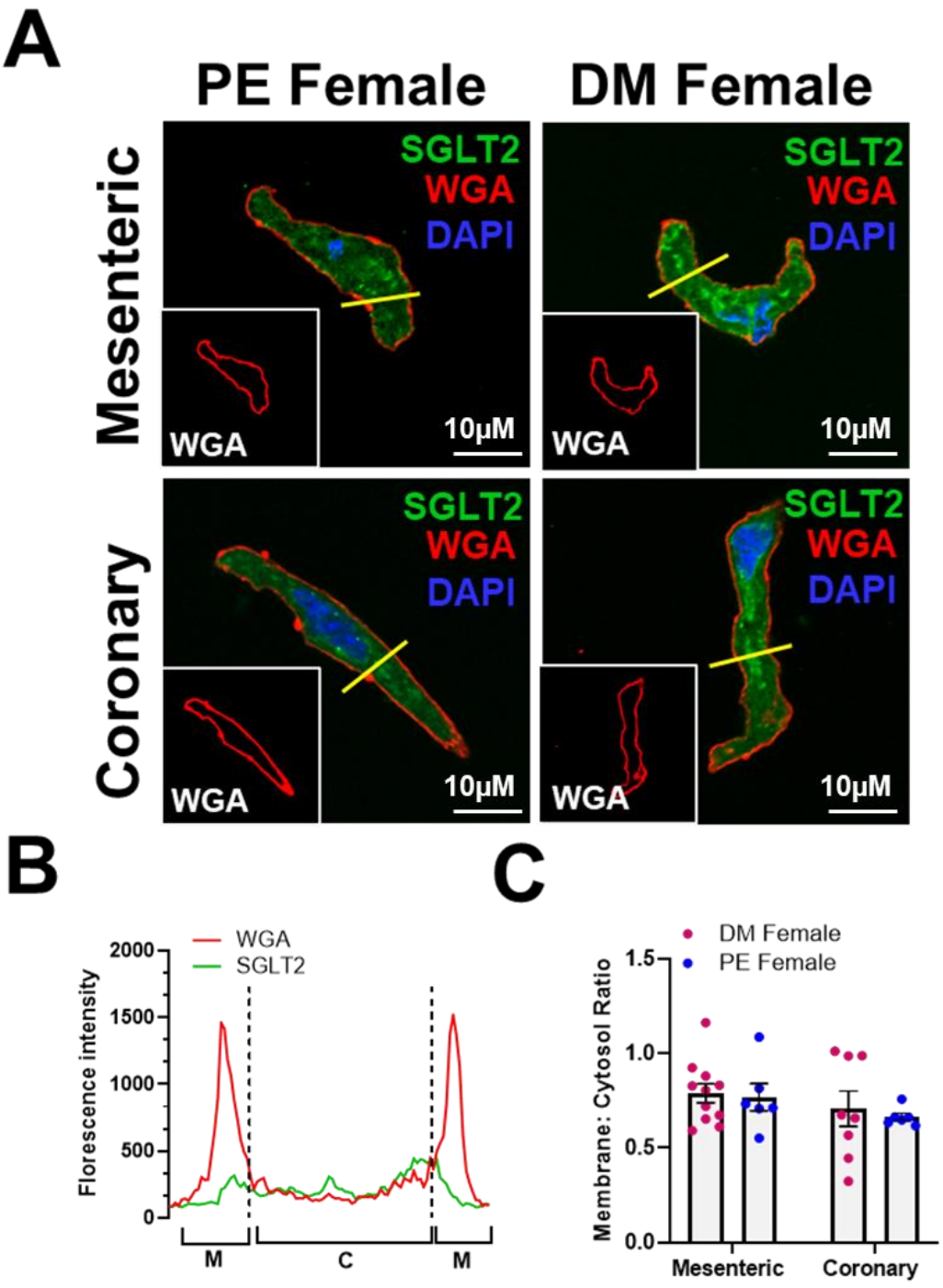


Figure 3.20: The membrane abundance and distribution of SGLT2 in the mesenteric, renal, and coronary arteries of DM and PE Female rats.
Representative staining of SGLT2 (green), DAPI (nuclear stain, blue) and membrane marker wheat germ agglutinin (WGA, red) in mesenteric and coronary arteries from PE and DM female rats (A). The line scan of SMIT1 expression and WGA staining across a cell can be seen in panel B, with M representing the cell's membrane and C representing the cell's cytosol.

The mean membrane cytosol ratio of SMIT1 in mesenteric and coronary arteries from DM female (blue) and PE female (pink) rats is in panel C (N=3 n=8-9). All values are expressed as mean ± SEM denoted by error bars, and a two-way ANOVA with post-hoc Bonferroni test was used to calculate significance (N= number of animals used, n=number of technical repeats).

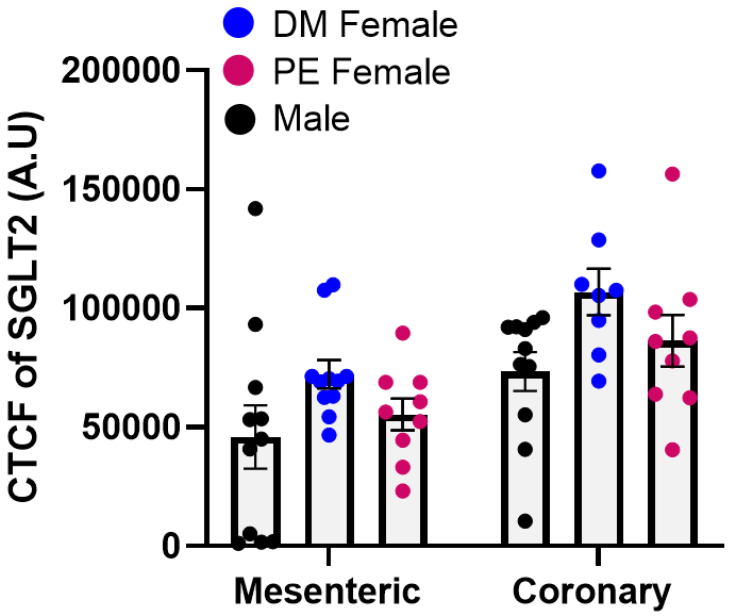


Figure 3.21: Comparison of the total expression of SGLT2 in mesenteric and coronary arteries from male, DM female and PE female rats.
The mean corrected total cell fluorescence intensity (CTCF) of SGLT2 in VSMCs from mesenteric and coronary arteries in male (black N=3 n=11), DM female (blue, N=3 n=10) and PE female (pink, N=3 n=9) rats. All values are expressed as mean ± SEM denoted by error bars, and a two-way ANOVA with post-hoc Bonferroni test was used to calculate significance (N= number of animals used, n=number of technical repeats).

3.4 | Discussion

This chapter investigated the expression and distribution of SLC5a proteins in the mesenteric, renal, and coronary arteries of male and female rats. This study found that SMIT1 encoded by Slc5a3 and SGLT2 splice variants encoded by Slc5a2 had the highest mRNA transcript abundance in mesenteric, renal and coronary arteries from male and female rats. The close relatives Slc5a1 and Slc5a11 had minimal mRNA expression in these arterial beds. SMIT1 protein was found in VSMCs and endothelial cell layers of whole mesenteric, renal and coronary arteries, whereas SGLT2 was only expressed in the VSMC layer. There was an oestrus cycle-dependent difference in the protein expression of SGLT2 and SMIT1 in isolated VSMCs. The expression of SMIT1 in isolated mesenteric and coronary arteries was greater in DM female rats compared to male and PE female rats. Comparatively, there was similar expression of SGLT2 in both male and female arteries, with the total SGLT2 expression being greater in coronary arteries of male and female rats than in mesenteric arteries; however, in male mesenteric arteries, there was a greater membrane abundance of SGLT2 compared to DM and PE females.

3.4.1 | Expression of SGLT2 and SMIT1 in different vascular beds

The arterial expression of SGLT2 and SMIT1 has only been investigated in a handful of papers. This study identified the expression of SMIT1, SMIT2, SGLT1 and SGLT2 in mesenteric, renal, coronary and cerebral arteries. The protein expression of SMIT1 and SGLT2 was found in vascular smooth muscle cells of mesenteric, renal and coronary arteries, and SMIT1 was also found in the endothelial cell layers of these vessels. These results support previous studies that found expression of SGLT2 in human and rat aortic VSMCs (Sukhanov et al., 2021; Takahashi et al., 2019), rat mesenteric arteries (Hasan, Menon, et al., 2022) and human adipose tissue arterioles (De Stefano et al., 2021). However, other groups identified SGLT2 expression in human aortic and coronary endothelial cells (Durante et al., 2021; Sukhanov et al., 2021b; Takahashi et al., 2019b; Uthman et al., 2019), whereas this study does not show any expression of SGLT2 in vascular endothelial cells from mesenteric, renal or coronary arteries. Strikingly, in the western bot experiments looking at the expression of SGTL2, two secondary bands

were seen in all samples at ~50kDa and ~35kDa. These bands have been identified in previous publications (Zhao et al., 2005 and Saponaro et al., 2020) and could be underpinned by the two SGLT2 splice variants found in RT-QPCR studies. However, the SGLT2 antibody used binds to the extracellular domain of SGLT2 of rat, mouse and human origin and raised against amino acids 226-268, which can bind to the splice variant X1 but not the shorter non-coding Slc5a2 X2 isomer. The lower molecular weight bands could result from cleavage products in these samples due to a high number of disulphide bonds in the protein structure, as previously shown in Saponaro et al., 2020 or the bands could be the translation product of the SGLT2 protein, as stated by Zhao et al., 2005. These similar bands were seen in SGLT2 western blot studies of the kidney tissue control by Hasan et al.,2022. However, they were not investigated further. Interestingly, qPCR experiments showed little overall Slc5a2 mRNA transcript abundance in all arterial beds, whereas ICC and western blot experiments identified high SGLT2 protein expression in mesenteric, renal and coronary arteries. The presence of mRNA transcript in a cell ultimately indicates that gene transcription has occurred, and this mRNA can thus be translated into a chain of amino acids to form a protein. The low Slc5a2 transcript could indicate a low turnover and long half-life of cellular SGLT2 proteins. However, previous literature has highlighted that transcript levels do not indicate genotype-phenotype relationships, with little correlation between mRNA levels and protein expression (Greenbaum et al., 2003 and Nie et al., 2006). Therefore, western blot, immunohistochemistry and immunocytochemistry experiments enabled confirmation that SGLT2 protein is expressed in VSMCs from mesenteric, renal and coronary arteries in male and female rats.

SMIT1 is known to be expressed in various tissues, including brain, lung, liver, heart and small intestine. Immunocytochemistry and immunohistochemical studies have previously shown that VSMCs from mesenteric, renal, (Barrese et al., 2020) and aortic arterial segments and endothelial cell layers in male rat aorta express SMIT1 (Grandperrin et al., 2024). This study supports these findings by showing SMIT1 expression in the VSMC and endothelial cell layers of the mesenteric, renal, coronary, and cerebral arteries. The expression of SMIT1 and SGLT2 in mesenteric, renal, and coronary arteries from DM and PE female rats has not previously been identified; hence, this study improves our understanding of the expression of sodium solute transporters in the vasculature.

3.4.2 | Sex differences in the arterial expression of SGLT2 and SMIT1

This study identified a sex-dependent difference in the expression of SMIT1 and SGLT2 in isolated mesenteric and coronary VSMCs. DM females had a greater expression of SMIT1 and SGLT2 in both mesenteric and coronary arteries than males and PE females. The expression of SMIT1 was also higher in coronary arteries from PE females than in males. This data corroborates Sabolić et al., 2012 who found that the expression of SGLT2 in the renal proximal tubule was significantly greater in female rats than in male rats. Moreover, further increases in female SGLT2 expression were seen after incubating in oestrogen, with a decrease in SGLT2 expression following testosterone incubation. However, the female rats in this study were not separated into high oestrogen (PE females) and low oestrogen (DM females) groups; hence, the oestrus cycle differences could not be investigated. Additionally, Sabolić et al. (2012) demonstrated a threefold increase in SGLT2 expression in females compared to males, significantly greater than that observed in the current study. SGLT1 expression has also previously been found to be higher in renal tissues of female rats than in males; however, this study did not investigate the expression of SGLT1 in female arteries (Sabolić et al., 2006). SGLT2 and SMIT1 staining in both DM and PE females were more cytosolic than male mesenteric and coronary VSMCs. This granulated cytosolic staining indicates the potential of SGLT2 proteins to be stored in intracellular compartments and translocate to the membrane following different stimuli similar to GLUT4 (Ralston & Ploug, 1996). However, further investigation is needed to confirm this hypothesis.

The results from this chapter found that the CTCF of SMIT1 and the membrane abundance in both mesenteric and coronary VSMCs was significantly greater in DM females compared to PE female rats. A combination of a decrease in the interaction of SMIT1 with the forward trafficking molecular chaperone protein HSP90 and an increase in SMIT1 protein degradation by ubiquitin ligase could underpin this. This has been shown in renal and mesenteric arteries, whereby Kv7.4 channel expression and membrane abundance were greater in DM females than PE female rats. This led to an overall increase in mesenteric and renal Kv7.4 channel activity from DM female rats, which was not seen in PE females (Baldwin

et al., 2022). However, this oestrus cycle difference in SMIT1 could also be due to other post-transcriptional differences in DM and PE vascular smooth muscle cells.

3.4.3 | Limitations

The results from this chapter were mainly generated using qPCR, immunocytochemistry and immunohistochemistry, which all have many limitations. Quantitative PCR (qPCR) experiments revealed the expression of Slc5a1, Slc5a2, Slc5a3, and Slc5a11 in mesenteric, renal, coronary, and cerebral arteries from male rats. However, obtaining sufficient coronary and cerebral arterial tissue for qPCR analysis proved challenging. Specifically, cDNA from the septal artery and the right and left coronary arteries of three individual animals was required to perform a single qPCR replicate (N=1). Consequently, it was not feasible to compare Slc5 gene expression between the left and right coronary and septal arteries. Therefore, the results obtained can only give a rough insight into the Slc5 gene expression in these arteries. To mitigate this, immunocytochemistry and immunohistochemistry experiments were conducted to examine SGLT and SMIT protein expression within VSMCs. The SGLT2 (Francis et al., 2004; Freeman et al., 2006; Magen et al., 2005; Rahmoune et al., 2005) and SMIT1 (Barrese et al., 2020; Berry et al., 1995; Wiese et al., 1996; Yamauchi et al., 1998) antibodies used in this study have been used in many publications. However, validating antibodies using SMIT1 and SGLT2 plasmid transfection, followed by comparative staining of un-transfected and transfected HEK293 cells, encountered several challenges. Specifically, both plasmids required vector insertion and sequencing results revealed that the SMIT1 plasmid exhibited homology within the first 100 amino acids, while the SGLT2 plasmid showed no priming. Morpholino-targeted SMIT1 knockdown shown in Chapter 6 did demonstrate a decrease in SMIT1 immunohistochemistry staining compared to scrambled control morpholino. However, alternative validation methods could have included using antigenic peptides corresponding to the SGLT2 and SMIT1 protein regions to assess antibody specificity or further knockdown studies of SMIT1 and SGLT2 expression. Moreover, western blot experiments showed protein expression of SGLT2 in mesenteric, renal and coronary arteries, but this could not be carried out using the SMIT1 antibody. Confirming that further validation of the SGLT2 and SMIT1 antibodies would have significantly improved the validity of this study.

Comparing the total expression of SMIT1 and SGLT2 in different arteries from male, DM female, and PE female rats did have statistical limitations, and there were no measurements of how functionally active the transporter was. Consequently, although the total fluorescence intensity of SMIT1 and SGLT2 transporters may be elevated in male and DM female arteries, this does not necessarily correlate with functional activity. The membrane abundance line scan analysis of SMIT1 and SGLT2 protein expression also has limitations. This study compared SMIT1 and SGLT2 membrane abundance between mesenteric and coronary arteries in male, DM female, and PE female rats by using a line scan and plotting the expression of SMIT1 and SGLT2 relative to the membrane marker WGA. This method can show that a protein is expressed localised similarly to WGA around the edge of a cell. However, it is not easy to distinguish between proteins expressed in the membrane and proteins expressed just outside the membrane in the cytosol due to the method used to measure the degree of fluorescence across the cell. Further experiments, such as surface biotinylation, bottom-up or top-down mass spectroscopy, or high-throughput flow cytometry, could better validate the expression of SMIT1 and SGLT2 in the VSMC membrane. Therefore, while this study provides novel insights into the differential expression of SMIT1 and SGLT2 in various arterial beds of male and female rats, the inherent limitations must be acknowledged.

3.4.4 | Conclusion

The expression of solute transporters is ill-defined in the vasculature. This study sought to characterise the expression of SLC5 transporters in different arteries from male and female rats. It is the first to identify that mesenteric, renal, coronary, and cerebral vascular smooth muscle cells predominantly expressed splice variants of SGLT2 and not the full-length form as well as SMIT1 in male and female rats. SMIT1 protein was also identified in the endothelial cell layer of whole mesenteric, renal, and coronary arteries from male rats. These findings will improve our understanding of the roles of transporters in regulating vascular reactivity and enable potential new targets in cardiovascular disease.

Chapter 4: Investigating the role of sensory nerves in SGLT2 inhibitor-induced relaxation.

4.1 | Introduction

Sodium/glucose transporter 2 (SGLT2 or Slc5A2) inhibitors are effective medications for lowering blood glucose levels through increased urinary glucose excretion (Grempler et al., 2012; Preda et al., 2024; Wright, 2021). The National Institute for Health and Care Excellence (NICE) has approved using SGLT2 inhibitors as efficacious therapeutic agents for managing heart failure with reduced left ventricular ejection fraction and chronic kidney disease, independent of raised glucose levels (McMurray et al., 2019; Nassif et al., 2019; Wheeler et al., 2021). Beyond the observed reductions in cardiac fluid retention, reactive oxygen species production, and mitigation of fibrosis (Preda et al., 2024), the cardioprotective benefits of SGLT2 inhibitors are also associated with a decrease in blood pressure by approximately 4 mmHg. However, the mechanism underlining this effect is unknown. SGLT2 inhibitors can promote glucosuria and natriuresis, leading to decreased circulatory volume, and, this blood pressure-lowering effect persists even under diminished glomerular filtration rates (Beal et al., 2023) . Therefore, another mode of action for these inhibitors is regulating blood pressure. Previous ex vivo studies showed that empagliflozin and dapagliflozin relaxed rabbit aortic rings, rat mesenteric arteries and rat left anterior descending coronary artery, but the underlying mechanisms were ill-defined and often contradictory. In rabbit aortic rings dapagliflozin- and empagliflozin-mediated relaxations were impaired by protein kinase G inhibitors and the non-specific Kv channel blocker 4-

aminopyridine (Li et al., 2018; Seo et al., 2020) but specific blockers of Kv subfamilies (Kv1.5, Kv2.1 and Kv7s) did not impair relaxations. In contrast, dapagliflozin, empagliflozin and canagliflozin relaxed mesenteric resistance arteries in an endothelium-independent manner that was suppressed, in part, by blockers of Kv1.5 and Kv7 potassium channels without an effect on protein kinase G (Hasan, Menon, et al., 2022; Hasan, Zerin, et al., 2022; Hasan & Hasan, 2021). In left anterior descending coronary arteries (LAD) from male Sprague Dawley rats, dapagliflozin only produced a significant relaxation at 500 μM that was endothelium-independent and not affected by a range of potassium channel blockers (Choi et al., 2023).

Peptidergic sensory nerves richly innervate the resistance arteries that dictate blood pressure (Kawasaki et al., 1988; Aalkjaer et al., 2021). The release of calcitonin gene-related peptide (CGRP) from these sensory nerves evokes vasodilation in many arteries (Brain et al., 1985; Ralevic et al., 2000; Shiraki et al., 2000). The specific impacts of SGLT2 inhibitors on arteries show some parallels with the vasodilatory effects induced by CGRP; for example, both relaxations were attenuated in the presence of pan-Kv7 channel blocker linopirdine(Hasan, Menon, et al., 2022; Hasan & Hasan, 2021; Stott et al., 2018). Kv7 channels are known downstream mediators of CGRP signalling (Chadha et al., 2014; Stott et al., 2018; Van Der Horst et al., 2020), and CGRP has been shown to increase NO production. CGRP serum levels are found to decrease in cardiovascular disease, and CGRP administration to hypertensive and heart failure patients improves patient outcomes (Taquet et al 1992 and Shekhar et al 1991). Hence, CGRP could protect the vasculature and myocardium against cardiovascular dysfunction, particularly heart failure and suggests a potential overlap in the mechanistic pathways of these two entities in modulating vascular tone. We hypothesise that SGLT2 inhibitors evoke relaxation by activating Kv7 channels and CGRP release. Therefore, this study sought to investigate:

1. If SGLT2 inhibitors directly activated Kv7 channels to evoke relaxation
2. If CGRP release is involved in the relaxations produced by SGLT2 inhibitors
3. How SGLT2 inhibitors drive CGRP release

4.2 | Methods

All aspects of the experiments carried out in this chapter are described in detail in Chapter 2. Kaitlyn Redford and Geoffrey Abbot (University of California, Irvine) provided data gathered from electrophysiological studies on Xenopus Oocytes expressing Kv7 channels. Voltage clamp data on HEK-293 cells expressing TRPV1 was produced by Miguel Benítez-Angeles and Tamara Rosenbaum at the Instituto de Fisiología Celular, Universidad Nacional Autónoma de México.

4.2.1 | Cell Cultures

HEK293 cells (ATCC® CRL-1573) were cultured in a complete growth medium containing Dulbecco's modified Eagle's medium with high-glucose (DMEM GibcoTM) complemented with 10% fetal bovine serum (HyCloneTM) and 100 U/ml of Penicillin-Streptomycin (GibcoTM). Cell cultures were maintained in a humidified incubator at 37°C with an atmosphere of 95% of air and 5% of CO2. Cells were subcultured every three days using 0.25% (w/V) Trypsin-EDTA solution (GibcoTM).

4.2.2 | Electrophysiology

The effect of various SGLT2 inhibitors was assessed on currents generated by the over-expression of Kv7 and TRPV1 genes in Xenopus laevis oocytes and HEK293 cells, respectively.

4.2.2.1 | Channel subunit cRNA preparation and Xenopus laevis oocyte injection.

cRNA transcripts encoding human Kv7.4, Kv7.5 and KCNE4 we generated by in vitro transcription using the message mMachine kit (Thermo Fisher Scientific, Waltham, MA, USA) according to manufacturer's instructions, after vector linearisation, from cDNA sub-cloned into expression vectors (pTLNx and pXOOM) incorporating Xenopus laevis β-globin 5' and 3' UTRs flanking the coding region to enhance translation and cRNA stability. Defolliculated stage V and VI Xenopus laevis oocytes (Xenoocyte, Dexter, MI, USA) were injected with Kv7 and KCNE4 cRNAs (2-10 ng) and incubated the oocytes at 16 °C in ND96 oocyte storage solution containing penicillin and streptomycin, with daily washing, for 2-5 days before two-electrode voltage-clamp (TEVC) recording.

4.2.3 | Two-electrode voltage clamp (TEVC)

TEVC was performed at room temperature using an OC-725C amplifier (Warner Instruments, Hamden, CT, USA) and pClamp10 software (Molecular Devices, Sunnyvale, CA, USA) 2-5 days after cRNA injection. Oocytes were placed in a small-volume oocyte bath (Warner) and viewed with a dissection microscope for cellular electrophysiology. Chemicals were sourced from Sigma-Aldrich (St. Louis, MO, USA). SGLT2 inhibitors were solubilised in bath solution (in mM): 96 NaCl, 4 KCl, 1 MgCl2, 1 CaCl2, 10 HEPES (pH 7.6). Compounds were introduced into the oocyte recording bath by gravity perfusion at a constant flow of 1 ml per minute for 3 minutes before recording. Pipettes were of 1-2 MΩ resistance when filled with 3 M KCl. Currents were recorded in response to voltage pulses between -80 mV and +40 mV at 20 mV intervals from a holding potential of -80 mV, to yield current-voltage relationships. Data were analyzed using Clampfit (Molecular Devices) and Graphpad Prism software (GraphPad, San Diego, CA, USA), stating values as mean ± SEM. Raw tail currents were plotted versus prepulse voltage and fitted with a single Boltzmann function:

Eq. 1:

$$g = \frac{(A_1 - A_2)}{\left\{1 + exp\,[V_{\frac{1}{2}} - V/Vs]\right\} y + A_2}$$

where g is the normalized tail conductance, A1 is the initial value at -∞, A2 is the final value at +∞, V1/2 is the half-maximal voltage of activation and Vs the slope factor.

4.2.4 | Transient cell transfection and patch-clamp

HEK-293 cells were seeded on poly-D-lysine (1 mg/ml, Sigma) coated coverslips for patch-clamp experiments. After 24 hrs, HEK293 cells were transfected with plasmids pcDNA3.1 containing the rat wild-type TRPV1 channel (1.5 µg) and pcDNA3.1 with green fluorescent protein (GFP, 500 ng) to identify successfully transfected cells using jetPEI™ Polyplus transfection reagent, per manufacturer's instructions.

TRPV1 currents were recorded from transiently transfected HEK-293 using the patch-clamp technique in the outside-out configuration (Hamill et al., 1981). Solutions were changed with an RSC-200 rapid solution changer (Molecular Kinetics). Currents were low-pass filtered at 2 kHz and sampled at 10 kHz with an EPC 10 amplifier (HEKA Elektronik) and were plotted and analysed with Igor Pro (Wavemetrics Inc.). Intracellular and extracellular recording solutions comprised of (in mM): 130 NaCl, 3 HEPES (pH 7.2) and 1 EDTA for experiments at pH 7.2 and HEPES was replaced by3 mM MES for experiments were TRPV1 was activated by pH 6. The capsaicin stock was prepared at 10 mM in absolute ethanol and then diluted to 250 nM in recording solution. Experiments were performed at room temperature (24 °C) and mean current values were measured after channel activation had reached the steady state. Pipettes were fabricated with borosilicate glass and had a resistance of 5 MΩ.

Currents were obtained using voltage protocols where the holding potential was 0 mV and then stepped from -120 to 120 mV for 100 ms using a square voltage protocol. Briefly, leak currents were obtained in the absence of agonists or dapagliflozin and then excised membrane patches containing TRPV1 channels were exposed to DAPA, capsaicin, capsaicin + dapagliflozin, pH 6 or pH 6 + dapagliflozin. All currents were leak-subtracted and normalized to currents activated either by capsaicin or pH alone.

4.3 | Results

4.3.1 | Characteristics of vasoconstrictor-induced contractions in mesenteric, renal and coronary arteries.

Two distinct myography protocols were used when exploring a potential vasorelaxant. The agent can either be administered to a contracted vessel, with subsequent recording of the percentage relaxation, or the vessel can be pre-incubated with the vasorelaxant drug, followed by recording the alteration in response to a contractile agent. Initial experiments were conducted to characterise the contractile reagents utilised in this investigation.

Mesenteric arteries were set to a resting basal tone until provoked via cumulative application of methoxamine, an alpha 1 adrenoreceptor agonist, or U46619, a thromboxane A2 receptor agonist from 1nM-30μM (figure 4.1). Both methoxamine and U46619 produced concentration-dependent contractions in mesenteric arteries with an EC50 value of 988.5±1.8 nM and 84.7±2.4 nM, respectively.

The response to methoxamine was completely ablated in the presence of an alpha-1 adrenoreceptor blocker, prazosin (100nM). Similarly, the response to U46619 was completely abolished in the presence of a thromboxane A2 antagonist, ICI192605 (1μM). Post application of either 300nM U46619 or 10μM methoxamine was added to the vessel to demonstrate the blocker specificity. figures 4.1 and 4.2 show the representative traces and mean data of methoxamine and U4619 curves in the presence and absence of their respective pharmacological blockers. The following experiments used EC80 concentrations of these vasocontractile agents of 10μM methoxamine and 300nM U46619.

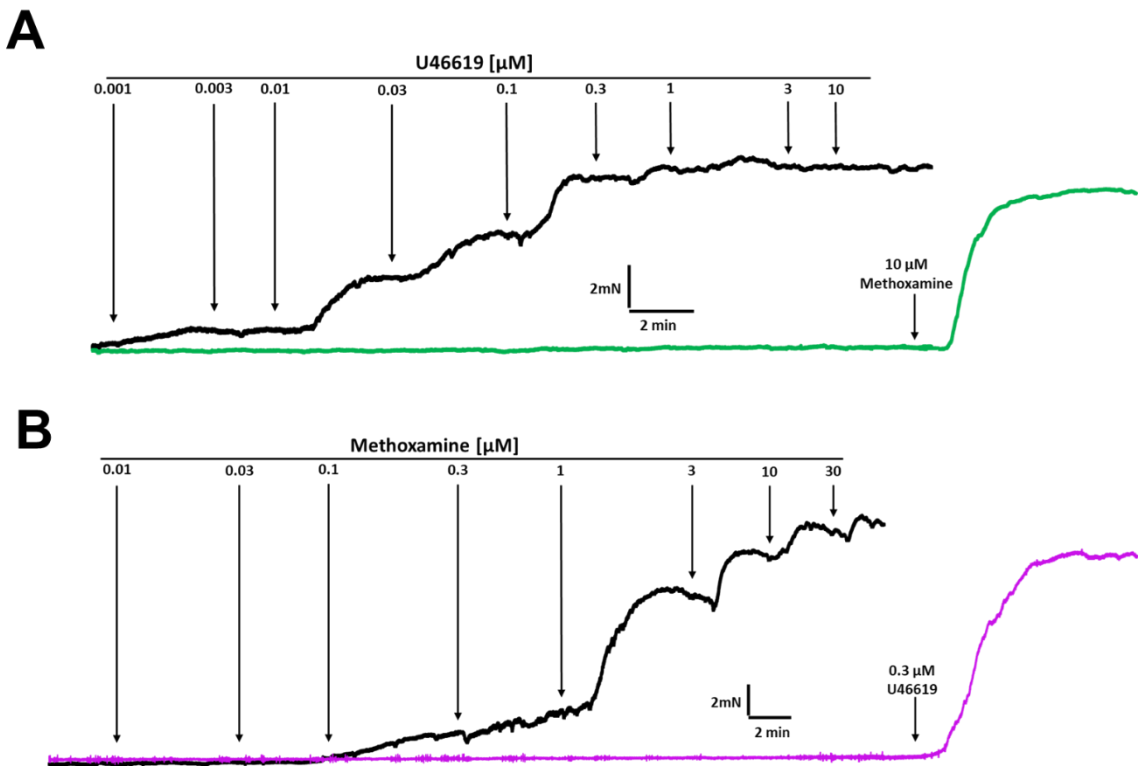


Figure 4.1: Representative traces of U46619 and methoxamine curves in the presence and absence of their respective blockers.
A- Representative trace of a concentration effect curve to U46619 in the presence (purple) and absence (black) of 1µM ICI192605. B- Representative trace of a concentration effect curve to methoxamine in the presence (green) and absence (black) of 100nM prazosin. Post-application of U46619 and methoxamine shows the blocking specificity of the drugs.

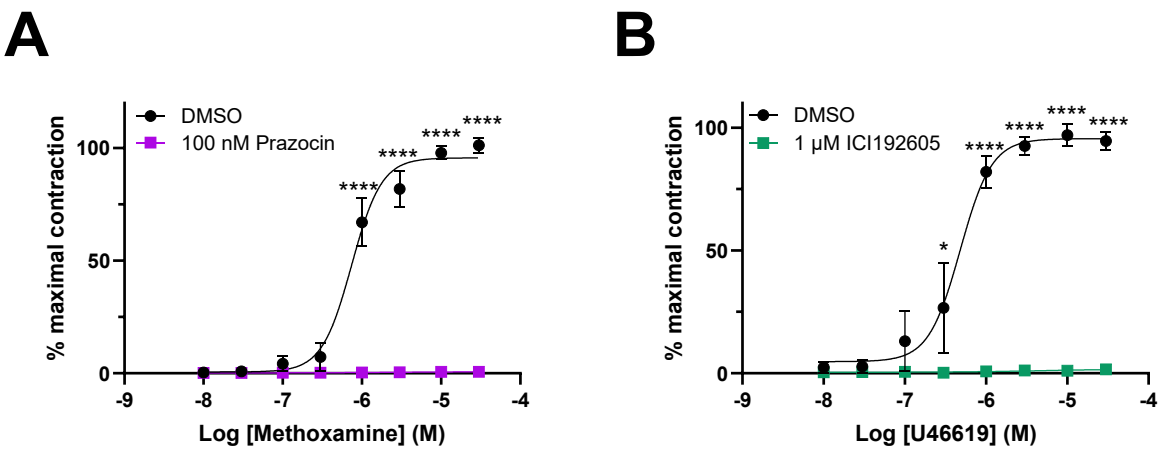


*Figure 4.2: Mean effect of prazosin and ICI192605 on vasocontractile agents: The mean effect of methoxamine in the presence (purple) and absence (black) of 100nM prazosin (A, N=8) and the mean effect of U46619 in the presence (green) and absence (black) of 1µM ICI192605 (B, N=7). Each point is the mean contractile tone, with error bars depicting the SEM. P values are calculated by a 2-way ANOVA with a Bonferroni post-Hoc test for multiple comparisons (*P<0.005, ****P<0.0001).*

4.3.2 | Effect of methoxamine and U46619 in coronary arteries.

The effect of methoxamine and U46619-induced contractions were compared in left anterior descending arteries. Methoxamine and U46619 were applied to the left anterior descending arteries (LAD) at resting basal tone from 10nM to 30µM, and the contractile response was recorded. Cumulative application of U46619 produced stable concentration-dependent contractions shown by an upward deflection in the trace (figure 4.3 A-B), whereas coronary arteries were less sensitive to methoxamine and produced smaller contractions (figure 4.3 C-D). Hence, U46619 was used for subsequent coronary artery experiments.

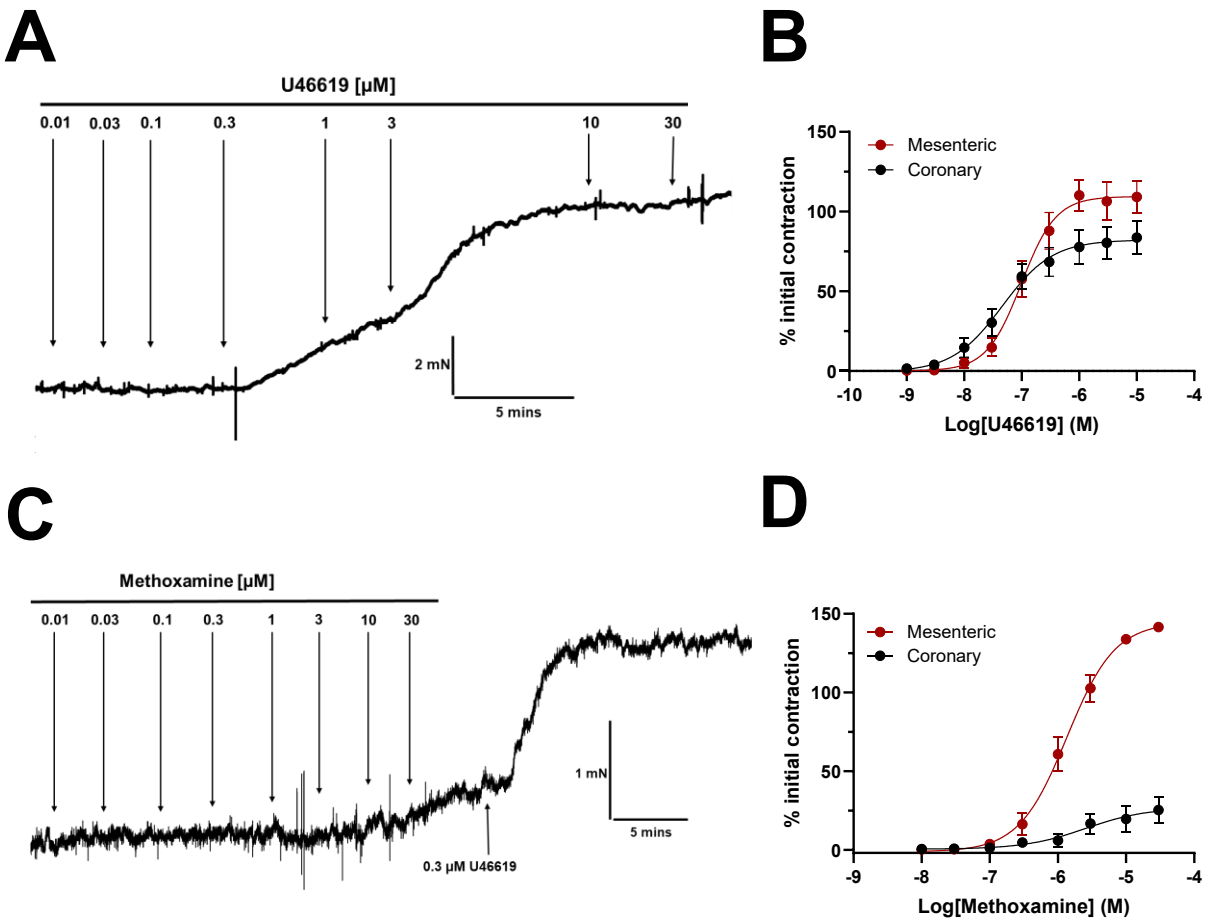


Figure 4.3: Effect of methoxamine and U46619 on coronary arteries.
A representative trace showing the response to cumulative application of alpha 1 adrenoreceptor agonist methoxamine (10nM - 30µM) followed by application of 300nM U46619 in coronary arteries (A). The mean effect of methoxamine is shown in panel B (N=5). A representative trace showing the response to U46619 from 10nM - 30µM (C) and the mean effect of U46619 is shown in panel D (N=6). All values are expressed as mean +- SEM denoted by the error bars, N= number of animals.

4.3.3 | The vasoconstrictor responses in mesenteric, renal, septal and LAD arteries.

Mesenteric, renal, and coronary arteries were normalised and set to a transmural pressure of 13.3kPa, while septal arteries, due to their size, were normalised to a target pressure of 10.7kPa. This normalisation produced a resting basal tone for each arterial bed, with renal arteries having the highest resting basal tone, as shown in figure 4.4. Vasoconstrictor responses to methoxamine and U46619 differed between mesenteric, renal, septal and LAD arterial beds. The peak

contraction (mN) to KCl, methoxamine and U46619 were similar in mesenteric and renal arteries, with slight variation between arterial segments. However, comparably smaller contractions were seen in both septal and LAD coronary arteries (figure 4.5). Mesenteric, septal and LAD arteries had similar sensitivities to the application of U46619. However, the sensitivity to the application of methoxamine was slightly different between all artery types, with renal arteries having the highest EC_{50} of 2751.7±0.01 nM and mesenteric arteries having the lowest at 988.5±1.8 nM. Table 5.1 summarises methoxamine and U46619-induced contraction data across all vessels.

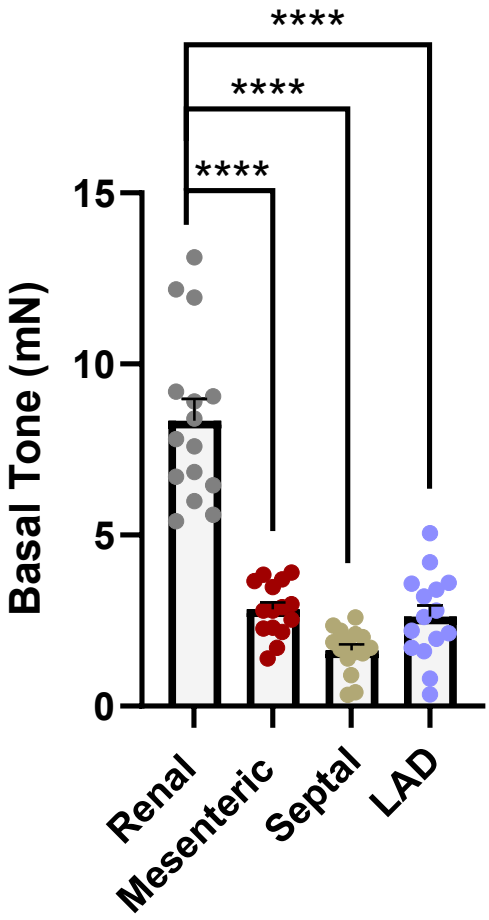


Figure 4.4: Comparison of the resting basal tone of mesenteric, renal, septal and left anterior descending artery.
*The mean resting basal tone (mN) of renal (grey), mesenteric (red), septal (beige) and left anterior descending (LAD, purple) arteries. All values are expressed as mean +- SEM, with N=15 denoted by the error bars, N= number of animals. P values are calculated by a one-way ANOVA (****P<0.0001).*

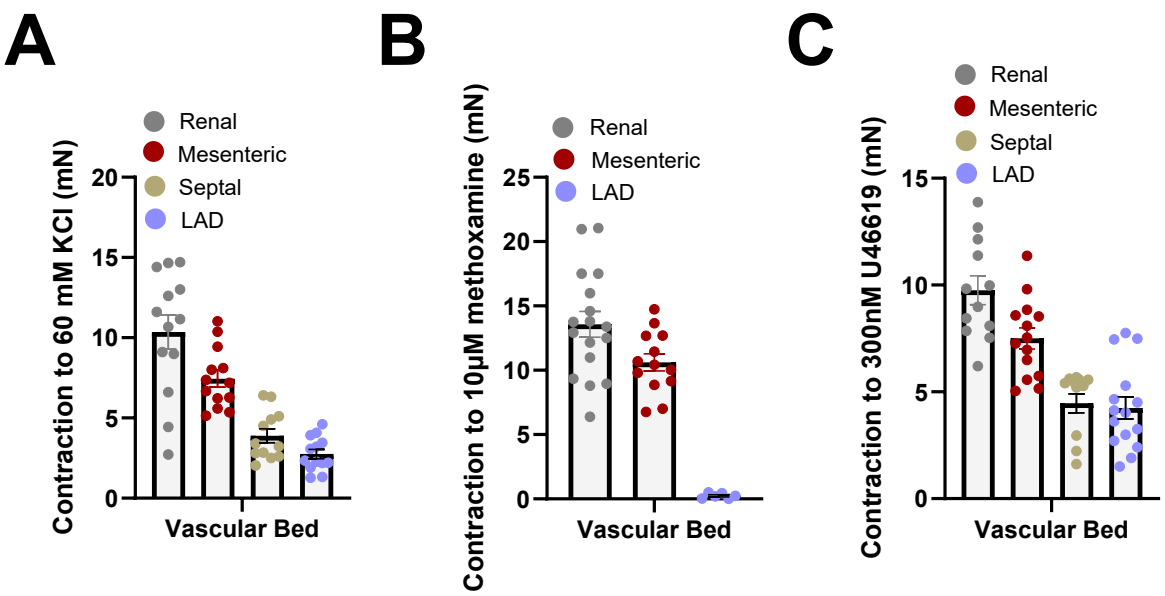


Figure 4.5: Comparison of mesenteric, renal, septal and LAD arterial contractions (mN).
The mean contraction in mN to 60mM KCl (A), methoxamine (B) and U46619 (C) in renal (grey, N=14-17), mesenteric (red, N=14), septal (beige, N=12) and left anterior descending (LED, purple, N=16) arteries. All values are expressed as mean +- SEM, with N=15 denoted by the error bars, N= number of animals.

Table 4.1 - Summary of vasoconstrictor responses in all arteries tested in myograph experiments.

Artery	Average methoxamine peak contraction (mN ±SEM)	Methoxamine EC50 (nM±SEM)	Average U46619 peak contraction (mN ±SEM)	U46619 EC50 (nM±SEM)	Average KCl peak contraction (mN ±SEM)
Mesenteric	10.6±0.7	988.5±1.8	6.9±0.8	84.7±2.4	7.4±0.5
Renal	13.1±1.2	2751.7±0.01	9.3±1.04	-	10.4±1.1
LAD	0.12±0.05	2364.7±0.01	4.3±0.5	72.7±0.02	2.8±0.3
Septal	-	-	4.5±0.5	-	3.9±0.4

4.3.4 | SGLT2 inhibitors relax mesenteric arteries in an endothelium-independent manner.

The vasorelaxant effect of 3 structurally different SGLT2 inhibitors (dapagliflozin, ertugliflozin and empagliflozin) and one SGLT1 inhibitor (mizagliflozin) was determined in second-order mesenteric arteries. Initial investigations focused on the cumulative application of dapagliflozin from 1μM-100μM, which produced a concentration-dependent relaxation represented by a downward deflection in the representative trace shown in figure 4.6. figure 4.6B shows the maximal inhibition was 60.27±4.9% and the approximate IC50 value was 9.5 μM. A vehicle control was produced to demonstrate the stable and sustained contraction to 10 μM methoxamine by applying DMSO at each interval.

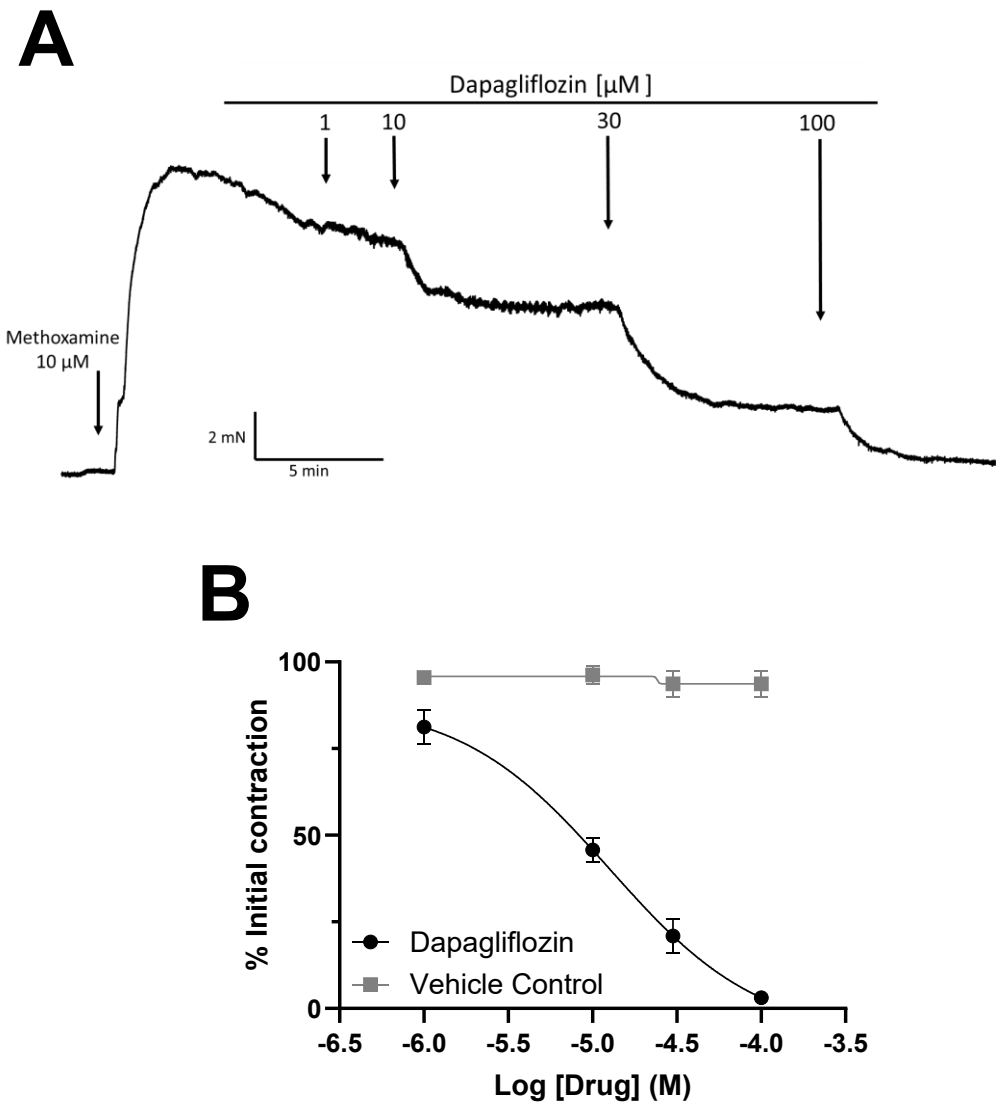


Figure 4.6: The effect of dapagliflozin on pre-contracted mesenteric arteries.
A representative trace showing the relaxation to dapagliflozin (1μM-30μM) in mesenteric arteries pre-contracted with 10μM methoxamine (A). The mean

response to dapagliflozin (black) is show in panel B with vehicle control (DMSO) in grey (N=6). All values are expressed as mean +- SEM denoted by the error bars, N= number of animals.

Cumulative application (1μM- 100μM) of empagliflozin, ertugliflozin and mizagliflozin also produced concentration-dependent relaxations with approximate IC50 values of 7.3 μM, 9.5 μM and 5.52 μM, respectively (figure 4.7; N=5). The vascular smooth muscle endothelium produces several vasoactive hormones acting as a key regulator of vascular homeostasis. Nitric oxide and prostacyclin are the main endothelial-derived relaxing factors. To identify if the relaxation produced by SGLT2 inhibitors was dependent on the presence of endothelium, the endothelium was denuded and the percentage relaxation produced by dapagliflozin and empagliflozin was determined. There was no significant difference between the relaxation produced by 30μM dapagliflozin and empagliflozin in endothelium intact and denuded mesenteric arteries as determined by the relaxant response to 10μM carbachol (figure 4.8). Hence, the relaxation evoked by each SGLT inhibitor was not dependent upon functional endothelium.

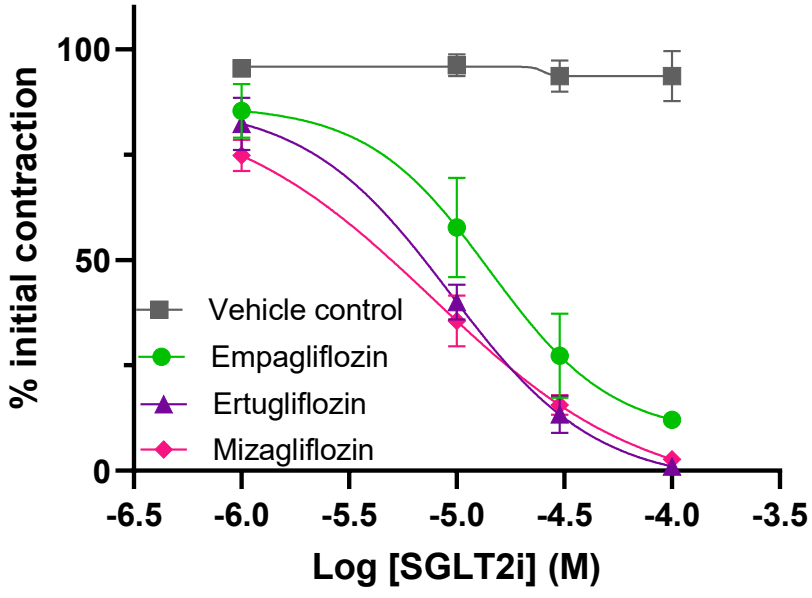


Figure 4.7: The effect of 2 structurally different SGLT2 inhibitors and one SGLT1 inhibitor on mesenteric arteries pre-contracted with 10 μM methoxamine.
The mean effect of empagliflozin (Green), ertugliflozin (purple), mizagliflozin (pink) with mean vehicle control in grey, N=5-6. All values are expressed as mean +- SEM denoted by the error bars, N= number of animals.

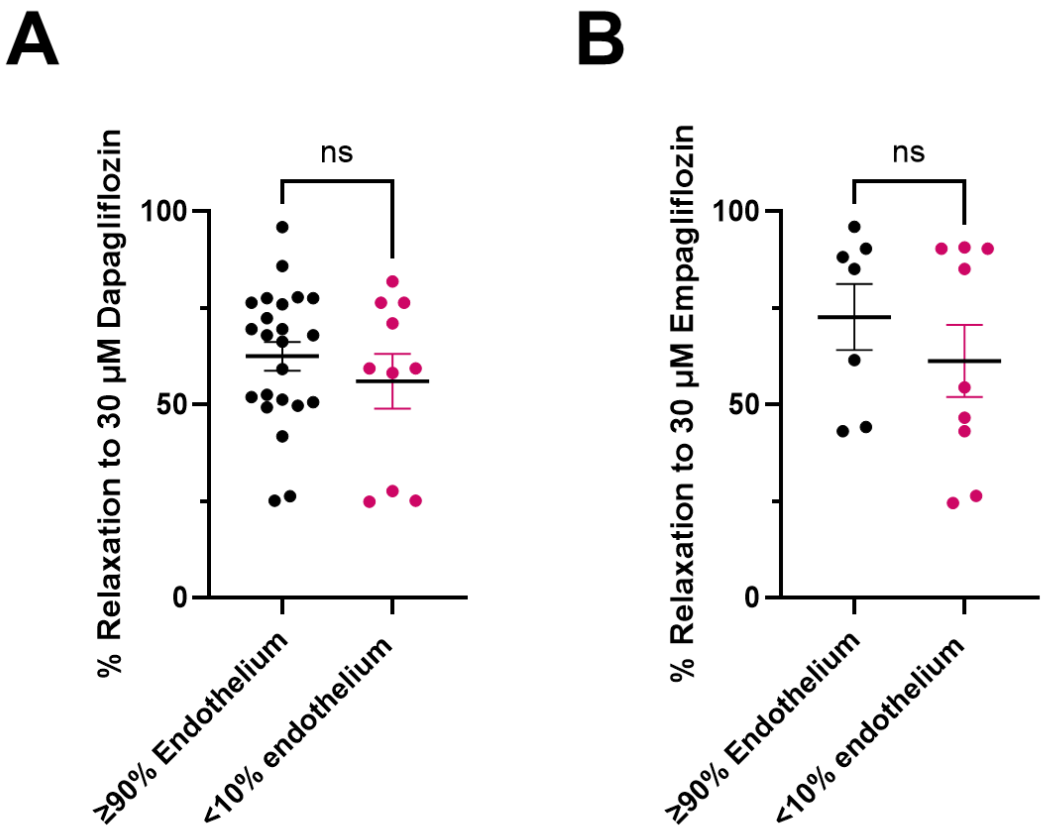


Figure 4.8: Lack of correlation between SGLT2 inhibitor and carbachol response in mesenteric arteries.
The percentage relaxation to 30uM dapagliflozin (A, N=30) and empagliflozin (B, N=16) in mesenteric arteries pre-contracted with 10µM methoxamine in > 90% endothelium and <10% endothelium. All values are expressed as mean +- SEM denoted by the error bars, N= number of animals.

4.3.5 | Effect of SGLT2 inhibitors in renal and septal arteries.

The effect of dapagliflozin and empagliflozin was compared in different arterial beds to see if the evoked relaxation was vascular bed-specific. Functional experiments revealed dapagliflozin and empagliflozin were mild relaxants of renal arteries (figure 4.9A-B), producing 28.3±7.1% and 19.4±6.9% at 30µM, respectively. Comparatively, dapagliflozin and empagliflozin were ineffective at relaxing septal arteries (figure 4.9C-D), whereby empagliflozin could only produce a maximum of 2.3±1.2% relaxation at 30µM and 10±2.3% relaxation at 100µM.

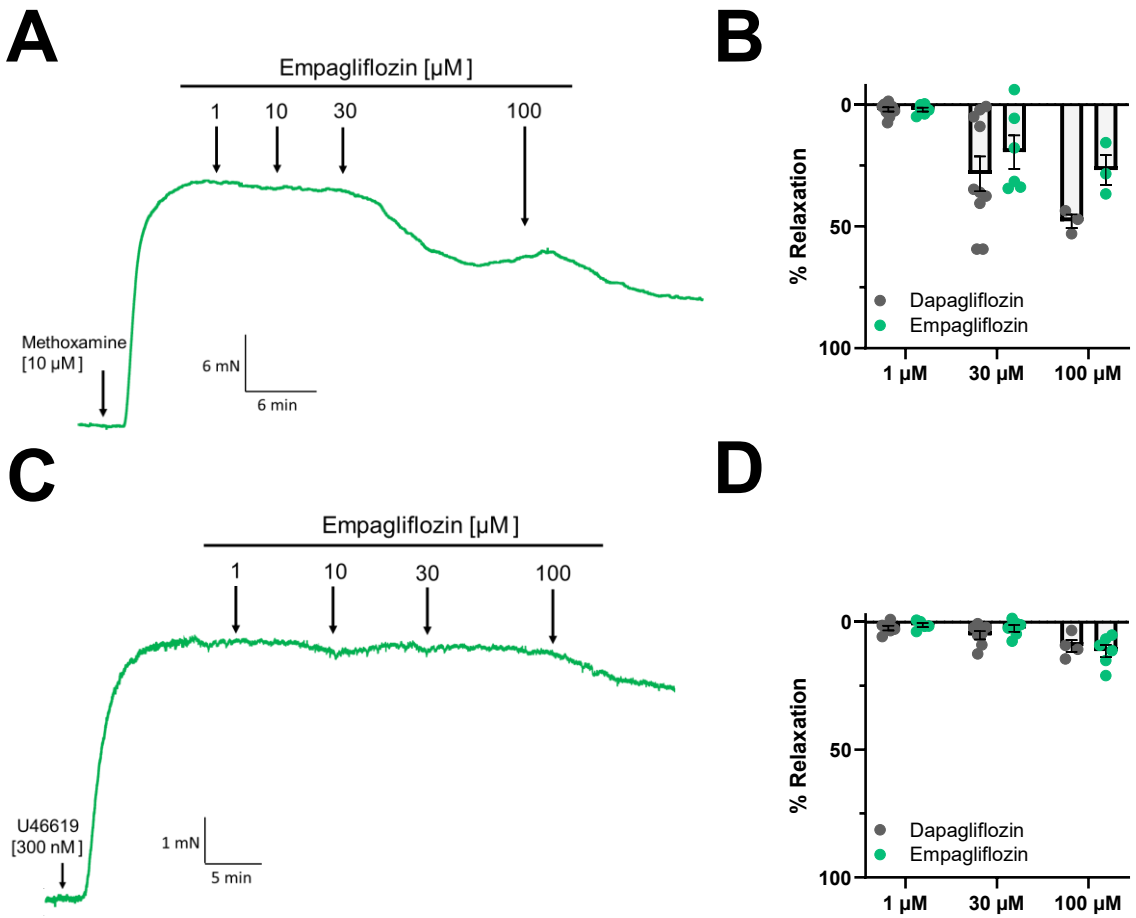


Figure 4.9: The effect of dapagliflozin and empagliflozin on renal and septal arteries.
A representative trace showing the effect of empagliflozin on pre-contracted renal arteries (A) with mean response to dapagliflozin and empagliflozin is shown in panel B (N=10). A representative trace showing the effect of empagliflozin in septal arteries (C) with mean response to dapagliflozin and empagliflozin is shown in panel D (N=5). All values are expressed as mean +- SEM denoted by the error bars, N= number of animals.

4.3.6 | Comparing the effect of dapagliflozin and empagliflozin in mesenteric, renal and septal arteries

The effect of 1μM —100μM of dapagliflozin and empagliflozin on mesenteric, renal, and septal arteries was compared. Mesenteric arteries exhibited significantly greater relaxation in response to both drugs compared to renal and septal arteries. At a concentration of 100μM, dapagliflozin induced a robust relaxation of 91.2% ±

2.4%, while empagliflozin produced a relaxation of 84.8% ± 2.3% in mesenteric arteries. Conversely, application of these drugs in renal arteries resulted in mild relaxation (45.8% ± 3% for dapagliflozin and 25.1% ± 3.2% for empagliflozin), while septal arteries did not respond to either drug (figure 4.10).

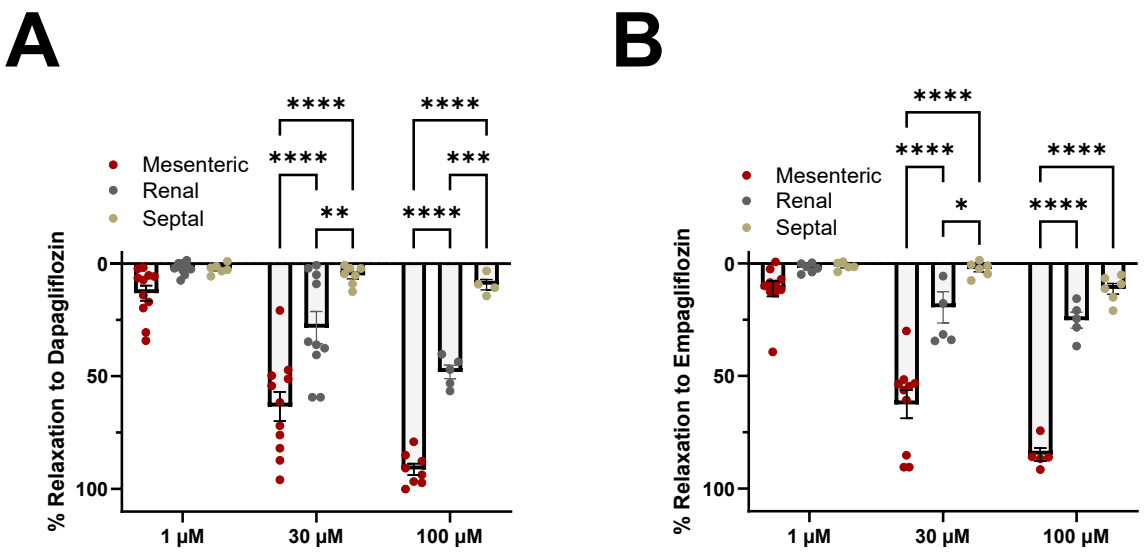


Figure 4.10: Comparison of the relaxation to dapagliflozin and empagliflozin in mesenteric and renal arteries pre-contracted with 10µM methoxamine.
*The mean relaxation to 1µM, 30µM and 100 µM dapagliflozin (A, N= 5-10) and empagliflozin (B, N= 5-6) in renal (grey), mesenteric (red) and septal (beige) arteries. All values are shown as mean +- SEM error bars. A 2-way ANOVA with post-hoc Sidack test was used to calculate significance values, where ****= P<0.0001, (N= Number of animals).*

4.3.7 | Characterising the expression of Kv7 ion channels in mesenteric and renal arteries

Previous literature has implicated voltage-gated potassium channels (Kv7) encoded by *KCNQ* genes and other Kv channels in the relaxant response to SGLT2 inhibitors in mesenteric arteries from male rats and rabbit aortic rings (Hasan, Menon, et al., 2022; Hasan & Hasan, 2021; Li et al., 2018; Seo et al., 2020). RT-QPCR experiments found that mesenteric, renal, coronary and cerebral

arteries had the highest transcript abundance of Kcnq4 and Kcnq5, encoding for Kv7.4 and Kv7.5, followed by Kcnq1 encoding Kv7.1 (figure 4.11).

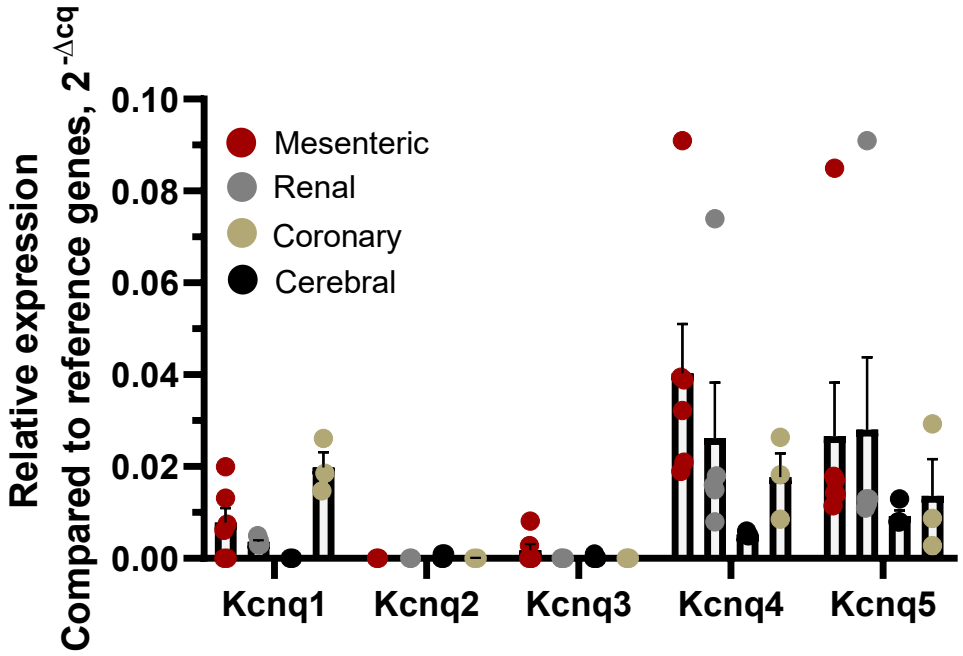


Figure 4.11: Expression of Kcnq1-5 in mesenteric and renal arteries.
QPCR relative transcript abundance of Kcnq1-5 genes in mesenteric (red), renal (grey), coronary (beige) and cerebral (black) arteries (N=6). All data values are shown as mean ±SEM, denoted by error bars (N = number of animals).

4.3.8 | Characterising Kv7 channel blockers in mesenteric and renal arteries

To ascertain a role for Kv7 channels in the relaxant responses, we observed experiments were performed with the pan Kv7 channel blocker linopirdine. To validate the use of this agent we investigated the effect of linopirdine on relaxations produced by the Kv7.2-7.5 channel activator, ML213. ML213 produced a concentration-dependent relaxation in both mesenteric and renal arteries, but ML213 was more effective in mesenteric arteries compared to renal arteries ($P<0.0001$), as shown in figure 4.12. These relaxations were completely ablated in the presence of 10uM linopirdine (figure 4.13). Demonstrating ML213 mediated relaxation works through linopirdine-sensitive mechanisms.

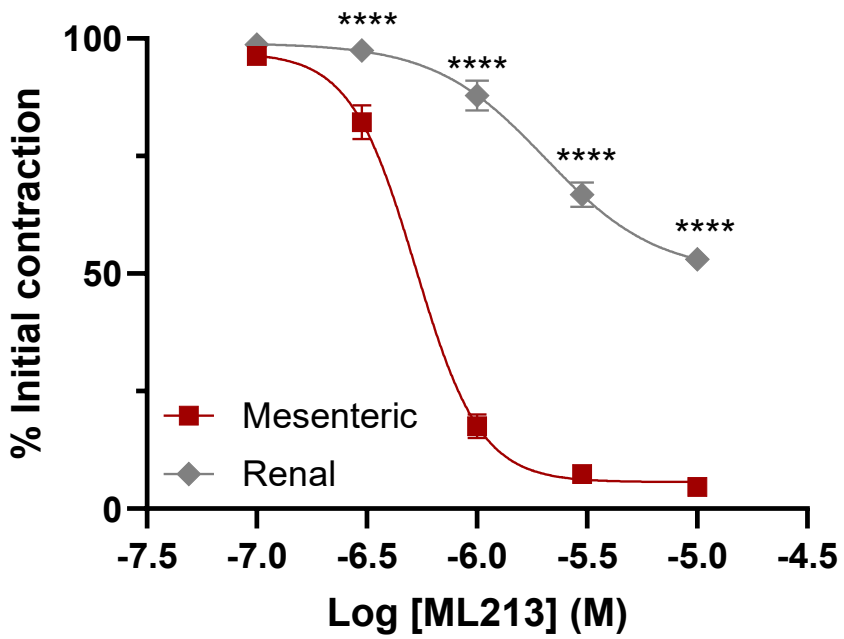


Figure 4.12: The relaxation to Pan Kv7 channel activator ML213.
*The relaxation to cumulative application of pan Kv7 channel activator, ML213 (100nM - 10μM) in mesenteric (red) and renal arteries (grey) pre-contracted with 10μM methoxamine (N=6). All values are expressed as mean±SEM. A two-way ANOVA with a post-hoc Bonferoni test was used to generate significant values (****= P<0.0001). (N=) number of animals used.*

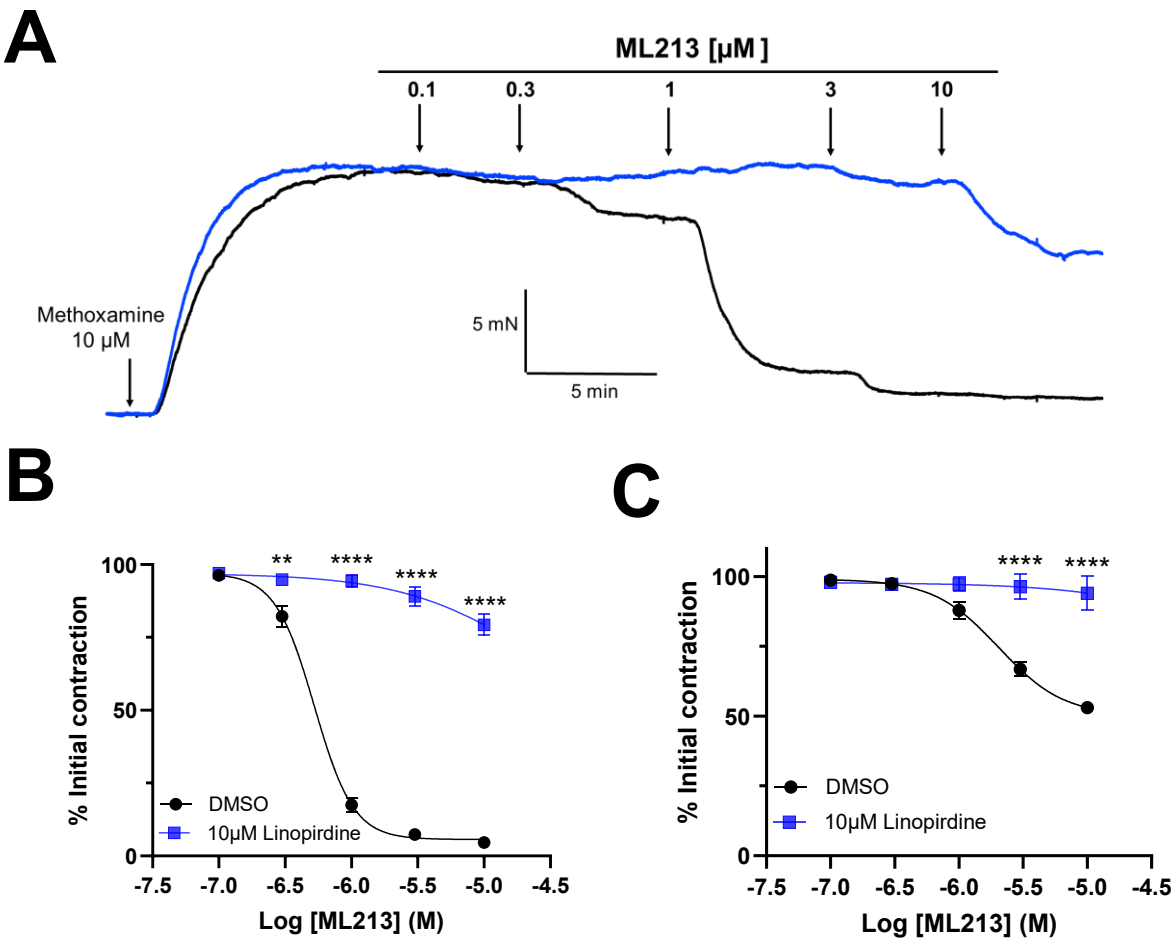


*Figure 4.13: Effect of linopirdine on the relaxant action of Kv7 activator ML213. Representative trace showing the effect of ML213 (100nM - 10µM) in mesenteric arteries pre-contracted with 10 µM methoxamine in the presence (blue) and absence (black) of 10µM linopirdine (A). The mean response to ML213 in mesenteric arteries pre-incubated with either DMSO or 10µM linopirdine is shown in panel B (N=6). The mean response to ML213 in pre-contracted renal arteries in the presence (blue) and absence (black) of 10µM linopirdine is shown in panel C (N=5). All values are expressed as mean±SEM. A two-way ANOVA with a post-hoc bonferoni test was used to generate significant values (** =P<0.01, ****= P<0.0001). (N=) number of animals used.*

4.3.9 | The role of Kv7 channels in SGLT2 inhibitor induced relaxations.

Functional experiments were conducted looking at the relaxant response to SGLT2 inhibitors in the presence and absence of 10 μM linopirdine, the pan-Kv7 blocker (Wang et al.,2000). The relaxation produced by dapagliflozin, empagliflozin and ertugliflozin in mesenteric arteries was attenuated significantly by pre-incubation with the linopirdine (10μM) when compared to DMSO control (figure 4.14; n=5-6). In contrast, the small relaxations produced by empagliflozin and dapagliflozin in renal arteries were unaffected by linopirdine (figure 4.15; N=7-12). Specific blockers of Kv7.1 (HMR1556), BK_{Ca} (iberiotoxin), K_{ATP} (glibenclamide) and the non-selective Kvchannel blockers 4-AP and TEA did not affect relaxations produced by SGLT2 inhibitors in mesenteric arteries as shown in figure 4.16 (N=7).

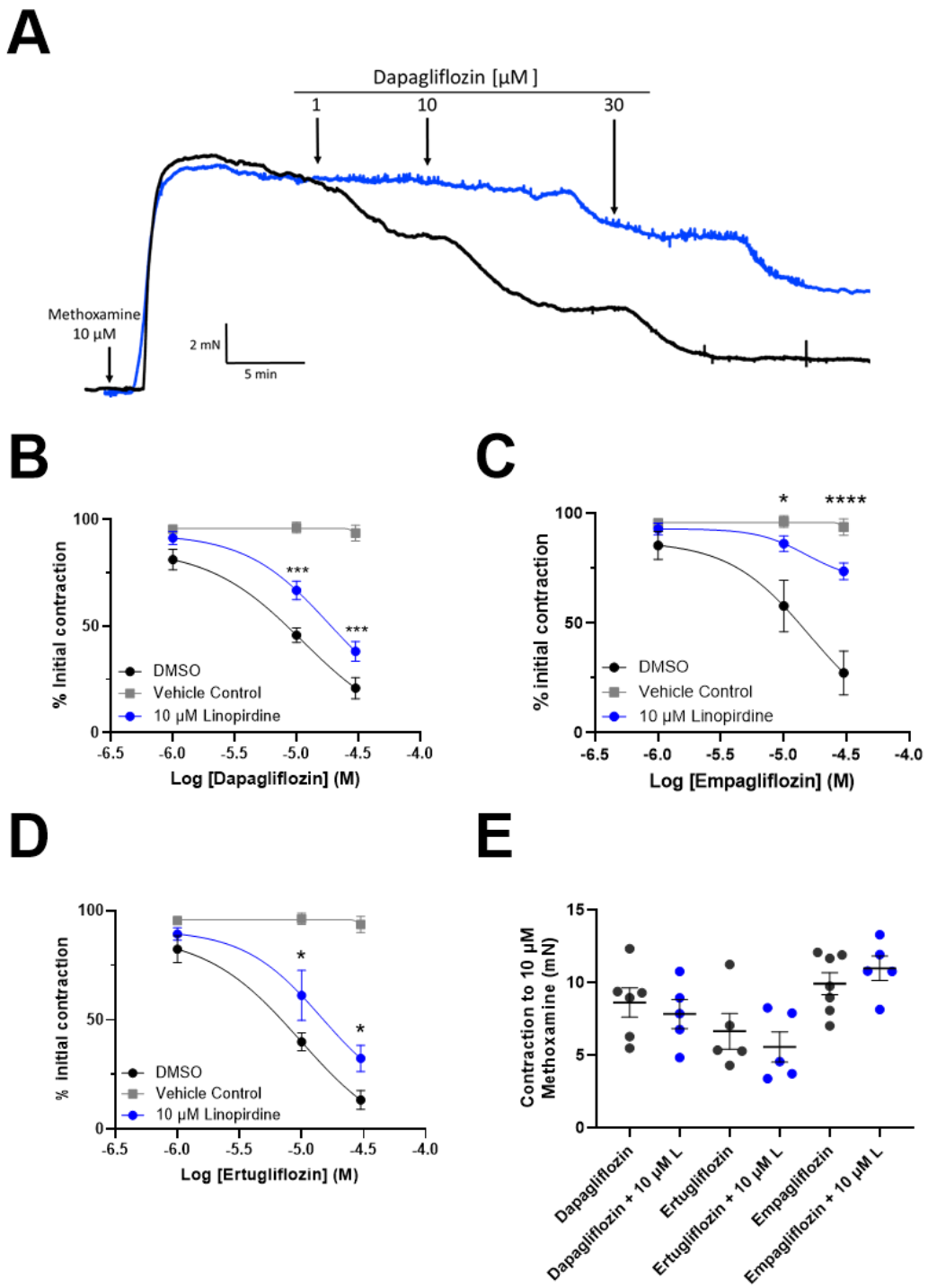


Figure 4.14: The effect of a pan Kv7 channel blocker linopirdine on SGLT2 inhibitor-induced relaxation:

A representative trace showing dapagliflozin-induced relaxation in mesenteric arteries pre-incubated in DMSO control (black) and 10µM linopirdine (blue)(A). The mean response to dapagliflozin (B, N=6), empagliflozin (C, N=5) and ertugliflozin (D, N=5) in mesenteric arteries pre-incubated with either DMSO (black) or 10µM linopirdine (blue). Vehicle control is shown in grey. The mean amplitude of the contraction produced by 10µM methoxamine under different conditions (E). All values are expressed as mean±SEM. A two-way ANOVA with a post-hoc bonferoni test was used to generate significant values (= P<0.05, ** = P<0.01, ***= P<0.001). (N=) number of animals used.*

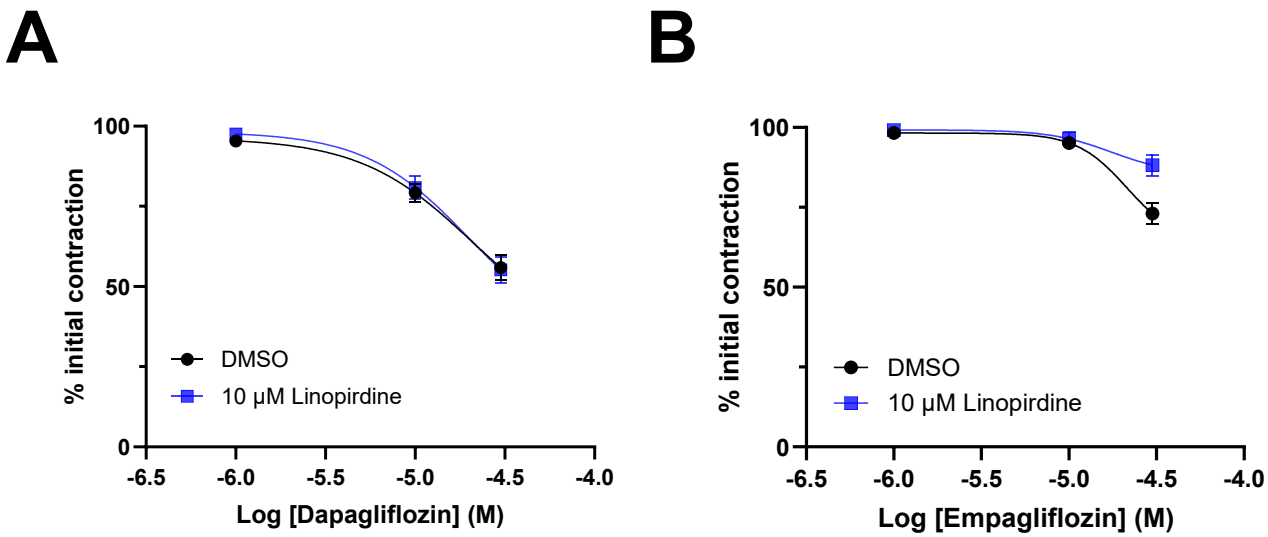


Figure 4.15: SGLT2 inhibitor-induced relaxation in renal arteries is not linopirdine sensitive.
The mean response to dapagliflozin (A, N=10) and empagliflozin (B, N=7) in renal arteries in the presence (blue) and absence (black) of 10μM linopirdine. All values are expressed as mean ±SEM, where (N=) number of animals used.

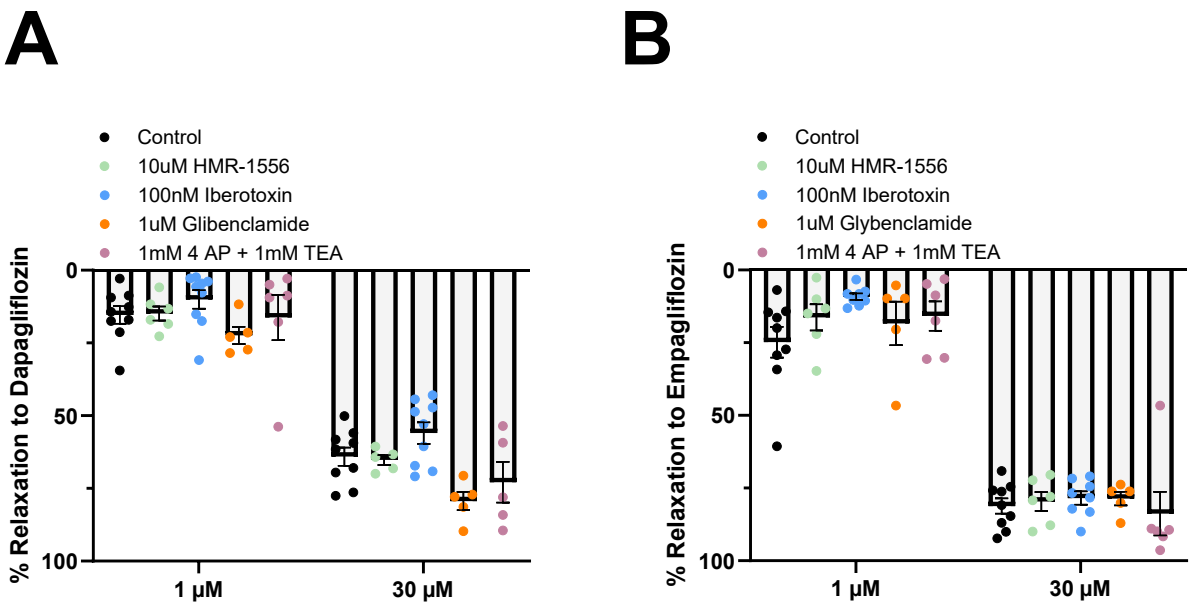


Figure 4.16: The effect of non-selective Kv blockers on the relaxation produced by dapagliflozin and empagliflozin in mesenteric arteries.
The effect of dapagliflozin (A) and empagliflozin (B) in the presence and absence of HMR1556 (green), Iberiotoxin (blue), 4-aminopyridine (AP) and tetraethylammonium (TEA, red) and glibenclamide (orange). All data values are shown as mean ±SEM, (N=5-6).

4.3.10 | Responses to SGLT inhibitors with different spasmogens.

The type of contractile agent used to pre-contract arteries can alter the effectiveness of the ability of a drug to evoke vasorelaxation (Askew Page et al., 2019). Hence, concentration-effect curves (1μM-30μM) to SGLT inhibitors were carried out in arterial segments pre-contracted with either 300nM U46619 or 10μM methoxamine, to determine whether the effect of SGLT inhibitors was spasmogen specific. The relaxation produced by dapagliflozin and ertugliflozin on mesenteric arteries was not affected by the pre-contractile agent. However, the SGLT1 inhibitor mizagliflozin showed a clear difference, depicted in figure 4.17 ($P<0.0001$). Vessels pre-contracted with 300nM U46619 produced only a 19.7%±3.4 relaxation in response to mizagliflozin at 30μM and was not linopirdine sensitive, whereas an 80.5%±3.1 relaxation was produced in vessels pre-contracted with 10uM methoxamine and was linopirdine sensitive (figure 4.18; N=5). This highlights that the effect of SGLT1 inhibitor mizagliflozin was dependent on the spasmogen used, whereas SGLT2 inhibitors dapagliflozin and ertugliflozin were not.

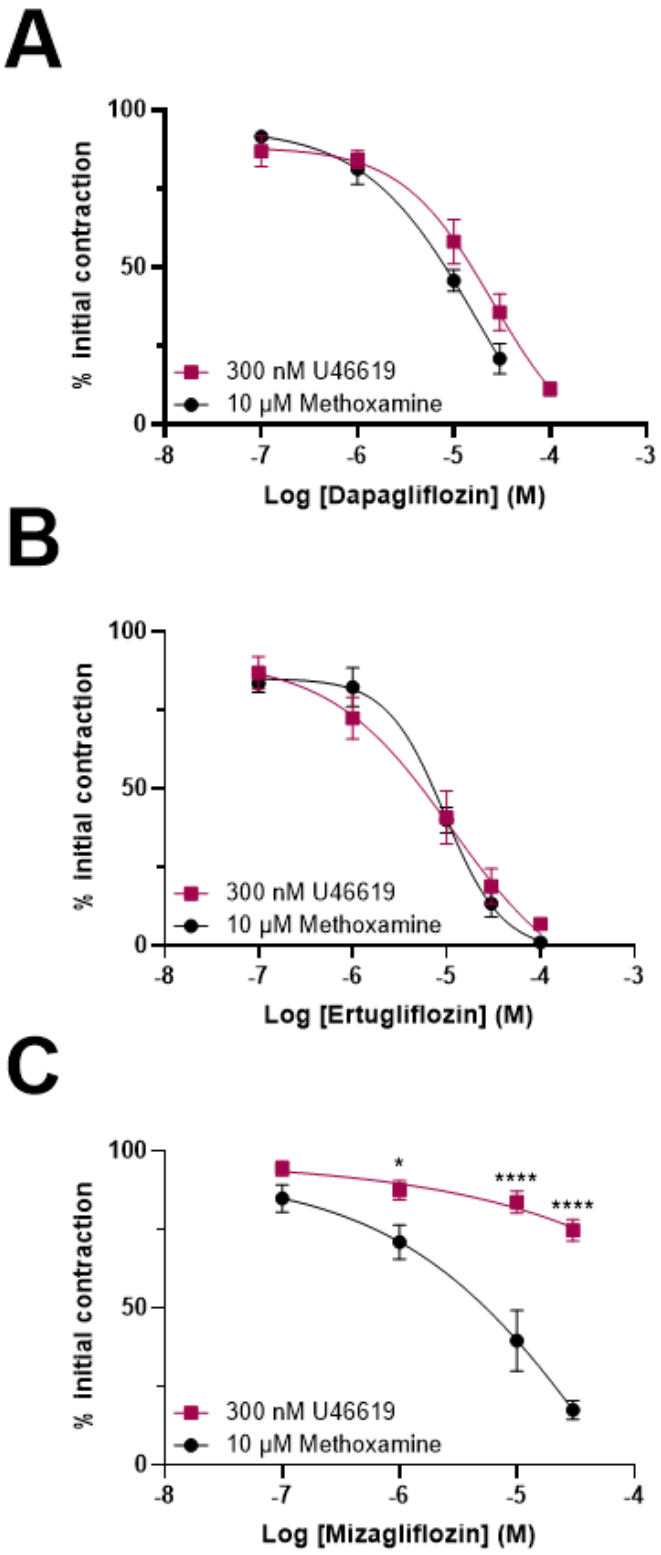


Figure 4.17: The effect of SGLT1 inhibitor, mizagliflozin on pre-contracted mesenteric arteries are spasmogen specific but SGLT2 inhibitors are not.
*The mean relaxation to dapagliflozin (A, N=6), ertugliflozin (B, N=5) and mizagliflozin (C, N=5) on mesenteric arteries pre-contracted with either 10μM methoxamine (black) or 300nM U46619 (pink). All values are expressed as mean +- SEM denoted by the error bars, N= number of animals. A two-way ANOVA with post-hoc Bonferroni test was used to generate significant values (****=P<0.0001).*

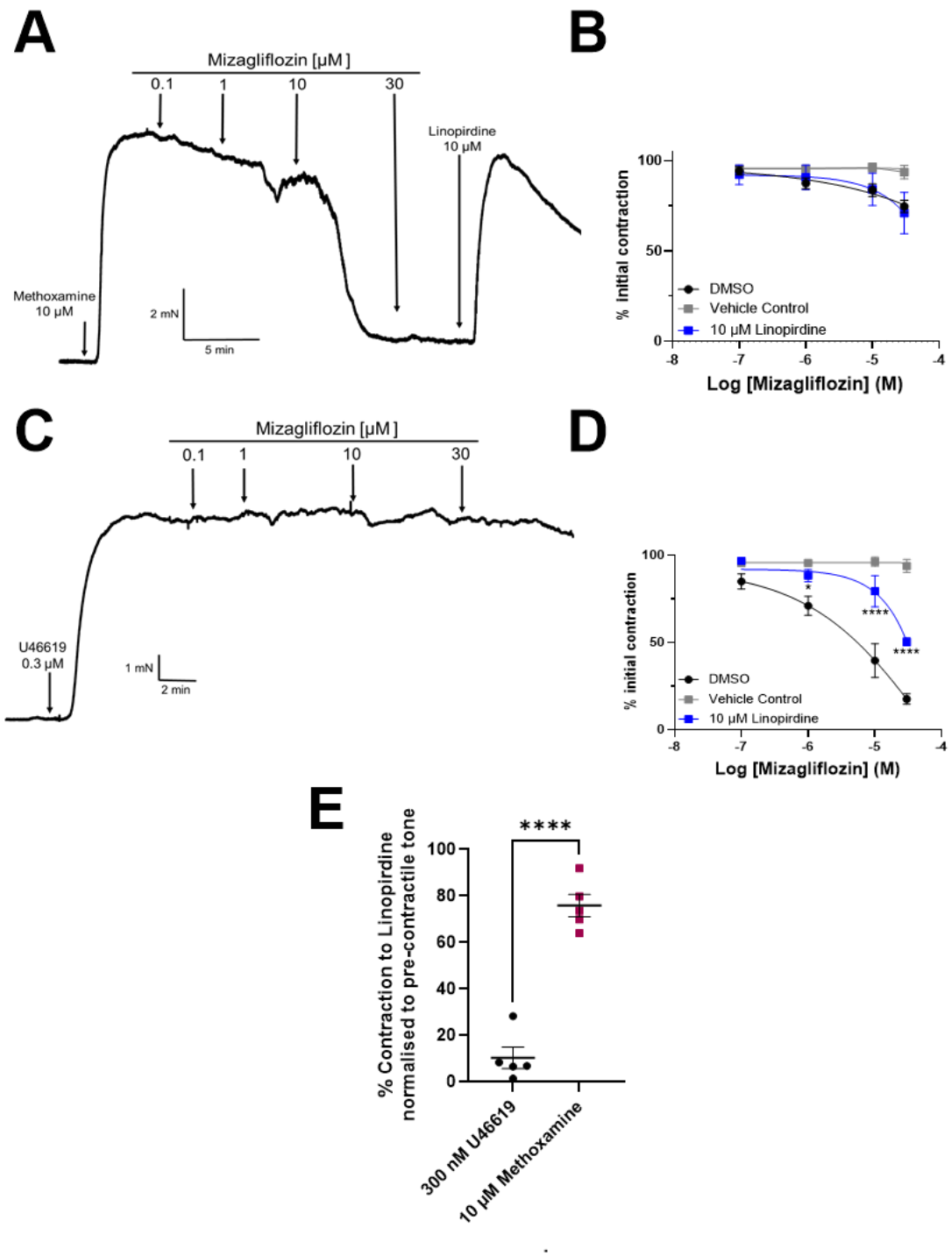


Figure 4.18: The effect of mizagliflozin is spasmogen dependent and linopirdine sensitive.

A representative trace showing the response to mizagliflozin (100nM-30µM) in mesenteric arteries pre-contracted with 300nM U46619 is shown in panel A. Mean response to mizagliflozin in mesenteric arteries pre-contracted with 300nM U46619 in the presence (blue) and absence (black) of 10µM linopirdine with vehicle control in grey (B, N=5). A representative trace showing the response to mizagliflozin in mesenteric arteries pre-contracted with 10µM methoxamine and a post-application of 10µM linopirdine is shown in panel C. Panel D shows the mean response to mizagliflozin in mesenteric arteries pre-contracted with 10µM methoxamine in the presence (blue) and absence (black) of 10µM linopirdine with vehicle control in

*grey (N=5). All concentration effect curve data is shown as mean+-SEM error bars. A two-way statistical ANOVA with a post-hoc bonferoni test was used to generate significant values (**=P<0.01, ***=P<0.001). The mean contraction produced by the post-application of 10μM linopirdine demonstrated in the trace in panel A shown in panel E (N=5). All data values are shown as mean ±SEM, denoted by error bars and a non-parametric t-test was used to generate significance value **** = P<0.0001, (N = number of animals).*

4.3.11 | SGLT2 inhibitors do not activate Kv7 channels

Due to SGLT2 inhibitor-induced relaxations being sensitive to Kv7 channel blockade electrophysiological experiments were performed on oocytes co-expressing KCNQ4/KCNQ5 and KCNE4 – a molecular combination found in most arterial smooth muscle (Barrese et al., 2018) as shown in figure 4.10. Neither dapagliflozin nor empagliflozin at 100 μM had any effect on the current amplitude nor the voltage-dependence of activation of the voltage-dependent potassium currents and neither agent affected the resting membrane potential (figure 4.19; N=6). Therefore, dapagliflozin and empagliflozin do not directly activate Kv7 channels. Consequently, the mechanism by which SGLT2 inhibitors induce downstream Kv7 channel activation and subsequent vasorelaxation must involve an alternative pathway.

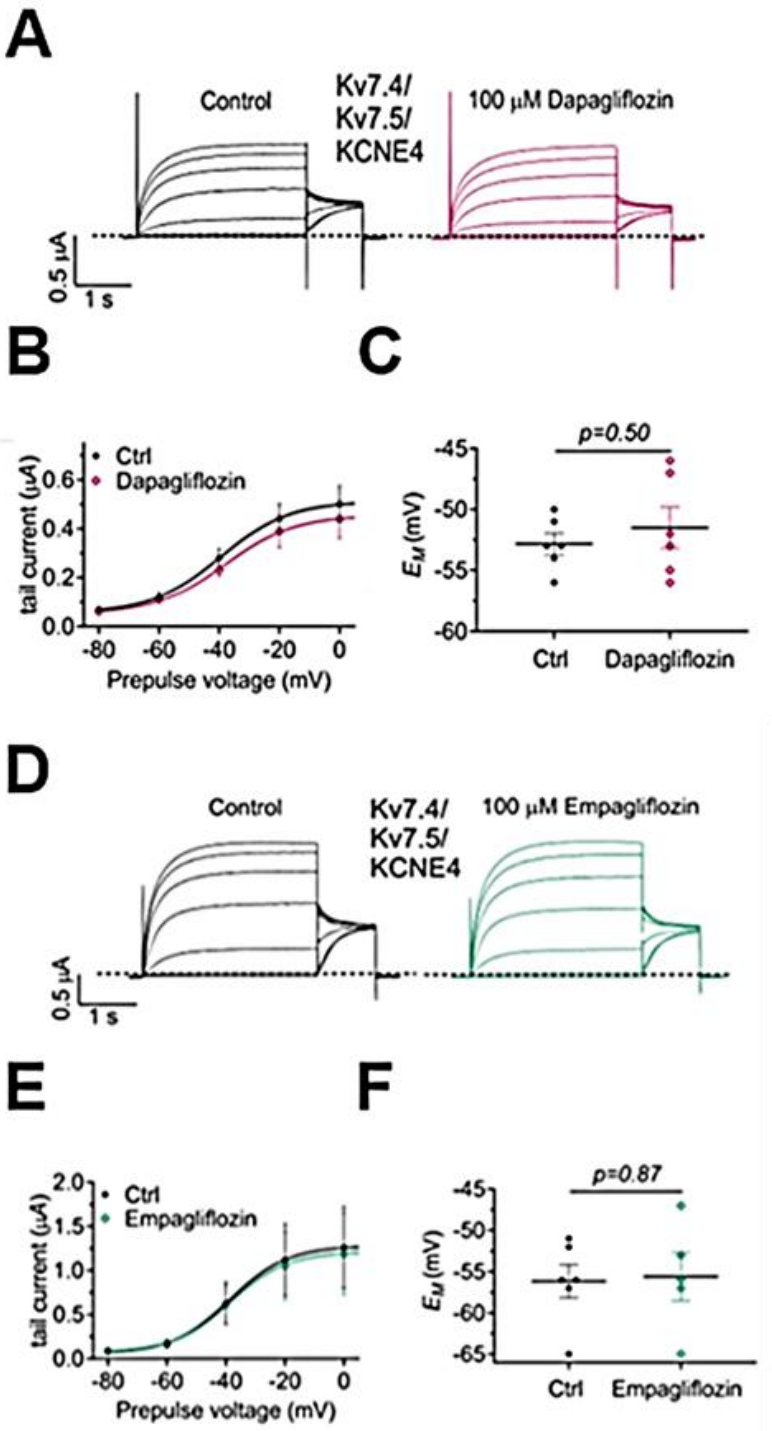


Figure 4.19: SGLT2 inhibitors do not activate Kv7.4/5 channels directly.
A-C shows currents produced by the co-expression of Kv7.4, Kv7.5 and KCNE4 in the absence and presence of 100 µM dapagliflozin. Representative traces in A, mean current-voltage relationship in B and mean membrane potential in C. The effect of 100 µM empagliflozin on currents produced by co-expression of Kv7.4, 7.5 and KCNE4 is shown in panels D-F. Representative traces in D, mean current-voltage relationship in E and mean membrane potential in F. Data are the mean of N=6 oocytes with error bars denoting the SD (Data courtesy of Prof Abbott, UCI).

4.3.12 | Sensory nerve contribution in mesenteric arteries compared to renal and septal arteries.

Functional experiments showed that the pan Kv7 channel blocker linopirdine reduced the relaxations produced by SGLT1 and SGLT2 inhibitors, but SGLT2 inhibitors did not directly activate Kv7 channels. Therefore, it is plausible that these agents promoted the release of an intermediate that recruits Kv7 channels (Chadha et al., 2014; Mondéjar-Parreño et al., 2019; Stott et al 2015). Since SGLT2 inhibitor-induced relaxations were not endothelium-dependent and the relaxation to SGLT2 inhibitors was dependent on the vascular bed, we focused on sensory nerve release of CGRP. We hypothesised that SGLT2 inhibitors induced relaxation through sensory nerve activation and CGRP release. Initial experiments compared the effect of CGRP in mesenteric and renal arteries. Cumulative application of CGRP (10 pM–10 nM) produced a maximal relaxation of 99.3±0.43% in pre-contracted mesenteric arteries (figure 4.20, N=5), which was abolished by the CGRP blocker BIBN-4096 (figure 4.21A). However, CGRP only produced minimal relaxation in renal arteries (figure 4.20, N=5). In line with our hypothesis, the pan Kv7 channel blocker linopirdine inhibited the relaxation in mesenteric arteries produced by exogenous CGRP to a similar degree as SGLT2 inhibitor-induced relaxations (figure 4.21A). These results suggest that mesenteric arteries exhibit significant sensitivity to relaxations induced by CGRP, however, renal arteries do not. Because of this, we hypothesised that SGLT2 inhibitors evoked relaxation in mesenteric arteries via CGRP release from sensory neurones.

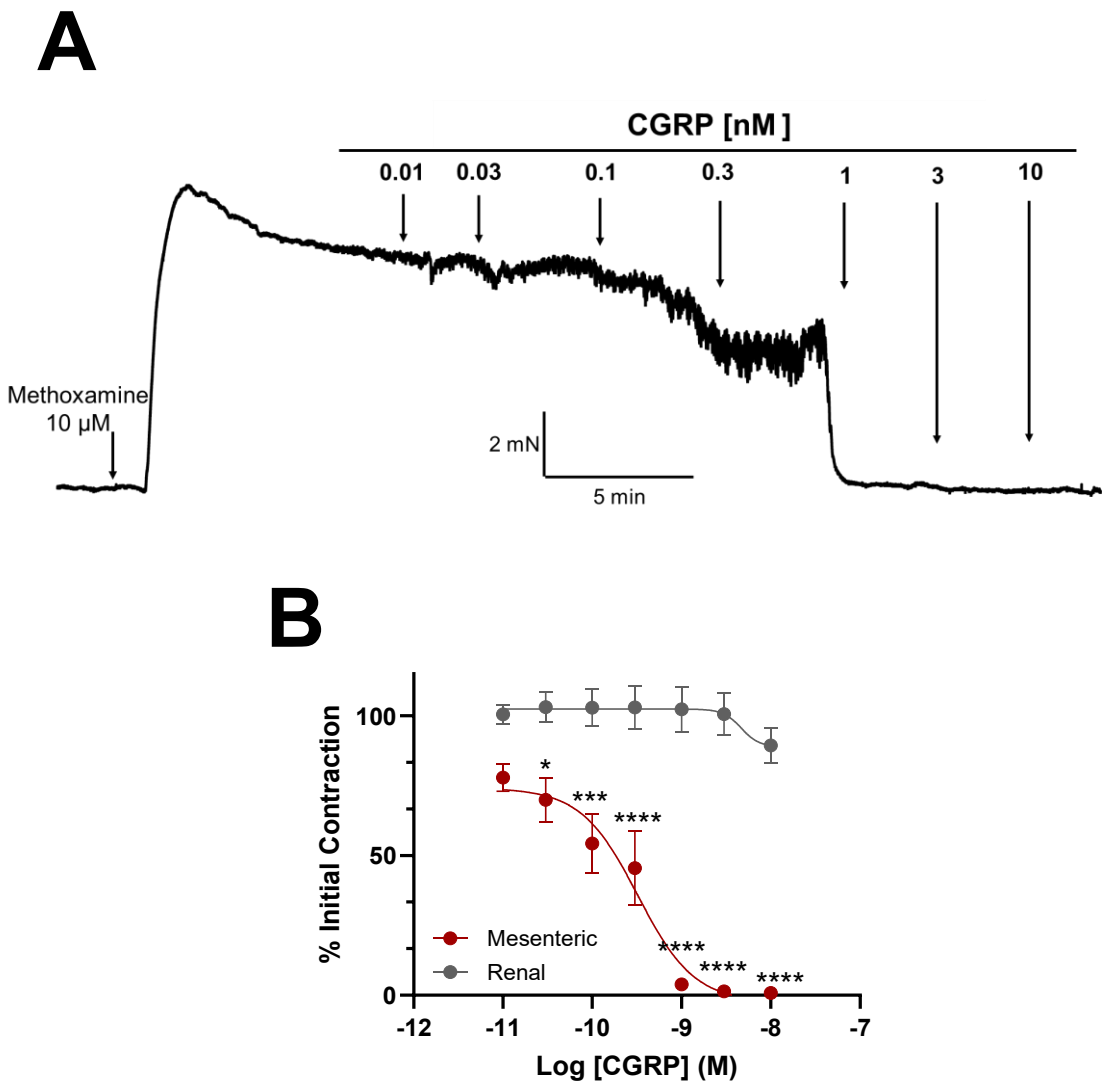


Figure 4.20: The effect of CGRP on mesenteric and renal arteries
Representative trace showing the relaxation produced by CGRP (10pmol·L^{-1}–10nmol·L^{-1}) in mesenteric arteries pre-contracted with 10µM methoxamine (A). The mean response to CGRP in mesenteric (red) and renal (grey) arteries is shown in panel B. All values are expressed as mean +- SEM denoted by the error bars, N= number of animals. A two-way ANOVA with post-hoc Bonferroni test was used to generate significant values (=P<0.05, ****=P<0.0001).*

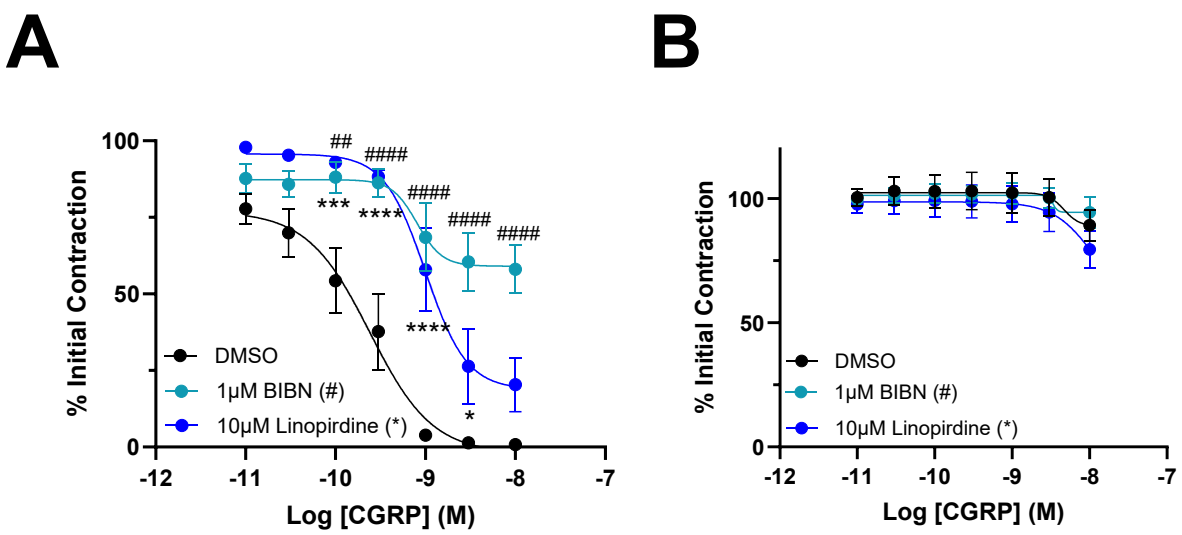


Figure 4.21: The effect of CGRP in mesenteric and renal arteries in the presence and absence of BIBN-4096 and linopirdine.
*The mean effect of CGRP in pre-contracted mesenteric arteries (A, N=6) and renal arteries (B, N=7) pre-incubated in either DMSO (control), 1μM BIBN-4096 or 10μM linopirdine. All values are expressed as mean +- SEM denoted by the error bars, N= number of animals. A two-way ANOVA with post-hoc Bonferroni test was used to generate significant values (**##=P<0.01, ***###=P<0.001, ****####=P<0.0001).*

4.3.13 | Mesenteric arteries are more sensitive to capsaicin and CGRP-induced relaxations than renal and septal arteries.

CGRP can be released from sensory neurons upon TRPV1 channel activation (Aalkjaer et al., 2021). Applying the TRPV1 activator capsaicin fully relaxed pre-contracted mesenteric arteries, which was significantly impaired by the CGRP receptor blocker BIBN-4096 (figure 4.22). Comparatively, capsaicin did not affect precontracted septal arteries and produced only a small relaxation in renal arteries (figure 4.23). The observed data indicates that the differential relaxation response to dapagliflozin and empagliflozin was potentially attributable to the differential contribution of sensory nerve-derived mediators.

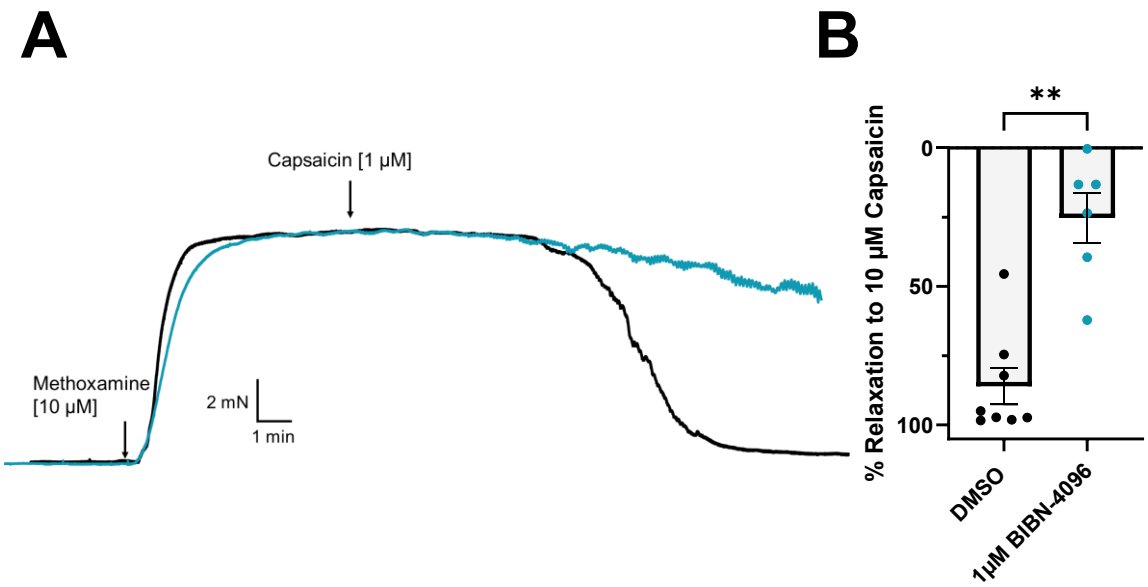


Figure 4.22: The effect of capsaicin on pre-contracted mesenteric arteries
*A representative trace showing the effect of 1µM capsaicin on mesenteric arteries pre-contracted with 10µM methoxamine in the presence (teal) and absence (black) of 1µM BIBN-4096 (A). Mean response to 1µM capsaicin in mesenteric arteries pre-incubated with either DMSO or 1µM BIBN-4096 (B). All values are shown as mean +- SEM error bars. A 2-way ANOVA with post-hoc Sidack test was used to calculate significance values, where ***= P<0.001, (N= Number of animals).*

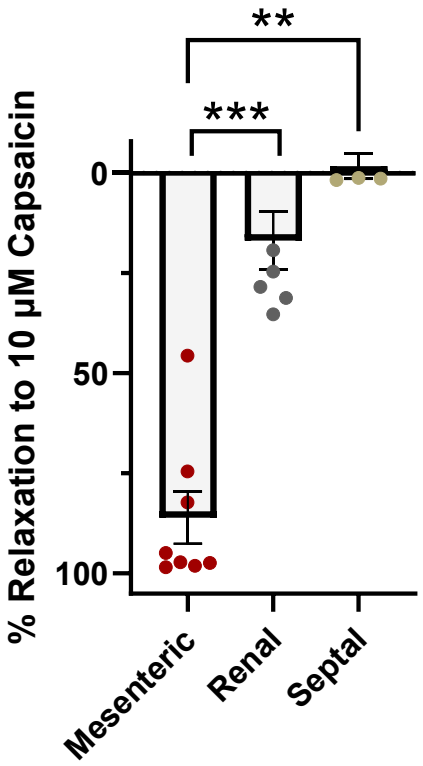


Figure 4.23: Mesenteric arteries produce greater relaxations to capsaicin compared to renal and septal arteries.
The response to 10µM capsaicin in pre-contracted mesenteric, renal and septal arteries (N=5-8). All values are shown as mean +- SEM error bars. A 2-way ANOVA

*with post-hoc Sidack test was used to calculate significance values, where **=P<0.01, ***= P<0.001, (N= Number of animals).*

4.3.14 | Comparing the CGRP and TRPV1 expression in the adventitial layer of whole arteries

Immunohistochemical studies were performed to ascertain the contribution of sensory nerves in mesenteric, renal and septal arteries. The artery's smooth muscle and endothelial layers were identified using myosin heavy chain (MHC) and CD31 antibodies that have been well-validated (Fang et al., 2022; Timraz et al., 2016; Wen et al., 2022) and shown in Chapter 4.

CGRP abundance was examined in mesenteric, renal and septal arterial beds with the TRPV1 antibody delineating sensory nerves. figure 4.24 shows robust TRPV1 and CGRP staining was observed in the adventitia of mesenteric arteries with comparatively little staining in the smooth muscle or endothelial layers as identified by MHC and CD31 staining (figure 4.26). In contrast, negligible TRPV1 or CGRP staining was identified in the adventitial, medial or inner layers of the renal artery (figure 4.25A and figure 4.26) and septal artery (figure 4.25B and figure 4.26). Thus, mesenteric arteries exhibit robust sensory nerve networks that were not present in renal or septal arteries. All three representative repeats for each artery are displayed in the appendix figures 9.1 and 9.2.

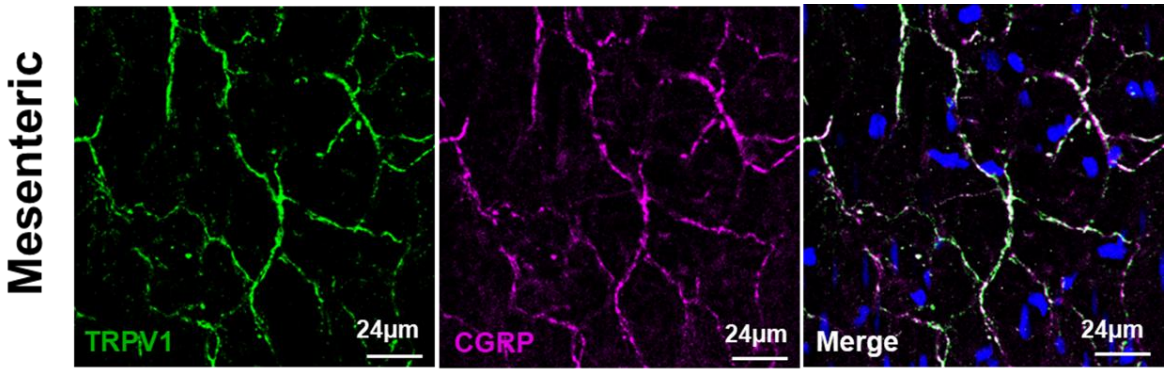


Figure 4.24: Expression of TRPV1 and CGRP in the adventitial layer of whole mesenteric arteries.
Representative labelling for TRPV1 (Green) and CGRP (magenta) indicative of sensory nerve presence in the adventitia of whole mesenteric arteries. Nuclei are labelled in blue (representative of 4 experiments).

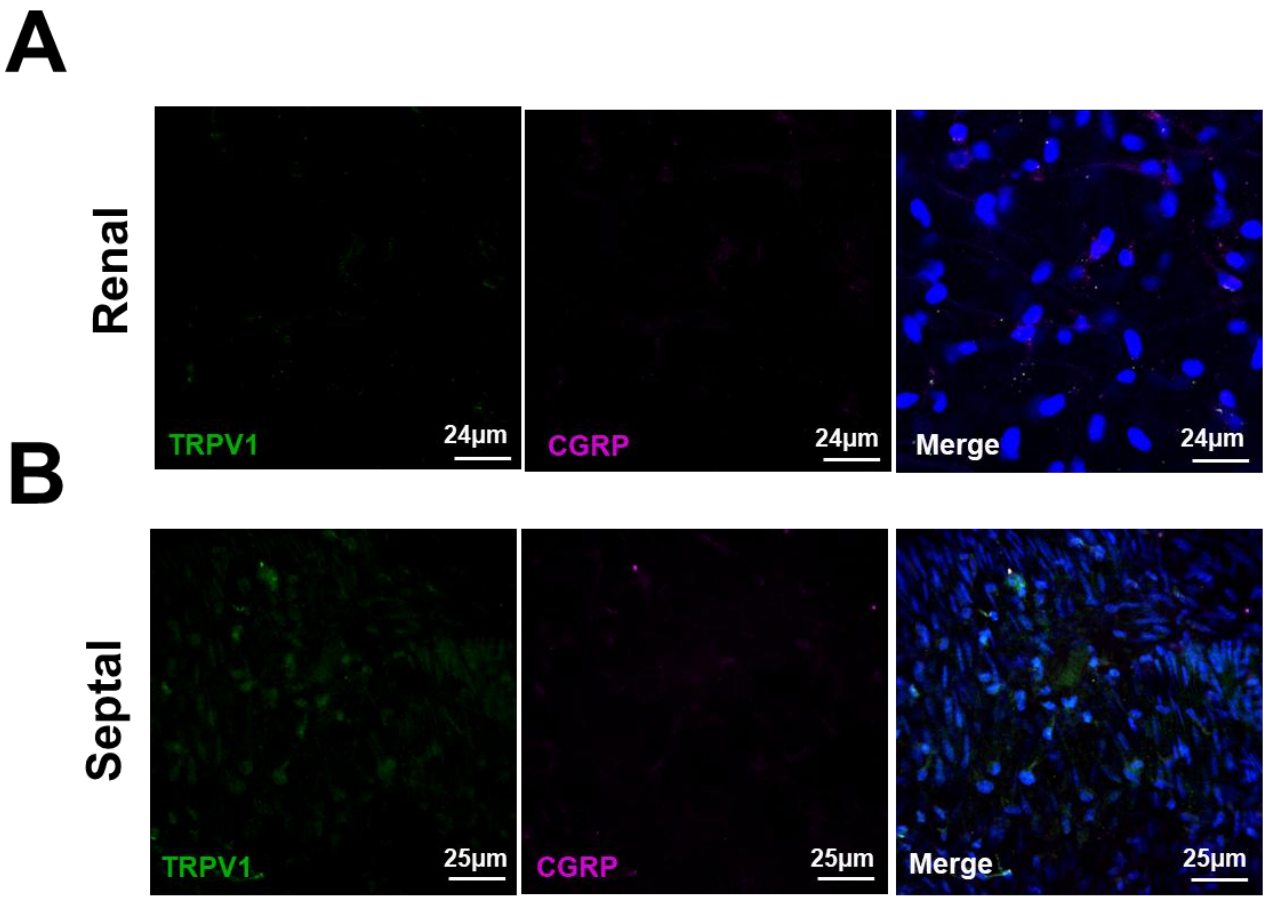


Figure 4.25: Expression of TRPV1 and CGRP in the adventitial layer of whole renal and septal arteries.

Representative labelling for TRPV1 (Green) and CGRP (magenta) indicative of sensory nerve presence in the adventitia of whole renal (A) and septal (B) arteries (N=4). Nuclei were labelled in blue, N = number of animals used.

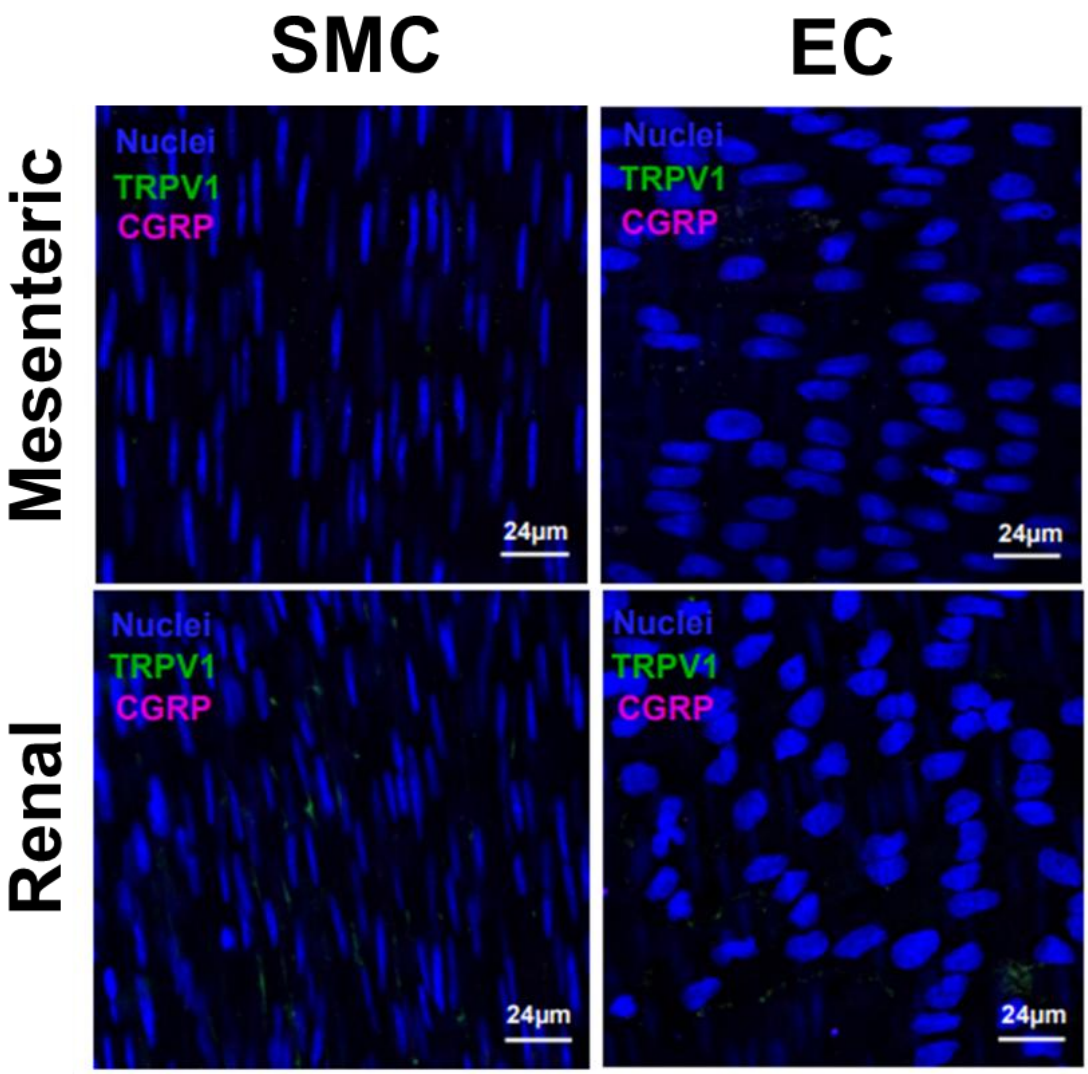


Figure 4.26: Lack of TRPV1 and CGRP expression in mesenteric and renal smooth muscle cells (SMC) and endothelial cell (EC) layers.
Representative labelling for TRPV1 (Green) and CGRP (magenta) in the smooth muscle cells and endothelial cells of whole mesenteric and renal arteries. Nuclei were labelled in blue (representative of 4 experiments).

4.3.15 | SGLT1 and SGLT2 inhibitor-induced relaxations are sensitive to CGRP blockade.

To identify a role for CGRP in SGLT2 inhibitor-induced relaxations, we applied dapagliflozin, empagliflozin and mizagliflozin to mesenteric arteries pre-incubated with either DMSO (control) or BIBN-4096 (1 µM). The relaxation produced by all three inhibitors was significantly attenuated by pre-incubation with the CGRP receptor blocker (figure 4.27). Hence, the relaxation produced by dapagliflozin, empagliflozin and mizagliflozin was impaired by CGRP receptor blockade.

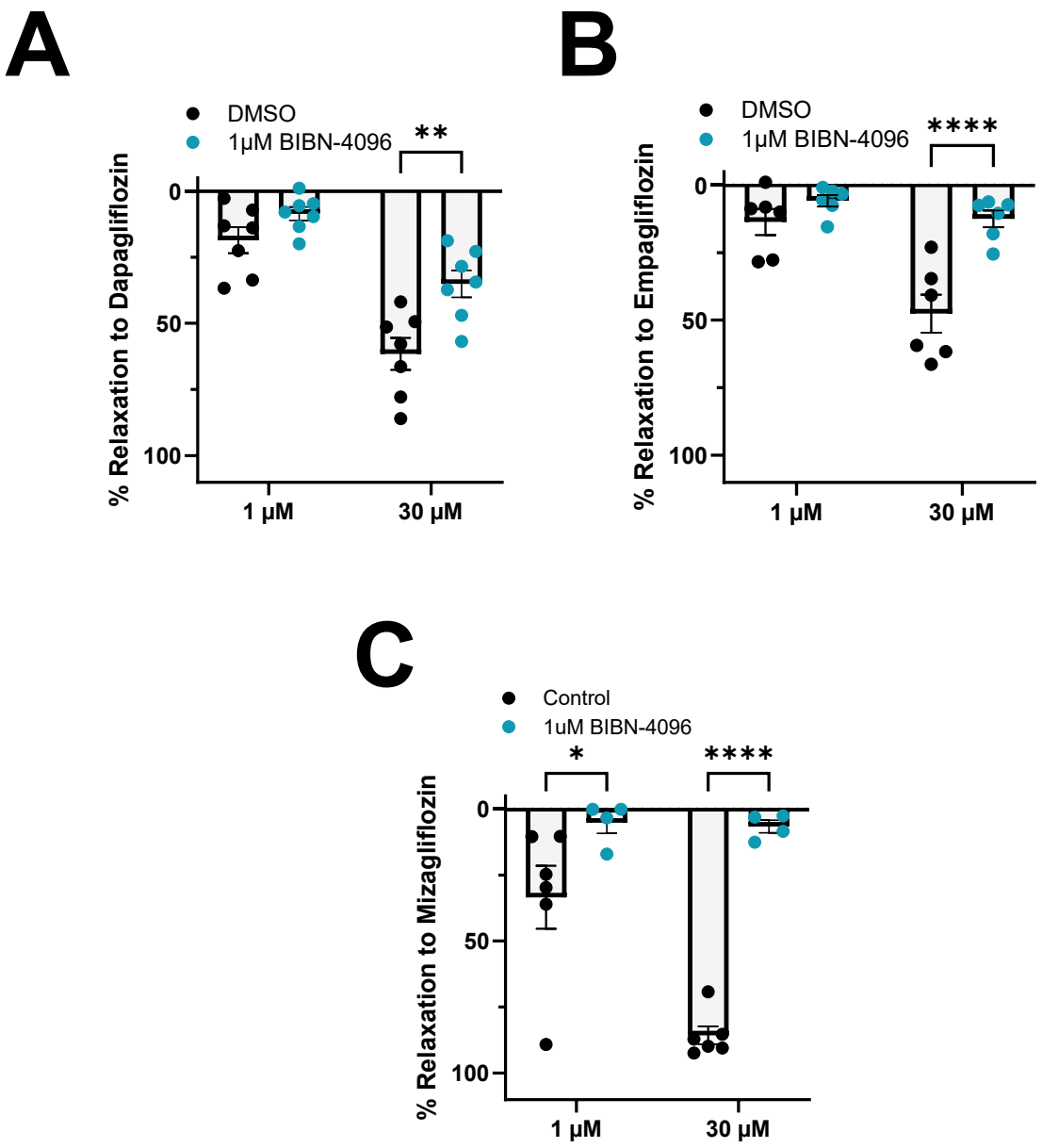


Figure 4.27: Dapagliflozin, empagliflozin and mizagliflozin relaxations are sensitive to CGRP blocker, BIBN-4096.
*The mean effect of dapagliflozin (A, N=6), empagliflozin (B, N=7) and mizagliflozin (C, N=5) on precontracted mesenteric arteries in the presence of DMSO (solvent control, grey) or 1 μM BIBN-4096 (teal). All values are expressed as mean ± SEM. A two-way statistical ANOVA with a post-hoc Sidak test was used to generate significant values (**=P<0.01, ***=P<0.001, ****=P<0.0001).*

4.3.16 | SGLT1 and SGLT2 evoked relaxations are sensitive to TRPV1 blockade.

We hypothesised that SGLT2 inhibitors relaxed mesenteric arteries by provoking CGRP release from sensory nerves. To confirm this, two methodological

approaches were used – depletion of CGRP stores through treatment with three 10-minute applications of capsaicin (10μM) followed by wash out of the bathing solution as shown in the methods chapter or direct blocking of TRPV1 with AMG-517 (1μM). Both approaches impaired the relaxation produced by 10μM capsaicin in pre-contracted mesenteric arteries, as seen in figure 4.28; N=5-6). The effect of these two treatments was also investigated on dapagliflozin-, empagliflozin- and mizagliflozin- induced relaxations.

Dapagliflozin and empagliflozin-induced relaxations were significantly attenuated after pre-treatment with capsaicin or incubation with AMG-517. (figure 4.29A-B). Mizagliflozin-induced relaxations were also sensitive to TRPV1 blockade (figure 4.29C). None of the pharmacological modulators altered the size of methoxamine-induced contractions (figure 4.30). Hence, relaxations induced by SGLT2 inhibitors were dependent upon the activation of the TRPV1 channel on perivascular sensory nerves and subsequent CGRP release.

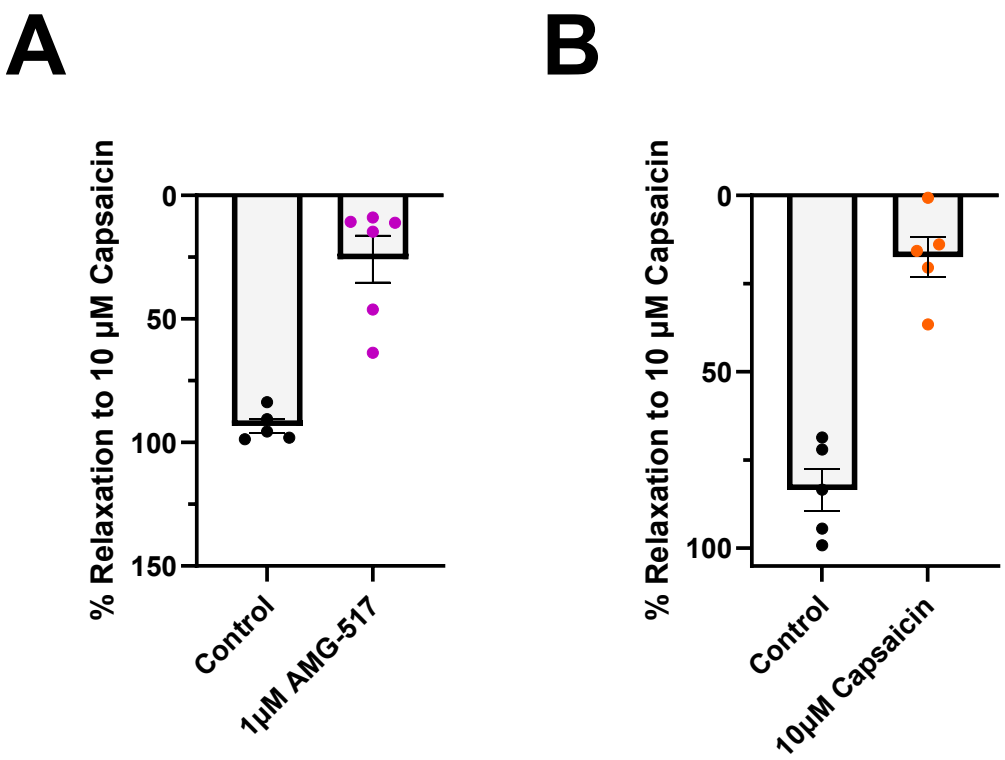


Figure 4.28: Effect of sensory nerve depletion and TRPV1 blockade on capsaicin-induced relaxations.
*The mean percentage relaxation to 10μM capsaicin in mesenteric arteries pre-contracted with 10 μM methoxamine in the presence of the TRPV1 blocker AMG-517 (A, Purple, N=5) or after sensory nerve depletion (B, orange, N=6). All values are expressed as mean ± SEM. A two-way statistical ANOVA with a post-hoc Sidak test was used to generate significant values (***=P<0.001, ****=P<0.0001). (N=) number of animals used.*

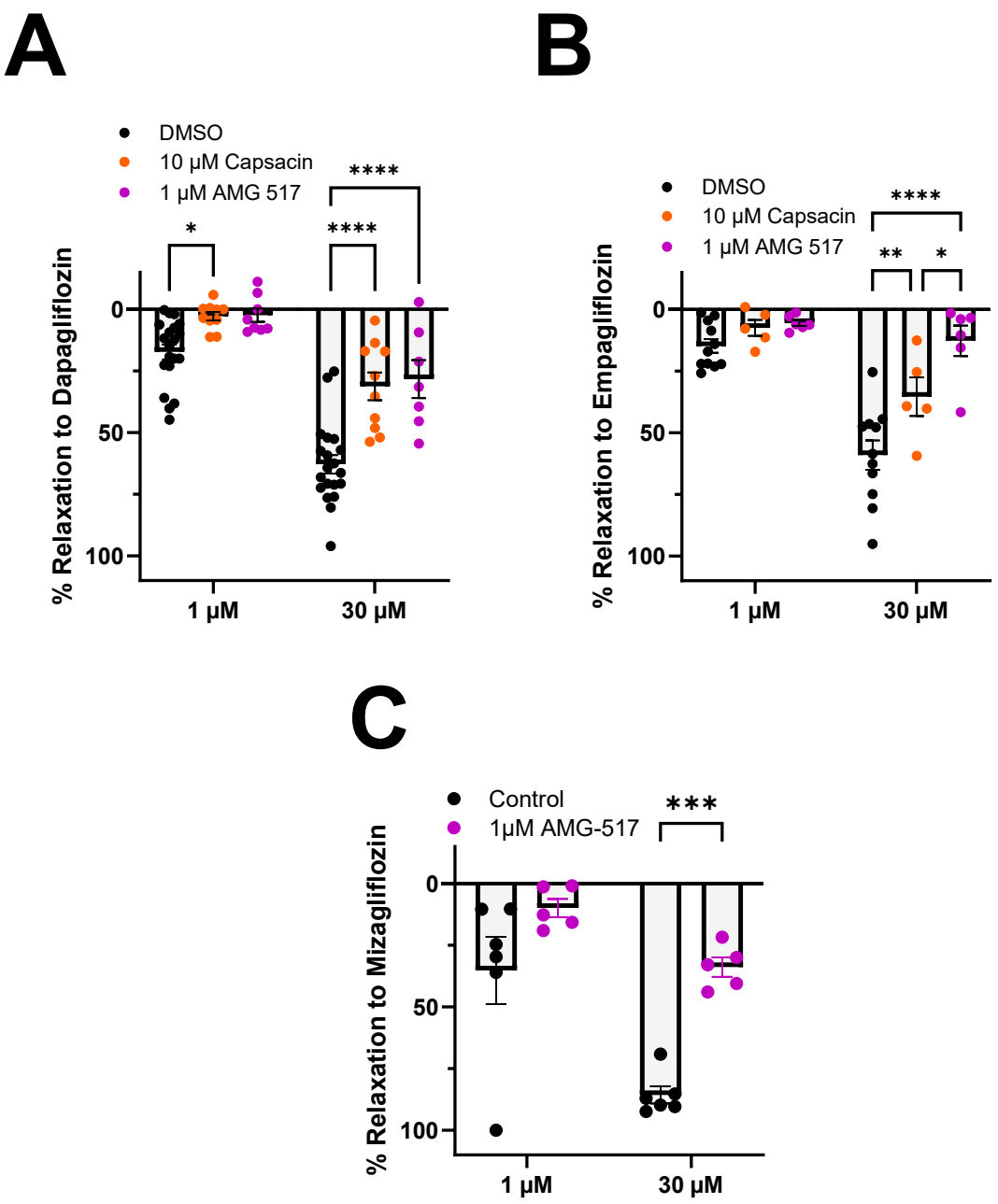


Figure 4.29: Dapagliflozin and empagliflozin-induced relaxations are impaired by sensory nerve depletion and TRPV1 blockade.
*The percentage relaxation to dapagliflozin (A, N=7-10), empagliflozin (B, N=6-10) and mizagliflozin (C, N=5) in mesenteric arteries pre-incubated in 1 μM AMG-517 (purple) or after sensory nerve depletion with 10μM capsaicin (orange). All values are expressed as mean ± SEM. A two-way statistical ANOVA with a post-hoc Sidak test was used to generate significant values (**=P<0.01, ***=P<0.001, ****=P<0.0001). (N=) number of animals used.*

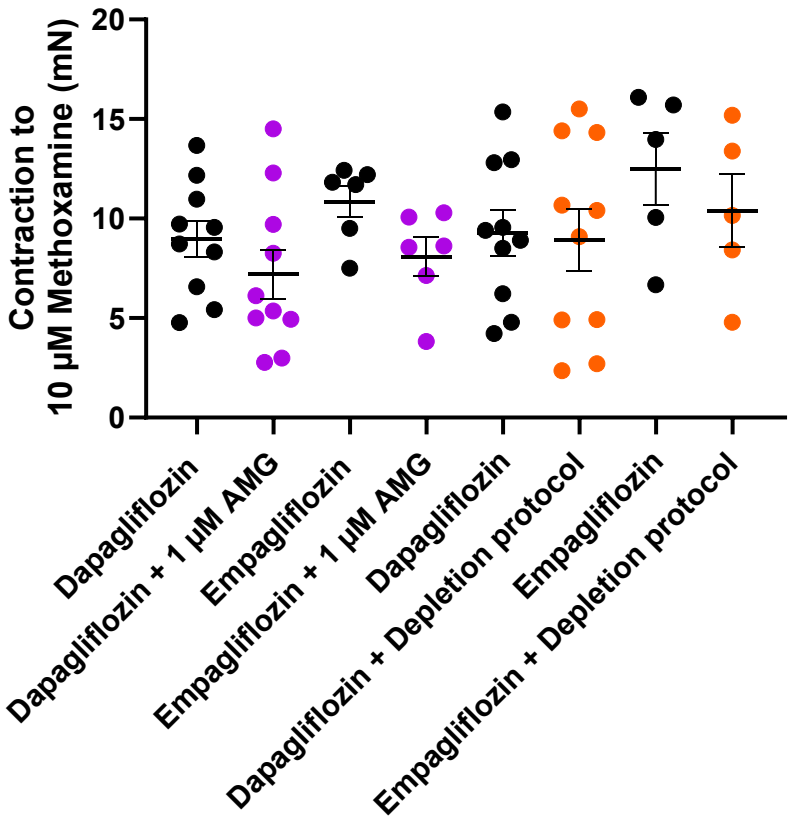


Figure 4.30: Mean amplitude of methoxamine evoked contractions.
The mean amplitude of the contraction produced by 10µM methoxamine under the different conditions pre-incubated with 10µM capsaicin or 1µM AMG-517 (N=5-10). Data is shown as mean contraction (mN) ±SEM, where N= number of animals.

4.3.17 | Dapagliflozin-induced relaxations are not sensitive to TRPA1 blockade.

TRPA1 channels exist on sensory nerves and can form hetromers with TRPA1 channels. Dapagliflozin relaxations were not affected by pre-incubation with the TRPA1 blocker AM0902 in mesenteric arteries (1µM or 10µM; figure 4.31). Suggesting that the relaxation produced by SGLT2 inhibitors was dependent on TRPV1 activation and not TRPA1.

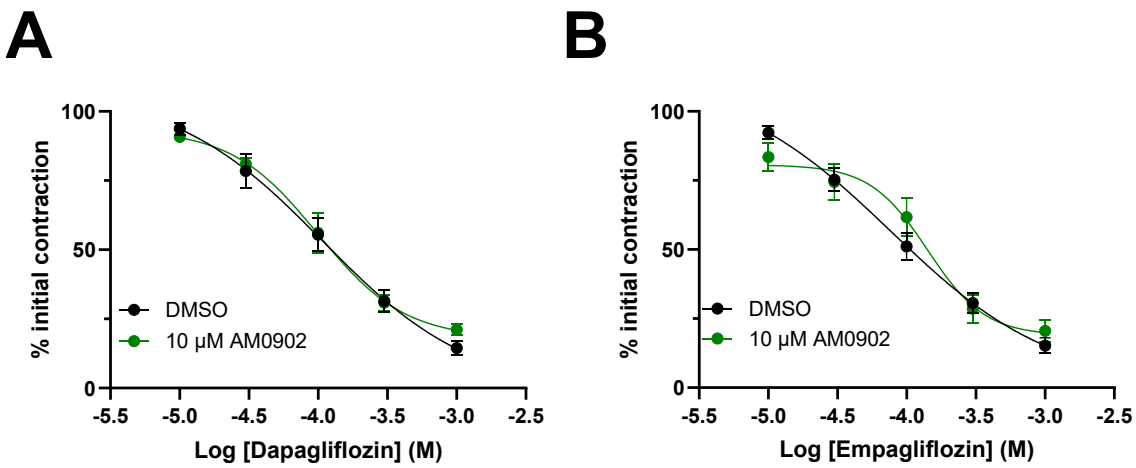


Figure 4.31: Effect of TRPA1 blocker AM0902 on dapagliflozin induced-relaxations. The mean response to 1μM and 30μM dapagliflozin in the presence (green) and absence (grey) of the TRPA1 blocker AM0902 (N=5-6). All values are expressed as mean ± SEM, where N=number of animals used.

4.3.18 | Effect of SGLT2 inhibitors on heterologously expressed TRPV1 currents.

Upon discovering SGLT1 and SGLT2 inhibitor-induced relaxation was sensitive to TRPV1 blockade, we sought to determine whether dapagliflozin or empagliflozin could directly activate TRPV1 channels. Patch-clamp experiments were performed using outside-out excised membrane patches of HEK293 cells expressing rat TRPV1 (rTRPV1) by Prof Tamara Rosenbaum, Mexico City University. As shown in figure 4.32, TRPV1 cation currents at -120 mV and +120mV were recorded in the absence and presence of either 30 μM (figure 4.32A) or 100 μM dapagliflozin (figure 4.32B) for 5 mins followed by 250 nM capsaicin. All currents were leak-subtracted and normalized to the current obtained at +120 mV (figure 4.32C). Currents after exposure to 30 μM dapagliflozin were 12.9±2.2% and 7.6±3.7% after 100 μM dapagliflozin of the currents elicited by the TRPV1 agonist, capsaicin (figure 4.32C, n=6). These data indicate that TRPV1 was not directly activated by dapagliflozin.

Next, we studied whether dapagliflozin and empagliflozin could potentiate capsaicin- or low pH -activated TRPV1 currents. For this set of experiments, TRPV1 in outside-out excised membrane patches was activated with either a sub-

saturating concentration of capsaicin (250 nM) or with a solution at pH 6. Stimuli were washed out to close the channels, and then 30 µM dapagliflozin was applied for 5 mins before the presence of 250 nM capsaicin or pH 6 solution was re-applied (figure 4.32D-G). The results from these experiments indicate that 30 µM dapagliflozin did not potentiate TRPV1 currents activated by 250 nM capsaicin (figure 4.32D and E; 84.1±13.5%, n = 5) or by low pH (figure 4.32F and G; 94±6.5%, n =5). A similar lack of effect on TRPV1 was also seen with empagliflozin, shown in figure 4.33. Thus, SGLT2 inhibitors neither activate TRPV1 directly nor sensitise the channel to known mediators.

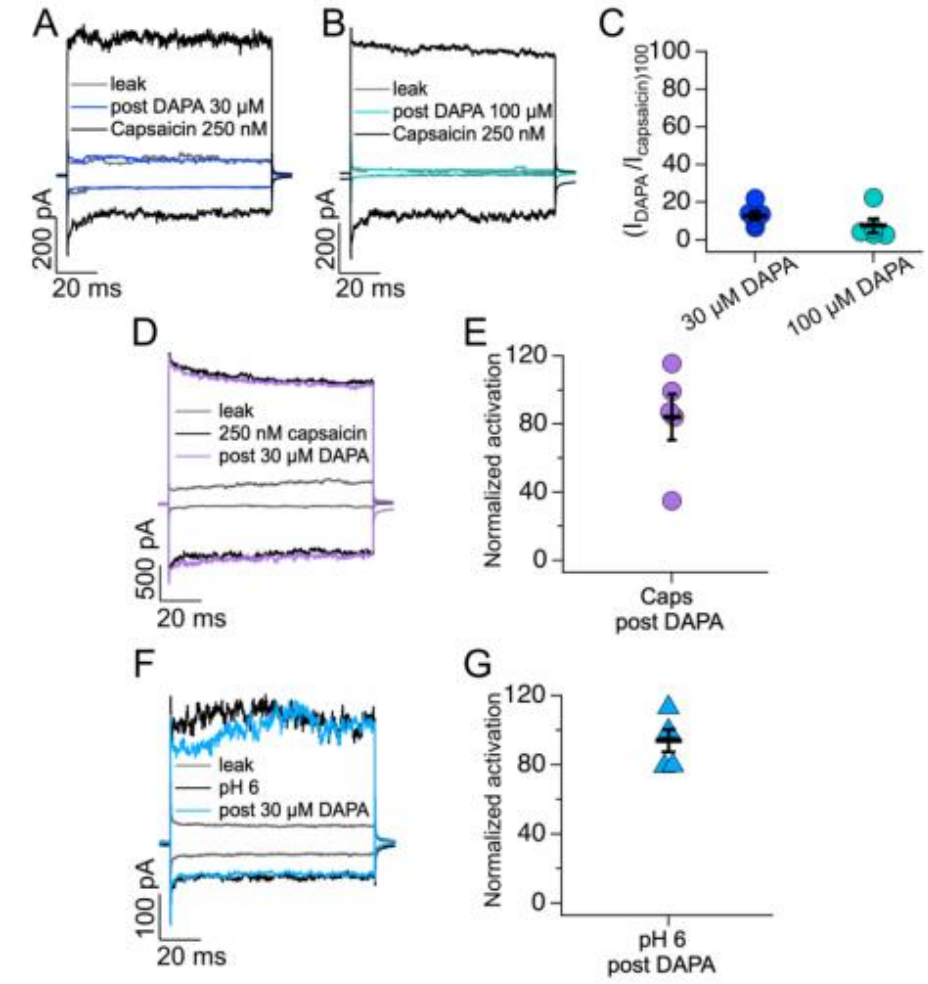


Figure 4.32: Dapagliflozin does not activate TRPV1 directly.
(A and B) Representative traces of currents at +120 and -120 mV from outside-out membrane patches of HEK293 cells expressing TRPV1. Leak currents were obtained in the absence of any agonist (grey) and after 5 min application of dapagliflozin (DAPA) 30 µM (blue traces, panel A) and 100 µM (green traces, panel B). Black trace shows the subsequent effect of 250 nM capsaicin. (C) Average data for experiments in (A and B). Currents were leak-subtracted, and data was normalized to activation by capsaicin 250 nM in the steady-state at +120 mV (N =

6 and N = 5 for DAPA 30 µM and 100 µM, respectively). (D) Representative traces of currents at +120 and -120 mV from outside-out membrane patches of HEK293 cells expressing TRPV1 in control conditions (grey), after application with 250 nM capsaicin (black traces) and after application of 250 nM capsaicin + 30 µM DAPA for 5 mins (lilac traces). (E) The data in (D) was normalized by dividing the currents obtained at +120 mV in response to 250 nM capsaicin + 30 µM DAPA by the currents in response to 250 nM capsaicin alone; (N = 5) (F) Representative traces of currents at +120 and -120 mV from outside-out membrane patches of HEK293 cells expressing TRPV1 under control conditions (grey), after activation of TRPV1 by pH 6 (black) and after 5 min application of 30 µM DAPA to pH 6 conditions (blue). (G) The data in (F) were normalized by dividing the currents obtained at +120 mV in response to pH 6 + 30 µM DAPA by the currents in response to pH 6 alone; (N = 6). Group data are reported as the mean ± standard error of the mean.

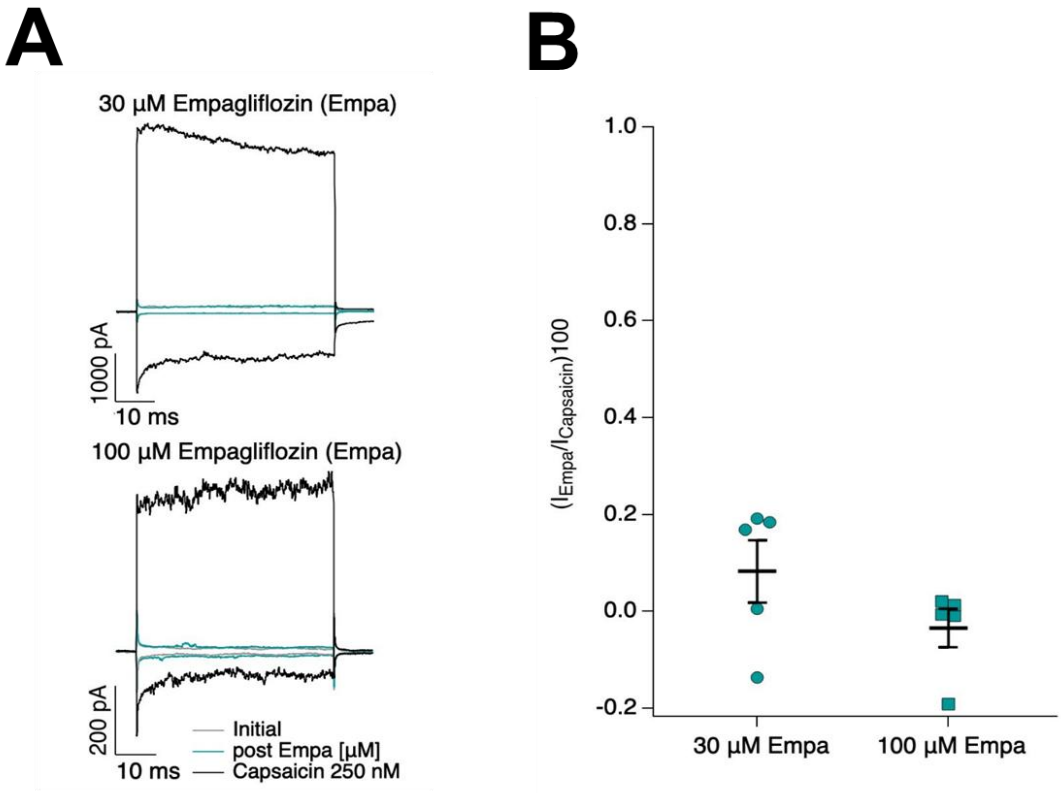


Figure 4.33: Empagliflozin does not activate TRPV1 directly
Representative traces of currents at +120 and -120 mV from outside-out membrane patches of HEK293 cells expressing TRPV1. Leak currents were obtained in the absence of any agonist (grey) and after 5 min application of 30 µM and 100 µM empagliflozin (Empa). Black trace shows the subsequent effect of 250 nM capsaicin (A). Average data for experiments in (B). Currents were leak-subtracted, and data was normalized to activation by capsaicin 250 nM in the steady-state at +120 mV (N = 6 and N = 5 for Empa 30 µM and 100 µM, respectively).

4.3.19 | NHE1 co-localises with TRPV1 in the adventitial layer

Various studies have shown that SGLT2 inhibitors block NHE isoforms (Baartscheer et al., 2017; Chung et al., 2023; De Stefano et al., 2021b; Uthman et al., 2018; Zuurbier et al., 2021). Since neither empagliflozin nor dapagliflozin-activated TRPV1 perse, we hypothesised that SGLT2 inhibitors promoted the release of CGRP from sensory nerves by inhibiting NHE and producing a localised pH change sufficient to activate TRPV1. NHE1 is the most commonly expressed NHE isoform, hence, initial experiments sought to characterise the expression and locality of NHE1 in mesenteric arteries. To do this, we fixed whole mesenteric and renal arteries, stained them with SGLT2 and NHE1 antibodies, and used TRPV1 to delineate the sensory nerves. In mesenteric arteries, prominent NHE1 staining was observed in the adventitia and smooth muscle cell layers co-localised with TRPV1, as shown in figure 4.34A-B. However, no staining of NHE1 was identified in the endothelial cell layers (figure 4.34C). SGLT2 was predominantly expressed in the smooth muscle cell layer of mesenteric arteries, as shown in figure 4.35. Negligible staining of SGLT2 was observed in the adventitial and endothelial layers (figure 4.35).

In the adventitial layers of renal arteries, traces of NHE1 staining were identified, but no staining was found in the smooth muscle cell or endothelial cell layers (figure 4.36A). No staining of SGLT2 was detected in renal artery adventitia or endothelial cells, but SGLT2 staining was detected in renal smooth muscle layers (figure 4.36B). The appendix shows all three representative repeats for each artery in figures 9.3-9.6. Therefore, these findings show NHE1 but not SGLT2 colocalised with TRPV1 in sensory nerves in the mesenteric artery. Therefore, we hypothesise that SGLT2 acts on NHE1 to evoke vasorelaxation via CGRP release from peptidergic sensory nerves.

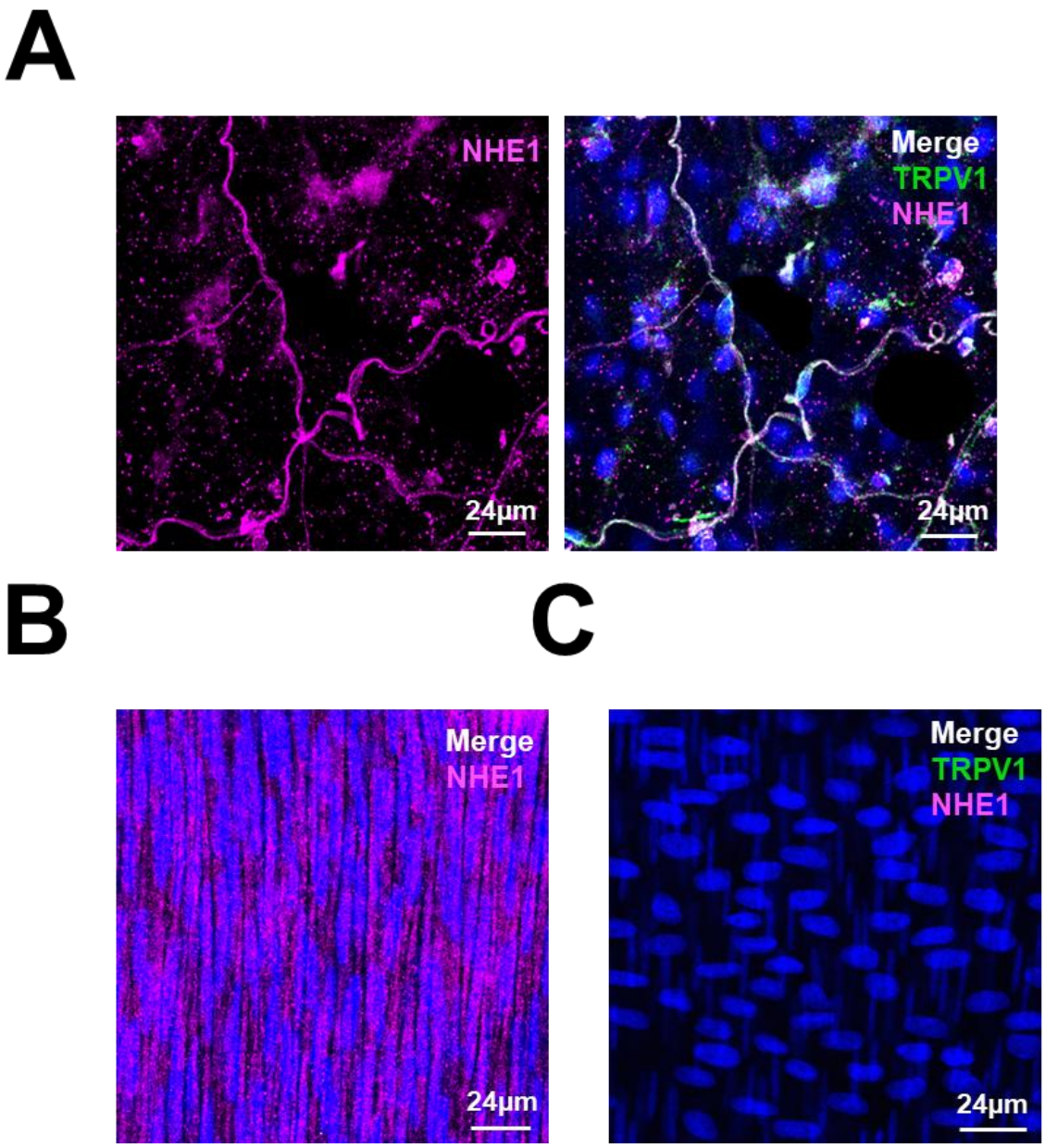


Figure 4.34: NHE1 expression is found in smooth muscle and adventitial cell layers but not endothelial cell layers of mesenteric arteries
Immunocytochemistry labelling of NHE1 (magenta) and TRPV1 (green) in the adventitia of whole mesenteric arteries (A). Immunocytochemistry labelling of NHE1 (magenta) in vascular smooth muscle cells (SM, B) and endothelial cells (EC, C). (representative of N=3) Nuclei were labelled in blue.

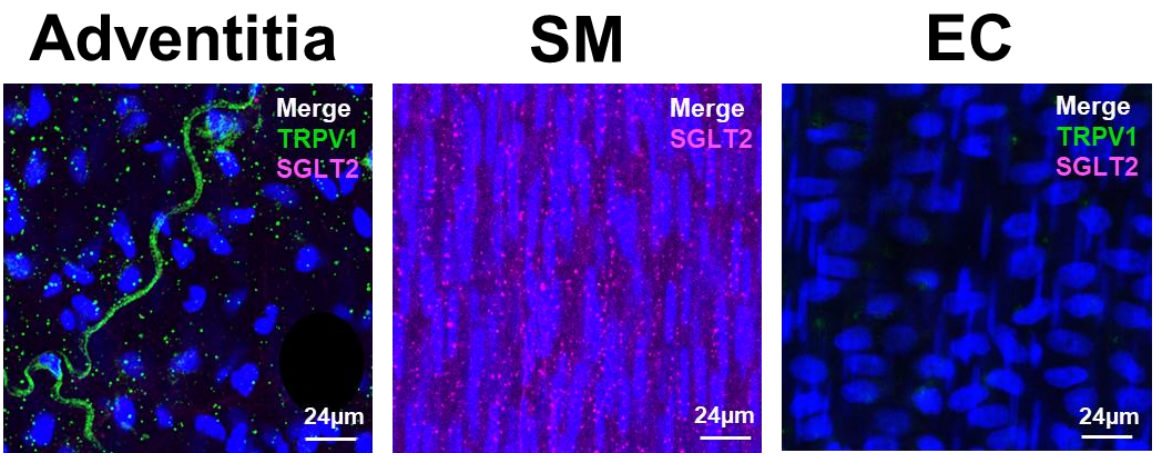


Figure 4.35: SGLT2 expression in the adventitial, smooth muscle, and endothelial cell layers of mesenteric arteries.
Immunocytochemistry labelling of SGLT2 (magenta) and TRPV1 (green) in the adventitia, smooth muscle (SM) and endothelial cell (EC) layers of whole mesenteric arteries (representative of N=3). Nuclei were labelled in blue.

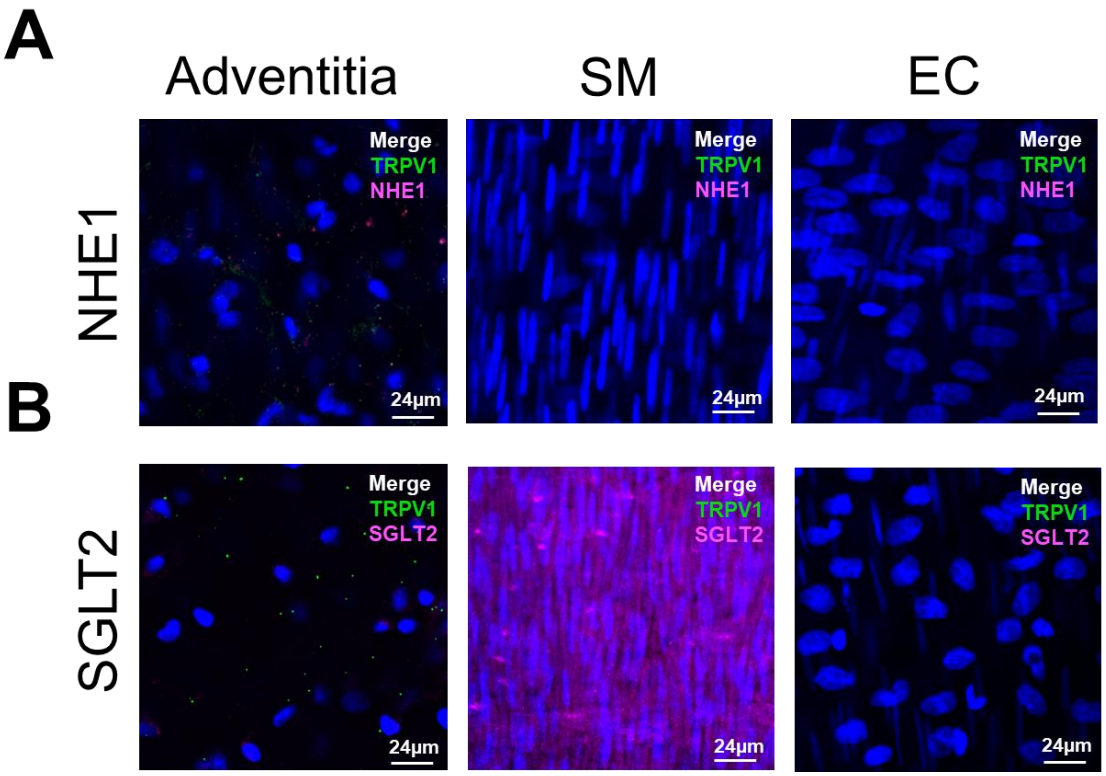


Figure 4.36: Expression of SGLT2 and NHE1 in renal artery adventitial, smooth muscle and endothelial cell layers.
Immunocytochemistry labelling for NHE1 (magenta, panel A) and SGLT2 (magenta, panel B) in the adventitia, smooth muscle (SM), and endothelial cell (EC) layers of whole renal arteries. (representative of 3 such experiments) Nuclei were labelled in blue.

4.3.20 | The effect of the NHE1 inhibitor cariporide in arteries.

Upon observing that NHE1 co-localises with TRPV1 in the sensory nerves of mesenteric arteries, functional experiments were conducted to explore the effect of NHE1 inhibitor cariporide on pre-contracted mesenteric arteries. The NHE1 inhibitor cariporide (1μM - 30μM) relaxed pre-contracted second-order mesenteric arteries, although to a lesser extent compared to the SGLT inhibitors (figure 4.37). Application of 30μM cariporide produced a 32.5±4.7% relaxation compared to 79.08±4.9% for dapagliflozin. Pre-incubation with 1 μM BIBN-4096 and AMG-517 in mesenteric arteries significantly attenuated cariporide induced-relaxations ($P<0.01$, figure 4.38). In contrast, cariporide was unable to evoke relaxations in pre-contracted renal or septal arteries (figure 4.35B, N=5-7).

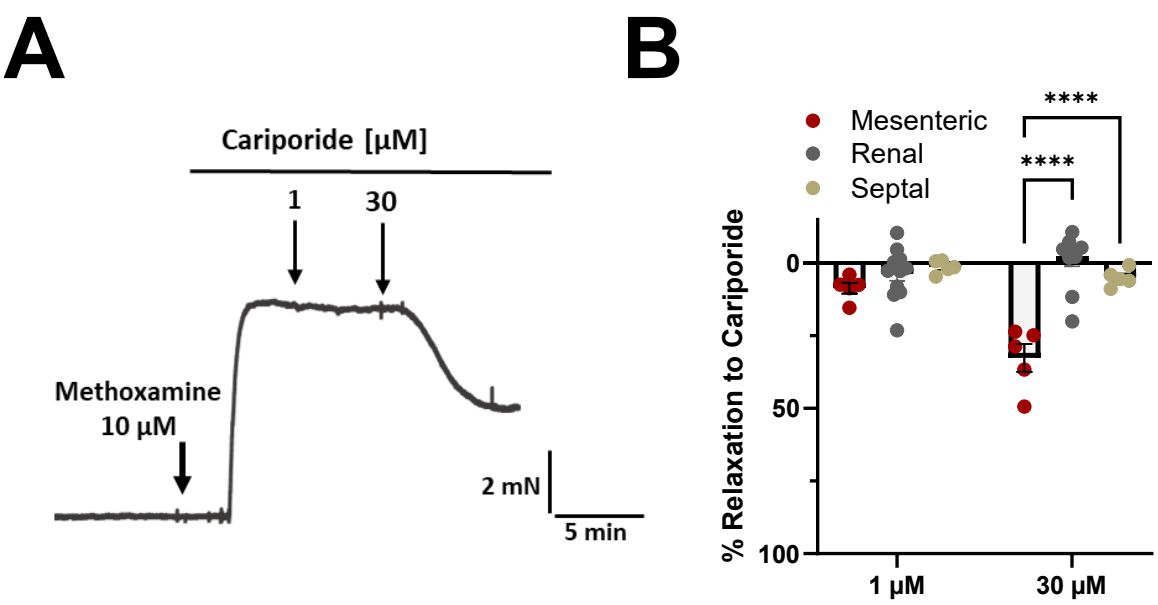


Figure 4.37: Comparison in the relaxation to cariporide in mesenteric and renal arteries pre-contracted with 10μM methoxamine.
*A representative trace showing the response to 1μM and 30μM cariporide in mesenteric arteries pre-contracted with 10μM methoxamine (A) and a comparison of the mean relaxation to cariporide in renal (grey), mesenteric (red) and septal (beige) arteries shown in panel B (N=5-8). All values are shown as mean +- SEM error bars. A 2-way ANOVA with post-hoc Sidack test was used to calcualte significance values, where ****= P<0.0001.*

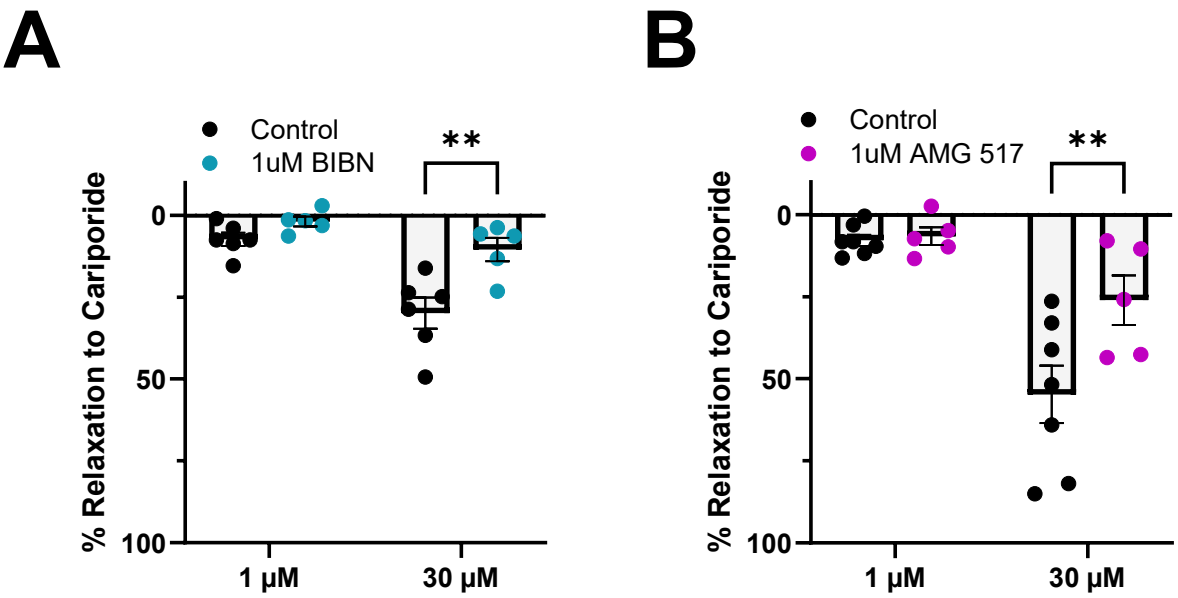


Figure 4.38: Cariporide induced relaxations are impaired by the CGRP blocker, BIBN and TRPV1 blocker, AMG-517.
*Mean relaxation produced by 1µM and 30µM cariporide in the presence (teal) and absence (black) of 1 µM BIBN (A, N=5-6). Mean relaxation produced by 1µM and 30µM cariporide in the presence (purple) and absence (black) of 1 µM AMG-517 (B, N=5-7). All values are expressed as mean ± SEM. A two-way statistical ANOVA with a post-hoc Sidak test generated significant values (**=P<0.01). (N=) number of animals used.*

4.3.21 | Cariporide prevents SGLT2 inhibitor-induced responses in mesenteric arteries.

Our functional assays elucidate that the NHE1 inhibitor, cariporide, induced relaxations in mesenteric arteries that were sensitive to TRPV1 and CGRP receptor blockers, like relaxations produced by SGLT2 inhibitors. This observation substantiates the hypothesis that SGLT2 inhibitors mediate vasorelaxation by inhibiting NHE1 on sensory nerves. Consequently, if cariporide mediates arterial relaxation via CGRP release, then the efficacy of SGLT2 inhibitors in inducing relaxation in pre-contracted mesenteric arteries may be compromised due to a depletion in CGRP reserves. This underscores the potential interplay between NHE1 inhibition, CGRP release, and the vasorelaxant effects of SGLT2 inhibitors.

In mesenteric arteries pretreated with 30µM cariporide, the relaxations to 30µM dapagliflozin or 30µM empagliflozin were significantly smaller ($p<0.001$) than relaxations produced in the time-matched control segments (figure 4.39A-C). The amplitude of methoxamine-induced contractions was not significantly different in

cariporide-treated arteries compared to DMSO-treated (figure 4.39D). These experiments support the hypothesis that the vasodilatory effects of SGLT2 inhibitors were mediated by NHE1 inhibition.

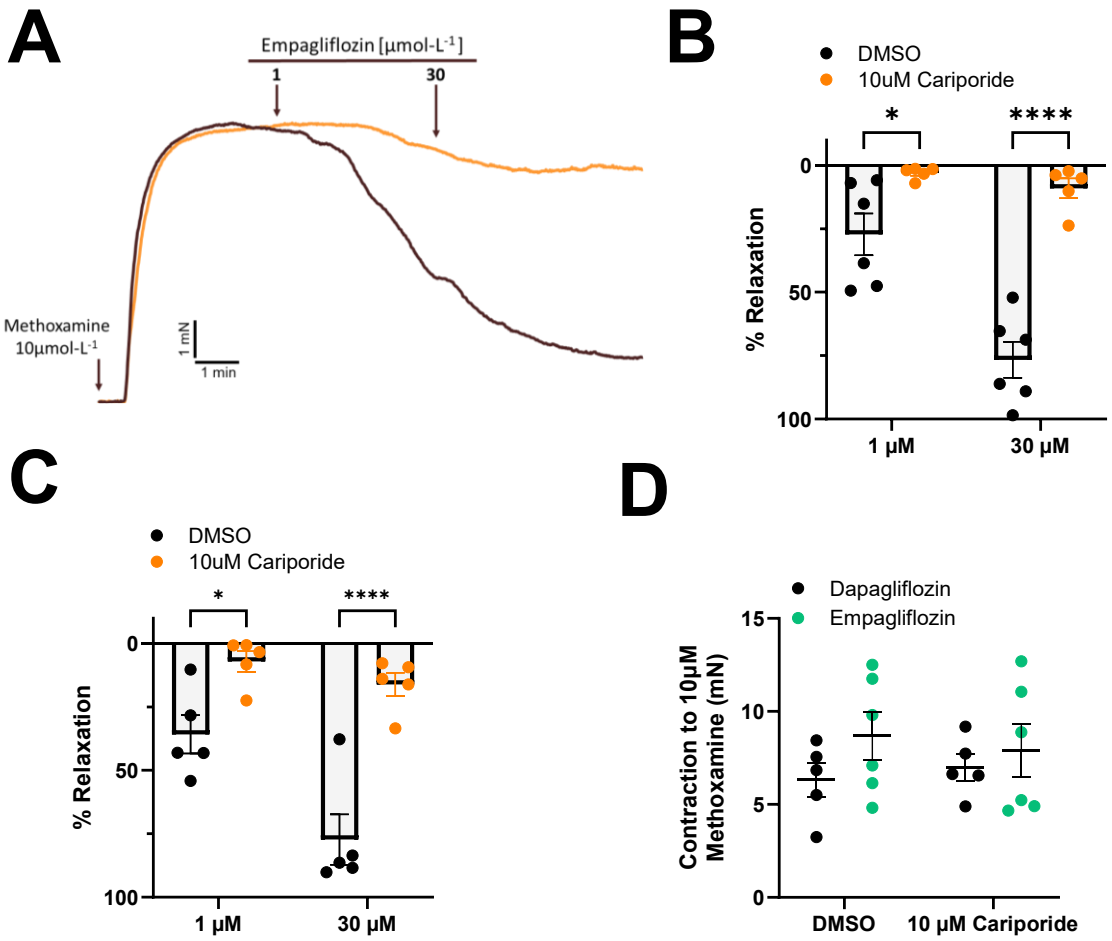


Figure 4.39: Effect of cariporide on SGLT2 inhibitor-induced relaxations.
A representative trace of the relaxation to empagliflozin in mesenteric arteries pre-contracted with 10µM methoxamine in the presence (orange) and absence (black) of cariporide (A). The mean data for the response to 1µM and 30µM empagliflozin (B, N=5) and dapagliflozin (C, N=5) in the presence (orange) and absence (grey) of 10µM cariporide is shown in Panel B and C. D shows the mean amplitude of the contraction produced by 10µM methoxamine under the different conditions. All values are expressed as mean ± SEM. A two-way statistical ANOVA with a post-hoc Sidak test was used to generate significant values (=P<0.05, **=P<0.01, ***=P<0.001, ****=P<0.0001). (N=) number of animals used.*

4.3.22 | Knock-down of NHE1 impairs the relaxation to dapagliflozin and empagliflozin.

To confirm that SGLT2-induced relaxations were mediated by NHE1 inhibition, morpholino-based molecular interference was used to reduce NHE1 protein expression in mesenteric arteries. For this knock-down to occur, local non-nuclear translation of NHE1 was needed, and previous studies have shown this occurs in sensory neurones (Gamarra et al., 2021). The effect of SGLT2 inhibitors on methoxamine contractions was compared in mesenteric arteries with NHE1 knock-down morpholino and scrambled control morpholino. Cumulative concentrations of methoxamine (10nM - 30μM) were applied to knock-down and scramble control arteries pre-incubated with either 30μM of dapagliflozin or empagliflozin. This protocol was chosen due to the lack of stable tone for methoxamine-induced contractions after incubation for 72 hours.

In control arteries transfected with non-targeting scrambled morpholinos, 5 min application of either 30μM empagliflozin or dapagliflozin reduced contractions produced by 10μM methoxamine by >70% (figure 4.40). However, in arteries transfected with translation-blocking morpholinos targeted against NHE1, empagliflozin or dapagliflozin had a negligible effect on methoxamine-induced contractions (figure 4.40). Immunohistochemical studies revealed that targeting morpholinos considerably reduced NHE1 staining in the adventitia compared to scrambled morpholinos (figure 4.41). These studies corroborate our hypothesis that SGLT2 inhibitors relax mesenteric arteries through NHE1-inhibition-induced release of CGRP.

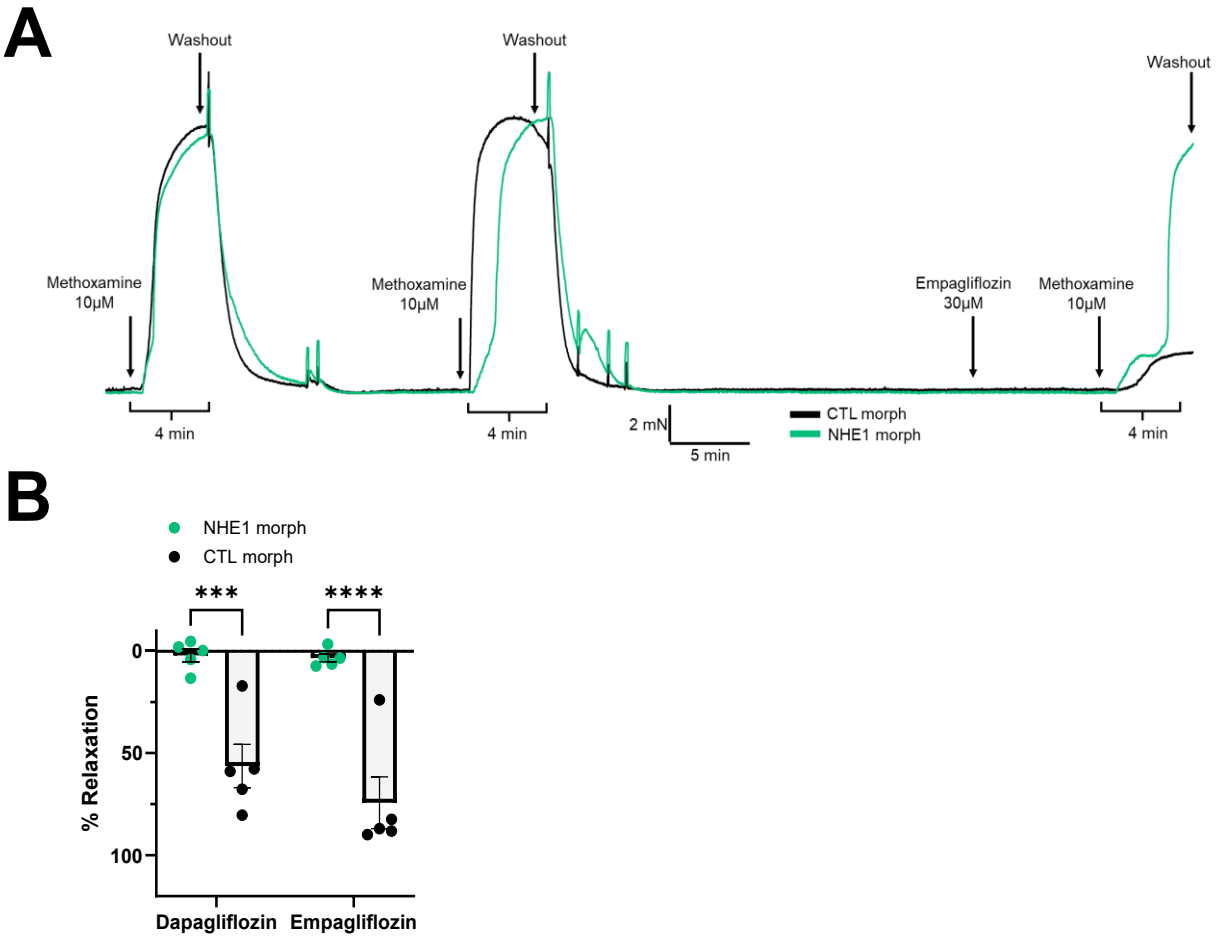


Figure 4.40: Knock-down of NHE1 impairs the relaxation to dapagliflozin and empagliflozin in mesenteric arteries.
*(A), representative trace of the contraction to 10μM methoxamine in the presence of 30μM empagliflozin in scrambled CTL morpholino (black) and knock-down NHE1 morpholino (green) arteries. (B), shows the mean data of the contraction to 10μM methoxamine in scrambled control morpholino (black) and knock down NHE1 morpholino (green) arteries when pre-incubated with 30μM dapagliflozin or 30μM empagliflozin (N=5). All data is represented as mean ±SEM denoted by the error bars. A two-way statistical ANOVA with a post-hoc Sidak test was used to generate significant values (***=P<0.001, ****=P<0.0001) (N= number of animals used).*

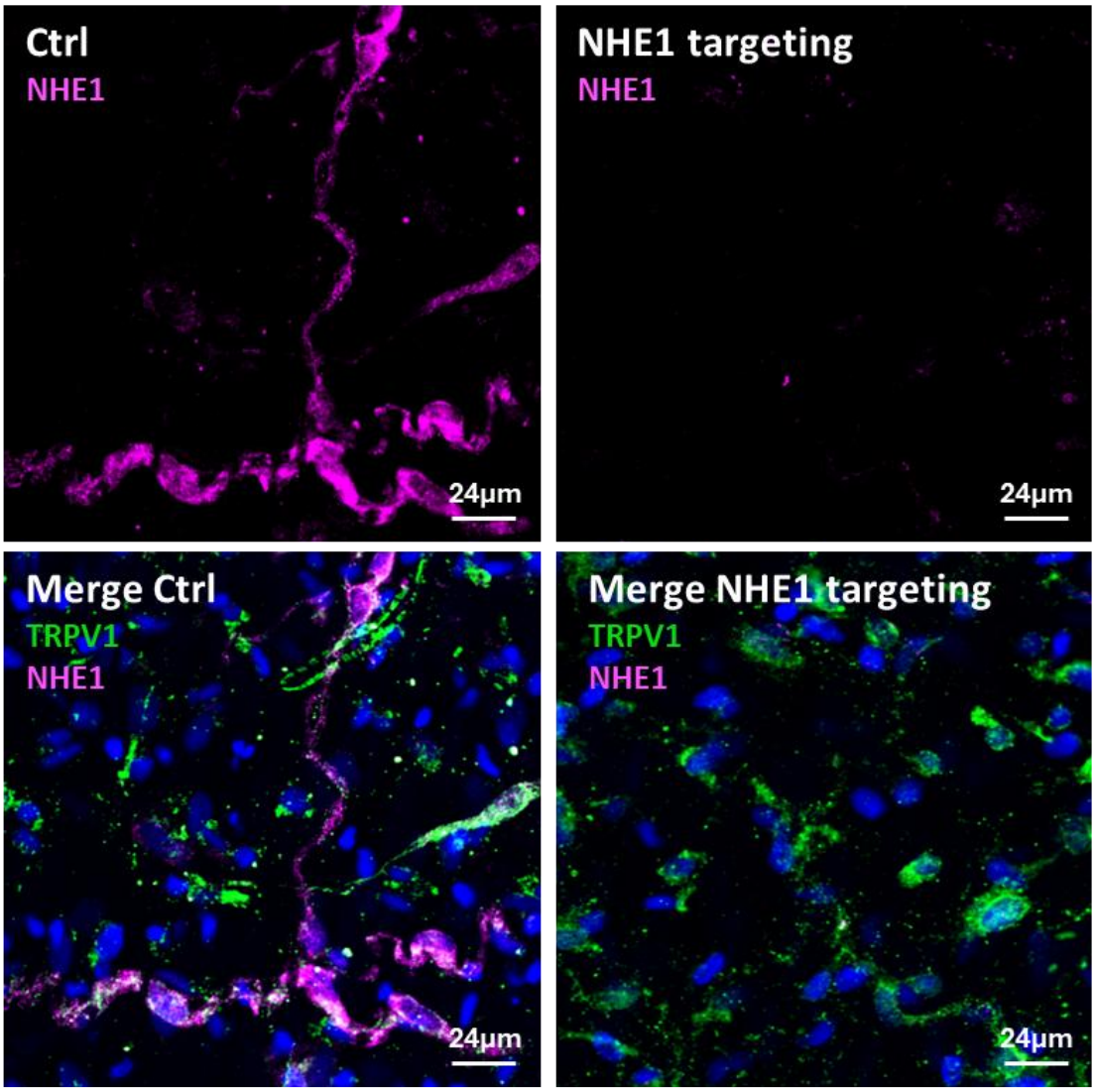


Figure 4.41: Representative labelling for TRPV1 (green) and NHE1 (magenta) in the adventitia of whole mesenteric arteries transfected with scrambled morpholino and NHE1 targeted morpholino.

4.4 | Discussion

This study investigated the underlying mechanism of SGLT2 inhibitor-induced relaxation of arteries and identified a role for CGRP release from sensory nerves mediated by NHE1 inhibition. The current investigation demonstrates that structurally distinct inhibitors of SGLT1 and SGLT2 relaxed mesenteric arterial segments equipotently in contrast to their ability to block SGLT2 mediated glucose transport where the Ki for ertugliflozin, dapagliflozin, empagliflozin and mizagliflozin is 0.88nM<1.1nM<3.1nM<27nM respectively (Grempler et al., 2012; Wright, 2021). The concentrations used in this study (10 μM to 100 μM) exceed the therapeutic plasma concentrations observed in humans, which are approximately 0.3 μM for a standard 10 mg dose of empagliflozin and 8 μM for the maximal administered dose of 800mg (Seman et al., 2013). Nonetheless, translating minor alterations in vascular tension to physiological implications on vascular resistance and blood flow presents challenges in an ex vivo context. Employing elevated drug concentrations in ex vivo experiments is a customary practice to elucidate underlying cellular mechanisms. The dosages applied within this study are consistent with those utilised in prior research involving mesenteric arteries, aortic rings, and coronary arterial tissues (Choi et al., 2023; Hasan, Menon, et al., 2022; Hasan & Hasan, 2021; H. Li et al., 2018; Seo et al., 2020).

This study shows that the relaxations produced by dapagliflozin and empagliflozin in mesenteric arteries were sensitive to TRPV1 and Kv7 channel blockade. However, electrophysiology recordings showed that SGLT2 inhibitors did not directly activate Kv7 and TRPV1 channels. Suggesting an ‘upstream’ mediator was involved. The consolidated view is that CGRP released from sensory nerves underpins the majority of the relaxation to SGLT inhibitors. This is based upon the following evidence: Relaxations to dapagliflozin and empagliflozin were attenuated markedly by CGRP receptor blockade or by depletion of sensory nerve neurotransmitters via capsaicin pre-treatment. Both agents were ineffective at producing relaxations in renal and septal arteries, where there was little to no staining of TRPV1 and CGRP in the adventitia of septal and renal arteries compared to mesenteric arteries. The NHE blocker cariporide also relaxed mesenteric arteries, which were sensitive to CGRP receptor and TRPV1 blockade, but had no effect in renal and septal arteries. Strikingly, NHE1 but not SGLT2 proteins colocalised with TRPV1 in the sensory nerves and pre-application of

cariporide or knock-down of NHE1 using targeted morpholino considerably attenuated the relaxations produced by empagliflozin and dapagliflozin.

Whilst SGLT2 was expressed in vascular smooth muscle cells, the functional data and imaging studies suggest that the relaxation produced by SGLT inhibitors is not due to direct action on SGLT2 but rather that SGLT2 inhibitors influence arterial reactivity by promoting the release of CGRP and potentially other neuropeptides from sensory nerves. This effect appeared to be mediated by the inhibition of NHE1, as reported previously (Baartscheer et al., 2017; De Stefano et al., 2021; Uthman et al., 2018) which was supported by the NHE1 knock-down functional studies. As the density of sensory nerves varies along the arterial bed and vasculature, this can explain the wide variability in the effectiveness of SGLT2 inhibitors to evoke relaxations shown in previous studies (Hasan, Menon, et al., 2022; Hasan, Zerin, et al., 2022; Hasan & Hasan, 2021).

4.4.1 | SGLT inhibitors induce arterial relaxations.

The effect of SGLT2 inhibitors on the vasculature has only recently been investigated, and their mechanism of action is ill-defined. Previous studies have looked at the effect of empagliflozin, dapagliflozin, and canagliflozin on rabbit aortic rings and rat mesenteric arteries, with a consensus that these inhibitors evoke vasorelaxation. However, different mechanisms have been proposed, and they are often contradictory. This study shows that the relaxations produced by dapagliflozin, empagliflozin and SGLT1 inhibitor mizagliflozin in pre-contracted mesenteric arteries were not sensitive to a range of K channel blockers (HMR-1556, iberiotoxin, 4-aminopyridine, tetraethylammonium and glibenclamide) but were sensitive to the pan-Kv7 channel blocker linopirdine, in agreement with earlier work in mesenteric arteries. However, our electrophysiological recordings showed that neither dapagliflozin nor empagliflozin directly enhanced potassium currents in oocytes expressing Kv7.4, Kv7.5 and KCNE4 (the combination in arterial smooth muscle, Barrese et al. 2018), suggesting that Kv7 channel activation is secondary to the direct action of SGLT2 inhibitors releasing a chemical intermediate.

This present study and past publications do show that the pan Kv7 blocker linopirdine impaired CGRP-induced relaxation in pre-contracted mesenteric and cerebral arteries (Chadha et al., 2014; Stott et al., 2018 and Van der Horst et al.,

2020). Therefore, these channels could be functional endpoints of the sensory nerve relaxation cascade that starts with TRPV1 in the sensory nerves and CGRP release. KATP and BKCa channels are known to be involved in CGRP-induced relaxation (Sheykhzade & Berg., 2001 and Norton & Segal., 2018), but recent studies have demonstrated that Kv7 channels and Gβγ subunit signalling play a more prominent role (Stott et al., 2018; Vries et al., 2024 & Chadha et al., 2014). Since this study did not demonstrate a complete inhibition of SGLT2-induced relaxation in the presence of linopirdine, it suggests that other signalling pathways, such as those involving Gβγ subunits or the inhibition of calcium channel activity, may also contribute to CGRP signalling and SGLT2 inhibitor-induced relaxations. To further investigate these mechanisms, experiments could be conducted to assess relaxations to SGLT2 inhibitors in the presence and absence of the Gβγ blocker Gallein. Additionally, calcium signalling in whole arteries could be recorded in the presence of dapagliflozin and empagliflozin.

4.4.2 | The role of CGRP release in SGLT1 and SGLT2 inhibitor-induced arterial relaxation

The present study hypothesises that the arterial relaxation produced by the structurally dissimilar SGLT2 and SGLT1 inhibitors was mediated predominantly by CGRP release from perivascular sensory nerves (Aalkjaer et al., 2021). The presence of dense sensory nerve innervation in the adventitia was confirmed in mesenteric arteries via immunohistochemistry with well-validated CGRP and TRPV1 antibodies, and this correlated with the artery's responsiveness to SGLT2 inhibitors. In contrast, SGLT2 inhibitors were poor or ineffective relaxants in renal and septal arteries, respectively, that correlated with negligible or no TRPV1 or CGRP staining in the adventitia. Dapagliflozin, empagliflozin and mizagliflozin-induced relaxations in mesenteric arteries were impaired by blocking the CGRP receptor with BIBN-4096. However, the lack of complete inhibition suggests other neuropeptides, such as substance P, may also be released. Interestingly, the effectiveness of Zinc Pyrithione, which also relaxes arteries through a release of CGRP from sensory nerves, was far greater in mesenteric arteries compared to renal and coronary arteries (Betrie et al., 2021).

TRPV1 is a polymodal cation channel that is regulated by various exogenous and endogenous activators. These include noxious chemicals (capsaicin or vanilloids), low pH (<6.0), high temperatures >43°C (Caterina et al. 1997), lipid mediators (i.e., anandamide), lipoxygenase products (e.g., LTB4) (Huang et al. 2002) and several signalling molecules (NGF, ATP and PAR-2 agonists)(Chuang et al. 2001; Fernandes et al. 2012). The influx of cations through TRPV1 channels triggers the fusion of synaptic vesicles that contain CGRP and other neuropeptides. The SGLT2 inhibitor-induced relaxations of mesenteric arteries were equally prevented by applying the TRPV1 blocker AMG-517 or by depletion of CGRP through capsaicin treatment but not by the TRPA1 inhibitor AM0902. This suggests that the recruitment of TRPV1 rather than TRPA1 channels in sensory nerves is a key step in SGLT2 inhibitor-induced relaxations in the mesenteric artery.

Our findings align with the idea that SGLT2 inhibitors induce relaxation in mesenteric arteries by facilitating the release of CGRP, a process that relies on TRPV1 channels. However, in HEK293 cells over-expressing rat TRPV1 dapagliflozin and empagliflozin failed to either activate TRPV1 currents or enhance the effect of low pH or capsaicin, suggesting that these agents do not work directly on the channel. Therefore, TRPV1 activation is a consequence of an additional mechanism. The calcium-sensing receptor (CaSR) expressed on perivascular sensory nerves induces arterial vasorelaxation upon increased extracellular calcium in mesenteric arteries. The activation of CaSR leads to CGRP release from sensory nerves and is found to be mediated by TRPV4/C1 channels through nitric oxide production (Greenberg et al., 2017, 2019). Recent findings have shown this CaSR relaxation was attenuated upon depletion of sensory nerves using the same capsaicin treatment employed in this study and incubation with BIBN-4096 and CGRP receptor blocker (Carlton-Carew et al., 2024). The similarities in these findings with the present study suggest that SGLT2 inhibitors could indirectly activate the CaSR on perivascular nerves, contributing to the SGLT2-induced relaxation seen in mesenteric arteries.

4.4.3 | NHE1 in arterial relaxation

NHE1 serves a crucial function in cardiomyocytes and vascular smooth muscle cells, primarily to regulate and maintain cellular pH levels around the physiological value of 7.2. Variations in the expression and activity of NHE have been associated

with major cardiac events. Specifically, during ischemic conditions, the alteration in pH triggers the activation of NHE, which subsequently leads to cardiac injury. Numerous cardioprotective effects of SGLT2 inhibitors have been associated with a decrease in sodium ion (Na+) load and the regulation of pH in cardiomyocytes, mediated through the influence on NHE1 (Baartscheer et al., 2017; Uthman et al., 2018a; De Stefano et al., 2021). However, this assertion has been contested by Chung et al. (2021), with the potential role of NHE1 suppression in the arterial benefits of SGLT2 inhibitors remaining undetermined, although De Stefano et al. (2021) have hypothesised a role for NHE1 inhibition in the relaxation of human visceral arteries induced by canagliflozin. Activation of NHE1 is associated with vasoconstriction, and it augments the myogenic response in the resistance arteries of mice (Artamonov et al., 2018). An escalation in NHE1 activity has also been implicated in the onset of pulmonary artery hypertension and the proliferation and remodelling processes (Lade et al., 2023). Upon identifying the presence of NHE1 in perivascular sensory nerves on mesenteric arteries, we postulated that NHE1 has a role in arterial function due to its influence on the activity of TRPV1 and subsequent vesicular release of potent vasodilators, including CGRP.

The current study corroborates this hypothesis as the NHE1 inhibitor, cariporide, induced relaxation in mesenteric arteries that was negated by the CGRP receptor antagonist, TRPV1 blocker, and the depletion of sensory nerves. Notably, the pre-application of cariporide and, importantly, the morpholino-based silencing of NHE1 nullified the response to dapagliflozin and empagliflozin. Intriguingly, only NHE1 was detected in sensory nerves, unlike in the proximal convoluted tubule where SGLT2 and NHE1 coexist in the same microdomain, and the inhibition of NHE1 in smooth muscle cells has also been found to exert some influence on the arterial contractile state. Boedtkjer et al., 2012 reported that NHE1 knockdown mice have lower mean arterial pressure and a 30% smaller media thickness, with a significantly reduced media thickness to lumen diameter ratio. These outcomes were associated with a shift in pH levels and a marked reduction in rho kinase-dependent VSMC Ca^{2+} sensitivity (Boedtkjer et al., 2012). This is supported by Boedtkjer et al., 2011 who showed that intracellular VSMC acidification increased arterial contractility by inhibiting rho kinase-dependent VSMC Ca^{2+} sensitivity as well as myosin light chain phosphatase phosphorylation. This further implies that the relaxation induced by SGLT2 inhibitors is not a result of SGLT2 activation but

rather the inhibition of NHE1, suggesting a critical interplay between NHE1 and TRPV1 in regulating vascular tone.

4.4.4 | Limitations

The results from this chapter were mainly generated from wire-myography experiments, which have many limitations. Isometric tension myography studies will record the change in arterial tone before and after applying a drug to the vessel's bath, allowing us to see the relaxation induced by SGLT2 inhibitors. However, pre-incubating in pharmacological antagonists such as BIBN-4096 and seeing a reduction in the relaxation is needed to identify the signalling mechanism responsible for the relaxation. This results in a reductionist approach as it becomes challenging to know whether the change in the concentration-effect curve produced is due to inhibiting CGRP receptors and, therefore, suggesting their involvement or whether the inhibition of TRPV1 channels is altering the activity of other vascular pathways indirectly affecting isometric tone. To negate this issue, patch clamp electrophysiology experiments were conducted in overexpressed HEK293 cells to investigate the effect of SGLT2 inhibitors on the activity of TRPV1 and Kv7 ion channels. HEK293 cells are relatively easy to culture and have a high transfection efficiency, allowing to record currents from individual ion channels. They also have low endogenous ion channel activity, reducing background noise in recordings. However, using HEK cells has drawbacks. For example, they lack native complex cellular environments such as ion channel protein expression and interactions that may affect the activity of the recorded ion channels. Hence, the results may lack physiological significance. Recording TRPV1 and Kv7.4/5 ion channel currents in the presence and absence of dapagliflozin and empagliflozin in whole isolated smooth muscle cells would curtail this limitation. Moreover, further electrophysiological experiments could have been carried out to examine the effect of SGLT2 inhibitors on calcium channel currents and other sensory neuronal pathways.

4.4.5 | Conclusion

This study reveals that SGLT2 inhibitors induce relaxation in mesenteric arteries. This is achieved through the release of CGRP, which is dependent on TRPV1 and is mediated by the inhibition of NHE1, as shown in figure 4.42 below (Forrester et

al., 2024). Hence, the beneficial effects of SGLT2 inhibitors in patients are derived from their capacity to release the cardioprotective CGRP into circulatory systems. The subsequent vasodilation, combined with the anti-inflammatory and anti-fibrotic properties of CGRP, contributes to maintaining adequate circulation and mitigating cardiovascular stress.

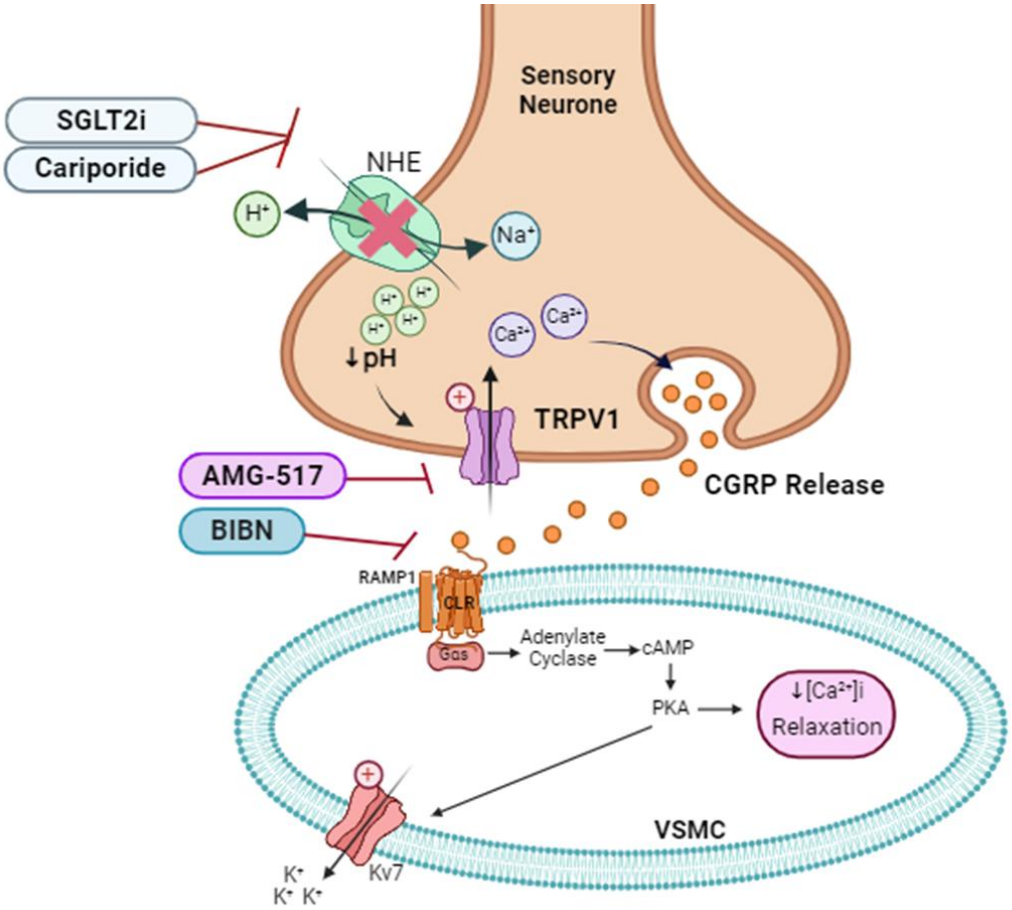


Figure 4.42: Pathway of SGLT2 induced relaxation in mesenteric arteries. *SGLT2 inhibitors acts on the sodium hydrogen exchanger (NHE) to induce vasorelaxation. Hydrogen (H), Sodium (Na), calcium (Ca2+), calcitonin-gene related peptide (CGRP), transient receptor potential vanilloid 1 (TRPV1), calcitonin receptor-like receptor (CLR), receptor activity-modifying protein 1 (RAMP1), cyclic guanosine monophosphate (cGMP), protein kinase A (PKA), voltage gated potassium channel (Kv7). From Forrester et al.,2024.*

Chapter 5: Characterising the functional role of sodium myo-inositol transporters in arteries

5.1 | Introduction

Myo-inositol is a vital organic osmolyte that, when transported, helps regulate osmotic balance without altering inorganic ion levels (Lang et al.,1998). Intracellular levels of myo-inositol are tightly controlled by sodium myo-inositol transporters 1 and 2 (SMIT1 and SMIT2) encoded by Slc5a3 and Slc5a11. Extracellular hypertonicity upregulates the membrane expression of SMIT and elevates the level of intracellular myo-inositol via activating the transcription factor, tonicity-responsive enhancer binding protein (TonEBP). In hypertonic conditions, there is an increase in phosphorylation of TonEBP transactivation domain and nucleocytoplasmic translocation (Tong et al., 2006), which results in TonEBP accumulating in the nucleus and the cytoplasm, stimulating transcription of Slc5a3 by binding to the genes enhancer region (Dai, Yu, Kruse, Traynor-Kaplan, & Hille, 2016). Other factors, such as serine/ threonine protein kinases (SGK) and ubiquitin ligases (NEDD), can also regulate SMIT1 expression (Klaus et al., 2008). In addition to its osmotic role, myo-inositol is metabolised to produce the secondary signalling molecule PIP_2 via phosphatidylinositol 4-kinase (PIP4K) and phosphatidylinositol 5-kinase (PIP5K), whereby if absent, cellular processes, including Kv7-encoded potassium channels (Rodriguez-Menchaca et al., 2012), inwardly rectifying potassium channels (Kir) (Xie et al., 2007), transient receptor potential channels (TRP) (Lemonnier et al., 2008) and epithelial sodium channels (ENaC) (Pochynyuk et al., 2007) will not function. As such, SMIT has a profound influence on the regulation of ion channel activity. Alterations in SMIT1 expression and myo-inositol metabolism have been linked to several diseases, including

Alzheimer's disease, down syndrome, epilepsy, and cardiovascular disease, opening new avenues for potential treatments and interventions.

In addition to transporting myo-inositol, SMIT1 forms complexes with Kv7 ion channels, which are essential in regulating cell excitability. SMIT1 physically interacts with Kv7.1 and Kv7.2 in the choroid plexus and forms complexes with Kv7.2/3 channels in the nodes of Ranvier (Neverisky and Abbott 2017, Dai et al.,2016, Abbott et al., 2017). These interactions enhance Kv7 channel activity independent of the movement of myo-inositol. In recent years, SMIT1 has been found to also physically interact with Kv7.4/5 ion channels in vascular smooth muscle cells, forming complexes that regulate arterial tone (Barrese et al., 2020). Increasing SMIT1 expression via raising extracellular tonicity increased the interaction of SMIT1 with Kv7.4/5 channels and auxiliary subunit KCNE4 in vascular smooth muscle cells and, in turn, elevated Kv7 channel currents, significantly reducing arterial contractility (Barrese et al., 2020). Comparatively, the knockdown of SMIT using Morpholino oligonucleotides increased the contractile response to methoxamine in renal arteries and impaired the effect of Kv7 channel activator ML213 but not any other potassium channel activators. Therefore, the interaction of SMIT1 with Kv7 channels is a novel mechanism that could explain the changes in vascular reactivity observed in cardiovascular diseases associated with hyperosmolarity, such as diabetes. However, the underlying function of SMIT1 in the vasculature is ill-defined.

Many changes in vascular reactivity are associated with hyper-osmolarity. Several papers identify hyperglycaemic type 2 diabetics have an increase in blood pressure, which leads to a higher risk of cardiovascular disease long-term (Davies et al., 2022; Roengrit et al., 2023; Sun et al., 2019) . However, other papers have identified that acute hyperglycaemia in healthy humans enhances vascular endothelial and cardiac microvascular function (Horton et al., 2022). Whereby 4 hours of intravenous-induced hyperglycaemia enhanced brachial artery flow-mediated dilatation and provoked cardiac and skeletal muscle microvascular function. Moreover, in patients with chronic kidney failure, the addition of glucose to dialysis fluid significantly decreased systolic and diastolic blood pressure (Sangill & Pedersen, 2006).

This chapter exploited the osmo-sensitivity of SMIT1 to explore its role in different arteries, following on from the findings obtained by Barrese et al.,2020, primarily focusing on the effect of hypertonicity and sex differences of SMIT1. We hypothesised that SMIT1 regulated arterial contractility and relaxation in male and female arteries. Hence, the aims of this study were to:

1. Investigate the effect of hypertonic medium on SMIT and Kv7 expression in mesenteric and coronary arteries
2. Ascertain the effect of hypertonic medium on vasoconstrictor and vasodilator responses.
3. Investigate how SMIT1 knockdown impacts upon arterial function.
4. Ascertain if there were any sex differences in SMIT1-mediated responses.

5.2 | Methods

Solution osmolarity was defined by the St George's Hospital Clinical Pathology unit using 4 plasma solutions as internal calibrations. In the following studies the osmolarity of the solutions used was (mOSm/ Kg); control PSS (271), PSS + 150 mM raffinose (480), PSS + 20 mM raffinose (319) and PSS + 20 mM glucose (306). Each value is the median of three recordings.

All other aspects of the experiments carried out in this chapter are described in detail in Chapter 2.

5.3 | Results

5.3.1 | The effect of SMIT1-specific morpholino oligonucleotide on vascular smooth muscle cell vasocontractile and relaxant responses

Barrese et al., 2020, investigated the effect of SMIT1-targeted knockdown in renal arteries using morpholino oligonucleotides. The present study sought to examine the impact of SMIT1 knockdown in mesenteric and coronary arteries to understand further the function of SMIT1 in regulating vascular tone. Mesenteric arteries were incubated with either a scrambled control morpholino or a SMIT1-targeted morpholino. The effects of various contractile and vasorelaxant agents were then investigated in SMIT1 knockdown vessels compared to control vessels. Immunohistochemistry staining was performed to show that incubation of mesenteric arteries with a SMIT1-specific morpholino oligonucleotide reduced SMIT1 expression in both endothelial and smooth muscle cell layers. An endothelial cell marker CD31 was used to denote the endothelial arterial layer (red), and DAPI was used as a nuclear stain (blue). SMIT1 staining (green) in mesenteric arteries transfected with a SMIT1-specific morpholino reduced by ~50% compared to control arteries (figure 5.1). The concentration-dependent response curve to methoxamine and U46619 shifted to the left compared to the control, and the raw contraction to methoxamine (figure 5.2) and U46619 (figure 5.3) was significantly greater in arteries transfected with SMIT1 targeted morpholino vessels compared to scrambled control. The EC_{50} of methoxamine in control morpholino vessels and SMIT1-targeted morpholino vessels was 2.5 µM and 2.3 µM, respectively, showing no shift in the sensitivity of the contraction to methoxamine. The EC_{50} of U46619 was 692.6 nM and 47.75 nM, respectively. Hence, the sensitivity to the U46619-induced contraction in SMIT1-targeted vessels shifted to the left. The contraction to 60 mM KCl was similar in both SMIT1-targeted morpholino and control arteries (figure 5.2C). This shows that there was no significant difference in the artery contractile mechanisms; therefore, the target sequences to knock down the SMIT1 gene were responsible for the contractile effect and not the scrambled control morpholino. Interestingly, SMIT1 knockdown had a considerably greater effect on U46619-mediated contractions than

methoxamine-induced contractions. Therefore, the knockdown of SMIT1 enhanced arterial sensitivity to different vasoconstrictive agents.

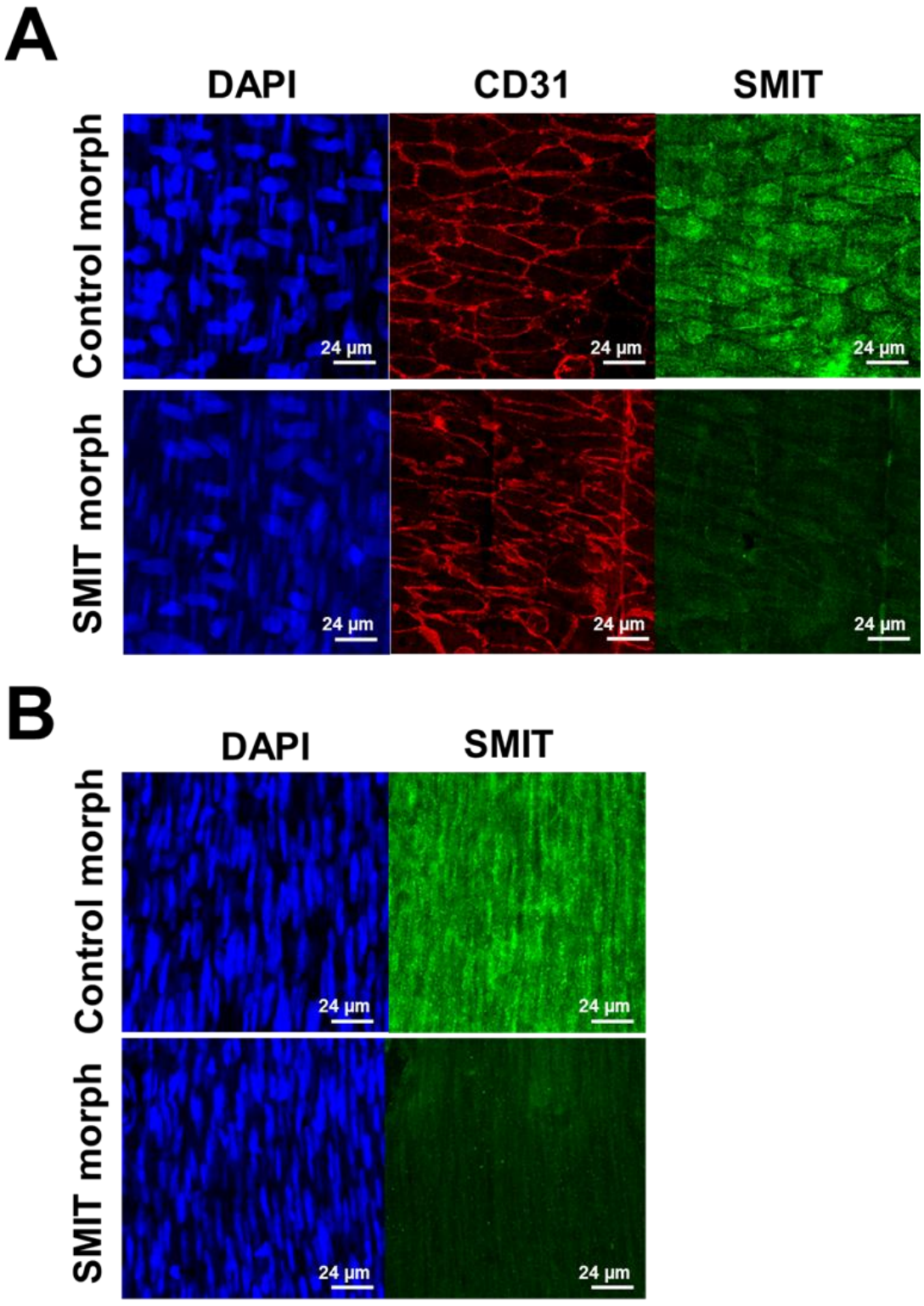


Figure 5.1: SMIT protein expression in control and knockdown smooth muscle cell and endothelial cell layers of whole mesenteric arteries

The expression of SMIT protein in the endothelial cell layer of mesenteric arteries transfected with scrambled control morpholino and SMIT1 targeted morpholino (A). The endothelial cells are stained with CD31, shown in red, with nuclear DAPI stain in blue and the SMIT1 protein stain in red. The expression of SMIT1 protein in

smooth muscle cell layers of mesenteric arteries transfected with scrambled control morpholino and SMIT1 targeted morpholino is shown in panel B.

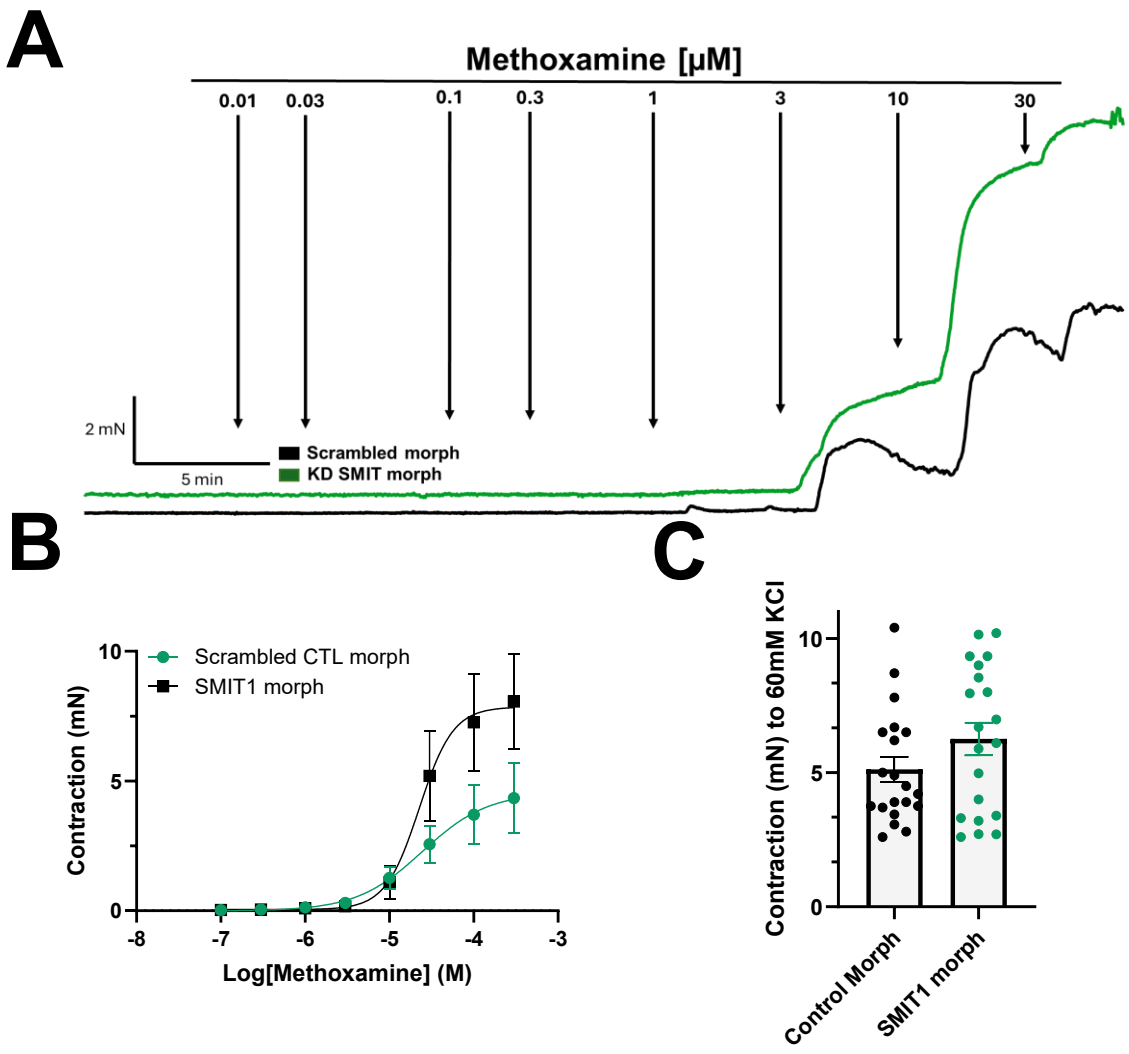


Figure 5.2: The contractile response to methoxamine and 60mM KCl in mesenteric arteries incubated with a scrambled control morpholino or SMIT1 knock-down morpholino

*A representative trace of the concentration-effect curve to methoxamine in mesenteric arteries incubated with either a scrambled control morpholino (black) or a SMIT1-targeting morpholino (green, A). The mean raw concentration-dependent contraction (mN) to methoxamine (10 nM – 10 µM) in mesenteric arteries incubated with either a scrambled control morpholino (black, EC_{50}= 2.45 µM) or a SMIT1 targeted morpholino (green, EC_{50}=2.26 µM) is shown in panel B (N=8). The contraction in mN to 60 mM KCl in mesenteric arteries incubated in scrambled control morpholino (black) or SMIT1 targeted morpholino (green, C) (N=20). All data points are shown as mean +-SEM denoted by error bars, and statistical values are determined by 2-way ANOVA with multiple comparisons are calculated using post hoc Bonferroni test where *=P<0.05, **=P<0.01, ***=P<0.001, ****=P<0.0001. (N= number of animals).*

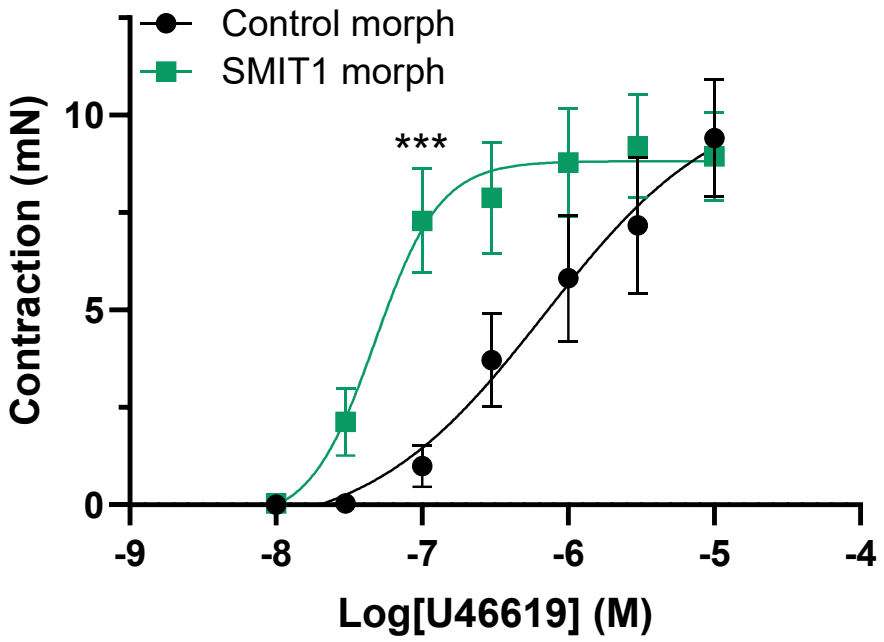


Figure 5.3: The contractile response to methoxamineU46619 in mesenteric arteries incubated with a scrambled control morpholino or SMIT1 knock-down morpholino
*The mean raw concentration-dependent contraction (mN) to U46619 (10 nM – 10 uM) in mesenteric arteries incubated with either a scrambled control morpholino (black, EC_{50} =692.6 nM) or a SMIT1 targeted morpholino (green, EC_{50} =477.5 nM) (N=8). All data points are shown as mean +-SEM denoted by error bars, and statistical values are determined by 2-way ANOVA with multiple comparisons are calculated using post hoc Bonferroni test where *=P<0.05, **=P<0.01, ***=P<0.001, ****=P<0.0001. (N= number of animals).*

5.3.2 | SMIT1 knock-down impaired the relaxation responses of CGRP and isoprenaline

Having established that SMIT1 modulated responses to vasoconstrictors, we evaluated whether SMIT1 knockdown affected the ability of arteries to relax in response to vasodilators. The effect of SMIT1 morpholino-induced knock-down on receptor-mediated vasodilation was investigated using agonists of two different G-protein-coupled receptors, namely isoprenaline (mixed β-adrenoreceptor) and CGRP. Both isoprenaline (1 nM—1 μM) and CGRP (10 ρM —1 nM) potently relaxed vessels transfected with a control morpholino (figure 5.4 and figure 5.5). These relaxations to both isoprenaline and CGRP were significantly impaired in arteries incubated in a SMIT1-targeted morpholino. A 36.7±5.1% reduction in the

relaxation to 30 nM isoprenaline and a 27.3±6% reduction to 1 nM CGRP were identified in SMIT1 targeted morpholino vessels. Additionally, the IC50 of isoprenaline shifted from 83.26 nM in control morpholino vessels to 303.9 nM in SMIT1-targeted vessels, suggesting that in SMIT1-targeted morpholino vessels had a reduced sensitivity to isoprenaline-induced relaxations shifting the curve to the right. Comparatively, the IC50 of CGRP in control morpholino vessels and SMIT1-targeted morpholino vessels was 151.3 ρM and 288.4 ρM, respectively, suggesting no change in the sensitivity of the CGRP response curve. This indicated that knocking down SMIT1 impairs the efficacy of several vasodilatory agents and enhances overall arterial contractility.

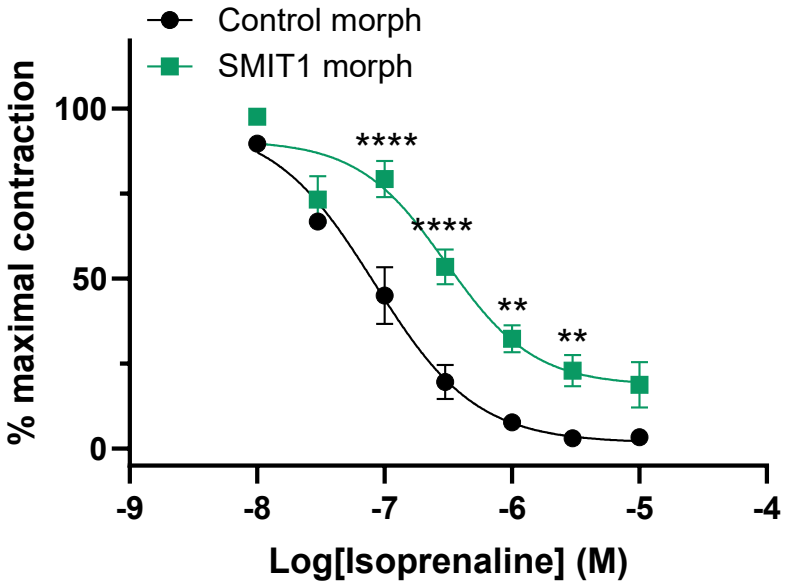


Figure 5.4: The relaxation response to the beta-adrenergic receptor agonist, isoprenaline in control and SMIT1 targeted morpholino vessels.
*The mean concentration-dependent relaxation (mN) to Isoprenaline (1 nM – 1 μM) in scrambled control morpholino (black, IC50 =83.26 nM) and SMIT1 targeted morpholino (green, IC50 =303.9 nM) mesenteric arteries pre-contracted with 300 nM U46619 (N=6). All data points are shown as mean +-SEM denoted by error bars, and statistical values are determined by 2-way ANOVA with multiple comparisons are calculated using post hoc Bonferroni test where *=P<0.05, **=P<0.01, ***=P<0.001, ****=P<0.0001.*

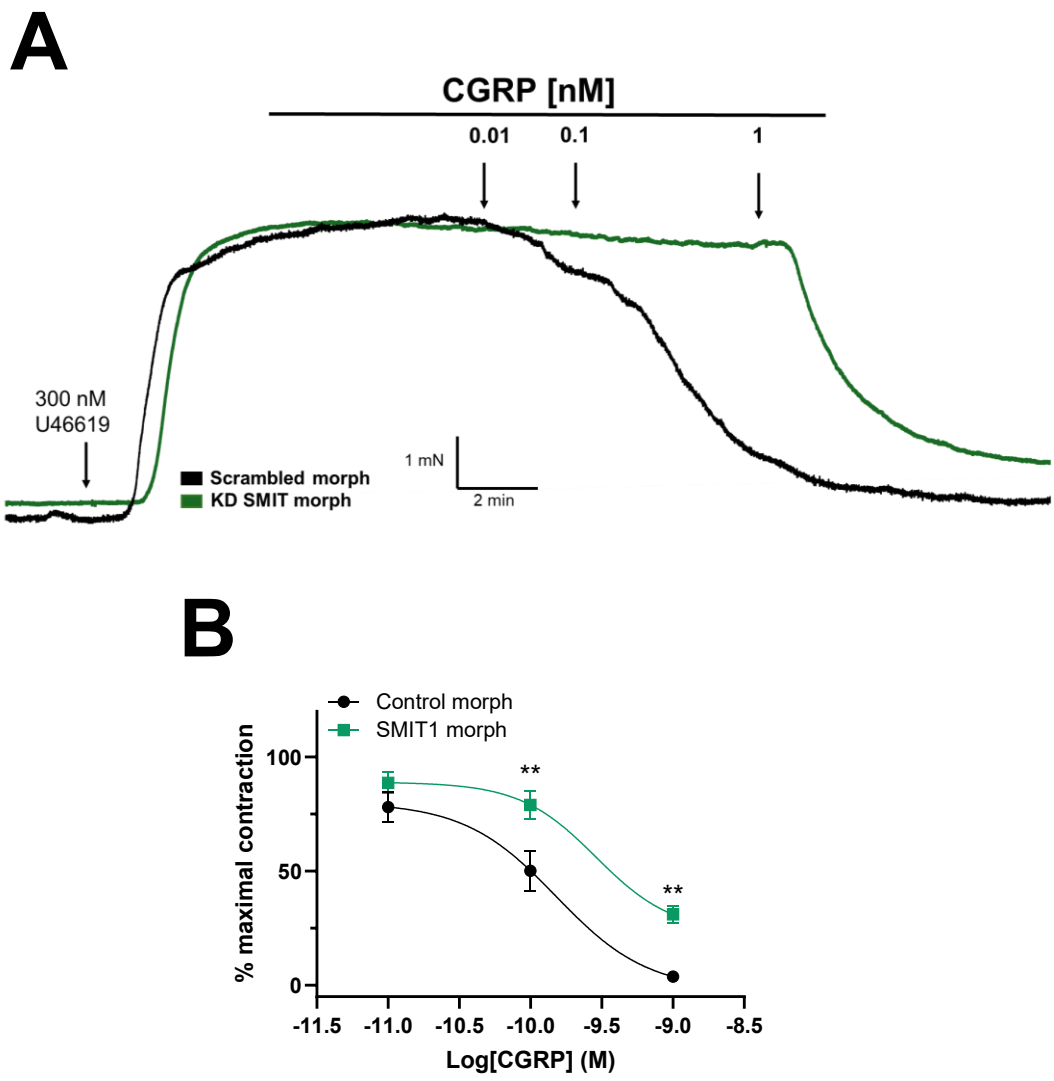


Figure 5.5: The relaxation response to CGRP receptor agonist in control and SMIT1 targeted morpholino vessels.

*A representative trace of the relaxation to CGRP in pre-contracted mesenteric arteries incubated in a scrambled control morpholino (black) or a SMIT1 targeted morpholino (green, A). The mean concentration-dependent relaxation (mN) to CGRP (10 pM – 1 nM) in scrambled control morpholino (black, IC50= 151.3 pM) and SMIT1 targeted morpholino (green, IC50 = 288.4 pM) mesenteric arteries pre-contracted with 300 nM U46619 is shown in panel B (N=7). All data points are shown as mean +-SEM denoted by error bars, and statistical values are determined by 2-way ANOVA with multiple comparisons are calculated using post hoc Bonferroni test where *=P<0.05, **=P<0.01, ***=P<0.001, ****=P<0.0001.*

5.3.3 | Raffinose incubation increased SMIT1 expression in isolated vascular smooth muscle cells

The effect of hypertonicity on SMIT1 expression in renal arteries has been previously investigated (Barrese et al., 2020). Using immunocytochemistry, these experiments ascertained the effect of bathing arteries in 150 mM raffinose on the expression of SMIT1 in mesenteric and coronary arteries from male rats. Arteries were incubated in control PSS or 150 mM raffinose PSS for 4 hours, and vascular smooth muscle cells were isolated. Raffinose increased total SMIT1 expression in both mesenteric and coronary arteries in male rats. The corrected total cell fluorescence (CTCF) intensity of SMIT1 in male mesenteric and coronary arteries increased approximately sevenfold when incubated in 150 mM raffinose for 4 hours (figure 5.6). The SMIT1 staining formed clusters around the VSMC membrane, increasing after raffinose incubation.

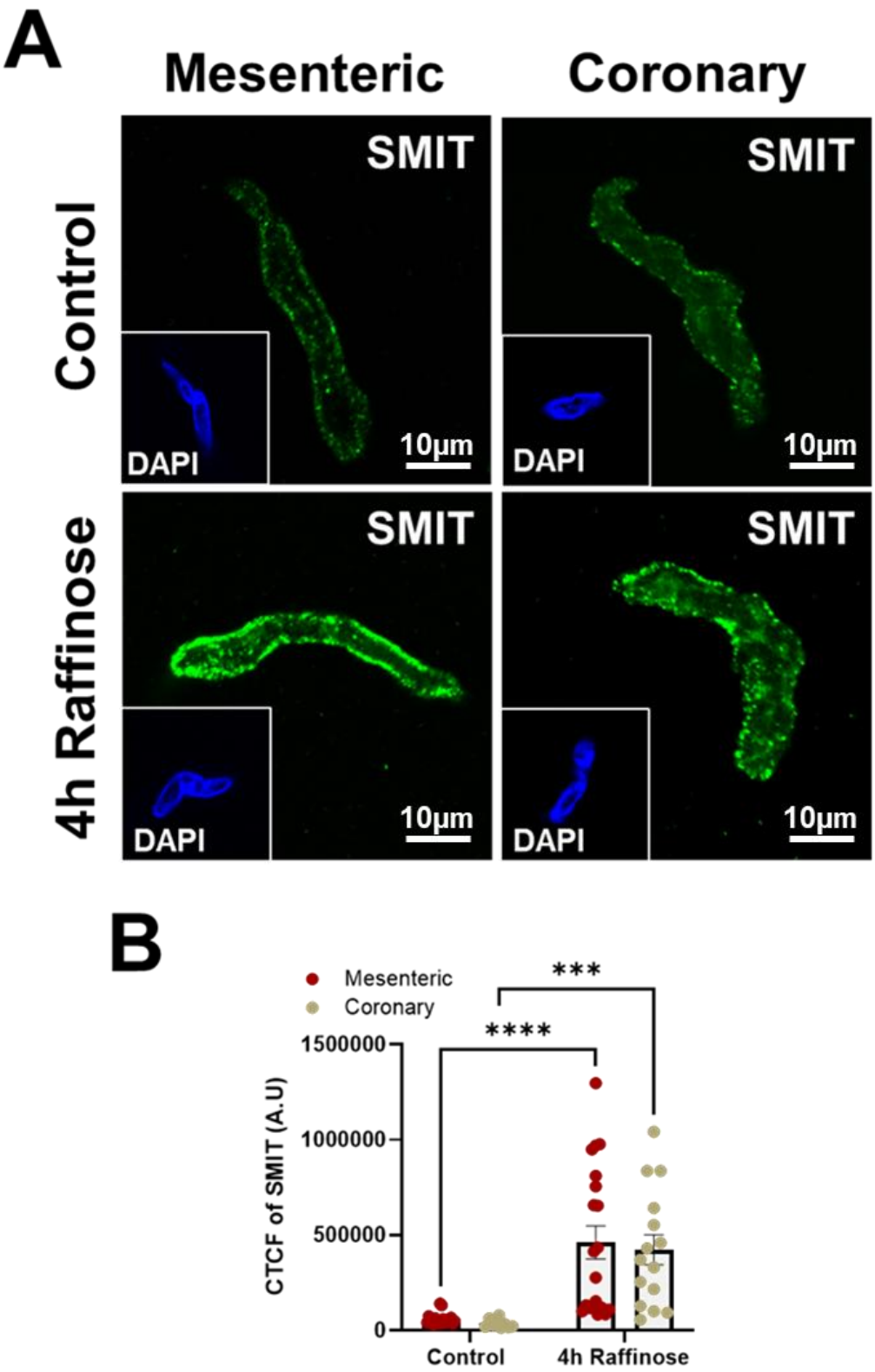


Figure 5.6- The expression of SMIT1 in VSMCs from mesenteric and coronary arteries isolated from male rats with and without incubating in raffinose for 4 hours: *Representative image of SMIT1 staining in isolated vascular smooth muscle cells from mesenteric and coronary arteries isolated from male rats in the presence and absence of incubating in 4 hours of 150 mM raffinose (A). Mean data showing the corrected total cell fluorescence (CTCF) intensity of SMIT1 in mesenteric (Red, N=4,n=20) and coronary arteries (Beige, N=3, n=15) before and after 4-hour incubation in raffinose. Data shown as mean+- SEM denoted by error bars and p-*

*values were calculated using a two way-ANOVA, and a post-Hoc Sidak test was used for multiple comparisons where ***=P<0.001, ****=P<0.0001. (N= number of animals used, n= number of technical repeats).*

5.3.3.1 | Augmented membrane abundance of SMIT1 after incubating in 150mM raffinose PSS

A line scan analysis using the membrane marker wheat germ agglutinin to denote membrane localisation identified the membrane abundance of SMIT1 in vascular smooth muscle cells. The membrane: cytosol ratio of SMIT1 was calculated in mesenteric and coronary smooth muscle cells incubated in control PSS and 150 mM raffinose PSS. The fluorescence intensity of SMIT1 and WGA measured across the cell shows two clear overlapping peaks, indicating the presence of SMIT1 in the membrane (figure 5.7A-B). There was a significant 2-fold increase in the membrane abundance of SMIT1 in male mesenteric arteries but not in coronary arteries (figure 5.7C). These results demonstrate that incubating arteries in raffinose increases the total protein expression and membrane abundance of SMIT1.

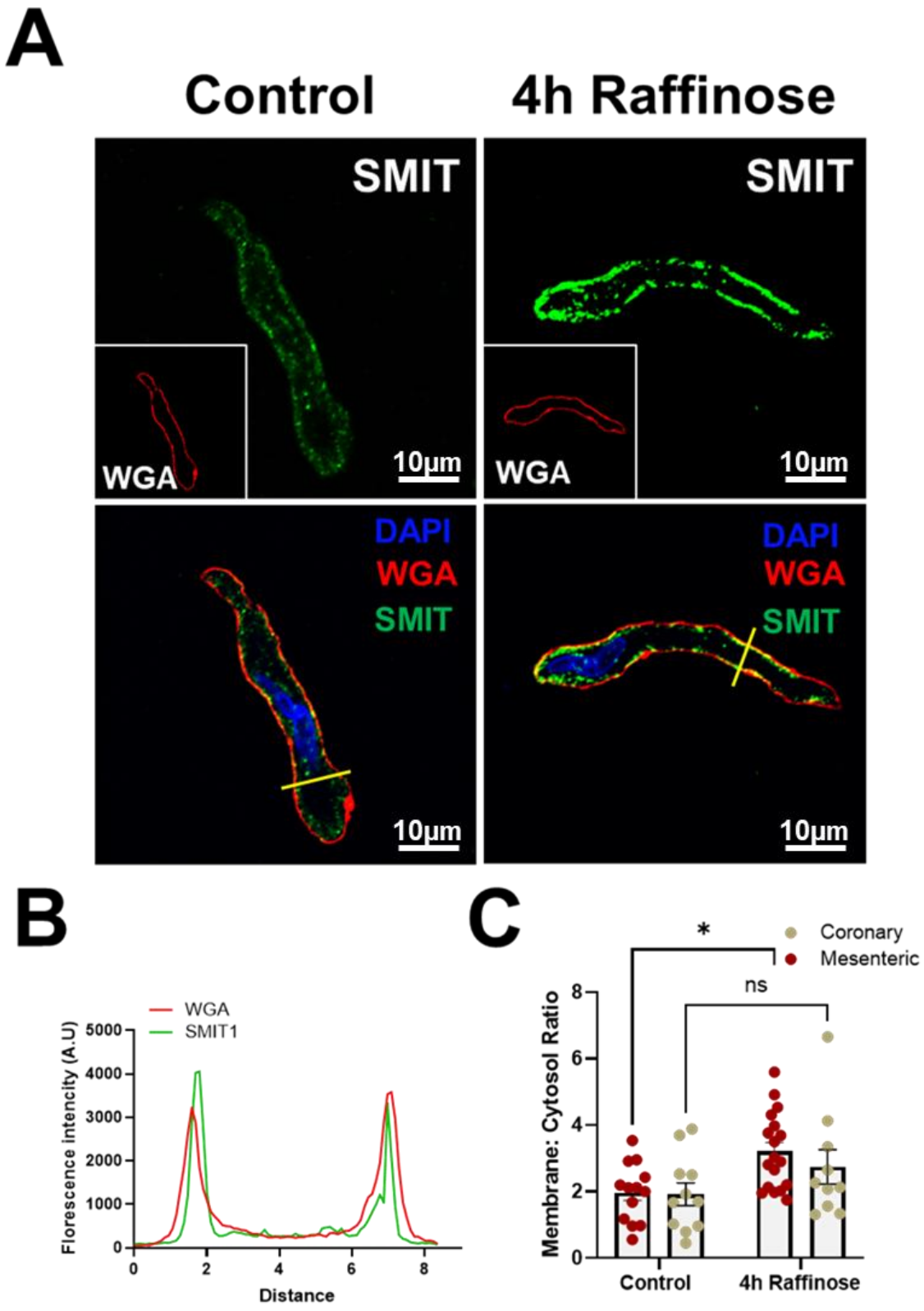


Figure 5.7: The change in membrane abundance of SMIT1 in male mesenteric and coronary arteries after incubating in 150 mM raffinose for 4-hours.

A representative image of male vascular smooth muscle cells stained with SMIT1 (green), membrane marker, wheat germ agglutinin (WGA, red) and nucleus stain with DAPI in control (A, left) and after 4 hours 150 mM raffinose (A, right). The fluorescence intensity of SMIT and WGA measured across a cell, marked by the yellow line, is shown in panel B. Mean membrane cytosol ratio of SMIT1 in

*mesenteric (red, N=3, n=15) and coronary (beige, N=3, n=10) arteries from male rats is shown in panel C. Data shown as mean+- SEM denoted by error bars and p-values were calculated using a two way-ANOVA, and a post-Hoc Sidak test was used for multiple comparisons where *=P<0.05. (N= number of animals used, n= number of technical repeats).*

5.3.4 | Augmenting membrane expression of SMIT1 attenuated the vasoconstrictor responses to methoxamine, U46619 and KCl

Having established that SMIT1 knockdown enhanced vasoconstrictor responses and impaired vasodilator responses, experiments were performed on arteries incubated in raffinose to ascertain the effect of increased SMIT1 expression on vasoconstrictor responses. Barrese et al (2020) showed that incubation of renal arteries with 150 mM raffinose overnight (~16h) caused considerable inhibition of methoxamine-mediated contractions and markedly shifted the sensitivity to the right. Overnight incubation of mesenteric and coronary arteries with 150 mM raffinose led to a similarly marked impairment of the contractile response to methoxamine with a concomitant rightward shift in the potency (figure 5.8). Subsequent experiments were performed to ascertain the time course of the effect of raffinose in mesenteric arteries by incubating in raffinose for different lengths of time (10 minutes, 30 minutes, 1 hour, 2 hours, 4 hours and 6 hours). Mesenteric arteries were incubated in 150mM raffinose PSS, which was then removed and replaced with fresh PSS, and the contractile response to methoxamine was recorded, as shown in the representative trace in figure 5.9A. Control vessels were incubated in PSS at a duration of 6 hours alongside the vessels incubated with 6-hour raffinose. Raffinose was added to the bath of other vessel segments at various time points throughout the 6-hour period, ensuring all experiments concluded at the 6-hour endpoint. Bathing mesenteric arteries in 150 mM raffinose produced an immediate contraction of 0.98±0.12 mN (n=15) that waned over 10 mins to a new level of 0.12±0.04 mN (figure 5.9A). Application of methoxamine after washout of raffinose incubated for 10 minutes, 30 minutes, 1 hour, and 2 hours resulted in contractions that were significantly smaller than the initial concentration response (figure 5.9B). Further incubating the arteries in raffinose PSS for 4 hours and 6 hours abolished the contractions to methoxamine, while incubating in raffinose overnight significantly reduced the sensitivity of the concentration-dependent

contraction to methoxamine greater than any other time point. The EC_{50} to methoxamine in control PSS arteries was 153.7 nM compared to 158.1 nM after 10 minutes in 150mM raffinose, 160.3 nM after 30 minutes, 227.6 nM after 1 hour, 708.5 nM after 2 hours, 5.01 µM after 4 hours and 2.37 µM after 6 hours in raffinose. Therefore, increasing SMIT1 membrane expression profoundly reduces the contractile response to methoxamine for durations as brief as 30 minutes in raffinose, with a right shift in the sensitivity to the concentration-dependent contraction to methoxamine after 2, 4 and 6 hours.

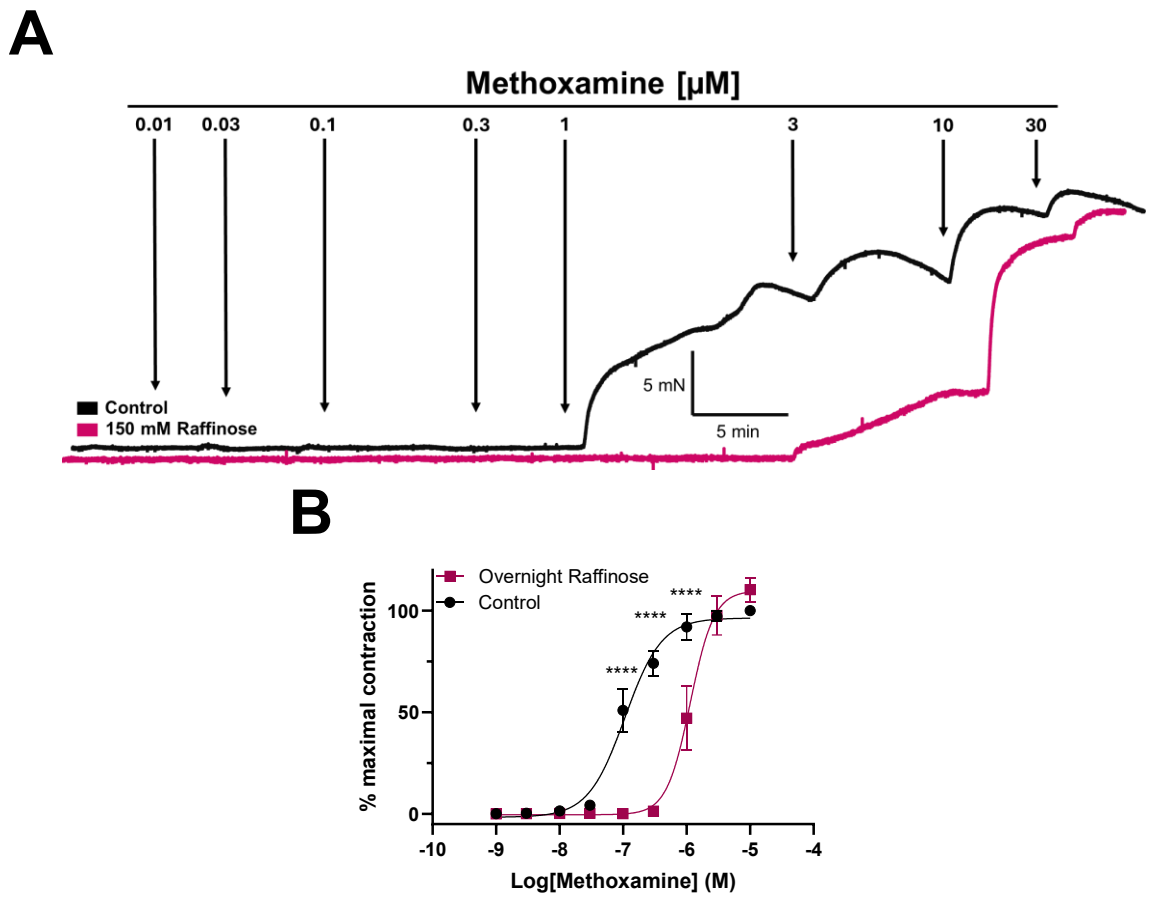


Figure 5.8: The concentration dependent contraction to methoxamine in mesenteric arteries after overnight incubation (~16h) in 150 mM raffinose.
*A representative trace of the contraction to methoxamine in mesenteric arteries incubated in control PSS (black) or 150 mM raffinose overnight (red, A). The mean response to methoxamine in mesenteric arteries incubated in either control PSS (black, EC_{50}=106.8 nM) or 150 mM raffinose overnight (pink, EC_{50} = 1.146 µM) is shown in panel B (N=5-7). All data points are shown as mean +-SEM denoted by error bars, and statistical values are determined by 2-way ANOVA with multiple comparisons are calculated using post hoc Bonferroni test where ****=P<0.0001.*

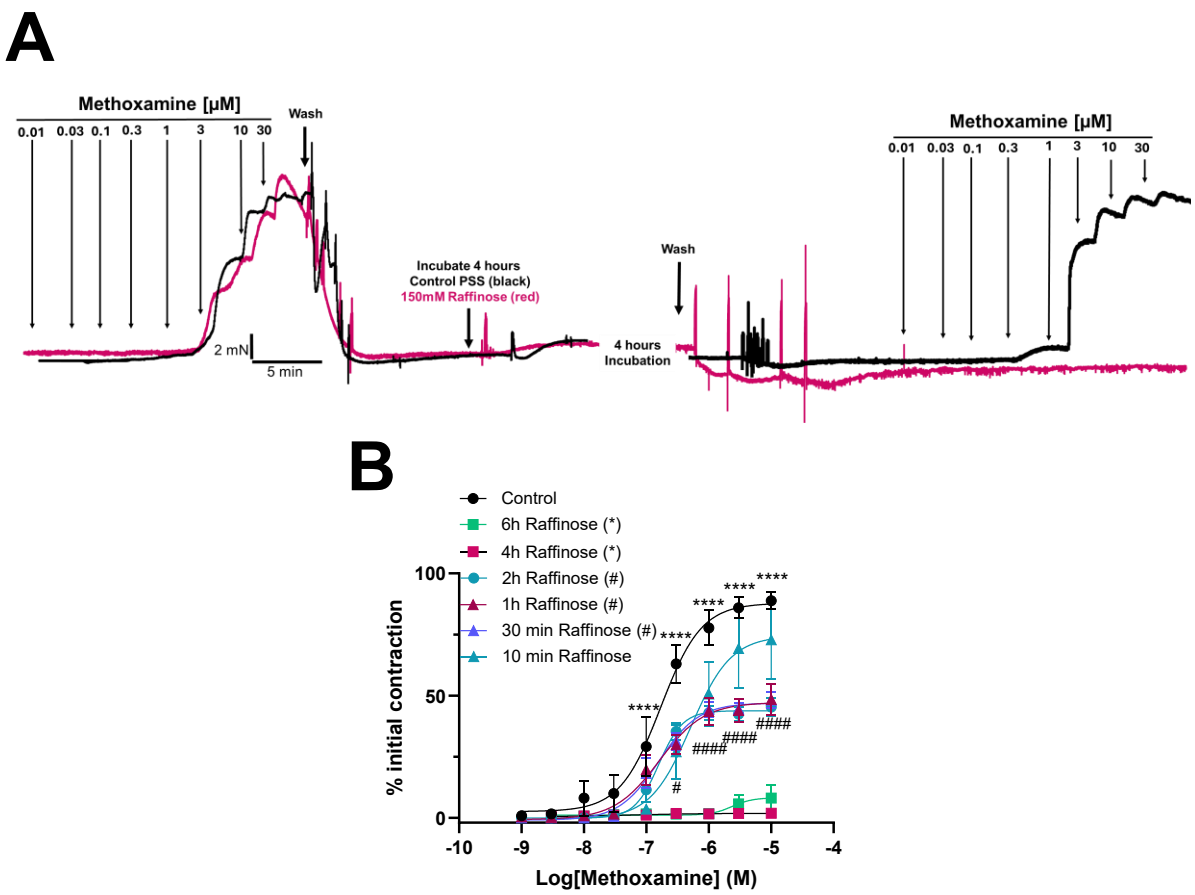


Figure 5.9: The concentration-dependent contraction to methoxamine after different timed interval incubations with 150 mM raffinose PSS.
*A representative trace of the contractile response to methoxamine (10 nM – 10 μM) in mesenteric arteries incubated in control PSS (black) or 150mM raffinose PSS for 4 hours (red)(A). The concentration-dependent contraction to methoxamine (10 nM – 10 μM) after incubating in 150mM raffinose for 10 minutes (turquoise), 30 minutes (blue), 1 hour (red), 2 hours (teal), 4 hours (red) and 6 hours (green) compared to control (black) (N=5-9)(B). All data points are shown as mean +-SEM denoted by error bars and statistical values are determined by 2-way ANOVA with multiple comparisons are calculated using post hoc Dunnets test where *=P<0.05, **=P<0.01, ***=P<0.001, ****=P<0.0001.*

Incubating in raffinose for 4 hours also reduced the U46619-evoked contraction, which was not dependent upon a functional endothelium (figure 5.10). The impairment in the concentration-dependent contraction to U46619 was equivalent to that of methoxamine. A similar reduction in the contractile response to U46619 in mesenteric arteries was seen in coronary arteries incubated in raffinose for 4 hours. A 63.82±8.4% impairment in the contraction to 10 μM U46619 and a right shift in the EC_{50} from 27.33 nM in control arteries to 308.5 nM in coronary arteries incubated for 4 hours in 150 mM raffinose PSS (figure 5.11). This data suggests

that incubating mesenteric arteries with raffinose for durations as brief as 10 to 30 minutes attenuates contractions induced by methoxamine and U46619. Prolonged incubation exceeding 4 hours markedly diminished the contractile responses of the arteries, an effect that is independent of the endothelium.

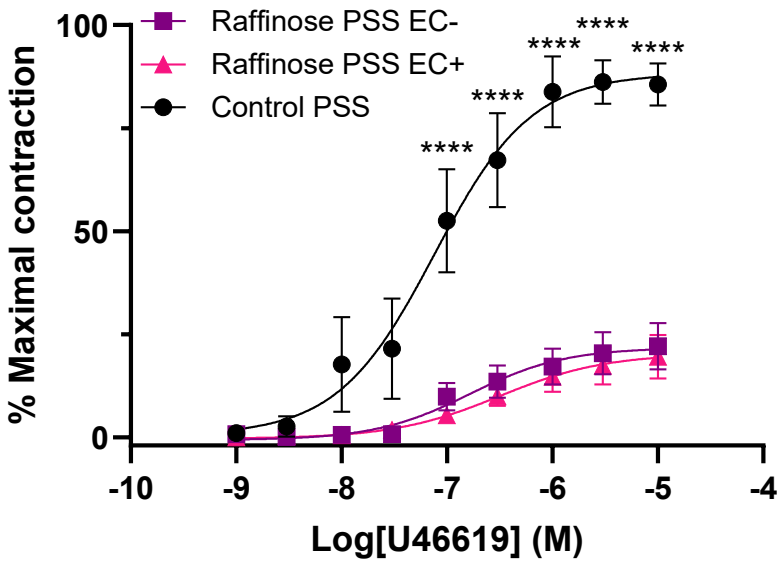


Figure 5.10: The concentration-dependent contraction to U46619 after 4 hours of raffinose incubation in mesenteric arteries with either positive endothelium or denuded.
*The mean response to U46619 when incubated in 150mM raffinose in mesenteric arteries with either positive endothelium (EC+, pink, EC_{50} = 165.6 nM) or denuded (EC-, dark purple, EC_{50} = 315.6 nM) compared to control PSS incubated vessels (black, EC_{50} = 76.05 nM). All data points are shown as mean +-SEM denoted by error bars with N=5, and statistical values are determined by 2-way ANOVA with multiple comparisons are calculated using post hoc Bonferroni test where *=P<0.05, **=P<0.01, ***=P<0.001, ****=P<0.0001.*

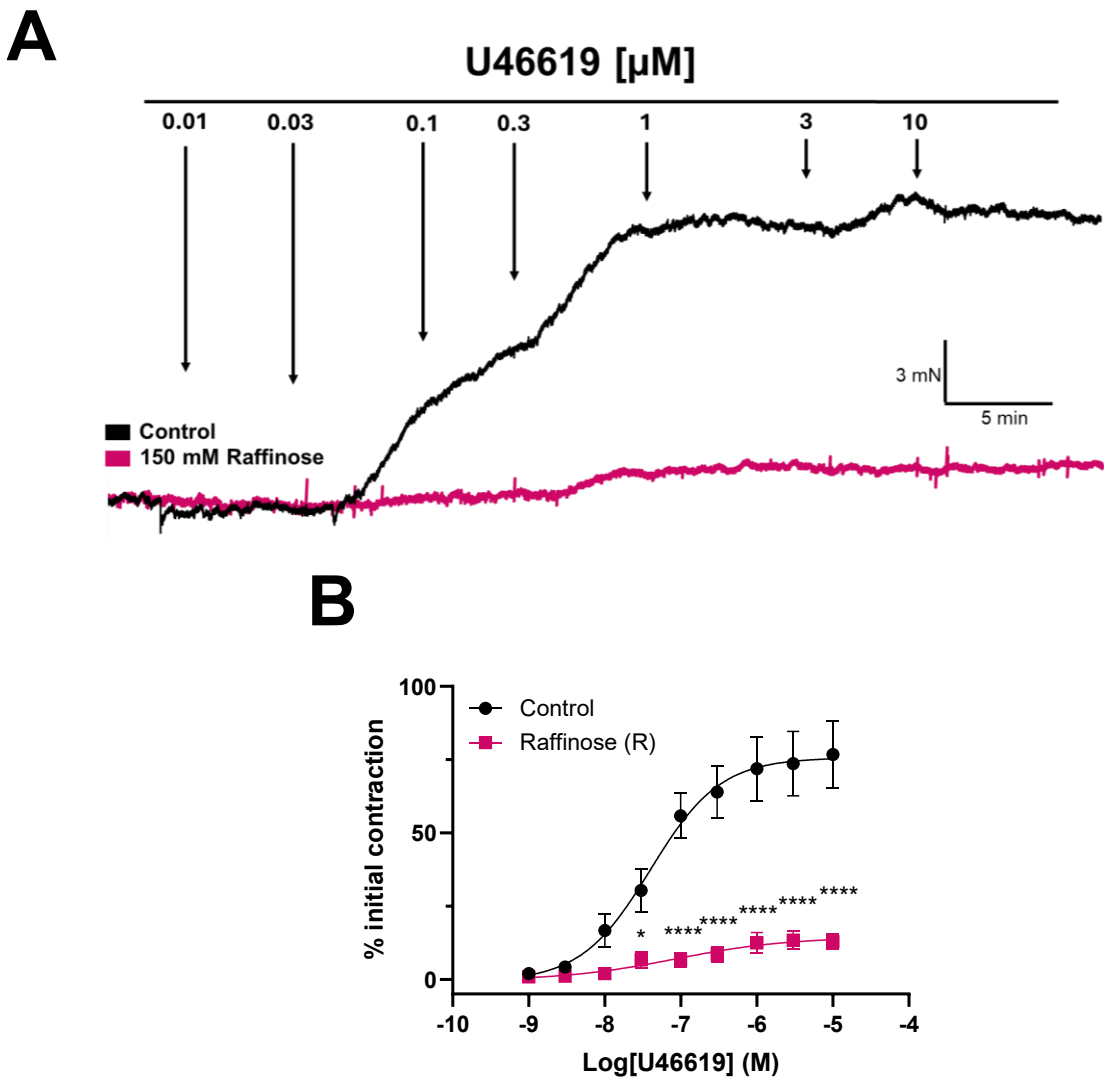


Figure 5.11: The contractile response to U46619 in coronary arteries from male rats when incubated in 150mM raffinose for 4-hours.
*A representative trace of the contraction to U46619 (1nM – 10µM) in the presence (red) and absence (black) incubating with 150mM raffinose PSS (A). The mean data of the U46619-induced contraction with (pink, EC_{50} = 308.5 nM) and without (black, EC_{50} = 27.33 nM) incubating in raffinose PSS can be seen in panel B (N=8). All data points are shown as mean +-SEM denoted by error bars and statistical values are determined by 2-way ANOVA with multiple comparisons are calculated using post hoc Bonferroni test where *=P<0.05, **=P<0.01, ***=P<0.001, ****=P<0.0001.*

5.3.5 | SMIT1 knock-down prevented the pro-relaxant effects of raffinose

To further investigate the role of SMIT1 in the concentration-dependent contraction response to methoxamine, experiments were conducted before and after incubation in 150 mM raffinose. Concentration-response curves to methoxamine

(ranging from 10 nM to 10 μM) were generated for both control and SMIT1 knock-down mesenteric arteries. These arteries were washed and incubated in 150 mM raffinose PSS for 4 hours. After removing the hypertonic PSS solution, the methoxamine response curves were repeated, and the resulting contractions were recorded (figure 5.12A). Incubation in 150 mM raffinose PSS significantly impaired the contractile response to methoxamine in mesenteric arteries treated with scrambled control morpholino, using the same protocol as shown in figure 5.9A. No reduction in the methoxamine-induced contraction was observed in arteries treated with SMIT1-targeted morpholino (figure 5.12). This confirms that the response to methoxamine post-raffinose incubation is sensitive to SMIT1 knockdown. Therefore, we used raffinose as a method of increasing SMIT1 expression in vascular smooth muscle cells and looked at the contractile and relaxant response in arteries post-raffinose incubation, further elucidating SMIT1 as a modulator of vascular reactivity.

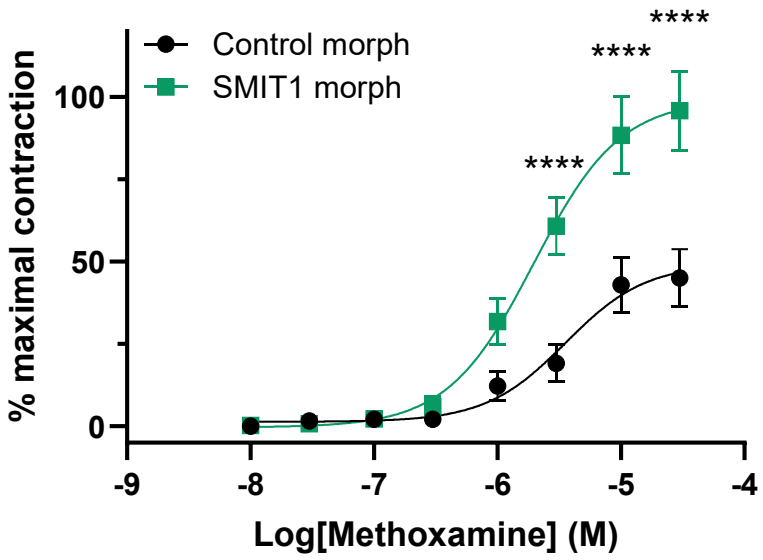


Figure 5.12: The effect of raffinose incubation on the contractile response to methoxamine in control and SMIT1 targeted morpholino vessels.
*The mean concentration-dependent contraction (mN) to methoxamine (10 nM – 10 uM) in scrambled control morpholino (black, EC_{50} = 3.56 μM) or a SMIT1 targeted morpholino (green, EC_{50} =1.97 μM) mesenteric arteries incubated in 150 mM raffinose (4 hours)(N=9). All data points are shown as mean +-SEM denoted by error bars and statistical values are determined by 2-way ANOVA with multiple comparisons calculated using post hoc Bonferroni test where ****=P<0.0001.*

5.3.5.1 | The impact of raffinose-induced upregulation of SMIT1 expression on KCl-induced contractions.

Upon identifying that augmenting SMIT expression attenuated vasoconstrictor responses in mesenteric and coronary arteries, the contractile response to KCl (10 mM – 120 mM) was investigated in the presence and absence of 150 mM raffinose PSS. This investigation aimed to elucidate SMIT's effect on K^+ channels. Incubation of mesenteric arteries with 150 mM raffinose PSS resulted in a reduction of the contraction response to KCl <60 mM, with a maximal reduction of 29.6±8.1% observed at 40 mM KCl (figure 5.13). These results suggest the involvement of K+ channels in mediating the effects of arterial contractility when the membrane expression of SMIT is increased.

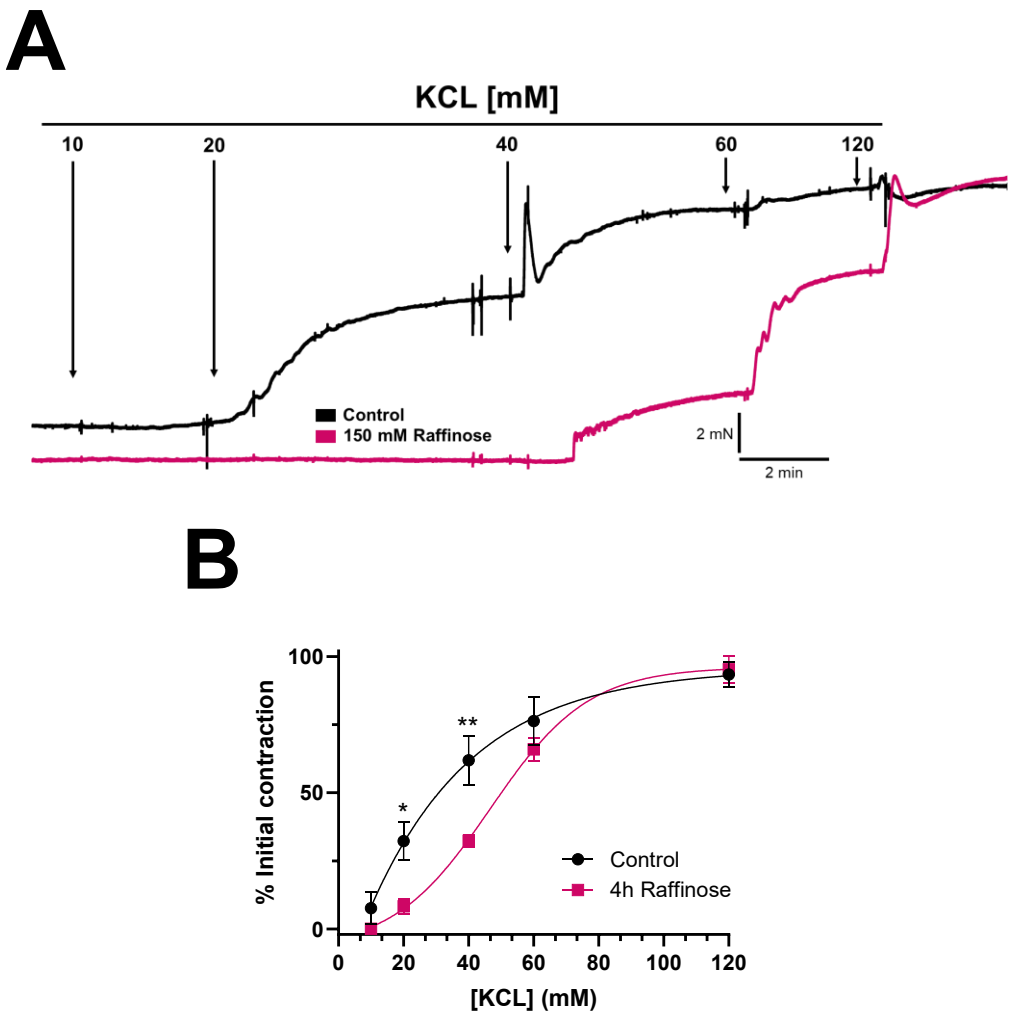


Figure 5.13: The effect of augmenting SMIT expression on KCL-induced contractions.
A representative trace of the contraction to KCl (10mM – 120mM) when incubated with (pink) and without (black) 150mM raffinose PSS (A). The mean concentration-dependent response to KCl in the presence (red) and absence (black) of incubating

*with 150mM raffinose is shown in panel B. All data points are shown as mean +- SEM denoted by error bars, with N=6 and statistical values are determined by 2-way ANOVA with multiple comparisons are calculated using post hoc Bonferroni test where *=P<0.05, **=P<0.01, ***=P<0.001, ****=P<0.0001.*

5.3.6 | The effect of augmented SMIT1 expression on Adenosine-induced relaxations in mesenteric arteries

Adenosine is a well-known relaxant of coronary arteries via activation of adenosine 2a and 2b receptors (Müller & Jacobson, 2011) that has negligible effect on mesenteric arteries. We speculated that raffinose incubation of mesenteric arteries would enhance the relaxation to adenosine. The impact of adenosine (1 nM - 10 μM) on mesenteric arteries pre-contracted with 300 nM U46619 was examined both in the presence and absence of the pan Kv7 channel blocker XE991. Under control conditions adenosine induced a concentration-dependent relaxation in mesenteric arteries, which was significantly attenuated by pre-incubation with 10μM XE991 (figure 5.14). These findings indicate that the activation of Kv7 channels was crucial in adenosine-mediated relaxation in mesenteric arteries, previously identified by (Khanamiri et al., 2013).

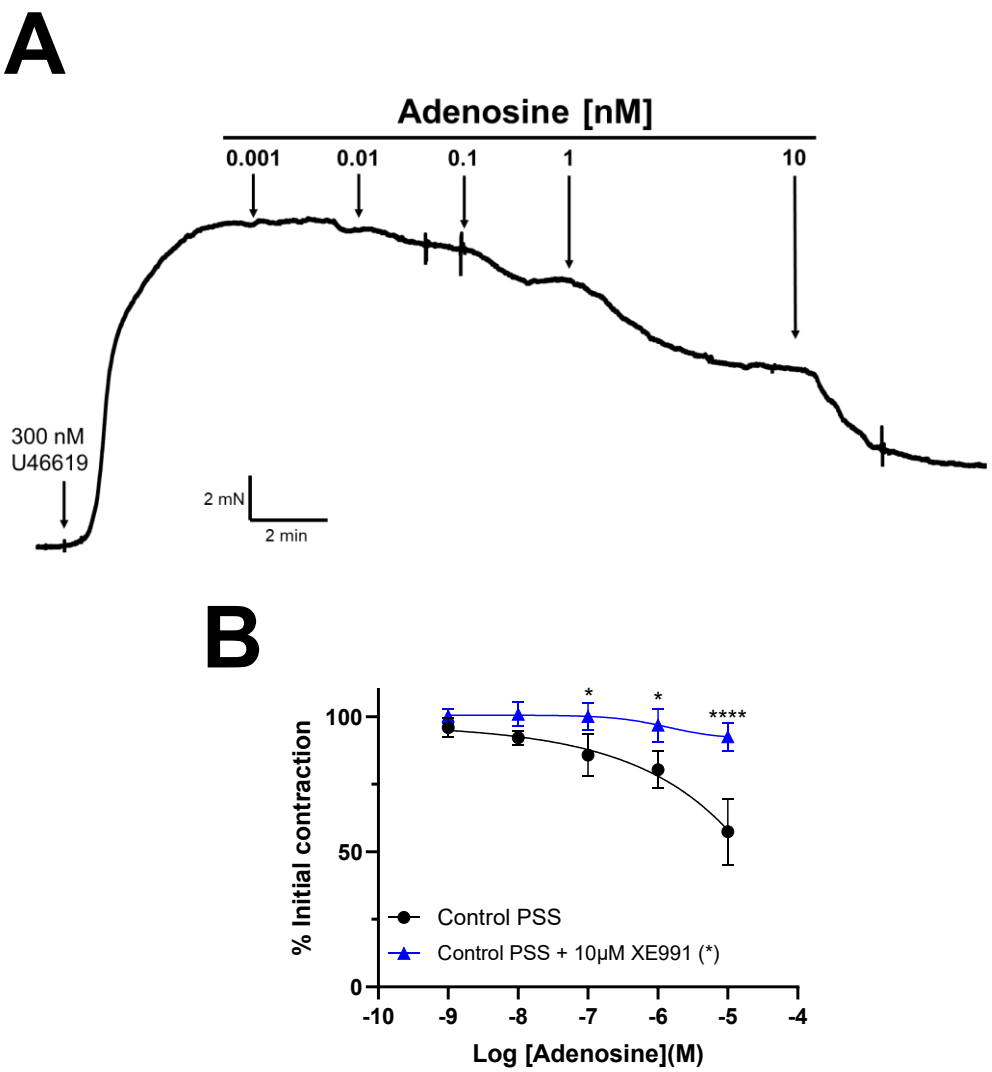


*Figure 5.14: Adenosine-mediated relaxation is sensitive to Kv7 channel blockade. A representative trace showing the relaxation to Adenosine (1nM - 10μM) in control PSS (A). The mean data of adenosine-induced relaxation in the presence (blue) and absence (black) of 10μM XE991 (B). All data points are shown as mean +- SEM denoted by error bars, with N=5 and statistical values are determined by 2-way ANOVA with multiple comparisons are calculated using post hoc Bonferroni test where *=P<0.05, **=P<0.01, ***=P<0.001, ****=P<0.0001.*

The relaxation response to adenosine was examined in mesenteric arteries with upregulated SMIT1 expression. Mesenteric arteries incubated for 2-hours in 150 mM raffinose PSS exhibited an enhanced concentration-dependent relaxation to adenosine, demonstrating a 37.2±1.9% greater relaxation in 150 mM raffinose-incubated vessels compared to the control, which was prevented by 10μM XE991 (figure 5.15A). Figure 5.15B showed the contraction to 300 nM U46619 compared to the percentage relaxation evoked by 10 μM adenosine in control and raffinose incubated vessel segments, where the starting contraction did not affect the

adenosine-induced relaxation. Overall, enhancing SMIT1 expression increased relaxation responses, whereas reducing SMIT1 expression using targeted morpholinos reduces relaxant responses, further suggesting SMIT1 regulates arterial vasodilation pathways.

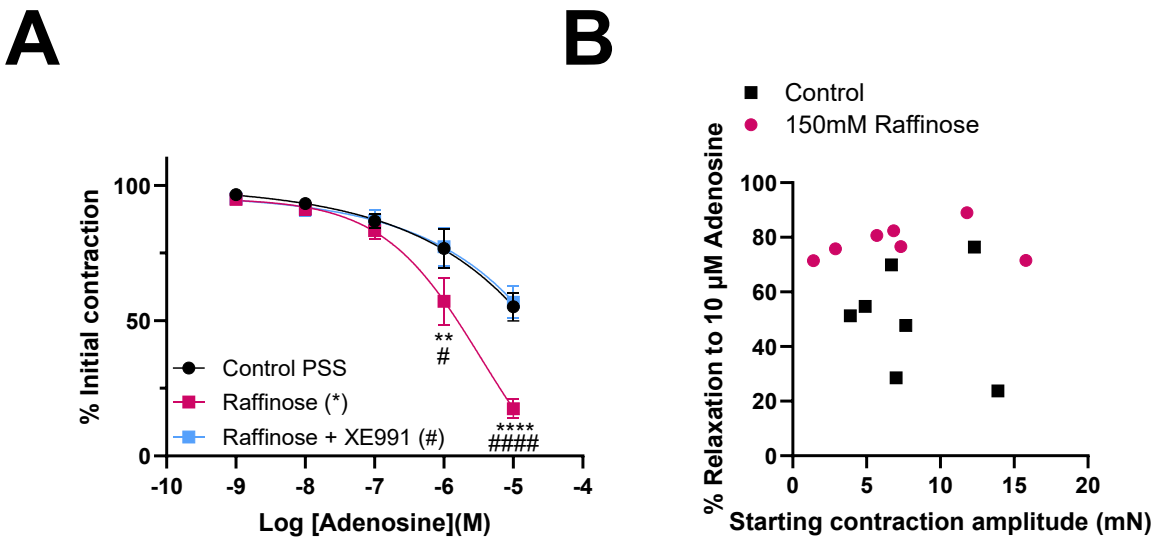


Figure 5.15: Adenosine-induced relaxations are enhanced in mesenteric arteries incubated in 150mM raffinose for 2-hours.
*The mean concentration-dependent relaxation to adenosine (1nM - 10µM) in mesenteric arteries when incubated in either control PSS (black), 150mM raffinose PSS (red) or 150mM raffinose and 10µM XE991 (blue) shown in panel A. The percentage relaxation to 10µM adenosine plotted against the starting contraction to 300nM U46619 in control (black) and 150mM raffinose incubated vessels (pink) (B). All data points are shown as mean +-SEM denoted by error bars, with N=4-7 and statistical values are determined by 2-way ANOVA with multiple comparisons are calculated using post hoc Bonferroni test where *=P<0.05, **=P<0.01, ***=P<0.001, ****=P<0.0001.*

5.3.7 | Expression of Kv7.4 in male mesenteric and coronary arteries post incubating in 150mM raffinose PSS

Kv7.4 channels are predominantly expressed in the vasculature and act as crucial regulators of vascular smooth muscle contractility (Barrese et al., 2018; Haick & Byron, 2016; Jepps et al., 2015). It has been established that the expression of the SMIT is upregulated in mesenteric and coronary arteries following incubation in 150 mM raffinose PSS. Therefore, experiments were carried out on mesenteric and coronary arteries to investigate whether the expression of Kv7.4 is similarly

altered after a 4-hour incubation in 150 mM raffinose PSS. Mesenteric and coronary arteries were incubated in either control PSS or 150 mM raffinose PSS. Subsequently, vascular smooth muscle cells from these arteries were isolated and subjected to immunocytochemistry staining using a previously validated Kv7.4 antibody. Incubation of male coronary and mesenteric arteries with 150 mM raffinose PSS increased the total cellular expression of Kv7.4 and an increase in clustering of SMIT1 staining predominantly in the cytosol (figure 5.16A-C). However, there was no significant alteration in the membrane-to-cytosol ratio of Kv7.4 staining (figure 5.16D-F), indicating that the membrane abundance of Kv7.4 remained unchanged following raffinose incubation.

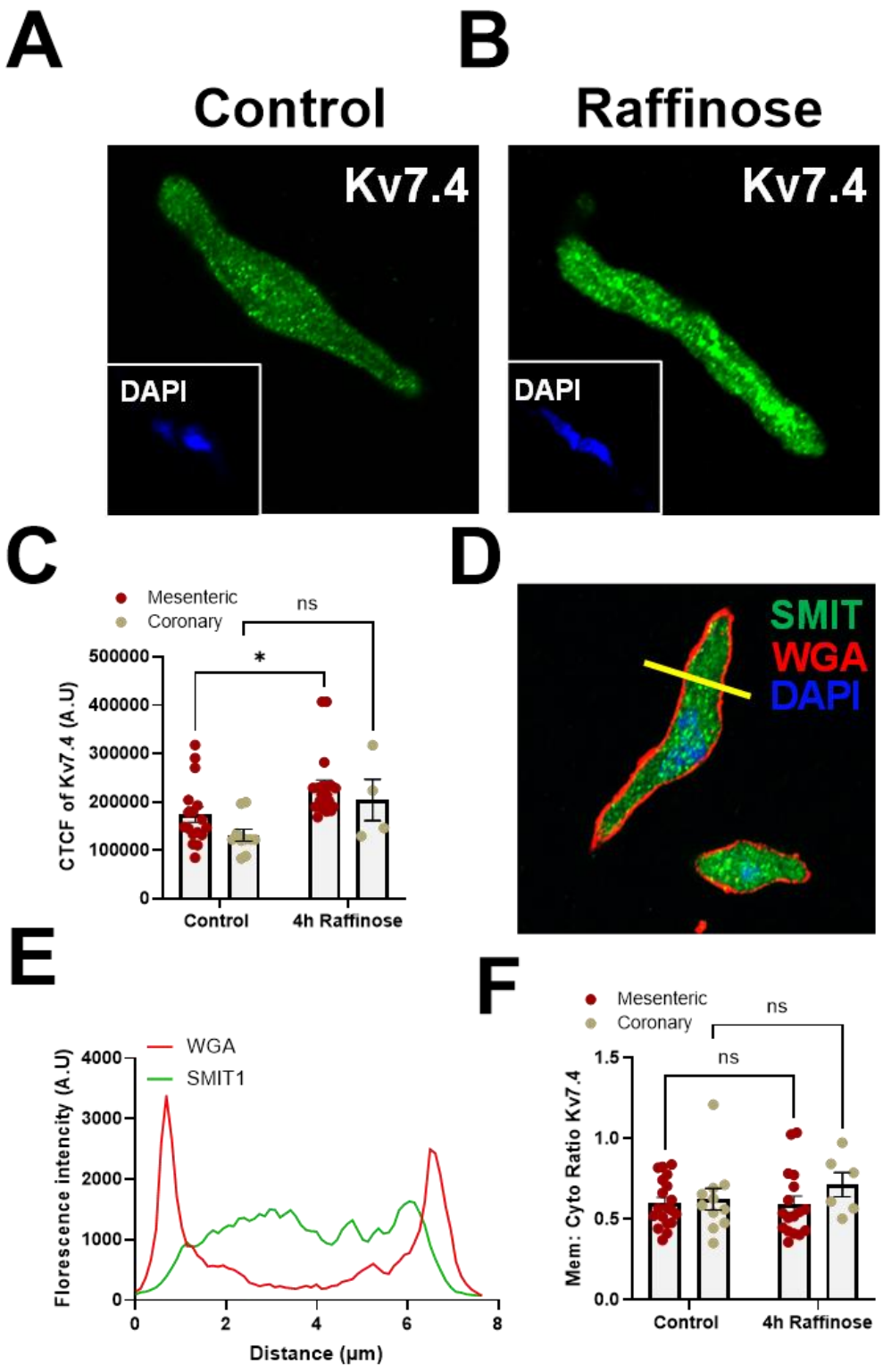


Figure 5.16 :Expression of Kv7.4 in male mesenteric and coronary arteries when incubated with either control PSS or 150 mM raffinose PSS for 4-hours.
A representative image of Kv7.4 staining (green) in male mesenteric arteries incubated in control PSS (A) or 150 mM raffinose PSS (B) with nuclear staining (DAPI) is shown in blue. The mean data of corrected total cell fluorescence (CTCF) of Kv7.4 in male mesenteric (red, N=3 n=15) and coronary (beige, N=3 n=9) arteries before and after 4h raffinose incubation is shown in panel C. A representative image of Kv7.4 staining (green), with the membrane marker wheat

*germ agglutinin (WGA, red) and nuclear stain (DAPI) in blue. The fluorescence intensity of Kv7.4 and WGA measured across a cell marked by the yellow line is shown in panel D. The graph of fluorescence intensity of SMIT and WGA measured across a cell, marked by the yellow line, is shown in panel E. The mean membrane cytosol ratio of Kv7.4 in mesenteric (red, N=4 n=20) and coronary (beige, N=3 n=10) arteries from male rats is shown in panel F. All data is shown as mean± SEM, where statistical P values were calculated using a 2-way ANOVA and multiple comparisons were made via a post hoc Sidak test where *=P<0.05, **=P<0.01, ***=P<0.001, ****=P<0.0001. (N= number of animals used, n= number of technical repeats).*

5.3.8 | SMIT physically interacts with Kv7.4 and Kv7.5 ion channels in mesenteric and coronary arteries

The interaction of SMIT with Kv7 ion channel proteins has been previously documented in the nodes of Ranvier, choroid plexus epithelium (Manville et al., 2017; Neverisky & Abbott, 2017) and, recently, in renal arteries (Barrese et al., 2020). However, little is understood about these interactions in the vasculature and their effect on arterial function. Initial experiments explored the interaction of SMIT with Kv7.4 and Kv7.5 ion channel proteins in mesenteric and coronary arteries from male rats. As shown in figure 5.17, SMIT1 was found to interact with Kv7.4 and Kv7.5 in isolated mesenteric and coronary smooth muscle cells from male rats via proximity ligation assay.

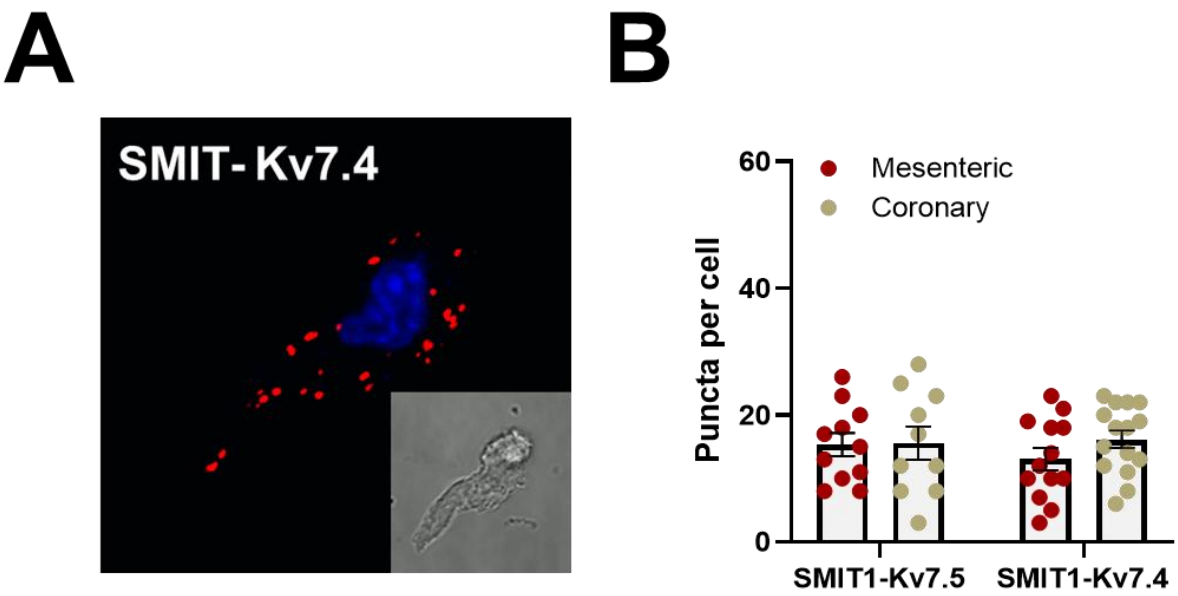


Figure 5.17: The interaction of SMIT with Kv7.4 and Kv7.5 in mesenteric and coronary arteries from male rats for 4-hours.

Proximity ligation assays (PLA) show the interaction of SMIT with Kv7.4 and Kv7.5 in vascular smooth muscle cells isolated from mesenteric and coronary arteries. Red dots indicate PLA puncta with nuclei DAPI staining in blue, and a brightfield image of the cell is shown below (A). The mean number of SMIT-Kv7.4 and SMIT-Kv7.5 Puncta per cell is shown in the bar graph for mesenteric (red, N=3 n=15) and coronary (beige, N=3 n=10) VSMCs (B). All data is shown as mean± SEM denoted by error bars (N= number of animals used, n= number of technical repeats).

To understand the functional changes that occur when SMIT expression is upregulated by raffinose, the interaction of SMIT with Kv7.4 and Kv7.5 was investigated in VSMCs isolated from mesenteric and coronary arteries that were incubated in either control PSS or 150 mM raffinose PSS. Enhancement of SMIT1 expression resulted in a significant increase in the number of SMIT-Kv7.4 puncta within mesenteric and coronary VSMCs, by approximately 63% and 55%, respectively, as indicated by elevated PLA staining shown in figure 5.18A-B. Similarly, the number of SMIT-Kv7.5 puncta in mesenteric and coronary VSMCs also increased upon enhancing SMIT1 expression (figure 5.18C). Therefore, this data suggests SMIT1 interactions with Kv7.4 and K7.5 increase in VSMCs from mesenteric and coronary arteries upon incubating in 150mM raffinose PSS.

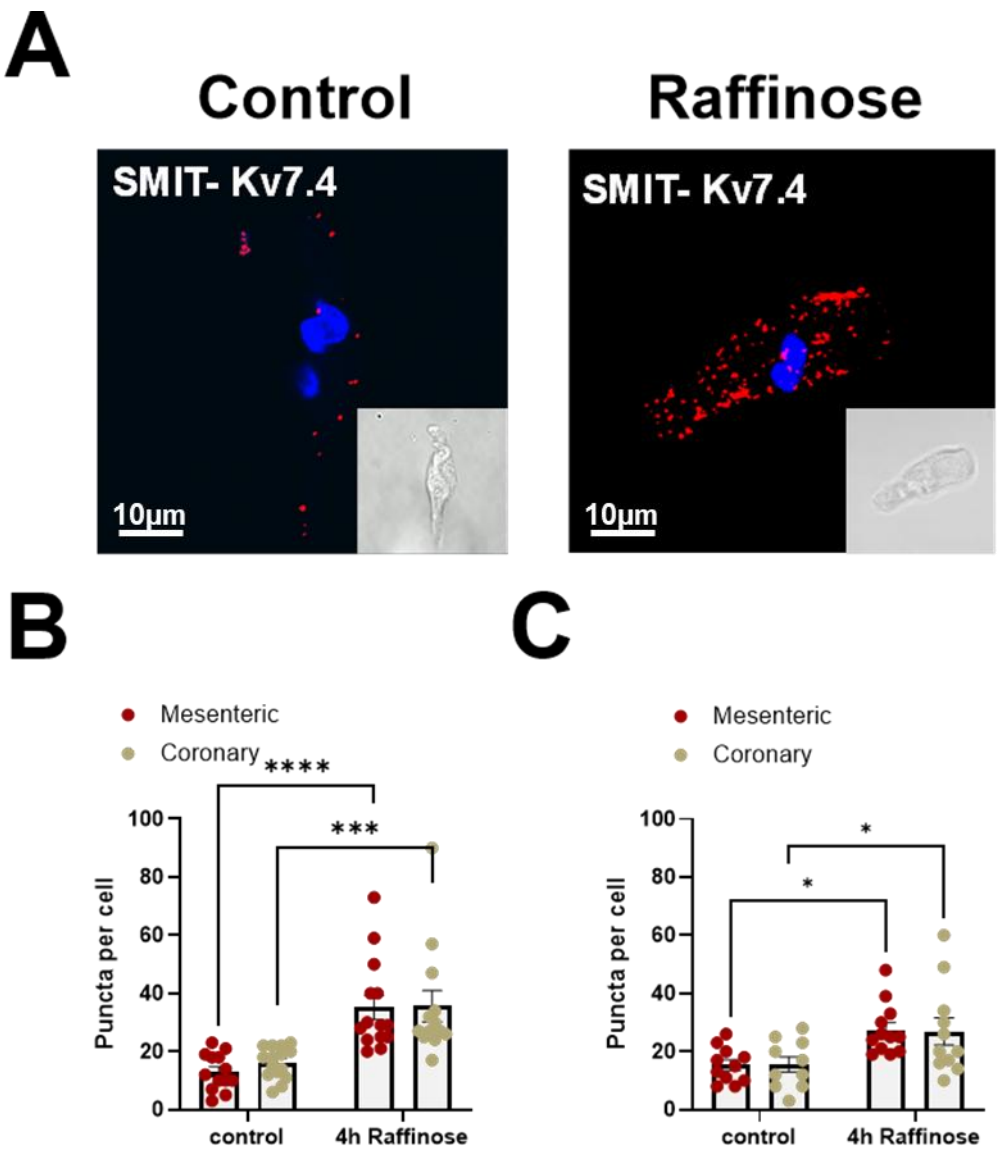


Figure 5.18: The interaction of SMIT with Kv7.4 and Kv7.5 in mesenteric and coronary VSMCs from male rats following 4-hour incubation in raffinose.
*PLA puncta show the interaction of SMIT with Kv7.4 in mesenteric VSMCs incubated in either control PSS or 150 mM raffinose PSS for 4 hours (A). Bar graph showing the mean number of PLA puncta for SMIT-Kv7.4 (B) and SMIT-Kv7.5 (C) in mesenteric (red, N=3 n=15) and coronary (beige, N=3 n=15) VSMCs incubated in either control PSS or 150 mM raffinose PSS for 4 hours. All data is shown as mean± SEM, where statistical P values were calculated using a 2-way ANOVA and multiple comparisons were made via a post hoc Sidak test where *=P<0.05, **=P<0.01, ***=P<0.001, ****=P<0.0001. (N= number of animals used, n= number of technical repeats).*

5.3.9 | Augmenting SMIT1 membrane expression increased ML213 relaxations in mesenteric and coronary arteries

SMIT1 has previously been shown to form complexes with Kv7 channels, altering the channel's voltage sensitivity and activation (Manville et al., 2017). Hence, the effect of 150mM raffinose on ML213-induced relaxations was investigated in mesenteric and coronary arteries from male rats to investigate if the increase in SMIT1 interactions with Kv7.4/5 proteins altered ML213-induced relaxations. Incubation of mesenteric arteries in 150 mM raffinose PSS for 1 hour significantly potentiated the vasorelaxation response to ML213 (figure 5.19A-B). Additionally, as illustrated in Figure 5.19C, the vasodilatory effect of 100 nM ML213 remained consistent regardless of whether the mesenteric arteries were incubated in 150 mM raffinose PSS for 10 minutes, 30 minutes or 1 hour (figure 5.19C). These results suggest that the functional effects of SMIT on vasorelaxation occur rapidly after its membrane expression was augmented by raffinose incubation. Interestingly, incubation of coronary arteries in 150 mM raffinose PSS resulted in an enhanced relaxation response to ML213 only at higher concentrations (1 μM to 10 μM, figure 5.20). In contrast, mesenteric arteries exhibited the most significant relaxation response at lower concentrations (10 nM to 300 nM) of ML213.

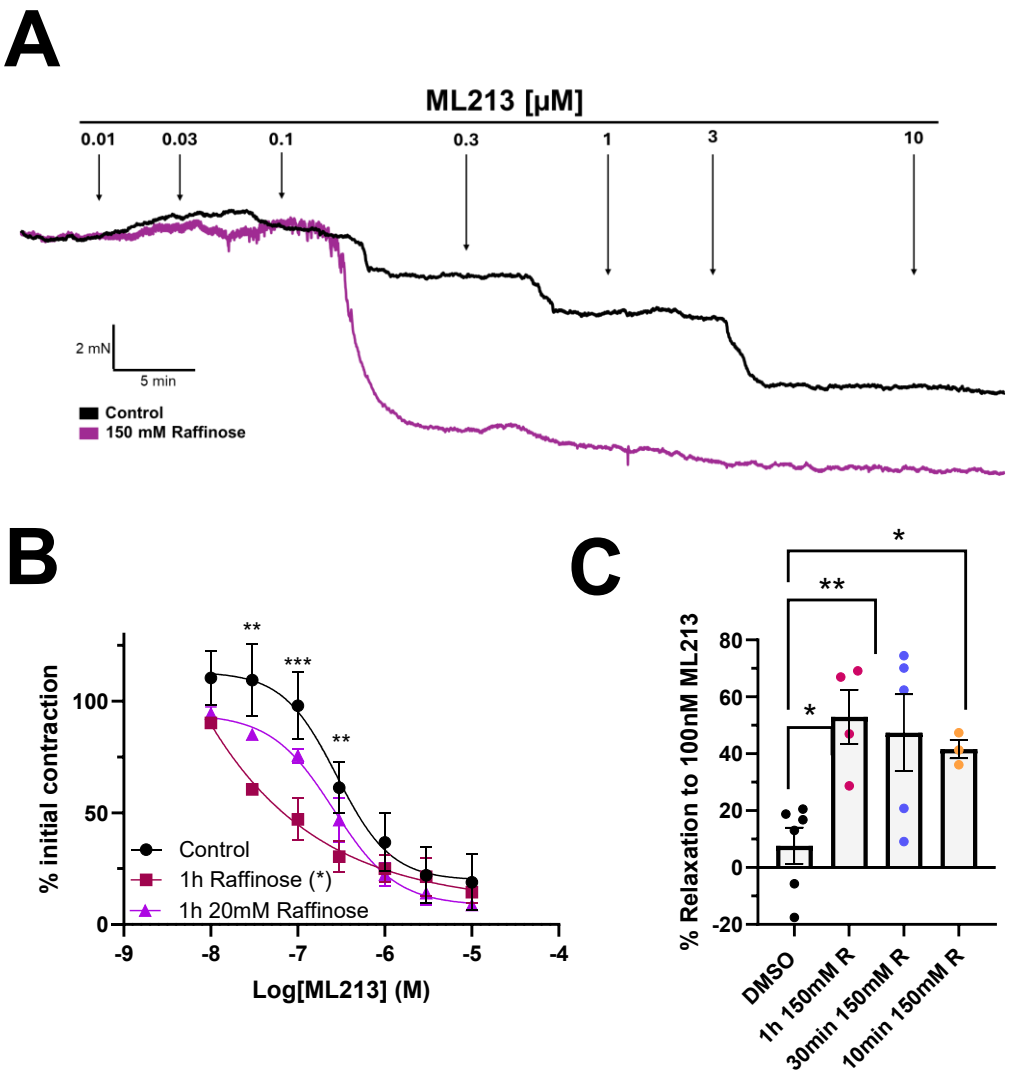


Figure 5.19: The relaxation to ML213 in mesenteric arteries when incubated in 150 mM raffinose for 10 minutes, 30 minutes and 1 hour.

*A representative trace of the response to ML213 (10nM – 10µM) in mesenteric arteries in the presence (pink) or absence (black) of 1 hour 150mM raffinose (A). The mean effect of ML213 in mesenteric arteries in control PSS (black, IC50 = 281.3 nM), 1 hour of 150mM raffinose PSS (red, IC50 = 17.9 nM) and 1 hour of 20 mM raffinose PSS (purple, IC50 = 259.0 nM) shown in panel B. The mean response to ML213 when incubated in control PSS (black), 10 minutes 150mM raffinose (orange), 30 minutes 150mM raffinose (blue) and 1-hour 150 mM raffinose (pink) in panel C (N=4-5). R represents raffinose in panel C. All data points are shown as mean +-SEM denoted by error bars, with N=5 and statistical values for concentration-response curves are determined by 2-way ANOVA with multiple comparisons calculated using post hoc Dunnets test and a non—non-parametric man-Whitney t-test was used to identify significance for the single response bar charts, where *=P<0.05, **=P<0.01, ***=P<0.001, ****=P<0.0001.*

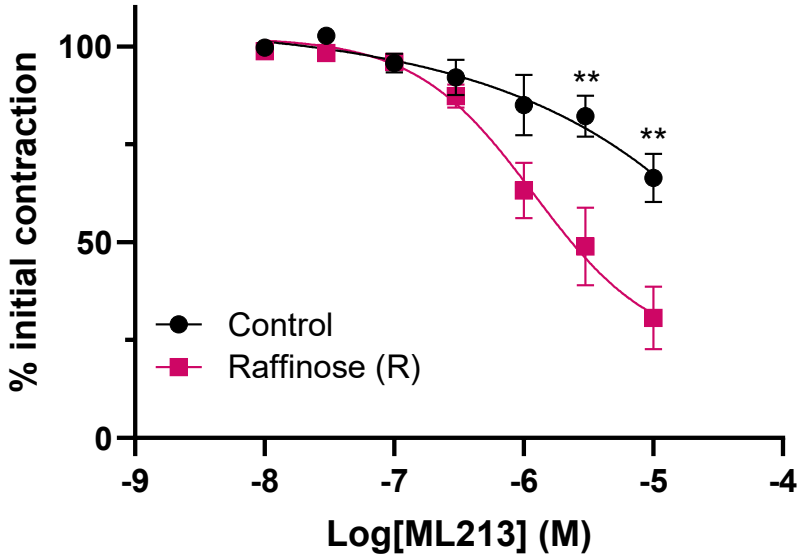


Figure 5.20: The relaxation to ML213 in coronary arteries when incubated in 150 mM raffinose for 2-hours.
*The response to ML213 on coronary arteries pre-contracted with 300 nM U46619 in the presence (purple, N=6) and absence (black, N=6) of 150mM raffinose (R). All data points are shown as mean +-SEM denoted by error bars, and statistical values are determined by 2-way ANOVA with multiple comparisons are calculated using post hoc Dunnets test where *=P<0.05, **=P<0.01, ***=P<0.001, ****=P<0.0001.*

5.3.9.1 | SMIT1 knock-down impaired the relaxation response of Kv7 activator ML213

The effect of the Kv7 channel activator ML213 was investigated in arteries transfected with a scrambled control morpholino or a targeted SMIT1 morpholino. Arteries with SMIT1 knock-down were significantly less sensitive to the concentration-dependent relaxation to ML213 than control vessels, whereby an 84.56±3.2% relaxation was produced to 1μM ML213 in scrambled control arteries with an IC_{50} of 2.77 μM, but only a 27.03±13.5% relaxation was produced in SMIT1 morpholino vessels with an IC50 of 167 μM (shown in figure 5.21). This data suggests that enhancing SMIT1 activity enhances ML213-induced relaxations, and reducing SMIT1 expression decreases ML213-induced relaxations. Hence, the level of SMIT1 activity can alter arterial relaxation responses.

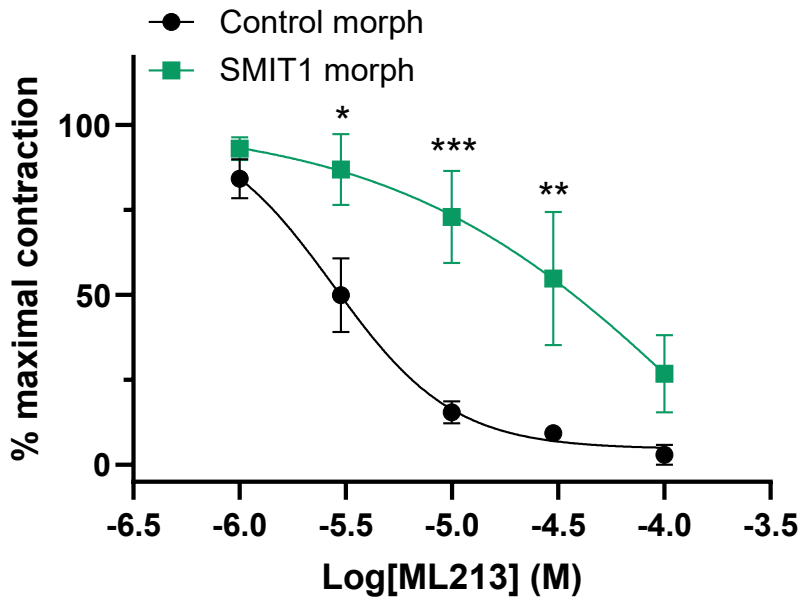


Figure 5.21: The relaxation response to Pan Kv7 channel activator ML213 in control and SMIT1 targeted morpholino vessels.
*The mean concentration-dependent relaxation (mN) to ML213 (10 nM – 10 μM) in scrambled control morpholino (black, EC_{50} = 2.77 nM) and SMIT1 targeted morpholino (green, EC_{50} =167 μM) mesenteric arteries pre-contracted with 300 nM U46619. All data points are shown as mean +-SEM denoted by error bars, with N=6 and statistical values are determined by 2-way ANOVA with multiple comparisons are calculated using post hoc Dunnets test where *=P<0.05, **=P<0.01, ***=P<0.001, ****=P<0.0001. (N= number of animals used).*

5.3.10 | SMIT1-Gβγ protein interactions in mesenteric and coronary arteries

Previous literature has shown SMIT1 interacts with Kv7 modulators, such as the auxiliary subunits KCNE2 and KCNE4 (Barrese et al., 2020; Manville et al., 2017; Neverisky & Abbott, 2017). Gβγ subunits positively regulate Kv7 channels and physically interact with Kv7.4, increasing current activation and amplitude (Stott, Povstyan, et al., 2015). Hence, initial experiments were conducted to identify if Kv7.4 and Gβγ interactions changed upon incubating in 150 mM raffinose. The number of interactions of Kv7.4 with Gβγ significantly increased by approximately 80% and 70%, respectively, in mesenteric and coronary arteries following 4-hour incubation in 150 mM raffinose PSS (figure 5.22). Therefore, the functional effects occurring because of SMIT knock-down and enhancing SMIT expression via raffinose could be due to more Kv7.4, Gβγ and SMIT interactions, forming one

large complex, positively regulating one another. To confirm this, we sought to identify whether SMIT interacted with Gβγ. PLA experiments identified that SMIT1 did interact with Gβγ in both mesenteric and coronary arteries from male rats, and the number of interactions increased following 4-hour raffinose incubation (figure 5.23). However, the quantity of puncta per cell and the fold increase following raffinose incubation was considerably less than Kv7.4-Gβγ.

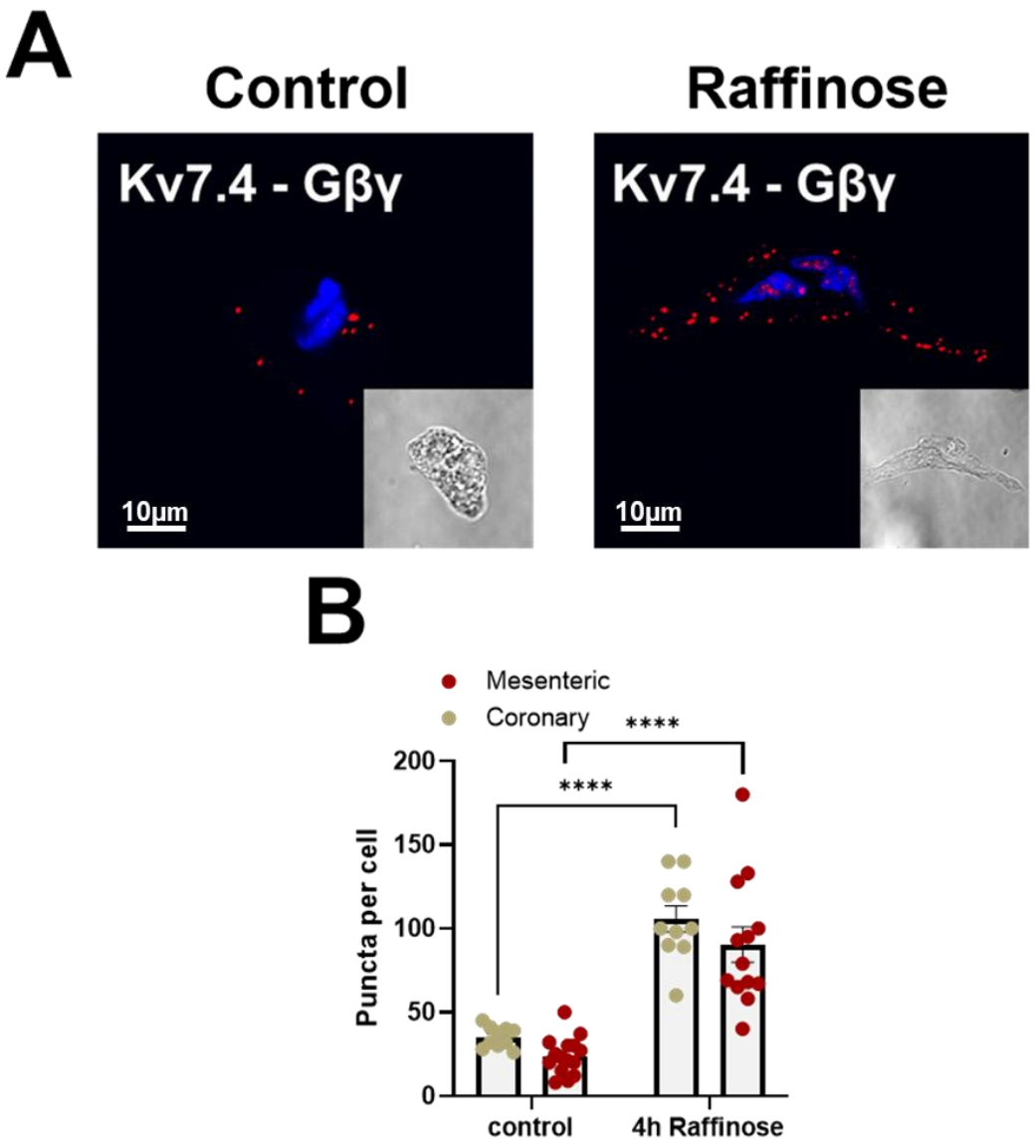


Figure 5.22: Kv7.4 and Gβγ interaction in mesenteric and coronary arteries incubated in either control PSS or 4-hours 150 mM raffinose PSS.
*PLA puncta staining of Kv7.4 and Gβγ in mesenteric arteries incubated in either control PSS or 150mM raffinose PSS. Bar chart showing the mean number of Kv7.4- Gβγ PLA puncta per cell in mesenteric (red, N=3 n=14) and coronary (beige, N=3 n=10) arteries incubated in either control PSS or 150mM raffinose PSS. All data is shown as mean± SEM, where statistical P values were calculated using a 2-way ANOVA and multiple comparisons were made via a post hoc Sidak test where *=P<0.05, **=P<0.01, ***=P<0.001, ****=P<0.0001. (N= number of animals used, n= number of technical repeats).*

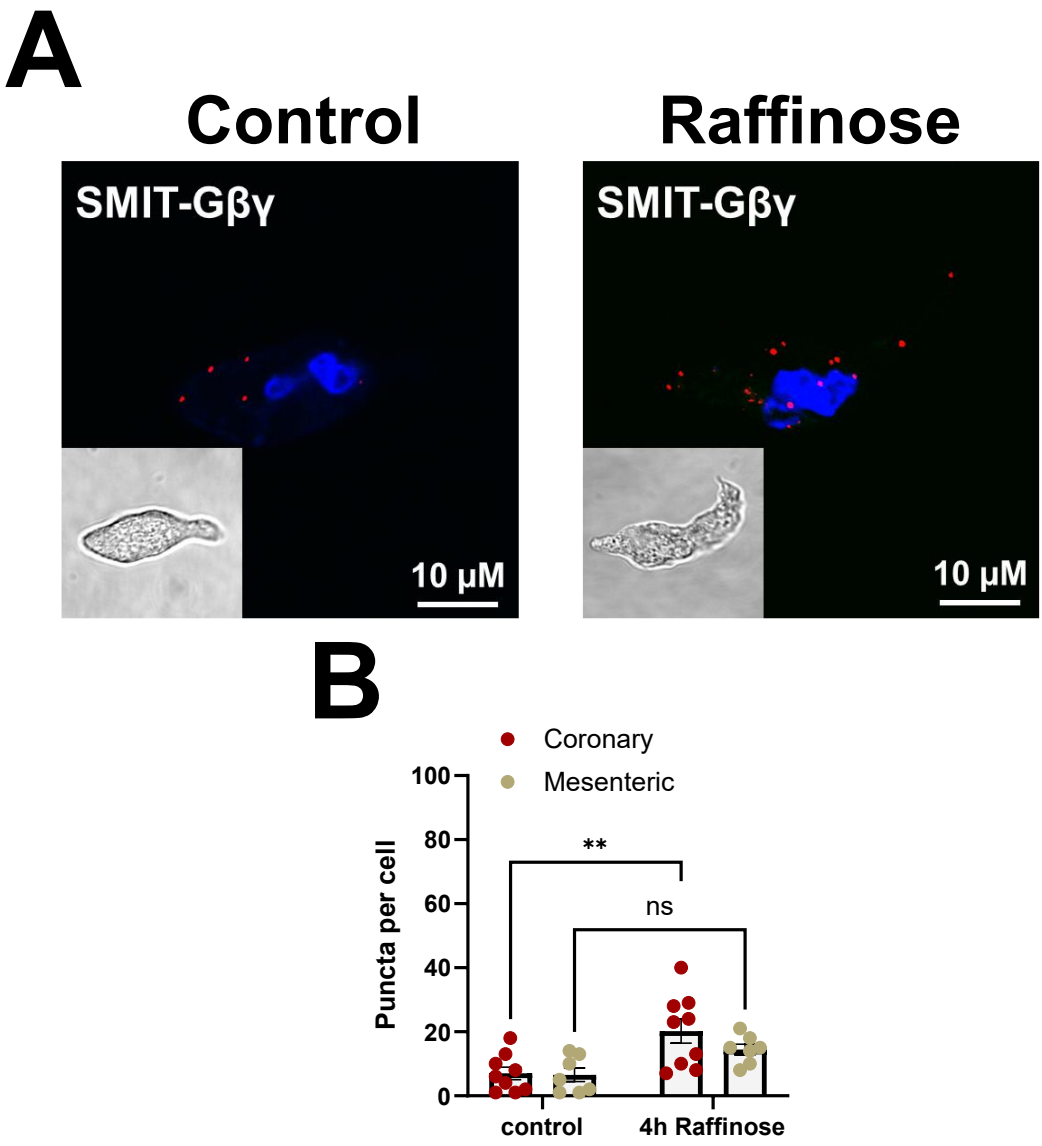


Figure 5.23: The interaction of SMIT1 with Gβγ in mesenteric and coronary arteries incubated in 150mM raffinose for 4-hours.
*PLA puncta of SMIT- Gβγ in mesenteric VSMCs incubated in either control PSS or 150 mM raffinose PSS (A). The mean number of SMIT- Gβγ PLA puncta in mesenteric (red, N=3 n=10) and coronary (beige, N=3 n=9) arteries incubated in either control PSS or 150mM raffinose PSS (B). All data is shown as mean± SEM, where statistical P values were calculated using a 2-way ANOVA and multiple comparisons were made via a post hoc Sidak test where *=P<0.05, **=P<0.01, ***=P<0.001, ****=P<0.0001. (N= number of animals used, n= number of technical repeats).*

5.3.11 | Inhibitors of the Kv7 channel and βγ subunits prevent the reduction of methoxamine-induced contractions in raffinose incubated vessels.

To elucidate the mechanism by which increased SMIT1 membrane expression reduces arterial contractility, mesenteric and coronary arteries incubated with 150 mM raffinose were treated with inhibitors of the Kv7 channel and Gβγ subunit. Subsequently, the contractile response to methoxamine was recorded. The Kv7 channel blocker XE991 and Gβγ subunit blocker gallein both significantly prevent the impairment of methoxamine-induced contraction (figure 5.24) caused by 150 mM raffinose incubation in mesenteric arteries. The concentration effect curve to methoxamine shifted to the left in the presence of raffinose with either XE991 or Gallien, such that the EC_{50} of methoxamine went from 2.136 µM to 574.9 nM in the presence of gallein and 716 nM in the presence of XE991. Similar results were seen in coronary arteries, with both agents preventing the impairment of the U46619-induced contraction (figure 5.25). However, the extent of reversal was less pronounced compared to mesenteric arteries. These findings suggest that Kv7 channels and Gβγ subunits are involved in the SMIT1-mediated relaxation.

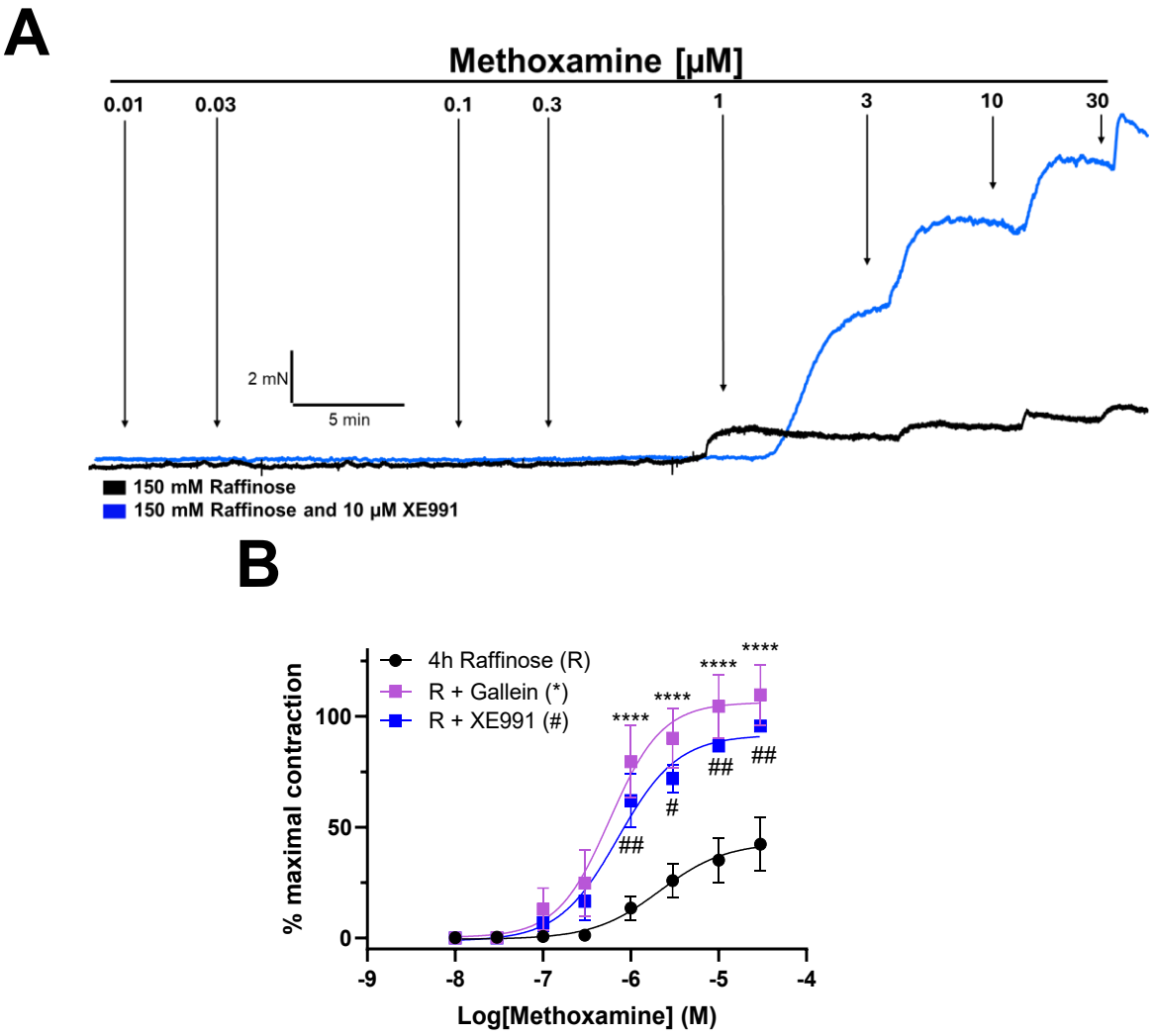


Figure 5.24: The effect of the concentration-dependent contraction to methoxamine in mesenteric arteries in raffinose (4-hours) when in the presence of a pan Kv7 channel, beta-gamma and SGK blocker.

*A representative trace of the contraction to methoxamine incubated in mesenteric arteries incubated with raffinose in the presence (blue) and absence (black) of XE991 (A). The amplitude contraction to methoxamine in the presence of 150 mM raffinose (black, EC_{50} =2.1 µM) with either XE991 (blue, EC_{50} =716 nM) or gallein (purple, EC_{50} = 574.9 nM) is shown in panel B (N=8). All data points are shown as mean +-SEM denoted by error bars and statistical values are determined by 2-way ANOVA with multiple comparisons are calculated using post hoc Bonferroni test where *=P<0.05, **=P<0.01, ***=P<0.001, ****=P<0.0001. (N= number of animals).*

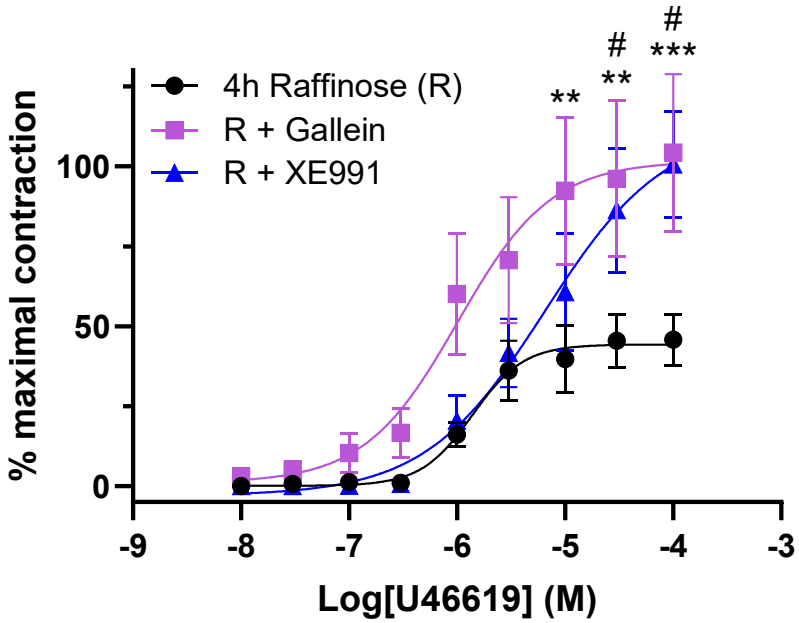


Figure 5.25: The concentration-dependent contraction to U46619 in coronary arteries in raffinose (4-hours) in the presence of either a pan Kv7 channel, beta-gamma or SGK blocker.

*The amplitude contraction to U46619 in the presence of 150 mM raffinose (black, EC_{50} = 1.38 nM) with either XE991 (blue, EC_{50} = 6.47 µM) or gallein (purple, EC_{50} = 1.0 µM). All data points are shown as mean +-SEM denoted by error bars, with N=5 and statistical values are determined by 2-way ANOVA with multiple comparisons are calculated using post hoc Bonferroni test where *=P<0.05, **=P<0.01, ***=P<0.001, ****=P<0.0001.*

5.3.12 | SGK1 regulates SMIT1 membrane expression

Serum- and glucocorticoid-inducible kinases (SGK) can activate SMIT1 and modulate SMIT1 post-translational expression. Klaus et al. 2008 have shown that SGK protein expression is upregulated upon hypertonic cell shrinkage and stabilises SMIT1 within the cellular membrane. The ubiquitin ligase Nedd4-2 removes SMIT1 from the membrane, reducing its activity; however, SGK1 has been found to deactivate Nedd4-2 via phosphorylation, leading to greater membrane SMIT1 expression (Debonneville et al., 2001a). Therefore, immunocytochemistry experiments were used to identify SMIT1 expression in raffinose-incubated arteries in the presence and absence of the SGK inhibitor EMD638683. Strikingly, the total cell fluorescence of SMIT1 in isolated mesenteric VSMCs (figure 5.26A) and the membrane abundance of SMIT1 (figure 5.26B) significantly decreased in raffinose and EMD638683 incubated arteries compared to raffinose alone. These results suggest that SGK1 regulated SMIT1 membrane expression.

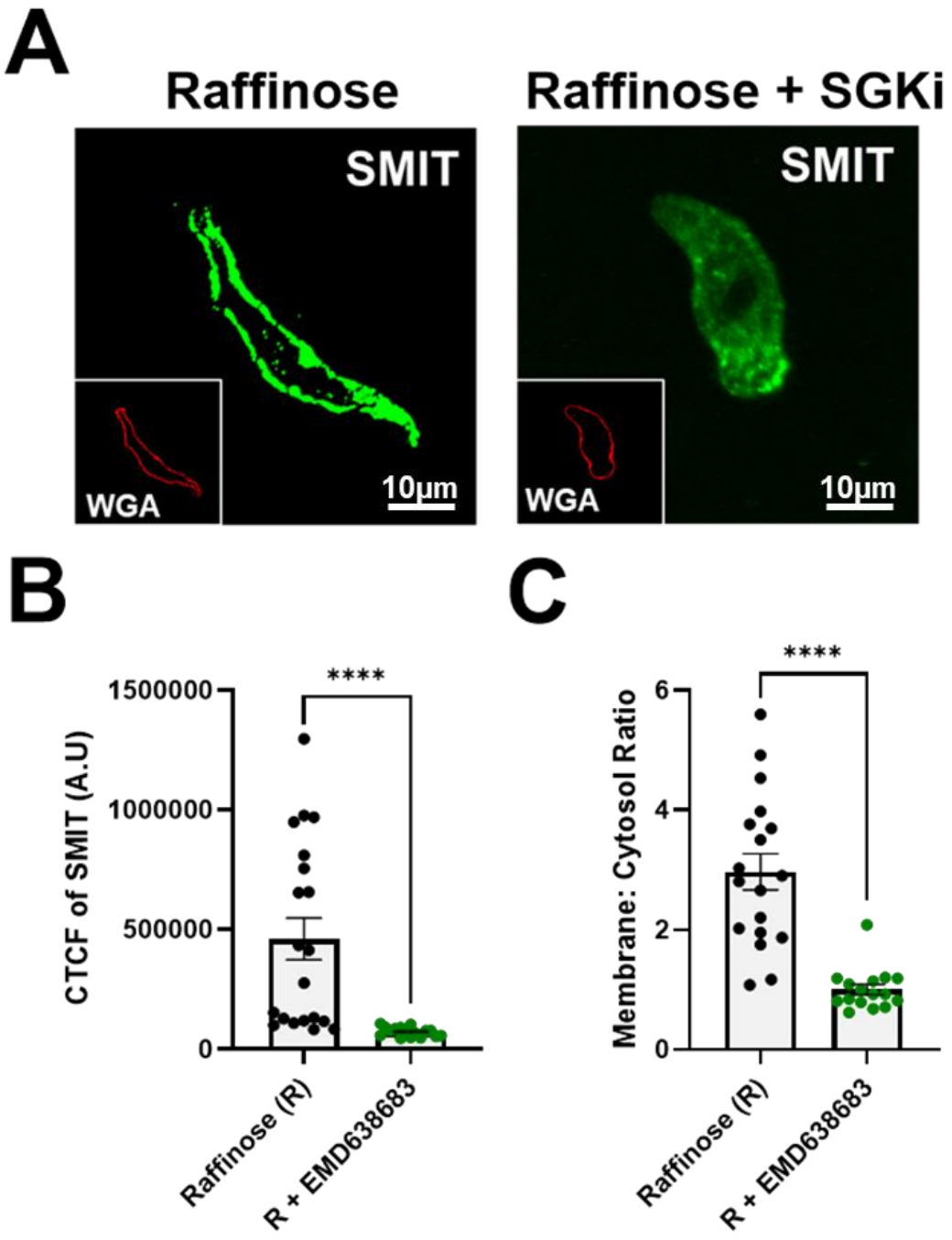


Figure 5.26: The expression of SMIT1 in mesenteric arteries incubated in raffinose for 4-hours with and without an SGK inhibitor.

*Representative staining of SMIT in raffinose (A, left) and in raffinose with EMD638683 (A, right). The mean corrected total cell fluorescence intensity (CTCF) of SMIT1 in mesenteric VSMCs incubated in raffinose alone (black, N=4 n=20) or with an SGK1 inhibitor EMD638683 (green, N=4 n=20) is shown in panel B. The mean membrane: cytosol ratio of SMIT1 staining in mesenteric VSMCs incubated with raffinose alone (black, N=4 n=18) or with EMD638683 (green, N=3 n=16) is shown in panel C. All data is shown as mean± SEM, where statistical P values were calculated using a 2-way ANOVA and multiple comparisons were made via a post hoc Sidak test where *=P<0.05, **=P<0.01, ***=P<0.001, ****=P<0.0001. (N= number of animals used, n= number of technical repeats).*

5.3.12.1 | SMIT1 interacts with SGK in mesenteric and coronary arteries

Upon identifying SGK regulates SMIT1 membrane expression. Experiments were conducted to determine if SGK physically interacted with SMIT1 to regulate SMIT1 activity. Proximity ligation assays identified that SGK did interact with SMIT in mesenteric and coronary arteries from male rats. However, there was a clear difference in the number of SMIT-SGK interactions innately, with coronary arteries having an 80% greater number of PLA puncta than mesenteric arteries, as shown in figure 5.27A,C and E. Interestingly, following a 4-hour incubation of mesenteric and coronary arteries with 150mM raffinose, SGK-SMIT interactions significantly increased in both arteries by 90% and 65%, respectively (figure 5.27E). These findings suggest that upon hypertonicity, SGK-SMIT interactions increase, leading to greater SMIT1 membrane expression and activity.

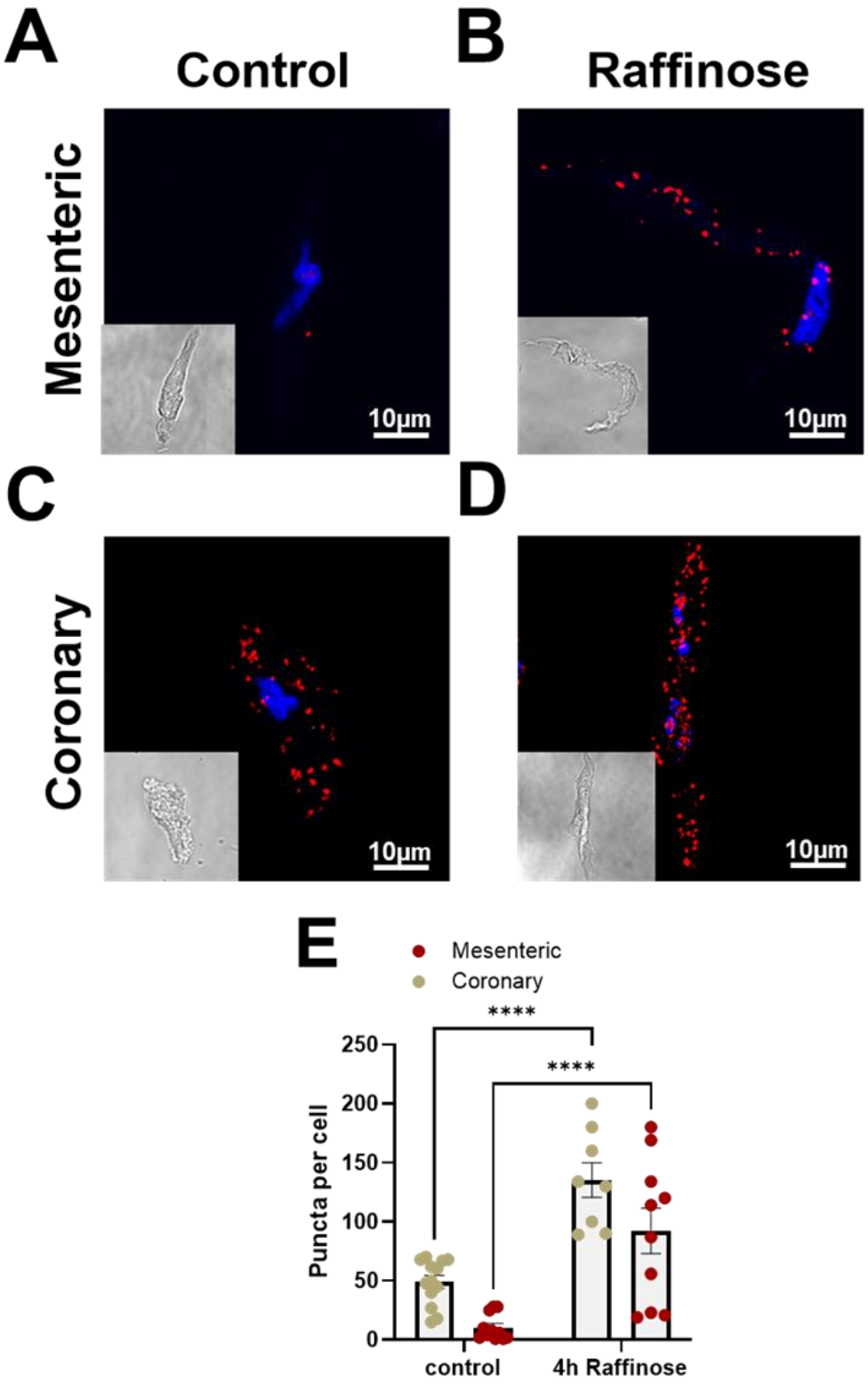


Figure 5.27:The interaction of SMIT1 with SGK in mesenteric and coronary arteries following 4-hour raffinose incubation.

*SMIT-SGK PLA puncta staining in mesenteric arteries incubated in either control PSS (A) or 150mM raffinose PSS (B) and coronary arteries incubated in either control PSS (C) or 150mM raffinose PSS (D). The mean number of PLA puncta in mesenteric (N=3 n=10) and coronary (N=3 n=10) arteries following 4-hour raffinose incubation in male rats is shown in panel E. All data is shown as mean± SEM, where statistical P values were calculated using a 2-way ANOVA and multiple comparisons were made via a post hoc Sidak test where *=P<0.05, **=P<0.01,*

****=P<0.001, ****=P<0.0001. (N= number of animals used, n= number of technical repeats).*

5.3.12.2 | Inhibitors of SGK1 prevent the reduction of methoxamine-induced contractions in raffinose incubated vessels.

Upon identifying that SGK interacts with SMIT1 and regulates SMIT1 membrane abundance. The effect on methoxamine-induced contractions following 4-hour raffinose incubation was investigated in mesenteric and coronary arteries in the presence and absence of the SGK inhibitor EMD638683. The SGK inhibitor significantly prevented the impairment of methoxamine-induced contraction in both mesenteric (figure 5.28A) and coronary (figure 5.28B) arteries. These results suggest that SGK can post-transcriptionally alter SMIT1 membrane expression and is involved in SMIT1-induced relaxations.

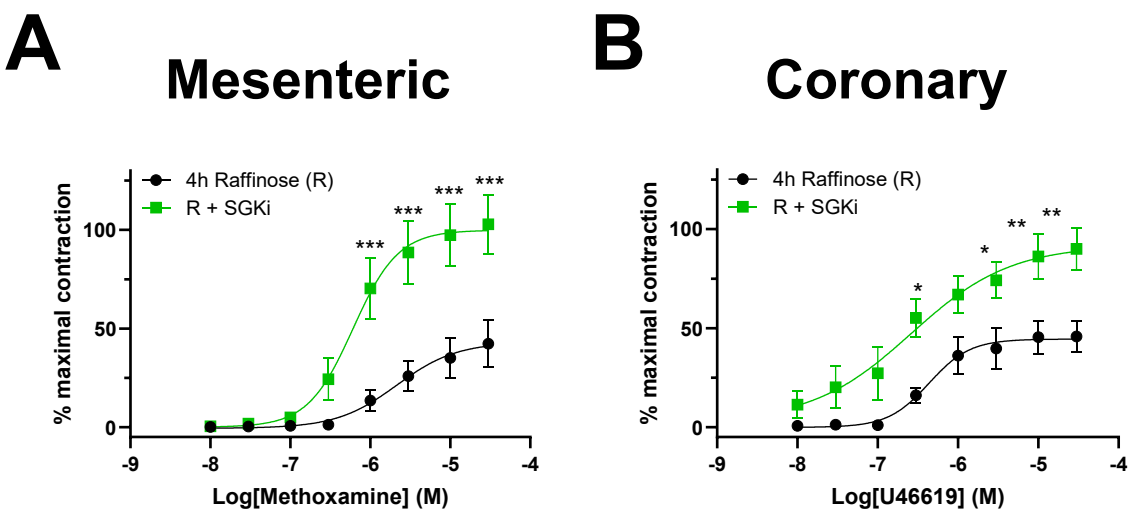


Figure 5.28: The effect of the concentration-dependent contraction to methoxamine in mesenteric and coronary arteries in raffinose (4-hours) when in the presence of the SGK inhibitor EMD638683.
*The contraction to methoxamine (10nM - 10μM) following 4-hour incubation in 150mM raffinose in the presence (green) and absence (black) of SGK inhibitor (SGKi) EMD638683 in mesenteric (A, N=7) and coronary (B, N=7) arteries. All data points are shown as mean +-SEM denoted by error bars, and statistical values are determined by 2-way ANOVA with multiple comparisons are calculated using post hoc Bonferroni test where *=P<0.05, **=P<0.01, ***=P<0.001, ****=P<0.0001. (N= number of animals used).*

5.3.13 | Change in SMIT expression in female mesenteric and coronary arteries when incubated in 150 mM raffinose

The effect of incubating mesenteric and coronary arteries in 150mM raffinose on SMIT1 expression was investigated in female rats using immunocytochemistry. Raffinose increased total SMIT1 expression in mesenteric and coronary arteries from both PE female (figure 5.29B) and DM female (figure 5.29C) rats. The corrected total cell fluorescence (CTCF) intensity of SMIT1 had the greatest increase in DM Female mesenteric arteries compared to PE females and males (figure 5.30). Meanwhile, SMIT1 expression in coronary arteries from both DM female and male rats increased approximately sevenfold when incubated in 150 mM raffinose for 4 hours (figure 5.30). Whereas, mesenteric and coronary arteries from PE females only saw a four-fold increase, which was significantly lower than both DM females and males (figure 5.30). This data suggests that arteries from DM female and male rats have an overall higher total fluorescence intensity of SMIT1 compared to PE females.

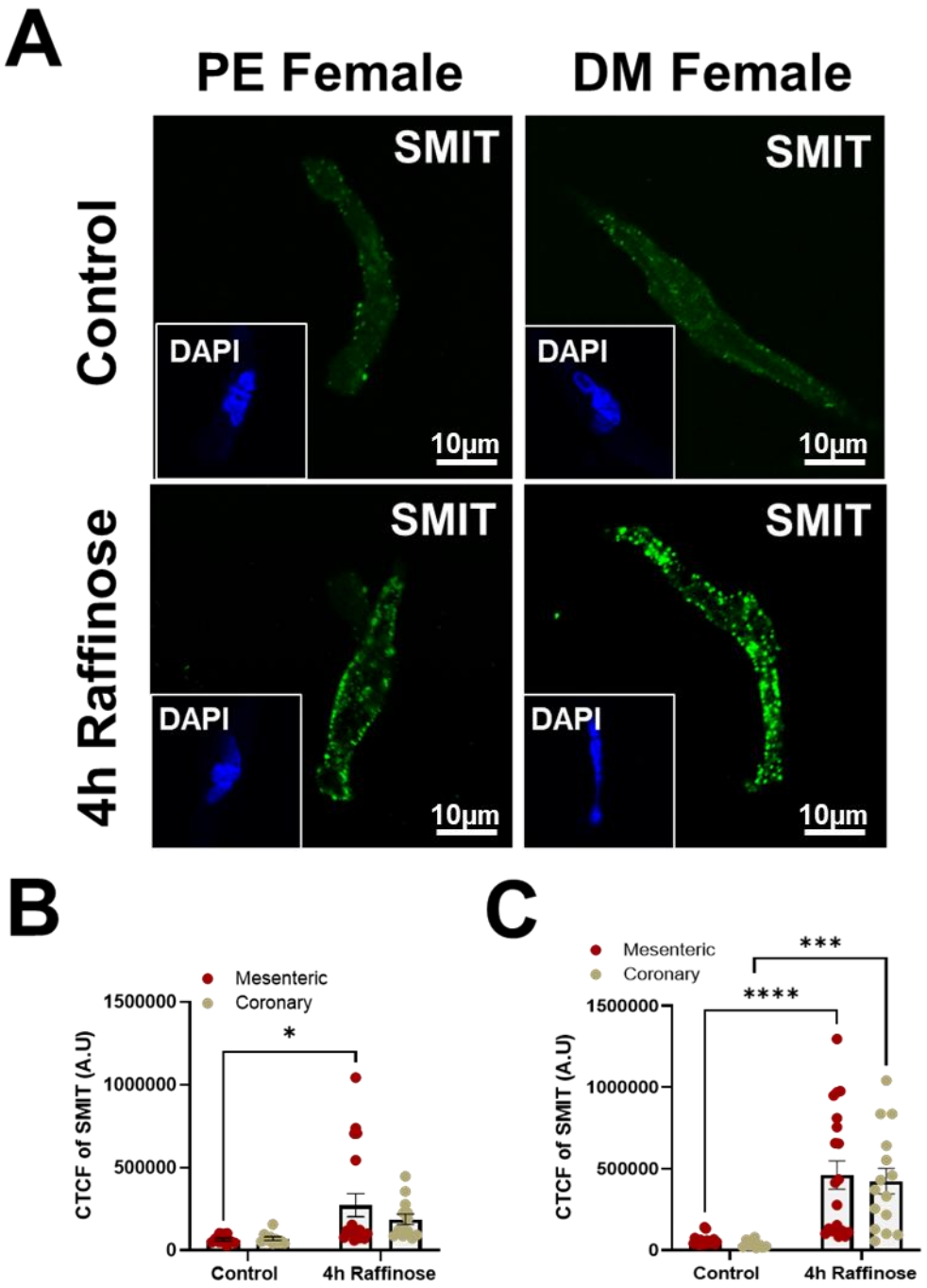


Figure 5.29: The expression of SMIT1 in mesenteric and coronary arteries from DM and PE female rats with and without incubating in raffinose for 4 hours:
*A representative image of SMIT1 staining in isolated vascular smooth muscle cells from mesenteric arteries in PE and DM female rats after incubating in 150 mM raffinose for 4h (A). Mean data showing the corrected total cell fluorescence (CTCF) intensity of SMIT1 in mesenteric (Red, N=4 n=20) and coronary arteries (beige, N=4 n=20) in PE female (B) and DM female rats (C) before and after 4-hour incubation in raffinose. Data shown as mean+- SEM denoted by error bars and p-values were calculated using a 2-way ANOVA, and a post-Hoc Sidak test was used for multiple comparisons where *=P<0.05, ***=P<0.001, ****=P<0.0001. (N= number of animals used, n= number of technical repeats).*

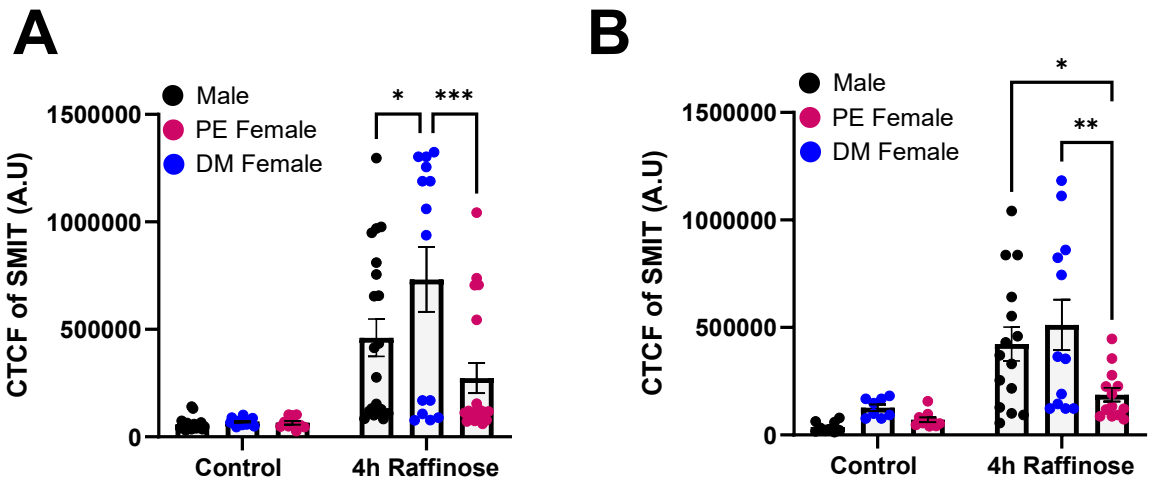


Figure 5.30: Expression of SMIT1 in mesenteric and coronary arteries from males, DM females and PE females in the presence and absence of 4-hour 150 mM raffinose incubation.
*The mean corrected total cell fluorescence (CTCF) intensity of SMIT1 staining in mesenteric (A) and coronary (B) arteries from male (black), DM female (blue) and PE female (pink) rats with and without incubating in 150 mM raffinose for 4 hours. The data is expressed as mean ±SEM denoted by error bars, and p-values were calculated using a 2-way ANOVA, and a post-Hoc Sidak test was used for multiple comparisons where *=P<0.05, **=P<0.01, ***=P<0.001.*

5.3.13.1 | Change in SMIT membrane abundance in female mesenteric and coronary arteries when incubated in 150 mM raffinose

The membrane: cytosol ratio of SMIT1 was calculated in mesenteric and coronary smooth muscle cells incubated in control PSS and 150 mM raffinose PSS. Interestingly, there was a significant increase in SMIT1 membrane abundance in mesenteric and coronary arteries following 150mM raffinose incubation in DM female rats (figure 5.31A-C) but not in PE females (figure 5.31D). The increase in DM female membrane abundance in mesenteric VSMC was similar to that of males (figure 5.32A). Comparatively, there was no increase in SMIT1 membrane protein expression in coronary arteries from male and PE female rats but a significant increase in DM females (figure 5.32B). Interestingly, when in the presence of 150 mM raffinose, the membrane abundance of SMIT was the greatest in male mesenteric arteries compared to DM and PE females. However, DM females had

a significantly greater membrane abundance of SMIT1 in coronary arteries than males and PE females, as shown in figure 5.34.

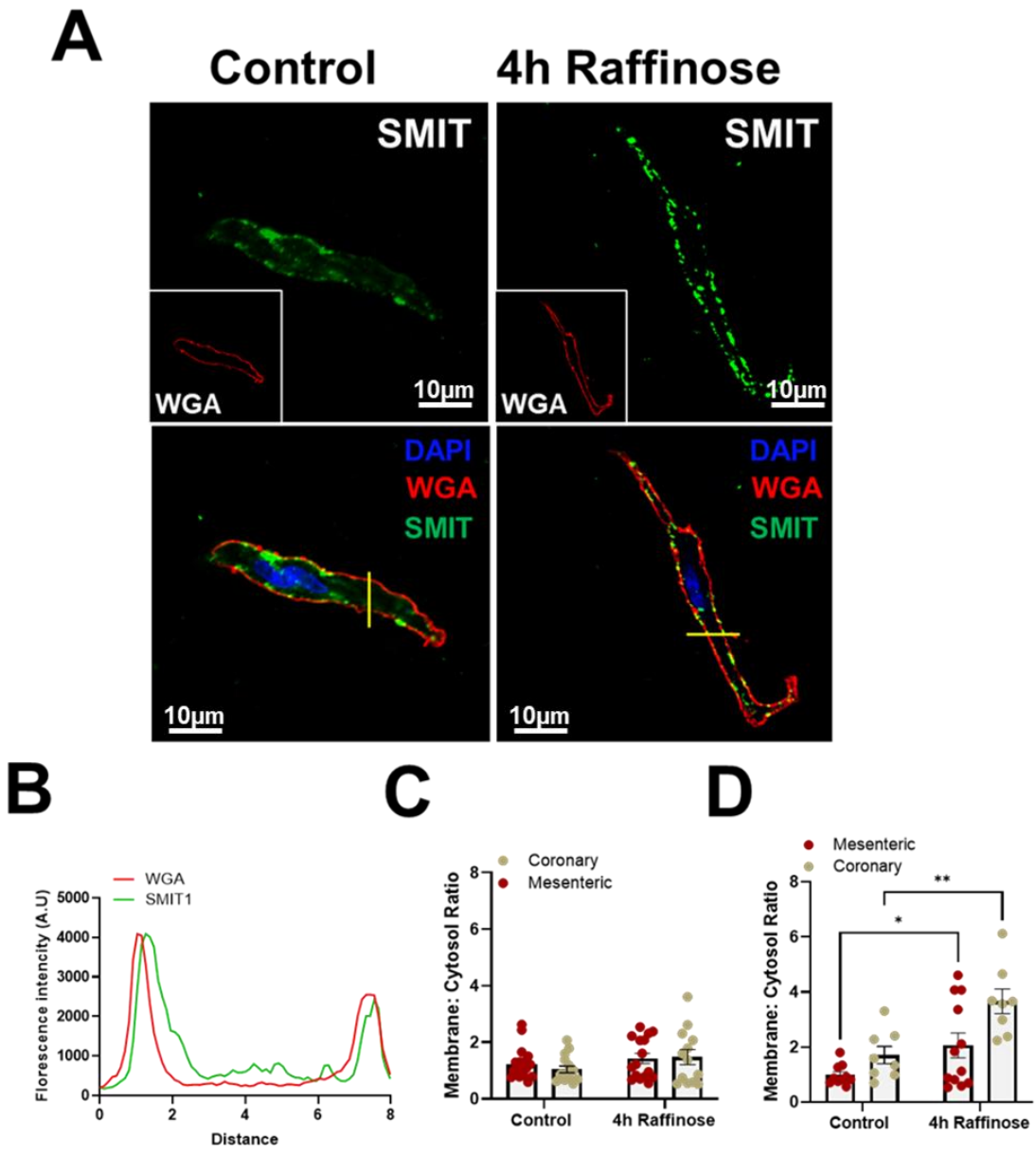


Figure 5.31: Membrane abundance of SMIT1 in female mesenteric and coronary arteries after a 4-hour raffinose incubation.
*A representative image of coronary smooth muscle cells stained with SMIT1 (green), membrane marker, wheat germ agglutinin (WGA, red) and nucleus stain with DAPI in control (A, left) and after 4-hours 150 mM raffinose (A, right). The fluorescence intensity of SMIT and WGA measured across a cell, marked by the yellow line, is shown in panel B. The mean membrane cytosol ratio of SMIT1 in mesenteric (red N=3 n=15) and coronary (beige, N=3 n=13) arteries from PE female (C) and DM female (D) rats is shown as mean± SEM, where statistical P values were calculated using a 2-way ANOVA and multiple comparisons, was made via a post hoc sidak test where *=P<0.05, **=P<0.01. (N= number of animals used, n= number of technical repeats).*

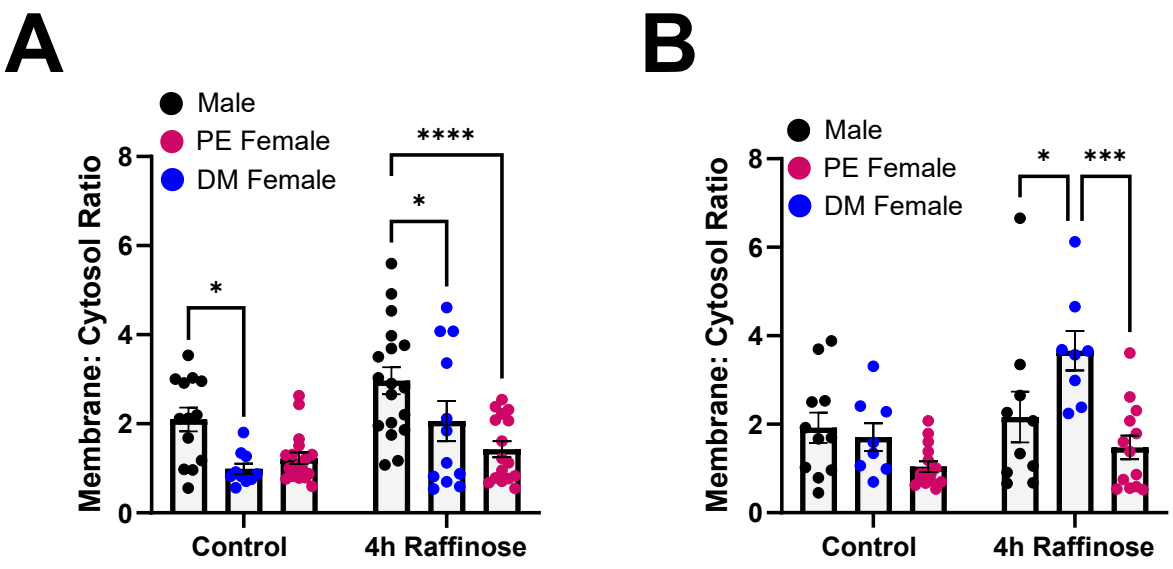


Figure 5.32: The membrane abundance of SMIT1 in mesenteric and coronary arteries from male, DM female and PE female rats.
*The mean membrane cytosol ratio of SMIT1 in mesenteric (A) and coronary (B) arteries from male (black), DM female (blue) and PE female (pink) rats in control vessels or vessels incubated with 150 mM raffinose for 4 hours. Data is shown as mean± SEM, where statistical P values were calculated using a 2-way ANOVA and multiple comparisons were made via a post hoc sidak test where *=P<0.05, **=P<0.01, ***=P<0.001, ****=P<0.0001.*

5.3.14 | The effect of increasing membrane SMIT1 expression on methoxamine-induced contractions in DM and PE female mesenteric arteries.

The membrane expression and functional activity of Kv7 channels in the vasculature changes between males and females and throughout the oestrus cycle (Baldwin et al.,2023) and the effect of SMIT1 function has not previously been investigated in female arteries. Consequently, the impact of incubation in 150 mM raffinose physiological saline solution (PSS) for 4 hours and overnight on methoxamine-induced contractions was examined in mesenteric arteries from female rats. Overnight incubation with raffinose induced a rightward shift in the concentration-response curve to methoxamine in mesenteric arteries from DM females, with the EC_{50} of methoxamine shifting from 622.3 nM to 1.22 µM (figure 5.33A). This effect was not observed in PE females (figure 5.33B). In comparison, the contractile response to methoxamine was attenuated in mesenteric arteries from both diestrus (DM) and proestrus (PE) female rats following 4-hour 150mM raffinose incubation (figure 5.34). In both female groups, there was a decreased sensitivity to methoxamine when incubated in 150mM raffinose, shown by a rightward shift in the methoxamine concentration-response curve with the EC_{50} going from 712.1 nM to 1.10 µM in DM females and 801.1 nM to 1.20 µM, respectively. Arteries from DM females demonstrated a greater shift in sensitivity compared to arteries from PE females. These findings indicate that increased membrane SMIT expression, achieved through raffinose incubation, reduces the sensitivity of mesenteric arteries to contractile agents in both males and females. However, the alteration in contractile tone and sensitivity is more pronounced in males and DM females compared to PE females.

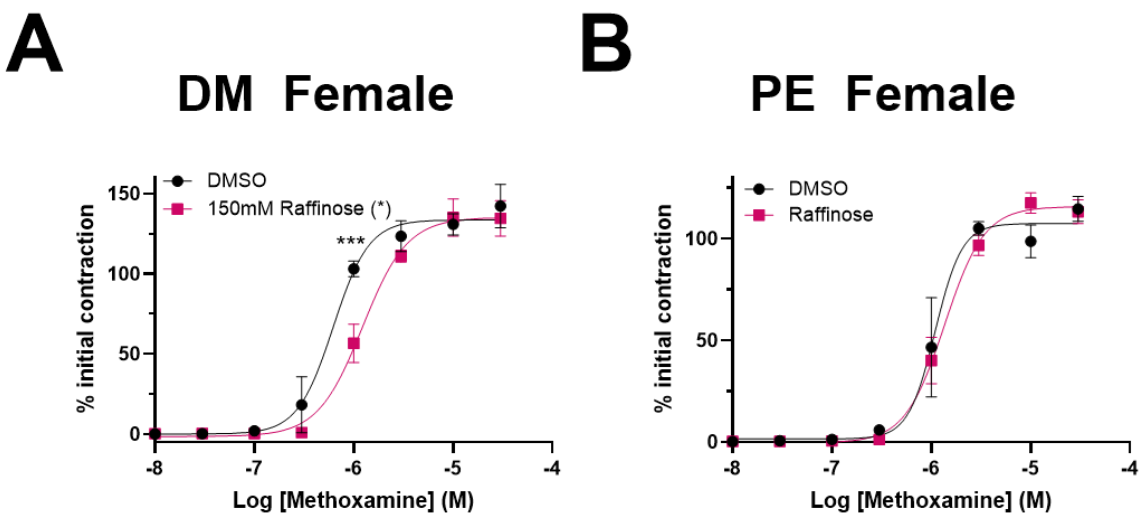


Figure 5.33: Effect of methoxamine-induced contractions on female mesenteric arteries when incubated overnight in raffinose PSS.
*The mean response to methoxamine in mesenteric arteries from DM (A) and PE female (B) arteries incubated in either control PSS (black, EC_{50} = 6.22 nM and 1.1 µM) or 150mM raffinose PSS (pink, EC_{50} = 1.2 µM and 1.4 µM). All data points are shown as mean +-SEM denoted by error bars, with N=5 and statistical values are determined by 2-way ANOVA with multiple comparisons are calculated using post hoc Bonferroni test where *=P<0.05, **=P<0.01, ***=P<0.001, ****=P<0.0001. (N= number of animals used).*

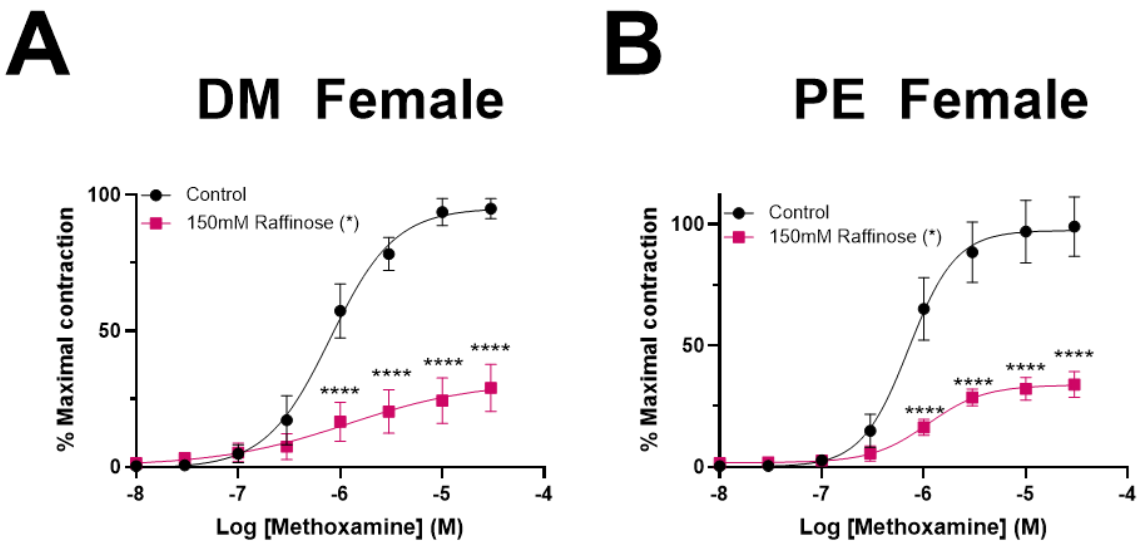


Figure 5.34: The concentration-dependent contraction to methoxamine in female mesenteric arteries incubated in either 20mM or 150mM raffinose for 4-hours.
*The mean concentration-dependent contraction to methoxamine (10nM - 30µM) in mesenteric arteries from DM (A) and PE females (B) incubated with either 150mM raffinose PSS (pink) or control PSS (black). All data points are shown as mean +-SEM denoted by error bars, with N=9 and statistical values are determined by 2-way ANOVA with multiple comparisons are calculated using post hoc Bonferroni test where *=P<0.05, **=P<0.01, ***=P<0.001, ****=P<0.0001.*

5.3.15 | Kv7.4 expression in males and females

Immunocytochemistry experiments showed Kv7.4 was expressed in mesenteric and coronary arteries from female rats (figure 5.31), similar to that seen in Baldwin et al.,2020. The expression of Kv7.4 in coronary and mesenteric arteries from PE females was markedly less than that of males and DM females; however, the expression in mesenteric arteries did not reach significance (figure 5.35A-B). Interestingly, the membrane: cytosol ratio of Kv7.4 was significantly greater in male and DM female mesenteric arteries compared to PE females, but no clear difference was seen in coronary arteries (figure 5.35). Therefore, males and DM females appear to have greater membrane abundance and total expression of Kv7.4 in mesenteric arteries and a greater total expression of Kv7.4 in coronary arteries compared to PE females.

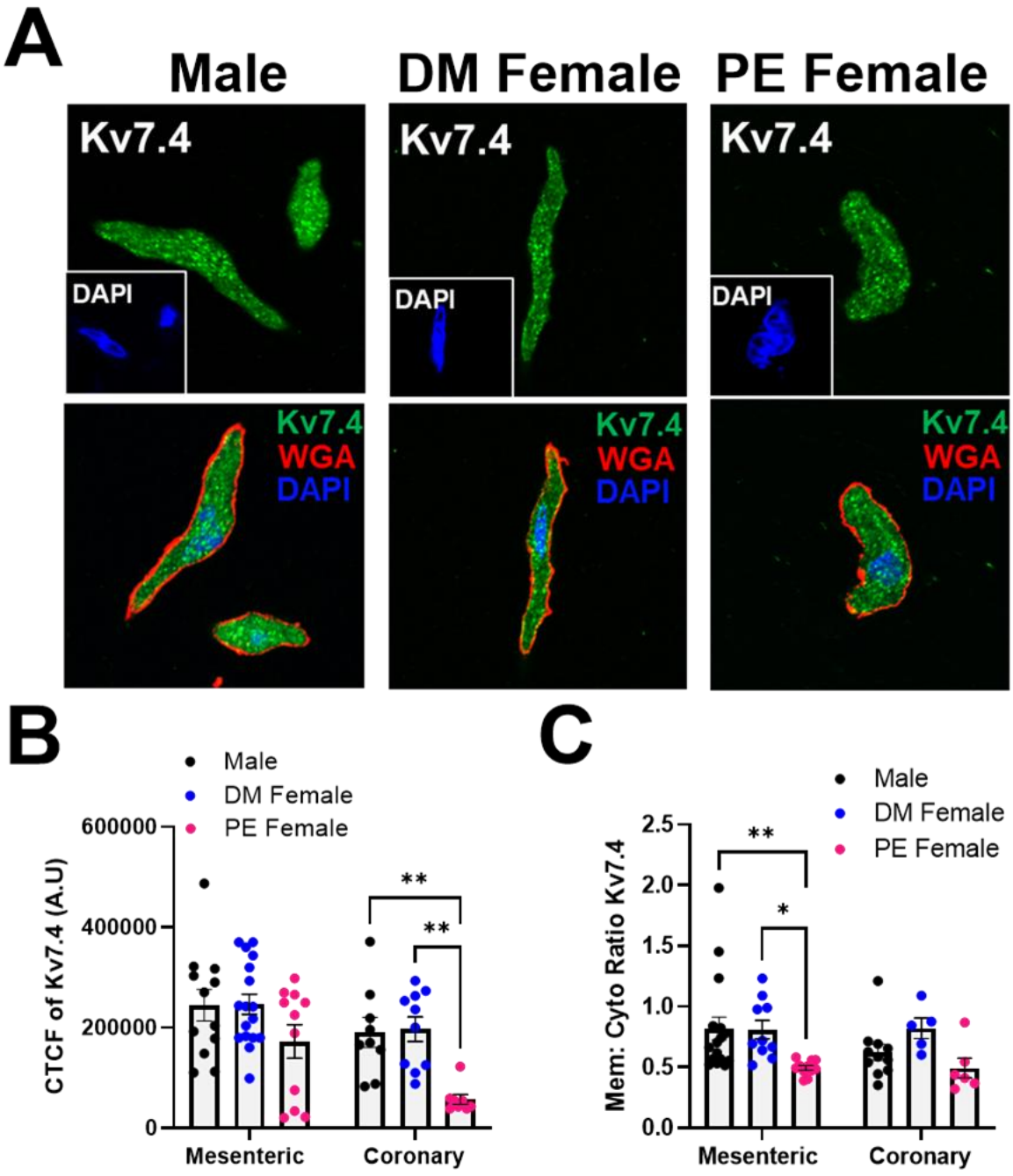


Figure 5.35: Expression of Kv7.4 in mesenteric and coronary arteries from male and female rats

*Panel A shows the representative staining of Kv7.4 in mesenteric arteries from male, DM female and PE female rats in green with a nuclear stain (DAPI) in blue and membrane marker Wheat germ agglutinin (WGA) in red. The mean total cell fluorescence (CTCF) of Kv7.4 in male (black), DM female (blue) and PE female (pink) mesenteric and coronary arteries is shown in panel B, and the mean membrane cytosol ratio of Kv7.4 staining is shown in panel C. All data is shown as mean± SEM, where statistical P values were calculated using a 2-way ANOVA and multiple comparisons were made via a post hoc Sidak test where *=P<0.05, **=P<0.01, ***=P<0.001, ****=P<0.0001.*

5.3.16 | Change in Kv7.4 expression in female mesenteric and coronary arteries when incubated in 150 mM raffinose

Alterations in Kv7.4 expression are seen throughout the female oestrus cycle (Baldwin et al., 2022; Baldwin et al., 2023). Hence, the expression of Kv7.4 in mesenteric and coronary arteries from female DM and PE rats incubated in either control PSS or 150 raffinose was investigated. Incubation with raffinose significantly upregulated Kv7.4 expression in mesenteric and coronary arteries from DM female rats (figure 5.36A-B) but not in PE female rats (figure 5.36A and C). Additionally, the membrane-to-cytosol ratio of Kv7.4 in smooth muscle cells of mesenteric and coronary arteries increased exclusively in DM females (figure 5.37A), with no significant change observed in PE females (figure 5.37B) and the shift in total Kv7.4 expression was more pronounced in DM females compared to their male and PE female counterparts. Therefore, this data suggests that Kv7.4 and SMIT expression both increase upon incubation with 150 mM raffinose PSS.

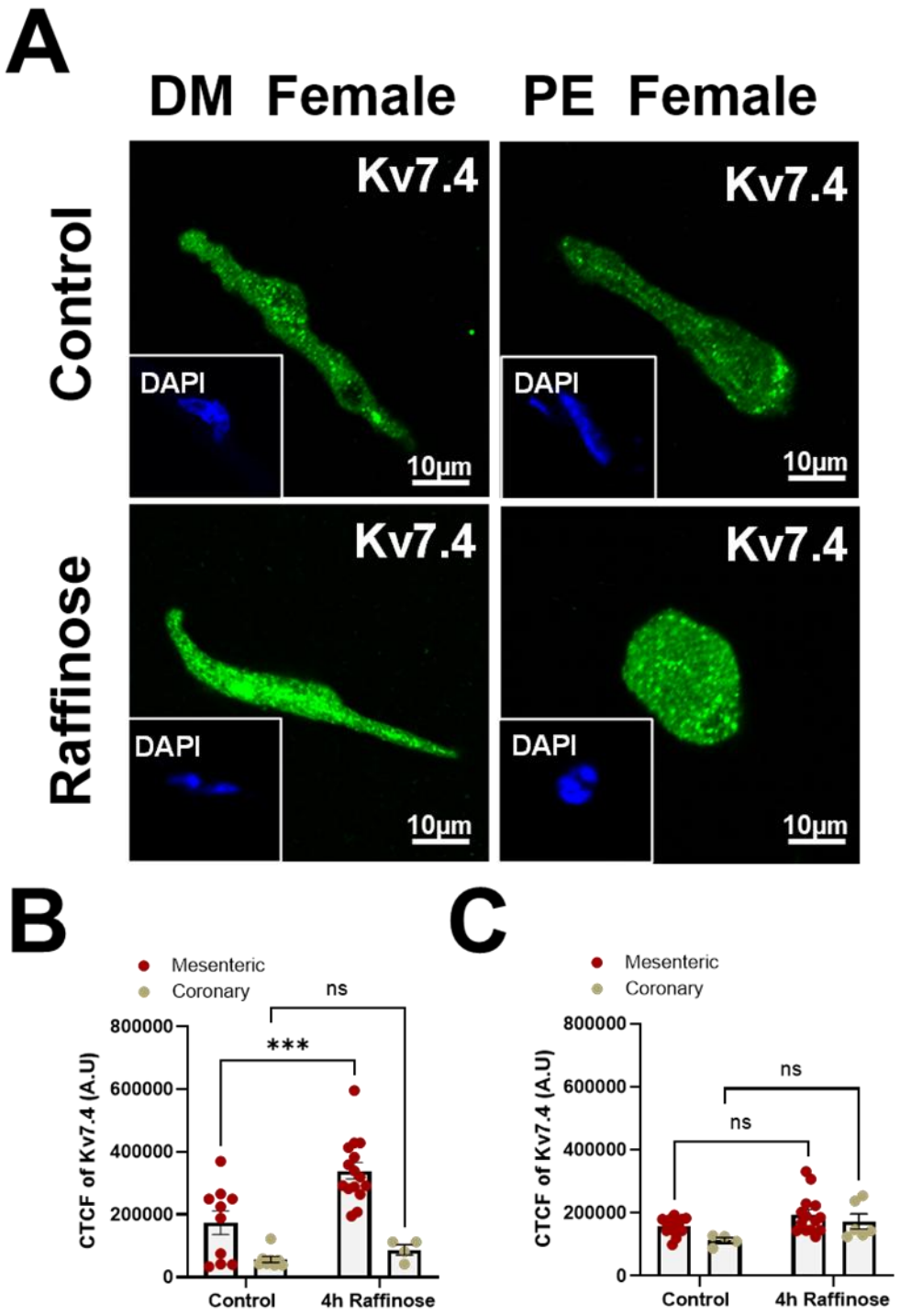


Figure 5.36: Expression of Kv7.4 in female mesenteric and coronary arteries when incubated in raffinose for 4-hours.

*A representative image of the expression of Kv7.4 (green) in mesenteric arteries from DM female and PE female rats, when incubated in either control PSS or 150 mM raffinose PSS, with the nuclear staining (DAPI), is shown in blue (A). The mean total cell fluorescence (CTCF) of Kv7.4 in mesenteric (red, N=3 n=15) and coronary (beige, N=3 n=9) arteries from DM female (B) and PE female (C) rats when incubated in control PSS or 150mM raffinose for 4-hours. All data is shown as mean± SEM, where statistical P values were calculated using a 2-way ANOVA and multiple comparisons were made via a post hoc Sidak test where *=P<0.05, **=P<0.01, ***=P<0.001, ****=P<0.0001. (N= number of animals used, n= number of technical repeats).*

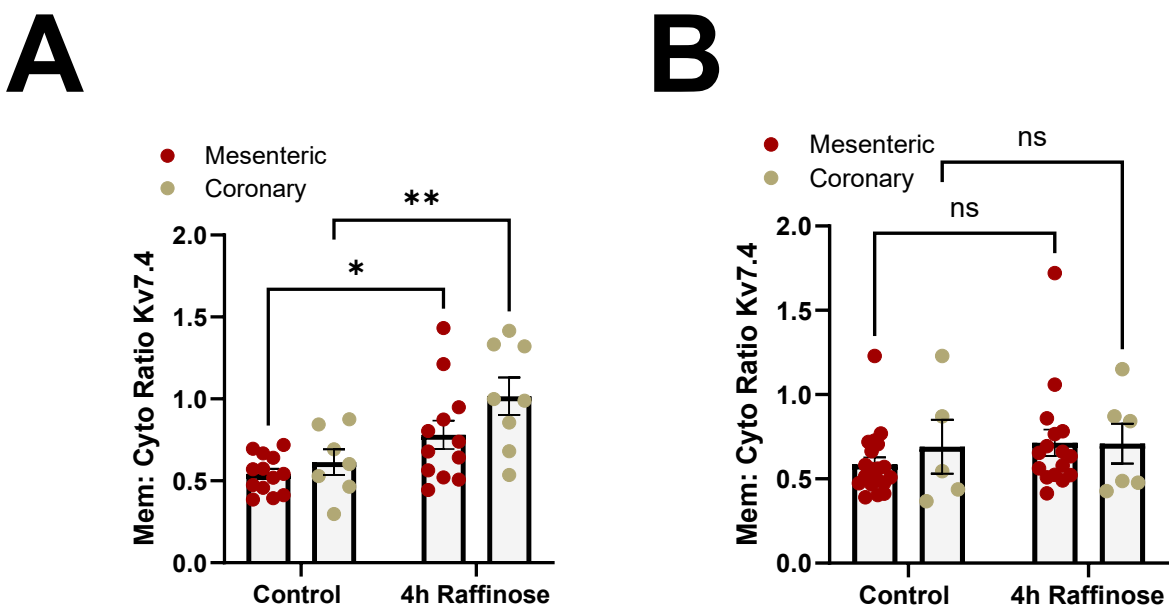


Figure 5.37: Membrane expression Kv7.4 in female mesenteric and coronary arteries when incubated in raffinose for 4-hours.
*The mean membrane cytosol ratio of Kv7.4 in mesenteric (red, N=3 n=15) and coronary (beige, N=3 n=9) arteries from DM female (A) and PE female (B) rats. All data is shown as mean± SEM, where statistical P values were calculated using a 2-way ANOVA and multiple comparisons were made via a post hoc Sidak test where *=P<0.05, **=P<0.01, ***=P<0.001, ****=P<0.0001. (N= number of animals used, n= number of technical repeats).*

5.3.17 | SMIT1 physically interacts with Kv7.4 and Kv7.5 ion channel proteins in mesenteric and coronary arteries from female rats

The interaction of SMIT1 with Kv7 ion channel proteins has not been investigated in arteries from female rats. Hence, PLA experiments exploring the interaction of SMIT1 with Kv7.4 and Kv7.5 proteins were carried out on mesenteric and coronary arteries from female rats. SMIT-Kv7.4 and SMIT-Kv7.5 interactions were identified in female mesenteric and coronary arteries (figure 5.38). DM female mesenteric VSMCs had the greatest SMIT-Kv7.4 and SMIT-Kv7.5 PLA puncta compared to males and PE females. Similarly, DM females had the highest number of SMIT-Kv7.4 PLA puncta in coronary arteries, but males had a comparably similar number of SMIT-Kv7.5 interactions.

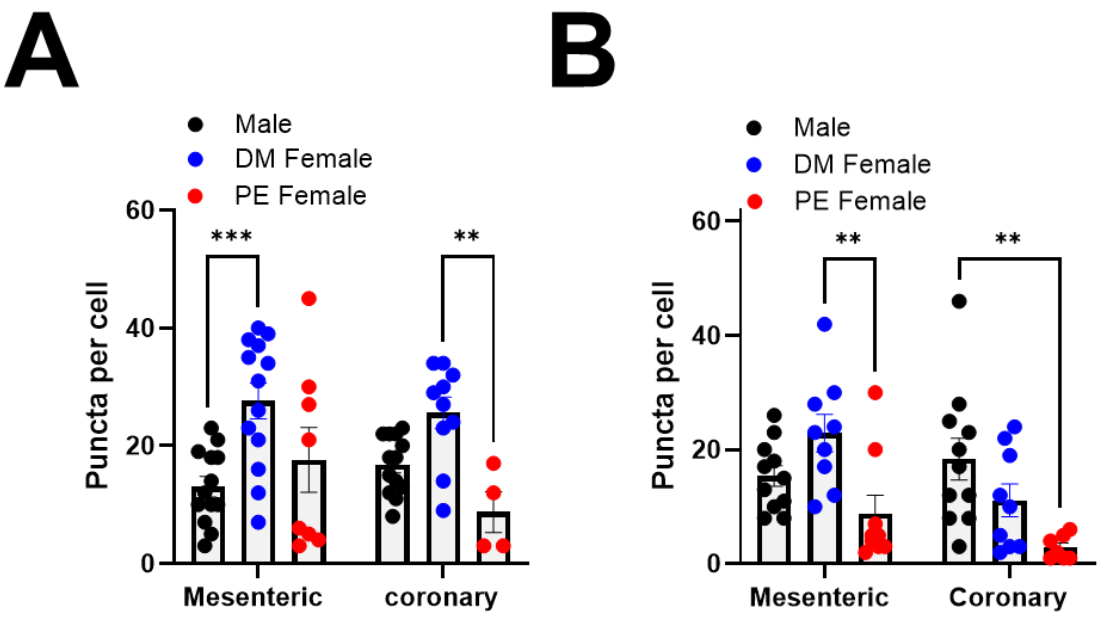


Figure 5.38: The interaction of SMIT with Kv7.4 and Kv7.5 in mesenteric and coronary VSMCs from male, DM female and PE female rats.
*Proximity ligation assays (PLA) showing the mean number of SMIT-Kv7.4 (A) and SMIT-Kv7.5 (B) puncta per cell in male (black, N=3 n=15), DM female (blue, N=3 n=12) and PE female (red, N=3 n=9) mesenteric and coronary VSMCs. All data is shown as mean± SEM, where statistical P values were calculated using a 2-way ANOVA and multiple comparisons were made via a post hoc Sidak test where *=P<0.05, **=P<0.01, ***=P<0.001, ****=P<0.0001. (N= number of animals used, n= number of technical repeats).*

Increasing SMIT1 protein expression via 4-hour raffinose incubation elevated SMIT1 interactions with Kv7.4 and Kv7.5 in mesenteric and coronary arteries from DM and PE females (figure 5.39). DM females exhibited a markedly greater increase in SMIT1-Kv7.4 and SMIT1-Kv7.5 PLA puncta in both mesenteric and coronary arteries compared to PE females and males. Specifically, SMIT1-Kv7.4 and SMIT1-Kv7.5 interactions in mesenteric arteries from DM females increased by approximately 70% and 80%, respectively, significantly greater than PE females (figure 5.39). The differences in SMIT1 interactions with Kv7.4 and Kv7.5 in coronary arteries from DM and PE females mirrored those observed in mesenteric arteries. This data suggests that SMIT1 interactions with Kv7.4 and K7.5 increase VSMCs from mesenteric and coronary arteries in both male and female rats following incubation in 150mM raffinose PSS. The increase in these interactions is most pronounced in arteries from DM females, followed by males and PE female rats.

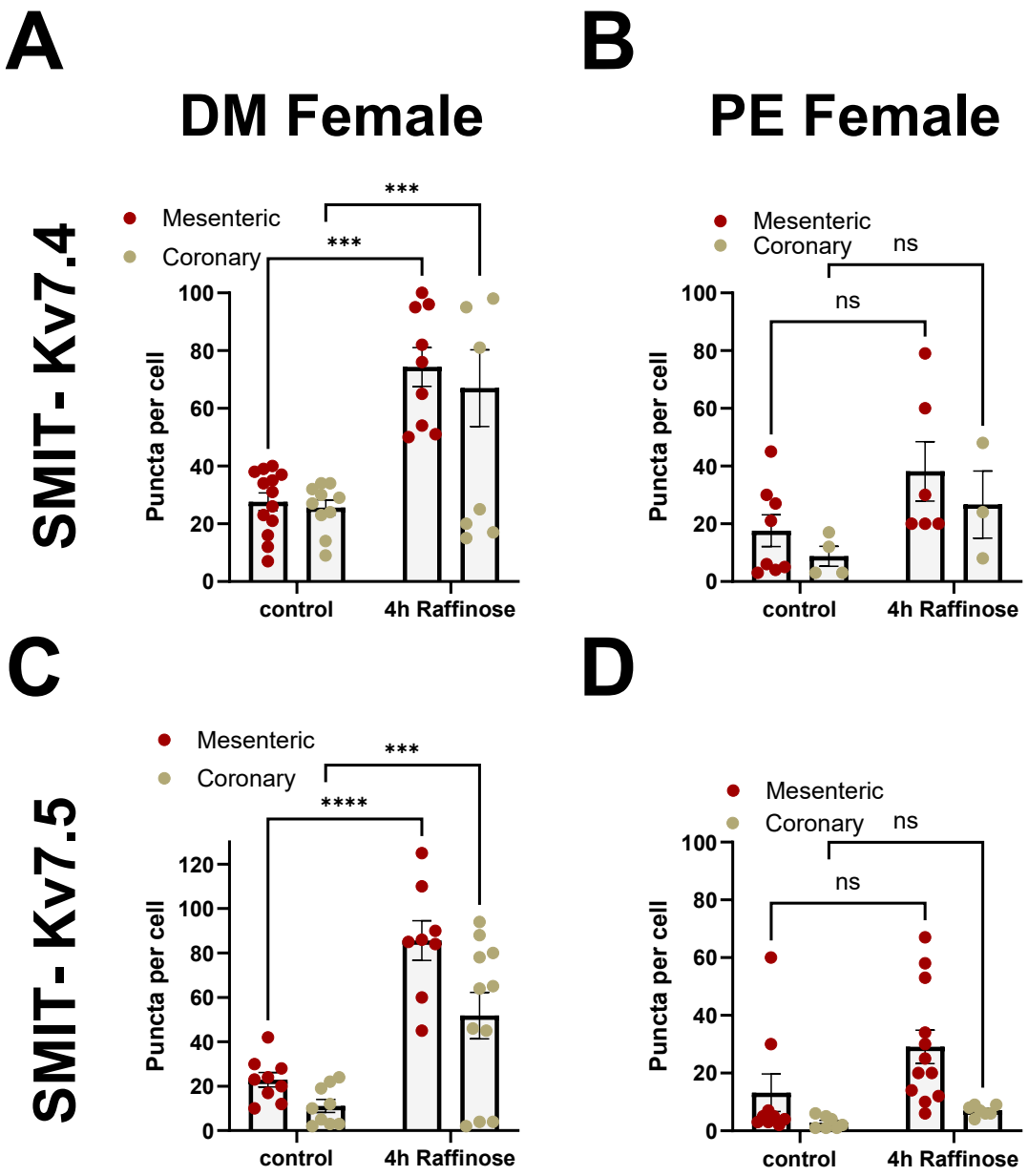


Figure 5.39: The interactions of SMIT1 with Kv7.4 and Kv7.5 in mesenteric and coronary VSMCs from DM female and PE female rats.
*Bar charts showing PLA puncta of SMIT1-Kv7.4 interactions in mesenteric (red) and coronary (beige) arteries from DM female (A, N=3 n=9) and PE female (B, N=2 n=8) rats. Also, bar charts showing PLA puncta of SMIT-Kv7.5 interactions in mesenteric (red) and coronary (beige) VSMCs from DM female (C) and PE female (D) rats. All data is shown as mean± SEM, where statistical P values were calculated using a 2-way ANOVA and multiple comparisons were made via a post hoc Sidak test where *=P<0.05, **=P<0.01, ***=P<0.001, ****=P<0.0001. (N= number of animals used, n= number of technical repeats).*

5.3.17.1 | SMIT1-Gβγ protein interactions in mesenteric and coronary arteries from female DM and PE rats.

DM females had significantly higher SMIT1- Gβγ PLA puncta in mesenteric and coronary arteries compared to both male and PE females, as shown in figure 5.29. Interestingly, PE females also had a greater number of SMIT- Gβγ PLA puncta in mesenteric VSMCs than males. Incubating mesenteric and coronary arteries from male rats with 150 mM raffinose PSS increased the number of SMIT- Gβγ interactions by ~50% and ~65%, respectively (figure 5.40). Raffinose incubation also increased SMIT1- Gβγ interactions in mesenteric and coronary arteries from DM and PE females (figure 5.41). However, only DM females produced a significant 3-fold increase in SMIT- Gβγ PLA puncta in coronary arteries (figure 5.41A, $P<0.0001$) compared to PE females and males (P =ns). DM females also produced a 3-fold increase in SMIT- Gβγ interactions in mesenteric VSMCs incubated in raffinose, greater than PE females and males. These findings suggest that the pro-relaxant effects of SMIT could also be due to Gβγ forming a complex with SMIT and Kv7.4/5 helping regulate vascular contractility.

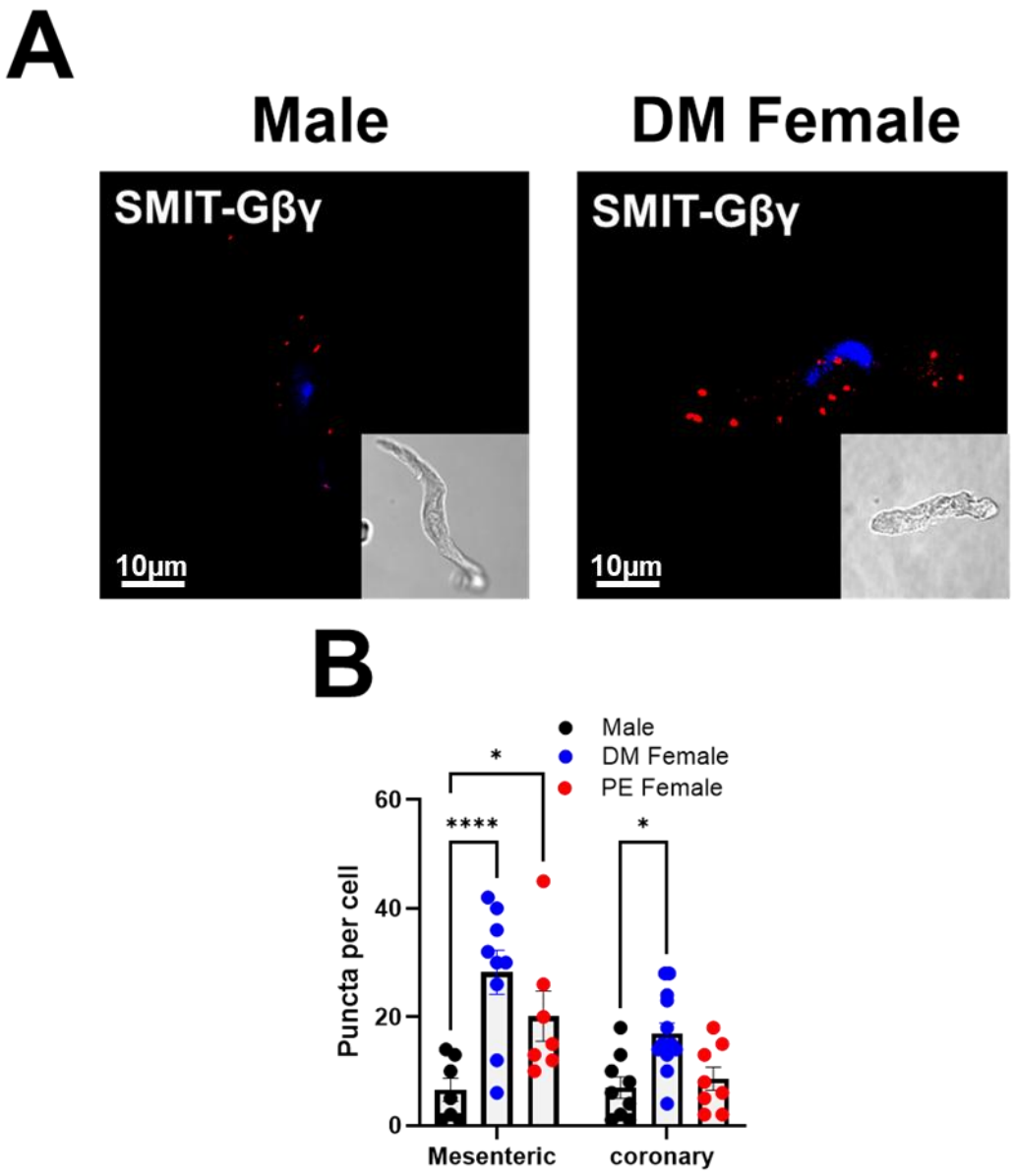


Figure 5.40: Interaction of SMIT1 with Gβγ in mesenteric and coronary arteries from male, DM female and PE female rats.
*PLA puncta staining (red) of SMIT1- Gβγ in mesenteric arteries from male and DM female rats (A). Bar chart showing the mean number of PLA puncta in mesenteric and coronary arteries from male (black, N=3 n=9), DM female (blue, N=3 n=9) and PE female (red, N=3 n=9) rats (B). All data is shown as mean± SEM, where statistical P values were calculated using a 2-way ANOVA and multiple comparisons were made via a post hoc Sidak test where *=P<0.05, **=P<0.01, ***=P<0.001, ****=P<0.0001. (N= number of animals used, n= number of technical repeats).*

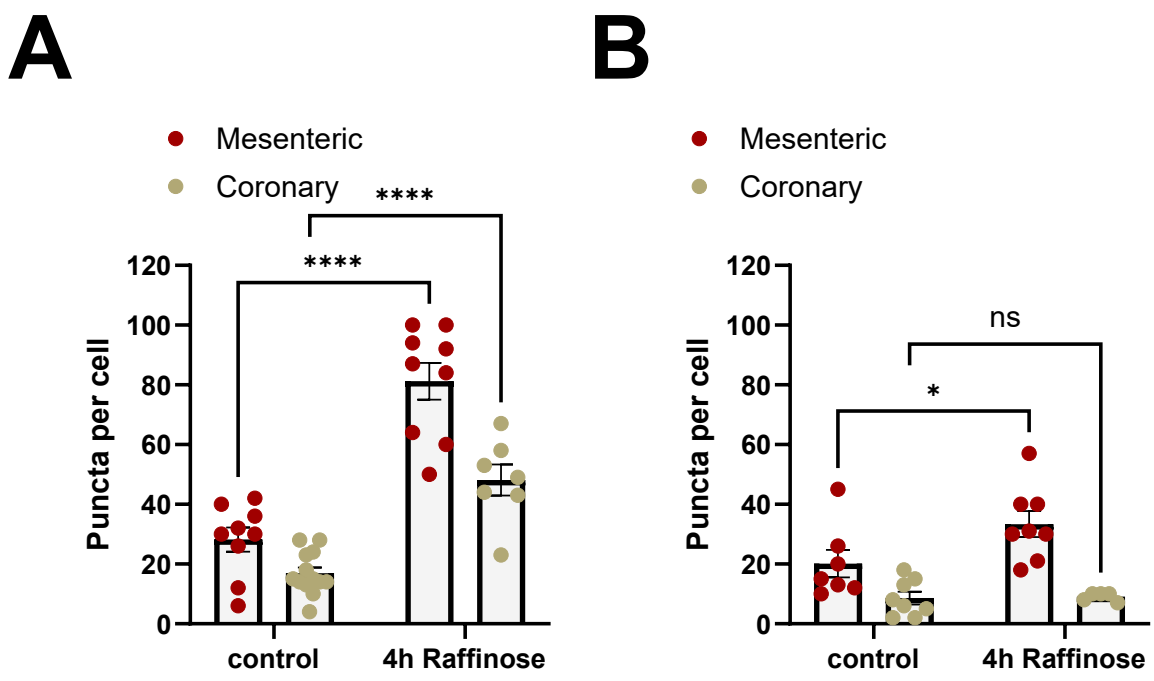


Figure 5.41: The interaction of SMIT with Gβγ in raffinose-incubated mesenteric and coronary arteries in DM and PE females.
Bar chart of the mean SMIT- Gβγ PLA puncta in control PSS and 4h 150mM raffinose PSS incubated mesenteric (red, N=3 n=9) and coronary (beige, N=3 n=9) arteries from DM female (A) and PE female (B) rats. (N= number of animals used, n= number of technical repeats).

5.3.18 | The effect of incubating mesenteric and coronary arteries in hyperglycaemic PSS

This results chapter has shown that incubating arteries in hypertonic 150 mM raffinose solution enhances SMIT1 membrane expression, reducing arterial contractility and increasing arterial-induced relaxations. However, do these effects occur in arteries exposed to hyperglycaemic PSS, giving a clinical perspective of the role of SMIT1 in diseases such as diabetes mellitus? Immunocytochemistry experiments were conducted to ascertain the change in SMIT and SGLT2 protein expression following a 4-hour incubation in hyperosmolar 20 mM glucose PSS (Glaser et al., 2022). Mesenteric and coronary vascular smooth muscle cells (VSMC) both exhibited increased SMIT1 expression predominantly in the cell membrane following a 4-hour incubation in 20 mM glucose PSS (figure 5.42). These findings show that hyperglycaemic PSS increases the total membrane abundance of SMIT in VSMCs. The clustering of the SMIT1 and SGLT2 staining

also increased when incubating in 20 mM glucose, as depicted in figures 5.42A and 5.43A. Interestingly, hyperglycaemic PSS did not change the protein expression or membrane abundance of SGLT2 in mesenteric arteries; however, a significant 3-fold increase in SGLT2 expression was found in coronary arteries incubated in hyperglycaemic PSS (figure 5.43).

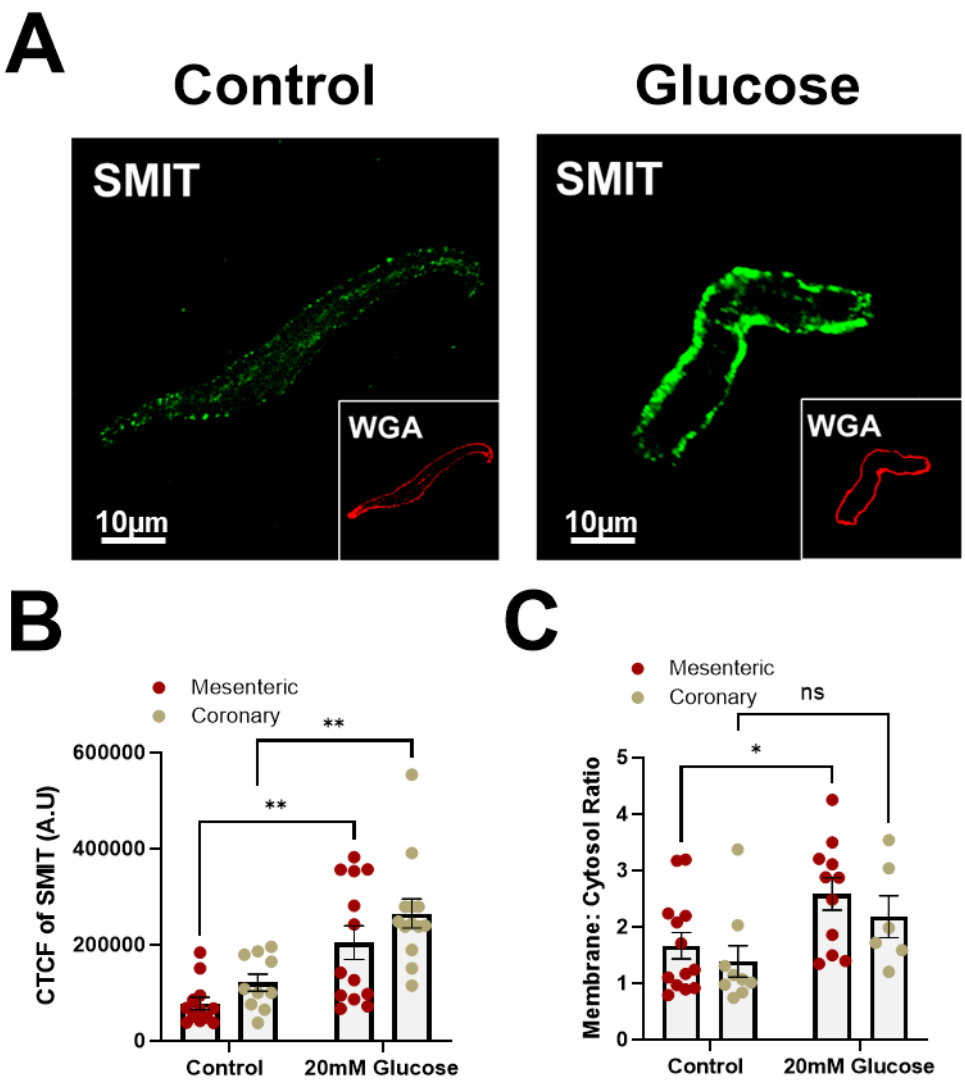


Figure 5.42: The change in the expression of SMIT1 in mesenteric and coronary arteries incubated in control or 4 hours of glucose PSS.
*Staining of SMIT (green) in mesenteric VSMCs incubated in either control PSS or 20mM glucose PSS, with a wheat germ agglutinin (WGA, red) membrane marker (A). The total fluorescence intensity (B) and membrane cytosol ratio (C) of SMIT1 in isolated mesenteric (red, N=3 n=12) and coronary (beige, N=3 n=8-10) arteries incubated in either control PSS or hyperglycaemic 20 mM glucose PSS. Data is shown as Mean +-SEM and P values were determined via a 2-way ANOVA with multiple comparisons calculated using a post hoc Sidak test where **=P<0.01, ***=P<0.001. (N= number of animals used, n= number of technical repeats).*

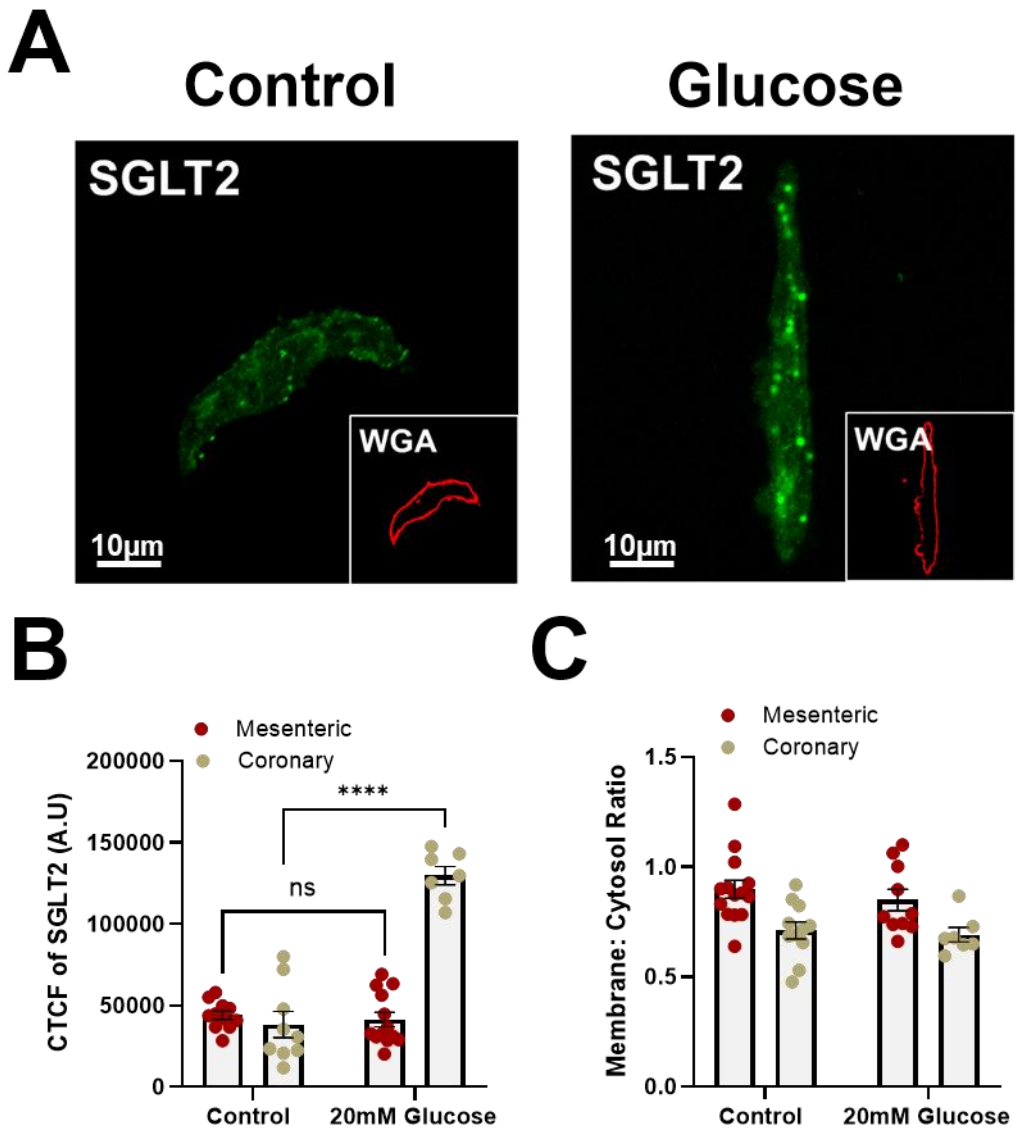


Figure 5.43: The change in the expression of SGLT2 in mesenteric and coronary arteries incubated in either control or 4 hours of 20 mM glucose PSS.
*Staining of SGLT2 protein in mesenteric VSMCs incubated in either control PSS or 20mM glucose PSS, with a wheat germ agglutinin (WGA, red) membrane marker (A). The total fluorescence intensity (B) and membrane cytosol ratio (C) of SGLT2 in isolated mesenteric (red, N=3 n=15) and coronary (beige, N=3 n=9) arteries incubated in either control PSS or hyperglycaemic 20 mM glucose PSS. Data is shown as Mean +-SEM and P values were determined via a 2-way ANOVA with multiple comparisons calculated using a post hoc Sidak test where **=P<0.01, ***=P<0.001. (N= number of animals used, n= number of technical repeats).*

5.3.18.1 | Overnight incubation in hyperglycaemic PSS shifted the sensitivity to methoxamine-induced contractions

Incubation in 150mM raffinose PSS markedly reduced arterial contractility in response to vasocontractile agents. Consequently, these experiments investigated the impact of overnight incubation in hyperglycaemic PSS on the contractility of mesenteric and coronary arteries in male and female rats. Mesenteric arteries were incubated overnight in either control PSS or 20 mM glucose PSS and then mounted on a wire myograph. A concentration-effect curve to methoxamine was produced, and the results were normalised to the initial vitality test contraction to methoxamine. Overnight incubation of mesenteric arteries with 20mM glucose PSS reduced the arterial contractility and produced a significant right shift in the concentration-effect curve to methoxamine (figure 5.44). Similarly, arteries from both DM and PE females exhibited a reduced contractile response to methoxamine, with a right shift in the concentration-effect curve (figure 5.45). Therefore, acute exposure to hyperglycaemic PSS leads to a reduction in the contractile response to methoxamine.

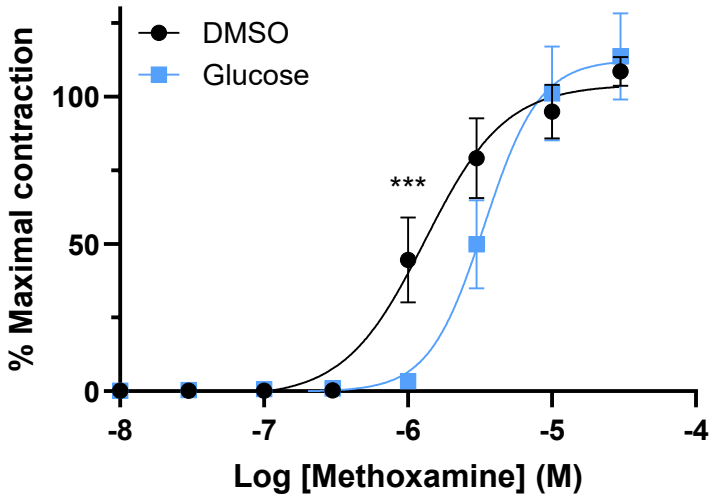


Figure 5.44: The concentration-dependent contraction to methoxamine in male mesenteric arteries incubated overnight in glucose PSS.
*A concentration effect curve to methoxamine (10 nM – 30 μM) in mesenteric arteries incubated overnight in either control PSS (Black, EC_{50} =1.1 μM) or 20 mM glucose PSS (blue, EC_{50} = 4.2 μM). All data points are shown as mean +-SEM denoted by error bars, with N=7 and statistical values are determined by 2-way ANOVA with multiple comparisons are calculated using post hoc Bonferroni test where *=P<0.05, **=P<0.01, ***=P<0.001, ****=P<0.0001. (N=number of animals).*

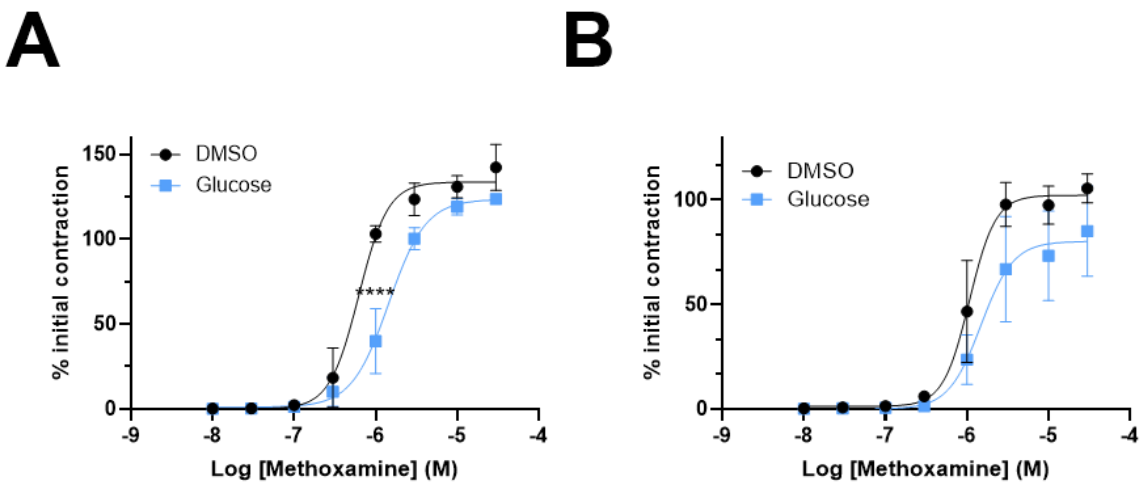


Figure 5.45: The contraction to methoxamine following overnight incubation in hyperglycaemic 20mM glucose PSS in female DM and PE mesenteric arteries.
*A concentration effect curve to methoxamine (10 nM – 30 μM) in mesenteric arteries from DM female (A) and PE female (B) rats incubated overnight in either control PSS (Black, EC_{50} = 622.3 nM and 1.1 μM respectively) or 20 mM glucose PSS (blue, EC_{50} = 1.45 μM and 1.3 μM respectively). All data points are shown as mean +-SEM denoted by error bars, with N=5 and statistical values are determined by 2-way ANOVA with multiple comparisons are calculated using post hoc Dunnets test where *=P<0.05, **=P<0.01, ***=P<0.001, ****=P<0.0001.*

To identify whether the reduction in the concentration-dependent contraction to methoxamine resulted from high glucose or osmolarity, the effect of 20 mM glucose (306 mOSm/ Kg) and 20 mM raffinose (319 mOSm/ Kg) PSS on methoxamine-induced contractions was investigated in mesenteric arteries from female rats. The concentration-dependent contraction to methoxamine was significantly impaired in mesenteric arteries from DM females following 20 mM glucose incubation, with a right shift in the sensitivity to methoxamine from an EC_{50} of 801.1 nM in control PSS arteries to 1.097 μM in glucose incubated arteries (figure 5.46A). PE females also exhibited an impairment in the contraction evoked by methoxamine; however, this was less pronounced than DM female mesenteric arteries (figure 5.46B). Incubating mesenteric arteries from DM and PE female rats in 20 mM raffinose attenuated the concentration-dependent contraction to methoxamine; however, not as strongly as 20 mM glucose. 20mM raffinose incubation in DM female arteries also produced a greater right shift in the methoxamine-effect curve with an EC_{50} of 2.13 μM compared to PE female arteries of 8.05 nM. These findings suggest that

the changes in arterial contractility are due to a combination of glucose activity and osmolarity.

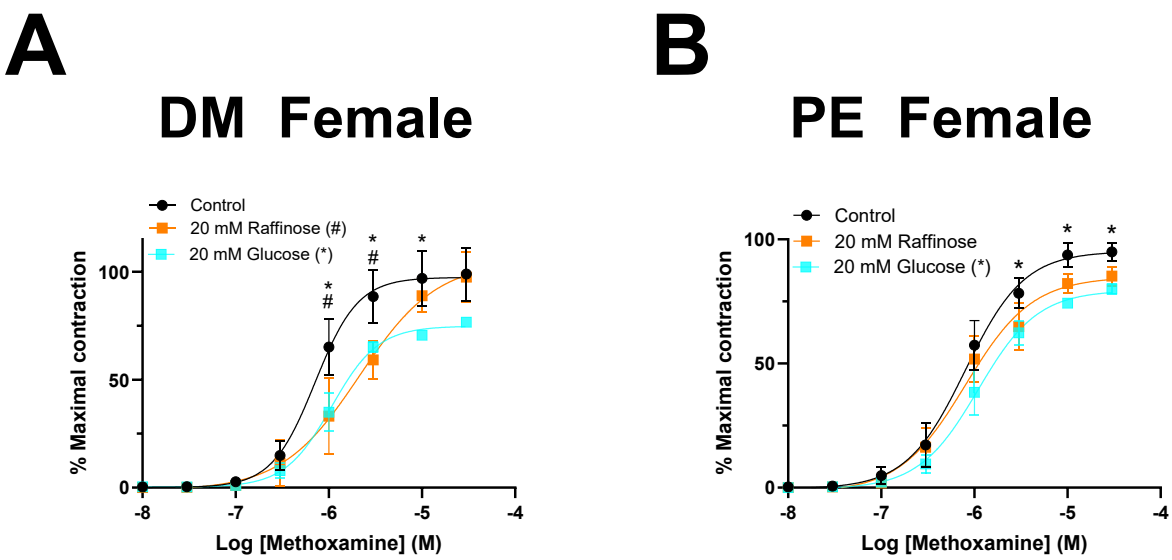


Figure 5.46: The contraction to methoxamine in female mesenteric arteries incubated in 20mM raffinose and 20mM glucose for 4-hours.
*The mean concentration-dependent contraction to methoxamine in mesenteric arteries from DM female (A, N=5) and PE female (B, N=6) rats following a 4-hour incubation in either control PSS (black), 20 mM glucose PSS (blue) and 20 mM raffinose PSS (orange). All data points are shown as mean +-SEM denoted by error bars, and statistical values are determined by 2-way ANOVA with multiple comparisons calculated using the post hoc Bonferroni test where *=P<0.05, **=P<0.01.*

5.4 | Discussion

This study investigated the functional role of SMIT in regulating vascular tone. The current results demonstrated that in arteries from both male and female rats, downregulation of SMIT1 expression through transfection with a SMIT1-targeted morpholino enhanced arterial contractility and a diminished relaxant response to ML213, isoprenaline, and CGRP. Conversely, upregulation of SMIT1 expression via hypertonic raffinose PSS led to reduced arterial contractility and an increased response to vasorelaxant agents independent of the presence of endothelium. After incubation with raffinose, an elevated membrane abundance of SMIT1 was observed in mesenteric and coronary vascular smooth muscle cells (VSMCs) from both male and female rats. Therefore, a clear correlation exists between alterations in SMIT1 expression and the vascular responses to contractile agents, implicating SMIT1 in regulating arterial tone. This regulatory effect of SMIT1 was partially mediated by Kv7.4/5 channels, Gβγ subunits, and SGK1. Inhibitors targeting these proteins attenuated the impairment of U46619-induced contraction observed under conditions of 150 mM raffinose incubation. Furthermore, Kv7.4/5 channels, Gβγ subunits, and SGK1 were found to physically interact with SMIT1 in VSMCs, with these interactions being enhanced in arteries incubated in 150 mM raffinose.

5.4.1 | SMIT1 induces vasorelaxation through activating Kv7.4/5 ion channels mediated by the Gβγ Subunit

Incubation in 150 mM raffinose PSS for 4 hours significantly impaired the contraction induced by lower concentrations of KCl (<60 mM), while contractions induced by higher concentrations of KCl remained unaffected. At these external [K] the membrane potential is effectively clamped at the theoretical equilibrium potential for potassium so no movement of the ion is possible. This is a recognised challenge for isolating a mechanism involving potassium channel opening. These findings are consistent with the results reported by Barrese et al. (2020). The lack of effect on high K contractions also rules out an effect on voltage-dependent calcium channels. These data implicate a role for enhanced potassium channel activity in the anti-contractile effect of raffinose with Kv7 channels being identified. Thus, the Pan-Kv7 blocker XE991 prevented raffinose-induced attenuation of vasoconstrictor responses and alterations in SMIT1 expression modified the

relaxation response to the Kv7 activator ML213. Specifically, mesenteric and coronary arteries exhibited enhanced relaxation in response to ML213 when incubated with 150 mM raffinose PSS. In contrast, arteries transfected with a SMIT1-targeted morpholino showed an attenuated relaxation response to the Kv7 activator. This suggests that increased SMIT1 expression may enhance the activity of Kv7.4/5 ion channels, thereby increasing sensitivity to vasorelaxants. Supporting this hypothesis, incubating with a pan Kv7 channel blocker XE991 prevented the reduction of the U46619 contraction in raffinose-incubated vessels. Additionally, previous electrophysiological studies in Xenopus oocytes (Manville et al., 2017) and CHO cells (Barrese et al., 2020) demonstrated that 150 mM raffinose incubation increased the speed of activation and current amplitude of Kv7.2/3 and Kv7.4/5 ion channels, respectively. Therefore, the absence of SMIT may result in a decreased activation of Kv7.4/5 ion channels, leading to reduced vasorelaxation. Both isoprenaline, CGRP, and adenosine induce vasorelaxation via downstream activation of Kv7 channels (Khanamiri et al. 2013; Chadha et al. 2014; Stott et al. 2018). In this study, the relaxation response to CGRP and isoprenaline was attenuated in mesenteric arteries transfected with a SMIT1-targeted morpholino. This shift was equivalent to that produced by linopirdine (Chadha et al., 2014; Stott et al., 2018). Conversely, adenosine-induced relaxation was enhanced in mesenteric arteries incubated in raffinose PSS. These findings suggest that modulating SMIT1 levels alters the activity of Kv7 ion channels and consequently affects vascular tone.

The interaction between SMIT1 and Kv7 ion channel proteins has been documented in the literature, demonstrating reciprocal regulation of each other’s activity independent of myo-inositol transport. Specifically, SMIT1 interacts with Kv7.2/3 and Kv7.1 ion channels in neurons and the choroid plexus KCNQ (Manville et al., 2017), as well as Kv7.4/5 ion channels in renal and mesenteric arteries (Barrese et al.,2020). The presence of SMIT1 negatively shifts the voltage dependence of these ion channels' currents, thereby enhancing their activity. The current study demonstrates that SMIT1 is localised in close proximity (<40 nm) to both Kv7.4 and Kv7.5 subunits in VSMCs from mesenteric and coronary arteries. Incubating mesenteric and coronary arteries in 150 mM raffinose increased SMIT-Kv7.4/5 interactions in mesenteric and coronary arteries in male, DM female and PE female rats. This increased SMIT1-Kv7.4/5 interaction would lead to enhanced

activity of these channels, resulting in vasorelaxation and the observed impairment of contractions in raffinose-incubated arteries. The total expression of Kv7.4 in mesenteric vascular smooth muscle cells (VSMCs) increased following raffinose incubation. This suggests a potential for enhanced interactions between SMIT1 and Kv7.4/5 channels on the VSMC membrane. However, the total expression of Kv7.4 in coronary VSMCs, as well as the membrane abundance of Kv7.4 in both mesenteric and coronary VSMCs, did not show an increase. Despite the Kv7.4 membrane-to-cytosol ratio remaining constant under both control and raffinose conditions, an overall increase in Kv7.4 protein in mesenteric VSMCs should theoretically result in greater membrane abundance. This observed discrepancy in Kv7.4 staining in mesenteric arteries warrants further investigation. Nonetheless, upregulating SMIT1 membrane expression could enhance the interaction between SMIT1 and the existing Kv7.4/5 channels in the VSMC membrane, thereby augmenting Kv7.4/5 channel activity.

Myo-inositol is a precursor for key signalling phosphoinositides, including phosphatidylinositol 4,5-bisphosphate (PIP_2), which binds to Kv7 channels and positively regulates their gating kinetics and activity. Under hypertonic conditions, the non-selective inhibitor of SMIT function phlorizin and the PI3K inhibitor wortmannin, which depletes PIP_2, both partially prevent the contractile effects of methoxamine produced by raffinose incubation seen in Barrese et al (2020). Additionally, altering SMIT activity regulates neuronal excitability via shifting PIP_2 levels (Dai et al., 2016). Therefore, the anti-contractile effects produced in raffinose-incubated vessels could be due to an elevation in SMIT1 myo-inositol transport and PIP_2 levels, positively upregulating Kv7.4/5 ion channel currents. However, no inositol was present in the external solution during the acute experiment or incubation periods.

Several Kv7 ion channel activity modulators exist, with Gβγ subunits recognised as crucial regulators of Kv7.4 ion channels. Stott et al. (2015) demonstrated that Gβγ and Kv7.4 interact, and Gβγ blocker gallein completely abolished the voltage-dependent activity of Kv7.4 channels. Furthermore, adding Gβγ subunits to HEK-293 cells overexpressing Kv7.4 significantly augmented the Kv7.4 whole-cell current amplitude (Stott et al., 2015). Auxiliary subunits such as the KCNE proteins also modulate Kv7 ion channels. Interestingly, KCNE2 and KCNE4, have been identified in complexes with SMIT in the choroid plexus epithelium, neurones and

renal arteries, respectively. SMIT can bind to heterologously expressed KCNQ1 and KCNQ2, enhancing both ion channel activity and myo-inositol transport. However, the binding of KCNE2 to this complex inhibits SMIT1 activity. Therefore, we hypothesised that SMIT may form a complex with Kv7.4/5 ion channels and Gβγ in vascular smooth muscle cells (VSMCs) to regulate arterial contractility. This study supported this by identifying Gβγ physically interacting with Kv7.4 and SMIT1 in smooth muscle cells from male and female rats arteries. These interactions all increased in VSMCs following a 4-hour incubation in raffinose-enriched PSS. Moreover, applying the Gβγ blocker gallein to raffinose incubated vessels prevented the impairment of U46619 contractions in mesenteric arteries to a similar extent as the Kv7 blocker XE991. As SMIT1 interacts with Gβγ, it is possible that the transporter co-ordinates the G-proteins to alter Kv7.4 activity. Hence, Kv7 ion channel proteins, SMIT and Gβγ could form one large complex to regulate arterial tone. However, more investigation into the underlying mechanism is needed to understand this new phenomenon.

To relate SMIT1 findings to clinical diseases such as diabetes mellitus, the effect of hyperglycaemia was investigated in mesenteric arteries from male and female rats. The expression of SMIT was upregulated in glucose-incubated mesenteric and coronary arteries, whereas the expression of SGLT2 only increased in coronary arteries following 20 mM glucose incubation. Acute overnight incubation of mesenteric arteries with hyperglycaemic 20 mM glucose PSS also impaired the concentration-dependent contraction to methoxamine in male and female rats. These findings align with previous literature that shows acute hyperglycaemia increased vasorelaxation and arterial blood flow in healthy human brachial arteries (Horton et al., 2022; Roberts-Thomson et al., 2022), rat skeletal muscle arterioles (De Clerck et al., 2005, 2006; Massett et al., 2000), rat cerebral arteries (Cipolla et al., 1997; Kam et al., 1993), rabbit coronary arteries (Keef & Ross, 1987) and monkey cerebral arteries (Toda et al., 1992). Several papers have indicated the involvement of BK_{Ca} channels and K_{ATP} channels (De Clerck et al., 2005; Massett et al., 2000) as the BK_{Ca} blocker iberiotoxin and the K_{ATP} blocker glibenclamide significantly reduced the hyperglycaemia-induced vasorelaxations in rats' skeletal arterioles (Massett et al., 2000). These papers suggest that hyperosmolarity evoked changes in calcium mobilisation, resulted in the activation of these potassium ion channels. Our recent findings indicate Kv7 ion channels are involved

in SMIT1-induced relaxations in arteries exposed to a hypertonic medium. This could also occur in arteries following acute hyperglycaemia. However, the role of Kv7 ion channels in hyperglycaemia-evoked relaxation has not been explored, so further research is needed to understand this pathway.

5.4.2 | Oestrus cycle differences in SMIT1-induced relaxations

Baldwin et al (2022 and 2023) identified oestrus cycle differences in Kv7 channel function separate from the sex-dependent differences in arterial contractility. They showed that Kv7 activators were less effective relaxants and membrane expression of Kv7.4 was reduced in high-oestrogen PE female arteries, resulting in pro-contractile vessels. This occurs due to oestrogen activating the membrane receptor GPER1 and preventing Kv7.4 from interacting with the chaperone protein HSP90, altering the forward trafficking of Kv7.4 and reducing its expression in the VSMC membrane. Comparatively, DM females had a high membrane expression of Kv7.4, producing pro-relaxant vessels and the pro-contractile responses seen in PE females could be replicated in DM female arteries upon applying exogenous E2 and the GPER1 agonist (G1). This study showed part of Baldwin et al.,2023 findings showing that PE females had a significantly lower total fluorescence intensity and membrane abundance of Kv7.4 before and after 150 mM raffinose incubation than DM females and males. This difference was also seen for SMIT1, whereby, the expression of SMIT1 in the presence and absence of 150 mM raffinose was considerably lower in smooth muscle cells from mesenteric and coronary arteries from PE female arteries compared to male and DM females, with DM females consistently having the greatest total fluorescence intensity of SMIT1 protein. Moreover, DM females consistently had a greater number of SMIT1 interactions with Kv7.4, Kv7.5 and Gβγ compared to males and PE females, with PE females overall having considerably fewer SMIT1 interactions in the presence and absence of raffinose. The alterations in Kv7.4 and SMIT1 channel expression and protein interactions in PE females may account for the contractile differences in functional experiments. Specifically, after overnight incubation in 150 mM raffinose, the sensitivity of the concentration-dependent contraction to methoxamine in mesenteric arteries from males and DM females but not PE females decreased. Additionally, a 4-hour incubation in 20 mM raffinose

significantly reduced the methoxamine-induced contraction in DM females, but this effect was not observed in PE females. Therefore, SMIT1-induced relaxations depend on Kv7.4 channel function, and there is a clear oestrus cycle difference in the expression and interactions of SMIT1 in DM female and PE female arteries.

5.4.3 | SGK1 regulates SMIT1 expression and functional effect

This study has highlighted that mesenteric arteries subjected to SMIT1-targeted knockdown exhibited a significantly greater contractile response compared to control arteries, and enhancing SMIT1 protein expression by incubating mesenteric and coronary arteries in 150 mM raffinose PSS reduces the contractile response to methoxamine, U46619 and KCl. We hypothesised that the changes in arterial contractility resulted from upregulated SMIT1 protein expression in VSMCs, which was supported by an increase in the total cell staining of SMIT1 in VSMCs incubated in raffinose PSS. The enhanced expression of SMIT1 may be due to the raffinose-mediated activation of the transcription factor TonEBP (tonicity-responsive enhancer binding protein), resulting in increased SMIT1 protein expression (Miyakawa et al., 1999; Rim et al., 1998). However, Miyakawa et al., 1999, showed that activation of TonEBP in response to hypertonicity is slow, with a detectible increase only occurring after approximately 3 hours. In contrast, this study observed that the effect of raffinose on contractility manifested rapidly, even after 10 minutes of incubating in high raffinose PSS. Therefore, other mechanisms could contribute to increased protein abundance of SMIT1, resulting in the observed anticontractile effects. SMIT1 staining in male and female vascular smooth muscle cells (VSMCs) is initially partially cytosolic and granulated. However, after a 4-hour incubation with raffinose, SMIT1 staining decreases in the cytosol and becomes localised around the membrane. This shift suggests increased protein trafficking to the membrane. Protein trafficking can occur rapidly, which may explain changes in arterial contractility observed within 10 to 30 minutes of raffinose incubation. After 4 hours of raffinose incubation, contractile responses to methoxamine and U46619 are abolished. This indicates that the increased membrane abundance of SMIT1 and Kv7.4/5 channel activity may result from SMIT1 trafficking coupled with increased SMIT1 production via TonEBP and reduced degradation. To confirm this, live cell imaging using fluorescently tagged

SMIT1, such as with GFP via time-lapse microscopy or bioluminescence resonance energy transfer (BRET) assays, could study the trafficking of SMIT upon raffinose incubation over a period of 24 hours.

Serum- and glucocorticoid-inducible kinases (SGK) are upregulated by hypertonicity (Waldegger et al., 1997) and are a known post-translational regulator of SMIT1. SGK and SMIT1 are co-expressed in many tissues, including the kidney and brain. Electrophysiological studies in Xenopus oocytes have identified that SMIT1-mediated myo-inositol transport currents are increased when co-expressed with SGK1 due to SMIT stabilising in the membrane, increasing its total membrane abundance (Klaus et al., 2008). This occurs by SGK phosphorylating and deactivating the ubiquitin ligase Nedd4-2, which removed SMIT1 from the cell membrane. There is also speculation that SGK can phosphorylate SMIT1 protein, leading to further SMIT1 membrane expression (Klaus et al., 2008; Schneider, 2015). This present study shows that the anti-contractile effect in raffinose incubated arteries is prevented by XE991, gallein and an SGK inhibitor, EMD638683. Strikingly, SGK1 was also found to closely interact with SMIT in mesenteric and coronary arteries, with the number of interactions increasing upon raffinose incubation. Consequently, the impaired arterial contractility and pro-relaxant arterial state could be caused by upregulated SGK activity upon hypertonicity enhancing SMIT1 protein expression (Klaus et al., 2008) and subsequently increasing SMIT1 interactions with Kv7.4/5 channels. Alternatively, numerous studies have demonstrated that SGK can regulate the membrane protein expression of various ion channels to modulate smooth muscle activity (Boehmer et al., 2003; Debonneville et al., 2001; Henke et al., 2004; Lamothe & Zhang, 2013; Maier et al., 2006; Wang et al., 2004). The human ether-a-go-go-related gene (hERG), which encodes the rapidly activating delayed rectifier potassium channel (I_{Kr}) in myocardial cells and the cardiac voltage-gated Na+ channel SCN5A ($Na_V1.5$) are critical ion channels involved in the cardiac action potential. Similar to its regulation of SMIT, SGK modulates the expression of hERG (Lamothe & Zhang, 2013; Maier et al., 2006) and $Na_V1.5$ (Boehmer et al., 2003) proteins in myocardial cell membranes by deactivating Nedd4-2, thereby preventing the retrograde trafficking of these channels and increasing their membrane abundance. Hence, SGK could also regulate the membrane expression

of Kv7.4/5 ion channel proteins and increase their membrane expression when vessels are exposed to hypertonic conditions.

5.4.4 | Limitations

The results of this chapter were largely obtained from myography isometric tension recordings, proximity ligation assays, and targeted translation morpholino knockdown. All of these experiments have limitations. Raffinose is used throughout this study to create a hypertonic environment in arteries. We have suggested that raffinose increases the protein expression of SMIT; hence, it is an effective model for looking at SMIT-mediated pathways evoking vasodilation as it is not transported between cells. However, by increasing tonicity, many other signalling pathways could be activated, making it very difficult to look at only SMIT-mediated signalling. Myography experiments were also conducted on arteries transfected with SMIT, targeting morpholinos to curtail this limitation. These two approaches did enable the study to examine the vascular effect on arteries with both enhanced SMIT expression and silenced SMIT1 expression.

The methodology for incubating arterial segments in raffinose varied between short-term (10 minutes to 6 hours) and overnight experiments. For the 10 minutes to 6 hours incubation, 150mM raffinose PSS was used in each myograph chamber, bubbled with 95% oxygen and 5% carbon dioxide at 37°C. The effects of various vasocontractile and relaxant agents were then tested on these vessels. For overnight incubation, mesenteric arteries were incubated in tubes containing either 150mM raffinose PSS or control PSS and stored in a humidified incubator with 5% CO2 at 37°C. The following day, these arteries were mounted on a wire myograph to investigate their contraction response to U46619 and methoxamine. This overnight incubation allowed for the study of long-term effects of raffinose on SMIT1 activity and arterial function, as well as responses in the absence of SMIT1 using SMIT1 targeting morpholinos in the same manner. However, these arteries were not normalised and stretched to 90mmHg unlike the experiments completed at 10 minutes – 6 hours. Therefore, the outcomes of overnight experiments cannot be directly compared to the effect of raffinose after 10 minutes – 6 hours.

Another difficulty when identifying the role of SMIT is using pharmacological antagonists such as the Kv7 blocker XE991 to determine the involvement of an ion channel in a vasoactive signalling pathway. This results in a reductionist approach

as it becomes challenging to know whether the change in the concentration-effect curve produced is due to inhibiting Kv7 channels and, therefore, suggesting their involvement or whether Kv7 channel inhibition is altering the activity of other vascular pathways indirectly affecting isometric tone. Future investigations will use electrophysiological patch-clamp recordings where XE991 sensitive Kv7 channel currents can be recorded in native smooth muscle cells (shown by Mackie et al. 2008; Stott et al. 2016) surrounded by hypertonic media (as shown in Barrese et al., 2020). Moreover, whilst negative and positive controls were used for the targeted antibodies chosen in molecular ICC, IHC and PLA experiments, they could have been validated further using transfected and un-transfected CHO/HEK293 cells to prove their specificity.

5.4.5 | Conclusion:

The study described in this chapter sought to identify the effect of hypertonic media on vasoconstrictor and vasorelaxant responses and the role of SMIT in regulating arterial tone. This chapter specifies how SMIT1 interacts with Kv7.4/5 ion channels and Gβγ to regulate arterial contractility in males and females, with these interactions increasing in a hypertonic environment. SGK also interacts with SMIT1, regulating its activity and increasing its protein localisation upon hypertonicity (summery shown in figure 5.49). These findings reveal a novel mechanism of SMIT1 regulating arterial contractility under changes in osmolarity irrespective of sex. This could explain the changes in vascular reactivity seen in several diseases involving hyperosmolarity, such as sepsis and diabetes mellitus.

Summary figure:

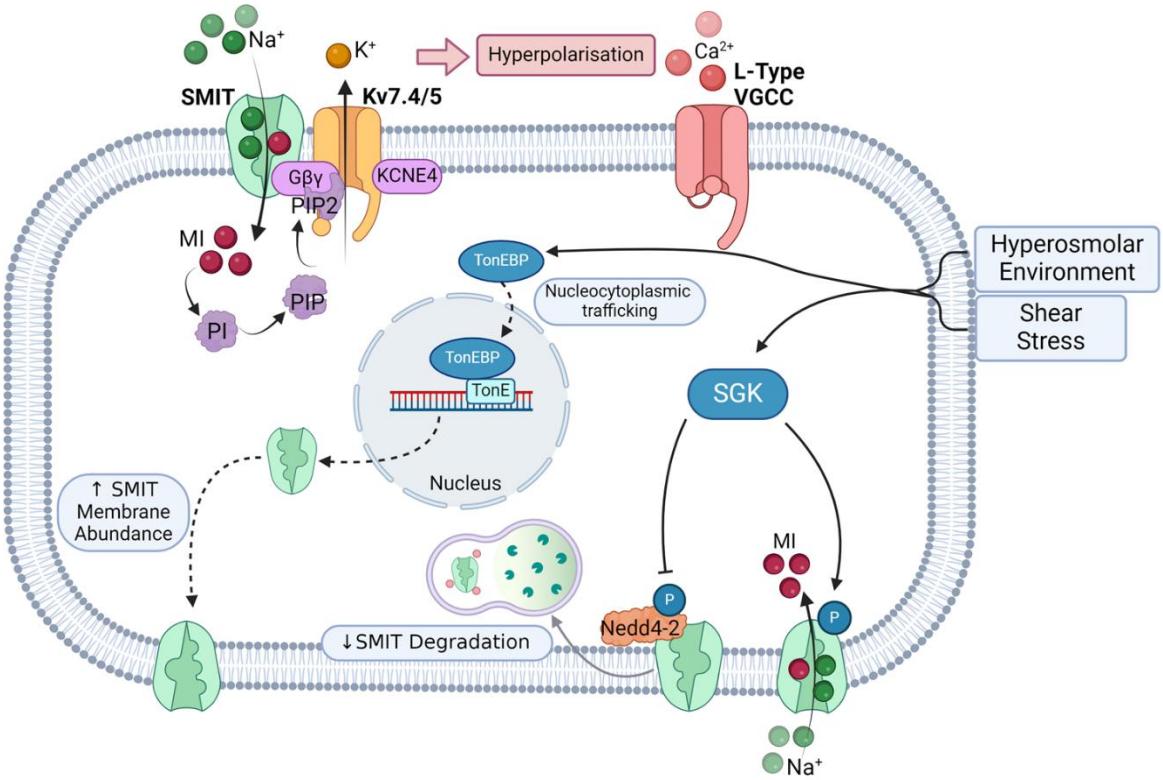


Figure 5.47 –Overview of SMIT1 activity in VSMCs
The tonicity-responsive enhancer binding protein (TonEBP) and serum-glucocorticoid kinase (SGK) sense a rise in extracellular hypertonicity and increase SMIT1 membrane abundance in VSMCs. SMIT1 interacts with Kv7.4/5, Gβγ, and KCNE4, promoting hyperpolarisation, VGCC inactivation, and vasorelaxation. (Source: Author using Biorender.com).

Chapter 6: Discussion

6.1 | Overview

This thesis reports the expression and role of Slc5 transporters in the vasculature. The first results chapter investigated the expression of SGLT1, SGLT2, SMIT1 and SMIT2 (encoded by Slc5a1, Slc5a2, Slc5a3 and Slc5a11) within various arteries. SMIT1 protein expression was found in VSMCs and endothelial cell layers of mesenteric, renal and coronary arteries from male and female rats, whereas SGLT2 protein was only found in the arteries VSMCs, with minimal transcript abundance of SGLT1 and SMIT2. To date, the expression of SGLT2 and SMIT1 in the vasculature has only been investigated in males, with SGLT2 expression identified in human and rat aortic VSMCs (Sukhanov et al., 2021a; Takahashi et al., 2019), rat mesenteric arteries (Hasan, Menon, et al., 2022), human adipose tissue arterioles (De Stefano et al., 2021) and human aortic coronary endothelial cells (Durante et al., 2021; Sukhanov et al., 2021; Takahashi et al., 2019; Uthman et al., 2019). Comparatively, SMIT1 expression in the cardiovascular system has only been found in VSMCs from mesenteric, renal, (Barrese et al., 2020) and aortic arterial segments and endothelial cell layers in male rat aorta (Grandperrin et al., 2024). This study is the first to investigate the expression of Slc5a transporters in arteries from female rats and demonstrate an oestrus cycle difference in SMIT1 expression, whereby the expression of SMIT1 in isolated mesenteric and coronary arteries was greater in DM female rats compared to male and PE female rats. Several limitations with the validity of the SMIT1 and SGLT2 antibodies used were highlighted in this results chapter; therefore, future investigations could include using antigenic peptides corresponding to the SGLT2 and SMIT1 protein regions to assess antibody specificity or further knockdown studies of SMIT1 and SGLT2 expression. Nevertheless, these findings highlight the distribution of Slc5a transporter expression in female arteries, which could contribute to the oestrus cycle differences in vascular physiology.

The second results chapter sought to investigate the mechanism of SGLT2-induced vasorelaxation to decipher how these agents contribute to the

improvement of heart failure and blood pressure outcomes in patients. This study found that SGLT2 inhibitor-induced relaxations were sensitive to Kv7 channel blockade, which corroborated the findings from Hasan et al., 2021, 2022a, and 2022b, however, electrophysiology recordings showed that dapagliflozin and empagliflozin did not directly activate Kv7 channels providing evidence that SGLT2 inhibitors relax arteries via an alternative 'upstream' mediator. Further investigations revealed that SGLT2 inhibitors relaxed mesenteric arteries that were markedly impaired by CGRP blockade, TRPV1 blockade and capsaicin pre-treatment but were ineffective relaxants of renal and septal arteries where there was little to no adventitial staining of TRPV1 and CGRP compared to mesenteric arteries. This led to the hypothesis that SGLT2 inhibitors induced relaxation via releasing CGRP from peptidergic sensory nerves mediated by NHE1 inhibition. This was supported by the NHE1 blocker cariporide relaxing mesenteric arteries and not renal or septal arteries, and pre-application of cariporide or knock-down of NHE1 using targeted morpholino considerably attenuated the relaxations produced by empagliflozin and dapagliflozin. The effect of NHE1 on vascular function has been previously documented. Inhibiting NHE1 decreases mean arterial pressure and reduces medial thickness (Boedtkjer et al., 2012), while activating NHE1 is associated with vasoconstriction and the development of hypertension (Artamonov et al., 2018; Lade et al., 2023). These outcomes are associated with NHE1's influence on TRPV1 activity by shifting cellular pH levels as well as decreasing rho-kinase-dependent VSMC calcium sensitivity. To further support these findings, the shift in pH could be measured via fluorescence dye in the sensory nerves. This would allow the pH change to be correlated with TRPV1 activity and subsequent CGRP release. However, these instruments were not available to us during the course of this study. The involvement of NHE1 in this relaxation pathway could also be validated by investigating SGLT2-induced vasorelaxation in NHE1 knock-out mice. However, conducting these experiments was not plausible due to the scarcity of NHE1 knock-out mice and their limited survival rate of only two weeks, which severely impedes data collection. Nevertheless, this chapter demonstrates that targeting Slc5 transporters can treat cardiovascular diseases. Hence, further research surrounding these transporters could identify new novel pathways to target in hypertensive and heart failure patients.

The final chapter of this thesis advanced our understanding of SMIT1's role in modulating vascular tone. The results show hypertonicity upregulated SMIT1 membrane expression in male and female arteries, reducing arterial contractility and increasing the response to vasorelaxant agents. These findings coincided with an increase in SMIT1 interacting with Kv7.4/5, Gβγ and SGK1 proteins. Inhibitors of these proteins attenuated the impairment of U46619-induced contraction observed under hypertonic conditions of 150 mM raffinose. Meanwhile, downregulation of SMIT1 expression through transfection with a SMIT1-targeted morpholino enhanced arterial contractility and diminished relaxant responses to ML213, isoprenaline, and CGRP. The present results in this chapter support the findings from Barrese et al., 2020, which is, to date, the only paper to investigate the effect of SMIT1 function on arterial contractility in male renal arteries. While this chapter does develop our knowledge of SMIT1 regulation via SGK and how it alters vascular contractility by forming complexes with Kv7.4/5 and Gβγ. The molecular mechanisms underlying these interactions and contractile pathways are still unknown. We hypothesise that SMIT1 forms complexes with Kv7.4/5 and Gβγ to alter Kv7.4 activity coupled with SGK, increasing SMIT1 interaction with ion channel proteins and potentially enhancing Kv7.4/5 channel activity. However, SGK is well-documented to regulate SMIT1 membrane expression by reducing its degradation through the proteasome via phosphorylating Nedd2-4, but upon finding SGK also interacts with SMIT1, it could be directly increasing SMIT1 and Kv7.4/5, channel activity on VSMC membranes too. To validate these findings, Western blot or flow cytometry assays could be employed to examine the required raffinose incubation time for the upregulation of SMIT1 protein and potential SGK1-mediated phosphorylation of SMIT1. Should SMIT1 expression levels remain unchanged within 10 minutes to 2 hours, it may indicate that SGK1 enhances SMIT1 membrane activity at the molecular level, independent of transcriptional upregulation of SMIT1 expression. Moreover, altering SMIT activity has been shown to regulate neuronal excitability via shifting PIP_2 levels (G. Dai et al., 2016) and the PI3K inhibitor wortmannin, which depletes PIP_2, partially prevented the contractile effects of methoxamine produced by raffinose incubation seen in Barrese et al (2020). Eluding that SMIT1 could also alter PIP_2 levels in VSMCs to regulate vascular tone.

Therefore, further research is needed to understand the molecular mechanisms involved in SMIT1-induced relaxations, characterise the interaction of SGK with SMIT1, and determine whether SGK also interacts with Kv7 channels, regulating their function during hypertonicity. Overall, this chapter shows the importance of characterising more transporters in the vasculature to understand their contribution to vascular function and open a new avenue for cardiovascular treatments.

6.2 | Oestrus cycle differences in vascular physiology

Research in males has dominated vascular physiology until recently, when sex and oestrus cycle differences have been at the forefront of research due to differences in cardiovascular disease prevalence. This thesis is the first to critically compare the expression and role of transporters in male and female DM and PE arteries and compare their function in vascular beds. The results from this study show that mesenteric and coronary arteries from PE females have a significantly lower SMIT1 protein expression and membrane abundance compared to DM females and males, with DM females having a greater total expression of SMIT1 than males. These findings correlate with previous literature whereby VSMCs from high-oestrogen PE female arteries had significantly reduced membrane expression of Kv7.4, resulting in pro-contractile vessels compared to DM female arteries (Baldwin et al., 2023). Moreover, under hypertonic conditions, the expression of SMIT1 and the number of SMIT1 interactions with Kv7.4, Kv7.5, and Gβγ were considerably lower in smooth muscle cells from mesenteric and coronary arteries from PE female arteries compared to male and DM females, with DM females consistently having the greatest number of SMIT1 interactions with Kv7.4, Kv7.5, and Gβγ compared to males and PE females. This expression data coincides with the pro-relaxant effect of SMIT1 impacting DM female and male arteries to a greater extent than PE female arteries. Hence, alterations in SMIT1 activity could be contributing to the sex-dependent differences in vascular contractility. Knock-down of SMIT1 in mesenteric and coronary arteries as well as renal arteries (Barrese et al., 2020) increases vasoconstriction and reduces the relaxation response to Kv7 activator ML213. These characteristics, as well as a downregulation of Kv7.4 channel expression and activity, were seen in the arteries of hypertensive animals (Jepps et al., 2011; Stott et al., 2015). Therefore, the alterations in SMIT1 and SGK may also underlie the decrease in Kv7 channel

expression and function overall leading to vascular complications seen in cardiovascular disease. A series of experiments investigating the role of SMIT1 in male and female spontaneously hypertensive rats (SHR) would confirm their role in vascular disease.

Current research indicates that the expression of SGLT1 and SGLT2 in the renal proximal tubule is higher in female animals than in males (Sabolić et al., 2012), however, there has been no comparison of Slc5 transporter expression across different stages of the oestrus cycle. Preliminary data gathered in this thesis demonstrate that SGLT2-inhibitors relax both PE and DM female mesenteric arteries, with PE females producing lower relaxation than DM females. Therefore, this gives plausible reasoning for continuing to research female vascular physiology as well as males to explore potential sex-dependent treatments for cardiovascular disease.

6.3 | Conclusion

This thesis has demonstrated that SLC5a transporters are expressed in male and female arteries and play a pivotal role in regulating vascular tone. This research highlights the benefits of targeting SMIT1 transporters in cardiovascular disease and the mechanism by which SGLT2 inhibitors induce relaxation in mesenteric arteries through CGRP release.

Chapter 7: Bibliography

Aalkjaer, C., Nilsson, H., & De Mey, JGR. (2021). Sympathetic and sensory-motor nerves in peripheral small arteries. *Physiological Reviews*, *101*(2), 495–544. https://doi.org/10.1152/PHYSREV.00007.2020

Aaronson, PI., & Smirnov, SV. (1996). Membrane ion channels in vascular smooth muscle excitation-contraction coupling. *The Pharmacology of Vascular Smooth Muscle*. https://doi.org/10.1093/ACPROF:OSO/9780192623874.003.0006

Abbott, GW., Tai, KK., Neverisky, DL., Hansler, A., Hu, Z., Roepke, TK., Lerner, DJ., Chen, Q., Liu, L., Zupan, B., Toth, M., Haynes, R., Huang, X., Demirbas, D., Buccafusca, R., Gross, SS., Kanda, V., & Berry, GT. (2014). KCNQ1, KCNE2, and Na+-Coupled Solute Transporters Form Reciprocally Regulating Complexes that Affect Neuronal Excitability. *Science signaling*, *7*(315), ra22. https://doi.org/10.1126/SCISIGNAL.2005025

Abramson, J., & Wright, EM. (2009). Structure and Function of Na+-Symporters with Inverted Repeats. *Current opinion in structural biology*, *19*(4), 425. https://doi.org/10.1016/J.SBI.2009.06.002

Agard, C., Rolli-Derkinderen, M., Dumas-de-La-Roque, E., Rio, M., Sagan, C., Savineau, J. P., Loirand, G., & Pacaud, P. (2009). Protective role of the antidiabetic drug metformin against chronic experimental pulmonary hypertension. *British Journal of Pharmacology*, *158*(5), 1285. https://doi.org/10.1111/J.1476-5381.2009.00445.X

Aickin, CC., & Vermuë, NA. (1983). Microelectrode measurement of intracellular chloride activity in smooth muscle cells of guinea-pig ureter. *Pflugers Archiv : European journal of physiology*, *397*(1), 25–28. https://doi.org/10.1007/BF00585163

Ajayi, AF., & Akhigbe, RE. (2020). Staging of the estrous cycle and induction of estrus in experimental rodents: an update. *Fertility Research and Practice*, *6*(1). https://doi.org/10.1186/S40738-020-00074-3

Alice Marino, A., Cumps, J., Guilbert, L., Baufays, C., Ginion, A., Ferté, L., Battault, S., Ambroise, J., Bearzatto, B., Zuurbier, C. J., Lezoualch, F., Pestiaux, C., Pyka, G., Kerckhofs, G., Tyteca, D., Bouzin, C., Bertrand, L., Horman, S., & Beauloye, C. (2023). Sodium myo-inositol cotransporter-1, SMIT1, promotes cardiac hypertrophy and fibrosis in pressure overloaded mouse hearts. *bioRxiv*, 2023.10.25.564086. https://doi.org/10.1101/2023.10.25.564086

Alonso-Carbajo, L., Kecskes, M., Jacobs, G., Pironet, A., Syam, N., Talavera, K., & Vennekens, R. (2017). Muscling in on TRP channels in vascular smooth muscle cells and cardiomyocytes. *Cell Calcium*, *66*, 48–61. https://doi.org/10.1016/J.CECA.2017.06.004

Anderson, PAW. (1996). The heart and development. *Seminars in Perinatology*, *20*(6), 482–509. https://doi.org/10.1016/S0146-0005(96)80064-4

Artamonov, MV., Sonkusare, SK., Good, ME., Momotani, K., Eto, M., Isakson, BE., Le, TH., Cope, EL., Derewenda, ZS., Derewenda, U., & Somlyo, AV. (2018). RSK2 contributes to myogenic vasoconstriction of resistance arteries by activating smooth muscle myosin and the Na+/H+ exchanger. *Science signaling*, *11*(554). https://doi.org/10.1126/SCISIGNAL.AAR3924

Artasensi, A., Pedretti, A., Vistoli, G., & Fumagalli, L. (2020). Type 2 Diabetes Mellitus: A Review of Multi-Target Drugs. *Molecules*, *25*(8). https://doi.org/10.3390/MOLECULES25081987

Aryan, L., Younessi, D., Zargari, M., Banerjee, S., Agopian, J., Rahman, S., Borna, R., Ruffenach, G., Umar, S., & Eghbali, M. (2020). The Role of Estrogen Receptors in Cardiovascular Disease. *International journal of molecular sciences*, *21*(12), 1–26. https://doi.org/10.3390/IJMS21124314

Askew Page, HR., Dalsgaard, T., Baldwin, SN., Jepps, TA., Povstyan, O., Olesen, SP., & Greenwood, IA. (2019). TMEM16A is implicated in the regulation of coronary flow and is altered in hypertension. *British Journal of Pharmacology*, *176*(11), 1635. https://doi.org/10.1111/BPH.14598

Baldwin, SN., Forrester, EA., Homer, NZM., Andrew, R., Barrese, V., Stott, JB., Isakson, BE., Albert, AP., & Greenwood, IA. (2023). Marked oestrous cycle-dependent regulation of rat arterial KV7.4 channels driven by GPER1. *British Journal of Pharmacology*, *180*(2), 174. https://doi.org/10.1111/BPH.15947

Baldwin, SN., Forrester, EA., McEwan, L., & Greenwood, IA. (2022). Sexual dimorphism in prostacyclin-mimetic responses within rat mesenteric arteries: A novel role for K V 7.1 in shaping IP receptor-mediated relaxation. *British journal of pharmacology*, *179*(7), 1338–1352. https://doi.org/10.1111/BPH.15722

Baldwin, SN., Jepps, TA., & Greenwood, IA. (2023). Cycling matters: Sex hormone regulation of vascular potassium channels. *Channels*, *17*(1). https://doi.org/10.1080/19336950.2023.2217637

Baldwin, SN., Sandow, SL., Mondéjar-Parreño, G., Stott, JB., & Greenwood, IA. (2020). KV7 Channel Expression and Function Within Rat Mesenteric Endothelial Cells. *Frontiers in Physiology*, *11*. https://doi.org/10.3389/FPHYS.2020.598779/FULL

Balen, D., Ljubojević, M., Breljak, D., Brzica, H., Žlender, V., Koepsell, H., & Sabolić, I. (2008). Revised immunolocalization of the Na+-D-glucose cotransporter SGLT1 in rat organs with an improved antibody. *American Journal of Physiology - Cell Physiology*, *295*(2). https://doi.org/10.1152/AJPCELL.00180.2008

Barata, R., Fila, M., Dalla-Vale, F., Bogarin, R., Nunes, P., Ramalho, J., Rueff, J., & Calado, J. (2023). Performance of the ACMG-AMP criteria in a large familial renal glucosuria cohort with identified SLC5A2 sequence variants. *Clinical genetics*, *104*(5), 582–586. https://doi.org/10.1111/CGE.14395

Barrese, V., Stott, JB., Baldwin, SN., Mondejar-Parreño, G., & Greenwood, IA. (2020). SMIT (Sodium-Myo-Inositol Transporter) 1 regulates arterial contractility through the modulation of vascular Kv7 Channels. *Arteriosclerosis, Thrombosis, and Vascular Biology*, *40*, 2468–2480. https://doi.org/10.1161/ATVBAHA.120.315096

Barrese, V., Stott, JB., & Greenwood, IA. (2018). KCNQ-Encoded Potassium Channels as Therapeutic Targets. I: *Annual Review of Pharmacology and*

Toxicology (Bd. 58, s. 625–648). Annual Reviews Inc. https://doi.org/10.1146/annurev-pharmtox-010617-052912

Beal, B., Schutte, AE., & Neuen, BL. (2023). Blood Pressure Effects of SGLT2 Inhibitors: Mechanisms and Clinical Evidence in Different Populations. *Current Hypertension Reports*, *25*(12), 429–435. https://doi.org/10.1007/S11906-023-01281-1/FIGURES/2

Beaney, KE., Smith, AJP., Folkersen, L., Palmen, J., Wannamethee, SG., Jefferis, BJ., Whincup, P., Gaunt, TR., Casas, JP., Ben-Shlomo, Y., Price, JF., Kumari, M., Wong, A., Ong, K., Hardy, R., Kuh, D., Wareham, N., Kivimaki, M., Eriksson, P., & Humphries, SE. (2017). Functional Analysis of the Coronary Heart Disease Risk Locus on Chromosome 21q22. *Disease Markers*, *2017*. https://doi.org/10.1155/2017/1096916

Berry, GT., Mallee, JJ., Kwon, HM., Rim, JS., Mulla, WR., Muenke, M., & Spinner, NB. (1995). The human osmoregulatory Na+/myo-inositol cotransporter gene (SLC5A3): molecular cloning and localization to chromosome 21. *Genomics*, *25*(2), 507–513. https://doi.org/10.1016/0888-7543(95)80052-N

Betrie, AH., Brock, JA., Harraz, OF., Bush, AI., He, GW., Nelson, MT., Angus, JA., Wright, CE., & Ayton, S. (2021). Zinc drives vasorelaxation by acting in sensory nerves, endothelium and smooth muscle. *Nature Communications*, *12*(1). https://doi.org/10.1038/S41467-021-23198-6

Bissonnette, P., Coady, MJ., & Lapointe, JY. (2004). Expression of the sodium–myo-inositol cotransporter SMIT2 at the apical membrane of Madin-Darby canine kidney cells. *The Journal of Physiology*, *558*(Pt 3), 759. https://doi.org/10.1113/JPHYSIOL.2004.064311

Boedtkjer, E., Damkier, HH., & Aalkjaer, C. (2012). NHE1 knockout reduces blood pressure and arterial media/lumen ratio with no effect on resting pHi in the vascular wall. *The Journal of Physiology*, *590*(Pt 8), 1895. https://doi.org/10.1113/JPHYSIOL.2011.227132

Boedtkjer, E., Praetorius, J., Matchkov, VV., Stankevicius, E., Mogensen, S., Füchtbauer, AC., Simonsen, U., Füchtbauer, EM., & Aalkjaer, C. (2011). Disruption of Na+,HCO_3^- cotransporter NBCn1 (slc4a7) inhibits NO-mediated vasorelaxation, smooth muscle Ca^{2+} sensitivity, and hypertension

development in mice. *Circulation*, *124*(17), 1819–1829. https://doi.org/10.1161/CIRCULATIONAHA.110.015974

Boehmer, C., Wilhelm, V., Palmada, M., Wallisch, S., Henke, G., Brinkmeier, H., Cohen, P., Pieske, B., & Lang, F. (2003). Serum and glucocorticoid inducible kinases in the regulation of the cardiac sodium channel SCN5A. *Cardiovascular Research*, *57*(4), 1079–1084. https://doi.org/10.1016/S0008-6363(02)00837-4/2/57-4-1079-FIG6.GIF

Bonner, C., Kerr-Conte, J., Gmyr, V., Queniat, G., Moerman, E., Thévenet, J., Beaucamps, C., Delalleau, N., Popescu, I., Malaisse, WJ., Sener, A., Deprez, B., Abderrahmani, A., Staels, B., & Pattou, F. (2015). Inhibition of the glucose transporter SGLT2 with dapagliflozin in pancreatic alpha cells triggers glucagon secretion. *Nature medicine*, *21*(5), 512–517. https://doi.org/10.1038/NM.3828

Bosch, A., Ott, C., Jung, S., Striepe, K., Karg, MV., Kannenkeril, D., Dienemann, T., & Schmieder, RE. (2019). How does empagliflozin improve arterial stiffness in patients with type 2 diabetes mellitus? Sub analysis of a clinical trial. *Cardiovascular Diabetology*, *18*(1), 1–12. https://doi.org/10.1186/S12933-019-0839-8/TABLES/7

Bradley, KK., Jaggar, JH., Bonev, AD., Heppner, TJ., Flynn, ERM., Nelson, M. T., & Horowitz, B. (1999). Kir2.1 encodes the inward rectifier potassium channel in rat arterial smooth muscle cells. *The Journal of physiology*, *515 (Pt 3)*(Pt 3), 639–651. https://doi.org/10.1111/J.1469-7793.1999.639AB.X

Bradshaw, HB., Raboune, S., & Hollis, JL. (2013). Opportunistic activation of TRP receptors by endogenous lipids: Exploiting lipidomics to understand TRP receptor cellular communication. *Life Sciences*, *92*(8–9), 404–409. https://doi.org/10.1016/J.LFS.2012.11.008

Brain, SD., Williams, TJ., Tippins, JR., Morris, HR., & MacIntyre, I. (1985). Calcitonin gene-related peptide is a potent vasodilator. *Nature 1985 313:5997*, *313*(5997), 54–56. https://doi.org/10.1038/313054a0

Brenner, R., Peréz, GJ., Bonev, AD., Eckman, DM., Kosek, JC., Wiler, SW., Patterson, AJ., Nelson, MT., & Aldrich, RW. (2000). Vasoregulation by the β1

subunit of the calcium-activated potassium channel. *Nature 2000 407:6806*, *407*(6806), 870–876. https://doi.org/10.1038/35038011

Brozovich, FV., Nicholson, CJ., Degen, CV., Gao, YZ., Aggarwal, M., & Morgan, K. G. (2016). Mechanisms of Vascular Smooth Muscle Contraction and the Basis for Pharmacologic Treatment of Smooth Muscle Disorders. *Pharmacological Reviews*, *68*(2), 476. https://doi.org/10.1124/PR.115.010652

Brueggemann, LI., Haick, JM., Cribbs, LL., & Byron, KL. (2014). Differential activation of vascular smooth muscle Kv7.4, Kv7.5, and Kv7.4/7.5 channels by ML213 and ICA-069673. *Molecular Pharmacology*, *86*(3), 330–341. https://doi.org/10.1124/MOL.114.093799/-/DC1

Byrne, NG., & Large, WA. (1987). Action of noradrenaline on single smooth muscle cells freshly dispersed from the rat anococcygeus muscle. *The Journal of physiology*, *389*(1), 513–525. https://doi.org/10.1113/JPHYSIOL.1987.SP016669

Baartscheer, A., Schumacher, CA., Wüst, RCI., Fiolet, JWT., Stienen, GJM., Coronel, R., & Zuurbier, CJ. (2017). Empagliflozin decreases myocardial cytoplasmic Na+ through inhibition of the cardiac Na+/H+ exchanger in rats and rabbits. *Diabetologia*, *60*(3), 568. https://doi.org/10.1007/S00125-016-4134-X

Calado, J., Soto, K., Clemente, C., Correia, P., & Rueff, J. (2004). Novel compound heterozygous mutations in SLC5A2 are responsible for autosomal recessive renal glucosuria. *Human genetics*, *114*(3), 314–316. https://doi.org/10.1007/S00439-003-1054-X

Carbó, R., & Rodríguez, E. (2023). Relevance of Sugar Transport across the Cell Membrane. *International Journal of Molecular Sciences 2023, Vol. 24, Page 6085*, *24*(7), 6085. https://doi.org/10.3390/IJMS24076085

Carlson, LJ., & Shaw, ND. (2019). Development of Ovulatory Menstrual Cycles in Adolescent Girls. *Journal of pediatric and adolescent gynecology*, *32*(3), 249–253. https://doi.org/10.1016/J.JPAG.2019.02.119

Carlton-Carew, SRE., Greenberg, HZE., Greenwood, IA., & Albert, AP. (2024). Stimulation of the calcium-sensing receptor induces relaxations through

CGRP and NK1 receptor-mediated pathways in male rat mesenteric arteries. *Physiological Reports*, *12*(12), 16125. https://doi.org/10.14814/PHY2.16125

Carvajal, K., Zarrinpashneh, E., Szarszoi, O., Joubert, F., Athea, Y., Mateo, P., Gillet, B., Vaulont, S., Viollet, B., Bigard, X., Bertrand, L., Ventura-Clapier, R., & Hoerter, JA. (2007). Dual cardiac contractile effects of the α2-AMPK deletion in low-flow ischemia and reperfusion. *American Journal of Physiology - Heart and Circulatory Physiology*, *292*(6), 3136–3147.

Celentano, C., Carotenuto, L., Miceli, F., Carleo, G., Corrado, B., Baroli, G., Iervolino, S., Vecchione, R., Taglialatela, M., & Barrese, V. (2024). Kv7 channel activation reduces brain endothelial cell permeability and prevents kainic acid-induced blood-brain barrier damage. American Journal of Physiology-Cell Physiology, 326(3), C893–C904. https://doi.org/10.1152/ajpcell.00709.2023

Cha, B., & Donowitz, M. (2008). The epithelial brush border Na+/H+ exchanger NHE3 associates with the actin cytoskeleton by binding to ezrin directly and via PDZ domain-containing Na+/H+ exchanger regulatory factor (NHERF) proteins. *Clinical and experimental pharmacology & physiology*, *35*(8), 863–871. https://doi.org/10.1111/J.1440-1681.2008.04931.X

Chadha, PS., Jepps, TA., Carr, G., Stott, JB., Zhu, HL., Cole, WC., & Greenwood, IA. (2014). Contribution of kv7.4/kv7.5 heteromers to intrinsic and calcitonin gene-related peptide-induced cerebral reactivity. *Arteriosclerosis, thrombosis, and vascular biology*, *34*(4), 887–893. https://doi.org/10.1161/ATVBAHA.114.303405

Chadha, PS., Zunke, F., Zhu, HL., Davis, AJ., Jepps, TA., Olesen, SP., Cole, WC., Moffatt, JD., & Greenwood, IA. (2012). Reduced KCNQ4-encoded voltage-dependent potassium channel activity underlies impaired β-adrenoceptor-mediated relaxation of renal arteries in hypertension. *Hypertension*, *59*(4), 877–884. https://doi.org/10.1161/HYPERTENSIONAHA.111.187427

Chang, AN., Kamm, KE., & Stull, J. T. (2016). Role of myosin light chain phosphatase in cardiac physiology and pathophysiology. *Journal of molecular and cellular cardiology*, *101*, 35. https://doi.org/10.1016/J.YJMCC.2016.10.004

Chen, J., Williams, S., Ho, S., Loraine, H., Hagan, D., Whaley, JM., & Feder, J. N. (2010). Quantitative PCR tissue expression profiling of the human SGLT2 gene and related family members. *Diabetes Therapy*, *1*(2), 57. https://doi.org/10.1007/S13300-010-0006-4

Chen, X., Li, W., Hiett, S. C., & Obukhov, A. G. (2016). Novel Roles for Kv7 Channels in Shaping Histamine-Induced Contractions and Bradykinin-Dependent Relaxations in Pig Coronary Arteries. PLOS ONE, 11(2), e0148569. https://doi.org/10.1371/journal.pone.0148569

Chiba, Y., Sugiyama, Y., Nishi, N., Nonaka, W., Murakami, R., & Ueno, M. (2020). Sodium/glucose cotransporter 2 is expressed in choroid plexus epithelial cells and ependymal cells in human and mouse brains. *Neuropathology : Official journal of the Japanese Society of Neuropathology*, *40*(5), 482–491. https://doi.org/10.1111/NEUP.12665

Choi, S., Haam, CE., Byeon, S., Oh, EY., Choi, SK., & Lee, YH. (2023). Investigating the Cardiovascular Benefits of Dapagliflozin: Vasodilatory Effect on Isolated Rat Coronary Arteries. *International Journal of Molecular Sciences*, *24*(23). https://doi.org/10.3390/IJMS242316873

Chrissobolis, S., & Sobey, CG. (2002). Inhibitory effects of protein kinase C on inwardly rectifying K+- and ATP-sensitive K+ channel-mediated responses of the basilar artery. *Stroke*, *33*(6), 1692–1697. https://doi.org/10.1161/01.STR.0000016966.89226.67

Chung, CC., Lin, YK., Chen, YC., Kao, YH., Yeh, YH., Trang, NN., & Chen, YJ. (2023). Empagliflozin suppressed cardiac fibrogenesis through sodium-hydrogen exchanger inhibition and modulation of the calcium homeostasis. *Cardiovascular Diabetology*, *22*(1), 27. https://doi.org/10.1186/S12933-023-01756-0

Cipolla, MJ., Porter, JM., & Osol, G. (1997). High glucose concentrations dilate cerebral arteries and diminish myogenic tone through an endothelial mechanism. *Stroke*, *28*(2), 405–411. https://doi.org/10.1161/01.STR.28.2.405

Claire, C., & Brading, AF. (1982). MEASUREMENT OF INTRACELLULAR CHLORIDE IN GUINEA-PIG VAS DEFERENS BY ION ANALYSIS,

36CHLORIDE EFFLUX AND MICRO-ELECTRODES. *J. Physiol*, *326*, 139–154.

Clay, JR. (2009). Determining K+ Channel Activation Curves from K+ Channel Currents Often Requires the Goldman–Hodgkin–Katz Equation. *Frontiers in Cellular Neuroscience*, *3*(DEC). https://doi.org/10.3389/NEURO.03.020.2009

Coady, MJ., El Tarazi, A., Santer, R., Bissonnette, P., Sasseville, LJ., Calado, J., Lussier, Y., Dumayne, C., Bichet, DG., & Lapointe, JY. (2017). MAP17 Is a Necessary Activator of Renal Na+/Glucose Cotransporter SGLT2. *Journal of the American Society of Nephrology : JASN*, *28*(1), 85. https://doi.org/10.1681/ASN.2015111282

Coady, MJ., Wallendorff, B., Gagnon, DG., & Lapointe, JY. (2002). Identification of a novel Na+/myo-inositol cotransporter. *Journal of Biological Chemistry*, *277*(38), 35219–35224. https://doi.org/10.1074/jbc.M204321200

Cole, WC., & Clément-Chomienne, O. (2003). ATP-sensitive K+ channels of vascular smooth muscle cells. *Journal of cardiovascular electrophysiology*, *14*(1), 94–103. https://doi.org/10.1046/J.1540-8167.2003.02376.X

Cole, WC., Malcolm, T., Walsh, MP., & Light, PE. (2000). Inhibition by protein kinase C of the K(NDP) subtype of vascular smooth muscle ATP-sensitive potassium channel. *Circulation research*, *87*(2), 112–117. https://doi.org/10.1161/01.RES.87.2.112

Cole, WC., & Welsh, DG. (2011). Role of myosin light chain kinase and myosin light chain phosphatase in the resistance arterial myogenic response to intravascular pressure. *Archives of Biochemistry and Biophysics*, *510*(2), 160–173. https://doi.org/10.1016/J.ABB.2011.02.024

Connelly, PJ., Casey, H., Montezano, AC., Touyz, RM., & Delles, C. (2021). Sex steroids receptors, hypertension, and vascular ageing. *Journal of Human Hypertension 2021 36:2*, *36*(2), 120–125. https://doi.org/10.1038/s41371-021-00576-7

Cora, MC., Kooistra, L., & Travlos, G. (2015). Vaginal Cytology of the Laboratory Rat and Mouse:Review and Criteria for the Staging of the Estrous Cycle Using

Stained Vaginal Smears. *Toxicologic Pathology*, *43*(6), 776–793. https://doi.org/10.1177/0192623315570339

Cox, RH. (2005). Molecular determinants of voltage-gated potassium currents in vascular smooth muscle. *Cell Biochemistry and Biophysics*, *42*(2), 167–195. https://doi.org/10.1385/CBB:42:2:167/METRICS

Dai, G., Yu, H., Kruse, M., Traynor-Kaplan, A., & Hille, B. (2016). Osmoregulatory inositol transporter SMIT1 modulates electrical activity by adjusting PI(4,5)P2 levels. *Proceedings of the National Academy of Sciences of the United States of America*, *113*(23), E3290–E3299. https://doi.org/10.1073/PNAS.1606348113/-/DCSUPPLEMENTAL

Dai, Z., Chung, SK., Miao, D., Lau, KS., Chan, AWH., & Kung, AWC. (2011). Sodium/myo-inositol cotransporter 1 and myo-inositol are essential for osteogenesis and bone formation. *Journal of Bone and Mineral Research*, *26*(3), 582–590. https://doi.org/10.1002/JBMR.240

Davies, MJ., Aroda, VR., Collins, BS., Gabbay, RA., Green, J., Maruthur, NM., Rosas, SE., Del Prato, S., Mathieu, C., Mingrone, G., Rossing, P., Tankova, T., Tsapas, A., & Buse, JB. (2022). Management of Hyperglycemia in Type 2 Diabetes, 2022. A Consensus Report by the American Diabetes Association (ADA) and the European Association for the Study of Diabetes (EASD). *Diabetes Care*, *45*(11), 2753–2786. https://doi.org/10.2337/DCI22-0034

De Clerck, I., Guyssens, B., Pannier, JL., & Van De Voorde, J. (2005). Hyperosmolarity causes BKCa-dependent vasodilatations in rat skeletal muscle arteries. *Medicine and Science in Sports and Exercise*, *37*(10), 1697–1703. https://doi.org/10.1249/01.MSS.0000176446.13607.B0

De Clerck, I., Pannier, JL., & Van de Voorde, J. (2006). K+ potentiates hyperosmolarity-induced vasorelaxations in rat skeletal muscle arterioles. *European Journal of Applied Physiology*, *96*(6), 679–685. https://doi.org/10.1007/S00421-005-0128-Y/FIGURES/4

de Jong, IEM., & Jepps, TA. (2018). Impaired Kv7 channel function in cerebral arteries of a tauopathy mouse model (rTg4510). *Physiological Reports*, *6*(23). https://doi.org/10.14814/PHY2.13920

De Stefano, A., Tesauro, M., Di Daniele, N., Vizioli, G., Schinzari, F., & Cardillo, C. (2021). Mechanisms of SGLT2 (Sodium-Glucose Transporter Type 2) Inhibition-Induced Relaxation in Arteries From Human Visceral Adipose Tissue. *Hypertension*, *77*(2), 729–738. https://doi.org/10.1161/HYPERTENSIONAHA.120.16466

Debonneville, C., Flores, SY., Kamynina, E., Plant, PJ., Tauxe, C., Thomas, MA., Münster, C., Chraïbi, A., Pratt, JH., Horisberger, JD., Pearce, D., Loffing, J., & Staub, O. (2001). Phosphorylation of Nedd4-2 by Sgk1 regulates epithelial Na(+) channel cell surface expression. *The EMBO journal*, *20*(24), 7052–7059. https://doi.org/10.1093/EMBOJ/20.24.7052

Dieter, M., Palmada, M., Rajamanickam, J., Aydin, A., Busjahn, A., Boehmer, C., Luft, FC., & Lang, F. (2004). Regulation of Glucose Transporter SGLT1 by Ubiquitin Ligase Nedd4-2 and Kinases SGK1, SGK3, and PKB. *Obesity Research*, *12*(5), 862–870. https://doi.org/10.1038/OBY.2004.104

Dora, KA., Gallagher, NT., McNeish, A., & Garland, CJ. (2008). Modulation of endothelial cell KCa3.1 channels during endothelium-derived hyperpolarizing factor signaling in mesenteric resistance arteries. *Circulation Research*, *102*(10), 1247–1255. https://doi.org/10.1161/CIRCRESAHA.108.172379/SUPPL_FILE/ZHH172379-SUPPL-3.MOV

Du, J., Gu, J., Deng, J., Kong, L., Guo, Y., Jin, C., Bao, Y., Fu, D., & Li, J. (2022). The expression and survival significance of sodium glucose transporters in pancreatic cancer. *BMC cancer*, *22*(1). https://doi.org/10.1186/S12885-021-09060-4

Durante, W., Behnammanesh, G., & Peyton, KJ. (2021). Effects of Sodium-Glucose Co-Transporter 2 Inhibitors on Vascular Cell Function and Arterial Remodeling. *International Journal of Molecular Sciences*, *22*(16). https://doi.org/10.3390/IJMS22168786

Dutka, M., Bobiński, R., Francuz, T., Garczorz, W., Zimmer, K., Ilczak, T., Ćwiertnia, M., & Hajduga, MB. (2022). SGLT-2 Inhibitors in Cancer Treatment-Mechanisms of Action and Emerging New Perspectives. *Cancers*, *14*(23). https://doi.org/10.3390/CANCERS14235811

Elfeber, K., Köhler, A., Lutzenburg, M., Osswald, C., Galla, HJ., Witte, OW., & Koepsell, H. (2004). Localization of the Na+-D-glucose cotransporter SGLT1 in the blood-brain barrier. *Histochemistry and cell biology*, *121*(3), 201–207. https://doi.org/10.1007/S00418-004-0633-9

Ellershaw, DC., Greenwood, IA., & Large, WA. (2000). Dual modulation of swelling-activated chloride current by NO and NO donors in rabbit portal vein myocytes. *The Journal of Physiology*, *528*(Pt 1), 15. https://doi.org/10.1111/J.1469-7793.2000.00015.X

Enyedi, P., & Czirják, G. (2010). Molecular background of leak K+ currents: two-pore domain potassium channels. *Physiological reviews*, *90*(2), 559–605. https://doi.org/10.1152/PHYSREV.00029.2009

Fang, S., Wu, J., Reho, JJ., Lu, KT., Brozoski, DT., Kumar, G., Werthman, AM., Silva, SD., Veitia, PCM., Wackman, KK., Mathison, AJ., Teng, BQ., Lin, CW., Quelle, FW., & Sigmund, CD. (2022). RhoBTB1 reverses established arterial stiffness in angiotensin II-induced hypertension by promoting actin depolymerization. *JCI insight*, *7*(9). https://doi.org/10.1172/JCI.INSIGHT.158043

Fei, YJ., Kanai, Y., Nussberger, S., Ganapathy, V., Leibach, FH., Romero, MF., Singh, SK., Boron, WF., & Hediger, MA. (1994). Expression cloning of a mammalian proton-coupled oligopeptide transporter. *Nature*, *368*(6471), 563–566. https://doi.org/10.1038/368563A0

Fleming, I. (2010). Molecular mechanisms underlying the activation of eNOS. *Pflugers Archiv European Journal of Physiology*, *459*(6), 793–806. https://doi.org/10.1007/S00424-009-0767-7/METRICS

Floyd, R., & Wray, S. (2007). Calcium transporters and signalling in smooth muscles. *Cell Calcium*, *42*(4–5), 467–476. https://doi.org/10.1016/J.CECA.2007.05.011

Forlenza, OV., De-Paula, VJR., & Diniz, BSO. (2014). Neuroprotective effects of lithium: implications for the treatment of Alzheimer's disease and related neurodegenerative disorders. *ACS chemical neuroscience*, *5*(6), 443–450. https://doi.org/10.1021/CN5000309

Foster, DB., Shen, LH., Kelly, J., Thibault, P., Van Eyk, JE., & Mak, AS. (2000). Phosphorylation of Caldesmon by p21-activated Kinase: IMPLICATIONS FOR THE Ca2+ SENSITIVITY OF SMOOTH MUSCLE CONTRACTION *. *Journal of Biological Chemistry*, *275*(3), 1959–1965. https://doi.org/10.1074/JBC.275.3.1959

Foster, MN., & Coetzee, WA. (2016). KATP Channels in the Cardiovascular System. *Physiological Reviews*, *96*(1), 177. https://doi.org/10.1152/PHYSREV.00003.2015

Forrester EA, Benítez-Angeles M, Redford KE, Rosenbaum T, Abbott GW, Barrese V, Dora K, Albert AP, Dannesboe J, Salles-Crawley I, Jepps TA, and Greenwood IA (2024). Crucial role for sensory nerves and Na/H exchanger inhibition in dapagliflozin and empagliflozin-induced arterial relaxation, *Cardiovascular Research*. doi:10.1093/cvr/cvae156.

Francis, J., Zhang, J., Farhi, A., Carey, H., & Geller, DS. (2004). A novel SGLT2 mutation in a patient with autosomal recessive renal glucosuria. *Nephrology, dialysis, transplantation : official publication of the European Dialysis and Transplant Association - European Renal Association*, *19*(11), 2893–2895. https://doi.org/10.1093/NDT/GFH426

Fredriksson, R., Nordström, K. JV., Stephansson, O., Hägglund, MGA., & Schiöth, HB. (2008). The solute carrier (SLC) complement of the human genome: phylogenetic classification reveals four major families. *FEBS letters*, *582*(27), 3811–3816. https://doi.org/10.1016/J.FEBSLET.2008.10.016

Fredriksson, S., Gullberg, M., Jarvius, J., Olsson, C., Pietras, K., Gústafsdóttir, SM., Östman, A., & Landegren, U. (2002). Protein detection using proximity-dependent DNA ligation assays. *Nature Biotechnology 2002 20:5*, *20*(5), 473–477. https://doi.org/10.1038/nbt0502-473

Freeman, SL., Bohan, D., Darcel, N., & Raybould, HE. (2006). Luminal glucose sensing in the rat intestine has characteristics of a sodium-glucose cotransporter. *American journal of physiology. Gastrointestinal and liver physiology*, *291*(3). https://doi.org/10.1152/AJPGI.00079.2006

Gamarra, M., de la Cruz, A., Blanco-Urrejola, M., & Baleriola, J. (2021). Local Translation in Nervous System Pathologies. *Frontiers in Integrative Neuroscience*, *15*. https://doi.org/10.3389/FNINT.2021.689208

Garcia, SM., Naik, JS., Resta, TC., & Jernigan, NL. (2023). Acid-sensing ion channel 1a activates IKCa/SKCa channels and contributes to endothelium-dependent dilation. *The Journal of General Physiology*, *155*(2). https://doi.org/10.1085/JGP.202213173

García-Morales, V., Cuíñas, A., Elíes, J., & Campos-Toimil, M. (2014). PKA and Epac activation mediates cAMP-induced vasorelaxation by increasing endothelial NO production. *Vascular pharmacology*, *60*(3), 95–101. https://doi.org/10.1016/J.VPH.2014.01.004

Gheibi, S., Jeddi, S., Kashfi, K., & Ghasemi, A. (2018). Regulation of vascular tone homeostasis by NO and H2S: Implications in hypertension. *Biochemical pharmacology*, *149*, 42. https://doi.org/10.1016/J.BCP.2018.01.017

Ghosal, A., Subramanian, VS., & Said, HM. (2011). Role of the putative N-glycosylation and PKC- phosphorylation sites of the human sodium-dependent multivitamin transporter (hSMVT) in function and regulation. *Biochimica et biophysica acta*, *1808*(8), 2073. https://doi.org/10.1016/J.BBAMEM.2011.04.014

Ghosh, D., Syed, AU., Prada, MP., Nystoriak, MA., Santana, LF., Nieves-Cintrón, M., & Navedo, MF. (2017). Calcium Channels in Vascular Smooth Muscle. *Advances in pharmacology (San Diego, Calif.)*, *78*, 49. https://doi.org/10.1016/BS.APHA.2016.08.002

Gisler, SM., Pribanic, S., Bacic, D., Forrer, P., Gantenbein, A., Sabourin, LA., Tsuji, A., Zhao, ZS., Manser, E., Biber, J., & Murer, H. (2003). PDZK1: I. a major scaffolder in brush borders of proximal tubular cells. *Kidney international*, *64*(5), 1733–1745. https://doi.org/10.1046/J.1523-1755.2003.00266.X

Glaser, N., Fritsch, M., Priyambada, L., Rewers, A., Cherubini, V., Estrada, S., Wolfsdorf, JI., & Codner, E. (2022). ISPAD clinical practice consensus guidelines 2022: Diabetic ketoacidosis and hyperglycemic hyperosmolar state. *Pediatric Diabetes*, *23*(7), 835–856. https://doi.org/10.1111/PEDI.13406

Gollasch, M., Löhn, M., Fürstenau, M., Nelson, MT., Luft, FC., & Haller, H. (2000). Ca2+ channels, Ca2+ sparks, and regulation of arterial smooth muscle function. *Zeitschrift fur Kardiologie*, *89 Suppl 2*(SUPPL. 2). https://doi.org/10.1007/S003920070095

Gong, D., Chi, X., Ren, K., Huang, G., Zhou, G., Yan, N., Lei, J., & Zhou, Q. (2018). Structure of the human plasma membrane Ca2+-ATPase 1 in complex with its obligatory subunit neuroplastin. *Nature Communications 2018 9:1*, *9*(1), 1–9. https://doi.org/10.1038/s41467-018-06075-7

Gonzalez-Cobos, JC., & Trebak, M. (2010). TRPC channels in smooth muscle cells. *Frontiers in bioscience : a journal and virtual library*, *15*(3), 1023. https://doi.org/10.2741/3660

Goto, K., Rummery, NM., Grayson, TH., & Hill, CE. (2004). Attenuation of conducted vasodilatation in rat mesenteric arteries during hypertension: role of inwardly rectifying potassium channels. *The Journal of physiology*, *561*(Pt 1), 215–231. https://doi.org/10.1113/JPHYSIOL.2004.070458

Grandperrin, A., Strock, E., Petit, L., Risdon, S., Boulghobra, D., Gayrard, S., Reboul, C., Walther, G., Battault, S., & Meyer, G. (2024). SMIT1 Expression in Arterial Tissue: A Potential New Trigger of Vascular Dysfunctions and ROS Production in Rats. *Arteriosclerosis, Thrombosis, and Vascular Biology*, *44*(5), E168–E170. https://doi.org/10.1161/ATVBAHA.123.320547/ASSET/AC0FE5E4-4F1D-4CFE-9C71-5976233E13A8/ASSETS/ATVBAHA.123.320547.FP.PNG

Greenbaum, D., Colangelo, C., Williams, K., & Gerstein, M. (2003). Comparing protein abundance and mRNA expression levels on a genomic scale. Genome Biology, 4(9), 117. https://doi.org/10.1186/gb-2003-4-9-117

Greenberg, HZE., Carlton-Carew, SRE., Khan, DM., Zargaran, AK., Jahan, KS., Vanessa Ho, WS., & Albert, AP. (2017). Heteromeric TRPV4/TRPC1 channels mediate calcium-sensing receptor-induced nitric oxide production and vasorelaxation in rabbit mesenteric arteries. *Vascular Pharmacology*, *96–98*, 53. https://doi.org/10.1016/J.VPH.2017.08.005

Greenberg, HZE., Carlton-Carew, SRE., Zargaran, A. K., Jahan, K. S., Birnbaumer, L., & Albert, A. P. (2019). Heteromeric TRPV4/TRPC1 channels

mediate calcium-sensing receptor-induced relaxations and nitric oxide production in mesenteric arteries: comparative study using wild-type and TRPC1−/- mice. *Channels*, *13*(1), 410. https://doi.org/10.1080/19336950.2019.1673131

Greenwood, I. A., & Large, W. A. (1998). Properties of a Cl- current activated by cell swelling in rabbit portal vein vascular smooth muscle cells. *The American journal of physiology*, *275*(5). https://doi.org/10.1152/AJPHEART.1998.275.5.H1524

Greenwood, IA., & Ohya, S. (2009). New tricks for old dogs: KCNQ expression and role in smooth muscle. *British Journal of Pharmacology*, *156*(8), 1196. https://doi.org/10.1111/J.1476-5381.2009.00131.X

Grempler, R., Thomas, L., Eckhardt, M., Himmelsbach, F., Sauer, A., Sharp, DE., Bakker, RA., Mark, M., Klein, T., & Eickelmann, P. (2012). Empagliflozin, a novel selective sodium glucose cotransporter-2 (SGLT-2) inhibitor: characterisation and comparison with other SGLT-2 inhibitors. *Diabetes, Obesity and Metabolism*, *14*(1), 83–90. https://doi.org/10.1111/J.1463-1326.2011.01517.X

Gronda, E., Jessup, M., Iacoviello, M., Palazzuoli, A., & Napoli, C. (2020). Glucose Metabolism in the Kidney: Neurohormonal Activation and Heart Failure Development. *Journal of the American Heart Association: Cardiovascular and Cerebrovascular Disease*, *9*(23), 18889. https://doi.org/10.1161/JAHA.120.018889

Guan, YY., Wang, GL., & Zhou, JG. (2006). The ClC-3 Cl- channel in cell volume regulation, proliferation and apoptosis in vascular smooth muscle cells. *Trends in pharmacological sciences*, *27*(6), 290–296. https://doi.org/10.1016/J.TIPS.2006.04.008

Gyimesi, G., Pujol-Giménez, J., Kanai, Y., & Hediger, MA. (2020). Sodium-coupled glucose transport, the SLC5 family, and therapeutically relevant inhibitors: from molecular discovery to clinical application. *Pflügers Archiv - European Journal of Physiology 2020 472:9*, *472*(9), 1177–1206. https://doi.org/10.1007/S00424-020-02433-X

Haick, JM., & Byron, KL. (2016). Novel treatment strategies for smooth muscle disorders: Targeting Kv7 potassium channels. *Pharmacology & Therapeutics*, *165*, 14–25. https://doi.org/10.1016/J.PHARMTHERA.2016.05.002

Haitin, Y., & Attali, B. (2008). The C-terminus of Kv7 channels: a multifunctional module. *The Journal of Physiology*, *586*(Pt 7), 1803. https://doi.org/10.1113/JPHYSIOL.2007.149187

Harada, S., Fujita (Hamabe), W., Shichi, K., & Tokuyama, S. (2009). The development of glucose intolerance after focal cerebral ischemia participates in subsequent neuronal damage. *Brain Research*, *1279*, 174–181. https://doi.org/10.1016/J.BRAINRES.2009.05.014

Harteneck, C., & Gollasch, M. (2011). Pharmacological Modulation of Diacylglycerol-Sensitive TRPC3/6/7 Channels. *Current Pharmaceutical Biotechnology*, *12*(1), 35. https://doi.org/10.2174/138920111793937943

Hasan, A., & Hasan, R. (2021). Empagliflozin Relaxes Resistance Mesenteric Arteries by Stimulating Multiple Smooth Muscle Cell Voltage-Gated K+ (KV) Channels. *International Journal of Molecular Sciences*, *22*(19), 10842. https://doi.org/10.3390/IJMS221910842

Hasan, A., Menon, SN., Zerin, F., & Hasan, R. (2022). Dapagliflozin induces vasodilation in resistance-size mesenteric arteries by stimulating smooth muscle cell KV7 ion channels. *Heliyon*, *8*(5), e09503. https://doi.org/10.1016/J.HELIYON.2022.E09503

Hasan, A., Zerin, F., Menon, SN., Alam, MA., & Hasan, R. (2022). Mechanism of canagliflozin-induced vasodilation in resistance mesenteric arteries and the regulation of systemic blood pressure. *Journal of pharmacological sciences*, *150*(4), 211–222. https://doi.org/10.1016/J.JPHS.2022.09.004

Hediger, MA., Coady, MJ., Ikeda, TS., & Wright, EM. (1987). Expression cloning and cDNA sequencing of the Na+/glucose co-transporter. *Nature*, *330*(6146), 379–381. https://doi.org/10.1038/330379A0

Hegyi, B., Mira Hernandez, J., Shen, EY., Habibi, NR., Bossuyt, J., & Bers, DM. (2022). Empagliflozin Reverses Late Na+Current Enhancement and Cardiomyocyte Proarrhythmia in a Translational Murine Model of Heart Failure

with Preserved Ejection Fraction. *Circulation*, *145*(13), 1029–1031. https://doi.org/10.1161/CIRCULATIONAHA.121.057237

Henke, G., Maier, G., Wallisch, S., Boehmer, C., & Lang, F. (2004). Regulation of the voltage gated K+ channel Kv1.3 by the ubiquitin ligase Nedd4-2 and the serum and glucocorticoid inducible kinase SGK1. *Journal of Cellular Physiology*, *199*(2), 194–199. https://doi.org/10.1002/JCP.10430

Hernandez, CC., Zaika, O., Tolstykh, GP., & Shapiro, MS. (2008). Regulation of neural KCNQ channels: signalling pathways, structural motifs and functional implications. *The Journal of Physiology*, *586*(Pt 7), 1811. https://doi.org/10.1113/JPHYSIOL.2007.148304

Hibino, H., Inanobe, A., Furutani, K., Murakami, S., Findlay, I., & Kurachi, Y. (2010). Inwardly rectifying potassium channels: their structure, function, and physiological roles. *Physiological reviews*, *90*(1), 291–366. https://doi.org/10.1152/PHYSREV.00021.2009

Holman, GD. (2020). Structure, function and regulation of mammalian glucose transporters of the SLC2 family. *Pflugers Archiv*, *472*(9), 1155. https://doi.org/10.1007/S00424-020-02411-3

Horowitz, A., Menice, CB., Laporte, R., & Morgan, KG. (1996). Mechanisms of smooth muscle contraction. *https://doi.org/10.1152/physrev.1996.76.4.967*, *76*(4), 967–1003. https://doi.org/10.1152/PHYSREV.1996.76.4.967

Horton, WB., Jahn, LA., Hartline, LM., Aylor, KW., Patrie, JT., & Barrett, EJ. (2022). Acute hyperglycaemia enhances both vascular endothelial function and cardiac and skeletal muscle microvascular function in healthy humans. *The Journal of physiology*, *600*(4), 949. https://doi.org/10.1113/JP281286

Hou, J., Speirs, HJL., Seckl, JR., & Brown, RW. (2002). Sgk1 Gene Expression in Kidney and Its Regulation by Aldosterone: Spatio-Temporal Heterogeneity and Quantitative Analysis. *Journal of the American Society of Nephrology*, *13*(5), 1190–1198. https://doi.org/10.1097/01.ASN.0000013702.73570.3B

Hu, S., Song, E., Tian, R., Ma, S., Yang, T., Mu, Y., Li, Y., Shao, C., Gao, S., & Gao, Y. (2009). Systematic analysis of a simple adaptor protein PDZK1: ligand identification, interaction and functional prediction of complex. *Cellular*

physiology and biochemistry : international journal of experimental cellular physiology, biochemistry, and pharmacology, *24*(3–4), 231–242. https://doi.org/10.1159/000233258

Hu, XQ., Xiao, D., Zhu, R., Huang, X., Yang, S., Wilson, S., & Zhang, L. (2011). Pregnancy upregulates large-conductance Ca 2+-activated K + channel activity and attenuates myogenic tone in uterine arteries. *Hypertension*, *58*(6), 1132–1139. https://doi.org/10.1161/HYPERTENSIONAHA.111.179952/SUPPL_FILE/179952_-_ONLINE_SUPPLEMENT.PDF

Huang, W., Alexander, GE., Daly, EM., Shetty, HU., Krasuski, JS., Rapoport, SI., & Schapiro, MB. (1999). High brain myo-inositol levels in the predementia phase of Alzheimer's disease in adults with Down's syndrome: A 1H MRS study. *American Journal of Psychiatry*, *156*(12), 1879–1886. https://doi.org/10.1176/AJP.156.12.1879/ASSET/IMAGES/LARGE/AT7F3.JPEG

Hwa, JJ., & Bevan, JA. (1986). Dihydropyridine calcium agonists selectively enhance resistance artery myogenic tone. *European Journal of Pharmacology*, *126*(3), 231–238. https://doi.org/10.1016/0014-2999(86)90052-X

Inoue, R., Okada, T., Onoue, H., Hara, Y., Shimizu, S., Naitoh, S., Ito, Y., & Mori, Y. (2001). The transient receptor potential protein homologue TRP6 is the essential component of vascular alpha(1)-adrenoceptor-activated Ca(2+)-permeable cation channel. *Circulation research*, *88*(3), 325–332. https://doi.org/10.1161/01.RES.88.3.325

Inoue, T., Takemura, M., Fushimi, N., Fujimori, Y., Onozato, T., Kurooka, T., Asari, T., Takeda, H., Kobayashi, M., Nishibe, H., & Isaji, M. (2017). Mizagliflozin, a novel selective SGLT1 inhibitor, exhibits potential in the amelioration of chronic constipation. *European Journal of Pharmacology*, *806*, 25–31. https://doi.org/10.1016/J.EJPHAR.2017.04.010

Islas, LD. (2016). Functional diversity of potassium channel voltage-sensing domains. I: *Channels* (Bd. 10, Nummer 3, s. 202–213). https://doi.org/10.1080/19336950.2016.1141842

Iwai, S., Motono, N., Oyama, T., Shioya, A., Yamada, S., & Uramoto, H. (2024). The Clinical Relevance of the Expression of SGLT2 in Lung Adenocarcinoma. *Oncology*, *102*(8). https://doi.org/10.1159/000536060

Jackson, WF. (2017). Potassium Channels in Regulation of Vascular Smooth Muscle Contraction and Growth. *Advances in pharmacology (San Diego, Calif.)*, *78*, 89. https://doi.org/10.1016/BS.APHA.2016.07.001

Jackson, WF., Konig, A., Dambacher, T., & Busse, R. (1993). Prostacyclin-induced vasodilation in rabbit heart is mediated by ATP-sensitive potassium channels. *The American journal of physiology*, *264*(1 Pt 2). https://doi.org/10.1152/AJPHEART.1993.264.1.H238

Jaggar, JH., Wellman, GC., Heppner, TJ., Porter, VA., Perez, GJ., Gollasch, M., Kleppisch, T., Rubart, M., Stevenson, AS., Lederer, WJ., Knot, HJ., Bonev, AD., & Nelson, MT. (1998). Ca2+ channels, ryanodine receptors and Ca(2+)-activated K+ channels: a functional unit for regulating arterial tone. *Acta physiologica Scandinavica*, *164*(4), 577–587. https://doi.org/10.1046/J.1365-201X.1998.00462.X

Je, HD., Gangopadhyay, SS., Ashworth, TD., & Morgan, KG. (2001). Calponin is required for agonist-induced signal transduction – evidence from an antisense approach in ferret smooth muscle. *The Journal of Physiology*, *537*(Pt 2), 567. https://doi.org/10.1111/J.1469-7793.2001.00567.X

Jepps, TA., Olesen, SP., Greenwood, IA., & Dalsgaard, T. (2016). Molecular and functional characterization of Kv7 channels in penile arteries and corpus cavernosum of healthy and metabolic syndrome rats. *British Journal of Pharmacology*, *173*(9), 1478–1490. https://doi.org/10.1111/BPH.13444

Jepps, TA., Carr, G., Lundegaard, PR., Olesen, SP., & Greenwood, IA. (2015). Fundamental role for the KCNE4 ancillary subunit in Kv7.4 regulation of arterial tone. *The Journal of Physiology*, *593*(24), 5325–5340. https://doi.org/10.1113/JP271286

Jepps, TA., Chadha, PS., Davis, AJ., Harhun, MI., Cockerill, GW., Olesen, SP., Hansen, RS., & Greenwood, IA. (2011). Downregulation of Kv7.4 channel activity in primary and secondary hypertension. *Circulation*, *124*(5), 602–611. https://doi.org/10.1161/CIRCULATIONAHA.111.032136

Jiao, J., Garg, V., Yang, B., Elton, TS., & Hu, K. (2008). Protein kinase C-epsilon induces caveolin-dependent internalization of vascular adenosine 5'-triphosphate-sensitive K+ channels. *Hypertension (Dallas, Tex. : 1979)*, *52*(3), 499–506. https://doi.org/10.1161/HYPERTENSIONAHA.108.110817

Johnson, TD., Marrelli, SP., Steenberg, ML., Childres, WF., & Bryan, RM. (1998). Inward rectifier potassium channels in the rat middle cerebral artery. *The American journal of physiology*, *274*(2). https://doi.org/10.1152/AJPREGU.1998.274.2.R541

Jojima, T., Wakamatsu, S., Kase, M., Iijima, T., Maejima, Y., Shimomura, K., Kogai, T., Tomaru, T., Usui, I., & Aso, Y. (2019). The SGLT2 Inhibitor Canagliflozin Prevents Carcinogenesis in a Mouse Model of Diabetes and Non-Alcoholic Steatohepatitis-Related Hepatocarcinogenesis: Association with SGLT2 Expression in Hepatocellular Carcinoma. *International journal of molecular sciences*, *20*(20). https://doi.org/10.3390/IJMS20205237

Joshi, S., Balan, P., & Gurney, AM. (2006). Pulmonary vasoconstrictor action of KCNQ potassium channel blockers. *Respiratory Research*, *7*(1), 31. https://doi.org/10.1186/1465-9921-7-31

Jung, HS., Seo, MS., An, JR., Heo, R., Kang, M., Han, ET., Park, H., Song, G., Son, YK., Jung, WK., Choi, IW., Na, SH., & Park, WS. (2021). The anti-diabetic drug alogliptin induces vasorelaxation via activation of Kv channels and SERCA pumps. *European Journal of Pharmacology*, *898*, 173991. https://doi.org/10.1016/J.EJPHAR.2021.173991

Kaji, K., Nishimura, N., Seki, K., Sato, S., Saikawa, S., Nakanishi, K., Furukawa, M., Kawaratani, H., Kitade, M., Moriya, K., Namisaki, T., & Yoshiji, H. (2018). Sodium glucose cotransporter 2 inhibitor canagliflozin attenuates liver cancer cell growth and angiogenic activity by inhibiting glucose uptake. *International journal of cancer*, *142*(8), 1712–1722. https://doi.org/10.1002/IJC.31193

Kam, KL., Pfaffendorf, M., & van Zwieten, P. ter A. (1993). The influence of high glucose levels and/or hyperosmolarity on rat isolated aorta. *Journal of Pharmacological and Toxicological Methods*, *30*(3), 153–157. https://doi.org/10.1016/1056-8719(93)90039-H

Kanai, Y., Lee, WS, You, G., Brown, D., & Hediger, MA. (1994). The human kidney low affinity Na+/glucose cotransporter SGLT2. Delineation of the major renal reabsorptive mechanism for D-glucose. *The Journal of clinical investigation*, *93*(1), 397–404. https://doi.org/10.1172/JCI116972

Kashiwagi, Y., Nagoshi, T., Yoshino, T., Tanaka, TD., Ito, K., Harada, T., Takahashi, H., Ikegami, M., Anzawa, R., & Yoshimura, M. (2015). Expression of SGLT1 in Human Hearts and Impairment of Cardiac Glucose Uptake by Phlorizin during Ischemia-Reperfusion Injury in Mice. *PLOS ONE*, *10*(6), e0130605. https://doi.org/10.1371/JOURNAL.PONE.0130605

Kathiresan, S., Voight, BF., Purcell, S., Musunuru, K., Ardissino, D., Mannucci, PM., Anand, S., Engert, JC., Samani, NJ., Schunkert, H., Erdmann, J., Reilly, MP., Rader, DJ., Morgan, T., Spertus, JA., Stoll, M., Girelli, D., McKeown, PP., Patterson, CC., … Siscovick, D. (2009). Genome-wide association of early-onset myocardial infarction with common single nucleotide polymorphisms, common copy number variants, and rare copy number variants. *Nature genetics*, *41*(3), 334. https://doi.org/10.1038/NG.327

Katz, B. (1949). Les constantes electriques de la membrane du muscle. *Arch Sci Physiol*, *2*, 285–299. https://cir.nii.ac.jp/crid/1574231874802068736

Katzmann, JL., Mason, AM., März, W., Kleber, ME., Niessner, A., Blüher, M., Speer, T., & Laufs, U. (2021). Genetic Variation in Sodium-glucose Cotransporter 2 and Heart Failure. *Clinical pharmacology and therapeutics*, *110*(1), 149–158. https://doi.org/10.1002/CPT.2153

Kawasaki, H., Takasaki, K., Saito, A., & Goto, K. (1988). Calcitonin gene-related peptide acts as a novel vasodilator neurotransmitter in mesenteric resistance vessels of the rat. *Nature 1988 335:6186*, *335*(6186), 164–167. https://doi.org/10.1038/335164a0

Keef, KD., & Ross, G. (1987). Relaxation induced by KCl, NaCl and sucrose in rabbit coronary arteries. *Pflugers Archiv : European journal of physiology*, *409*(3), 308–313. https://doi.org/10.1007/BF00583481

Khanamiri, S., Soltysinska, E., Jepps, TA., Bentzen, BH., Chadha, PS., Schmitt, N., Greenwood, IA., & Olesen, SP. (2013). Contribution of KV7 channels to

basal coronary flow and active response to ischemia. *Hypertension*, *62*(6), 1090–1097. https://doi.org/10.1161/HYPERTENSIONAHA.113.01244

Kim, DM., & Nimigean, CM. (2016). Voltage-gated potassium channels: A structural examination of selectivity and gating. *Cold Spring Harbor Perspectives in Biology*, *8*(5). https://doi.org/10.1101/cshperspect.a029231

Kim, HW., Li, H., Kim, HS., Shin, SE., Jung, WK., Ha, KS., Han, ET., Hong, SH., Choi, IW., Firth, AL., Bang, H., & Park, WS. (2016). The anti-diabetic drug repaglinide induces vasorelaxation via activation of PKA and PKG in aortic smooth muscle. *Vascular Pharmacology*, *84*, 38–46. https://doi.org/10.1016/J.VPH.2016.07.005

Kim, MY., Liang, GH., Kim, JA., Park, SH., Hah, JS., & Suh, SH. (2005). Contribution of Na+-K+ pump and KIR currents to extracellular pH-dependent changes of contractility in rat superior mesenteric artery. *American Journal of Physiology - Heart and Circulatory Physiology*, *289*(2 58-2). https://doi.org/10.1152/AJPHEART.00050.2005

Kitamura, K., & Yamazaki, J. (2001). Chloride channels and their functional roles in smooth muscle tone in the vasculature. *Japanese journal of pharmacology*, *85*(4), 351–357. https://doi.org/10.1254/JJP.85.351

Klaus, F., Palmada, M., Lindner, R., Laufer, J., Jeyaraj, S., Lang, F., & Boehmer, C. (2008). Up-regulation of hypertonicity-activated myo-inositol transporter SMIT1 by the cell volume-sensitive protein kinase SGK1. *The Journal of Physiology*, *586*(Pt 6), 1539. https://doi.org/10.1113/JPHYSIOL.2007.146191

Knot, HJ., & Nelson, MT. (1998a). Regulation of arterial diameter and wall [Ca2+] in cerebral arteries of rat by membrane potential and intravascular pressure. *The Journal of Physiology*, *508*(Pt 1), 199. https://doi.org/10.1111/J.1469-7793.1998.199BR.X

Knot, HJ., Zimmermann, PA., & Nelson, MT. (1996). Extracellular K(+)-induced hyperpolarizations and dilatations of rat coronary and cerebral arteries involve inward rectifier K(+) channels. *The Journal of physiology*, *492 (Pt 2)*(Pt 2), 419–430. https://doi.org/10.1113/JPHYSIOL.1996.SP021318

Ko, EA., Park, WS., Firth, AL., Kim, N., Yuan, JX. J., & Han, J. (2010). Pathophysiology of voltage-gated K+ channels in vascular smooth muscle cells: Modulation by protein kinases. *Progress in Biophysics and Molecular Biology*, *103*(1), 95–101. https://doi.org/10.1016/J.PBIOMOLBIO.2009.10.001

Koepsell, H. (2017). The Na+-D-glucose cotransporters SGLT1 and SGLT2 are targets for the treatment of diabetes and cancer. *Pharmacology & Therapeutics*, *170*, 148–165. https://doi.org/10.1016/J.PHARMTHERA.2016.10.017

Koller, A., Schlossmann, J., Ashman, K., Uttenweiler-Joseph, S., Ruth, P., & Hofmann, F. (2003). Association of phospholamban with a cGMP kinase signaling complex. *Biochemical and Biophysical Research Communications*, *300*(1), 155–160. https://doi.org/10.1016/S0006-291X(02)02799-7

Kuang, Q., Purhonen, P., & Hebert, H. (2015). Structure of potassium channels. *Cellular and Molecular Life Sciences*, *72*(19), 3677. https://doi.org/10.1007/S00018-015-1948-5

Kuo, IY., & Ehrlich, BE. (2015). Signaling in Muscle Contraction. *Cold Spring Harbor Perspectives in Biology*, *7*(2). https://doi.org/10.1101/CSHPERSPECT.A006023

Kwan, HY., Shen, B., Ma, X., Kwok, YC., Huang, Y., Man, YB., Yu, S., & Yao, X. (2009). TRPC1 Associates With BKCa Channel to Form a Signal Complex in Vascular Smooth Muscle Cells. *Circulation Research*, *104*(5), 670–678. https://doi.org/10.1161/CIRCRESAHA.108.188748

Lade, JM., Andrade, MR., Undem, C., Walker, J., Jiang, H., Yun, X., & Shimoda, LA. (2023). Hypoxia enhances interactions between Na+/H+ exchanger isoform 1 and actin filaments via ezrin in pulmonary vascular smooth muscle. *Frontiers in Physiology*, *14*. https://doi.org/10.3389/FPHYS.2023.1108304

Lahjouji, K., Aouameur, R., Bissonnette, P., Coady, MJ., Bichet, DG., & Lapointe, J. Y. (2007). Expression and functionality of the Na+/myo-inositol cotransporter SMIT2 in rabbit kidney. *Biochimica et Biophysica Acta (BBA) - Biomembranes*, *1768*(5), 1154–1159. https://doi.org/10.1016/J.BBAMEM.2007.01.007

Lambert, R., Srodulskic, S., Peng, X., Margulies, KB., Despa, F., & Despa, S. (2015). Intracellular Na+ Concentration ([Na+]i) Is Elevated in Diabetic Hearts Due to Enhanced Na+–Glucose Cotransport. *Journal of the American Heart Association: Cardiovascular and Cerebrovascular Disease*, *4*(9). https://doi.org/10.1161/JAHA.115.002183

Lamothe, SM., & Zhang, S. (2013). The Serum- and Glucocorticoid-inducible Kinases SGK1 and SGK3 Regulate hERG Channel Expression via Ubiquitin Ligase Nedd4-2 and GTPase Rab11. *The Journal of Biological Chemistry*, *288*(21), 15075. https://doi.org/10.1074/JBC.M113.453670

Lang, F., Busch, GL., & Völkl, H. (1998). The Diversity of Volume Regulatory Mechanisms. *Cellular Physiology and Biochemistry*, *8*(1–2), 1–45. https://doi.org/10.1159/000016269

Leblanc, N., Forrest, AS., Ayon, RJ., Wiwchar, M., Angermann, JE., Pritchard, HA. T., Singer, CA., Valencik, ML., Britton, F., & Greenwood, IA. (2015). Molecular and functional significance of Ca(2+)-activated Cl(-) channels in pulmonary arterial smooth muscle. *Pulmonary circulation*, *5*(2), 244–268. https://doi.org/10.1086/680189

Ledoux, J., Taylor, MS., Bonev, AD., Hannah, RM., Solodushko, V., Shui, B., Tallini, Y., Kotlikoff, MI., & Nelson, MT. (2008). Functional architecture of inositol 1,4,5-trisphosphate signaling in restricted spaces of myoendothelial projections. *Proceedings of the National Academy of Sciences of the United States of America*, *105*(28), 9627–9632. https://doi.org/10.1073/PNAS.0801963105/SUPPL_FILE/0801963105SI.PDF

Lee, S., Yang, Y., Tanner, MA., Li, M., & Hill, MA. (2015). Heterogeneity in Kv7 channel function in the Cerebral and Coronary Circulation. *Microcirculation (New York, N.Y. : 1994)*, *22*(2), 109. https://doi.org/10.1111/MICC.12183

Lee, TI., Chen, YC., Lin, YK., Chung, CC., Lu, YY., Kao, YH., & Chen, YJ. (2019). Empagliflozin Attenuates Myocardial Sodium and Calcium Dysregulation and Reverses Cardiac Remodeling in Streptozotocin-Induced Diabetic Rats. *International Journal of Molecular Sciences*, *20*(7), 1680. https://doi.org/10.3390/IJMS20071680

Lee, WS., Kanais, Y., Wells, RG., & Hedigefl, MA. (1994). *THE JOURNAL OF BIOLOGICAL CHEMISTRY The High Affinity Na+/Glucose Cotransporter RE-EVALUATION OF FUNCTION AND DISTRIBUTION OF EXPRESSION**. *269*(16), 12032–12039. https://doi.org/10.1016/S0021-9258(17)32677-7

Lemonnier, L., Trebak, M., & Putney, JW. (2008). Complex regulation of the TRPC3, 6 and 7 channel subfamily by diacylglycerol and phosphatidylinositol-4,5-bisphosphate. *Cell calcium*, *43*(5), 506–514. https://doi.org/10.1016/J.CECA.2007.09.001

Lepore, E., Lauretta, R., Bianchini, M., Mormando, M., Di Lorenzo, C., & Unfer, V. (2021). Inositols Depletion and Resistance: Principal Mechanisms and Therapeutic Strategies. *International Journal of Molecular Sciences*, *22*(13). https://doi.org/10.3390/IJMS22136796

Li, C., & Yang, Y. (2023). Advancements in the study of inward rectifying potassium channels on vascular cells. *Channels*, *17*(1). https://doi.org/10.1080/19336950.2023.2237303

Li, H., Shin, SE., Seo, MS., An, JR., Choi, IW., Jung, WK., Firth, AL., Lee, DS., Yim, MJ., Choi, G., Lee, JM., Na, SH., & Park, WS. (2018). The anti-diabetic drug dapagliflozin induces vasodilation via activation of PKG and Kv channels. *Life Sciences*, *197*, 46–55. https://doi.org/10.1016/J.LFS.2018.01.032

Li, T., Wu, K., Yue, Z., Wang, Y., Zhang, F., & Shen, H. (2021). Structural Basis for the Modulation of Human KCNQ4 by Small-Molecule Drugs. *Molecular Cell*, *81*(1), 25-37.e4. https://doi.org/10.1016/J.MOLCEL.2020.10.037

Li, Y., Gamper, N., Hilgemann, DW., & Shapiro, MS. (2005). Regulation of Kv7 (KCNQ) K+ channel open probability by phosphatidylinositol 4,5-bisphosphate. *The Journal of neuroscience : the official journal of the Society for Neuroscience*, *25*(43), 9825–9835. https://doi.org/10.1523/JNEUROSCI.2597-05.2005

Li, Z., Agrawal, V., Ramratnam, M., Sharma, RK., D'Auria, S., Sincoular, A., Jakubiak, M., Music, ML., Kutschke, WJ., Huang, XN., Gifford, L., & Ahmad, F. (2019). Cardiac sodium-dependent glucose cotransporter 1 is a novel mediator of ischaemia/reperfusion injury. *Cardiovascular Research*, *115*(11), 1646. https://doi.org/10.1093/CVR/CVZ037

Lin, H., Guan, L., Meng, L., Uzui, H., & Guo, H. (2021). SGLT1 Knockdown Attenuates Cardiac Fibroblast Activation in Diabetic Cardiac Fibrosis. *Frontiers in Pharmacology*, *12*. https://doi.org/10.3389/FPHAR.2021.700366/FULL

Lin, JH., Scullion, L., Garland, CJ., & Dora, K. (2023). Gβγ subunit signalling underlies neuropeptide Y-stimulated vasoconstriction in rat mesenteric and coronary arteries. *British Journal of Pharmacology*, *180*(23), 3045–3058. https://doi.org/10.1111/BPH.16192

Lin, X., Ma, L., Fitzgerald, RL., & Ostlund, RE. (2009). Human sodium/inositol cotransporter 2 (SMIT2) transports inositols but not glucose in L6 cells. *Archives of Biochemistry and Biophysics*, *481*(2), 197–201. https://doi.org/10.1016/J.ABB.2008.11.008

Lopatin, AN., Makhina, EN., & Nichols, CG. (1994). Potassium channel block by cytoplasmic polyamines as the mechanism of intrinsic rectification. *Nature 1994 372:6504*, *372*(6504), 366–369. https://doi.org/10.1038/372366a0

Lu, Y., Hanna, ST., Tang, G., & Wang, R. (2002). Contributions of Kv1.2, Kv1.5 and Kv2.1 subunits to the native delayed rectifier K+ current in rat mesenteric artery smooth muscle cells. *Life Sciences*, *71*(12), 1465–1473. https://doi.org/10.1016/S0024-3205(02)01922-7

Lucas-Herald, AK., Alves-Lopes, R., Montezano, AC., Ahmed, SF., & Touyz, RM. (2017). Genomic and non-genomic effects of androgens in the cardiovascular system: clinical implications. *Clinical Science (London, England : 1979)*, *131*(13), 1405. https://doi.org/10.1042/CS20170090

Lusk, KA., Benitez, RM., Carter, J., Diocee, H., Snoga, JL., Lusk, KA., Benitez, RM., Carter, J., Diocee, H., & Snoga, JL. (2022). The role of SGLT2 inhibitors in heart failure. *American Journal of Pharmacotherapy and Pharmaceutical Sciences*, *1*, 2. https://doi.org/10.25259/AJPPS_5_2021

Ma, D., Gaynullina, D., Schmidt, N., Mladenov, M., & Schubert, R. (2020). The Functional Availability of Arterial Kv7 Channels Is Suppressed Considerably by Large-Conductance Calcium-Activated Potassium Channels in 2- to 3-Month Old but Not in 10- to 15-Day Old Rats. *Frontiers in Physiology*, *11*, 1644. https://doi.org/10.3389/FPHYS.2020.597395/BIBTEX

Mackie, AR., Brueggemann, LI., Henderson, KK., Shiels, AJ., Cribbs, LL., Scrogin, KE., & Byron, KL. (2008). Vascular KCNQ Potassium Channels as Novel Targets for the Control of Mesenteric Artery Constriction by Vasopressin, Based on Studies in Single Cells, Pressurized Arteries, and in Vivo Measurements of Mesenteric Vascular Resistance. *The Journal of pharmacology and experimental therapeutics*, *325*(2), 475. https://doi.org/10.1124/JPET.107.135764

MacKinnon ÃR., Heijne, von, Rydstro, J., & Brzezinski, P. (2003). Potassium channels. *FEBS Letters*, *555*(1), 62–65. https://doi.org/10.1016/S0014-5793(03)01104-9

Magen, D., Sprecher, E., Zelikovic, I., & Skorecki, K. (2005). A novel missense mutation in SLC5A2 encoding SGLT2 underlies autosomal-recessive renal glucosuria and aminoaciduria. *Kidney international*, *67*(1), 34–41. https://doi.org/10.1111/J.1523-1755.2005.00053.X

Maier, G., Palmada, M., Rajamanickam, J., Shumilina, E., Böhmer, C., & Lang, F. (2006). Upregulation of HERG Channels by the Serum and Glucocorticoid Inducible Kinase Isoform SGK3. *Cellular Physiology and Biochemistry*, *18*(4–5), 177–186. https://doi.org/10.1159/000097666

Manville, R., Neverisky, DL., & Abbott, GW. (2017). SMIT1 Modifies KCNQ Channel Function and Pharmacology by Physical Interaction with the Pore. *Biophysical Journal*, *113*(3), 613. https://doi.org/10.1016/J.BPJ.2017.06.055

Marino, M., Galluzzo, P., & Ascenzi, P. (2006). Estrogen Signaling Multiple Pathways to Impact Gene Transcription. *Current Genomics*, *7*(8), 497–508. https://doi.org/10.2174/138920206779315737

Martinez, FA., Serenelli, M., Nicolau, JC., Petrie, MC., Chiang, CE., Tereshchenko, S., Solomon, SD., Inzucchi, SE., Køber, L., Kosiborod, MN., Ponikowski, P., Sabatine, MS., Demets, DL., Dutkiewicz-Piasecka, M., Bengtsson, O., Sjöstrand, M., Langkilde, AM., Jhund, PS., & McMurray, JJV. (2020). Efficacy and Safety of Dapagliflozin in Heart Failure With Reduced Ejection Fraction According to Age. *Circulation*, 100–111. https://doi.org/10.1161/CIRCULATIONAHA.119.044133

Massett, MP., Koller, A., & Kaley, G. (2000). Hyperosmolality dilates rat skeletal muscle arterioles: role of endothelial K(ATP) channels and daily exercise. *Journal of applied physiology (Bethesda, Md.: 1985)*, *89*(6), 2227–2234. https://doi.org/10.1152/JAPPL.2000.89.6.2227

Matsuda, H., Saigusa, A., & Irisawa, H. (1987). Ohmic conductance through the inwardly rectifying K channel and blocking by internal Mg2+. *Nature*, *325*(7000), 156–159. https://doi.org/10.1038/325156A0

McMurray, JJV., Solomon, SD., Inzucchi, SE., Køber, L., Kosiborod, MN., Martinez, FA., Ponikowski, P., Sabatine, MS., Anand, IS., Bělohlávek, J., Böhm, M., Chiang, CE., Chopra, VK., Boer, RA. de, Desai, AS., Diez, M., Drozdz, J., Dukát, A., Ge, J., Langkilde, AM. (2019). Dapagliflozin in Patients with Heart Failure and Reduced Ejection Fraction. *https://doi.org/10.1056/NEJMoa1911303*, *381*(21), 1995–2008. https://doi.org/10.1056/NEJMOA1911303

Mishra, JS., More, AS., Gopalakrishnan, K., & Kumar, S. (2019). Testosterone plays a permissive role in angiotensin II-induced hypertension and cardiac hypertrophy in male rats. *Biology of Reproduction*, *100*(1), 139. https://doi.org/10.1093/BIOLRE/IOY179

Miyakawa, H., Woo, SK., Dahl, SC., Handler, JS., & Kwon, HM. (1999). Tonicity-responsive enhancer binding protein, a Rel-like protein that stimulates transcription in response to hypertonicity. *Proceedings of the National Academy of Sciences of the United States of America*, *96*(5), 2538. https://doi.org/10.1073/PNAS.96.5.2538

Moiseenkova-Bell, VY., Stanciu, LA., Serysheva, II., Tobe, BJ., & Wensel, TG. (2008). Structure of TRPV1 channel revealed by electron cryomicroscopy. *Proceedings of the National Academy of Sciences of the United States of America*, *105*(21), 7451–7455. https://doi.org/10.1073/PNAS.0711835105

Mondéjar-Parreño, G., Barreira, B., Callejo, M., Morales-Cano, D., Barrese, V., Esquivel-Ruiz, S., Olivencia, MA., MacÍas, M., Moreno, L., Greenwood, IA., Perez-Vizcaino, F., & Cogolludo, A. (2020). Uncovered contribution of Kv7 channels to pulmonary vascular tone in pulmonary arterial hypertension.

Hypertension, 1134–1146. https://doi.org/10.1161/HYPERTENSIONAHA.120.15221

Mondéjar-Parreño, G., Moral-Sanz, J., Barreira, B., De la Cruz, A., Gonzalez, T., Callejo, M., Esquivel-Ruiz, S., Morales-Cano, D., Moreno, L., Valenzuela, C., Perez-Vizcaino, F., & Cogolludo, A. (2019). Activation of Kv7 channels as a novel mechanism for NO/cGMP-induced pulmonary vasodilation. *British Journal of Pharmacology*, *176*(13), 2131. https://doi.org/10.1111/BPH.14662

Moo Kwon, H., Yamauchi, A., Uchida, S., Preston, AS., Garcia-Perez$, A., Burg$, MB., & Handler8, JS. (1992). Cloning of the cDNa for a Na+/myo-Inositol Cotransporter, a Hypertonicity Stress Protein*. *THE JOURNAL OF BIOLOGICAL CHEMISTRY*, *267*(9), 6297–6301. https://doi.org/10.1016/S0021-9258(18)42695-6

Moosmang, S., Schulla, V., Welling, A., Feil, R., Feil, S., Wegener, J. W., Hofmann, F., & Klugbauer, N. (2003). Dominant role of smooth muscle L-type calcium channel Cav1.2 for blood pressure regulation. *The EMBO Journal*, *22*(22), 6027. https://doi.org/10.1093/EMBOJ/CDG583

Morales-Cano, D., Moreno, L., Barreira, B., Pandolfi, R., Chamorro, V., Jimenez, R., Villamor, E., Duarte, J., Perez-Vizcaino, F., & Cogolludo, A. (2015). Kv7 channels critically determine coronary artery reactivity: left–right differences and down-regulation by hyperglycaemia. *Cardiovascular Research*, *106*(1), 98–108. https://doi.org/10.1093/CVR/CVV020

Morgado, M., Cairrão, E., Santos-Silva, AJ., & Verde, I. (2011). Cyclic nucleotide-dependent relaxation pathways in vascular smooth muscle. *Cellular and Molecular Life Sciences 2011 69:2*, *69*(2), 247–266. https://doi.org/10.1007/S00018-011-0815-2

Morth, JP., Pedersen, BP., Toustrup-Jensen, MS., Sørensen, TLM., Petersen, J., Andersen, JP., Vilsen, B., & Nissen, P. (2007). Crystal structure of the sodium-potassium pump. *Nature*, *450*(7172), 1043–1049. https://doi.org/10.1038/NATURE06419

Mueckler, M., & Thorens, B. (2013). The SLC2 (GLUT) Family of Membrane Transporters. *Molecular aspects of medicine*, *34*(0), 121. https://doi.org/10.1016/J.MAM.2012.07.001

Mustafa, AK., Sikka, G., Gazi, SK., Steppan, J., Jung, SM., Bhunia, AK., Barodka, VM., Gazi, FK., Barrow, RK., Wang, R., Amzel, LM., Berkowitz, DE., & Snyder, SH. (2011). Hydrogen sulfide as endothelium-derived hyperpolarizing factor sulfhydrates potassium channels. *Circulation research*, *109*(11), 1259–1268. https://doi.org/10.1161/CIRCRESAHA.111.240242

Myeong, J., Ko, J., Kwak, M., Kim, J., Woo, J., Ha, K., Hong, C., Yang, D., Kim, HJ., Jeon, JH., & So, I. (2018). Dual action of the Gαq-PLCβ-PI(4,5)P2 pathway on TRPC1/4 and TRPC1/5 heterotetramers. *Scientific Reports 2018 8:1*, *8*(1), 1–13. https://doi.org/10.1038/s41598-018-30625-0

Müller, CE., & Jacobson, KA. (2011). Recent developments in adenosine receptor ligands and their potential as novel drugs. *Biochimica et Biophysica Acta (BBA) - Biomembranes*, *1808*(5), 1290–1308. https://doi.org/10.1016/J.BBAMEM.2010.12.017

MaassenVanDenBrink, A., Meijer, J., Villalón, CM., & Ferrari, MD. (2016). Wiping Out CGRP: Potential Cardiovascular Risks. *Trends in Pharmacological Sciences*, *37*(9), 779–788. https://doi.org/10.1016/J.TIPS.2016.06.002

Nagai, K., Yoshida, S., & Konishi, H. (2014a). Gender differences in the gene expression profiles of glucose transporter GLUT class I and SGLT in mouse tissues. *Pharmazie*, *69*(11), 856–859. https://doi.org/10.1691/PH.2014.4647

Nagar, D., Liu, XT., & Rosenfeld, CR. (2005). Estrogen regulates β1-subunit expression in Ca 2+-activated K+ channels in arteries from reproductive tissues. *American Journal of Physiology - Heart and Circulatory Physiology*, *289*(458-4),1417–1427. https://doi.org/10.1152/AJPHEART.01174.2004/ASSET/IMAGES/LARGE/ZH40100561881009.JPEG

Nappi, P., Miceli, F., Soldovieri, M. V., Ambrosino, P., Barrese, V., & Taglialatela, M. (2020). Epileptic channelopathies caused by neuronal Kv7 (KCNQ) channel dysfunction. Pflügers Archiv - European Journal of Physiology, 472(7), 881–898. https://doi.org/10.1007/s00424-020-02404-2.

Nassif, M., Windsor, S., Tang, F., Khariton, Y., Husain, M., Inzucchi, S., McGuire, D., Pitt, B., Scirica, B., Austin, B., Drazner, M., Fong, M., Givertz, M., Gordon, R., Jermyn, R., Katz, S., Lamba, S., Lanfear, D., LaRue, S., … Cox, J. (2019).

Dapagliflozin Effects on Biomarkers, Symptoms, and Functional Status in Patients With Heart Failure With Reduced Ejection Fraction. *Circulation*, *140*(18). https://doi.org/10.1161/CIRCULATIONAHA.119.042929

Neverisky, DL., & Abbott, G. W. (2015). Ion channel-transporter interactions. *Critical reviews in biochemistry and molecular biology*, *51*(4), 257. https://doi.org/10.3109/10409238.2016.1172553

Neverisky, DL., & Abbott, GW. (2017). KCNQ-SMIT complex formation facilitates ion channel-solute transporter cross talk. *FASEB Journal*, *31*(7), 2828–2838. https://doi.org/10.1096/FJ.201601334R/-/DC1

Ng, FL., Davis, AJ., Jepps, TA., Harhun, MI., Yeung, SY., Wan, A., Reddy, M., Melville, D., Nardi, A., Khong, TK., & Greenwood, IA. (2011). Expression and function of the K+ channel KCNQ genes in human arteries. *British Journal of Pharmacology*, *162*(1), 42. https://doi.org/10.1111/J.1476-5381.2010.01027.X

Ng, LC., Mccormack, MD., Airey, JA., Singer, CA., Keller, PS., Shen, XM., & Hume, JR. (2009). TRPC1 and STIM1 mediate capacitative Ca2+ entry in mouse pulmonary arterial smooth muscle cells. *The Journal of Physiology*, *587*(Pt 11), 2429. https://doi.org/10.1113/JPHYSIOL.2009.172254

Nie, L., Wu, G., & Zhang, W. (2006). Correlation of mRNA Expression and Protein Abundance Affected by Multiple Sequence Features Related to Translational Efficiency in Desulfovibrio vulgaris: A Quantitative Analysis. Genetics, 174(4), 2229–2243. https://doi.org/10.1534/genetics.106.065862

Nilsson, ME., Vandenput, L., Tivesten, Å., Norlén, AK., Lagerquist, M.K., Windahl, SH., Börjesson, AE., Farman, HH., Poutanen, M., Benrick, A., Maliqueo, M., Stener-Victorin, E., Ryberg, H., & Ohlsson, C. (2015). Measurement of a Comprehensive Sex Steroid Profile in Rodent Serum by High-Sensitive Gas Chromatography-Tandem Mass Spectrometry. *Endocrinology*, *156*(7), 2492–2502. https://doi.org/10.1210/EN.2014-1890

Noma, A. (1983). ATP-regulated K+ channels in cardiac muscle. *Nature*, *305*(5930), 147–148. https://doi.org/10.1038/305147A0

Nordio, M., & Pajalich, R. (2013). Combined treatment with Myo-inositol and selenium ensures euthyroidism in subclinical hypothyroidism patients with autoimmune thyroiditis. *Journal of Thyroid Research*, *2013*. https://doi.org/10.1155/2013/424163

Norton, C. E., & Segal, S. S. (2018). Calcitonin gene-related peptide hyperpolarizes mouse pulmonary artery endothelial tubes through KATP channel activation. AJP Lung Cellular and Molecular Physiology, 315(2), L212–L226. https://doi.org/10.1152/ajplung.00044.2018

Nuedling, S., Karas, RH., Mendelsohn, ME., Katzenellenbogen, JA., Katzenellenbogen, BS., Meyer, R., Vetter, H., & Grohé, C. (2001). Activation of estrogen receptor beta is a prerequisite for estrogen-dependent upregulation of nitric oxide synthases in neonatal rat cardiac myocytes. *FEBS letters*, *502*(3), 103–108. https://doi.org/10.1016/S0014-5793(01)02675-8

Oceandy, D., Stanley, PJ., Cartwright, EJ., & Neyses, L. (2007). The regulatory function of plasma-membrane Ca(2+)-ATPase (PMCA) in the heart. *Biochemical Society transactions*, *35*(Pt 5), 927–930. https://doi.org/10.1042/BST0350927

Ohya, S., Sergeant, GP., Greenwood, IA., & Horowitz, B. (2003). Molecular variants of KCNQ channels expressed in murine portal vein myocytes: A role in delayed rectifier current. *Circulation Research*, *92*(9), 1016–1023. https://doi.org/10.1161/01.RES.0000070880.20955.F4

Ortega, R., Collado, A., Selles, F., Gonzalez-Navarro, H., Sanz, MJ., Real, JT., & Piqueras, L. (2019). SGLT-2 (Sodium-Glucose Cotransporter 2) Inhibition Reduces Ang II (Angiotensin II)–Induced Dissecting Abdominal Aortic Aneurysm in ApoE (Apolipoprotein E) Knockout Mice. *Arteriosclerosis, Thrombosis, and Vascular Biology*, *39*(8), 1614–1628. https://doi.org/10.1161/ATVBAHA.119.312659

Ostlund, RE., Seemayer, R., Gupta, S., Kimmel, R., Ostlund, EL., & Sherman, WR. (1996). A stereospecific myo-inositol/D-chiro-inositol transporter in HepG2 liver cells: Identification with D-chiro- [3-3H] inositol. *Journal of Biological Chemistry*, *271*(17), 10073–10078.

https://doi.org/10.1074/JBC.271.17.10073/ASSET/72F6EAB1-E3DB-4988-801A-835EB9BEAB79/MAIN.ASSETS/GR9.JPG

Ottolia, M., John, S., Hazan, A., & Goldhaber, JI. (2021). The Cardiac Na+-Ca2+ Exchanger: From Structure to Function. *Comprehensive Physiology*, *12*(1), 2681. https://doi.org/10.1002/CPHY.C200031

Pabbidi, MR., Kuppusamy, M., Didion, SP., Sanapureddy, P., Reed, JT., & Sontakke, SP. (2018). Sex differences in the vascular function and related mechanisms: role of 17β-estradiol. *American journal of physiology. Heart and circulatory physiology*, *315*(6), H1499–H1518. https://doi.org/10.1152/AJPHEART.00194.2018

Park, WS., Son, YK., Kim, N., Ko, JH., Kang, SH., Warda, M., Earm, YE., Jung, ID., Park, YM., & Han, J. (2007). Acute hypoxia induces vasodilation and increases coronary blood flow by activating inward rectifier K(+) channels. *Pflugers Archiv : European journal of physiology*, *454*(6), 1023–1030. https://doi.org/10.1007/S00424-007-0269-4

Pearson, LJ., Yandle, TG., Nicholls, MG., & Evans, JJ. (2008). Regulation of endothelin-1 release from human endothelial cells by sex steroids and angiotensin-II. *Peptides*, *29*(6), 1057–1061. https://doi.org/10.1016/j.peptides.2008.02.003

Perland, E., & Fredriksson, R. (2017). Classification Systems of Secondary Active Transporters. *Trends in Pharmacological Sciences*, *38*(3), 305–315. https://doi.org/10.1016/J.TIPS.2016.11.008

Pesch, B., Casjens, S., Woitalla, D., Dharmadhikari, S., Edmondson, DA., Zella, MA. S., Lehnert, M., Lotz, A., Herrmann, L., Muhlack, S., Kraus, P., Yeh, CL., Glaubitz, B., Schmidt-Wilcke, T., Gold, R., van Thriel, C., Brüning, T., Tönges, L., & Dydak, U. (2019). Impairment of Motor Function Correlates with Neurometabolite and Brain Iron Alterations in Parkinson's Disease. *Cells*, *8*(2), 96. https://doi.org/10.3390/CELLS8020096

Pessoa, TD., Campos, LCG., Carraro-Lacroix, L., Girardi, ACC., & Malnic, G. (2014). Functional role of glucose metabolism, osmotic stress, and sodium-glucose cotransporter isoform-mediated transport on Na+ /H+ exchanger isoform 3 activity in the renal proximal tubule. *Journal of the American Society*

of Nephrology, *25*(9), 2028–2039. https://doi.org/10.1681/ASN.2013060588/-/DCSUPPLEMENTAL

Pochynyuk, O., Tong, Q., Staruschenko, A., & Stockand, JD. (2007). Binding and direct activation of the epithelial Na+ channel (ENaC) by phosphatidylinositides. *The Journal of physiology*, *580*(Pt. 2), 365–372. https://doi.org/10.1113/JPHYSIOL.2006.127449

Poppe, R., Karbach, U., Gambaryan, S., Wiesinger, H., Lutzenburg, M., Kraemer, M., Witte, O. W., & Koepsell, H. (1997). Expression of the Na+-D-glucose cotransporter SGLT1 in neurons. *Journal of neurochemistry*, *69*(1), 84–94. https://doi.org/10.1046/J.1471-4159.1997.69010084.X

Pouleur, AC., Menghoum, N., Cumps, J., Marino, A., Badii, M., Lejeune, S., Legault, JT., Boucher, G., Gruson, D., Roy, C., Battault, S., Mahrouche, L., Pedneault-Gagnon, V., Charpentier, D., Furtos, A., Hussin, J., Rhainds, D., Tardif, JC., Bertrand, L., … Beauloye, C. (2024). Plasma myo-inositol elevation in heart failure: clinical implications and prognostic significance. Results from the BElgian and CAnadian MEtabolomics in HFpEF (BECAME-HF) research project. *eBioMedicine*, *107*. https://doi.org/10.1016/j.ebiom.2024.105264

Powell, DR., DaCosta, CM., Gay, J., Ding, ZM., Smith, M., Greer, J., Doree, D., Jeter-Jones, S., Mseeh, F., Rodriguez, LA., Harris, A., Buhring, L., Platt, KA., Vogel, P., Brommage, R., Shadoan, MK., Sands, AT., & Zambrowicz, B. (2013). Improved glycemic control in mice lacking Sglt1 and Sglt2. *American journal of physiology. Endocrinology and metabolism*, *304*(2). https://doi.org/10.1152/AJPENDO.00439.2012

Preda, A., Montecucco, F., Carbone, F., Camici, GG., Lüscher, TF., Kraler, S., & Liberale, L. (2024). SGLT2 inhibitors: from glucose-lowering to cardiovascular benefits. *Cardiovascular Research*, *120*(5), 443–460. https://doi.org/10.1093/CVR/CVAE047

Qiao, YN., He, WQ., Chen, CP., Zhang, CH., Zhao, W., Wang, P., Zhang, L., Wu, Y. Z., Yang, X., Peng, YJ., Gao, JM., Kamm, K. E., Stull, JT., & Zhu, MS. (2014). Myosin Phosphatase Target Subunit 1 (MYPT1) Regulates the Contraction and Relaxation of Vascular Smooth Muscle and Maintains Blood

Pressure. *The Journal of Biological Chemistry*, *289*(32), 22512. https://doi.org/10.1074/JBC.M113.525444

Quayle, JM., Bonev, AD., Brayden, JE., & Nelson, MT. (1994). Calcitonin gene-related peptide activated ATP-sensitive K+ currents in rabbit arterial smooth muscle via protein kinase A. *The Journal of Physiology*, *475*(1), 9. https://doi.org/10.1113/JPHYSIOL.1994.SP020045

Rahmoune, H., Thompson, PW., Ward, JM., Smith, CD., Hong, G., & Brown, J. (2005). Glucose transporters in human renal proximal tubular cells isolated from the urine of patients with non-insulin-dependent diabetes. *Diabetes*, *54*(12), 3427–3434. https://doi.org/10.2337/DIABETES.54.12.3427

Ralevic, V., Kendall, DA, Randall, MD., Zygmunt, PM., Movahed, P., & Högestätt, ED. (2000). Vanilloid receptors on capsaicin-sensitive sensory nerves mediate relaxation to methanandamide in the rat isolated mesenteric arterial bed and small mesenteric arteries. *British Journal of Pharmacology*, *130*(7), 1483. https://doi.org/10.1038/SJ.BJP.0703456

Ralston, E., & Ploug, T. (1996). GLUT4 in cultured skeletal myotubes is segregated from the transferrin receptor and stored in vesicles associated with TGN. Journal of Cell Science, 109(13), 2967–2978. https://doi.org/10.1242/jcs.109.13.2967

Rattan, S., Phillips, BR., & Maxwell, PJ. (2010). RhoA/Rho-Kinase: Pathophysiological and Therapeutic Implications in Gastrointestinal Smooth Muscle Tone and Relaxation. *Gastroenterology*, *138*(1), 13. https://doi.org/10.1053/J.GASTRO.2009.11.016

Ravera, S., Reyna-Neyra, A., Ferrandino, G., Amzel, LM., & Carrasco, N. (2017). The Sodium/Iodide Symporter (NIS): Molecular Physiology and Preclinical and Clinical Applications. *Annual review of physiology*, *79*, 261. https://doi.org/10.1146/ANNUREV-PHYSIOL-022516-034125

Reading, SA., Earley, S., Waldron, BJ., Welsh, DG., & Brayden, JE. (2005). TRPC3 mediates pyrimidine receptor-induced depolarization of cerebral arteries. *American journal of physiology. Heart and circulatory physiology*, *288*(5). https://doi.org/10.1152/AJPHEART.00861.2004

Rim, JS., Atta, MG., Dahl, SC., Berry, GT., Handler, JS., & Kwon, HM. (1998). Transcription of the Sodium/myo-Inositol Cotransporter Gene Is Regulated by Multiple Tonicity-responsive Enhancers Spread over 50 Kilobase Pairs in the 5′-Flanking Region. *The Journal of biological chemistry*, *273*(32), 20615. https://doi.org/10.1074/JBC.273.32.20615

Ripatti, S., Tikkanen, E., Orho-Melander, M., Havulinna, AS., Silander, K., Sharma, A., Guiducci, C., Perola, M., Jula, A., Sinisalo, J., Lokki, ML., Nieminen, MS., Melander, O., Salomaa, V., Peltonen, L., & Kathiresan, S. (2010). A multilocus genetic risk score for coronary heart disease: case-control and prospective cohort analyses. *Lancet*, *376*(9750), 1393. https://doi.org/10.1016/S0140-6736(10)61267-6

Robert, R., Norez, C., & Becq, F. (2005). Disruption of CFTR chloride channel alters mechanical properties and cAMP-dependent Cl- transport of mouse aortic smooth muscle cells. *The Journal of physiology*, *568*(Pt 2), 483–495. https://doi.org/10.1113/JPHYSIOL.2005.085019

Robert, R., Thoreau, V., Norez, C., Cantereau, A., Kitzis, A., Mettey, Y., Rogier, C., & Becq, F. (2004). Regulation of the cystic fibrosis transmembrane conductance regulator channel by beta-adrenergic agonists and vasoactive intestinal peptide in rat smooth muscle cells and its role in vasorelaxation. *The Journal of biological chemistry*, *279*(20), 21160–21168. https://doi.org/10.1074/JBC.M312199200

Robertson, BE., Schubert, R., Hescheler, J., & Nelson, MT. (1993). cGMP-dependent protein kinase activates Ca-activated K channels in cerebral artery smooth muscle cells. *The American journal of physiology*, *265*(1 Pt 1). https://doi.org/10.1152/AJPCELL.1993.265.1.C299

Robertson, Blair E., Bonev, AD., & Nelson, MT. (1996). Inward rectifier K+ currents in smooth muscle cells from rat coronary arteries: block by Mg2+, Ca2+, and Ba2+. *The American journal of physiology*, *271*(2 Pt 2). https://doi.org/10.1152/AJPHEART.1996.271.2.H696

Roberts-Thomson, KM., Parker, L., Betik, AC., Wadley, GD., Gatta, PAD., Marwick, TH., & Keske, MA. (2022). Oral and intravenous glucose administration elicit opposing microvascular blood flow responses in skeletal

muscle of healthy people: role of incretins. *The Journal of Physiology*, *600*(7), 1667. https://doi.org/10.1113/JP282428

Rodriguez-Menchaca, AA., Adney, SK., Tang, QY., Meng, XY., Rosenhouse-Dantsker, A., Cui, M., & Logothetis, DE. (2012). PIP_2 controls voltage-sensor movement and pore opening of Kv channels through the S4-S5 linker. *Proceedings of the National Academy of Sciences of the United States of America*, *109*(36), E2399–E2408. https://doi.org/10.1073/PNAS.1207901109

Roengrit, T., Sri-Amad, R., Huipao, N., Phababpha, S., & Prasertsri, P. (2023). Impact of Fasting Blood Glucose Levels on Blood Pressure Parameters among Older Adults with Prediabetes. *The Scientific World Journal*, *2023*(1), 1778371. https://doi.org/10.1155/2023/1778371

Roepke, TK., Kanda, VA., Purtell, K., King, EC., Lerner, DJ., & Abbott, GW. (2011). KCNE2 forms potassium channels with KCNA3 and KCNQ1 in the choroid plexus epithelium. *The FASEB Journal*, *25*(12), 4264. https://doi.org/10.1096/FJ.11-187609

Rogue, PJ., Humbert, JP., Meyer, A., Freyermuth, S., Krady, MM., & Malviya, AN. (1998). cAMP-dependent protein kinase phosphorylates and activates nuclear Ca2+-ATPase. *Proceedings of the National Academy of Sciences of the United States of America*, *95*(16), 9178. https://doi.org/10.1073/PNAS.95.16.9178

Sabolić, I., Škarica, M., Gorboulev, V., Ljubojević, M., Balen, D., Herak-Kramberger, CM., & Koepsell, H. (2006). Rat renal glucose transporter SGLT1 exhibits zonal distribution and androgen-dependent gender differences. *American Journal of Physiology - Renal Physiology*, *290*(4), 913–926. https://doi.org/10.1152/AJPRENAL.00270.2005/ASSET/IMAGES/LARGE/ZH20040642490013.JPEG

Sabolić, I., Vrhovac, I., Eror, DB., Gerasimova, M., Rose, M., Breljak, D., Ljubojevic, M., Brzica, H., Sebastiani, A., Thal, SC., Sauvant, C., Kipp, H., Vallon, V., & Koepsell, H. (2012). Expression of Na+-d-glucose cotransporter SGLT2 in rodents is kidney-specific and exhibits sex and species differences. *American Journal of Physiology - Cell Physiology*, *302*(8), C1174. https://doi.org/10.1152/AJPCELL.00450.2011

Sakmann, B., & Trube, G. (1984). Conductance properties of single inwardly rectifying potassium channels in ventricular cells from guinea-pig heart. *The Journal of Physiology*, *347*(1), 641. https://doi.org/10.1113/JPHYSIOL.1984.SP015088

Sala-Rabanal, M., Ghezzi, C., Hirayama, BA., Kepe, V., Liu, J., Barrio, JR., & Wright, EM. (2018). Intestinal absorption of glucose in mice as determined by positron emission tomography. *The Journal of Physiology*, *596*(13), 2473–2489. https://doi.org/10.1113/JP275934

Sala-Rabanal, M., Hirayama, BA., Ghezzi, C., Liu, J., Huang, SC., Kepe, V., Koepsell, H., Yu, A., Powell, DR., Thorens, B., Wright, EM., & Barrio, JR. (2016). Revisiting the physiological roles of SGLTs and GLUTs using positron emission tomography in mice. *The Journal of physiology*, *594*(15), 4425–4438. https://doi.org/10.1113/JP271904

Saleh, SN., Albert, AP., Peppiatt-Wildman, CM., & Large, WA. (2008). Diverse properties of store-operated TRPC channels activated by protein kinase C in vascular myocytes. *The Journal of Physiology*, *586*(Pt 10), 2463. https://doi.org/10.1113/JPHYSIOL.2008.152157

Samanta, A., Hughes, TET., & Moiseenkova-Bell, VY. (2018). Transient Receptor Potential (TRP) Channels. *Sub-cellular biochemistry*, *87*, 141. https://doi.org/10.1007/978-981-10-7757-9_6

Sampson, LJ., Davies, LM., Barrett-Jolley, R., Standen, NB., & Dart, C. (2007). Angiotensin II-activated protein kinase C targets caveolae to inhibit aortic ATP-sensitive potassium channels. *Cardiovascular Research*, *76*(1), 61–70. https://doi.org/10.1016/J.CARDIORES.2007.05.020/2/76-1-61-FIG6.GIF

Sancho, M., & Kyle, BD. (2021). The Large-Conductance, Calcium-Activated Potassium Channel: A Big Key Regulator of Cell Physiology. *Frontiers in Physiology*, *12*, 750615. https://doi.org/10.3389/FPHYS.2021.750615

Sangill, M., & Pedersen, EB. (2006). The Effect of Glucose Added to the Dialysis Fluid on Blood Pressure, Blood Glucose, and Quality of Life in Hemodialysis Patients: A Placebo-Controlled Crossover Study. *American Journal of Kidney Diseases*, *47*(4), 636–643. https://doi.org/10.1053/J.AJKD.2006.01.007

Saponaro, C., Mühlemann, M., Acosta-Montalvo, A., Piron, A., Gmyr, V., Delalleau, N., Moerman, E., Thévenet, J., Pasquetti, G., Coddeville, A., Cnop, M., Kerr-Conte, J., Staels, B., Pattou, F., & Bonner, C. (2020). Interindividual Heterogeneity of SGLT2 Expression and Function in Human Pancreatic Islets. *Diabetes*, *69*(5), 902–914. https://doi.org/10.2337/DB19-0888

Sarma, GN., Moody, IS., Ilouz, R., Phan, RH., Sankaran, B., Hall, RA., & Taylor, SS. (2015). D-AKAP2:PKA RII:PDZK1 ternary complex structure: Insights from the nucleation of a polyvalent scaffold. *Protein Science*, *24*(1), 105–116. https://doi.org/10.1002/PRO.2593

Sasseville, LJ., Longpré, JP., Wallendorff, B., & Lapointe, JY. (2014). The transport mechanism of the human sodium/myo-inositol transporter 2 (SMIT2/SGLT6), a member of the LeuT structural family. *American Journal of Physiology - Cell Physiology*, *307*(5), C431. https://doi.org/10.1152/AJPCELL.00054.2014

Sausbier, M., Arntz, C., Bucurenciu, I., Zhao, H., Zhou, XB., Sausbier, U., Feil, S., Kamm, S., Essin, K., Sailer, CA., Abdullah, U., Krippeit-Drews, P., Feil, R., Hoffmann, F., Knaus, HG., Kenyon, C., Shipston, MJ., Storm, JF., Neuhuber, W., Ruth, P. (2005). Elevated Blood Pressure Linked to Primary Hyperaldosteronism and Impaired Vasodilation in BK Channel–Deficient Mice. *Circulation*, *112*(1), 60–68. https://doi.org/10.1161/01.CIR.0000156448.74296.FE

Scafoglio, C., Hirayama, BA., Kepe, V., Liu, J., Ghezzi, C., Satyamurthy, N., Moatamed, NA., Huang, J., Koepsell, H., Barrio, J. R., & Wright, E. M. (2015). Functional expression of sodium-glucose transporters in cancer. *Proceedings of the National Academy of Sciences of the United States of America*, *112*(30), E4111–E4119. https://doi.org/10.1073/PNAS.1511698112/-/DCSUPPLEMENTAL

Schneider, S. (2015). Inositol transport proteins. *FEBS Letters*, *589*(10), 1049–1058. https://doi.org/10.1016/J.FEBSLET.2015.03.012

Sędzikowska, A., & Szablewski, L. (2021). Human Glucose Transporters in Renal Glucose Homeostasis. *International Journal of Molecular Sciences*, *22*(24). https://doi.org/10.3390/IJMS222413522

Seman, L., Macha, S., Nehmiz, G., Simons, G., Ren, B., Pinnetti, S., Woerle, HJ., & Dugi, K. (2013). Empagliflozin (BI 10773), a Potent and Selective SGLT2 Inhibitor, Induces Dose-Dependent Glucosuria in Healthy Subjects. *Clinical Pharmacology in Drug Development*, *2*(2), 152–161. https://doi.org/10.1002/CPDD.16

Seo, MS., Jung, HS., An, JR., Kang, M., Heo, R., Li, H., Han, ET., Yang, SR., Cho, EH., Bae, YM., & Park, WS. (2020). Empagliflozin dilates the rabbit aorta by activating PKG and voltage-dependent K+ channels. *Toxicology and Applied Pharmacology*, *403*, 115153. https://doi.org/10.1016/J.TAAP.2020.115153

Shah, AJ., Vorla, M., Jafri, SH., & Kalra, DK. (2024). Sglt2 Inhibitors In Women And Cardiovascular Outcomes - Meta-analysis Of Sex Differences In Eleven Randomized Clinical Trials. *Journal of Cardiac Failure*, *30*(1), 252. https://doi.org/10.1016/J.CARDFAIL.2023.10.320

Shekhar, YC., Anand, IS., Sarma, R., Ferrari, R., Wahi, PL. and Poole-Wilson, PA. (1991). Effects of prolonged infusion of human alpha calcitonin gene-related peptide on hemodynamics, renal blood flow and hormone levels in congestive heart failure. *The American Journal of Cardiology*, 67(8), pp.732–736. doi:https://doi.org/10.1016/0002-9149(91)90531-o.

Sheng, J., Ella, S., Davis, MJ., Hill, MA., & Braun, AP. (2009). Openers of SKCa and IKCa channels enhance agonist-evoked endothelial nitric oxide synthesis and arteriolar vasodilation. *The FASEB Journal*, *23*(4), 1138. https://doi.org/10.1096/FJ.08-120451

Shiraki, H., Kawasaki, H., Tezuka, S., Nakatsuma, A., & Kurosaki, Y. (2000). Endogenous calcitonin gene-related peptide (CGRP) mediates adrenergic-dependent vasodilation induced by nicotine in mesenteric resistance arteries of the rat. *British Journal of Pharmacology*, *130*(5), 1083. https://doi.org/10.1038/SJ.BJP.0703376

Solaro, RJ. (2000). Myosin Light Chain Phosphatase. *Circulation Research*, *87*(3), 173–175. https://doi.org/10.1161/01.RES.87.3.173

Soldovieri, MV., Miceli, F., & Taglialatela, M. (2011). Driving with no brakes: Molecular pathophysiology of Kv7 potassium channels. *Physiology*, *26*(5), 365–376.

https://doi.org/10.1152/PHYSIOL.00009.2011/ASSET/IMAGES/LARGE/PHY0051100760003.JPEG

Stott, JB., Barrese, V., & Greenwood, IA. (2016). Kv7 Channel Activation Underpins EPAC-Dependent Relaxations of Rat Arteries. *Arteriosclerosis, Thrombosis, and Vascular Biology*, *36*(12), 2404–2411. https://doi.org/10.1161/ATVBAHA.116.308517

Stott, JB., Barrese, V., Jepps, TA., Leighton, EV., & Greenwood, IA. (2015). Contribution of Kv7 channels to natriuretic peptide mediated vasodilation in normal and hypertensive rats. *Hypertension*, *65*(3), 676–682. https://doi.org/10.1161/HYPERTENSIONAHA.114.04373

Stott, JB., Barrese, V., Suresh, M., Masoodi, S., & Greenwood, IA. (2018). Investigating the role of Gβγ in Kv7 dependent relaxations of the rat vasculature. *Arteriosclerosis, thrombosis, and vascular biology*, *38*(9), 2091. https://doi.org/10.1161/ATVBAHA.118.311360

Stott, JB., Povstyan, OV., Carr, G., Barrese, V., & Greenwood, IA. (2015). G-protein βγ subunits are positive regulators of Kv7.4 and native vascular Kv7 channel activity. *Proceedings of the National Academy of Sciences of the United States of America*, *112*(20), 6497–6502. https://doi.org/10.1073/PNAS.1418605112/-/DCSUPPLEMENTAL

Sukhanov, S., Higashi, Y., Yoshida, T., Mummidi, S., Aroor, AR., Jeffrey Russell, J., Bender, SB., DeMarco, VG., & Chandrasekar, B. (2021). The SGLT2 inhibitor Empagliflozin attenuates interleukin-17A-induced human aortic smooth muscle cell proliferation and migration by targeting TRAF3IP2/ROS/NLRP3/Caspase-1-dependent IL-1β and IL-18 secretion. *Cellular signalling*, *77*, 109825. https://doi.org/10.1016/J.CELLSIG.2020.109825

Sun, D., Zhou, T., Heianza, Y., Li, X., Fan, M., Fonseca, VA., & QiL. (2019). Type 2 Diabetes and Hypertension: A Study on Bidirectional Causality. *Circulation Research*, *124*(6), 930–937. https://doi.org/10.1161/CIRCRESAHA.118.314487/SUPPL_FILE/CIRCRES_CIRCRES-2018-314487D_SUPP1.PDF

Søgaard, R., Ljungstrøm, T., Pedersen, KA., Olesen, SP., & Skaaning Jensen, BO. (2001). KCNQ4 channels expressed in mammalian cells: Functional characteristics and pharmacology. *American Journal of Physiology - Cell Physiology*, *280*(4 49-4). https://doi.org/10.1152/AJPCELL.2001.280.4.C859/ASSET/IMAGES/LARGE/H00410379007.JPEG

Saadat, S., Noureddini, M., Mahjoubin-Tehran, M., Nazemi, S., Shojaie, L., Aschner, M., Maleki, B., Abbasi-kolli, M., Rajabi Moghadam, H., Alani, B., & Mirzaei, H. (2021). Pivotal Role of TGF-β/Smad Signaling in Cardiac Fibrosis: Non-coding RNAs as Effectual Players. *Frontiers in Cardiovascular Medicine*, *7*. https://doi.org/10.3389/FCVM.2020.588347/FULL

Sheykhzade, M & Berg, C. (2001). Mechanism of CGRP-induced relaxation in rat intramural coronary arteries. British Journal of Pharmacology, 132(6), 1235–1246. https://doi.org/10.1038/sj.bjp.0703936

Taguchi, K., Kaneko, K., & Kubo, T. (2000). Protein kinase C modulates Ca2+-activated K+ channels in cultured rat mesenteric artery smooth muscle cells. *Biological & pharmaceutical bulletin*, *23*(12), 1450–1454. https://doi.org/10.1248/BPB.23.1450

Takahashi, H., Nomiyama, T., Terawaki, Y., Horikawa, T., Kawanami, T., Hamaguchi, Y., Tanaka, T., Motonaga, R., Fukuda, T., Tanabe, M., & Yanase, T. (2019). Combined treatment with DPP-4 inhibitor linagliptin and SGLT2 inhibitor empagliflozin attenuates neointima formation after vascular injury in diabetic mice. *Biochemistry and Biophysics Reports*, *18*. https://doi.org/10.1016/J.BBREP.2019.100640

Tan, SY., Mei Wong, JL., Sim, YJ., Wong, SS., Mohamed Elhassan, SA., Tan, SH., Ling Lim, GP., Rong Tay, NW., Annan, NC., Bhattamisra, SK., & Candasamy, M. (2019). Type 1 and 2 diabetes mellitus: A review on current treatment approach and gene therapy as potential intervention. *Diabetes & Metabolic Syndrome: Clinical Research & Reviews*, *13*(1), 364–372. https://doi.org/10.1016/J.DSX.2018.10.008

Tano, JY., & Gollasch, M. (2014). Calcium-activated potassium channels in ischemia reperfusion: A brief update. *Frontiers in Physiology*, *5*(OCT), 109935. https://doi.org/10.3389/FPHYS.2014.00381/BIBTEX

Taquet H, Komajda M, Grenier O., Belas F., Landault C, Carayon A, Lechat P, Grosgogeat Y, & Legrand JC. (1992). Plasma calcitonin gene-related peptide decreases in chronic congestive heart failure. European Heart Journal, 13(11), 1473–1476. https://doi.org/10.1093/oxfordjournals.eurheartj.a060088

Tennant, BP., Cui, Y., Tinker, A., & Clapp, LH. (2006). Functional expression of inward rectifier potassium channels in cultured human pulmonary smooth muscle cells: evidence for a major role of Kir2.4 subunits. *The Journal of membrane biology*, *213*(1), 19. https://doi.org/10.1007/S00232-006-0037-Y

Thakore, P., & Earley, S. (2019). Transient Receptor Potential Channels and Endothelial Cell Calcium Signaling. *Comprehensive Physiology*, *9*(3), 1249. https://doi.org/10.1002/CPHY.C180034

Thomas-Gatewood, C., Neeb, ZP., Bulley, S., Adebiyi, A., Bannister, JP., Leo, MD., & Jaggar, JH. (2011). Tmem16a channels generate Ca 2+-activated Cl - currents in cerebral artery smooth muscle cells. *American Journal of Physiology - Heart and Circulatory Physiology*, *301*(5), 1819–1827. https://doi.org/10.1152/AJPHEART.00404.2011/ASSET/IMAGES/LARGE/ZH40111101140005.JPEG

Tian, C., Zhu, R., Zhu, L., Qiu, T., Cao, Z., & Kang, T. (2014). Potassium Channels: Structures, Diseases, and Modulators. *Chemical Biology & Drug Design*, *83*(1), 1–26. https://doi.org/10.1111/CBDD.12237

Tian, J., Zhang, M., Suo, M., Liu, D., Wang, X., Liu, M., Pan, J., Jin, T., & An, F. (2021). Dapagliflozin alleviates cardiac fibrosis through suppressing EndMT and fibroblast activation via AMPKα/TGF-β/Smad signalling in type 2 diabetic rats. *Journal of Cellular and Molecular Medicine*, *25*(16), 7642. https://doi.org/10.1111/JCMM.16601

Tian, L., Coghill, LS., McClafferty, H., MacDonald, SHF., Antoni, FA., Ruth, P., Knaus, HG., & Shipston, MJ. (2004). Distinct stoichiometry of BKCa channel tetramer phosphorylation specifies channel activation and inhibition by cAMP-dependent protein kinase. *Proceedings of the National Academy of Sciences*

of the United States of America, *101*(32), 11897–11902. https://doi.org/10.1073/PNAS.0402590101

Timraz, SBH., Farhat, IAH., Alhussein, G., Christoforou, N., & Teo, JCM. (2016). In-depth evaluation of commercially available human vascular smooth muscle cells phenotype: Implications for vascular tissue engineering. *Experimental cell research*, *343*(2), 168–176. https://doi.org/10.1016/J.YEXCR.2016.04.004

Toda, N., Ayajiki, K., Toda, H., Hatano, Y., & Okamura, T. (1992). Mechanism underlying mannitol-induced relaxation in isolated monkey cerebral arteries. *The American journal of physiology*, *262*(3 Pt 2). https://doi.org/10.1152/AJPHEART.1992.262.3.H897

Tong, EHY., Guo, JJ., Huang, AL., Liu, H., Hu, CD., Chung, SSM., & Ko, BCB. (2006). Regulation of Nucleocytoplasmic Trafficking of Transcription Factor OREBP/TonEBP/NFAT5. *Journal of Biological Chemistry*, *281*(33), 23870–23879. https://doi.org/10.1074/JBC.M602556200

Touyz, RM., Alves-Lopes, R., Rios, FJ., Camargo, LL., Anagnostopoulou, A., Arner, A., & Montezano, AC. (2018). Vascular smooth muscle contraction in hypertension. *Cardiovascular Research*, *114*(4), 529. https://doi.org/10.1093/CVR/CVY023

Uthman, L., Baartscheer, A., Bleijlevens, B., Schumacher, CA., Fiolet, JWT., Koeman, A., Jancev, M., Hollmann, MW., Weber, NC., Coronel, R., & Zuurbier, CJ. (2018). Class effects of SGLT2 inhibitors in mouse cardiomyocytes and hearts: inhibition of Na+/H+ exchanger, lowering of cytosolic Na+ and vasodilation. *Diabetologia*, *61*(3), 722. https://doi.org/10.1007/S00125-017-4509-7

Uthman, L., Homayr, A., Juni, RP., Spin, EL., Kerindongo, R., Boomsma, M., Hollmanna Benedikt Preckel, MW., Koolwijk, P., Van Hinsbergh, VWM., Zuurbier, CJ., Albrecht, M., & Weber, NC. (2019). Empagliflozin and dapagliflozin reduce ROS generation and restore no bioavailability in tumor necrosis factor α-stimulated human coronary arterial endothelial cells. *Cellular Physiology & Biochemistry*, *53*(5), 865–886. https://doi.org/10.33594/000000178

Vadlapudi, AD., Vadlapatla, RK., & Mitra, AK. (2012). Sodium Dependent Multivitamin Transporter (SMVT): A Potential Target for Drug Delivery. *Current drug targets*, *13*(7), 994. https://doi.org/10.2174/138945012800675650

Vaithianathan, T., Bukiya, A., Liu, J., Liu, P., Asuncion-Chin, M., Fan, Z., & Dopico, A. (2008). Direct regulation of BK channels by phosphatidylinositol 4,5-bisphosphate as a novel signaling pathway. *The Journal of general physiology*, *132*(1), 13–28. https://doi.org/10.1085/JGP.200709913

Vallon, V., Platt, KA., Cunard, R., Schroth, J., Whaley, J., Thomson, SC., Koepsell, H., & Rieg, T. (2011). SGLT2 mediates glucose reabsorption in the early proximal tubule. *Journal of the American Society of Nephrology : JASN*, *22*(1), 104–112. https://doi.org/10.1681/ASN.2010030246

Van Den Heuvel, LP., Assink, K., Willemsen, M., & Monnens, L. (2002). Autosomal recessive renal glucosuria attributable to a mutation in the sodium glucose cotransporter (SGLT2). *Human Genetics*, *111*(6), 544–547. https://doi.org/10.1007/S00439-002-0820-5/METRICS

Van Der Horst, J., Manville, RW., Hayes, K., Thomsen, MB., Abbott, GW., & Jepps, TA. (2020). Acetaminophen (Paracetamol) metabolites induce vasodilation and hypotension by activating Kv7 potassium channels directly and indirectly. *Arteriosclerosis, thrombosis, and vascular biology*, *40*(5), 1207. https://doi.org/10.1161/ATVBAHA.120.313997

Van Steenbergen, A., Balteau, M., Ginion, A., Ferté, L., Battault, S., Ravenstein, CDM. De, Balligand, JL., Daskalopoulos, EP., Gilon, P., Despa, F., Despa, S., Vanoverschelde, JL., Horman, S., Koepsell, H., Berry, G., Hue, L., Bertrand, L., & Beauloye, C. (2017). Sodium-myoinositol cotransporter-1, SMIT1, mediates the production of reactive oxygen species induced by hyperglycemia in the heart. *Scientific Reports 2017 7:1*, *7*(1), 1–14. https://doi.org/10.1038/srep41166

Vrhovac, I., Eror, DB., Klessen, D., Burger, C., Breljak, D., Kraus, O., Radović, N., Jadrijević, S., Aleksic, I., Walles, T., Sauvant, C., Sabolić, I., & Koepsell, H. (2015). Localizations of Na(+)-D-glucose cotransporters SGLT1 and SGLT2 in human kidney and of SGLT1 in human small intestine, liver, lung, and heart.

Pflugers Archiv : European journal of physiology, *467*(9), 1881–1898. https://doi.org/10.1007/S00424-014-1619-7

Vries, T, Sieneke Labruijere, Rivera-Mancilla, E., Garrelds, IM., René de Vries, Schutter, D., van, Poyner, DR., Ladds, G., Danser, J., & MaassenVanDenBrink, A. (2024). Intracellular pathways of calcitonin gene-related peptide-induced relaxation of human coronary arteries: A key role for Gβγ subunit instead of cAMP. British Journal of Pharmacology, 181(15), 2478–2491. https://doi.org/10.1111/bph.16372

Waldegger, S., Barth, P., Raber, G., & Lang, F. (1997). Cloning and characterization of a putative human serine/threonine protein kinase transcriptionally modified during anisotonic and isotonic alterations of cell volume. *Proceedings of the National Academy of Sciences of the United States of America*, *94*(9), 4440–4445. https://doi.org/10.1073/PNAS.94.9.4440

Walker, RL., Hume, JR., & Horowitz, B. (2001). Differential expression and alternative splicing of TRP channel genes in smooth muscles. *American journal of physiology. Cell physiology*, *280*(5). https://doi.org/10.1152/AJPCELL.2001.280.5.C1184

Wang, GX., McCrudden, C., Dai, YP., Horowitz, B., Hume, JR., & Yamboliev, IA. (2004). Hypotonic activation of volume-sensitive outwardly rectifying chloride channels in cultured PASMCs is modulated by SGK. *American Journal of Physiology - Heart and Circulatory Physiology*, *287*(2 56-2), 533–544. https://doi.org/10.1152/AJPHEART.00228.2003/ASSET/IMAGES/LARGE/ZH40080432290007.JPEG

Wang, HS., Pan, Z., Shi, W., Brown, BS., Wymore, RS., Cohen, IS., Dixon, JE., & McKinnon, D. (1998). KCNQ2 and KCNQ3 potassium channel subunits: Molecular correlates of the M-channel. *Science*, *282*(5395), 1890–1893. https://doi.org/10.1126/SCIENCE.282.5395.1890/ASSET/A3A4D147-037F-4706-86C3-C314B3A1F102/ASSETS/GRAPHIC/SE4887055004.JPEG

Wang, Q., & Michalak, M. (2020). Calsequestrin. Structure, function, and evolution. *Cell Calcium*, *90*, 102242. https://doi.org/10.1016/J.CECA.2020.102242

Wang, Y., Yang, L., Mao, L., Zhang, L., Zhu, Y., Xu, Y., Cheng, Y., Sun, R., Zhang, Y., Ke, J., & Zhao, D. (2022). SGLT2 inhibition restrains thyroid cancer growth via G1/S phase transition arrest and apoptosis mediated by DNA damage response signaling pathways. *Cancer Cell International*, *22*(1). https://doi.org/10.1186/S12935-022-02496-Z

Webb, RC. (2003). Smooth muscle contraction and relaxation. *American Journal of Physiology - Advances in Physiology Education*, *27*(1–4), 201–206. https://doi.org/10.1152/ADVAN.00025.2003

Wehbe, N., Nasser, SA., Al-Dhaheri, Y., Iratni, R., Bitto, A., El-Yazbi, AF., Badran, A., Kobeissy, F., Baydoun, E., & Eid, AH. (2020). EPAC in Vascular Smooth Muscle Cells. *International Journal of Molecular Sciences*, *21*(14), 1–14. https://doi.org/10.3390/IJMS21145160

Wellman, GC., Nathan, DJ., Saundry, CM., Perez, G., Bonev, AD., Penar, PL., Tranmer, BI., & Nelson, MT. (2002). Ca2+ sparks and their function in human cerebral arteries. *Stroke*, *33*(3), 802–808. https://doi.org/10.1161/HS0302.104089

Wen, X., Peng, Y., Gao, M., Zhu, Y., Zhu, Y., Yu, F., Zhou, T., Shao, J., Feng, L., & Ma, X. (2022). Endothelial Transient Receptor Potential Canonical Channel Regulates Angiogenesis and Promotes Recovery After Myocardial Infarction. *Journal of the American Heart Association*, *11*(6). https://doi.org/10.1161/JAHA.121.023678

Wenceslau, CF., McCarthy, CG., Earley, S., England, SK., Filosa, JA., Goulopoulou, S., Gutterman, DD., Isakson, BE., Kanagy, NL., Martinez-Lemus, LA., Sonkusare, SK., Thakore, P., Trask, AJ., Watts, SW., & Clinton Webb, R. (2021). Guidelines in Cardiovascular Research: Guidelines for the measurement of vascular function and structure in isolated arteries and veins. *American Journal of Physiology - Heart and Circulatory Physiology*, *321*(1), H77. https://doi.org/10.1152/AJPHEART.01021.2020

Wheeler, DC., Stefánsson, BV., Jongs, N., Chertow, GM., Greene, T., Hou, FF., McMurray, JJV., Correa-Rotter, R., Rossing, P., Toto, RD., Sjöström, C. D., Langkilde, AM., & Heerspink, HJ.L. (2021). Effects of dapagliflozin on major adverse kidney and cardiovascular events in patients with diabetic and non-

diabetic chronic kidney disease: a prespecified analysis from the DAPA-CKD trial. *The lancet. Diabetes & endocrinology*, *9*(1), 22–31. https://doi.org/10.1016/S2213-8587(20)30369-7

White, RE., Han, G., Maunz, M., Dimitropoulou, C., El-Mowafy, AM., Barlow, RS., Catravas, JD., Snead, C., Carrier, GO., Zhu, S., & Yu, X. (2002). Endothelium-independent effect of estrogen on Ca(2+)-activated K(+) channels in human coronary artery smooth muscle cells. *Cardiovascular research*, *53*(3), 650–661. https://doi.org/10.1016/S0008-6363(01)00428-X

Wiese, TJ., Matsushita, K., Lowe, WL., Stokes, JB., & Yorek, MA. (1996). Localization and regulation of renal Na+/myo-inositol cotransporter in diabetic rats. *Kidney international*, *50*(4), 1202–1211. https://doi.org/10.1038/KI.1996.429

Williams, DM., & Evans, M. (2020). Are SGLT-2 Inhibitors the Future of Heart Failure Treatment? The EMPEROR-Preserved and EMPEROR-Reduced Trials. *Diabetes Therapy*, *11*(9), 1925. https://doi.org/10.1007/S13300-020-00889-9

Wilson, AJ., Jabr, RI., & Clapp, LH. (2000). Calcium modulation of vascular smooth muscle ATP-sensitive K(+) channels: role of protein phosphatase-2B. *Circulation research*, *87*(11), 1019–1025. https://doi.org/10.1161/01.RES.87.11.1019

Wiviott, SD., Raz, I., Bonaca, MP., Mosenzon, O., Kato, ET., Cahn, A., Silverman, MG., Bansilal, S., Bhatt, DL., Leiter, LA., McGuire, DK., Wilding, JP., Gause-Nilsson, IA., Langkilde, AM., Johansson, PA., & Sabatine, MS. (2018). The design and rationale for the Dapagliflozin Effect on Cardiovascular Events (DECLARE)–TIMI 58 Trial. *American Heart Journal*, *200*, 83–89. https://doi.org/10.1016/J.AHJ.2018.01.012

Wooldridge, AA., MacDonald, JA., Erdodi, F., Ma, C., Borman, MA., Hartshorne, DJ., & Haystead, TAJ. (2004). Smooth muscle phosphatase is regulated in Vivo by exclusion of phosphorylation of threonine 696 of MYPT1 by phosphorylation of serine 695 in response to cyclic nucleotides. *Journal of Biological Chemistry*, *279*(33), 34496–34504. https://doi.org/10.1074/jbc.M405957200

Worley, PF., Zeng, W., Huang, GN., Yuan, JP., Kim, JY., Lee, MG., & Muallem, S. (2007). TRPC channels as STIM1-regulated store-operated channels. *Cell calcium*, *42*(2), 205–211. https://doi.org/10.1016/J.CECA.2007.03.004

Wright, EM. (2021). SGLT2 Inhibitors: Physiology and Pharmacology. *Kidney360*, *2*(12), 2027–2037. https://doi.org/10.34067/KID.0002772021

Wright, EM., Ghezzi, C., & Loo, DDF. (2017). Novel and Unexpected Functions of SGLTs. *Physiology*, *32*(6), 435. https://doi.org/10.1152/PHYSIOL.00021.2017

Wright, EM., Loo, DDF., & Hirayama, BA. (2011). Biology of human sodium glucose transporters. *Physiological reviews*, *91*(2), 733–794. https://doi.org/10.1152/PHYSREV.00055.2009

Wright, SH. (2004). Generation of resting membrane potential. *American Journal of Physiology - Advances in Physiology Education*, *28*(4), 139–142. https://doi.org/10.1152/ADVAN.00029.2004/ASSET/IMAGES/LARGE/ZU10040402360001.JPEG

Wärntges, S., Friedrich, B., Henke, G., Duranton, C., Lang, P., Waldegger, S., Meyermann, R., Kuhl, D., Speckmann, E., Obermüller, N., Witzgall, R., Mack, A., Wagner, H., Wagner, C., Bröer, S., & Lang, F. (2001). Cerebral localization and regulation of the cell volume-sensitive serum- and glucocorticoid-dependent kinase SGK1. *Pflügers Archiv - European Journal of Physiology 2001 443:4*, *443*(4), 617–624. https://doi.org/10.1007/S00424-001-0737-1

Xi, Q., Adebiyi, A., Zhao, G., Chapman, KE., Waters, CM., Hassid, A., & Jaggar, JH. (2008). IP3 Constricts Cerebral Arteries via IP3 Receptor–Mediated TRPC3 Channel Activation and Independently of Sarcoplasmic Reticulum Ca2+ Release. *Circulation research*, *102*(9), 1118. https://doi.org/10.1161/CIRCRESAHA.108.173948

Xie, LH., John, SA., Ribalet, B., & Weiss, JN. (2007). Activation of inwardly rectifying potassium (Kir) channels by phosphatidylinositol-4,5-bisphosphate (PIP2): interaction with other regulatory ligands. *Progress in biophysics and molecular biology*, *94*(3), 320–335. https://doi.org/10.1016/J.PBIOMOLBIO.2006.04.001

Xu, B., Li, S., Kang, B., Fan, S., Chen, C., Li, W., Chen, J., He, Z., Tang, F., & Zhou, J. (2023). Role of SLC5A2 polymorphisms and effects of genetic polymorphism on sodium glucose cotransporter 2 inhibitorsinhibitor response. *Molecular biology reports*, *50*(11), 9637–9647. https://doi.org/10.1007/S11033-023-08836-0

Xu, C., Lu, Y., Tang, G., & Wang, R. (1999). Expression of voltage-dependent K+ channel genes in mesenteric artery smooth muscle cells. *American Journal of Physiology - Gastrointestinal and Liver Physiology*, *277*(5 40-5). https://doi.org/10.1152/AJPGI.1999.277.5.G1055/ASSET/IMAGES/LARGE/AGIJ31113006Y.JPEG

Yamauchi, A., Sugiura, T., Kitamura, H., Matsuoka, Y., Imai, E., & Hori, M. (1998). Expression of the Na+/myo-inositol cotransporter in the juxtaglomerular region. *Kidney international. Supplement*, *67*(67). https://doi.org/10.1046/J.1523-1755.1998.06741.X

Yamazaki, J., Duan, D., Janiak, R., Kuenzli, K., Horowitz, B., & Hume, JR. (1998). Functional and molecular expression of volume-regulated chloride channels in canine vascular smooth muscle cells. *The Journal of physiology*, *507 (Pt 3)*(Pt 3), 729–736. https://doi.org/10.1111/J.1469-7793.1998.729BS.X

Yamazaki, Y., Harada, S., & Tokuyama, S. (2012). Post-ischemic hyperglycemia exacerbates the development of cerebral ischemic neuronal damage through the cerebral sodium-glucose transporter. *Brain Research*, *1489*, 113–120. https://doi.org/10.1016/J.BRAINRES.2012.10.020

Yamazaki, Y., Harada, S., Wada, T., Yoshida, S., & Tokuyama, S. (2016). Sodium transport through the cerebral sodium–glucose transporter exacerbates neuron damage during cerebral ischaemia. *Journal of Pharmacy and Pharmacology*, *68*(7), 922–931. https://doi.org/10.1111/JPHP.12571

Yamazaki, Y., Ogihara, S., Harada, S., & Tokuyama, S. (2015). Activation of cerebral sodium-glucose transporter type 1 function mediated by post-ischemic hyperglycemia exacerbates the development of cerebral ischemia. *Neuroscience*, *310*, 674–685. https://doi.org/10.1016/J.NEUROSCIENCE.2015.10.005

Yan, J., & Aldrich, RW. (2012). BK potassium channel modulation by leucine-rich repeat-containing proteins. *Proceedings of the National Academy of Sciences of the United States of America*, *109*(20), 7917–7922. https://doi.org/10.1073/PNAS.1205435109/-/DCSUPPLEMENTAL

Yang, Q., Underwood, MJ., & He, GW. (2012). Calcium-activated potassium channels in vasculature in response to ischemia-reperfusion. *Journal of Cardiovascular Pharmacology*, *59*(2), 109–115. https://doi.org/10.1097/FJC.0B013E318210FB4B

Yang, Y., Shi, Y., Guo, S., Zhang, S., Cui, N., Shi, W., Zhu, D., & Jiang, C. (2008). PKA-dependent activation of the vascular smooth muscle isoform of KATP channels by vasoactive intestinal polypeptide and its effect on relaxation of the mesenteric resistance artery. *Biochimica et biophysica acta*, *1778*(1), 88. https://doi.org/10.1016/J.BBAMEM.2007.08.030

Yeung, SYM., Pucovský, V., Moffatt, JD., Saldanha, L., Schwake, M., Ohya, S., & Greenwood, IA. (2007). Molecular expression and pharmacological identification of a role for Kv7 channels in murine vascular reactivity. *British Journal of Pharmacology*, *151*(6), 758. https://doi.org/10.1038/SJ.BJP.0707284

Yeung, Shuk Yin M., Lange, W., Schwake, M., & Greenwood, I. A. (2008). Expression profile and characterisation of a truncated KCNQ5 splice variant. *Biochemical and Biophysical Research Communications*, *371*(4), 741–746. https://doi.org/10.1016/j.bbrc.2008.04.129

You, G., Lee, W. Sen, Barros, EJG., Kanai, Y., Huo, TL., Khawaja, S., Wells, RG., Nigam, SK., & Hediger, MA. (1995). Molecular characteristics of Na(+)-coupled glucose transporters in adult and embryonic rat kidney. *The Journal of biological chemistry*, *270*(49), 29365–29371. https://doi.org/10.1074/JBC.270.49.29365

Yu, AS., Hirayama, BA., Timbol, G., Liu, J., Diez-Sampedro, A., Kepe, V., Satyamurthy, N., Huang, SC., Wright, EM., & Barrio, JR. (2013). Regional distribution of SGLT activity in rat brain in vivo. *American journal of physiology. Cell physiology*, *304*(3). https://doi.org/10.1152/AJPCELL.00317.2012

Yu, L., Flynn, AN., Turner, JR., & Buret, AG. (2005). SGLT-1-mediated glucose uptake protects intestinal epithelial cells against LPS-induced apoptosis and barrier defects: a novel cellular rescue mechanism? *The FASEB Journal*, *19*(13), 1822–1835. https://doi.org/10.1096/FJ.05-4226COM

Yu, Linda., Turner, JR., & Buret, AG. (2006). LPS/CD14 activation triggers SGLT-1-mediated glucose uptake and cell rescue in intestinal epithelial cells via early apoptotic signals upstream of caspase-3. *Experimental Cell Research*, *312*(17), 3276–3286. https://doi.org/10.1016/J.YEXCR.2006.06.023

Yu, X., Ma, H., Barman, SA., Liu, AT., Sellers, M., Stallone, JN., Prossnitz, ER., White, RE., & Han, G. (2011). Activation of G protein-coupled estrogen receptor induces endothelium-independent relaxation of coronary artery smooth muscle. *American Journal of Physiology - Endocrinology and Metabolism*, *301*(5), E882. https://doi.org/10.1152/AJPENDO.00037.2011

Yu, X., Zhang, Q., Zhao, Y., Schwarz, BJ., Stallone, JN., Heaps, CL., & Han, G. (2017). Activation of G protein-coupled estrogen receptor 1 induces coronary artery relaxation via Epac/Rap1-mediated inhibition of RhoA/Rho kinase pathway in parallel with PKA. *Plos one*, *12*(3), e0173085–e0173085. https://doi.org/10.1371/JOURNAL.PONE.0173085

Yuan, JP., Zeng, W., Huang, GN., Worley, PF., & Muallem, S. (2007). STIM1 heteromultimerizes TRPC channels to determine their function as store-operated channels. *Nature cell biology*, *9*(6), 636. https://doi.org/10.1038/NCB1590

Zannad, F., Ferreira, JP., Pocock, SJ., Anker, SD., Butler, J., Filippatos, G., Brueckmann, M., Ofstad, AP., Pfarr, E., Jamal, W., & Packer, M. (2020). SGLT2 inhibitors in patients with heart failure with reduced ejection fraction: a meta-analysis of the EMPEROR-Reduced and DAPA-HF trials. *Lancet (London, England)*, *396*(10254), 819–829. https://doi.org/10.1016/S0140-6736(20)31824-9

Zaydman, MA., & Cui, J. (2014). PIP2 regulation of KCNQ channels: biophysical and molecular mechanisms for lipid modulation of voltage-dependent gating. *Frontiers in physiology*, *5*. https://doi.org/10.3389/FPHYS.2014.00195

Zelniker, TA., Bonaca, MP., Furtado, RHM., Mosenzon, O., Kuder, JF., Murphy, SA., Bhatt, DL., Leiter, LA., McGuire, DK., Wilding, JPH., Budaj, A., Kiss, RG., Padilla, F., Gause-Nilsson, I., Langkilde, AM., Raz, I., Sabatine, MS., & Wiviott, SD. (2020). Effect of Dapagliflozin on Atrial Fibrillation in Patients With Type 2 Diabetes Mellitus. *Circulation*, 1227–1234. https://doi.org/10.1161/CIRCULATIONAHA.119.044183

Zeuthen, T., Gorraitz, E., Her, K., Wright, EM., & Loo, DDF. (2016). Structural and functional significance of water permeation through cotransporters. *Proceedings of the National Academy of Sciences of the United States of America*, *113*(44), E6887–E6894. https://doi.org/10.1073/PNAS.1613744113

Zhang, M., Ma, Y., Ye, X., Zhang, N., Pan, L., & Wang, B. (2023). TRP (transient receptor potential) ion channel family: structures, biological functions and therapeutic interventions for diseases. *Signal Transduction and Targeted Therapy 2023 8:1*, *8*(1), 1–38. https://doi.org/10.1038/s41392-023-01464-x

Zhang, Y., Lin, X., Chu, Y., Chen, X., Du, H., Zhang, H., Xu, C., Xie, H., Ruan, Q., Lin, J., Liu, J., Zeng, J., Ma, K., & Chai, D. (2021). Dapagliflozin: a sodium–glucose cotransporter 2 inhibitor, attenuates angiotensin II-induced cardiac fibrotic remodeling by regulating TGFβ1/Smad signaling. *Cardiovascular Diabetology*, *20*(1), 121. https://doi.org/10.1186/S12933-021-01312-8

Zhang, YP., Ye, LL., Yuan, H., & Duan, DD. (2021). CFTR plays an important role in the regulation of vascular resistance and high-fructose/salt-diet induced hypertension in mice. *Journal of Cystic Fibrosis*, *20*(3), 516–524. https://doi.org/10.1016/j.jcf.2020.11.014

Zhao, Y., Gao, P., Sun, F., Li, Q., Chen, J., Yu, H., Li, L., Wei, X., He, H., Lu, Z., Wei, X., Wang, B., Cui, Y., Xiong, S., Shang, Q., Xu, A., Huang, Y., Liu, D., & Zhu, Z. (2016). Sodium Intake Regulates Glucose Homeostasis through the PPARδ/Adiponectin-Mediated SGLT2 Pathway. *Cell Metabolism*, *23*(4), 699–711. https://doi.org/10.1016/J.CMET.2016.02.019/ATTACHMENT/4766A9A8-C2FC-4E70-839D-9AD7078CFBCD/MMC2.PDF

Zhou, JG., Ren, JL., Qiu, QY., He, H., & Guan, YY. (2005). Regulation of intracellular Cl- concentration through volume-regulated ClC-3 chloride

channels in A10 vascular smooth muscle cells. *The Journal of biological chemistry*, *280*(8), 7301–7308. https://doi.org/10.1074/JBC.M412813200

Zhou, L., Cryan, EV., D'Andrea, MR., Belkowski, S., Conway, BR., & Demarest, KT. (2003a). Human cardiomyocytes express high level of Na+/glucose cotransporter 1 (SGLT1). *Journal of Cellular Biochemistry*, *90*(2), 339–346. https://doi.org/10.1002/JCB.10631

Zhou, L., Cryan, EV., D'Andrea, MR., Belkowski, S., Conway, BR., & Demarest, KT. (2003b). Human cardiomyocytes express high level of Na+/glucose cotransporter 1 (SGLT1). *Journal of Cellular Biochemistry*, *90*(2), 339–346. https://doi.org/10.1002/JCB.10631

Zhao, FQ., McFadden, TB., Wall, EH., Dong, B., & Zheng, YC. (2005). Cloning and Expression of Bovine Sodium/Glucose Cotransporter SGLT2. Journal of Dairy Science, 88(8), 2738–2748. https://doi.org/10.3168/jds.s0022-0302(05)72953-2

Zimdahl, H., Haupt, A., Brendel, M., Bour, L., Machicao, F., Salsali, A., Broedl, UC., Woerle, HJ., Häring, HU., & Staiger, H. (2017). Influence of common polymorphisms in the SLC5A2 gene on metabolic traits in subjects at increased risk of diabetes and on response to empagliflozin treatment in patients with diabetes. *Pharmacogenetics and genomics*, *27*(4), 135–142. https://doi.org/10.1097/FPC.0000000000000268

Zinman, B., Wanner, C., Lachin, J., Fitchett, D., Bluhmki, E., Hantel, S., Mattheus, M., Devins, T., Johansen, O., Woerle, H., Broedl, U., & Inzucchi, S. (2015). Empagliflozin, Cardiovascular Outcomes, and Mortality in Type 2 Diabetes. *The New England journal of medicine*, *373*(22), 17–18. https://doi.org/10.1056/NEJMOA1504720

Zuurbier, CJ., Baartscheer, A., Schumacher, CA., Fiolet, JWT., & Coronel, R. (2021). Sodium-glucose co-transporter 2 inhibitor empagliflozin inhibits the cardiac Na+/H+ exchanger 1: persistent inhibition under various experimental conditions. *Cardiovascular Research*, *117*(14), 2699–2701. https://doi.org/10.1093/CVR/CVAB129

Chapter 8: Appendices

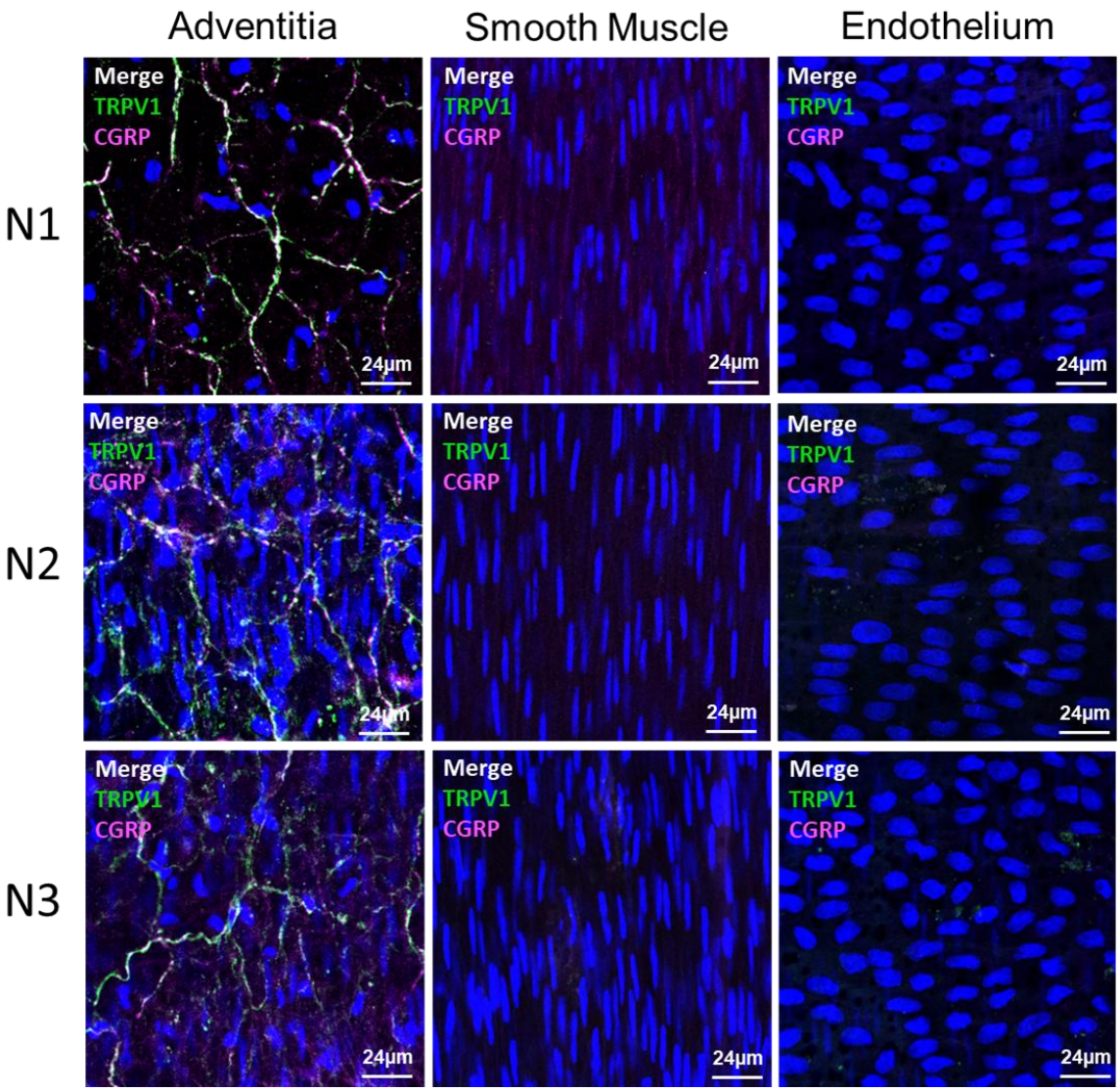


Figure 8.1: Representative labelling for TRPV1 (Green) and CGRP (magenta) in mesenteric arteries, showing all three representative repeats.

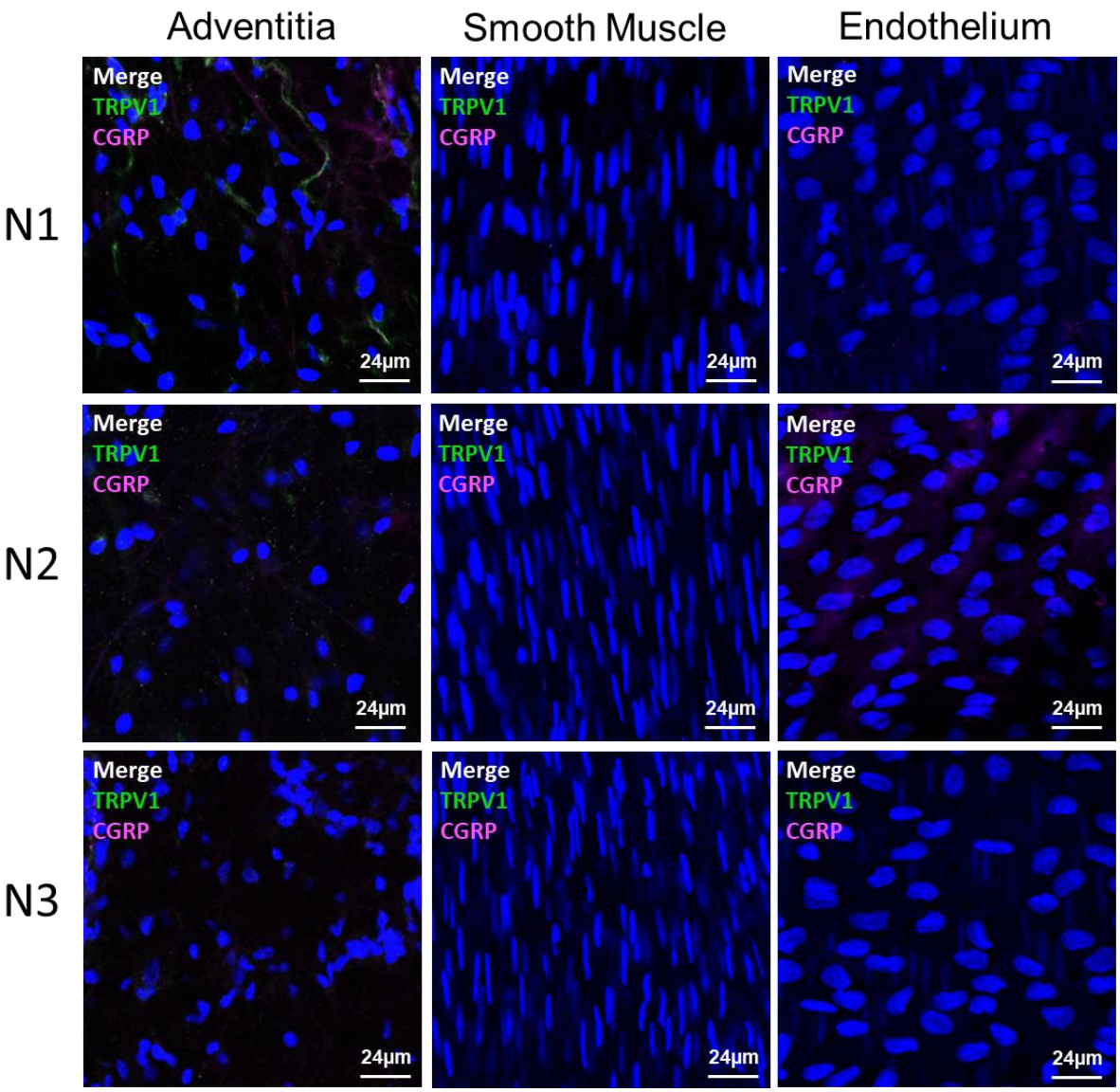


Figure 8.2: Representative labelling for TRPV1 (Green) and CGRP (magenta) in renal arteries, showing all three representative repeats.

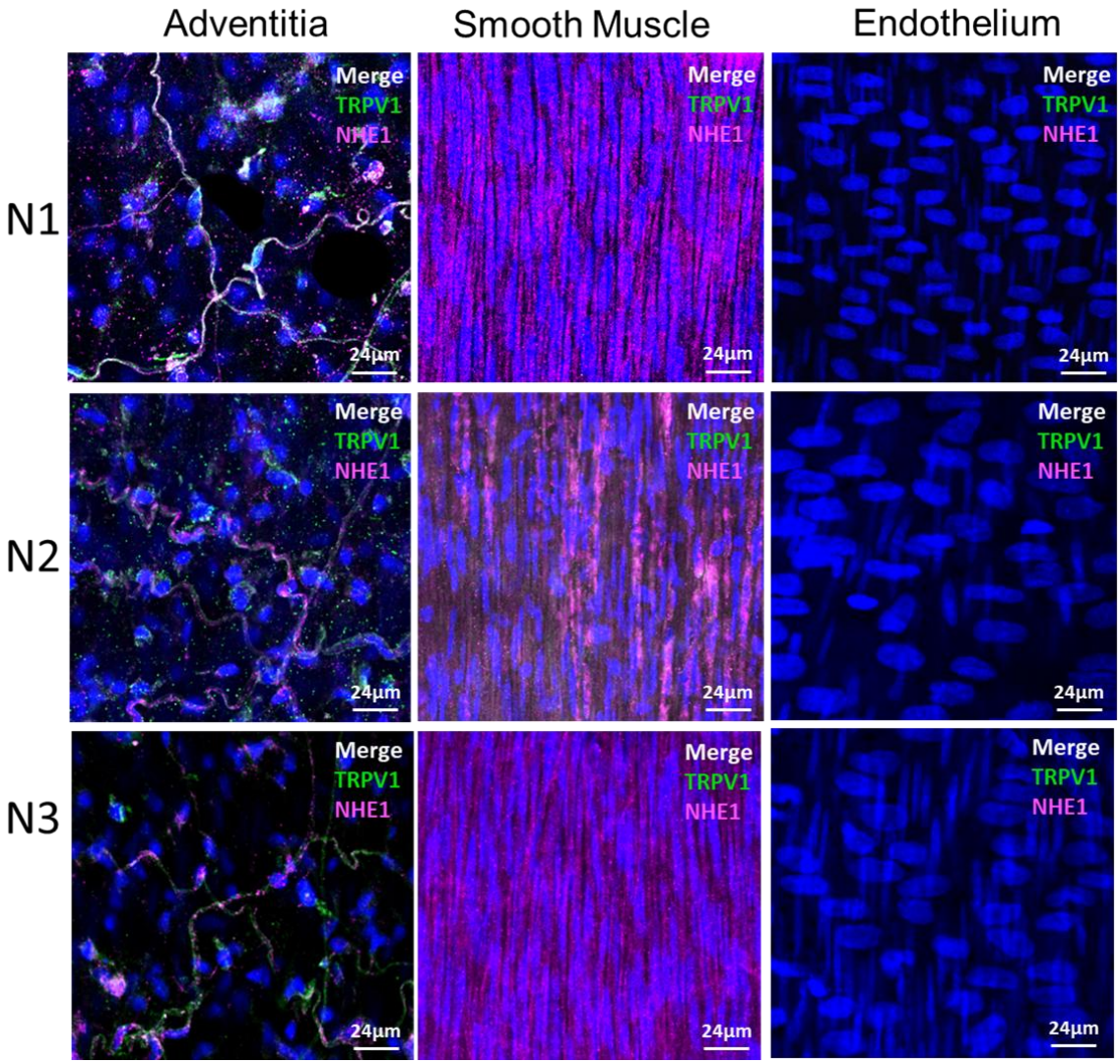


Figure 8.3: Representative labelling for TRPV1 (Green) and NHE1 (magenta) in mesenteric arteries, showing all three representative repeats.

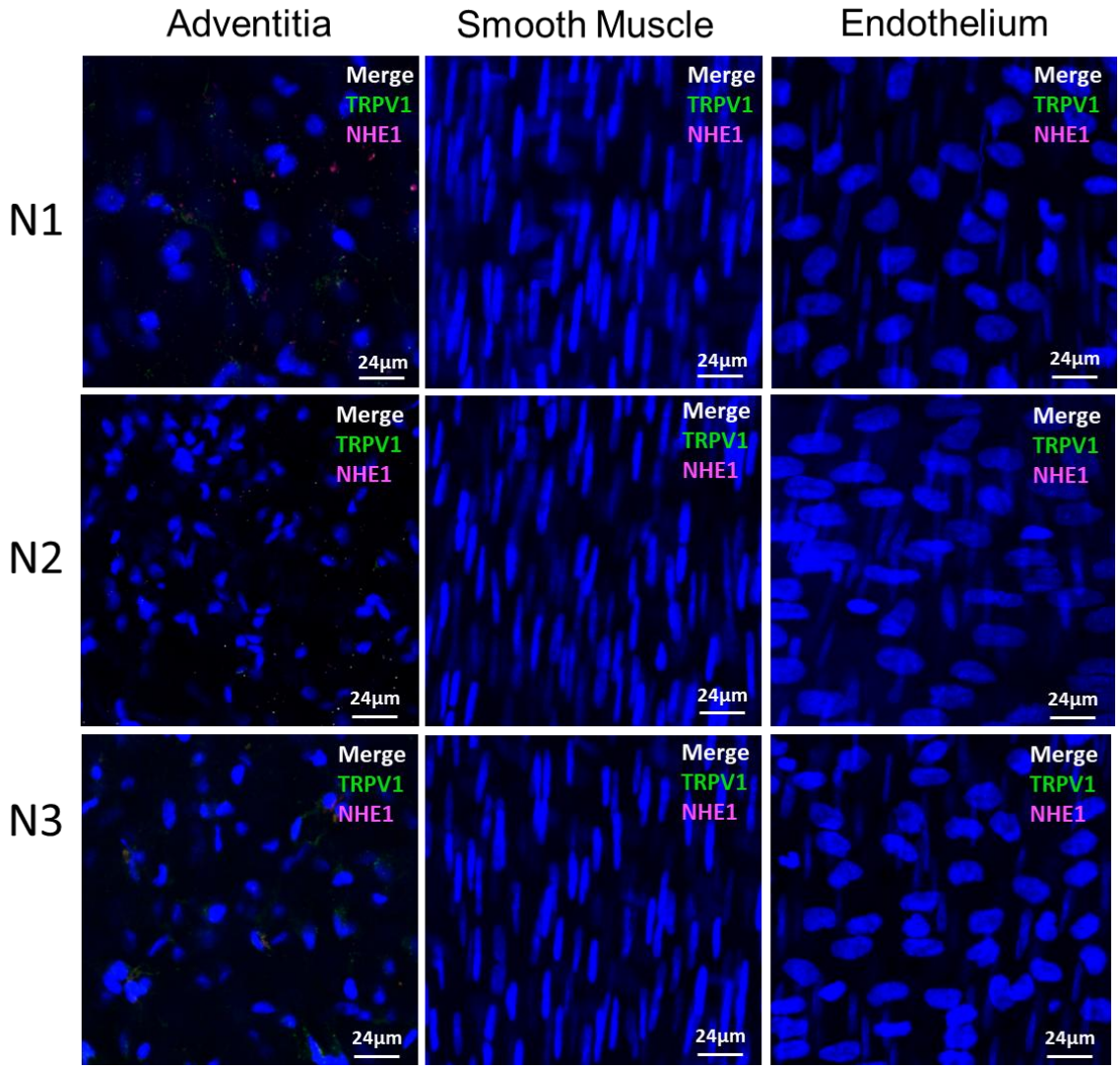


Figure 8.4: Representative labelling for TRPV1 (Green) and NHE1 (magenta) in renal arteries, showing all three representative repeats.

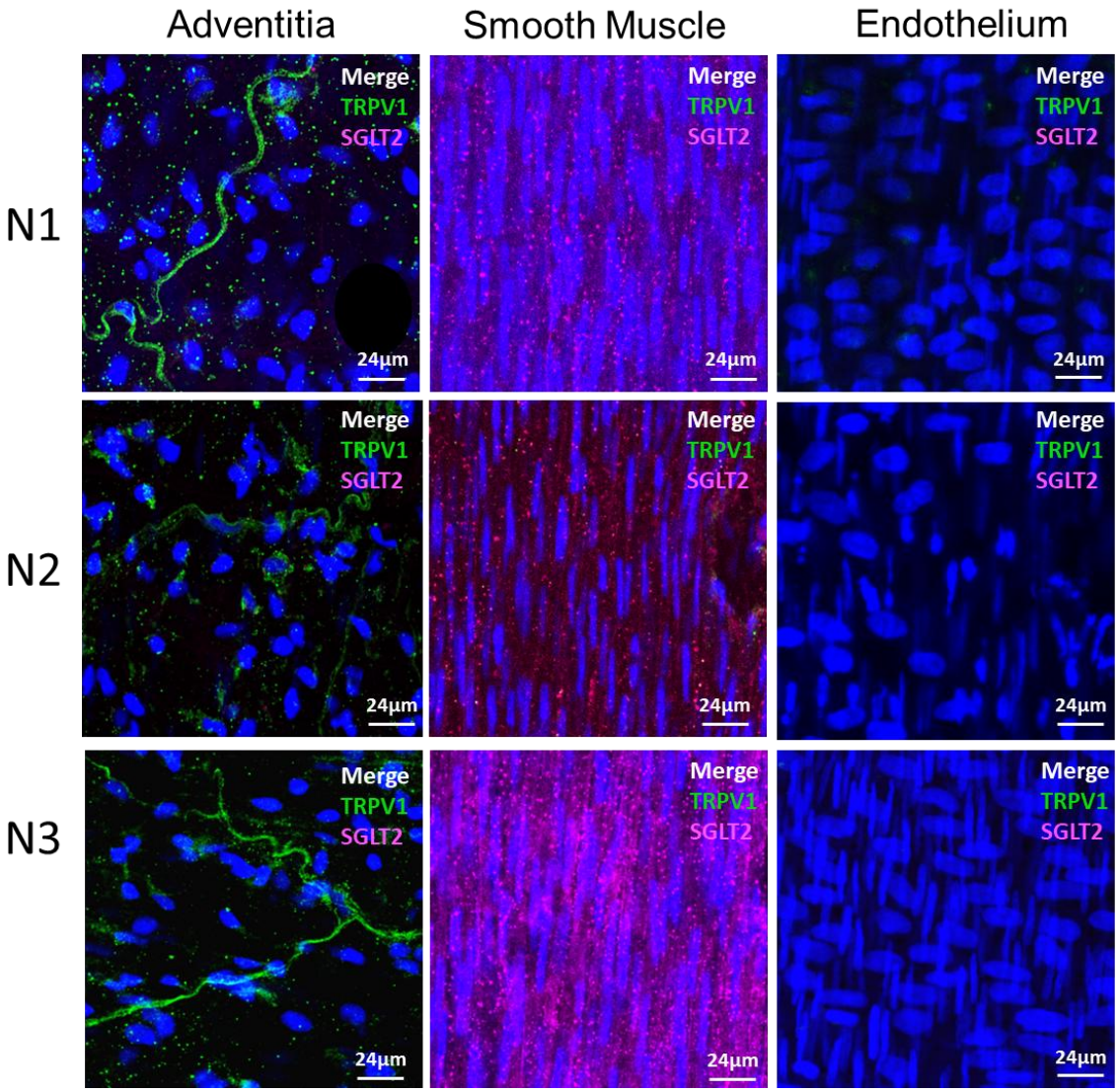


Figure 8.5: Representative labelling for TRPV1 (Green) and SGLT2 (magenta) in mesenteric arteries, showing all three representative repeats.

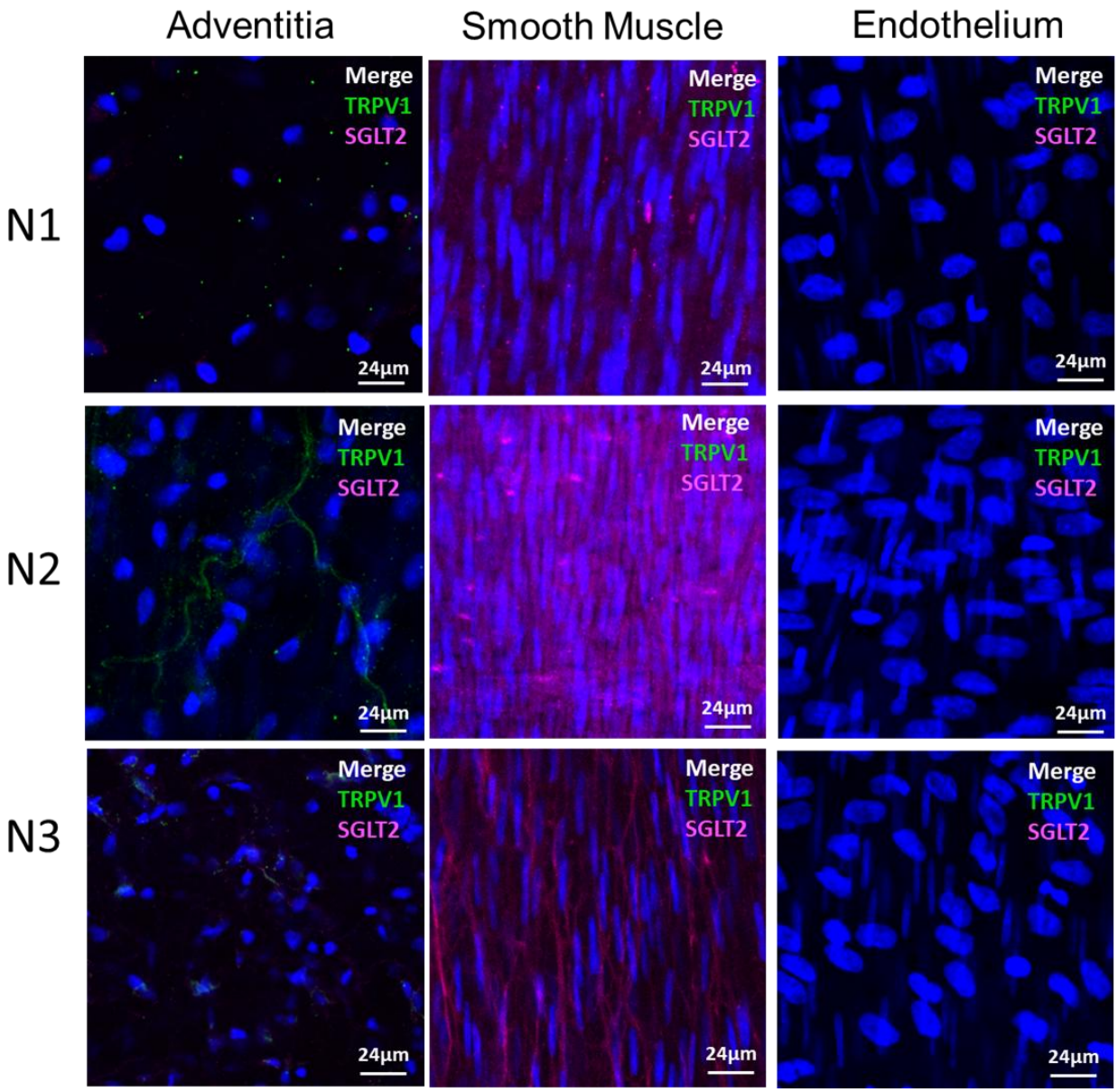


Figure 8.6: Representative labelling for TRPV1 (Green) and SGLT2 (magenta) in renal arteries, showing all three representative repeats.

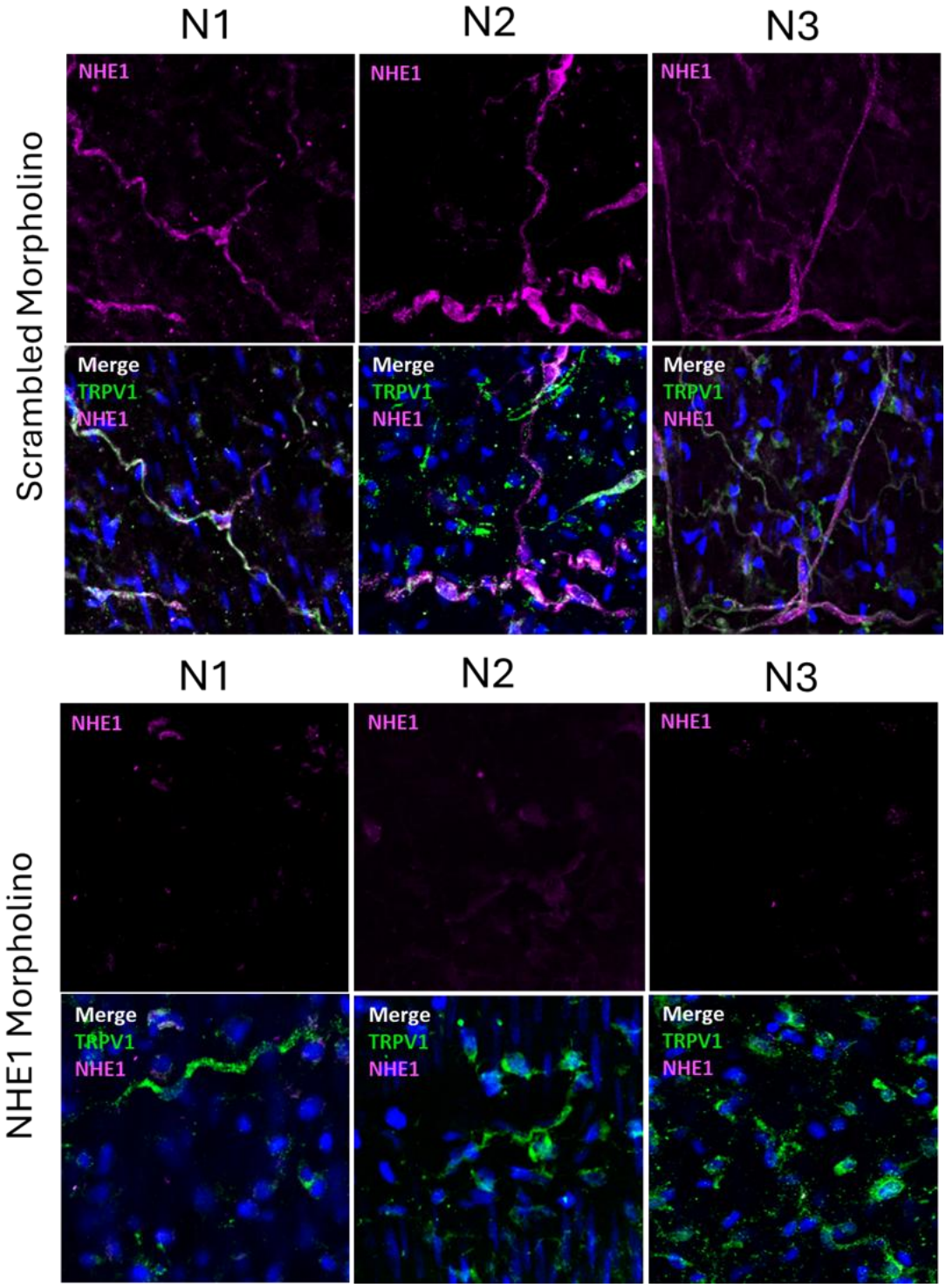


Figure 8.7: Representative labelling for TRPV1 (green) and NHE1 (magenta) in the adventitia of whole mesenteric arteries transfected with scrambled morpholino (Top) and NHE1 targeted morpholino (Bottom), showing all three representative repeats.

ESC European Society of Cardiology

Cardiovascular Research (2024) **120**, 1811–1824
https://doi.org/10.1093/cvr/cvae156

Crucial role for sensory nerves and Na/H exchanger inhibition in dapagliflozin- and empagliflozin-induced arterial relaxation

Elizabeth A. Forrester[1], Miguel Benítez-Angeles[2], Kaitlyn E. Redford[3], Tamara Rosenbaum[2], Geoffrey W. Abbott[3], Vincenzo Barrese [4], Kim Dora[5], Anthony P. Albert[1], Johs Dannesboe[6], Isabelle Salles-Crawley[1], Thomas A. Jepps[6], and Iain A. Greenwood [1]*

[1]Vascular Biology Section, Molecular & Clinical Sciences Research Institute, St George's University, Cranmer Terrace, London SW17 ORE, UK; [2]I Instituto de Fisiología Celular, Universidad Nacional Autónoma de México, Mexico City, Mexico; [3]Bioelectricity Lab, Department of Physiology & Biophysics, School of Medicine, University of California, Irvine, USA; [4]Department of Neuroscience, Reproductive Sciences and Dentistry, University of Naples Federico II, Naples, Italy; [5]Department of Pharmacology, Oxford University, Oxford, UK; and [6]Biomedical Sciences, Panum Institute, University of Copenhagen, Copenhagen, Denmark

Received 19 March 2024; revised 6 June 2024; accepted 5 July 2024; online publish-ahead-of-print 26 July 2024

Time of primary review: 37 days

Aims Sodium/glucose transporter 2 (SGLT2 or SLC5A2) inhibitors lower blood glucose and are also approved treatments for heart failure independent of raised glucose. Various studies have showed that SGLT2 inhibitors relax arteries, but the underlying mechanisms are poorly understood and responses variable across arterial beds. We speculated that SGLT2 inhibitor-mediated arterial relaxation is dependent upon calcitonin gene-related peptide (CGRP) released from sensory nerves independent of glucose transport.

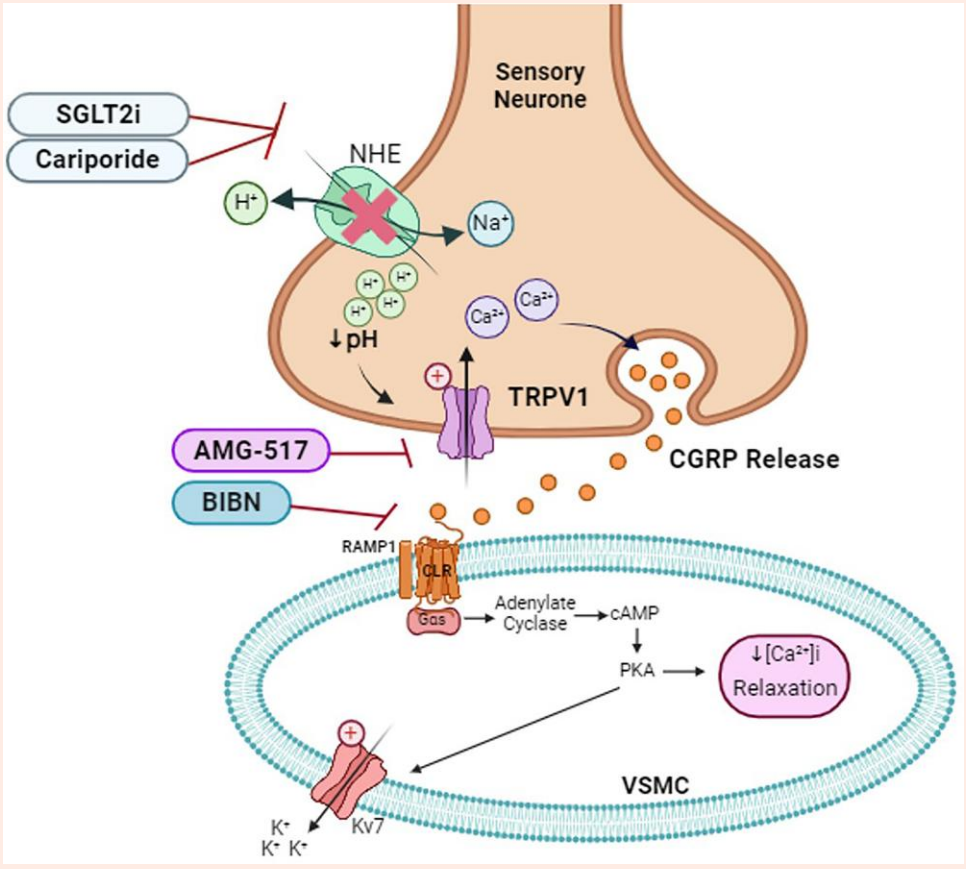
Methods and results The functional effects of SGLT1 and 2 inhibitors (mizagliflozin, dapagliflozin, and empagliflozin) and the sodium/hydrogen exchanger 1 (NHE1) blocker cariporide were determined on pre-contracted resistance arteries (mesenteric and cardiac septal arteries) as well as main renal conduit arteries from male Wistar rats using wire myography. SGLT2, CGRP, TRPV1, and NHE1 expression was determined by western blot and immunohistochemistry. Kv7.4/5/KCNE4 and TRPV1 currents were measured in the presence and absence of dapagliflozin and empagliflozin. All SGLT inhibitors (1–100 μM) and cariporide (30 μM) relaxed mesenteric arteries but had negligible effect on renal or septal arteries. Immunohistochemistry with TRPV1 and CGRP antibodies revealed a dense innervation of sensory nerves in mesenteric arteries that were absent in renal and septal arteries. Consistent with a greater sensory nerve component, the TRPV1 agonist capsaicin relaxed mesenteric arteries more effectively than renal or septal arteries. In mesenteric arteries, relaxations to dapagliflozin, empagliflozin, and cariporide were attenuated by the CGRP receptor antagonist BIBN-4096, depletion of sensory nerves with capsaicin, and blockade of TRPV1 or Kv7 channels. Neither dapagliflozin nor empagliflozin activated heterologously expressed TRPV1 channels or Kv7 channels directly. Sensory nerves also expressed NHE1 but not SGLT2 and cariporide pre-application as well as knockdown of NHE1 by translation stop morpholinos prevented the relaxant response to SGLT2 inhibitors.

Conclusion SGLT2 inhibitors relax mesenteric arteries by promoting the release of CGRP from sensory nerves in a NHE1-dependent manner.

Downloaded from https://academic.oup.com/cardiovascres/article/120/14/1811/7721236 by guest on 10 January 2025

* Corresponding author. Tel: +442077252857, E-mail: grenwood@sgul.ac.uk
© The Author(s) 2024. Published by Oxford University Press on behalf of the European Society of Cardiology.
This is an Open Access article distributed under the terms of the Creative Commons Attribution License (https://creativecommons.org/licenses/by/4.0/), which permits unrestricted reuse, distribution, and reproduction in any medium, provided the original work is properly cited.

Graphical Abstract



Pathway of SGLT2 inhibitor-induced relaxation in mesenteric arteries. SGLT2 inhibitors act on the sodium/hydrogen exchanger (NHE) to induce vasorelaxation. H, hydrogen; Na, sodium; Ca^{2+}, calcium; CGRP, calcitonin gene-related peptide; TRPV1, transient receptor potential vanilloid 1; CLR, calcitonin receptor-like receptor; RAMP1, receptor activity-modifying protein 1; cGMP, cyclic guanosine monophosphate; PKA, protein kinase A; Kv7, voltage-gated potassium channel.

Keywords Sodium/glucose transporter 2 • Sodium/hydrogen exchanger • Calcitonin-gene related peptide • Sensory nerves • Vasodilatation

1. Introduction

Inhibitors of sodium-dependent glucose transporter 2 (SGLT2 encoded by *SLC5A2*), such as dapagliflozin or empagliflozin,[1,2] lower blood glucose levels through increased urinary excretion of glucose.[3] The UK National Institute for Health and Care Excellence also recommend SGLT2 inhibitors for treatment of heart failure with reduced ejection fraction and chronic kidney disease independent of raised blood glucose.[3–5] In addition to decreased cardiac fluid retention, reduced reactive oxygen species generation, and lessened fibrosis (summarized in Preda *et al.*[3]), the cardioprotective effect of SGLT2 inhibitors has been linked to a reduction in blood pressure (~4 mmHg). Still, the mechanism underlying this effect is not known.[6] Some of the initial effects may be due to a decrease in circulatory volume due to increased natriuresis, but SGLT2 inhibitors still lower blood pressure at low glomerular filtration rates.[6] The main non-natriuretic mechanism is the relaxation of arterial smooth muscle and the associated reduction in peripheral resistance. Previous *ex vivo* studies showed that empagliflozin and dapagliflozin relaxed rabbit aortic rings, rat mesenteric arteries, and rat left anterior descending coronary artery, but the underlying mechanisms were ill defined and often contradictory. In rabbit aortic rings, dapagliflozin- and empagliflozin-mediated relaxations were impaired by protein kinase G inhibitors and the non-specific Kv channel blocker 4-aminopyridine (4-AP),[7,8] but specific blockers of Kv subfamilies (Kv1.5, Kv2.1, and Kv7s) did not impair relaxations. In contrast, SGLT2 inhibitors relaxed mesenteric resistance arteries in an endothelium-independent manner that was sensitive to blockers of Kv1.5 and Kv7 potassium channels[9–11] without an effect on protein kinase G. In the left anterior descending coronary arteries, a significant relaxation was only observed with a high concentration of dapagliflozin (500 μM) and the relaxation was not affected by a range of potassium channel blockers.[12] In this study, we aimed to investigate whether SGLT2 inhibitors were acting via a shared upstream mechanism that could explain the vascular-dependent effects observed in many of the trials, as well as the artery-specific differences that have been reported.

Resistance arteries that dictate blood pressure are richly innervated with peptidergic sensory nerves.[13,14] Release of calcitonin gene-related peptide (CGRP) from sensory nerves has a pronounced vasodilatory effect in many arteries.[15–17] CGRP has been shown to have beneficial effects in hypertensive and heart failure patients. Animal studies suggest that CGRP has vascular-dependent and vascular-independent processes by which it could protect the vasculature and myocardium against cardiovascular

Downloaded from https://academic.oup.com/cardiovascres/article/120/14/1811/7721236 by guest on 10 January 2025

dysfunction, particularly heart failure,[18] to a similar extent as the SGLT2 inhibitors. The artery-specific effects of SGLT2 inhibitors reported previously are somewhat in line with CGRP-induced relaxation. Kv7 channels have been shown to be downstream mediators of CGRP signaling,[19–21] and CGRP can increase NO production. The present study aimed to ascertain whether SGLT2 inhibitors promoted CGRP release from perivascular sensory nerves, which would explain not only the vascular-dependent cardiovascular protective effects of SGLT2 inhibitors but also the vascular-independent protective effects.

2. Methods

2.1 Animals

Experiments were performed on second-order mesenteric and cardiac septal resistance arteries as well as conduit renal arteries from male rats aged 11–14 weeks and weighing 175–300 g. Animals were maintained under an institutional site licence and sacrificed by a Schedule 1 method (cervical dislocation) in accordance with the UK Animal (Scientific Procedures) Act 1986; therefore, no approval from a local or university ethics review board was required. This investigation conforms to Directive 2010/63/EU of the European Parliament on the protection of animals used for scientific purposes.

2.2 Myography

Arteries were cut into ~2 mm segments and mounted on 40 μm stainless steel wires in a myograph (DMT, Aarhus, Denmark). The myograph chambers contained physiological salt solution (composition in Supplementary material online, *Section S1.9*) that was bubbled with 95% oxygen and 5% carbon dioxide at 37°C. Tension in each segment was recorded using LabChart Pro Software (ADInstruments, Oxford, UK). All vessels were subject to a normalization procedure[22] to standardize the experimental conditions, and arteries were set to an internal circumference 90% of the diameter at *in vivo* transmural pressure (13.3 or 10.3 kPa for septal arteries). Endothelial integrity was estimated by the response to 10 μM carbachol applied to arteries constricted with 10 μM of the α1-adrenoreceptor agonist, methoxamine. The endothelium was denuded by mechanical abrasion with an eyebrow hair, and effectiveness of removal was ascertained by a carbachol challenge in all experiments with septal arteries.

Arterial segments were pre-contracted with 10 μM methoxamine and dapagliflozin, empagliflozin, or mizagliflozin applied cumulatively (1–100 μM). The Ki for these agents to inhibit SGLT2 is 1.2, 3.1, and 8170 nM, respectively.[1,23] Similar experiments were performed with the NHE1 inhibitor cariporide (1 and 30 μM), CGRP (10 pM–10 nM), and capsaicin (10 μM). To identify possible underlying mechanisms, arteries were pre-incubated with a variety of agents for 15 min including the following: solvent control dimethyl sulfoxide (DMSO), linopirdine (pan-Kv7 channel blocker, 10 μM), BIBN-4096 (CGRP receptor blocker, 1 μM), capsaicin (TRPV1 agonist, 10 μM), AMG-517 (TRPV1 blocker, 1 μM), AM0902 (TRPA1 channel blocker, 10 μM), HMR-1556 (Kv7.1 channel blocker, 10 μM), iberiotoxin (BK_{Ca} channel blocker, 100 nM), 4-AP (1 mM), tetraethylammonium (TEA, 1 mM), and glibenclamide (K_{ATP} channel blocker, 1 and 3 μM). To confirm that sensory nerve-derived mediators were involved with SGLT inhibitor responses, we used repeated challenges of the TRPV1 agonist capsaicin (10 μM) to deplete CGRP content in sensory nerves.[14,16] Capsaicin (10 μM) was applied to relaxed arteries for 5 min followed by washout to remove any released CGRP. Two further challenges of capsaicin were applied followed by extensive washout over 10 min before contraction with methoxamine (depletion protocol).

2.3 Immunohistochemistry

After completion of functional myography experiments, arterial segments were fixed *in situ* in myograph chambers with 4% paraformaldehyde (J61899, Thermo Scientific) for 1 h at room temperature. Arteries were then incubated for 90 min at room temperature with blocking buffer containing permeabilization agents [1% bovine serum albumin (BSA), 0.5% Triton X-100, 0.05% Tween 20 in phosphate buffered saline (PBS), composition in Supplementary material online, *Section S1.9*] and incubated overnight at 4°C with guinea pig anti-TRPV1 (Ab10295, 1:1000, Abcam), goat anti-CGRP (Ab36001, 1:1000, Abcam), rabbit anti-NHE1 (PA5115917, 1:1000, Invitrogen), mouse anti-SGLT2 (sc-393350, 1:200, Santa Cruz), rabbit anti-smooth muscle myosin heavy chain 11 (ab125884, 1:500, Abcam), and goat anti-mouse CD31/PECAM-1 (AF3628-SP, 1:150, R&D Systems) diluted in blocking buffer. This was followed by a secondary antibody incubation with either goat anti-guinea pig (Alexa Fluor 488, A11073, Life Technologies), donkey anti-goat (Alexa Fluor 633, A21082, Life Technologies), donkey anti-rabbit (Alexa Fluor 488, A21206, Life Technologies), or donkey anti-mouse (Alexa Fluor 594, A21203, Invitrogen) diluted in blocking buffer for 90 min at room temperature. Arteries were then placed in mounting medium (Vectashield Plus Antifade, Vector Laboratories) and laid flat between two glass coverslips. Arteries were excited at 405, 488, 536, and 635 nm, and fluorescence was acquired through a water immersion objective (1024 × 1024 pixels; ×40, 1.15 NA objective, Olympus) using a FV1000 laser scanning confocal microscope (Olympus, Southend-on-Sea, UK). Z-stacks were acquired through each artery wall in 1 μm increments using Fluoview (version 4.1, Olympus) software and analysed offline using Imaris (version 8.0.2, Bitplane) software.

2.4 Western blot and immunocytochemistry

SGLT2 expression was identified by western blot and immunocytochemistry (ICC). Protein lysates were prepared from whole mesenteric arcade, right and left renal arteries, and a combination of septal and left anterior descending artery using Triton buffer (Fisher Scientific) supplemented with protease and phosphatase inhibitors (cOmplete, mini, and PhosSTOP from Roche). Protein concentrations were determined via the Pierce™ BCA Protein Assay Kit (Thermo Fisher Scientific, Loughborough, UK). Ten micrograms of each artery sample was run under reducing conditions with 4–12% Bolt™ Bis-Tris Plus pre-cast gels (Invitrogen), and proteins were transferred to a nitrocellulose membrane. Membranes were blocked for at least 0.5 h in 3% BSA–PBS and incubated overnight at 4°C with the primary SGLT2 mouse monoclonal antibody (D-6, sc-393350, 1/200 dilution, Santa Cruz). The membranes were incubated with highly adsorbed horseradish peroxidase-conjugated goat anti-mouse IgG (A16078, Fisher Scientific) for 1 h at room temperature and developed using Immobilon™ Western Chemiluminescent HRP Substrate (Millipore). Full quantification protocol is in the Supplementary material. For ICC, vascular smooth muscle cells (VSMCs) were isolated from six mesenteric branches, right and left main renal arteries, and whole septal arteries (protocol and solution composition in Supplementary material online, *Section S1.9*), and SGLT2 localization was identified using a mouse anti-SGLT2 antibody (dilution 1:200, Santa Cruz, TX, USA) with a donkey anti-mouse secondary antibody conjugated to Alexa Fluor 488 (dilution 1:100, Thermo Fisher, Paisley, UK). Wheat Germ Agglutinin (WGA) Texas Red was used as a membrane stain before permeabilization.

2.5 Electrophysiology

A possible direct effect of dapagliflozin and empagliflozin was assessed on currents generated by the over-expression of Kv7 and TRPV1 genes in *Xenopus laevis* oocytes and HEK293 cells, respectively. Cell culture and channel expression methods are described fully in the Supplementary material. Potassium currents generated by the expression of KCNQ4, KCNQ5, and KCNE4 (accepted molecular combination in arterial smooth muscle[24]) were recorded using two-electrode voltage clamp at room temperature using an OC-725C amplifier (Warner Instruments, Hamden, CT, USA) and pClamp10 software (Molecular Devices, Sunnyvale, CA, USA) 2–5 days after cRNA injection. TRPV1 currents were recorded from transiently transfected HEK293 cells using the patch-clamp technique in the outside-out configuration. TRPV1-dependent currents were activated using a sub-saturating concentration (250 nM) of capsaicin (see Ortíz-Rentería

Downloaded from https://academic.oup.com/cardiovascres/article/120/14/1811/7721236 by guest on 10 January 2025

et al.[25]). Currents were low-pass filtered at 2 kHz and sampled at 10 kHz with an EPC 10 amplifier (HEKA Elektronik) and were plotted and analysed with Igor Pro (WaveMetrics Inc.). All internal and external solutions are shown in the Supplementary material online, *Section S1.9*.

2.6 Morpholino studies

As NHE1 knockout mice have a short lifespan,[26] studies were performed *ex vivo* using translation-stopping morpholinos to reduce NHE1 expression with the assumption that local translation of mRNA occurred in the sensory neurites like in motor nerves.[27] Knockdown of NHE1 in mesenteric arteries was performed by transfection with morpholino oligonucleotides targeting NHE1 or a scrambled control as described previously.[28] All morpholino oligonucleotides (5 μM; Gene Tools, Oregon, USA) were mixed in Opti-MEM and transfected using Lipofectamine 2000 (Thermo Fisher, Paisley, UK). Arteries were then incubated in DMEM/F-12 with 1% penicillin/streptomycin for 48 h. Transfected arteries tended to lose tone in the continued presence of methoxamine so a modified protocol was used to study the effect of SGLT2 inhibitors in these conditions. Methoxamine (10 μM) was applied for 4 min followed by washout for 20 min. This was repeated, and then 30 μM empagliflozin or dapagliflozin was applied 5 min before the third application of methoxamine. Arteries were fixed *in situ* and permeabilized, and NHE1 staining was detected to ascertain NHE1 knockdown.

2.7 Data and statistical analysis

All values from functional experiments are expressed as mean ± standard error of the mean (SEM) with no less than five individual data points, each representing a biological repeat. Measurements of total cell florescence during ICC involved five biological repeats with a minimum of five cells to be recorded per sample. For quantification of SGLT2 protein via western blot, a minimum of three biological repeats were obtained. For functional experiments, cumulative concentration effect curves were produced, whereby the contraction produced by 10 μM methoxamine at stable tone was taken as the maximal contraction of 100%. The tone of the artery was recorded after each subsequent addition of the pharmacological agent, and the values were formulated as a percentage of the maximum contraction. Using GraphPad Prism (RRID:SCR_002798, Version 9.0.0), a transformed data set of mean values was generated using $X = \text{Log}(X)$ to reduce representative skew. A four-parametric linear regression analysis was then performed to produce a concentration effect curve on a log(x) graph with the SEM. When comparing multiple groups, a two-way analysis of variance (ANOVA) was performed followed by a *post hoc* Bonferroni or Dunnett's test. For data comparing two groups, an unpaired parametric t-test was performed. Significance values are represented as $^{*}P < 0.05$, $^{**}P < 0.01$, $^{***}P < 0.001$ and $^{****}P < 0.0001$, and data sets subject to statistical analysis contained at least five animals per group, where N = number of independent values.

3. Results

3.1 Expression of SGLT2 in mesenteric and renal arteries from male Wister rats

The expression of SGLT2 within the vasculature is ill defined; hence, we characterized its expression in different vascular beds. A band at the expected molecular weight for SGLT2 (~75 kDa) was detected in protein lysates from kidney (positive control), mesenteric, renal, and coronary arteries (*Figure 1A* and *B*). Additional bands of ~49and ~33 kDa were also detected corresponding to the presence of the other known isoform for SGLT2 and/or products of degradation. Immunocytochemical studies on VSMCs showed a strong co-localization of SGLT2 with the plasma membrane marker WGA, suggesting a robust expression in the membrane of VSMCs (*Figure 1C–E*). We performed immunohistochemistry experiments with well-validated CGRP and TRPV1 antibodies to delineate sensory nerves in the different arteries. *Figure 1F* shows robust TRPV1 and CGRP staining in the adventitia of mesenteric arteries with comparatively little staining in the smooth muscle or endothelial layers (see Supplementary material online, *Figure S1*). In contrast, negligible TRPV1 or CGRP staining was identified in the adventitial layer of the renal artery (*Figure 1G*; Supplementary material online, *Figure S1*), and none was detected in a septal artery (*Figure 1H*). Thus, mesenteric arteries exhibit robust sensory nerve networks that were not present in renal or cardiac septal arteries.

3.2 SGLT2 inhibitors relax mesenteric arteries

In rat mesenteric artery segments, dapagliflozin and empagliflozin, as well as a SGLT1 inhibitor, mizagliflozin, produced concentration-dependent relaxations (1–100 μM), with approximate IC_{50} values of 9.5, 7.3 and 5.5 μM, respectively (*Figure 2A* and *B*; $n = 5–6$). The relaxation elicited by each SGLT inhibitor was not affected by the size of the induced contraction and not dependent upon a functional endothelium (see Supplementary material online, *Figures S2* and *S3*). In contrast to their effect on mesenteric arteries, dapagliflozin and empagliflozin were significantly poorer relaxants of pre-contracted renal arteries and were ineffective relaxants of septal arteries (up to 100 μM; *Figure 2C* and *D*).

3.3 Role of Kv7 channels in SGLT2 inhibitor-induced relaxations

Previous studies implicated Kv channels encoded by *KCNQ* genes (Kv7 channels) in the relaxant response to different SGLT2 inhibitors.[9–11] In the present study, the relaxation of mesenteric arteries produced by dapagliflozin, empagliflozin, and mizagliflozin was significantly attenuated by pre-incubation with the pan-Kv7 channel inhibitor linopirdine (10 μM) when compared to DMSO control (*Figure 3A* and *B*; $n = 5–6$). Specific blockers of Kv7.1 (HMR1556), BK_{Ca} (iberiotoxin), K_{ATP} (glibenclamide), and the non-selective K channel blockers 4-AP and TEA had no effect on relaxations produced by SGLT2 inhibitors (*Figure 3C* and *D*; Supplementary material online, *Figure S5*). However, electrophysiological experiments on oocytes co-expressing KCNQ4/KCNQ5 and KCNE4—a molecular combination found in most arterial smooth muscle[24] showed that neither dapagliflozin nor empagliflozin at 100 μM had any effect on the current amplitude nor the voltage dependence of activation of the Kv currents and neither agent affected the resting membrane potential (*Figure 3E–J*). Thus, dapagliflozin and empagliflozin do not activate Kv7 channels directly.

3.4 Sensory nerve contribution in mesenteric and renal arteries

Kv7 blockers attenuate arterial relaxations produced by several agonists of Gs-linked receptors.[19–21] As Kv7 channels are not directly activated by SGLT2 inhibitors, a logical conclusion is that these agents promoted the release of a mediator that recruited Kv7 channels. As dapagliflozin- and empagliflozin-mediated relaxations were not endothelium dependent (see Supplementary material online, *Figure S3*), we focused on CGRP released from the sensory nerves and the different effects of the SGLT2 inhibitors between mesenteric and renal or septal arcades were due to a differential abundance of sensory nerves (see *Figure 1*). CGRP can be released from sensory neurones upon TRPV1 channel activation.[14] Applying the TRPV1 activator capsaicin fully relaxed pre-contracted mesenteric arteries (*Figure 4A*), which was abrogated by the CGRP receptor blocker BIBN-4096 (see Supplementary material online, *Figure S4A*). Consistent with the lack of sensory nerves (*Figure 1F* and *G*), capsaicin had no effect in pre-contracted renal or septal arteries (*Figure 4A*). Linopirdine inhibited mesenteric artery relaxations produced by exogenous CGRP or SGLT2 inhibitors to a similar extent (*Figure 4B*), consistent with our hypothesis that SGLT2 inhibitor-induced relaxations are mediated by CGRP.

Downloaded from https://academic.oup.com/cardiovascres/article/120/14/1811/7721236 by guest on 10 January 2025

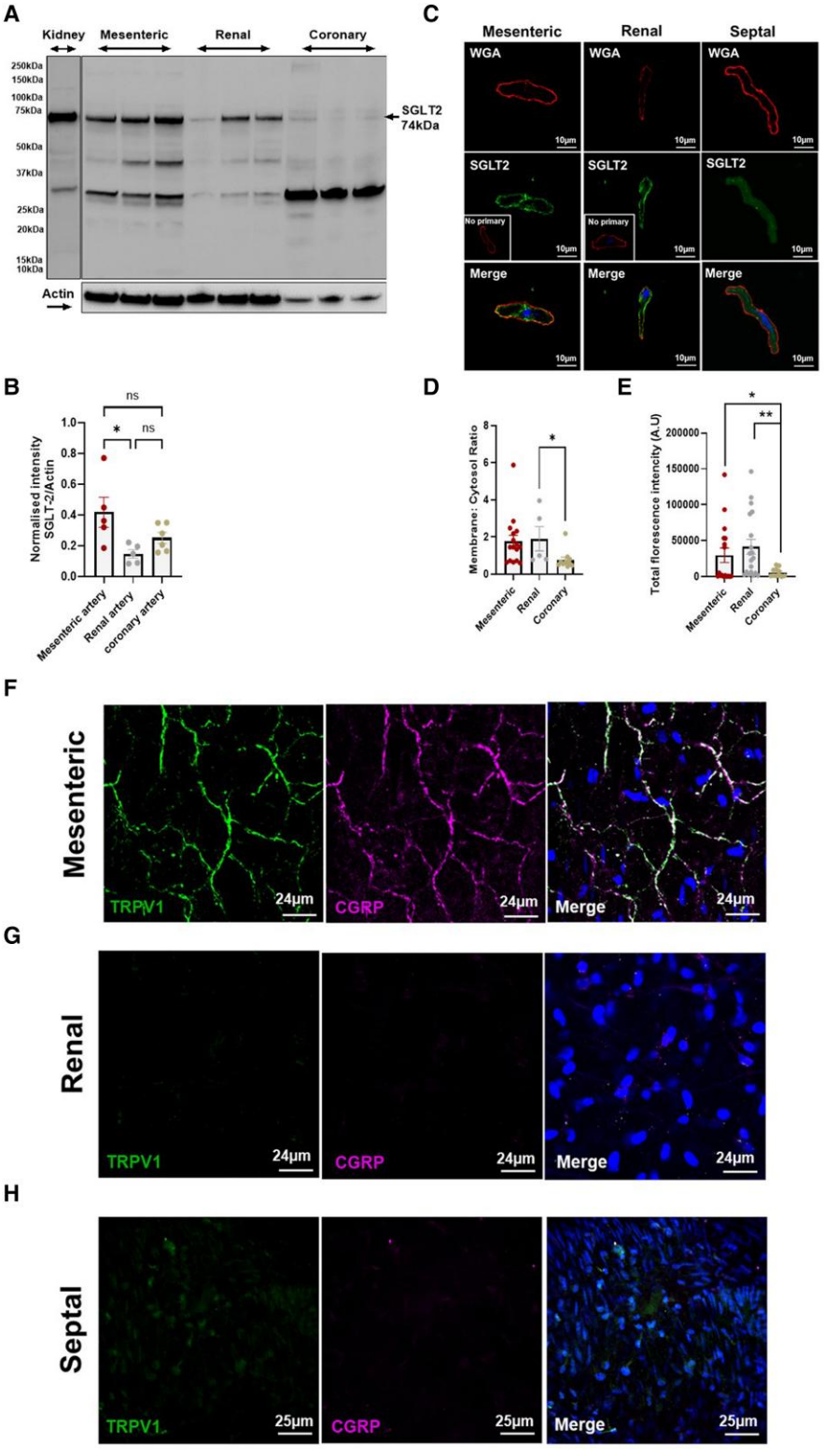


Figure 1 SGLT2 expression in mesenteric, renal, and coronary arteries. (*A*) Western blot quantification of SGLT2 protein in mesenteric, renal, and coronary arteries with whole kidney as a positive control ($N = 3$). Quantification of the western blot in mesenteric (left), renal (centre), and coronary (right) arteries shown in (*B*). (*C*) Representative staining of SGLT2 (middle row) and membrane stain WGA (top row) in isolated mesenteric, renal, and septal coronary VSMCs ($N = 5$, $n = 25$) with total cell fluorescence in (*D*) and membrane-to-cytosol ratio of SGLT2 expression in each artery in (*E*). All values were shown as mean ± SEM denoted by error bars, and a one-way ANOVA was used to calculate significance where $^{*}P < 0.05$ and $^{**}P < 0.01$. (*F–H*) show representative labelling for TRPV1 (green, left column) and CGRP (magenta, middle column) indicative of sensory nerve presence in the adventitia of whole mesenteric (*F*), renal arteries (*G*), and septal arteries (*H*). Nuclei were labelled in blue. Similar images seen in arteries from 4 animals). Non-significance is shown by ns.

Downloaded from https://academic.oup.com/cardiovascres/article/120/14/1811/7721236 by guest on 10 January 2025

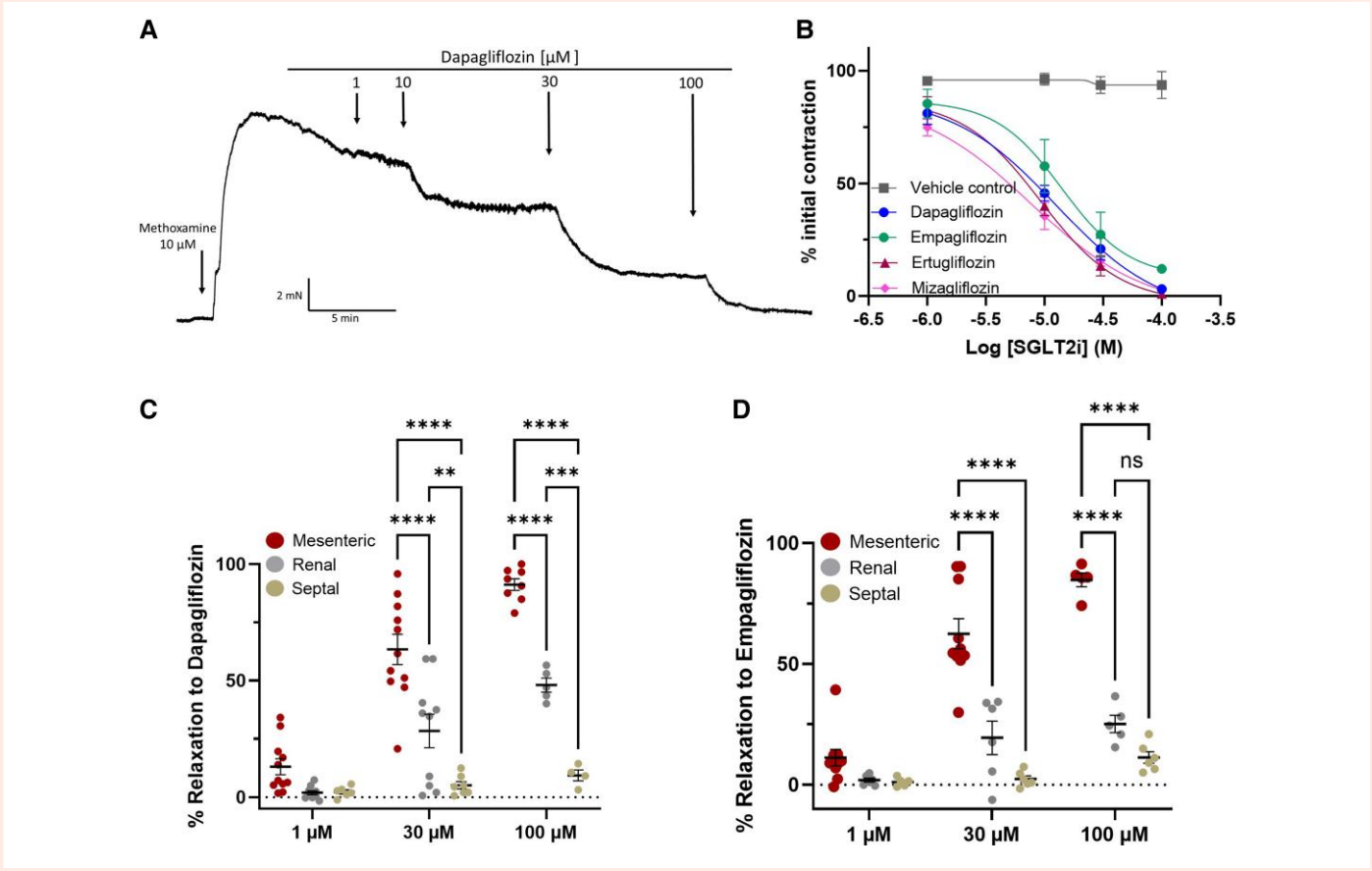


Figure 2 The effect of SGLT2 and SGLT1 inhibitors on mesenteric, renal, and septal arterial tones. (*A*) A representative trace of the effect of dapagliflozin in mesenteric arteries pre-contracted with 10 μM methoxamine. (*B*) Mean effect of dapagliflozin (blue), empagliflozin (green), and mizagliflozin (purple), with mean vehicle control in grey, *N*= 5–6. All values are shown as mean ± SEM denoted by the error bars (*N* = 6–8). (*C* and *D*) show the relaxation of dapagliflozin and empagliflozin in renal mesenteric (left hand data set), renal (middle data set), and septal (right hand data set) arteries. All data are individual experiments and a two-way ANOVA with a *post hoc* Sidak test was used to calculate significance values where **, ***, and **** denote $P < 0.01$, 0.001 and 0.0001 respectively. Non-significance is shown by ns.

3.5 Dapagliflozin- and empagliflozin-evoked relaxations are sensitive to CGRP and TRPV1 blockade

To identify a role for CGRP in SGLT2 inhibitor-induced relaxations, we applied dapagliflozin, empagliflozin, and mizagliflozin to mesenteric arteries pre-incubated with either DMSO (control) or BIBN-4096 (1 μM). The relaxation to all three agents was significantly attenuated by 1 μM BIBN-4096 (*Figure 4C–E*). To confirm that SGLT2 inhibitors relaxed mesenteric arteries through provoking CGRP release from sensory nerves, we depleted CGRP stores through treatment with three 5-min applications of capsaicin (10 μM) followed by washout of the bathing solution or directly blocked TRPV1 with AMG-517 (1 μM). Both treatments prevented the relaxation produced by 1 μM capsaicin (see Supplementary material online, *Figure S4B and C*). The relaxations produced by both dapagliflozin and empagliflozin were significantly attenuated after treatment with capsaicin or incubation with the TRPV1 blocker, AMG-517 (*Figure 4F* and *G*, *N* = 6–10). The mizagliflozin-induced relaxation was also sensitive to AMG-517 (*Figure 4H*). The relaxation to dapagliflozin was not affected by pre-application of the TRPA1 blocker AM0902 (1 or 10 μM, Supplementary material online, *Figure S5*). Neither the TRP blockers nor capsaicin pre-treatment affected methoxamine-induced contraction amplitude (see Supplementary material online, *Figure S6*). Hence, relaxations induced by SGLT2 inhibitors were dependent upon activation of the TRPV1 channel on perivascular sensory nerves and subsequent CGRP release.

3.6 Effect of SGLT2 inhibitors on heterologously expressed TRPV1 currents

To determine whether dapagliflozin could activate TRPV1 channels directly, we performed patch-clamp experiments using outside-out excised membrane patches of HEK293 cells expressing rat TRPV1 (rTRPV1). As shown in *Figure 5*, we first obtained the leak currents (in the absence of agonist, grey traces) elicited by a square voltage pulse to −120 mV followed by a pulse to 120 mV, then used the same voltage protocol to assess currents after exposing the patches to either 30 μM (*Figure 5A*) or 100 μM dapagliflozin (*Figure 5B*) for 5 min and, finally, to 250 nM capsaicin alone (black traces). All currents were leak subtracted and normalized to the current obtained at +120 mV (*Figure 5C*). Currents after exposure to 30 μM dapagliflozin were 12.9 ± 2.2 and 7.6 ± 3.7% after 100 μM dapagliflozin of the currents elicited by the TRPV1 agonist, capsaicin (*Figure 5C*, *n* = 6). These data indicate that TRPV1 is not directly activated by dapagliflozin.

Next, we studied whether dapagliflozin could potentiate capsaicin- or low pH-activated TRPV1 currents. For this set of experiments, we first recorded leak currents (grey traces), then activated TRPV1 in outside-out excised membrane patches of HEK293 cells with either a sub-saturating concentration (250 nM) of capsaicin or with a solution at pH 6, then washed the membrane patches to close the channels and exposed the patches to 30 μM dapagliflozin for 5 min and remeasured the currents in the presence of 250 nM capsaicin or solution with low

Downloaded from https://academic.oup.com/cardiovascres/article/120/14/1811/7721236 by guest on 10 January 2025

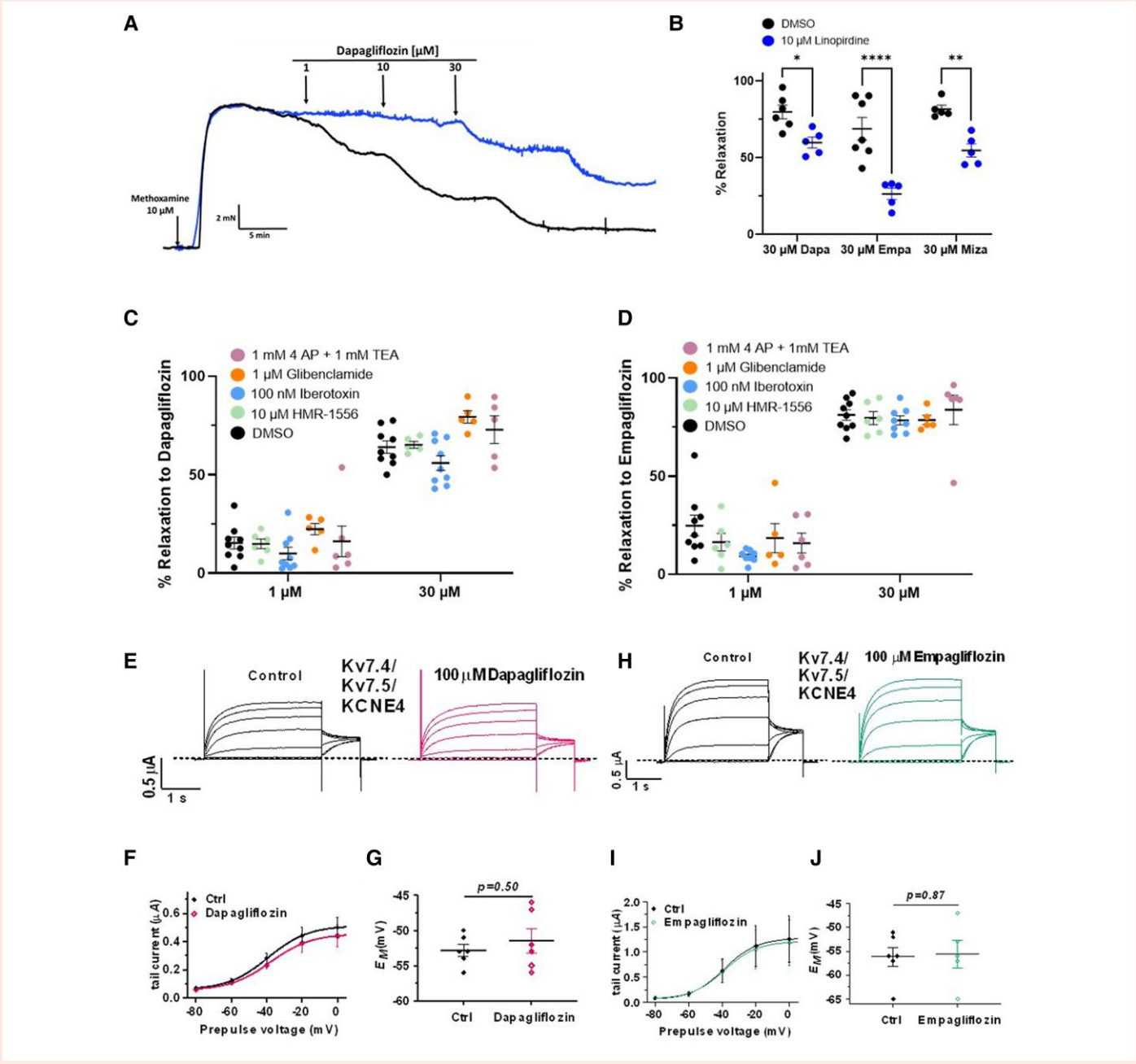


Figure 3 SGLT2 inhibitors and Kv7 channels. (*A*) Representative trace of the effect of dapagliflozin on pre-contracted mesenteric arteries in the presence (upper trace/blue) and absence (lower trace) of 10 μM linopirdine. (*B*) Mean data for relaxations to dapagliflozin, empagliflozin, and mizagliflozin (30 μM) in solvent control (left data set) and when pre-incubated with 10 μM linopirdine (right data set/blue) ($N = 5–6$). All values are individual experiments with mean ± SEM denoted by the error bars. A two-way statistical ANOVA with a *post hoc* Sidak test was used to generate significant values (*$P < 0.05$, **$P < 0.01$, and ****$P < 0.0001$). The effect of dapagliflozin (*C*) and empagliflozin (*D*) in the absence and presence of HMR1556, iberiotoxin, 4-AP, TEA, and glibenclamide (data sets left to right respectively). All data values are shown as mean ± SEM ($N = 5–6$). (*E–G*) show currents produced by the co-expression of Kv7.4, Kv7.5, and KCNE4 in the absence and presence of 100 μM dapagliflozin. Representative traces in (*E*), mean current–voltage relationship in (*F*), and mean membrane potential in (*G*). The effect of 100 μM empagliflozin on currents produced by co-expression of Kv7.4, 7.5, and KCNE4 is shown in (*H–J*). Representative traces in (*H*), mean current–voltage relationship in (*I*), and mean membrane potential in (*J*). Data are the mean of *N* oocytes with error bars denoting the SD.

extracellular pH (*Figure 5D–G*). The results from these experiments indicate that 30 μM dapagliflozin did not potentiate TRPV1 currents activated by 250 nM capsaicin (*Figure 5D* and *E*; 84.1 ± 13.5%, $n = 5$) or by low pH (*Figure 5F* and *G*; 94 ± 6.5%, $n = 5$). Thus, SGLT2 inhibitors neither activate TRPV1 directly nor sensitize the channel to known mediators.

3.7 NHE1 co-localizes with TRPV1 and cariporide prevents SGLT2 inhibitor-induced responses

Various studies have shown that SGLT2 inhibitors block NHE isoforms[29–34] with *in silico* studies predicting a binding site in the extracellular

Downloaded from https://academic.oup.com/cardiovascres/article/120/14/1811/7721236 by guest on 10 January 2025

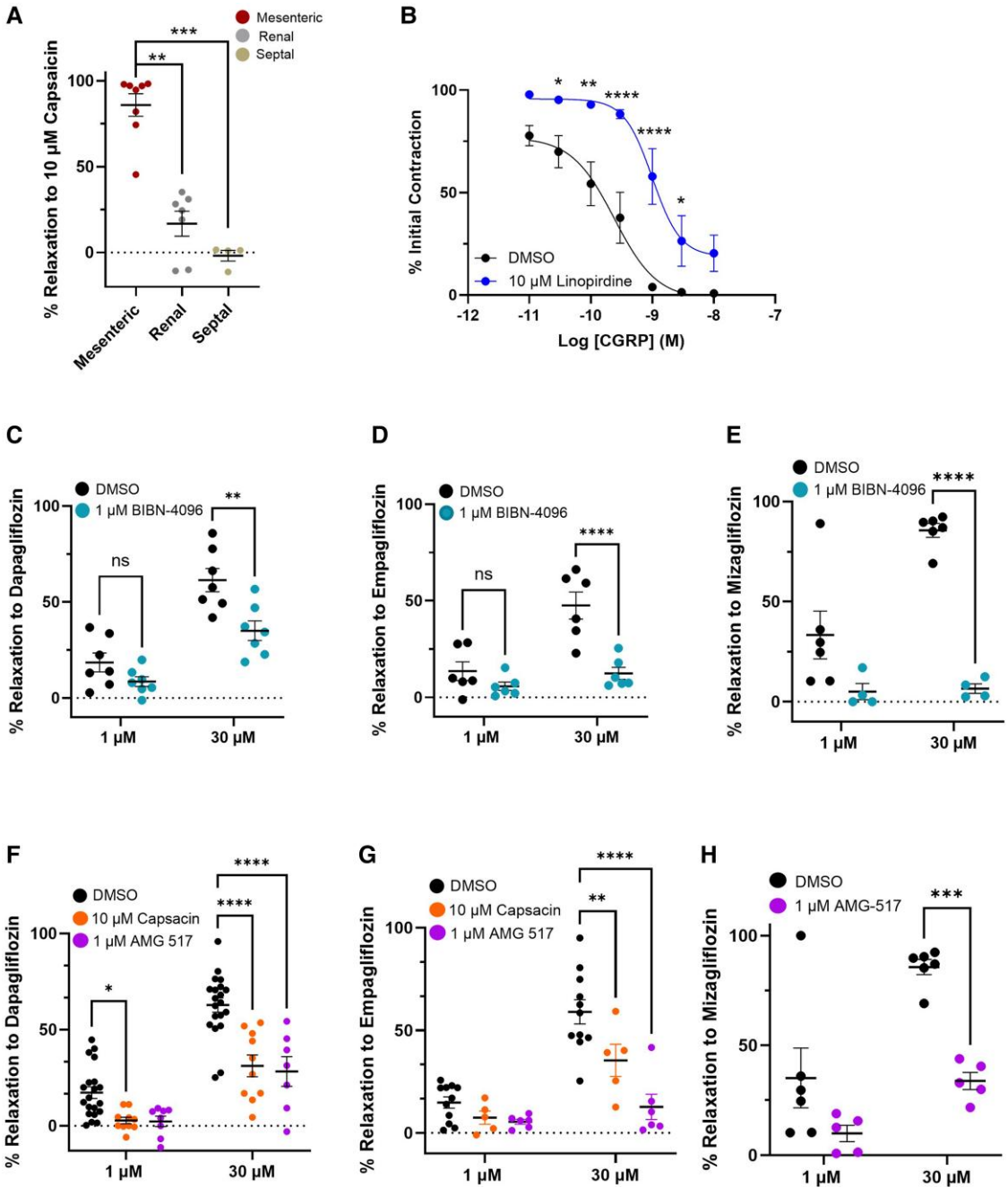


Figure 4 Dapagliflozin-, empagliflozin-, and mizagliflozin-induced relaxations are blocked by CGRP receptor antagonist and TRPV1 blockade. (*A*) shows the percentage relaxation to 10 μM capsaicin in mesenteric (left hand data set), renal (middle data set), and septal arteries (right hand data set) ($N = 6$–8). (*B*) shows the mean relaxation to CGRP in the absence and presence of 10 μM linopirdine (blue, $N = 5$–8). All data points are represented as mean ± SEM denoted by the error bars. A two-way statistical ANOVA with a *post hoc* Bonferroni test was used to generate significant values (*$P < 0.05$, **$P < 0.01$, ***$P < 0.001$, and ****$P < 0.0001$). The mean effect of dapagliflozin (*C*, $N = 6$), empagliflozin (*D*, $N = 7$), and mizagliflozin (*E*, $N = 5$) on pre-contracted mesenteric arteries in the presence of DMSO (left data set) and 1 μM BIBN (right data set). The mean relaxations produced by 1 and 30 μM dapagliflozin (*F*, $N = 7$–10) and empagliflozin (*G*, $N = 6$–10) in mesenteric arteries pre-incubated in DMSO (solvent control, black), 1 μM AMG-517 (right hand data set), or after sensory nerve depletion with 10 μM capsaicin (centre data set). The relaxation to mizagliflozin in theabsence and presence of TRPV1 blocker AMG-517 (right hand data set) is shown in (*H*) ($N = 5$). All values are expressed as mean ± SEM. A two-way statistical ANOVA with a *post hoc* Sidak test was used to generate significant values (*$P < 0.05$, **$P < 0.01$, ***$P < 0.001$, and ****$P < 0.0001$).

sodium-binding pocket of NHE1.[29] We postulated that SGLT2 inhibitors promoted release of CGRP from sensory nerves by inhibiting NHE and producing a localized pH change sufficient to activate TRPV1. Functional experiments revealed that the NHE1 inhibitor cariporide[29] relaxed mesenteric arteries, which were markedly impaired by BIBN-4096 or AMG-517 pre-treatment (*Figure 6A* and *C*). Cariporide was ineffective at relaxing

Downloaded from https://academic.oup.com/cardiovascres/article/120/14/1811/7721236 by guest on 10 January 2025

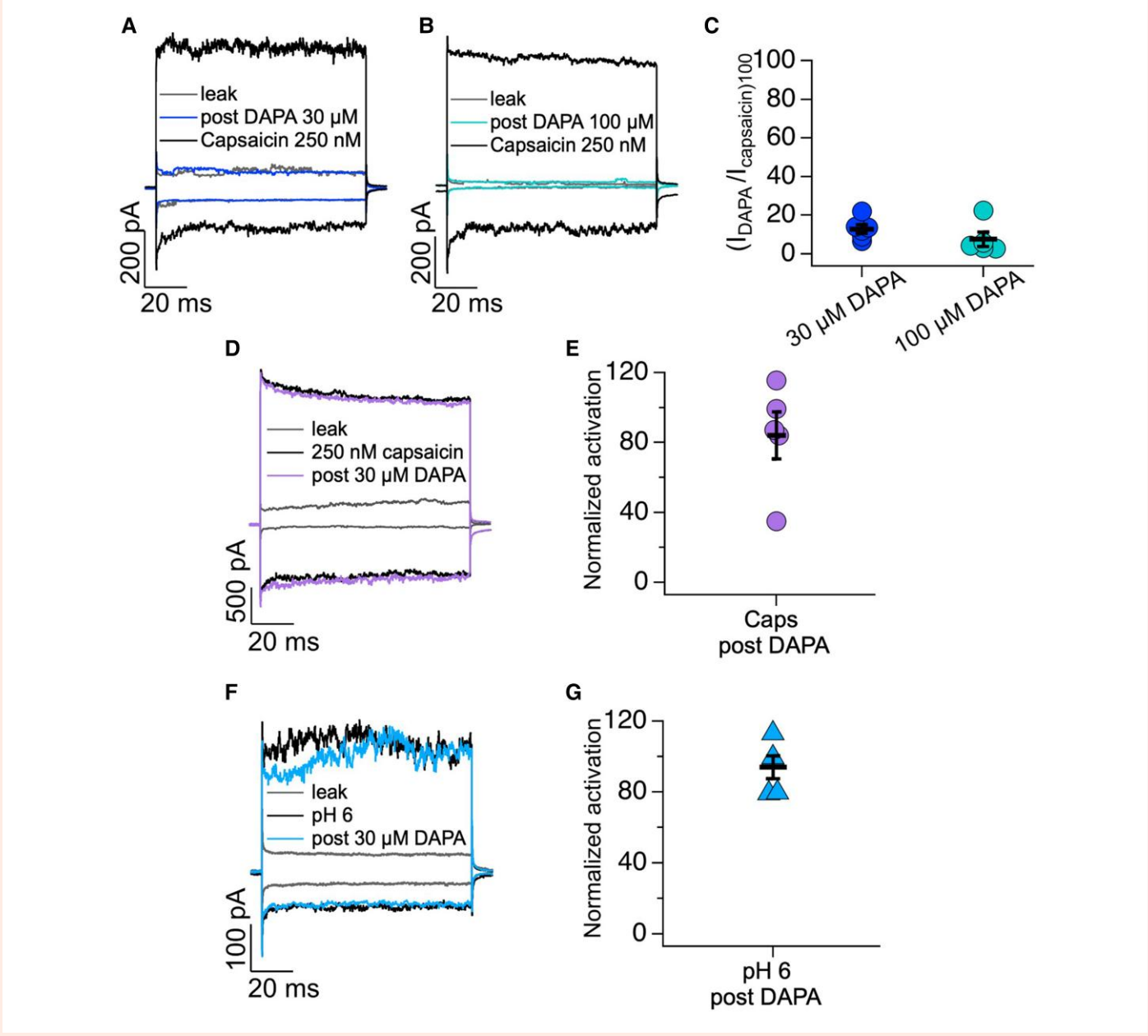


Figure 5 SGLT2 inhibitors do not activate TRPV1 directly. (*A* and *B*) Representative traces of currents at +120 and −120 mV from outside-out membrane patches of HEK293 cells expressing TRPV1. Leak currents were obtained in the absence of any agonist and after 5-min application of dapagliflozin (DAPA) 30 μM (blue traces, *A*) and 100 μM (green traces, *B*). The top and bottom traces shows the subsequent effect of 250 nM capsaicin. (*C*) Average data for experiments in (*A* and *B*). Currents were leak subtracted, and data were normalized to activation by capsaicin 250 nM in the steady state at +120 mV ($N = 6$ and $N = 5$ for DAPA 30 and 100 μM, respectively). (*D*) Representative traces of currents at +120 and −120 mV from outside-out membrane patches of HEK293 cells expressing TRPV1 in control conditions (grey), after application with 250 nM capsaicin (black traces) and after application of 250 nM capsaicin + 30 μM DAPA for 5 min (lilac traces). (*E*) The data in (*D*) were normalized by dividing the currents obtained at +120 mV in response to 250 nM capsaicin + 30 μM DAPA by the currents in response to 250 nM capsaicin alone; ($N = 5$). (*F*) Representative traces of currents at +120 and −120 mV from outside-out membrane patches of HEK293 cells expressing TRPV1 under control conditions (grey), after activation of TRPV1 by pH 6 (black) and after 5-min application of 30 μM DAPA to pH 6 conditions (blue). (*G*) The data in (*F*) were normalized by dividing the currents obtained at +120 mV in response to pH 6 + 30 μM DAPA by the currents in response to pH 6 alone ($N = 6$). Group data are reported as the mean ± SEM.

pre-contracted renal or septal arteries (*Figure 6B*). We stained mesenteric arteries with SGLT2 and NHE1 antibodies and used TRPV1 to delineate the sensory nerves. As shown in *Figure 6D*, prominent NHE1 staining was observed in the adventitia of mesenteric arteries co-localized with TRPV1 and some staining in the smooth muscle and endothelial layers (see Supplementary material online, *Figure S7*). In contrast, negligible staining of SGLT2 was observed in the adventitial and endothelial layers, but traces of staining were identified in the smooth muscle layer of mesenteric arteries (see Supplementary material online, *Figure S7*), consistent with the staining identified in dispersed single smooth muscle cells (*Figure 1C–E*). No staining

Downloaded from https://academic.oup.com/cardiovascres/article/120/14/1811/7721236 by guest on 10 January 2025

for NHE1 or SGLT2 was detected in renal artery adventitia (*Figure 6E*; Supplementary material online, *Figure S8*). Therefore, NHE1 co-localized with TRPV1 in sensory nerves in the mesenteric artery, but SGLT2 was only found in the smooth muscle layer. In mesenteric arteries, pre-treatment with 30 μM cariporide reduced the relaxations to 30 μM dapagliflozin or 30 μM empagliflozin significantly ($P < 0.001$; *Figure 6F–H*). These experiments suggest that vasodilatory effects of SGLT2 inhibitors were mediated by NHE1 inhibition. To confirm this, we used morpholino-based molecular interference to reduce NHE1 protein expression in mesenteric arteries. In control arteries transfected with non-targeting scrambled morpholinos, 5-min application of either 30 μM empagliflozin or dapagliflozin reduced contractions produced by the subsequent application of 10 μM methoxamine by >70% (*Figure 7A* and *B*; Supplementary material online, *Figure S9*). However, in arteries transfected with translation-blocking morpholinos targeted against NHE1, empagliflozin or dapagliflozin had a negligible effect on methoxamine-induced contractions (*Figure 7A* and *B*). Immunohistochemical studies on the same arteries revealed that targeting morpholinos reduced NHE1 staining in the adventitia considerably compared to scrambled morpholinos (*Figure 7C*). These studies corroborate our hypothesis that SGLT2 inhibitors relax mesenteric arteries through NHE1 inhibition-induced release of CGRP.

4. Discussion

This study investigated the underlying mechanism of SGLT2 inhibitor-induced vasorelaxation and identified a role for CGRP release from sensory nerves secondary to NHE1 inhibition. We show that structurally different SGLT inhibitors relaxed mesenteric arteries equipotently, divergent from their ability to block SGLT2 (or SGLT1)-mediated glucose transport.[1,23] Relaxations produced by SGLT inhibitors were sensitive to TRPV1 and Kv7 channel blockade; however, electrophysiology recordings showed that SGLT2 inhibitors did not activate vascular Kv7 or TRPV1 channels directly. In addition, relaxations to dapagliflozin, empagliflozin, and the SGLT1 inhibitor mizagliflozin were attenuated by CGRP receptor blockade or by depletion of sensory nerve transmitters through capsaicin challenge. In contrast, SGLT2 inhibitors were poor relaxants of pre-contracted conduit renal and ineffective in septal resistance arteries where sensory nerves, evinced by staining for CGRP and TRPV1 in the adventitia, were absent compared to mesenteric arteries. The NHE1 blocker cariporide also relaxed mesenteric arteries, which was prevented by CGRP receptor and TRPV1 blockade, but had no effect in renal or septal arteries. Strikingly, NHE1 but not SGLT2 proteins co-localized with TRPV1 in the sensory nerves, and pre-application of cariporide or transfection with NHE1-targeted morpholino attenuated the inhibitory effects of empagliflozin and dapagliflozin.

The study provides strong evidence that SGLT2 inhibitors influence arterial reactivity by promoting the release of CGRP from sensory nerves. As the density of sensory nerve innervation varies across the vasculature and within an artery (see staining in *Figure 1*), this seminal finding explains much of the variability in data seen in previous publications.[9–11] Interestingly, the effectiveness of zinc pyrithione, which also relaxes arteries through a release of CGRP from sensory nerves, was far greater in mesenteric arteries compared to renal and coronary arteries[35] consistent with our observations with SGLT inhibitors. While SGLT2 is present in arterial smooth muscles, our pharmacological studies and comparative imaging suggest that the effects of the gliflozins are not mediated by an action on SGLT2 *per se* but via an additional effect of these agents on NHE1, as reported previously.[29–31] This hypothesis was corroborated here by molecular knockdown of NHE1. Interestingly, a previous study in human visceral adipose arteries speculated NHE1 may be involved in the moderate relaxation produced by canaglifozin.[31]

4.1 SGLT2 inhibitors induce arterial relaxations

The present study shows that SGLT2 inhibitors relaxed pre-contracted mesenteric arteries at concentrations between 10 and 100 μM, in general agreement with previous work in mesenteric arteries and aortic rings.[7–11] This is slightly higher than the therapeutic plasma concentrations in humans, which for empagliflozin is about 0.3 μM for the commonly prescribed dose of 10 mg and 8 μM for the maximum dose of 800 mg.[36] But in an *ex vivo* setting, small changes in tension are hard to relate to the physiological impact of resistance and flow. It is common to use higher concentrations of drugs in *ex vivo* studies to delineate cellular processes. The present study shows that the mesenteric artery relaxations produced by dapagliflozin and empagliflozin, as well as mizagliflozin, were not sensitive to a range of K channel blockers (HMR-1556, iberiotoxin, 4-AP, TEA, and glibenclamide) but were sensitive to the pan-Kv7 channel blocker linopirdine, in agreement with earlier work in mesenteric arteries.[9–11] However, our electrophysiological recordings showed that neither dapagliflozin nor empagliflozin directly enhanced potassium currents in oocytes expressing Kv7.4, Kv7.5, and KCNE4 (the combination in arterial smooth muscle[24]), suggesting that Kv7 channel activation is secondary to the release of a chemical intermediate. We have previously found that Kv7 channel-specific blockers impaired CGRP-induced relaxations in cerebral and mesenteric arteries[19–21] so we propose that these channels are a functional endpoint of a relaxant cascade that involves CGRP release from sensory nerves.

4.2 The role of CGRP in arterial effects of SGLT2 inhibitors

Our hypothesis is that the arterial relaxation produced by the structurally dissimilar SGLT2 and SGLT1 inhibitors was mediated predominantly by CGRP release from perivascular sensory nerves.[14] Thus, empagliflozin, dapagliflozin, or mizagliflozin relaxed mesenteric arteries that were impaired by blocking the CGRP receptor with BIBN-4096, although the lack of complete inhibition suggests other neuropeptides such as substance P may also be released. Immunohistochemistry with validated antibodies for TRPV1 or CGRP showed that mesenteric arteries had dense sensory nerve networks in the adventitia. In contrast, SGLT2 inhibitors were poor or ineffective relaxants in renal and septal arteries, respectively, that correlated with negligible or no TRPV1 or CGRP staining in the adventitia. The SGLT2 inhibitor-induced relaxations of mesenteric arteries were equally prevented by the application of the TRPV1 blocker AMG-517 or by depletion of CGRP through capsaicin treatment but not by the TRPA1 inhibitor AM0902. This suggests that the recruitment of TRPV1 rather than TRPA1 channels in sensory nerves is a key step in SGLT2 inhibitor-induced relaxations in the mesenteric artery.

TRPV1 is a polymodal cation channel regulated by various exogenous and endogenous activators. These include noxious chemicals (capsaicin or vanilloids), low pH (<6.0), high temperatures >43°C,[37] lipid mediators (i.e. anandamide), lipoxygenase products (e.g. LTB4),[38] and several signalling molecules (NGF, ATP, and PAR-2 agonists).[39,40] The subsequent influx of cations through TRPV1 is sufficient to promote fusion of synaptic vesicles containing CGRP and other neuropeptides. Our data are consistent with SGLT2 inhibitors relaxing mesenteric arteries by promoting CGRP release in a manner dependent upon TRPV1 channels. However, in over-expression systems, dapagliflozin and empagliflozin failed to either activate TRPV1 currents or enhance the effect of low pH or capsaicin, suggesting that these agents do not work directly on the channel. Therefore, TRPV1 activation is a consequence of an additional mechanism.

4.3 NHE1 and arterial relaxation

NHE1 plays a primary role in cardiomyocytes and VSMCs to maintain cellular pH levels at ~7.2.[41,42] Altered NHE expression and activity have been linked to severe cardiac events, where during ischaemia, the pH change activates NHE, leading to cardiac injury.[42] Many of the cardioprotective effects of SGLT2 inhibitors have been linked to reduced Na^+ load and pH development in cardiomyocytes through an effect on NHE1,[29–31] although this has been disputed.[43] However, an arterial role for NHE1 suppression in the clinical benefit of SGLT2 inhibitors has not been demonstrated, although a role for NHE1 inhibition in relaxations of human visceral arteries by canagliflozin was speculated.[31] NHE1 activation is linked to vasoconstriction and enhances the myogenic response in mouse

Downloaded from https://academic.oup.com/cardiovascres/article/120/14/1811/7721236 by guest on 10 January 2025

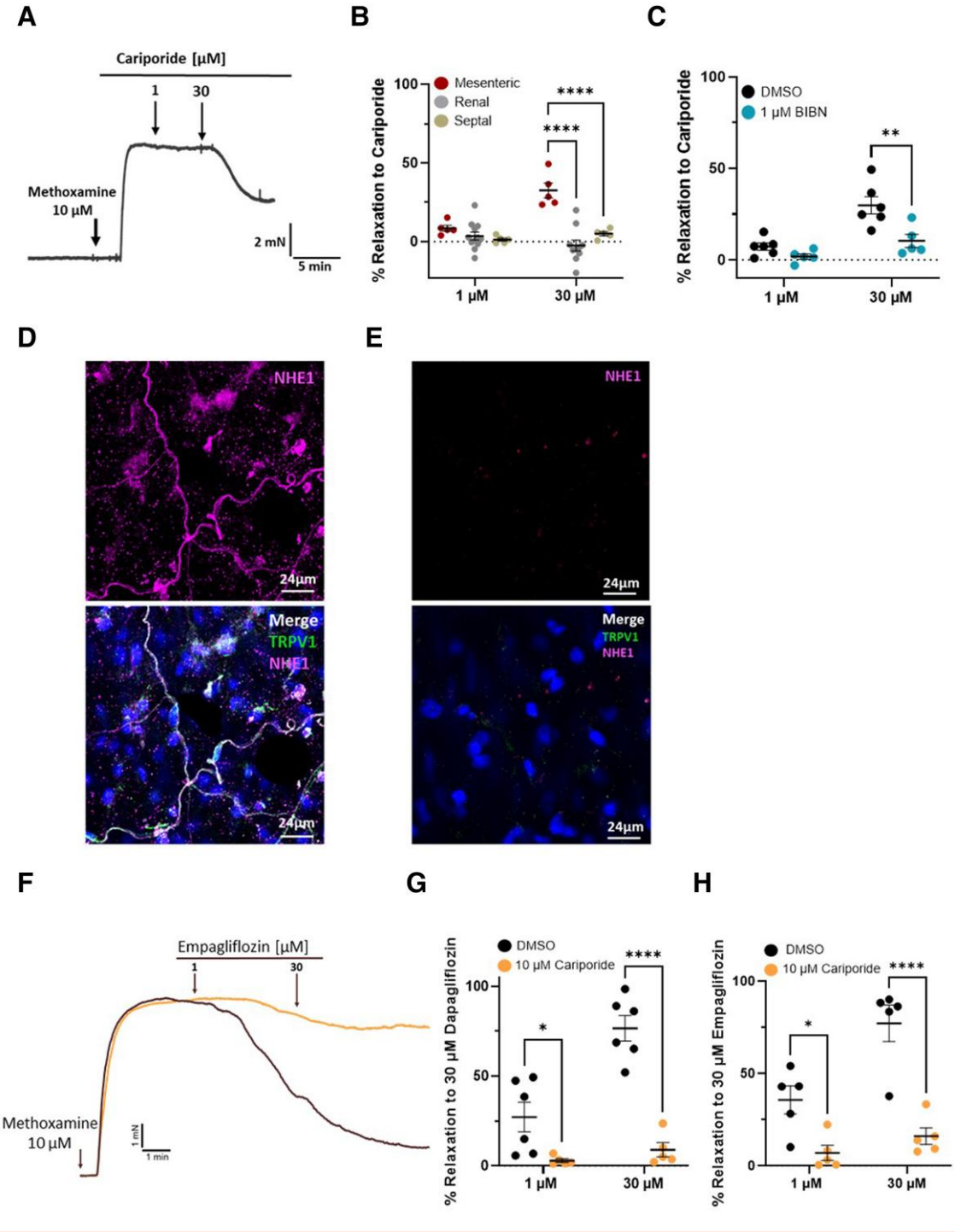


Figure 6 Effect of cariporide and NHE1 localization in mesenteric arteries. (*A*) A representative trace of the relaxation to 1 and 30 μM cariporide in mesenteric arteries pre-contracted with 10 μM methoxamine. (*B*) Mean percentage relaxation to 1 and 30 μM cariporide in mesenteric (left hand data), renal (middle data set), and septal arteries (right hand data set) ($N = 6$–10). (*C*) shows the mean percentage relaxation to cariporide (1–30 μM) in pre-contracted mesenteric arteries when incubated with DMSO (left) and 1 μM BIBN (right) ($N = 5$–6). (*D* and *E*) show representative labelling for TRPV1 alone (green, top) and with NHE1 (magenta, bottom) in the adventitia of whole mesenteric (*D*, $N = 3$) and renal (*E*, $N = 4$) arteries. Nuclei were labelled in blue. (*F*) Representative trace of the relaxation to empagliflozin (1–30 μM) in mesenteric arteries pre-contracted with 10 μM methoxamine in the presence (orange) and absence (black) of cariporide. The mean data for the response to 1 and 30 μM dapagliflozin ($N = 5$) and empagliflozin ($N = 5$) in the presence (top trace) and absence (bottom trace) of 10 μM cariporide are shown in (*G* and *H*). All data are individual experiments with the mean ± SEM denoted by the error bars. A two-way statistical ANOVA with a *post hoc* Sidak test was used to generate significant values (*$P < 0.05$, **$P < 0.01$, and ****$P < 0.0001$).

Downloaded from https://academic.oup.com/cardiovascres/article/120/14/1811/7721236 by guest on 10 January 2025

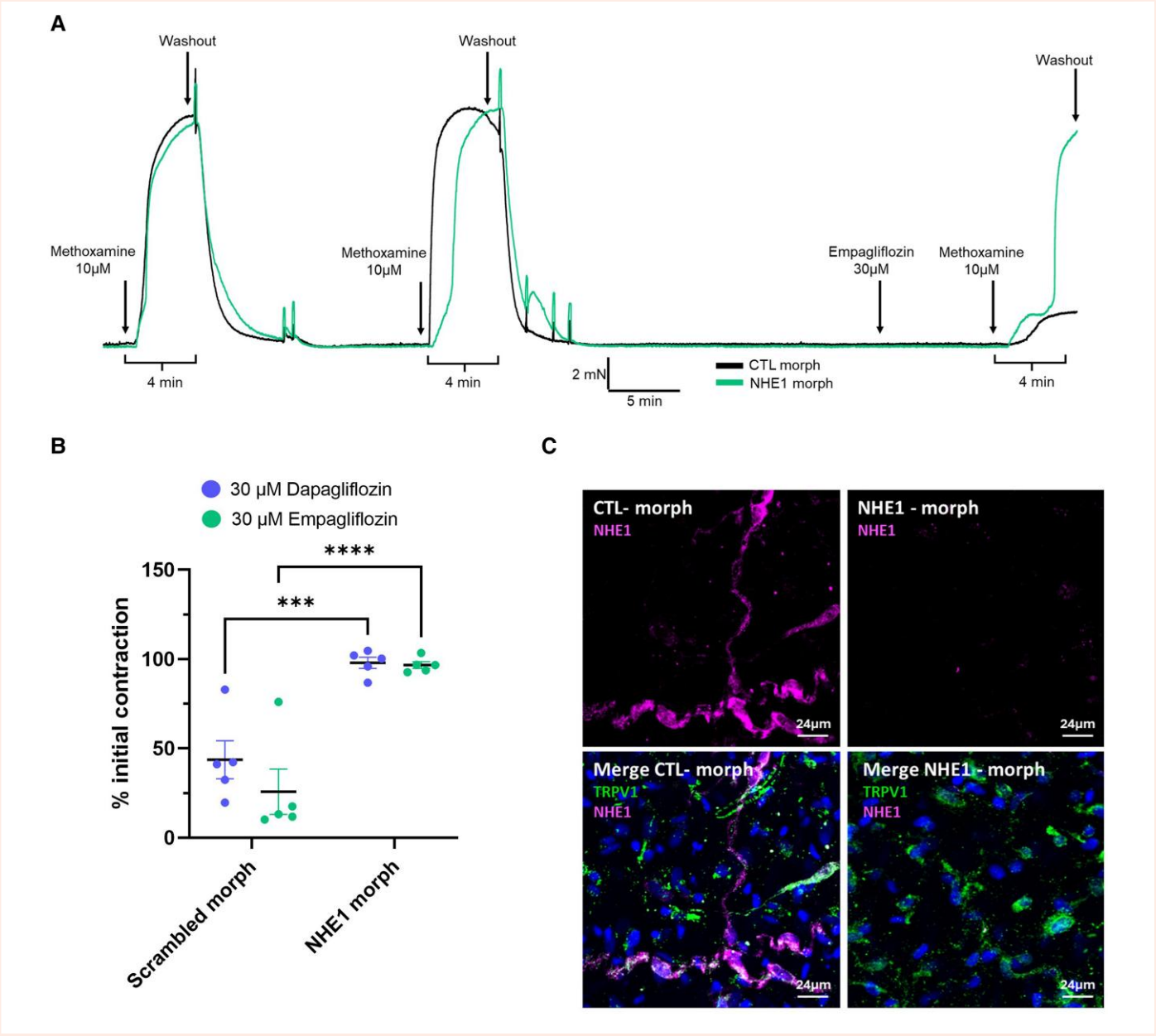


Figure 7 Knockdown of NHE1 impairs the relaxation of dapagliflozin and empagliflozin in mesenteric arteries. (*A*) A representative trace of the contraction to 10 μM methoxamine in the presence of 30 μM empagliflozin in scrambled control morpholino (black) and knockdown NHE1 morpholino (green/lighter line) arteries. (*B*) shows the mean data of the contraction to 10 μM methoxamine in scrambled control morpholino and knockdown NHE1 morpholino arteries when pre-incubated with 30 μM dapagliflozin or 30 μM empagliflozin. All data are represented as mean ± SEM denoted by the error bars. A two-way statistical ANOVA with a *post hoc* Sidak test was used to generate significant values (***$P < 0.001$ and ****$P < 0.0001$). (*C*) shows representative labelling for NHE1 alone (top image) and with TRPV1 (lower image) in the adventitia of whole mesenteric arteries transfected with scrambled morpholino (Ctrl) and NHE1-targeted morpholino (right hand column). Representative of 4 such experiments.

resistance arteries.[44] Increased NHE1 activity is also implicated in pulmonary artery hypertension, proliferation, and remodelling,[45] with the protein regulating pH or acting as a protein anchor. We propose that NHE1 located in the sensory nerves also has a profound effect in arteries because they influence TRPV1 activity and the subsequent cation influx precipitates vesicular release of potent vasodilators including CGRP. Thus, in the present study, relaxations to SGLT2 inhibitors and the NHE1 blocker cariporide[30] were prevented by a CGRP receptor antagonist and TRPV1 blocker. Moreover, pre-application of cariporide and, crucially, morpholino-based knockdown of NHE1 abrogated the response to dapagliflozin and empagliflozin. Interestingly, only NHE1 was identified in sensory nerves, unlike in the proximal convoluted tubule, where SGLT2 and NHE1 co-habit in the same microdomain.[46] Inhibition of NHE1 in the smooth muscle cells would also influence the contractile state to some degree (see Boedtkjer *et al.*[26]), but our work provides robust evidence that SGLT2 inhibitors relax mesenteric arteries via TRPV1-dependent release of CGRP following NHE1 inhibition. Future studies will ascertain the precise mechanisms linking NHE1 inhibition and CGRP release.

Downloaded from https://academic.oup.com/cardiovascres/article/120/14/1811/7721236 by guest on 10 January 2025

Translational perspective

SGLT2 inhibitors like empagliflozin are effective hypoglycaemic agents but are also recommended treatments for heart failure and chronic kidney disease independent of circulating glucose. However, the mechanisms underlying the cardiovascular benefit are ill defined. The present study reveals that SGLT2 inhibitors relax arteries *ex vivo* via the release of calcitonin gene related peptide (CGRP) from sensory nerves, which is mediated by inhibition of sodium/hydrogen exchangers. The ensuing vasodilatation allied to anti-inflammatory, anti-fibrotic, and pro-inotropic actions of CGRP will ameliorate cardiovascular stress. This understanding of the mechanisms that underlie the arterial vasodilatation by these agents may inform future use.

5. Conclusion

CGRP is a potent vasodilator of many vascular beds,[14] is a safeguard against cardiac ischaemia, and promotes cardiac contractility in failing hearts.[18] Our data reveal that the beneficial effects of SGLT2 inhibitors likely stem from an ability to release cardioprotective CGRP into stressed circulations. The ensuing vasodilatation allied to anti-inflammatory, anti-fibrotic, and pro-inotropic actions of CGRP will support effective circulation and help to ameliorate cardiovascular stress.

Supplementary material

Supplementary material is available at *Cardiovascular Research* online.

Authors' contributions

E.A.F. generated and analysed data, and wrote the manuscript. M.B.-A. and K.E.R. generated and analysed electrophysiological data. K.D. supervised generation of whole artery staining. V.B. and I.S.-C. supervised the PCR, WB, and ICC data and edited the manuscript. A.P.A., T.A.J., G.W.A., and T.R. edited the manuscript. I.A.G. supervised the project, edited the manuscript, and provided the funding for the project.

Acknowledgements

Dr Lillian Wallis at the Department of Pharmacology, Oxford University, provided expertise in whole artery immunohistochemistry and Itzel Llorente from the Instituto de Fisiología Celular at UNAM performed cell culture and transfection of HEK293 cells with TRPV1. Thanks to Professor Christian Aalkjaer, University of Arhus, for his insightful comments about sensory nerves and sodium/hydrogen exchangers.

Conflict of interest: none declared.

Funding

This work was supported by a PhD studentship for E.A.F. (FS/PhD/21/2912) from the British Heart Foundation awarded to I.A.G. G.W.A. was supported by the National Institute of General Medical Sciences (GM130377). K.E.R. was supported by the National Institute of Neurological Disorders and Stroke (T32NS045540). T.A.J. was funded by the Lundbeck Foundation (grant R323-2018-3674), and T.R. was funded by Dirección General de Asuntos del Personal Académico (DGAPA)-Programa de Apoyo a Proyectos de Investigación e Innovación Tecnológica (PAPIIT) (IN200423).

Data availability

The data underlying this article will be shared on reasonable request to the corresponding author.

References

1. Grempler R, Thomas L, Eckhardt M, Himmelsbach F, Sauer A, Sharp DE, Bakker RA, Mark M, Klein T, Eickelmann P. Empagliflozin, a novel selective sodium glucose cotransporter-2 (SGLT-2) inhibitor: characterisation and comparison with other SGLT-2 inhibitors. *Diabetes Obes Metab* 2012;**14**:83–90.
2. Wright EM. SGLT2 inhibitors: physiology and pharmacology. *Kidney360* 2021;**2**:2027–2037.
3. Preda A, Montecucco F, Carbone F, Camici GG, Lüscher TF, Kraler S, Liberale L. SGLT2 inhibitors: from glucose-lowering to cardiovascular benefits. *Cardiovasc Res* 2024;**120**:443–460.
4. McMurray JJV, Solomon SD, Inzucchi SE, Køber L, Kosiborod MN, Martinez FA, Ponikowski P, Sabatine MS, Anand IS, Bělohlávek J, Böhm M, Chiang CE, Chopra VK, Boer RA, de Desai AS, Diez M, Drozdz J, Dukát A, Ge J, Howlett JG, Katova T, Kitakaze M, Ljungman CEA, Merkely B, Nicolau JC, O'Meara E, Petrie MC, Vinh PN, Schou M, Tereshchenko S, Verma S, Held C, DeMets DL, Docherty KF, Jhund PS, Bengtsson O, Sjöstrand M, Langkilde AM. Dapagliflozin in patients with heart failure and reduced ejection fraction. *NEJM* 2019;**381**:1995–2008.
5. Nassif ME, Windsor S, Tang F, Khariton Y, Husain M, Inzucchi S, McGuire D, Pitt B, Scirica B, Austin B, Drazner M, Fong M, Givertz M, Gordon R, Jermyn R, Katz S, Lamba S, Lanfear D, LaRue S, Lindenfeld JA, Malone M, Margulies K, Mentz R, Kannan Mutharasan R, Pursley M, Umpierrez G, Kosiborod M, Malik A, Wenger N, Ogunniyi M, Vellanki P, Murphy B, Newman J, Hartupee J, Gupta C, Goldsmith M, Baweja P, Montero M, Gottlieb S, Costanzo MR, Hoang T, Warnock A, Allen L, Tang W, Chen H, Cox J. Dapagliflozin effects on biomarkers, symptoms, and functional status in patients with heart failure with reduced ejection fraction. *Circulation* 2019;**140**:1463–1476.
6. Beal B, Schutte AE, Neuen BL. Blood pressure effects of SGLT2 inhibitors: mechanisms and clinical evidence in different populations. *Curr Hypertens Rep* 2023;**25**:429–435.
7. Li H, Shin SE, Seo MS, An JR, Choi IW, Jung WK, Firth AL, Lee DS, Yim MJ, Choi G, Lee JM, Na SH, Park WS. The anti-diabetic drug dapagliflozin induces vasodilation via activation of PKG and Kv channels. *Life Sci* 2018;**197**:46–55.
8. Seo MS, Jung HS, An JR, Kang M, Heo R, Li H, Han ET, Yang SR, Cho EH, Bae YM, Park WS. Empagliflozin dilates the rabbit aorta by activating PKG and voltage-dependent K+ channels. *Toxicol Appl Pharmacol* 2020;**403**:115153.
9. Hasan A, Hasan R. Empagliflozin relaxes resistance mesenteric arteries by stimulating multiple smooth muscle cell voltage-gated K+ (KV) channels. *Int J Mol Sci* 2021;**22**:10842.
10. Hasan A, Menon SN, Zerin F, Hasan R. Dapagliflozin induces vasodilation in resistance-size mesenteric arteries by stimulating smooth muscle cell KV7 ion channels. *Heliyon* 2022;**8**:e09503.
11. Hasan A, Zerin F, Menon SN, Alam MA, Hasan R. Mechanism of canagliflozin-induced vasodilation in resistance mesenteric arteries and the regulation of systemic blood pressure. *J Pharm Sci* 2022;**150**:211–222.
12. Choi S, Haam CE, Byeon S, Oh EY, Choi SK, Lee YH. Investigating the cardiovascular benefits of dapagliflozin: vasodilatory effect on isolated rat coronary arteries. *Int J Mol Sci* 2023;**24**:16873.
13. Kawasaki H, Takasaki K, Saito A, Goto K. Calcitonin gene-related peptide acts as a novel vasodilator neurotransmitter in mesenteric resistance vessels of the rat. *Nature* 1988;**335**:164–167.
14. Aalkjaer C, Nilsson H, De Mey JGR. Sympathetic and sensory-motor nerves in peripheral small arteries. *Physiol Rev* 2021;**101**:495–544.
15. Brain SD, Williams TJ, Tippins JR, HR M, MacIntyre I. Calcitonin gene-related peptide is a potent vasodilator. *Nature* 1985;**313**:54–56.
16. Ralevic V, Kendall DA, Randall MD, Zygmunt PM, Movahed P, Högestätt ED. Vanilloid receptors on capsaicin-sensitive sensory nerves mediate relaxation to methanandamide in the rat isolated mesenteric arterial bed and small mesenteric arteries. *Brit J Pharmacol* 2000;**130**:1483.
17. Shiraki H, Kawasaki H, Tezuka S, Nakatsuma A, Kurosaki Y. Endogenous calcitonin gene-related peptide (CGRP) mediates adrenergic-dependent vasodilation induced by nicotine in mesenteric resistance arteries of the rat. *Brit J Pharmacol* 2000;**130**:1083.
18. MaassenVanDenBrink A, Meijer J, Villalón CM, Ferrari MD. Wiping out CGRP: potential cardiovascular risks. *TiPS* 2016;**37**:779–788.
19. Chadha PS, Jepps TA, Carr G, Stott JB, Zhu HL, Cole WC, Greenwood IA. Contribution of kv7.4/kv7.5 heteromers to intrinsic and calcitonin gene-related peptide-induced cerebral reactivity. *ATVB* 2014;**34**:887–893.
20. Stott JB, Barrese V, Suresh M, Masoodi S, Greenwood IA. Investigating the role of Gβγ in Kv7 dependent relaxations of the rat vasculature. *ATVB* 2018;**38**:2091.
21. van der Horst J, Manville RW, Hayes K, Thomsen MB, Abbott GW, Jepps TA. Acetaminophen (paracetamol) metabolites induce vasodilation and hypotension by activating Kv7 potassium channels directly and indirectly. *ATVB* 2020;**40**:1207–1219.
22. Mulvany MJ, Halpern W. Contractile properties of small arterial resistance vessels in spontaneously hypertensive and normotensive rats. *Circ Res* 1977;**41**:19–26.

Downloaded from https://academic.oup.com/cardiovascres/article/120/14/1811/7721236 by guest on 10 January 2025

23. Inoue T, Takemura M, Fushimi N, Fujimori Y, Onozato T, Kurooka T, Asari T, Takeda H, Kobayashi M, Nishibe H, Isaji M. Mizagliflozin, a novel selective SGLT1 inhibitor, exhibits potential in the amelioration of chronic constipation. *Eur J Pharmacol* 2017;**806**:25–31.
24. Barrese V, Stott JB, Greenwood IA. KCNQ-encoded potassium channels as therapeutic targets. *Annu Rev Pharmacol Toxicol* 2018;**58**:625–648.
25. Ortíz-Rentería M, Juárez-Contreras R, González-Ramírez R, Islas LD, Sierra-Ramírez F, Llorente I, Simon SA, Hiriart M, Rosenbaum T, Morales-Lázaro SL. TRPV1 channels and the progesterone receptor Sig-1R interact to regulate pain. *PNAS* 2018;**115**:E1657–E1666.
26. Boedtkjer E, Damkier HH, Aalkjaer C. NHE1 knockout reduces blood pressure and arterial media/lumen ratio with no effect on resting pHi in the vascular wall. *J Physiol* 2012;**590**:1895–1906.
27. Gamarra M, de la Cruz A, Blanco-Urrejola M, Baleriola J. Local translation in nervous system pathologies. *Front Integr Neurosci* 2021;**15**:689208.
28. Barrese V, Stott JB, Baldwin SN, Mondejar-Parreño G, Greenwood IA. SMIT (sodium-myo-inositol transporter) 1 regulates arterial contractility through the modulation of vascular Kv7 channels. *ATVB* 2020;**40**:2468–2480.
29. Baartscheer A, Schumacher CA, Wüst RCI, Fiolet JWT, Stienen GJM, Coronel R, Zuurbier CJ. Empagliflozin decreases myocardial cytoplasmic Na+ through inhibition of the cardiac Na+/H+ exchanger in rats and rabbits. *Diabetologia* 2017;**60**:568.
30. Uthman L, Baartscheer A, Bleijlevens B, Schumacher CA, Fiolet JWT, Koeman A, Jancev M, Hollmann MW, Weber NC, Coronel R, Zuurbier CJ. Class effects of SGLT2 inhibitors in mouse cardiomyocytes and hearts: inhibition of Na+/H+ exchanger, lowering of cytosolic Na+ and vasodilation. *Diabetologia* 2018;**61**:722.
31. De Stefano A, Tesauro M, Di Daniele N, Vizioli G, Schinzari F, Cardillo C. Mechanisms of SGLT2 (sodium-glucose transporter type 2) inhibition-induced relaxation in arteries from human visceral adipose tissue. *Hypertension* 2021;**77**:729–738.
32. Zuurbier CJ, Baartscheer A, Schumacher CA, Fiolet JWT, Coronel R. Sodium-glucose cotransporter 2 inhibitor empagliflozin inhibits the cardiac Na+/H+ exchanger 1: persistent inhibition under various experimental conditions. *Cardiovasc Res* 2021;**117**:2699–2701.
33. Uthman L, Li X, Baartscheer A, Schumacher CA, Baumgart P, Hermanides J, Preckel B, Hollmann MW, Coronel R, Zuurbier CJ, Weber NC. Empagliflozin reduces oxidative stress through inhibition of the novel inflammation/NHE/[Na+]c/ROS-pathway in human endothelial cells. *Biomed Pharmacother* 2022;**146**:112515.
34. Chung CC, Lin YK, Chen YC, Kao YH, Yeh YH, Trang NN, Chen YJ. Empagliflozin suppressed cardiac fibrogenesis through sodium-hydrogen exchanger inhibition and modulation of the calcium homeostasis. *Cardiovasc Diabetol* 2023;**22**:27.
35. Betrie AH, Brock JA, Harraz OF, Bush AI, He GW, Nelson MT, Angus JA, Wright CE, Ayton S. Zinc drives vasorelaxation by acting in sensory nerves, endothelium and smooth muscle. *Nat Commun* 2021;**12**:3296.
36. Seman L, Macha S, Nehmiz G, Simons G, Ren B, Pinnetti S, Woerle HJ, Dugi K. Empagliflozin (BI 10773), a potent and selective SGLT2 inhibitor, induces dose-dependent glucosuria in healthy subjects. *Clin Pharmacol Drug Dev* 2013;**2**:152–161.
37. Caterina MJ, Schumacher MA, Tominaga M, Rosen TA, Levine JD, Julius D. The capsaicin receptor: a heat-activated ion channel in the pain pathway. *Nature* 1997;**389**:816–824.
38. Huang SM, Bisogno T, Trevisani M, Al-Hayani A, De Petrocellis L, Fezza F, Tognetto M, Petros TJ, Krey JF, Chu CJ, Miller JD, Davies SN, Geppetti P, Walker JM, Di Marzo V. An endogenous capsaicin-like substance with high potency at recombinant and native vanilloid VR1 receptors. *PNAS* 2002;**99**:8400.
39. Chuang HH, Prescott ED, Kong H, Shields S, Jordt SE, Basbaum AI, Chao MV, Julius D. Bradykinin and nerve growth factor release the capsaicin receptor from PtdIns(4,5)P2-mediated inhibition. *Nature* 2001;**411**:957–962.
40. Fernandes ES, Fernandes MA, Keeble JE. The functions of TRPA1 and TRPV1: moving away from sensory nerves. *Brit J Pharmacol* 2012;**166**:510.
41. Karmazyn M, Gan XT, Humphreys RA, Yoshida H, Kusumoto K. The myocardial Na+-H+ exchange. *Circ Res* 1999;**85**:777–786.
42. Wichaiyo S, Saengklub N. Alterations of sodium-hydrogen exchanger 1 function in response to SGLT2 inhibitors: what is the evidence? *Heart Fail Rev* 2022;**27**:1973–1990.
43. Chung YJ, Park KC, Tokar S, Eykyn TR, Fuller W, Pavlovic D, Swietach P, Shattock MJ. Off-target effects of sodium-glucose co-transporter 2 blockers: empagliflozin does not inhibit Na+/H+ exchanger-1 or lower [Na+]i in the heart. *Cardiovasc Res* 2021;**117**:2794–2806.
44. Artamonov MV, Sonkusare SK, Good ME, Momotani K, Eto M, Isakson BE, Le TH, Cope EL, Derewenda ZS, Derewenda U, Somlyo AV. RSK2 contributes to myogenic vasoconstriction of resistance arteries by activating smooth muscle myosin and the Na+/H+ exchanger. *Sci Signal* 2018;**11**:eaar3924.
45. Lade JM, Andrade MR, Undem C, Walker J, Jiang H, Yun X, Shimoda LA. Hypoxia enhances interactions between Na+/H+ exchanger isoform 1 and actin filaments via ezrin in pulmonary vascular smooth muscle. *Front Physiol* 2023;**14**:1108304.
46. Pessoa TD, Campos LCG, Carraro-Lacroix L, Girardi ACC, Malnic G. Functional role of glucose metabolism, osmotic stress, and sodium-glucose cotransporter isoform-mediated transport on Na+/H+ exchanger isoform 3 activity in the renal proximal tubule. *J Am Soc Nephrol* 2014;**25**:2028–2039.

Downloaded from https://academic.oup.com/cardiovascres/article/120/14/1811/7721236 by guest on 10 January 2025

Check for updates

Received: 12 August 2022 | Revised: 4 January 2023 | Accepted: 4 January 2023

DOI: 10.14814/phy2.15583

ORIGINAL ARTICLE

The Physiological Society | american physiological society | Physiological Reports

Key role for Kv11.1 (ether-a-go-go related gene) channels in rat bladder contractility

Vincenzo Barrese[1,2] | **Zena Wehbe**[1] | **Alice Linden**[1] | **Sarah McDowell**[3] | **Elizabeth Forrester**[1] | **Oleksander Povstyan**[4] | **Karen D. McCloskey**[3] | **Iain A. Greenwood**[1]

[1]Vascular Biology Research Centre, Molecular and Clinical Sciences Research Institute, St George's University of London, London, UK

[2]Department of Neuroscience, Reproductive Sciences and Dentistry, University of Naples Federico II, Naples, Italy

[3]Patrick G. Johnston Centre for Cancer Research, School of Medicine, Dentistry and Biomedical Sciences, Queen's University Belfast, Belfast, UK

[4]Institute of Medicine, University of Leeds, Leeds, UK

Correspondence
Iain A. Greenwood, Vascular Biology Research Centre, Molecular and Clinical Sciences Research Institute, St George's University of London, London SW17 0RE, UK.
Email: grenwood@sgul.ac.uk

Abstract

In addition, to their established role in cardiac myocytes and neurons, ion channels encoded by ether-a-go-go-related genes (ERG1-3 or *kcnh2,3* and *6*) (*kcnh*2) are functionally relevant in phasic smooth muscle. The aim of the study was to determine the expression and functional impact of ERG expression products in rat urinary bladder smooth muscle using quantitative polymerase chain reaction, immunocytochemistry, whole-cell patch-clamp and isometric tension recording. *kcnh*2 was expressed in rat bladder, whereas *kcnh*6 and *kcnh*3 expression were negligible. Immunofluorescence for the *kcnh2* expression product Kv11.1 was detected in the membrane of isolated smooth muscle cells. Potassium currents with voltage-dependent characteristics consistent with Kv11.1 channels and sensitive to the specific blocker E4031 (1 μM) were recorded from isolated detrusor smooth muscles. Disabling Kv11.1 activity with specific blockers (E4031 and dofetilide, 0.2–20 μM) augmented spontaneous contractions to a greater extent than BK_{Ca} channel blockers, enhanced carbachol-driven activity, increased nerve stimulation-mediated contractions, and impaired β-adrenoceptor-mediated inhibitory responses. These data establish for the first time that Kv11.1 channels are key determinants of contractility in rat detrusor smooth muscle.

KEYWORDS

BK channels, detrusor smooth muscle, ether-a-go-go-related genes, *kcnh2* gene, Kv11.1

1 | INTRODUCTION

The ether-a-go-go-related gene (ERG) family comprises three members in humans, *ERG1,2,3* (*KCNH2*, *KCNH6*, and *KCNH7*, HUGO gene nomenclature) that encode for tetrameric voltage-dependent potassium channels (Kv11.1–Kv11.3, respectively) (Gutman et al., 2005). Kv11 channels exhibit distinctive voltage-dependent kinetics due to a dominant C-type inactivation that is relieved quicker than channel deactivation by membrane hyperpolarization (Dai & Zagotta, 2017; Hoshi & Armstrong, 2013; Spector et al., 1996).

KCNH2 is expressed predominantly in cardiac myocytes and congenital mutations in this gene result in gross perturbation of the normal cardiac electrical activity associated with hereditary long QT syndrome (London

This is an open access article under the terms of the Creative Commons Attribution License, which permits use, distribution and reproduction in any medium, provided the original work is properly cited.
© 2023 The Authors. *Physiological Reports* published by Wiley Periodicals LLC on behalf of The Physiological Society and the American Physiological Society.

et al., 1997; Vandenberg et al., 2001). *KCNH6* and *KCNH7* expression are restricted mainly to neuronal cells, where the expression products contribute to resting membrane conductance (Bauer & Schwarz, 2018). However, several studies have identified Kv11 channels as important dampeners of cellular excitability in several smooth muscles. *KCNH2* expression has been detected by qPCR and immunocytochemistry in rodent stomach, portal vein, and myometrium (Greenwood et al., 2009; Ohya, Asakura, et al., 2002; Ohya, Horowitz, et al., 2002). Moreover, currents with kinetics characteristic of Kv11 channels have been recorded in opossum esophagus, mouse portal vein, and nonpregnant mouse and human myometrium (Akbarali et al., 1999; Greenwood et al., 2009; Ohya, Horowitz, et al., 2002; Parkington et al., 2014; Yeung & Greenwood, 2007). In addition, selective Kv11 channel blockers like E4031 or dofetilide depolarise membrane potential and increase contractility in opossum esophagus, rat stomach, mouse gall bladder, equine and human jejunum, mouse portal vein, bovine epididymis, mouse and human myometrium (Akbarali et al., 1999; Farrelly et al., 2003; Greenwood et al., 2009; Lillich et al., 2003; Mewe et al., 2008; Ohya, Asakura, et al., 2002; Ohya, Horowitz, et al., 2002; Parkington et al., 2014; Parr et al., 2003; Yeung & Greenwood, 2007). Common to all these smooth muscles is the exhibition of spontaneous, phasic contractile behavior associated with action potential discharge.

The detrusor smooth muscle of the urinary bladder also exhibits spontaneous contractions which, in tension recordings from bladder strips, manifest as low-amplitude contractions in contrast to much larger nerve-evoked or agonist-evoked (e.g., acetylcholine or ATP) contractions (Drake et al., 2018). The genesis of spontaneous contractions is a source of debate with both inherent myogenicity and urothelial-derived or mucosal mediators being implicated (Brading, 1997; Drake et al., 2018). Their role is considered to provide a degree of tone and dynamic adjustment of optimal bladder shape during filling so that the bladder can be effectively emptied from any volume (Turner & Brading, 1997). During bladder filling, mechanisms that limit the amplitude of spontaneous contractions are essential for the bladder to expand and act as a reservoir. Detrusor smooth muscle expresses a panel of potassium channels that act as brakes on contractility through repolarization of the action potential and control of the resting membrane potential (Petkov, 2011). Of the myriad potassium channels, there is substantial evidence for the functional expression of BK (Petkov, 2014), Kv (Maylz & Petkov, 2020), and Kv7 channels (Anderson et al., 2013; Bientinesi et al., 2017; Provence et al., 2018; Svalo et al., 2015) and their contribution to spontaneous contractions. There is a paucity of work supporting the expression of *ERG* in a bladder and to the best of our knowledge, only one paper on ERG channel function where increased spontaneous contraction amplitude and corresponding decreased frequency in guinea-pig bladder strips by the ERG channel blocker, E4031 was reported (Imai et al., 2001). The goal of the present study was to determine the molecular expression of *Kcnh* genes in rat detrusor smooth muscle and to ascertain the functional impact of ERG channels in detrusor contractility using various pharmacological selective modulators.

2 | MATERIALS AND METHODS

2.1 | Ex vivo bladder preparation techniques

Whole bladders were dissected from male Wistar rats (200–250 g) killed by cervical dislocation in accordance with the 1986 UK Animals Scientific Procedures Act (1986). Bladders were dissected free of fat and connective tissue then cut into transverse bands of 1 mm thickness from the mid-region of the bladder, while submerged in an ice-cold physiological saline solution (PSS) of the following composition (mmol/L); 1.25 $CaCl_2$, 5 glucose, 25 $NaHCO_3$, 1.18 NaH_2PO_4, 1.17 $MgSO_4$, 4.5 KCl, 119 NaCl. The bands were then mounted on micro-pins within the tissue chambers of a myograph capable of isometric tension recording. Bands were set to an initial tension of 2 mN and reset to this level over a 1-h equilibration period. Tissue viability was then assessed by a 60 mM KCl challenge. The effect of two structurally different, open channel blockers of Kv11.1, E4031 and dofetilide (Spector et al., 1996) was investigated using single concentrations per tissue. In a separate experimental series, carbachol was added cumulatively to all bladder bands. After the washout of carbachol, tissue bands were incubated with one of the following agents: dimethyl sulphoxide (DMSO) (0.2%) as the vehicle control or 2 μM E4031 and 20 μM E4031.

For isoprenaline experiments, the level of spontaneous activity was enhanced by the application of 20 mM KCl. Isoprenaline was applied cumulatively from 0.001 to 1 μM. After washout, tissue bands were preincubated with one of the following channel modulators: 20 μM E4031, 10 μM XE991 (Kv7 channel blocker),100 nM Iberiotoxin (BK_{Ca} blocker), or DMSO as vehicle control (0.2%) and isoprenaline was re-applied.

All drugs were obtained from HelloBio except iberiotoxin (Alomone).

For electrical field stimulation (EFS) studies, transverse bands (1 mm thickness) were mounted in vertical baths attached to force transducers via wire hooks. EFS was delivered via silver/silver chloride electrodes placed at the top

2051817x, 2023, 3, Downloaded from https://physoc.onlinelibrary.wiley.com/doi/10.14814/phy2.15583 by Test, Wiley Online Library on [10/01/2025]. See the Terms and Conditions (https://onlinelibrary.wiley.com/terms-and-conditions) on Wiley Online Library for rules of use; OA articles are governed by the applicable Creative Commons License

and bottom of the vertical organ baths using a Grass stimulator (Grass) and the following parameters, 0.3 ms pulse width, 10 s duration, 30–40 V, 0.5–32 Hz frequency range. Organ baths were perfused with oxygenated PSS (solution as above) at 37°C at a rate of 2–3 mL/min; drugs were delivered via the perfusion system. Recordings were made via an AD/DA converter (National Instruments) and a personal computer running Chart software (University of Strathclyde, Dr J Dempster).

Contractions were measured in Clampfit (pClamp software; Axon Instruments) and data were collated in Excel (Microsoft Office) and analyzed in GraphPad Prism software. EFS contraction amplitudes were normalized to a control contraction evoked by 60 mM K^+ Krebs solution for each experiment. Data are presented as mean ± standard error of the mean (SEM), and data sets were tested with two-way analysis of variance (ANOVA) and Bonferroni post-hoc tests with $p < 0.05$ considered significant.

Spontaneous contractions were recorded using LabChart software. The parameters that were then measured and analyzed, included baseline tone, amplitude and frequency of individual phasic contractions, and maximum change in contractility. Baseline tone is the lowest point of the trace from which phasic contractions develop. Maximum change in baseline contractility was measured for the highest crest amplitude and compared with the initial baseline tone. Amplitude was calculated as the average force (mN) of the peaks of the amplitudes 2 min prior to the addition of the next drug. Frequency was calculated as the average number of individual contractions occurring per minute.

2.2 | Quantitative real-time polymerase chain reaction assay

cDNA was produced by reverse transcription of messenger RNA extracted from the intact bladder tissue samples. Quantitative real-time polymerase chain reaction (qPCR) was performed using specific primers for rat *Kcnh*2, *Kcnh*2-L, *Kcnh*6, and *Kcnh*7 (Table 1) and SYBR Green Master Mix from Primer design. Two isoforms are known for Kcnh2 (erg1) gene: a full-length isoform, encoding a protein composed of 1163 amino acids (previously termed erg1 long or erg1a), and a short one (erg1 short or erg1b), missing the first 5 exons of full-length Erg1 and encoding an 821 amino acid protein with a different N-terminus with respect to Erg1a, encoded by an alternative exon 5 (Vandenberg et al., 2012).

Therefore, to evaluate the expression in rat bladder of the different isoforms, we used two sets of primers targeting the *Kcnh2* gene; these sequences were designed to amplify a common region of Kcnh2 found in the two transcripts variant (here defined as "*Kcnh2* primers"), and a specific sequence that can be found only in the longer variant of the same gene (here called "*Kcnh2-L* primers").

The reaction was carried out in a clean, designated environment to minimize the risk of contamination. Primer and SYBR Green Mix were prepared and added to a 96-well plate, and the prepared cDNA template was added. Control wells containing no cDNA were used to detect the possible occurrence of contamination of the samples. qPCR reaction was performed using a CFX96 Real-Time PCR machine (Biorad) according to the following protocol: 95°C for 10 min (enzyme activation), then 40 cycles at 95°C for 15 s and 60°C for 60 s (denaturation and data collection). A melt curve to check for nonspecific PCR products was performed at the end of the reaction. Results were then collected and analyzed using BioRad CFX Manager Software. Data were normalized to the housekeeping gene Cytochrome C1 (CYC1) and expressed using the $2^{-\Delta Ct}$ formula.

2.3 | Electrophysiology

Single smooth muscle cells (SMCs) were isolated from the whole bladder by enzymatic dispersal. Tissues were carefully cleaned of the mucosal layer (comprising urothelium, lamina propria, small blood vessels, and connective

TABLE 1 Primers used for qPCR experiments.

Gene	*Kcnh2*	*Kcnh2-L*	*Kcnh6*	*Kcnh7*	*cyc1*
Primer sequence Forward	5′-CCCCTCCA TCAAGG ACAAGT-3′	5′-CCTCGACACCA TCATCCGCA-3′	5′-GTGGATGTGGT CCCTGTGAA-3′	5′-GCCCGGGC TCAACC TGAAGA-3′	5′-TCGAAAACGCA TGGGACTCA-3′
Primer sequence Reverse	5′-TGAGCATG ACACAG ATGGAG-3′	5′-AGGAAATCGCA GGTGCAGGG-3′	5′-AGAGCCCAGGA AGCTGTGTG-3′	5′-TGGCCTGG ATGTCC GTTGTC-3′	5′-TGACCACTTAT GCCGCTTCA-3′
Amplicon size (base pairs)	128	156	141	169	85
Target sequence region	2145–2272	369–533	328–468	3012–3180	889–973

20518171x, 2023, 3, Downloaded from https://physoc.onlinelibrary.wiley.com/doi/10.14814/phy2.15583 by Test, Wiley Online Library on [10/01/2025]. See the Terms and Conditions (https://onlinelibrary.wiley.com/terms-and-conditions) on Wiley Online Library for rules of use; OA articles are governed by the applicable Creative Commons License

tissues) and bathed for 10 min in nominally Ca^{2+}-free PSS. The vessels were then incubated at 37°C in Ca^{2+}-free PSS-containing collagenase type IA (2 mg/mL) and protease type X (1 mg/mL) for 25–30 min followed by a 10 min wash in Ca^{2+}-free PSS at room temperature (RT). Single cells were liberated by gentle mechanical agitation of tissues with a wide-bore Pasteur pipette and the suspension was transferred to experimental chambers. All experiments were performed at RT using the whole-cell patch-clamp technique. The solution used for recordings was of the following composition (mM): KCl 60, NaCl 66, $MgCl_2$ 1.2, $CaCl_2$ 0.1, D-glucose 12, and HEPES 10, pH was adjusted to 7.35 with NaOH. The solution was supplemented with paxilline (1 μM) and nicardipine (5 μM). Patch pipettes were fire-polished and had resistances of 4–8 MΩ when filled with the pipette solution containing (in mmol/L): 110 K gluconate, 30 KCl, 0.5 $MgCl_2$, 5 HEPES, and 0.5 EGTA. The electrical signals were recorded using an Axopatch 200B patch-clamp amplifier (Molecular Devices). Electrical signals were generated and digitized at 1 kHz using a Digidata 1322A hosted by a PC running pClamp 9.0 software (Axon Instruments). Data were analyzed and plotted using pClamp and MicroCal Origin software. All data are presented as mean ± SEM. To isolate Kv11 channel currents, we employed a protocol used previously (Greenwood et al., 2009; Ohya, Asakura, et al., 2002) that took advantage of the biophysical properties of the channel. Cells were held at 0 mV, where Kv11.1 channels were in an inactive state and then stepped to hyperpolarized potentials from −120 to −20 mV every 5 s. Steps to hyperpolarized voltages remove the inactivation that is followed by channel closure (deactivation). This results in a distinctive "hooked" appearance as both the recovery from inactivation and deactivation is faster at more hyperpolarized potentials (Ohya, Horowitz, et al., 2002; Smith et al., 1996).

2.4 | Immunocytochemistry

Bladder SMC were fixed with 3% paraformaldehyde solution at 22–24°C (RT) for 10 min, treated with 0.1 M glycine in phosphate-buffered saline (PBS) for 5 min, and incubated in blocking solution (PBS containing 0.1% Triton X-100 and 1% bovine serum albumin) for 1 h at RT. Subsequently, cells were incubated overnight at 4°C with goat polyclonal anti-HERG antibody (dilution 1:100), which had been validated previously using overexpression systems (Barrese et al., 2017) now discontinued or with mouse monoclonal anti-HERG antibody (1:100; sc-377388), and mouse monoclonal anti-α-smooth muscle actin antibody (dilution 1:1000) (Cat.#: A5228; Sigma). Samples were washed with PBS and incubated for 1 h with donkey antigoat secondary antibody conjugated to Alexa Fluor 568 (Cat.#: A-11057) and donkey antimouse secondary antibody conjugated to Alexa Fluor 488 (Cat.#: A32766) (dilution 1:100) (ThermoFisher). All antibodies were diluted in the blocking solution. No primary antibody was used as a negative control. Coverslips were mounted on glass slides; images were acquired using a Nikon A1R confocal microscope (Nikon Instruments Europe BV).

2.5 | Data analysis

Data were presented as mean ± SEM. For most graphical presentations, data were normalized and given as a percentage increase from resting conditions or as a percentage difference from the control group. Data processing and presentation utilized Microsoft Excel and Prism GraphPad software. Statistical analysis was carried out with one-way and two-way ANOVAs, where statistically significant values *, **, ***, **** represent $p < 0.05$, $p < 0.01$, $p < 0.001$, $p < 0.0001$, respectively. The number of tissues utilized in an experiment is referred to as "*n*," whereas the number of rats culled is denoted by "*N*."

3 | RESULTS

3.1 | Kv11.1 transcript (Kcnh) is expressed in rat detrusor smooth muscle

qPCR using primers specific for all three *Kcnh* isoforms revealed robust expression of *Kcnh2* but the minimal expression of Kcnh6 and Kcnh7 in the intact rat detrusor (Figure 1a). Of the two known variants of *Kcnh2* (London et al., 1997), the rat detrusor predominantly expressed the longer form (Figure 1a). Immunofluorescence experiments using anti-Kv11.1 antibodies were undertaken to assess the expression of *Kcnh2* products in detrusor muscle. SMCs were identified by co-staining with α-smooth muscle actin. In these cells, anti-Kv11.1 immunofluorescence showed peripheral distribution, indicative of plasma membrane localization of Kv11.1 channels (Figure 1b). Similar staining was seen with the goat anti-HERG polyclonal validated by Barrese et al. (2017).

Whole-cell electrophysiology was performed to determine if functional Kv11.1 currents could be recorded from isolated detrusor SMC using a protocol utilized previously (Greenwood et al., 2009; Ohya, Horowitz, et al., 2002) that takes advantage of the distinctive properties of the Kv11.1 channel. When isolated detrusor SMC were hyperpolarized from a holding potential to −120 mV a large, slowly developing inward current was recorded. This current was the HCN-encoded mixed cation current known as the "funny" current that is responsible for sino-atrial node pacing and

2051817x, 2023, 3, Downloaded from https://physoc.onlinelibrary.wiley.com/doi/10.14814/phy2.15583 by Test, Wiley Online Library on [10/01/2025]. See the Terms and Conditions (https://onlinelibrary.wiley.com/terms-and-conditions) on Wiley Online Library for rules of use; OA articles are governed by the applicable Creative Commons License

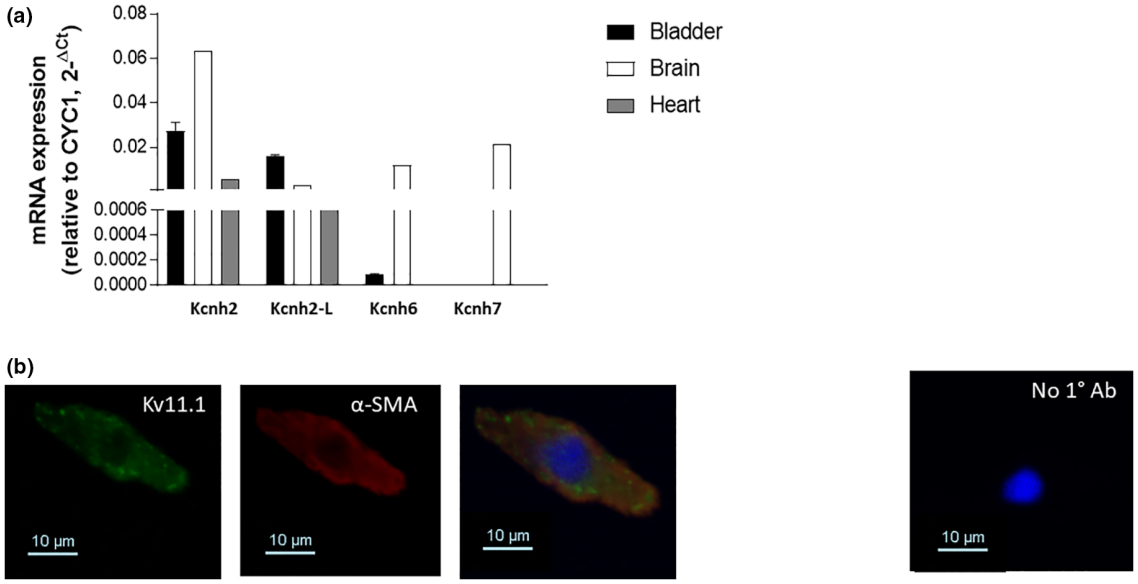


FIGURE 1 Expression of Kcnh2 channels in rat detrusor. (a) Quantitative PCR experiments showing the expression of total Kcnh2, long Kcnh2 isoform (Kcnq2-L), Kcnh6 and Kcnh7 mRNAs in rat detrusor, normalized to the housekeeping gene Cyc1. The rat brain and heart were used as positive controls. Data are expressed as mean ± standard error of the mean. $N = 5$. (b) Fluorescent images of smooth muscle cells isolated from rat detrusor and labeled with a mouse monoclonal Kv11.1 antibody (left column) and α-smooth muscle actin (α-SMA, middle column). Cells where primary antibodies were omitted (incubated with secondary antibodies only) are also shown (right panel). Each image is representative of five separate dispersals. Scale bar = 10 µm.

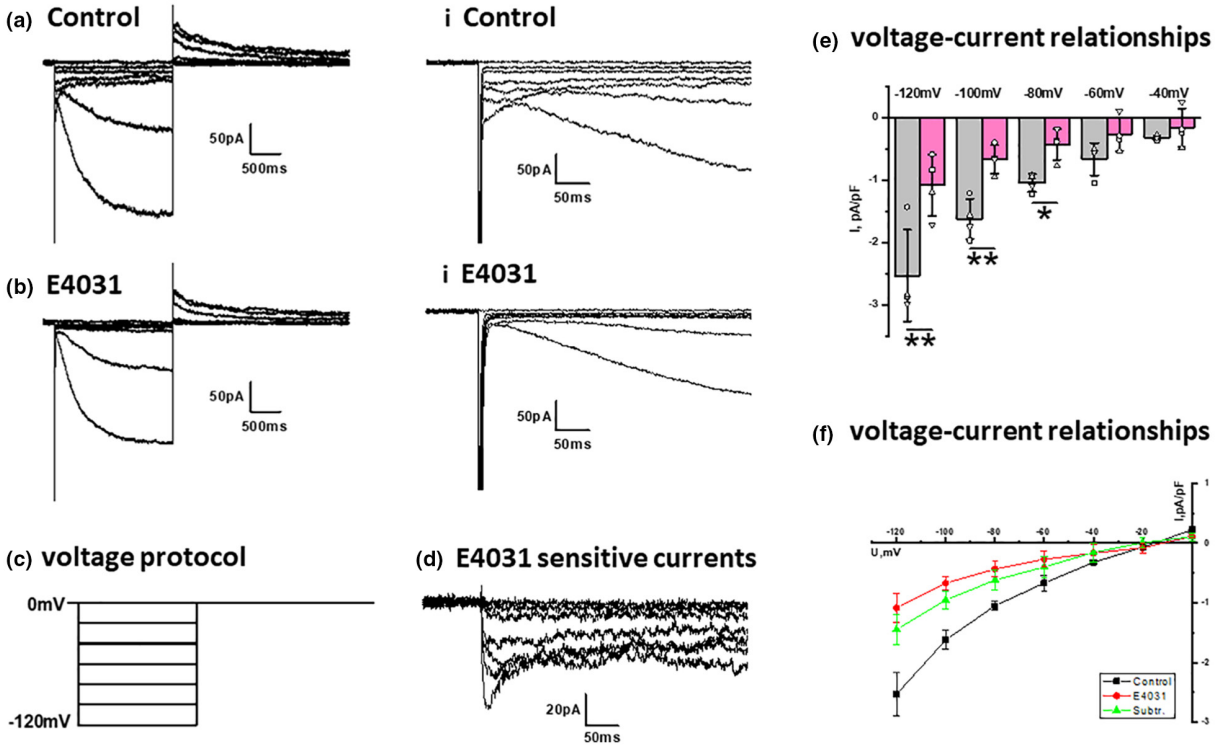


FIGURE 2 Whole-cell electrophysiology of isolated detrusor smooth muscle cells. (a, b) Show currents evoked by the protocol shown in (c) in the absence (a) and presence (b) of E4031 (2 µM). The right-hand panels (a.i, b.i) show a zoom of the initial 200 ms of the test step to highlight the E4031-sensitive current. (d) Shows a representative set of E4031-sensitive currents. (e, f) Show the mean current amplitude at different test potentials in the absence and presence of E4031. Data were taken from 8 to 12 cells from four animals ($N = 4$, $^{*}p < 0.05$, $^{**}p < 0.01$, one-way analysis of variance, error bars represent standard error of the mean).

20511817x, 2023, 3, Downloaded from https://physoc.onlinelibrary.wiley.com/doi/10.14814/phy2.15583 by Test, Wiley Online Library on [10/01/2025]. See the Terms and Conditions (https://onlinelibrary.wiley.com/terms-and-conditions) on Wiley Online Library for rules of use; OA articles are governed by the applicable Creative Commons License

that has been characterized in rat bladder and mouse portal vein previously (Green et al., 1996; Greenwood & Prestwich, 2002). The HCN channel current was preceded by an inward current with a prominent "hook" (Figure 2) that decayed rapidly and was abrogated by the Kv11.1-specific blocker E4031 (Figure 2a–f) ($N = 4$, $p < 0.05$). The kinetics of the development and subsequent decay of the E4031-sensitive current were voltage-dependent becoming slower at less negative potentials (Figure 2d). These kinetics are consistent with the voltage-dependent properties of inactivation recovery and deactivation exhibited by Kv11.1 channels (Ohya, Horowitz, et al., 2002; Spector et al., 1996).

3.2 | Kv11.1 blockers affect detrusor contractility

Transverse bands of the bladder exhibited spontaneous phasic contractile activity that was sustained through the duration of typical recordings. The addition of two structurally different Kv11.1-specific blockers, E4031 and dofetilide (Yeung & Greenwood, 2007), augmented detrusor contractility considerably in a concentration-dependent manner (Figure 3). In an intact bladder (in which the mucosa is retained), application of 2 μM E4031 or 2 μM dofetilide did not increase basal tone, whereas 20 μM E4031 caused a significant increase (+0.6 ± 0.1, $N = 5$, $p < 0.001$), as did 20 μM dofetilide (+0.56 ± 0.18, $N = 5$, $p < 0.05$) (Figure 3b.i,ii). To confirm if neuronal input modulated the effect of E4031 on baseline tone, 1 μM of tetrodotoxin (TTX) was added prior to 20 μM E4031 to prevent neurotransmitter release. E4031 still increased baseline tone even in the presence of TTX (+0.14 ± 0.01, $N = 5$) and this was not significantly different from its corresponding control (Figure 3b.iii).

Phasic contraction amplitude was significantly increased in the presence of 2 μM E4031 (566.7% ± 54.21%, $N = 5$, $p < 0.001$) and 20 μM E4031 (734.5% ± 106.8%, $N = 5$, $p < 0.0001$) in an intact detrusor (Figure 3c.i). Similarly, 2 and 20 μM dofetilide also increased phasic contraction amplitude by 560.4% (±131.7%, $N = 5$, $p < 0.05$) and 695.1% (±110.1%, $N = 5$, $p < 0.01$), respectively (Figure 3c.ii). This heightened contractile activity was unaltered over a 5-h experimental period. E4031 still increased the amplitude of spontaneous contractions in the presence of TTX (+355.2% ± 67.9, $N = 5$) (Figure 3c.iii). These data show that Kv11.1 channels have a considerable impact on spontaneous activity in the rat detrusor and that this effect is not likely mediated via neuronal stimulation.

3.3 | Kv11.1 blockers and carbachol-mediated contractions

Application of the muscarinic receptor agonist, carbachol (1–10 μM) (CCh) evoked concentration-dependent contractions that were manifest as enhanced baseline superimposed by individual contractions (Figure 4a,b). All bladder strips were exposed to increasing concentrations of CCh followed by a washout with PSS and this served as the internal control for each strip. The washout was

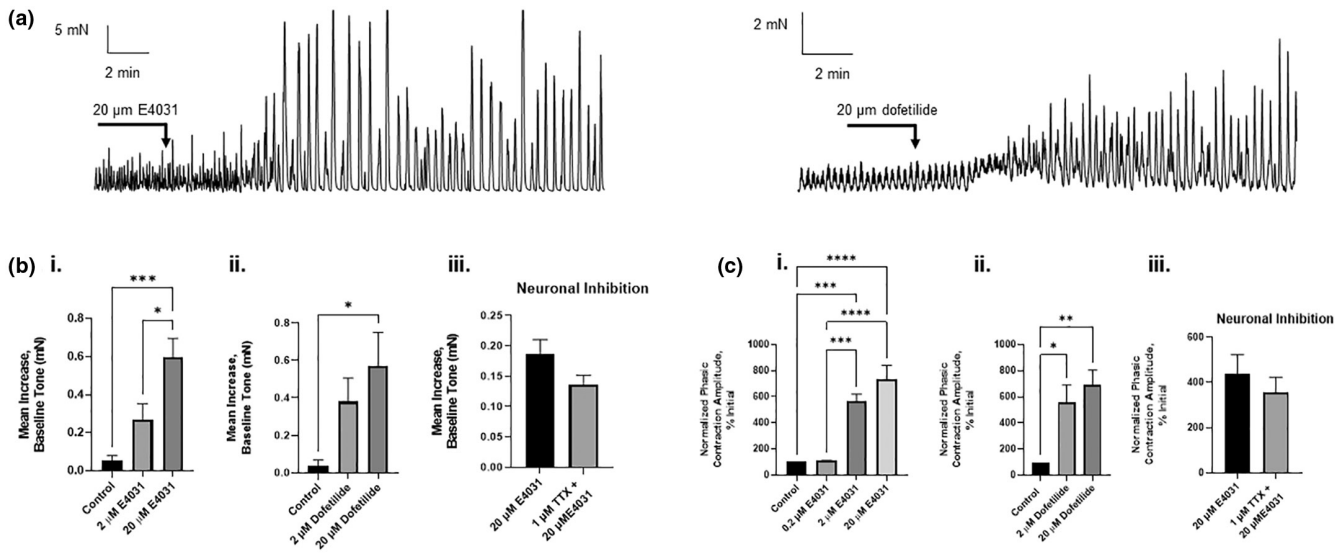


FIGURE 3 Effect of Kv11.1 channel inhibitors on spontaneous contractile activity. (a) Representative trace of basal tone and phasic contraction amplitudes after the addition of 20 μM of the Kv11.1 inhibitors, E4031 (left) and Dofetilide (right). (b) The maximum increase in baseline tone at various concentrations of Kv11.1 inhibitors E4031 (i) and dofetilide (ii), and in the presence of neuronal inhibition with TTX (iii) ($N = 5$). (c) Percent increase in the amplitude of phasic contractions compared with the control, in the presence of Kv11.1 inhibitors, E4031 (i) and dofetilide (ii), and in the presence of neuronal inhibition (iii) ($N = 5$) (*$p < 0.05$, **$p < 0.01$, ***$p < 0.001$, ****$p < 0.0001$, one-way analysis of variance, error bars represent standard error of the mean).

20518117x, 2023, 3, Downloaded from https://physoc.onlinelibrary.wiley.com/doi/10.14814/phy2.15583 by Test, Wiley Online Library on [10/01/2025]. See the Terms and Conditions (https://onlinelibrary.wiley.com/terms-and-conditions) on Wiley Online Library for rules of use; OA articles are governed by the applicable Creative Commons License

followed by a second application of CCh either with the prior incubation with 2 μM, 20 μM E4031, or vehicle control. The subsequent increase in baseline tone, contractile amplitude, or area under the curve was measured as the change from its internal control (first exposure to CCh). Preapplication of E4031 (2 μM) enhanced the effect of CCh on the amplitude of phasic contractions and further enhancement was observed with 20 μM (Figure 4c). Neither concentration of E4031 affected the force integral of the carbachol response measured as the area under curve during the first 3 min of the CCh response (Figure 4d).

3.4 | Kv11.1 blockers and nerve-mediated contractions

Electrical field stimulation (EFS, 0.5–32 Hz) evoked frequency-dependent contractions (Figure 5a), which were inhibited by the voltage-gated sodium channel blocker tetrodotoxin (see Campbell et al., 2017). E4031 (20 μM) caused small but significant increases in EFS contraction amplitude across all frequencies (0.5, 1, 2, 4, 8, and 16 Hz; $p < 0.05$, $N = 5$) (Figure 5b.i). EFS contraction amplitudes in each experiment were normalized to a control contraction evoked by 60 mM K^+ Krebs solution, prior to calculations of means, SEM, or statistical analysis. The addition of TTX (1 μM) eliminated EFS contractions (30 V, 30 Hz), and they were not restored upon the addition of 20 μM E4031 (Figure 5b.ii).

3.5 | Kv11.1 blockers on contractions of a denuded bladder

The bladder was denuded in order to test the efficacy of E4031 on phasic and EFS contractions in the absence of the mucosa (Figure 6a). There was still a significant increase in baseline tone (+0.13 ± 0.01, $N = 5$, $p < 0.05$) (Figure 6b.i) and phasic contraction amplitude, relative to control (556.3% ± 63.9, N = 5, $p < 0.001$) in a denuded bladder (Figure 6b.ii). E4031 (20 μM) induced a significant increase in EFS contraction amplitude across low frequencies (0.5, 2, 4 Hz; $p < 0.05$, $N = 5$), but had no effect at higher frequencies (Figure 6b.iii). EFS contraction amplitudes were

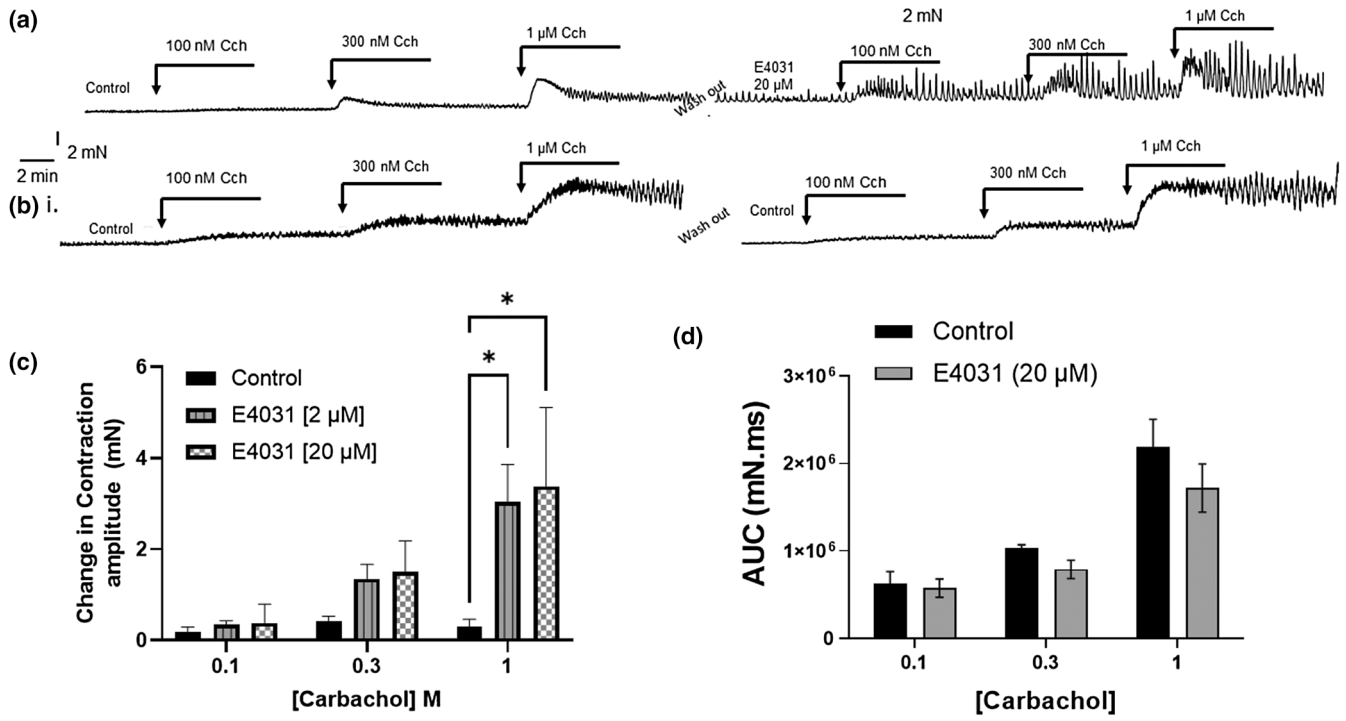


FIGURE 4 Assessing amplitude of phasic contractions in response to carbachol in the presence and absence of potassium channel inhibitors. (a) Representative traces of contraction amplitudes in response to carbachol before and after the addition of the Kv11.1 inhibitor, E4031 (20 μM) within the same tissue (internal control). (b) Representative traces of contraction amplitudes in response to carbachol before and after the addition of vehicle control (dimethyl sulphoxide). (c) The change in the mean amplitude of contractions taken over a 2-min period when the effect of Cch reaches a plateau and prior to the addition of the next concentration. The greatest change in amplitude, compared with control was observed in the presence of E4031 with 1 μM CCh ($N = 5$), *$p < 0.05$, error bars represent SEM; statistical analysis using two-way ANOVA, with Bonferroni multiple comparison test. (d) The area under the curve analysis carried out at the maximum change in baseline tone after the addition of each concentration of Cch, in the presence of 20 μM E4031 ($N = 5$; two-way ANOVA; error bars represent SEM). ANOVA, analysis of variance; SEM, standard error of the mean.

20518171x, 2023, 3, Downloaded from https://physoc.onlinelibrary.wiley.com/doi/10.14814/phy2.15583 by Test, Wiley Online Library on [10/01/2025]. See the Terms and Conditions (https://onlinelibrary.wiley.com/terms-and-conditions) on Wiley Online Library for rules of use; OA articles are governed by the applicable Creative Commons License

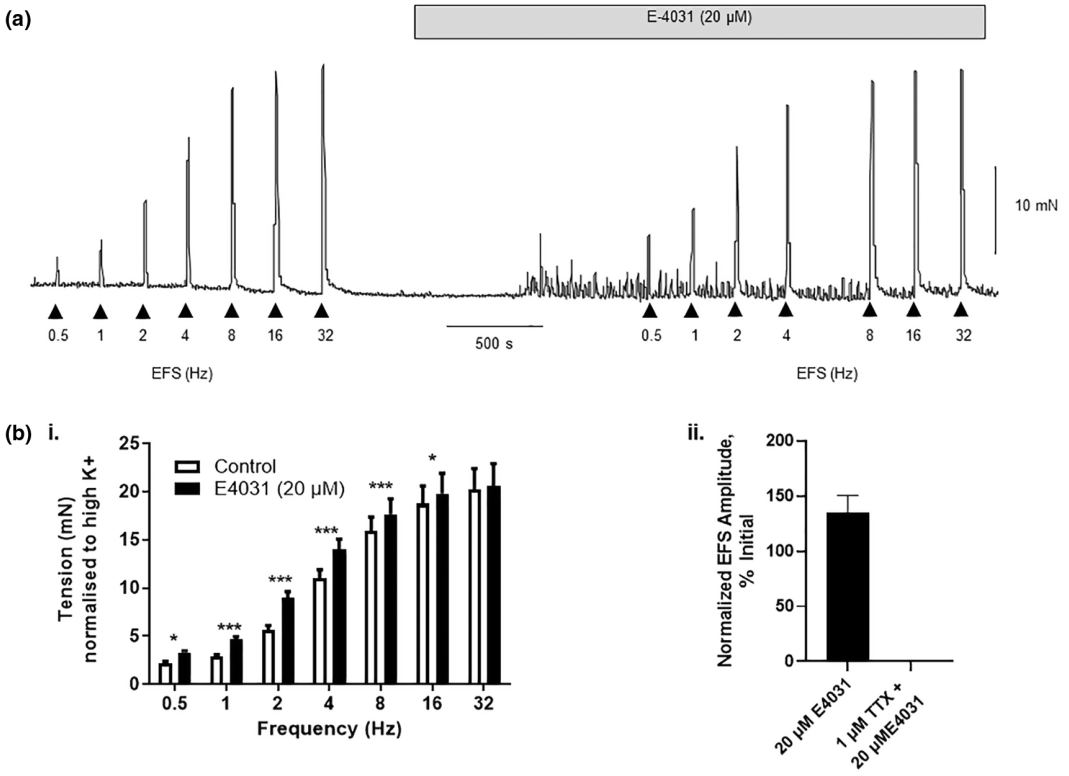


FIGURE 5 Effect of E-4031 on nerve-evoked contractions. (a) Electrical field stimulation (EFS) across the frequency range 0.5, 1, 2, 4, 8, 16, and 32 Hz evoked frequency-dependent contractions. Following treatment with E4031 (20 μM), the stimulation protocol was repeated. Note the enhancement of spontaneous contractions in the presence of E4031. (b.i) Summary data from experimental series (N = 5), normalized to high K+ (60 mM) contraction. (b.ii) Mean data showing the effect of E4031 on EFS (30 Hz, 30 V) with and without prior incubation with TTX (*t* test). *$p < 0.05$, ***$p < 0.0001$; error bars represent standard error of the mean. (Two-way analysis of variance with Bonferroni post-hoc test).

normalized to a control contraction induced by 60 mM K^+ Krebs solution before calculating means and SEM.

3.6 | The effect of Kv11.1 activators on EFS-evoked and spontaneous contractions

The effects of two structurally dissimilar Kv11.1 activators PD118057 and NS1643 (Casis et al., 2006; Zhou et al., 2005) were assessed on spontaneous and nerve-evoked contractions. PD118057 significantly reduced spontaneous contractions to ~40% of basal levels ($N = 5$, $p < 0.05$) (Figure 7). NS1643 also reduced spontaneous contractions but this did not reach significance (not shown). Both NS1643 and PD118057 had no significant effect on nerve-evoked contractions.

3.7 | Comparison of BK and Kv11.1 blockers on spontaneous activity

BK channels are considered to have significant roles in bladder SMC physiology (Meredith et al., 2004; Petkov, 2014) and have been studied extensively in tissue myography and single-cell patch-clamp recordings (Cotton et al., 1996; Herrera & Nelson, 2002). Here, we investigated the impact of blocking BK and Kv11.1 channels on bladder spontaneous contractions (Figure 8). Application of the BK channel blocker, iberiotoxin (IbTX, 300 nM) increased the amplitude of spontaneous contractions amplitude by 156.6 ± 15.90% (SEM, $N = 5$) that was associated with a small (0.13 mN ± 0.04) increase in basal tone (Figure 8b,c). Subsequent addition of E4031 (20 μM) augmented the amplitude of spontaneous contractions (606.3 ± 76.42%, N = 5), similar to the increase induced by E4031 (20 μM) alone (~634% ± 82.89). Application of E4031 to tissues incubated in IbTX increased resting tension (0.50 ± 0.0.078 mN) to a level similar to that seen with E4031 (20 μM) alone (~0.5 ± 0.09) (Figure 8b,c).

3.8 | Isoprenaline-mediated relaxations are affected by Kv11.1 blockade

Stimulation of cAMP-linked β-adrenoceptors (predominantly β3) reduces detrusor smooth muscle

2051817x, 2023, 3, Downloaded from https://physoc.onlinelibrary.wiley.com/doi/10.14814/phy2.15583 by Test, Wiley Online Library on [10/01/2025]. See the Terms and Conditions (https://onlinelibrary.wiley.com/terms-and-conditions) on Wiley Online Library for rules of use; OA articles are governed by the applicable Creative Commons License

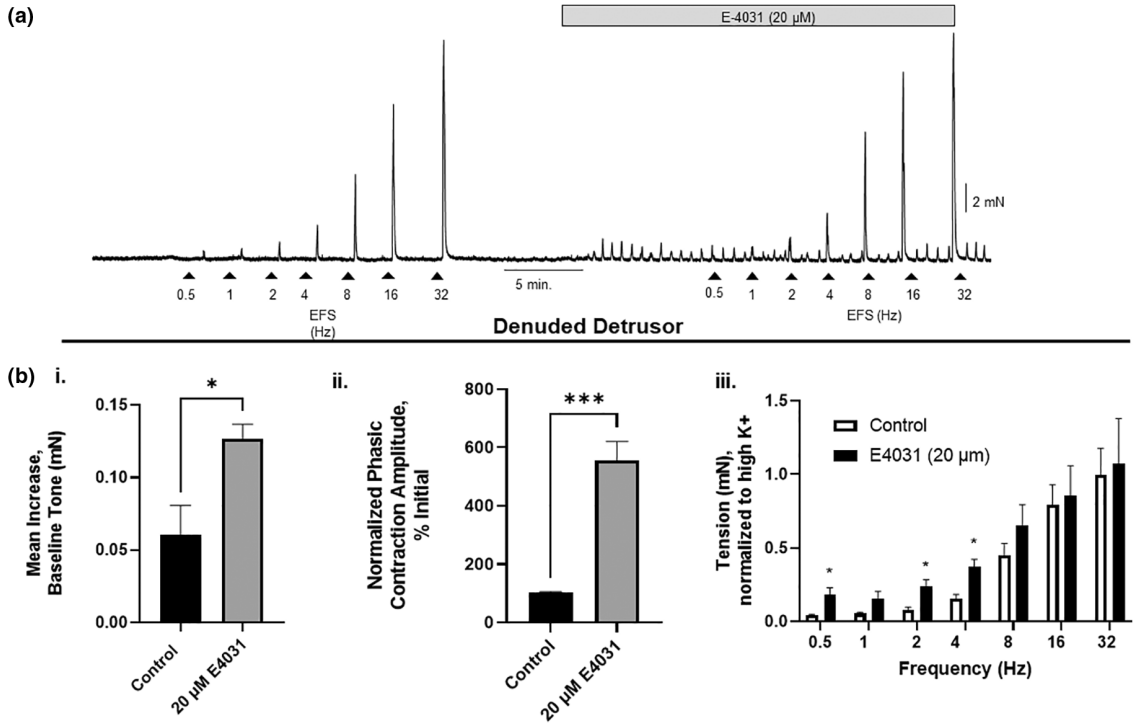


FIGURE 6 Effect of E-4031 on contractile activity of a denuded bladder. (a) Electric field stimulation (EFS) of a denuded bladder across a range of frequencies (0.5, 1, 2, 4, 8, 16, 32 Hz). The protocol was conducted before and after incubation with E4031 (20 μM). (b.i) Mean data indicating an increase in baseline tone in the absence (control) and presence of E4031. (b.ii) Average data of increase in phasic contractile amplitude after the addition of E4031 or in the presence of the vehicle (control) (*t* test). (B.iii) Summary data of EFS-induced contractions (normalized to K+ (60 mM). $*p < 0.05$, $***p < 0.0001$, $N = 5$, error bars represent standard error of the mean).

contractility. As Kv11.1 channel activity is enhanced by cAMP-dependent protein kinase A (e.g., Chen et al., 2010) we speculated if Kv11 channels contributed functionally to β-adrenoceptor-mediated responses. Application of the general β-adrenoceptor agonist isoprenaline produced a concentration-dependent inhibition of spontaneous activity that had been augmented by the addition of 20 mM KCl (Figure 9a). The presence of E4031 (2 μM) attenuated the inhibitory effect of isoprenaline markedly (Figure 9a). BK and Kv7 channels have also been implicated in relaxations produced by agonists of cAMP-linked receptors (e.g., Huang & Kwok, 1997; Stott et al., 2018; Van der Horst et al., 2020). In contrast to the effect of E4031 on isoprenaline-mediated responses, neither IBTX (100 nM) nor the Kv7 channel blocker XE991 (10 μM) altered the inhibitory effect of isoprenaline (Figure 9b). These data suggest that Kv11.1 channels provide a functional endpoint for β-adrenoceptor-related actions on bladder contractility.

4 | DISCUSSION

This study demonstrated that male rat bladders expressed both known variants of *Kcnh2* but not *Kcnh6* or *Kcnh7*. Immunocytochemistry established that the *Kcnh2* expression product, Kv11.1, was located predominantly at the cell membrane and patch-clamp experiments demonstrated potassium currents with distinctive hooked kinetics sensitive to the selective Kv11.1 blocker, E4031, were present in bladder SMCs. In tension recordings, the blockade of Kv11.1 by two structurally different agents, E4031 and dofetilide, enhanced the contractile activity of the detrusor. In addition, Kv11.1 blockers augmented the contractile response of the muscarinic receptor agonist carbachol and attenuated the relaxant effect of the β-adrenoceptor agonist, isoprenaline.

Blockade of Kv11.1 channels with two structurally different agents enhanced the spontaneous contractile activity of rat bladders similar to preliminary data published by Imai et al. (2001) in guinea pig bladder. These effects far exceeded those produced by blockers of BK_{Ca} and Kv7 channels (IBTX and XE991, respectively) and were manifest as an increase in the amplitude and duration of spontaneous events leading to a tonic increase in tension. These data are consistent with Kv11.1 channels contributing to the resting membrane potential and repolarization of the action potential associated with spontaneous contractions (Hashitani & Brading, 2003). These pronounced effects of Kv11.1 blockers have also been observed in opossum esophagus, mouse gall bladder,

2051817x, 2023, 3, Downloaded from https://physoc.onlinelibrary.wiley.com/doi/10.14814/phy2.15583 by Test, Wiley Online Library on [10/01/2025]. See the Terms and Conditions (https://onlinelibrary.wiley.com/terms-and-conditions) on Wiley Online Library for rules of use; OA articles are governed by the applicable Creative Commons License

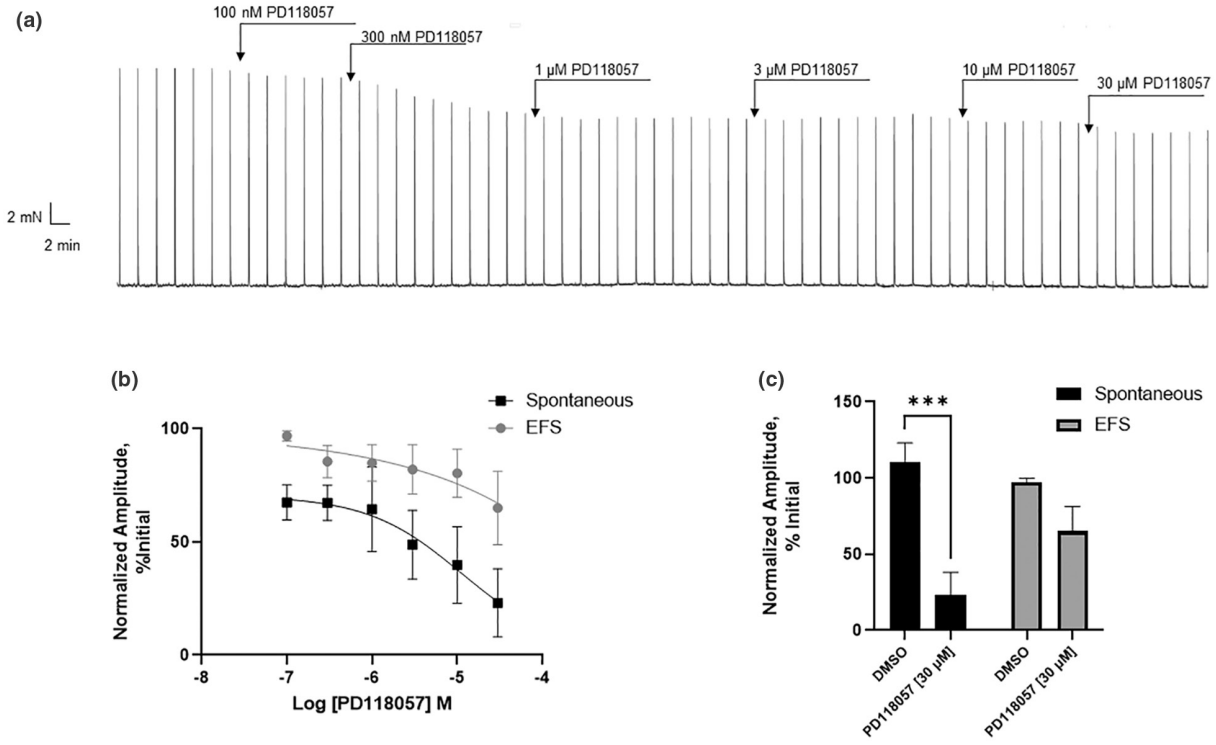


FIGURE 7 Effect of the Kv11.1 activator, PD118057 on the amplitude of spontaneous and EFS (electric field-stimulated) contractions (20 Hz). (a) Representative trace of cumulative concentration of PD118057. (b) Normalized amplitudes of spontaneous and EFS contractions at increasing concentrations of PD118057. (c) Normalized amplitudes of spontaneous and EFS contractions in response to PD118057, relative to the vehicle. $N = 5$, Error bars represent standard error of the mean, $^{***}p < 0.001$. Statistical analysis using two-way analysis of variance.

equine and human jejunum, bovine epididymis, mouse and human myometrium (Akbarali et al., 1999; Farrelly et al., 2003; Greenwood et al., 2009; Lillich et al., 2003; Mewe et al., 2008; Parkington et al., 2014; Parr et al., 2003). In many tissues, the application of Kv11.1 blockers can convert mechanically quiescent smooth muscle to actively contracting tissues suggesting the contractile activity of the tissue may be dictated by the relative dominance of Kv11.1 channels. As this study demonstrated, the effects of Kv11.1 blockers on bladder contractility were mediated via detrusor SMCs, as even in the absence of a mucosa, phasic contraction amplitude was still significantly elevated. Moreover, inhibition of neuronal activation via TTX did not prevent the effect of E4031 on detrusor phasic contractility. However, this does not rule out that E4031 may also be affecting urothelial, interstitial cells, or neuronal depolarization and remains to be further investigated in future studies. Of note, Kv11.1 channels have been identified in neurons and they are involved in mediating the neuronal resting current (e.g., Sanchez-Conde et al., 2022).

Moreover, Kv11.1 protein was identified in the plasma membrane of α-smooth muscle actin-positive cells and E4031-sensitive currents with the distinctive voltage-dependent kinetics that is inherent to the channels were recorded from isolated SMCs. Kv11.1 currents have previously been recorded in SMCs isolated from opossum esophagus, mouse portal vein, and myometrium from mice and humans (Akbarali et al., 1999; Greenwood et al., 2009; Ohya, Horowitz, et al., 2002; Parkington et al., 2014; Yeung & Greenwood, 2007). The voltage-dependent kinetics recorded in the present study were remarkably similar to those recorded in the other cell types. The combined data suggest that Kv11.1 is expressed by the detrusor SMCs and it contributes markedly to the regulation of smooth muscle contractility. There are two known rat isoforms of Kv11.1, previously known as erg1a and 1b. With respect to erg1a, erg1b lacks 373 amino acids and has a different N-terminus. The N-terminal region of erg1a forms the protein domain responsible for the characteristic deactivation kinetics of the channel, and the so-called "PAS domain," which defines the ether-a-go-go subfamily of voltage-gated potassium channels. Erg1a and Erg1b co-assemble in the endoplasmic reticulum to form a tetrameric channel that mediates the "native" current in cardiac myocytes. Heteromeric erg1a/1b channels show faster activation, deactivation, and recovery from inactivation than channels formed by erg1a alone, a characteristic consistent with the lack of the N-terminal region responsible for the deactivation kinetics in erg1b. On the other hand, erg1b

2051817x, 2023, 3, Downloaded from https://physoc.onlinelibrary.wiley.com/doi/10.14814/phy2.15583 by Test, Wiley Online Library on [10/01/2025]. See the Terms and Conditions (https://onlinelibrary.wiley.com/terms-and-conditions) on Wiley Online Library for rules of use; OA articles are governed by the applicable Creative Commons License

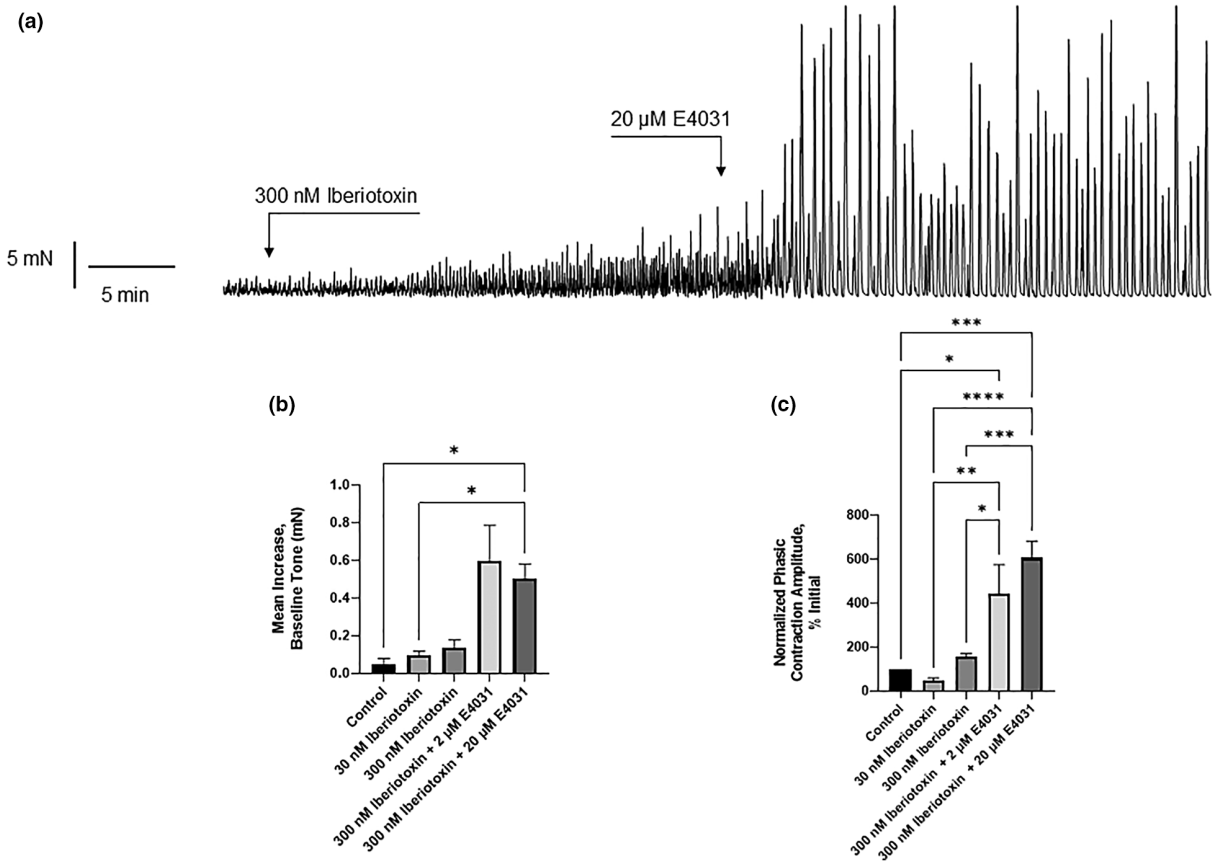


FIGURE 8 Characterization of baseline tone and phasic contraction amplitude in the presence of BK channel inhibitors in the presence and absence of E4031. (a) Representative trace of basal tone and phasic contraction amplitudes after the addition of 20 μm of the Kv11.1 inhibitor, following preincubation with 300 nM of the BK inhibitor iberiotoxin. (b) Maximum increase in baseline tone in the presence of iberiotoxin with and without E4031 ($N = 5$). (c) Percent increase in the amplitude of phasic contractions compared with control, in the presence of the Kv11.1 inhibitor, E4031 with and without prior incubation with iberiotoxin ($N = 5$). *$p < 0.05$, **$p < 0.01$, ***$p < 0.001$, ****$p < 0.0001$, error bars represent SEM. Statistical testing using one-way ANOVA (N = 5, one-way ANOVA, **p < 0.01, error bars represent SEM). ANOVA, analysis of variance; SEM, standard error of the mean.

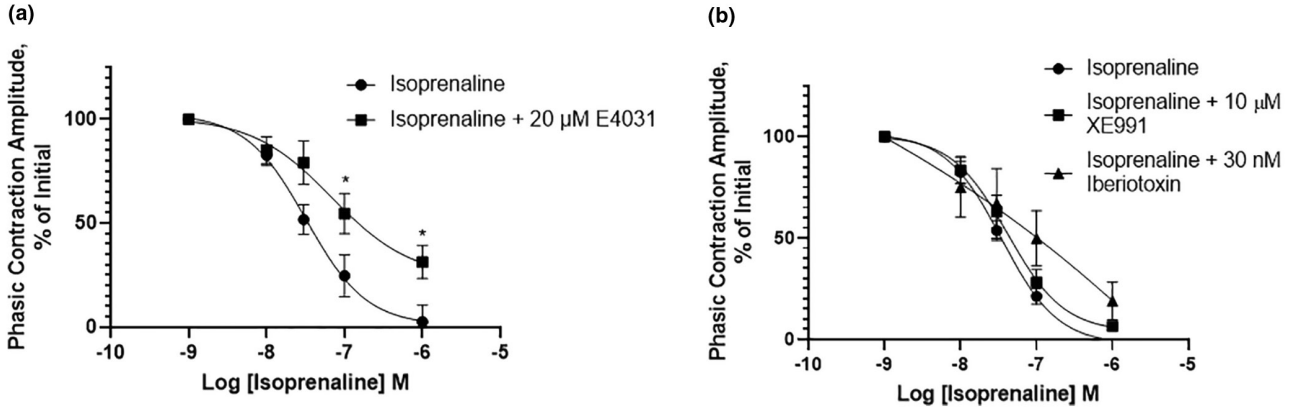


FIGURE 9 The effect of isoprenaline in the presence of potassium channel inhibitors. (a) Decrease in phasic contraction amplitude of detrusor muscle strips upon treatment with Isoprenaline. The relaxation effect of Isoprenaline is significantly counteracted upon pretreatment with E4031 (b) Preincubation with either XE991 or Iberiotoxin did not significantly alter the adrenergic effect of Isoprenaline ($N = 5$), *$p < 0.05$; error bars represent standard error of the mean, statistical analysis using two-way analysis of variance, with Bonferroni multiple comparison test.

2051817x, 2023, 3, Downloaded from https://physoc.onlinelibrary.wiley.com/doi/10.14814/phy2.15583 by Test, Wiley Online Library on [10/01/2025]. See the Terms and Conditions (https://onlinelibrary.wiley.com/terms-and-conditions) on Wiley Online Library for rules of use; OA articles are governed by the applicable Creative Commons License

modulates channel trafficking and response to hormones and other endogenous agonists (Vanderberg et al., 2012). While the molecular composition of the Kv11.1 channel in the bladder remains to be defined the relative lack of the shorter isoform suggests a heterotetramer is unlikely.

In addition to verifying the expression of *Kcnh2* and characterizing the role of Kv11.1, we also compared its effect to the large conductance voltage-activated and Ca^{2+}-activated (BK) channels. The BK channel is activated by both voltage and Ca^{2+} and is well expressed in the detrusor (Petkov, 2011). Consistent with previous studies application of the BK channel blocker, IBTX, enhanced spontaneous activity; however, its impact was substantially smaller than that of the Kv11.1 inhibitors. Application of E4031 in the continued presence of iberiotoxin produced a striking enhancement of contractile activity reinforcing the view that Kv11.1 channels provide considerable capacity for suppressing bladder contractions and are major determinants of resting activity. It should be noted that detrusor SMCs also express a variety of other K+ channels, which collectively modulate and contribute to resting membrane potential and repolarization (Malysz & Petkov, 2020). For example, SK channels, which are Ca^{2+} sensitive but voltage insensitive, are activated after the hyperpolarization phase and are present in much less abundance compared with BK channels. Pharmacological inhibition of these channels is associated with increased phasic contraction frequency (Herrera et al., 2003). Other channels that have been detected on the DSM include inward-rectifying ATP-sensitive K+ channels (K_{ATP}). These channels are activated at low intracellular concentrations of ATP, whereas they are inhibited at higher concentrations. Future studies will elaborate on the interplay of Kv11.1 channels with other K channels expressed in the bladder.

E4031 also enhanced carbachol-induced contractility by ~25%, suggesting that Kv11.1 is not only important in regulating baseline tone and spontaneous activity but also limits the amplitude of receptor-operated contractions. Our finding that EFS-mediated, neurogenic contractions could also be augmented by E4031, shows that Kv11.1 activity may provide a protective limit to bladder contraction amplitude during micturition. This would maintain metabolic homeostasis and also provide a further tuning mechanism for appropriate contraction amplitude. Such a mechanism might be expected to react to the relaxation of bladder smooth muscle and this was tested in the present study using, isoprenaline, a nonspecific β-adrenergic receptor agonist, that induced a concentration-dependent relaxation, almost abolishing spontaneous contractions. Notably, E4031 but not blockers of BK or Kv7 channels blunted the relaxation effect of isoprenaline. Activation of β-adrenergic receptors stimulates Kv11.1 channels via a cAMP-PKA mechanism (Kiehl, 2000; Vandenberg et al., 2012); furthermore, Kv11.1 protein contains numerous protein kinase A (PKA) phosphorylation sites within its intracellular domain, and, within cardiac myocytes, the interaction activates the channel enabling greater channel activation (Kiehl, 2000; Vandenberg et al., 2012). Thus, Kv11.1 may also have an important role in mediating β-adrenergic receptor bladder relaxation.

Dual actions of Kv11.1 blockers enhancing contraction (spontaneous, neurogenic, and muscarinic receptor-operated) and impairing relaxation (β-adrenergic receptor-operated) reveal the versatility of Kv11.1-mediated signaling in bladder physiology. While the complexity of mechanisms is not yet understood, Kv11.1 function is a promising area of study. Bladder dysfunction and lower urinary tract symptoms are common and represent many diverse pathophysiologies. Many targets have been identified and investigated for clinical translation, notably, drugs-targeting muscarinic receptors and β3-adrenergic receptor agonists are used clinically. BK channel activators were considered to be promising to reduce detrusor overactivity; however, the finding that BK is underexpressed in the neurogenic bladder impeded further development. Interestingly, gene therapies to restore BK channel expression in the neurogenic bladder have been in clinical trials and may bring benefits to patients. With the known key function of Kv11.1 channels in cardiac myocytes (Sanguinetti et al., 1996), their importance is especially notable in individuals with congenital defects in Kv11.1 channels, where resulting cardiac arrhythmia may lead to sudden death. Mutations in *KCNH2* are responsible for approximately 25% of hereditary arrhythmias that present with QT interval prolongation (Sanguinetti et al., 1996); it is not known whether this has consequences for bladder function. All drugs are screened for activity against Kv11.1 to avoid adverse cardiac effects and this might suggest that Kv11.1 could not be progressed as a target to treat bladder dysfunction. Research directed at the characterization of bladder Kv11.1 protein structure, subtypes and pharmacological profile compared with cardiac channels may provide the opportunity to progress bladder-selective drugs. It is also important to discover whether existing bladder dysfunction treatments have actions on bladder Kv11.1 in addition to their known targets.

In conclusion, the findings of the study reveal functional expression of *kcnh*2 transcript as Kv11.1 ion channels in rat bladder smooth muscle. Pharmacological modulators reveal that Kv11.1 are key determinants of bladder contractility and may represent a more powerful brake on excitability than BK or other Kv channels. The findings show the participation of Kv11.1 in spontaneous, neurogenic, and receptor-mediated contractions, suggesting a central role in bladder physiology. It is not yet known whether *kcnh*2 mutations are linked with bladder dysfunction or

2051817x, 2023, 3, Downloaded from https://physoc.onlinelibrary.wiley.com/doi/10.14814/phy2.15583 by Test, Wiley Online Library on [10/01/2025]. See the Terms and Conditions (https://onlinelibrary.wiley.com/terms-and-conditions) on Wiley Online Library for rules of use; OA articles are governed by the applicable Creative Commons License

whether Kv11.1 modulators could restore normal contractility if developed with a cardiac-safe profile; we highlight this as an important area for further research.

AUTHOR CONTRIBUTIONS

Vincenzo Barrese performed molecular research. Alice Linden, Karen D. McCloskey, Sarah McDowell, and Zena Wehbe performed functional research. Zena Wehbe performed immunocytochemistry. Oleksander Povstyan conducted electrophysiology research. Zena Wehbe and Iain A. Greenwood wrote the manuscript. Iain A. Greenwood designed the research study. All authors contributed to the manuscript and approved the submitted version.

ACKNOWLEDGMENTS

We would like to acknowledge the help with immunocytochemistry from Dr. Alice Esseola and Sandra Ashton.

FUNDING INFORMATION

There are no funders for this research.

CONFLICT OF INTEREST STATEMENT

The authors declare that they have no conflict of interest.

DECLARATION OF TRANSPARENCY AND SCIENTIFIC RIGOR

We declare that our paper adheres to the principles for transparent reporting and scientific rigor of preclinic research as stated in the BJP guidelines for Natural Products Research, Design and Analysis, Immunoblotting and Immunochemistry, and Animal Experimentations, as recommended by funding agencies, publishers, and other organizations engaged with supporting research.

ETHICS APPROVAL STATEMENT

Animals used in the following investigation were handled in strict accordance with the Animal (Scientific Procedures) Act 1986.

ORCID

Zena Wehbe https://orcid.org/0000-0003-0154-0247
Iain A. Greenwood https://orcid.org/0000-0002-0603-0492

REFERENCES

Akbarali, H. I., Thatte, H., He, X. D., Giles, W. R., & Goyal, R. K. (1999). Role of HERG-like K(+) currents in opossum esophageal circular smooth muscle. *The American Journal of Physiology*, *277*, C1284–C1290.

Anderson, U. A., Carson, C., Johnston, L., Joshi, S., Gurney, A. M., & McCloskey, K. D. (2013). Functional expression of KCNQ (Kv7) channels in Guinea pig bladder smooth muscle and their contribution to spontaneous activity. *British Journal of Pharmacology*, *169*, 1290–1304.

Barrese, V., Cidad, P., Yeung, S. Y., López-López, J. R., McNeish, A. J., Ohya, S., Pérez-García, M. T., & Greenwood, I. A. (2017). Proliferative role of Kv11 channels in murine arteries. *Frontiers in Physiology*, *8*, 500.

Bauer, C. K., & Schwarz, J. R. (2018). Ether-à-go-go K. *The Journal of Physiology*, *596*, 769–783.

Bientinesi, R., Mancuso, C., Martire, M., Bassi, P. F., Sacco, E., & Currò, D. (2017). KV7 channels in the human detrusor: channel modulator effects and gene and protein expression. *Naunyn-Schmiedeberg's Archives of Pharmacology*, *390*, 127–137.

Brading, A. F. (1997). A myogenic basis for the overactive bladder. *Urology*, *50*, 57–67; discussion 68–73.

Campbell, P. C., McDonnell, B., Monaghan, K. P., Baysting, L., Little, O., & McCloskey, K. D. (2017). Mucosal modulation of contractility in bladder strips from normal and overactive rat models and the effect of botulinum toxin a on overactive bladder strips. *Neurourology and Urodynamics*, *36*, 1052–1060.

Casis, O., Olesen, S. P., & Sanguinetti, M. C. (2006). Mechanism of action of a novel human ether-a- go-go-related gene channel activator. *Molecular Pharmacology*, *69*, 658–665.

Chen, J., Chen, K., Sroubek, J., Wu, Z. Y., Thomas, D., Bian, J. S., & McDonald, T. V. (2010). Post-transcriptional control of human ether-a-go-go-related gene potassium channel protein by alpha-adrenergic receptor stimulation. *Molecular Pharmacology*, *78*(2), 186–197.

Cotton, K. D., Hollywood, M. A., Thornbury, K. D., & McHale, N. G. (1996). Effect of purinergic blockers on outward current in isolated smooth muscle cells of the sheep bladder. *The American Journal of Physiology*, *270*, C969–C973.

Dai, G., & Zagotta, W. N. (2017). Molecular mechanism of voltage-dependent potentiation of *kcnh* potassium channels. *eLife*, *6*, e26355.

Drake, M. J., Fry, C. H., Hashitani, H., Kirschner-Hermanns, R., Rahnama'i, M. S., Speich, J. E., Tomoe, H., Kanai, A. J., & McCloskey, K. D. (2018). What are the origins and relevance of spontaneous bladder contractions? ICI-RS 2017. *Neurourology and Urodynamics*, *37*, S13–S19.

Farrelly, A. M., Ro, S., Callaghan, B. P., Khoyi, M. A., Fleming, N., Horowitz, B., Sanders, K. M., & Keef, K. D. (2003). Expression and function of *kcnh*2 (HERG) in the human jejunum. *American Journal of Physiology. Gastrointestinal and Liver Physiology*, *284*, G883–G895.

Green, M. E., Edwards, G., Kirkup, A. J., Miller, M., & Weston, A. H. (1996). Pharmacological characterization of the inwardly-rectifying current in the smooth muscle cells of the rat bladder. *British Journal of Pharmacology*, *119*, 1509–1518.

Greenwood, I. A., & Prestwich, S. A. (2002). Characteristics of hyperpolarization-activated cation currents in portal vein smooth muscle cells. *American Journal of Physiology Cell Physiology*, *282*(4), C744–C753.

Greenwood, I. A., Yeung, S. Y., Tribe, R. M., & Ohya, S. (2009). Loss of functional K+ channels encoded by ether-à-go-go-related genes in mouse myometrium prior to labour onset. *The Journal of Physiology*, *587*, 2313–2326.

Gutman, G. A., Chandy, K. G., Grissmer, S., Lazdunski, M., McKinnon, D., Pardo, L. A., Robertson, G. A., Rudy, B., Sanguinetti, M. C., Stuhmer, W., & Wang, X. (2005). International Union of Pharmacology. LIII. Nomenclature and molecular relationships of voltage-gated potassium channels. *Pharmacological Reviews*, *57*, 473–508.

2051817x, 2023, 3, Downloaded from https://physoc.onlinelibrary.wiley.com/doi/10.14814/phy2.15583 by Test, Wiley Online Library on [10/01/2025]. See the Terms and Conditions (https://onlinelibrary.wiley.com/terms-and-conditions) on Wiley Online Library for rules of use; OA articles are governed by the applicable Creative Commons License

Hashitani, H., & Brading, A. F. (2003). Ionic basis for the regulation of spontaneous excitation in detrusor smooth muscle cells of the Guinea-pig urinary bladder. *British Journal of Pharmacology*, *140*, 159–169.

Herrera, G. M., & Nelson, M. T. (2002). Differential regulation of SK and BK channels by Ca(2+) signals from Ca(2+) channels and ryanodine receptors in Guinea-pig urinary bladder myocytes. *The Journal of Physiology*, *541*, 483–492.

Herrera, G. M., Pozo, M. J., Zvara, P., Petkov, G. V., Bond, C. T., Adelman, J. P., & Nelson, M. T. (2003). Urinary bladder instability induced by selective suppression of the murine small conductance calcium-activated potassium (SK3) channel. *The Journal of Physiology*, *551*(Pt 3), 893–903. https://doi.org/10.1113/jphysiol.2003.045914

Hoshi, T., & Armstrong, C. M. (2013). C-type inactivation of voltage-gated K+ channels: Pore constriction or dilation? *The Journal of General Physiology*, *141*, 151–160.

Huang, Y., & Kwok, K. H. (1997). Effects of putative K+ channel blockers on beta-adrenoceptor-mediated vasorelaxation of rat mesenteric artery. *Journal of Cardiovascular Pharmacology*, *29*(4), 515–519.

Imai, T., Okamoto, T., Yamamoto, Y., Tanaka, H., Koike, K., Shigenobu, K., & Tanaka, Y. (2001). Effects of different types of K+ channel modulators on the spontaneous myogenic contraction of Guinea-pig urinary bladder smooth muscle. *Acta Physiologica Scandinavica*, *173*, 323–333.

Kiehl, J. (2000). Regulation of the cardiac repolarizing HERG potassium channel by protein kinase A. *Trends in Cardiovascular Medicine*, *10*, 205–209.

Lillich, J. D., Rakestraw, P. C., Roussel, A. J., Finley, M. R., Ganta, S., & Freeman, L. C. (2003). Expression of the ether-a-go-go (ERG) potassium channel in smooth muscle of the equine gastrointestinal tract and influence on activity of jejunal smooth muscle. *American Journal of Veterinary Research*, *64*, 267–272.

London, B., Trudeau, M. C., Newton, K. P., Beyer, A. K., Copeland, N. G., Gilbert, D. J., Jenkins, N. A., Satler, C. A., & Robertson, G. A. (1997). Two isoforms of the mouse ether-a-go-go-related gene coassemble to form channels with properties similar to the rapidly activating component of the cardiac delayed rectifier K+ current. *Circulation Research*, *81*, 870–878.

Malysz, J., & Petkov, G. V. (2020). Urinary bladder smooth muscle ion channels: Expression, function, and regulation in health and disease. *American Journal of Physiology. Renal Physiology*, *319*, F257–F283.

Meredith, A. L., Thorneloe, K. S., Werner, M. E., Nelson, M. T., & Aldrich, R. W. (2004). Overactive bladder and incontinence in the absence of the BK large conductance Ca2+−activated K+ channel. *The Journal of Biological Chemistry*, *279*, 36746–36752.

Mewe, M., Wulfsen, I., Schuster, A. M., Middendorff, R., Glassmeier, G., Schwarz, J. R., & Bauer, C. K. (2008). Erg K+ channels modulate contractile activity in the bovine epididymal duct. *American Journal of Physiology. Regulatory, Integrative and Comparative Physiology*, *294*, R895–R904.

Ohya, S., Asakura, K., Muraki, K., Watanabe, M., & Imaizumi, Y. (2002). Molecular and functional characterization of ERG, KCNQ, and KCNE subtypes in rat stomach smooth muscle. *American Journal of Physiology. Gastrointestinal and Liver Physiology*, *282*, G277–G287.

Ohya, S., Horowitz, B., & Greenwood, I. A. (2002). Functional and molecular identification of ERG channels in murine portal vein myocytes. *American Journal of Physiology. Cell Physiology*, *283*, C866–C877.

Parkington, H. C., Stevenson, J., Tonta, M. A., Paul, J., Butler, T., Maiti, K., Chan, E. C., Sheehan, P. M., Brennecke, S. P., Coleman, H. A., & Smith, R. (2014). Diminished hERG K+ channel activity facilitates strong human labour contractions but is dysregulated in obese women. *Nature Communications*, *5*, 4108.

Parr, E., Pozo, M. J., Horowitz, B., Nelson, M. T., & Mawe, G. M. (2003). ERG K+ channels modulate the electrical and contractile activities of gallbladder smooth muscle. *American Journal of Physiology. Gastrointestinal and Liver Physiology*, *284*, G392–G398.

Petkov, G. V. (2011). Role of potassium ion channels in detrusor smooth muscle function and dysfunction. *Nature Reviews. Urology*, *9*(1), 30–40. https://doi.org/10.1038/nrurol.2011.194

Petkov, G. V. (2014). Central role of the BK channel in urinary bladder smooth muscle physiology and pathophysiology. *American Journal of Physiology, Regulatory, Integrative and Comparative Physiology*, *307*, R571–R584.

Provence, A., Angoli, D., & Petkov, G. V. (2018). KV7 channel pharmacological activation by the novel activator ML213: Role for heteromeric KV7.4/KV7.5 channels in guinea pig detrusor smooth muscle function. *The Journal of Pharmacology and Experimental Therapeutics*, *364*(1), 131–144.

Sanchez-Conde, F. G., Jimenez-Vazquez, E. N., Auerbach, D. S., & Jones, D. K. (2022). The ERG1 K^+ channel and its role in neuronal health and disease. *Frontiers in Molecular Neuroscience*, *15*, 890368. https://doi.org/10.3389/fnmol.2022.890368

Sanguinetti, M. C., Curran, M. E., Spector, P. S., & Keating, M. T. (1996). Spectrum of HERG K+-channel dysfunction in an inherited cardiac arrhythmia. *Proceedings of the National Academy of Sciences of the United States of America*, *93*, 2208–2212.

Smith, P. L., Baukrowitz, T., & Yellen, G. (1996). The inward rectification mechanism of the HERG cardiac potassium channel. *Nature*, *379*(6568), 833–836.

Spector, P. S., Curran, M. E., Keating, M. T., & Sanguinetti, M. C. (1996). Class III antiarrhythmic drugs block HERG, a human cardiac delayed rectifier K+ channel. Open-channel block by methanesulfonanilides. *Circulation Research*, *78*(3), 499–503.

Stott, J. B., Barrese, V., Suresh, M., Masoodi, S., & Greenwood, I. A. (2018). Investigating the role of G protein $\beta\gamma$ in Kv7-dependent relaxations of the rat vasculature. *Arteriosclerosis, Thrombosis, and Vascular Biology*, *38*(9), 2091–2102.

Svalo, J., Sheykhzade, M., Nordling, J., Matras, C., & Bouchelouche, P. (2015). Functional and molecular evidence for Kv7 channel subtypes in human detrusor from patients with and without bladder outflow obstruction. *PLoS One*, *10*, e0117350.

Turner, W. H., & Brading, A. F. (1997). Smooth muscle of the bladder in the normal and the diseased state: Pathophysiology, diagnosis and treatment. *Pharmacology & Therapeutics*, *75*, 77–110.

Vandenberg, J. I., Perry, M. D., Perrin, M. J., Mann, S. A., Ke, Y., & Hill, A. P. (2012). hERG K(+) channels: structure, function, and clinical significance. *Physiological Reviews*, *92*(3), 1393–1478.

Vandenberg, J. I., Walker, B. D., & Campbell, T. J. (2001). HERG K+ channels: Friend and foe. *Trends in Pharmacological Sciences*, *22*, 240–246.

van der Horst, J., Greenwood, I. A., & Jepps, T. A. (2020). Cyclic AMP-dependent regulation of Kv7 voltage-gated potassium channels. *Frontiers in Physiology*, *11*, 727.

20518171x, 2023, 3, Downloaded from https://physoc.onlinelibrary.wiley.com/doi/10.14814/phy2.15583 by Test, Wiley Online Library on [10/01/2025]. See the Terms and Conditions (https://onlinelibrary.wiley.com/terms-and-conditions) on Wiley Online Library for rules of use; OA articles are governed by the applicable Creative Commons License

Yeung, S. Y., & Greenwood, I. A. (2007). Pharmacological and biophysical isolation of K+ currents encoded by ether-à-go-go-related genes in murine hepatic portal vein smooth muscle cells. *American Journal of Physiology. Cell Physiology*, *292*, C468–C476.

Zhou, J., Augelli-Szafran, C. E., Bradley, J. A., Chen, X., Koci, B. J., Volberg, W. A., Sun, Z., & Cordes, J. S. (2005). Novel potent human *ether-a-go-go*-related gene (hERG) potassium channel enhancers and their *in vitro* antiarrhythmic activity. *Molecular Pharmacology*, *68*, 876–884.

How to cite this article: Barrese, V., Wehbe, Z., Linden, A., McDowell, S., Forrester, E., Povstyan, O., McCloskey, K. D., & Greenwood, I. A. (2023). Key role for Kv11.1 (ether-a-go-go related gene) channels in rat bladder contractility. *Physiological Reports*, *11*, e15583. https://doi.org/10.14814/phy2.15583

2051817x, 2023, 3, Downloaded from https://physoc.onlinelibrary.wiley.com/doi/10.14814/phy2.15583 by Test, Wiley Online Library on [10/01/2025]. See the Terms and Conditions (https://onlinelibrary.wiley.com/terms-and-conditions) on Wiley Online Library for rules of use; OA articles are governed by the applicable Creative Commons License

Check for updates

Received: 14 November 2021 | Revised: 21 June 2022 | Accepted: 20 July 2022

DOI: 10.1111/bph.15947

RESEARCH ARTICLE

Marked oestrous cycle-dependent regulation of rat arterial $K_V7.4$ channels driven by GPER1

Samuel N. Baldwin[1] | Elizabeth A. Forrester[1] | Natalie Z. M. Homer[2] | Ruth Andrew[2,3] | Vincenzo Barrese[4] | Jennifer B. Stott[1] | Brant E. Isakson[5] | Anthony P. Albert[1] | Iain A. Greenwood[1]

[1]Vascular Biology Research Centre, Institute of Molecular and Clinical Sciences, St George's University of London, London, UK

[2]Mass Spectrometry Core Laboratory, Edinburgh Clinical Research Facility, Queen's Medical Research Institute, University of Edinburgh, Edinburgh, UK

[3]BHF Centre for Cardiovascular Science, Queen's Medical Research Institute, University of Edinburgh, Edinburgh, UK

[4]Department of Neuroscience, Reproductive Sciences and Dentistry, University of Naples Federico II, Naples, Italy

[5]Department of Molecular Physiology and Biophysics, Robert M. Berne Cardiovascular Research Centre, University of Virginia School of Medicine, Charlottesville, Virginia, USA

Correspondence
Iain A. Greenwood, Vascular Biology Research Centre, Institute of Molecular and Clinical Sciences, St George's University of London, London, UK.
Email: grenwood@sgul.ac.uk

Funding information
British Heart Foundation, Grant/Award Numbers: #FS/18/41/33762, FS/18/41/33762

Background and Purpose: *Kcnq*-encoded K_V7 channels (termed $K_V7.1–5$) regulate vascular smooth muscle cell (VSMC) contractility at rest and as targets of receptor-mediated responses. However, the current data are mostly derived from males. Considering the known effects of sex, the oestrous cycle and sex hormones on vascular reactivity, here we have characterised the molecular and functional properties of K_V7 channels from renal and mesenteric arteries from female Wistar rats separated into di-oestrus and met-oestrus (F-D/M) and pro-oestrus and oestrus (F-P/E).

Experimental Approach: RT-qPCR, immunocytochemistry, proximity ligation assay and wire myography were performed in renal and mesenteric arteries. Circulating sex hormone concentrations were determined by liquid chromatography–tandem mass spectrometry. Whole-cell electrophysiology was undertaken on cells expressing $K_V7.4$ channels in association with G-protein-coupled oestrogen receptor 1 (GPER1).

Key Results: The $K_V7.2–5$ activators S-1 and ML213 and the pan-K_V7 inhibitor linopirdine were more effective in arteries from F-D/M compared with F-P/E animals. In VSMCs isolated from F-P/E rats, exploratory evidence indicates reduced membrane abundance of $K_V7.4$ but not $K_V7.1$, $K_V7.5$ and Kcne4 when compared with cells from F-D/M. Plasma oestradiol was higher in F-P/E compared with F-D/M, and progesterone showed the converse pattern. Oestradiol/GPER1 agonist G-1 diminished $K_V7.4$ encoded currents and ML213 relaxations and reduced the membrane abundance of $K_V7.4$ and interaction between $K_V7.4$ and heat shock protein 90 (HSP90), in arteries from F-D/M but not F-P/E.

Conclusions and Implications: GPER1 signalling decreased $K_V7.4$ membrane abundance in conjunction with diminished interaction with HSP90, giving rise to a 'pro-contractile state'.

Abbreviations: BK_{Ca}, large conductive calcium activated potassium channel; E2, oestradiol; EC(−), endothelium denuded; EC(+), endothelium intact; ECs, endothelial cells; F-D/M, di-oestrus and met-oestrus; F-P/E, pro-oestrus and oestrus; FSH, follicular stimulating hormone; GPER1, G-protein-coupled oestrogen receptor 1; HEK-$K_V7.4$, human embryonic kidney 293B stably expressing $K_V7.4$; HEK-$K_V7.4$-GPER1, HEK-$K_V7.4$ cells transiently transfected with *GPER1*; HSP90, heat shock protein 90; K^+PSS, high K^+ physiological salt solution; K_{ATP}, ATP-sensitive potassium channel; K_V, voltage-gated potassium channel; LC–MS/MS, liquid chromatography–tandem mass spectrometry; LH, luteinising hormone; PLA, proximity ligation assay; PSS, physiological salt solution; VGCC, voltage-gated calcium channels; VSMCs, vascular smooth muscle cells.

This is an open access article under the terms of the Creative Commons Attribution License, which permits use, distribution and reproduction in any medium, provided the original work is properly cited.
© 2022 The Authors. *British Journal of Pharmacology* published by John Wiley & Sons Ltd on behalf of British Pharmacological Society.

1 | INTRODUCTION

Sexual dimorphisms in cardiovascular physiology and pathophysiology are a well-documented phenomenon (Pabbidi et al., 2018). Premenopausal women exhibit greater coronary and cerebral blood flow, and the incidence of adverse cardiovascular events is significantly lower (Pabbidi et al., 2018). As the female cardioprotective phenotype decreases after the menopause, the most likely candidates that drive sexual dimorphisms within the vasculature are sex hormones, primarily oestrogens. However, the role of oestrogens within the cardiovascular system remains enigmatic, as they have been shown to be both protective and detrimental to the vasculature (Hulley et al., 1998, 2002; Yang & Reckelhoff, 2011).

Within rodent and human arteries, *KCNQ*-encoded **K_V7** channels are key regulators of vascular reactivity, whereby activation of the channel mediates hyperpolarisation of the membrane and closure of voltage-gated calcium channels (VGCC). In vascular smooth muscle, of the five subtypes, ***KCNQ1***, ***KCNQ4*** and ***KCNQ5*** are the principally expressed genes (Ng et al., 2011; Ohya et al., 2003), **$K_V7.4$** is the predominantly expressed protein (Ng et al., 2011; Yeung et al., 2007) and the $K_V7.4$/**$K_V7.5$** heterotetramer is purported to be the most common channel species (Chadha et al., 2014). Pharmacological and molecular evidence shows that activity of $K_V7.4$/$K_V7.5$ channels regulates resting membrane potential (Mackie et al., 2008) and is functionally important for **cAMP**- and **cGMP**-linked receptor-mediated vasorelaxation (Chadha et al., 2012, 2014; Mondéjar-Parreño et al., 2019; Stott et al., 2015) and **PKC**-mediated contraction (Brueggemann et al., 2006). Notably, $K_V7.4$ channels are downregulated in hypertensive rats (Jepps et al., 2011) via post-transcriptional mechanisms affecting protein synthesis, trafficking and degradation (Barrese, Stott, Figueiredo, et al., 2018; Carr et al., 2016) and are associated with the hypertensive phenotype (Barrese, Stott, & Greenwood, 2018).

To date, data on vascular K_V7 channels focuses primarily on arteries from male animals. On the basis of known sexual dimorphisms in vascular reactivity and the growing recognition of sex as an experimental factor (Docherty et al., 2019), we aimed to address this deficit. We have characterised the functional and molecular properties of K_V7 channels in arteries from female Wistar rats. In light of previously demonstrated oestrous cycle-dependent changes in vascular reactivity (Jaimes et al., 2019), the oestrous cycle was a key consideration in the following study. The rat oestrous cycle lasts only 4–5 days, with different durations for each stage, as follows: (1) pro-oestrus, 14 h; (2) oestrus, 24–48 h; (3) met-oestrus, 6–8 h; and (4) di-oestrus, 48–72 h (Cora et al., 2015). As sex hormones peak in pro-oestrus (Nilsson et al., 2015), female rats were separated into two groups, those in pro-oestrus and oestrus (F-P/E) and those in di-oestrus and met-oestrus (F-D/M) stages of the oestrous cycle. The observations detailed here demonstrate a remarkable oestrous cycle-related reduction in $K_V7.4$ membrane abundance, mediated through oestradiol (**E2**) signalling via G-protein-coupled oestrogen receptor 1 (**GPER1**), which underlies a pro-contractile vascular state.

What is already known

- Vascular K_V7 channels are key components of resting tone and endogenous vasoactive responses.
- The oestrous cycle regulates vascular reactivity.

What does this study add

- Oestrous cycle-dependent reduction in $K_V7.4$ membrane abundance and function coincided with a pro-contractile phenotype.
- GPER1 activation negatively regulates $K_V7.4$ forward trafficking and function.

What is the clinical significance

- Oestrogenic signalling decreases vascular K_V7 channel function.
- Negative regulation of $K_V7.4$ may contribute to the detrimental attributes of hormone replacement therapy.

2 | METHODS

2.1 | Animal model

All animal care and experimental procedures complied with the requirements of the UK Animal (Scientific Procedures) Act (ASPA) 1986 and were approved by the Institutional Animal Ethics Committee. Animal studies are reported in compliance with the ARRIVE guidelines (Percie du Sert et al., 2020) and with the recommendations made by the *British Journal of Pharmacology* (Lilley et al., 2020). Experiments were performed with male and female Wistar rats (RRID:RGD_734476; Charles River, Margate, UK) aged 11–15 weeks (200–300 g) kept at the Biological Research Facility at St George's University (London). The animals were housed in cages with free access to water and food (RM1; Dietex International, UK) on a 12-h light/dark cycle and maintained at a constant temperature and humidity (21°C ± 1°C; 50% ± 10% humidity) in accordance with the ASPA 1986. Animals were kept in a bedding of LSB Aspen woodchip. Female rats were housed separately from males to ensure standard progression through the oestrous cycle. Animals were killed humanely by cervical dislocation with secondary confirmation via femoral artery severance, in accordance with Schedule 1 of the ASPA 1986. Organs were harvested and immediately placed in ice-cold physiological salt solution (PSS) of the following composition ($mmol \cdot L^{-1}$): 119 NaCl, 4.5 KCl, 1.17 $MgSO_4 \cdot 7H_20$, 1.18 NaH_2PO_4, 25 $NaHCO_3$, 5 glucose and 1.25 $CaCl_2$ balanced to a

14765381, 2023, 2, Downloaded from https://bpspubs.onlinelibrary.wiley.com/doi/10.1111/bph.15947 by Test, Wiley Online Library on [10/01/2025]. See the Terms and Conditions (https://onlinelibrary.wiley.com/terms-and-conditions) on Wiley Online Library for rules of use; OA articles are governed by the applicable Creative Commons License

pH of 7.4 by perfusion of 95% O_2 and 5% CO_2. Blood (2 ml) was collected during femoral artery severance, into vials containing EDTA (100 μl of 0.5M in H_2O). Samples were then centrifuged at 2000 x *g* for 20 min. Plasma was extracted and stored at −80°C.

2.2 | Oestrous cycle stage determination

Following humane killing, PSS (50 μl) was inserted into the vaginal canal via a 2–200 μl tip and flushed 4–6 times to liberate cells from the surface of the cervix. PSS was removed from the vaginal canal, and 25 μl of the cervical cell suspension was mounted on a glass slide and examined under light microscopy. Variation in the population of three principal cell types - large keratinised (cornified) epithelial cells, nucleated epithelial cells and leukocytes - were used to identify each stage, as previously described (Cora et al., 2015), which was the primary tool used for cycle stage determination during the course of this study. Representative images from each cycle stage are shown in Figure S1. To generate the representative images in Figure S1, samples of cervical cell suspension (50 μl) were plated on glass slides and left to adhere for 1 h at room temperature. Then the slide was flooded with toluidine blue O (1ml, 0.1% in H_2O, passed through a 0.2-μm syringe filter). Cells were left in the dye solution for 45 s, before being washed in distilled water on a rotating plate (20 rpm) for 1 min. Cells were left to dry and then imaged via Nikon Eclipse Ni. Cycle stage determination was performed after the experiment, during functional investigation, as a means of blinding. Such blinding was not possible during molecular techniques.

2.3 | Wire myography

Arterial segments (∼2 mm) of the main renal, second-order mesenteric, basilar and left anterior descending coronary arteries were mounted on either 100 μm pins (renal) or 40 μm tungsten wire (mesenteric, coronary and cerebral arteries) within a myograph chamber (Danish Myo Technology, Arhus, Denmark) containing PSS (5 ml) oxygenated with 95% O_2 and 5% CO_2 at 37°C. Vessels then underwent a passive force normalisation process to achieve an internal luminal circumference at a transmural pressure of 100 mmHg (13.3 kPa) to standardise pre-experimental conditions (Mulvany & Halpern, 1976). Force generated was amplified by a PowerLab (ADInstruments, Oxford, UK) and then recorded via LabChart software (RRID:SCR_017551; ADInstruments). Vessels were then left to rest for 10 min. A minimal time interval that was applied between all separate challenges to the vessels. Isotonic high K^+ physiological salt solution (K^+PSS) of the following composition (mmol·L^{-1}): 63.5 NaCl, 60 KCl, 1.17 $MgSO_4{\cdot}7H_20$, 1.18 NaH_2PO_4, 25 $NaHCO_3$, 5 glucose and 1.25 $CaCl_2$ balanced to a pH of 7.4 by gassing with 95% O_2 and 5% CO_2, was then added to bath to determine vessel viability. After the contraction had stabilised, the vessels were washed in normal PSS until they returned to baseline. Vessels were then challenged again with K^+PSS to ensure maximal contraction had been achieved. Endothelial cell (EC) integrity was determined by relaxation of pre-constricted arterial tone (**methoxamine**, 10 μmol·L^{-1}) in response to **carbachol** (10 μmol·L^{-1}). Only vessels that generated ≥80% relaxation were used and considered endothelium-positive.

When generating concentration–effect curves in response to the TXA_2 receptor agonist **U46619** (0.003–3 μmol·L^{-1}), logarithmically increasing concentrations of an agent were added to the bath following the 'warm-up' protocol, with incremental increase in tension allowed to plateau before the next concentration was added. Upon completion of the curve, vessels were washed in standard PSS and allowed to return to baseline tension. Vessels were then pre-incubated in either DMSO (≤0.1%) as the solvent control, **linopirdine** (10 μmol·L^{-1}) or **HMR-1556** (10 μmol·L^{-1}) for 10 min, before starting a second concentration–effect curve. All contractions were then normalised to the peak, stable contraction generated in response to K^+PSS. In contrast, when investigating vasorelaxants, vessels were first pre-constricted with U46619 (300 nmol·L^{-1}). Once tone had stabilised, logarithmically increasing concentrations of either **isoprenaline** (0.003–3 μmol·L^{-1}), **S-1** (0.1–10 μmol·L^{-1}), **ML213** (0.01/0.1–10 μmol·L^{-1}), **NS11021** (0.1–30 μmol·L^{-1}), **pinacidil** (0.1–30 μmol·L^{-1}) or **nicardipine** (0.001–1 μmol·L^{-1}) were then added to the bath. With regard to isoprenaline, vessels were then washed and pre-incubated in either DMSO (≤0.1%), linopirdine (10 μmol·L^{-1}) or HMR-1556 (10 μmol·L^{-1}) for 10 min, and a second curve was generated. With experiments involving vasorelaxation in response to ion channel modulators, only one curve could be generated as these drugs do not readily wash out. EC denudation was achieved by mechanical abrasion of the lumen of the arterial segment with human hair and was validated by loss of the relaxation of pre-contracted arterial tone (10 μmol·L^{-1} methoxamine) in response to carbachol.

2.4 | RT-qPCR procedures

Relative fold changes in expression levels of *Kcnq1–5*, *Kcne1–5*, *Esr1–2*, *Gper1*, *Acta2 and Cd31* transcripts were determined in main renal and mesenteric arteries and whole brain, heart and uterine samples via RT-qPCR. In addition, endothelium intact (EC(+)) and endothelium denuded (EC(−)) lysates of mesenteric arteries were prepared. EC(−) samples were prepared as previously described (Askew Page et al., 2019).

mRNA was extracted and converted to cDNA using Monarch Total RNA Miniprep Kit (New England BioLabs, Ipswich, MA, USA) then LunaScript RT SuperMix Kit (New England BioLabs), respectively. Quantitative analysis of target genes was assessed via CFX-96 Real-Time PCR Detection System (RRID:SCR_018064; BioRad, Hertfordshire, UK). Samples were run in BrightWhite qPCR plates (Primer Design, Camberley, UK) in combination with PrecisionPLUS qPCR Master Mix (Primer Design), 300 nmol·L^{-1} of gene-specific target primer (Thermofisher Scientific, Waltham, MA, USA) and 10 ng cDNA, according to the manufacturer's instructions. Quantification cycles (Cq) were determined via Bio-Rad CFX96 Manager 3.0. Cq was

14765381, 2023, 2, Downloaded from https://bpspubs.onlinelibrary.wiley.com/doi/10.1111/bph.15947 by Test, Wiley Online Library on [10/01/2025]. See the Terms and Conditions (https://onlinelibrary.wiley.com/terms-and-conditions) on Wiley Online Library for rules of use; OA articles are governed by the applicable Creative Commons License

normalised to the average of two housekeeping genes, chosen from ubiquitin C (*Ubc*), polyamine transporter 1 (*Tpo-1*), cytochrome C1 (*Cyc1*), calnexin (*Canx*) and glyceraldehyde 3-phosphate dehydrogenase (*Gapdh*) and expressed using either formula $2^{-\Delta Cq}$ or $2^{-\Delta\Delta Cq}$ for analysis of relative abundance or relative fold changes as stated (Jepps et al., 2011). A list of the primers used (Thermo-Fisher, Paisley, UK) in the experiments described here is given in Table 1. Primers for housekeeping genes were provided by Primer Design; such sequences cannot be disclosed for proprietary reasons.

2.5 | Vascular smooth muscle cell isolation

Renal and mesenteric arteries were incubated in isolation PSS of the following composition (mmol·L^{-1}): 120 NaCl, 6 KCl, 12 glucose, 10 HEPES and 1.2 $MgCl_2$ balanced to a pH of 7.4 with NaOH, supplemented with 1.75 mg·ml^{-1} collagenase type IA, 0.9 mg·ml^{-1} protease, 1 mg·ml^{-1} trypsin inhibitor and 1 mg·ml^{-1} bovine serum albumin (Sigma, UK) at 37°C for 30 min (renal artery) or 17 min (mesenteric artery). Next, vessels were gently triturated with a wide-bore glass pipette to liberate vascular smooth muscle cells (VSMCs) from their extracellular matrix. The subsequent cell suspension was supplemented with 2.5 mmol·L^{-1} Ca^{2+} and left to adhere on 25 mm glass coverslips for 1 h in an incubator at 37°C in 95% O_2 + 5% CO_2. Isolated myocytes were then either fixed immediately afterwards or incubated in 1 ml isolation PSS containing solvent control (DMSO or ethanol, final solvent concentrations were ≤0.1%), or the following - **oestradiol** (E2; 10 nmol·L^{-1}), G-36 (1 μmol·L^{-1}) or **G-1** (1 μmol·L^{-1}) for 10 or 30 min as stated.

TABLE 1 Primers used in RT-qPCR analyses

Gene	(+) Forward primer sequence (−) Reverse primer sequence	Gene accession number	Amplicon (bp)
Kcnq1	TGGGTCTCATCTTCTCCTCC GTAGCCAATGGTGGTGACTG	NM_032073	124
Kcnq2	AAGAGCAGCATCGGCAAAAA GGTGCGTGAGAGGTTAGTAGCA	NM_133322	101
Kcnq3	CAGCAAAGAACTCATCACCG ATGGTGGCCAGTGTGATCAG	AF091247	161
Kcnq4	GAATGAGCAGCTCCCAGAAG AAGCTCCAGCTTTTCTGCAC	XM_233477.8	133
Kcnq5	AACTGATGAGGAGGTCGGTG GATGACCGTGACCTTCCAGT	XM_001071249.3	120
Kcne1	GTTTCCCCAAATCTCTCCATT AGCACACACTTCCCATTTCAA	NM_008424.3	111
Kcne2	CCTGGTATTTAACTGAGTTGGACAT GCACTGGGGGCTCTTGAAT	NM_133603.2	97
Kcne3	CTCAACCATATCAAGCCACAGT GCCTATCAGTCCCTCTTCTCT	NM_022235.2	99
Kcne4	GGAGGAGGGGGCTGATGA CTGGTGGATGTTCTCGGAAGA	NM_212526.1	88
Kcne5	GCACGAAGAGACCTCAGACAT GGACAGGAAACAAGAACACCAT	NM_001101003.1	146
Esr1	TTCACCTTCTGGAGTGTGCC ACTTGACGTAGCCAGCAACA	NM_012689.1	173
Esr2	TGCCGACTTCGCAAGTGTTA ACCGTTTCTCTTGGCTTTGC	NM_012754.2	138
Gper1	TCATCGGCCTGTGCTATTCC GAAGACAAGGACCACTGCGA	NM_133573	119
Cd31	CTCCTAAGAGCAAAGAGCAACTTC TACACTGGTATTCCATGTCTCTGG	NM_031591.1	100
Acta2	ATCCGATAGAACACGGCATC AGGCATAGAGGGACAGCACA	NM_031004.2	228

14765381, 2023, 2, Downloaded from https://bpspubs.onlinelibrary.wiley.com/doi/10.1111/bph.15947 by Test, Wiley Online Library on [10/01/2025]. See the Terms and Conditions (https://onlinelibrary.wiley.com/terms-and-conditions) on Wiley Online Library for rules of use; OA articles are governed by the applicable Creative Commons License

2.6 | Immunocytochemistry

The immuno-related procedures used comply with the recommendations made by the *British Journal of Pharmacology* (Alexander et al., 2018). Isolated VSMCs were fixed in 3% paraformaldehyde (PFA) containing phosphate buffered serum (PBS) for 15 min at room temperature (Barrese, Stott, Figueiredo, et al., 2018). For membrane staining, cells were incubated in Alexa Fluor 488-conjugated wheat germ agglutinin (WGA; Thermo-Fisher; dil. 1:200 in PBS) for 10 min, washed in 0.1 mmol·L^{-1} glycine in PBS for 5 min and incubated in blocking solution (0.1% Triton X-100, 10% fetal bovine serum in PBS) for 1 h. Cells were incubated overnight in either rabbit anti-K_V7.4 (RRID:AB_2341042; #APC-164; Alomone, Jerusalem, Israel; dil. 1:200), rabbit anti-K_V7.1 (Pineda, Antikörber-Service, Germany; dil. 1:100), rabbit anti-K_V7.5 (RRID:AB_210806; #ABN1372; Millipore, Temecula, CA, USA; dil. 1:100) or rabbit anti-**Kcne4** (RRID:AB_1079170; #HPA011420; Atlas Antibodies, Sweden; dil. 1:200) at 4°C. Cells were then washed in PBS and incubated in goat anti-rabbit secondary antibody conjugated to Alexa Fluro 568 (RRID:AB_143157; A11036; Thermo-Fisher; dil. 1:100), and then mounted in Vectashield (P4170; Sigma) medium containing 4′,6-diamidino-2-phenylindole (DAPI). All antibodies were diluted in blocking solution. Cells were then imaged via Nikon A1R confocal microscope (inverted) on Ti2 chassis (Image Resource Facility, St George's University, London). For experiments determining the membrane:cytosol ratio for K_V7.4 expression, fluorescence intensity profiles for K_V7.4 and WGA were plotted across three randomly drawn lines spanning the width of the cell measured in arbitrary units (A.U.) using ImageJ software (RRID:SCR_003070; https://imagej.nih.gov/ij/). Fluorescence intensity ≥ 200 A.U. was considered as the plasma membrane, and below the threshold was considered as the cytosol. The membrane:cytosol ratio for K_V7.4 expression was calculated by measuring the average fluorescence intensity of K_V7.4 within the membrane and dividing it by the average fluorescence intensity of K_V7.4 within cytosol in 10–12 cells per n. Total cell fluorescence was measured by via ImageJ software (https://imagej.nih.gov/ij/). Validation of rabbit anti-K_V7.4 (#APC-164) is demonstrated in Figure S2.

2.7 | Plasma concentration of sex hormones

Steroid analysis was performed by targeted liquid chromatography–tandem mass spectrometry (LC–MS/MS), following extraction of samples through automated supported liquid extraction (SLE) on an Extrahera liquid handling robot (Biotage, Uppsala, Sweden), adapted from Boulton et al. (2021). The method has an intra- and inter-assay coefficient variation between 4.9% and 7.2% for the five steroids measured: E2, **aldosterone**, **testosterone**, **androstenedione** and **progesterone.** Analysis was performed on an I-class Acquity UPLC (Waters, Wilmslow, UK) interfaced to a QTRAP 6500+ (AB Sciex, Warrington, UK) mass spectrometer. Instrument control and data acquisition were achieved using Analyst® 1.6.3 Software. Data were integrated and evaluated using MultiQuant® 2.3.1 (AB Sciex). Chromatographic separation was achieved on a Kinetex C18 (2.1 × 150 mm; 2.6 μm particle size), column fitted with a KrudKatcher Ultra In-Line Filter (0.5 μm porosity) both from Phenomenex, UK. The mobile phase system comprised mobile phase A - water with ammonium fluoride (50 μM) and mobile phase B – methanol with ammonium fluoride (50 μM) pumped at a flow rate of 0.3 ml·min^{-1} over 16 min, starting at 55% B for 2 min, rising to 100% B over 6 min, held for 2 min, before returning to 55% B over 0.1 min and equilibrating for 4.9 min, all held at a temperature of 50°C. The solvent flow was diverted to waste from 0 to 2 min and 11 to 16 min.

The mass spectrometer was operated in electrospray ionisation mode with polarity switching using a TurboIonSpray source, and data were collected in unit resolution (0.7 *m/z* full width at half maximum). The source was operated at 600°C with polarity switching with an IonSpray voltage of 5.5 kV/−4.5 kV, a curtain gas of 30 psi, nitrogen nebuliser ion source gas 1 and heater ion source gas 2 of 40 and 60 psi, respectively. Multiple reaction monitoring transitions for steroids and their isotopically labelled internal standards are as follows with chromatographic retention time: negative ions following −4.5 kV IonSpray voltage for 17β-oestradiol (7.0 min) *m/z* 271.0 → 144.9, 182.9 at −21 and −19 V, $^{13}C_3$-[2,3,4]-oestradiol (7.0 min) *m/z* 274.0 → 147.9 at −29 V, aldosterone (2.6 min) *m/z* 359.1 → 188.9, 331.0 at −21 and −35 V and d8-aldosterone (2.6 min) *m/z* 367.2 → 193.9 at −21 V; and positive ions for testosterone (7.6 min) *m/z* 289.1 → 97.0, 109.2 at 12 and 6 V, $^{13}C_3$-[2,3,4]-testosterone (7.6 min) *m/z* 292.1 → 100.0 at −12 V, androstenedione (6.8 min) *m/z* 287.1 → 97.0, 78.9 at 14 and 10 V, $^{13}C_3$-[2,3,4]-androstenedione (6.8 min) *m/z* 290.2 → 100.1 at −14 V and progesterone (8.9 min) *m/z* 315.0 → 97.1, 109.1 at 25 and 27 V and 2,2,4,6,6,17α,21,21,21-d9-progesterone (8.9 min) *m/z* 324.1 → 100.0, 109.1 at 15 V.

Calibration ranges (between 0.0025 and 100 ng·ml^{-1}) for each steroid were plotted as the peak area ratio of the analyte divided by the relevant internal standard versus amount of steroid. Amounts of steroid were calculated using the calibration lines of best fit, which were considered acceptable if the regression coefficient, r, was >0.99, with 1/x weighting.

Plasma concentrations of **luteinising hormone (LH)** and **follicular stimulating hormone (FSH)** were determined at the University of Virginia Ligand Core for clinical and basic scientific research. Hormones were analysed via an own in-house enzyme-linked immunoblot assay (ELISA) protocol. LH was measured in plasma by a two-step sandwich immunoassay using monoclonal antibodies against bovine LH (no. 581B7) and against the **human LH-β subunit** (no. 5303: Medix Kauniainen, Finland) as described previously (Haavisto et al., 1993). FSH was assayed by RIA using mouse FSH reference prep AFP5308D for assay standards and mouse FSH antiserum (guinea pig; AFP-1760191). See https://med.virginia.edu/research-in-reproduction/ligand-assay-analysis-core/ for further detail.

14765381, 2023, 2, Downloaded from https://bpspubs.onlinelibrary.wiley.com/doi/10.1111/bph.15947 by Test, Wiley Online Library on [10/01/2025]. See the Terms and Conditions (https://onlinelibrary.wiley.com/terms-and-conditions) on Wiley Online Library for rules of use; OA articles are governed by the applicable Creative Commons License

2.8 | Single-cell electrophysiology

Human embryonic kidney 293B (HEK293B) cells stably expressing human $K_V7.4$ (HEK-$K_V7.4$; Copenhagen, Denmark) were grown in Dulbecco's modified Eagle's medium (DMEM)/F-12 (Sigma) supplemented in 1% penicillin/streptomycin in 5% CO_2 at 37°C. HEK-$K_V7.4$ cells were transiently transfected with *GPER1* (HEK-$K_V7.4$-GPER1; HG11264-ACG; pCMV3-GPER1-GFPSpark; 4 μg; Sino Biological, Eschborn, Germany) via Lipofectamine 3000 reagent (ThermoFisher Scientific), according to the manufacturer's instructions. HEK-$K_V7.4$-GPER1 and same-day non-transfected controls were mounted on glass coverslips and left to attach for 1 h at room temperature. Cells were then incubated in either solvent, E2 (10 nmol·L^{-1}) or G-1 (1 μmol·L^{-1}), for 30 min prior to generating ruptured whole-cell current recordings.

Coverslips were mounted on an inverted microscope fitted with a Nikon C-SHG mercury lamp. Cells were bathed in an external solution composed of (in mmol·L^{-1}) 140 NaCl, 4 KCl, 2 $CaCl_2$, 10 HEPES and 1 $MgCl_2$ balanced to a pH of 7.4 with NaOH at room temperature. Glass pipettes (Plowden & Thompson) were pulled in-house via PP-830 (Narishige, Japan) to a resistance of 6–10 MΩ. Pipettes were filled with an internal solution composed of (in mmol·L^{-1}) 110 K gluconate, 30 KCl, 0.5 MgCl, 5 HEPES, 0.5 EGTA and 1 Na_2ATP balanced to a pH of 7.2 with CsOH. All currents in the following investigation were recorded using an AXOpatch 200B amplifier (Axon Instruments), and whole-cell electrical signals were made and digitised via Digidata 1550A series operated by pClamp 10.7 (Molecular Devices). After membrane rupture, cells were held at −50 mV and pulsed to +20 mV every 20 s for 200 ms. Once currents had stabilised, current voltage relationships (*IV*) were constructed by stepping from −50 mV to 'test voltages' ranging from −70 to +40 mV for 1.5 s. Peak current amplitude normalised to cell size, $I_{(pA/pF)}$, was measured following plateau at each voltage step. Voltage was stepped down to an inactivation step of -40 mV after each test and measured as a 'tail current'.

2.9 | Proximity ligation assay

The interaction of $K_V7.4$ and heat shock protein 90 (HSP90) was determined by proximity ligation assay (PLA), as described by Barrese, Stott, Figueiredo et al., (2018). Mesenteric VSMCs were isolated, incubated in either ethanol (≤0.1%) or E2 (10 nmol·L^{-1}), diluted in 1 ml of isolation PSS for 30 min at 37°C and fixed as above. Cells were washed in 0.1 mmol·L^{-1} glycine containing PSS for 10 min, permeabilised via 0.1% Triton X-100 for 5 min and blocked via Duolink blocking solution for 1 h at 37°C, and then incubated in a combination of rabbit anti-$K_V7.4$ (APC-164, Alomone; dil. 1:200) and mouse-anti-HSP90 (RRID:AB_300396; ab13492, Abcam, Cambridge, UK; dil. 1:200) overnight at 4°C. The following morning, cells were incubated in a combination of Duolink In situ PLA probes, anti-mouse MINUS (RRID:AB_2713942; DUO92004; Sigma-Aldrich, St. Louis, MO, USA) and anti-rabbit PLUS (RRID:AB_2810940; DUO92002; Sigma-Aldrich) for 1 h at 37°C, according to the manufacturer's instructions. Using Duolink In situ detection reagents (DUO92008; Sigma-Aldrich), samples underwent ligation (30 min at 37°C) and amplification (100 min at 37°C), according to the manufacturer's instructions. Cells were then mounted on cover slides in Vectashield (P4170; Sigma) containing DAPI. All antibodies and probes were diluted in blocking solution. Cells were then imaged in the Image Resource Facility, St George's University, London.

2.10 | Data analysis

Figures show mean data from at least five repeats ± SEM. For functional experiments involving cumulative concentrations, a transformed data set was generated using X = Log(X) to reduce representative skew, following which a four-parametric linear regression analysis was performed using the following equation: (Log (Agonist) vs. response − Variable slope (four parameters bottom/Hillslope/top/EC_{50})), using GraphPad Prism (RRID:SCR_002798; Version 8.2.0) to fit a concentration–effect curve to the figure. For data comparing multiple groups, a one-way analysis of variance (ANOVA) was performed, or two-way ANOVA followed by a post hoc Bonferroni/Dunnett's test to account for type 1 errors in multiple comparisons was performed for comparison of mean values. Multiple comparisons include condition A versus condition B at varying concentrations. Values of $P \leq 0.05$ were considered to show significant effects. Some groups compared were of unequal numbers because of technical failure or an artefact of cycle stage determination, after the experiment, during functional investigations. Immunocytochemistry data was derived from 10-15 cells from only 3 animals, therefore statistical analysis could not be performed. The data and statistical analysis comply with the recommendations of the *British Journal of Pharmacology* on experimental design and analysis in pharmacology (Curtis et al., 2018).

2.11 | Materials

The reagents used in the present study were S-1 and ML213, as specific activators of $K_V7.2$–5 channels (Baldwin et al., 2020; Jepps et al., 2014); the pan-K_V7 channel blocker, linopirdine (10 μmol·L^{-1}; Schnee & Brown, 1998); HMR-1556, the specific blocker of $K_V7.1$ channels (Thomas et al., 2003); the activator of large conductance calcium-activated calcium channels (BK_{Ca}), NS11021 (0.1–10 μmol·L^{-1}); the activator of ATP-sensitive potassium channel (K_{ATP}), pinacidil (0.1–10 μmol·L^{-1}); the inhibitor of VGCC channels, nicardipine (0.001–1 μmol·L^{-1}); U46619 (0.003–3 μmol·L^{-1}); β-adrenoceptor agonist isoprenaline (0.003–3 μmol·L^{-1}); E2 (0.01 μmol·L^{-1}); the specific GPER1 agonist G-1 (Dennis et al., 2009); and the specific GPER1 antagonist G-36 (Dennis et al., 2011). All drugs for isometric tension recordings were obtained from Tocris Bioscience (Oxford, UK) except for S-1 which was obtained from NeuroSearch (Ballerup, Denmark) and E2, which was purchased from Sigma-Aldrich. Drugs were

14765381, 2023, 2, Downloaded from https://bpspubs.onlinelibrary.wiley.com/doi/10.1111/bph.15947 by Test, Wiley Online Library on [10/01/2025]. See the Terms and Conditions (https://onlinelibrary.wiley.com/terms-and-conditions) on Wiley Online Library for rules of use; OA articles are governed by the applicable Creative Commons License

dissolved in DMSO or ethanol (E2), and diluted in PSS during isometric tension recording, isolation PSS during prior to cell fixing for immunocytoschemistry or external solution during single cell electrophysiology, final vehicle concentrations were ≤0.1%.

2.12 | Nomenclature of targets and ligands

Key protein targets and ligands in this article are hyperlinked to corresponding entries in http://www.guidetopharmacology.org and are permanently archived in the Concise Guide to PHARMACOLOGY 2021/22 (Alexander, Christopoulos et al.; 2021; Alexander, Cidlowski et al., 2021; Alexander, Fabbro et al., 2021; Alexander, Mathie et al., 2021).

3 | RESULTS

3.1 | Oestrous cycle-dependent changes in sensitivity to K^+ channel modulators

The $K_V7.2–5$ channel activator S-1 (0.1–10 μmol·L^{-1}) evoked concentration-dependent relaxation of pre-constricted arterial tone (300 nmol·L^{-1} U46619) in arteries from both F-D/M and F-P/E (see representative traces in Figure 1a,b). S-1 was approximately 10-fold more potent in renal arteries from F-D/M (EC_{50} = 0.45 ± 0.07 μmol·L^{-1}) rats when compared with arteries from F-P/E rats (EC_{50} = 4 ± 0.3 μmol·L^{-1}; Figure 1c). The same oestrous cycle-dependent differences were observed with mesenteric, coronary and cerebral arteries (Figure 1d–f).

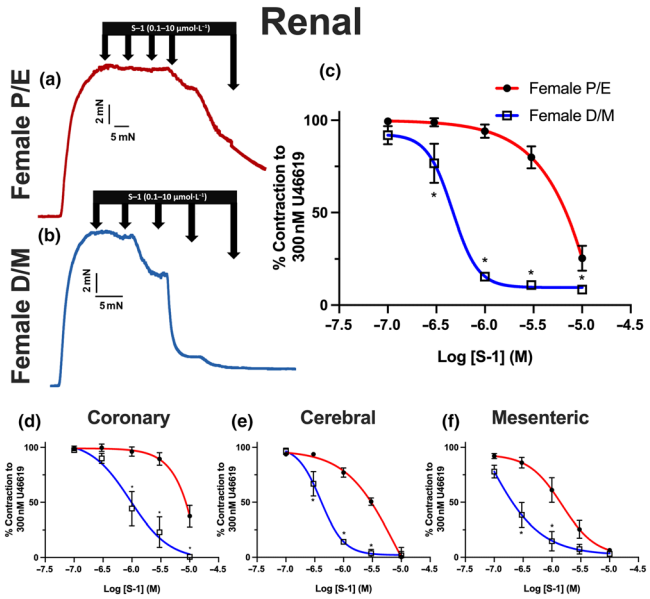


FIGURE 1 Oestrous cycle-dependent differences in S-1-mediated relaxation of pre-contracted tone within arteries from female (P/E2) and female (D/M) Wistar rats. Representative traces of relaxation of pre-contracted arterial tone (U46619; 300 nmol·L^{-1}) in renal arteries from female pro-oestrus/oestrus (P/E; a) and female di-oestrus/met-oestrus (D/M; b) in response to $K_V7.2–5$ activator S-1 (0.1–10 μmol·L^{-1}). Mean data of S-1-mediated relaxation in renal (n = 5–8; c), coronary (n = 4–8; d), cerebral (n = 5–7; e) and mesenteric (n = 5–6; f) arteries. Data shown are means ± SEM; n = number of animals (c–f). *$P \leq 0.05$, significantly different from female P/E; two-way ANOVA with post hoc Bonferroni test.

The structurally dissimilar $K_V7.2–7.5$ activator ML213 (0.1–10 μmol·L^{-1}) was also significantly more potent within arteries from F-D/M rats when compared with arteries from F-P/E rats (Figure 2a, b). Inhibitors of K_V7 channels depolarise VSMC membrane potential and produce contraction (Mackie et al., 2008). The pan-K_V7 blocker linopirdine (10 μmol·L^{-1}) contracted arteries from F-D/M rats more effectively than arteries from F-P/E rats (Figure 2c–e). In all groups, no contraction was produced by application of HMR-1556 (10 μmol·L^{-1}), a specific blocker of $K_V7.1$ channels (Figure 2c,d), consistent with previous reports (Chadha et al., 2012). These data revealed an oestrous cycle-dependent contribution of $K_V7.2–7.5$ channels to arterial reactivity.

In contrast, pinacidil- and nicardipine-dependent relaxations of pre-contracted renal arteries were independent of oestrous cycle stage (Figure 3b,c), whereas NS11021 was ineffective in any stage (Figure 3a). In mesenteric arteries, NS11021 and nicardipine relaxed pre-contracted tone, independent of oestrous cycle stage (Figure 3d,f). Pinacidil was more potent in mesenteric arteries from F-D/M rats compared with F-P/E (Figure 3e; $P \leq 0.05$). No significant differences were observed in the stable pre-contracted tone in response to 300 nmol·L^{-1} U46619 (ΔmN; Figure S3) in either mesenteric or renal arteries taken from F-P/E or F-D/M Wistar rats.

3.2 | Diminished K_V7 channel contribution to receptor-mediated responses underlies oestrous cycle-dependent changes in vascular reactivity

K_V7 channel blockers, such as linopirdine, enhance receptor-mediated contractions (Brueggemann et al., 2006) and diminish cAMP-PKA-dependent β-adrenoreceptor-mediated vaso-relaxation (Chadha et al., 2012). Within this study, contraction mediated by U46619 (0.003–3 μmol·L^{-1}) was less potent in renal arteries from F-D/M compared with F-P/E rats (Figure 4a,b). Linopirdine significantly augmented the sensitivity of U46619-mediated vasoconstriction within vessels from F-D/M, but not F-P/E rats (Figure 4a,b). In arteries from F-D/M rats pre-incubated in linopirdine, the response to U46619 was equipotent to arteries from F-P/E rats pre-incubated in both DMSO solvent control and linopirdine (Figure 4b). In contrast, pre-incubation with linopirdine had no effect in arteries from F-P/E rats, and HMR-1556 had no effect within any group (Figure 4a,b).

Isoprenaline was significantly less potent in renal arteries from F-P/E when compared with vessels from F-D/M rats (Figure 4c, d). As previously reported (Chadha et al., 2012), linopirdine

14765381, 2023, 2, Downloaded from https://bpspubs.onlinelibrary.wiley.com/doi/10.1111/bph.15947 by Test, Wiley Online Library on [10/01/2025]. See the Terms and Conditions (https://onlinelibrary.wiley.com/terms-and-conditions) on Wiley Online Library for rules of use; OA articles are governed by the applicable Creative Commons License

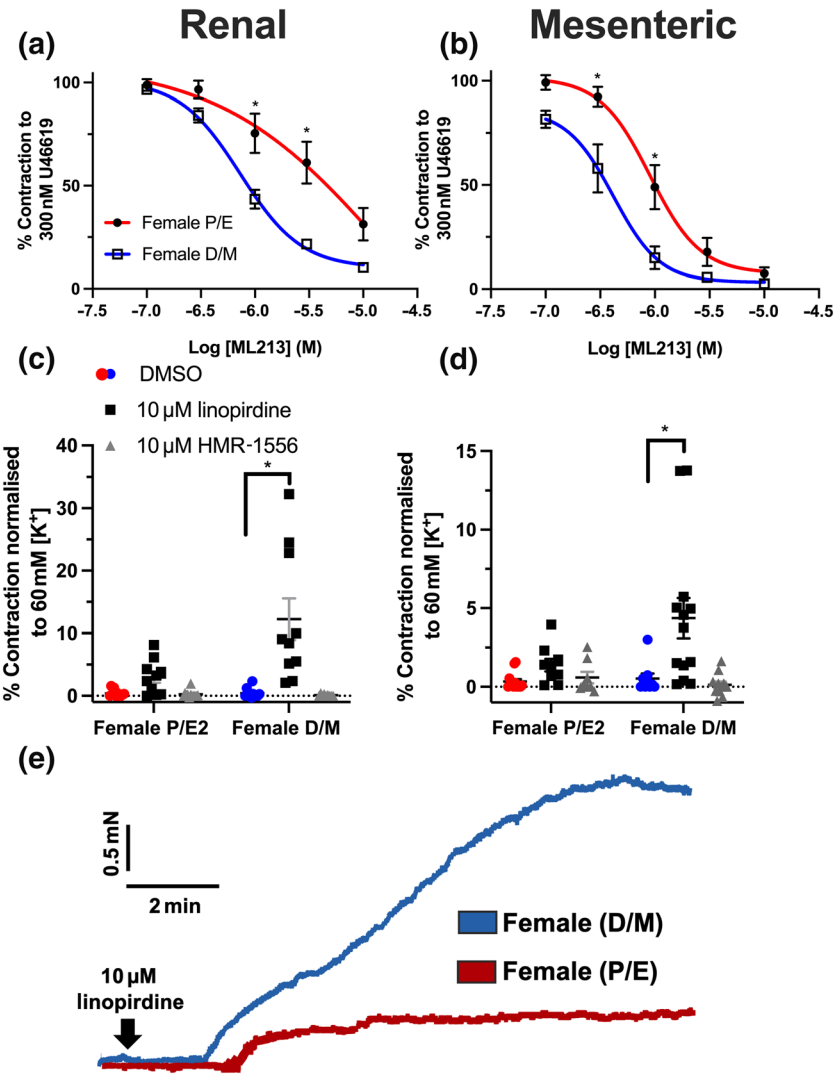


FIGURE 2 K_V7 channel modulators are more efficacious and potent on arteries from female D/M, when compared with female P/E Wistar rats. Mean data of relaxation of pre-contracted tone (U46619; 300 nmol·L^{-1}) in response to ML213 (0.01–10 µmol·L^{-1}) in renal (n = 5–6; a) and mesenteric (n = 5–6; b) arteries from female pro-oestrus/oestrus (P/E) and female di-oestrus/met-oestrus (D/M) rats. Mean data of increases in basal tone in response to solvent control (DMSO), linopirdine (10 µmol·L^{-1}) and HMR-1556 (10 µmol·L^{-1}) in renal (n = 10–12; c) and mesenteric arteries (n = 10–13; d). Representative traces of contraction of renal arteries from female P/E and female D/M rats in response to pan-K_V7 channel blocker linopirdine (10 µmol·L^{-1}; e). Data shown are means ± SEM; n = number of animals used. *$P \leq 0.05$, significantly different from female D/M rats; two-way ANOVA with post hoc Bonferroni (a, b) or Dunnett (c, d) correction.

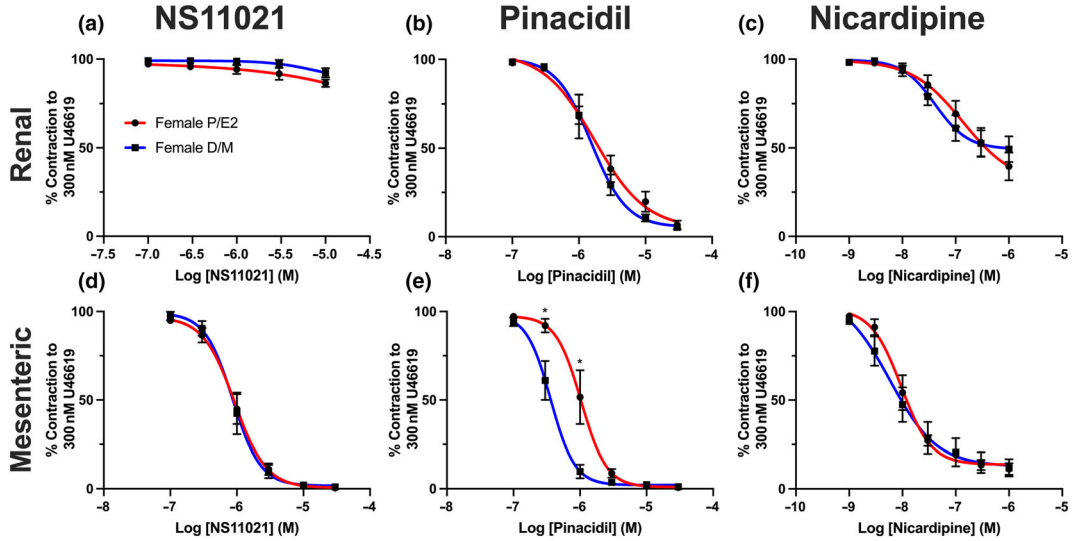


FIGURE 3 Effect of different ion channel modulators in renal arteries from female (P/E) and female (D/M) Wistar rats. NS11021 (0.1–30 µmol·L^{-1}; a, d), pinacidil (0.1–30 µmol·L^{-1}; b, e) and nicardipine (0.001–1 µmol·L^{-1}; c, f) mediated relaxation of pre-constricted arterial tone (300 nmol·L^{-1} U46619) in renal (a–c) and mesenteric (d–f) arteries from female pro-oestrus/oestrus (P/E; red; n = 5) and female di-oestrus/met-oestrus (D/M; blue; n = 5–7) Wistar rats. Data shown are means ± SEM; n = number of animals used. * $P \leq 0.05$, significantly different from D/M; two-way ANOVA with post hoc Bonferroni test.

14765381, 2023, 2, Downloaded from https://bpspubs.onlinelibrary.wiley.com/doi/10.1111/bph.15947 by Test, Wiley Online Library on [10/01/2025]. See the Terms and Conditions (https://onlinelibrary.wiley.com/terms-and-conditions) on Wiley Online Library for rules of use; OA articles are governed by the applicable Creative Commons License

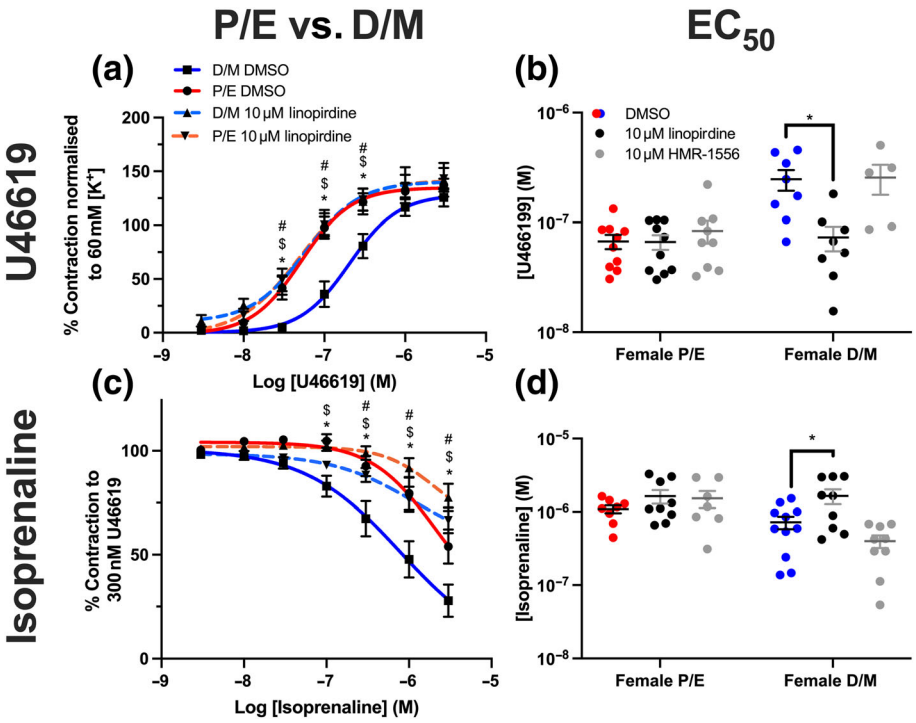


FIGURE 4 Linopirdine alters receptor-mediated responses in renal arteries from female D/M, but not female P/E Wistar rats. Mean data of contraction in response to U46619 (0.003–3 μmol·L^{-1}; n = 7–10; a) and relaxation of pre-contracted arterial tone (300 nmol·L^{-1} U46619) in response to isoprenaline (0.003–3 μmol·L^{-1}; n = 9–10; c) in renal arteries from F-D/M and F-P/E rats, pre-incubated in DMSO solvent control or linopirdine (10 μmol·L^{-1}). Scatter graph representing the raw EC_{50} values of U46619-mediated contraction (b) or isoprenaline-mediated relaxation (d) in renal arteries of the mean data to the left, in addition to vessels pre-incubated in K_V7.1-specific blocker HMR-1556 (10 μmol·L^{-1}). Data shown are means ± SEM; n = number of animals used. In (a, c), * $P \leq 0.05$, D/M DMSO significantly different from P/E DMSO; # $P \leq 0.05$, D/M DMSO significantly different from D/M 10 μmol·L^{-1} linopirdine; $ $P \leq 0.05$, D/M DMSO significantly different from P/E 10 μmol·L^{-1} linopirdine; in (b, d), * $P \leq 0.05$, significantly different as indicated; two-way ANOVA with a post hoc Bonferroni (a, c) or Dunnett (b, d) correction.

significantly attenuated isoprenaline-mediated vasorelaxation in arteries from F-D/M rats (Figure 4c, d). By contrast, the effect of linopirdine on isoprenaline-mediated vasorelaxation in arteries from F-P/E rats was smaller (Figure 4c, d). The response to isoprenaline in arteries from F-D/M rats pre-incubated in linopirdine was equipotent to arteries from F-P/E rats pre-incubated in either DMSO solvent control or linopirdine (Figure 4d). Moreover, in all vessels, pre-incubation with HMR-1556 had no effect (Figure 4d). See Figure S4 for U46619-mediated contraction and Figure S5 for isoprenaline-mediated relaxation within mesenteric, cerebral and coronary arteries from F-P/E and F-D/M rats. Within these arteries, where linopirdine sensitivity was observed, significant differences in control conditions between F-D/M and F-P/E rats were also observed.

The aggregated findings indicate that the K_V7.2–5 channel contribution to isoprenaline- and U46619-mediated vascular response was diminished within arteries from F-P/E rats. This finding potentially underlies the observed oestrous cycle-dependent increased sensitivity to TXA2 receptor-mediated contraction and decreased sensitivity to β-adrenoreceptor-mediated relaxation in arteries from F-P/E, when compared with F-D/M rats.

3.3 | Identification of K_V7 channel transcript and protein expression in arteries from female Wistar rats

The molecular characteristics of the candidates for vascular K_V7 function were subsequently determined. RT-qPCR revealed no significant differences in *Kcnq1–5* nor β-auxiliary subunit *Kcne1–5* relative transcript abundance within renal and mesenteric arteries from both groups ($2^{-\Delta Cq}$; Figure S6A–D). Positive control samples (brain and heart) for transcript expression of target genes can also be seen in Figure S5 (Figure S6E–H).

Immunostaining of K_V7.4 was performed in VSMCs isolated from renal and mesenteric arteries, with 8-12 cells imaged per rat. Preliminary data indicated K_V7.4-associated fluorescence to be predominantly in the periphery, overlapping with the membrane marker WGA in VSMCs from F-D/M rats. In contrast, K_V7.4 staining was diffuse throughout the cytosol of VSMCs from F-P/E rats (Figure 5a,b). When comparing biological replicates, membrane:cytosol ratio for K_V7.4 changed from 1.2 ± 0.19 and 1.8 ± 0.2 in renal and mesenteric artery myocytes from F-D/M rats, respectively, to 0.5 ± 0.03 and 0.8 ± 0.02 in the corresponding cells from F-P/E rats (Figure 5c). A reduction in total cell fluorescence (A.U.) was

14765381, 2023, 2, Downloaded from https://bpspubs.onlinelibrary.wiley.com/doi/10.1111/bph.15947 by Test, Wiley Online Library on [10/01/2025]. See the Terms and Conditions (https://onlinelibrary.wiley.com/terms-and-conditions) on Wiley Online Library for rules of use; OA articles are governed by the applicable Creative Commons License

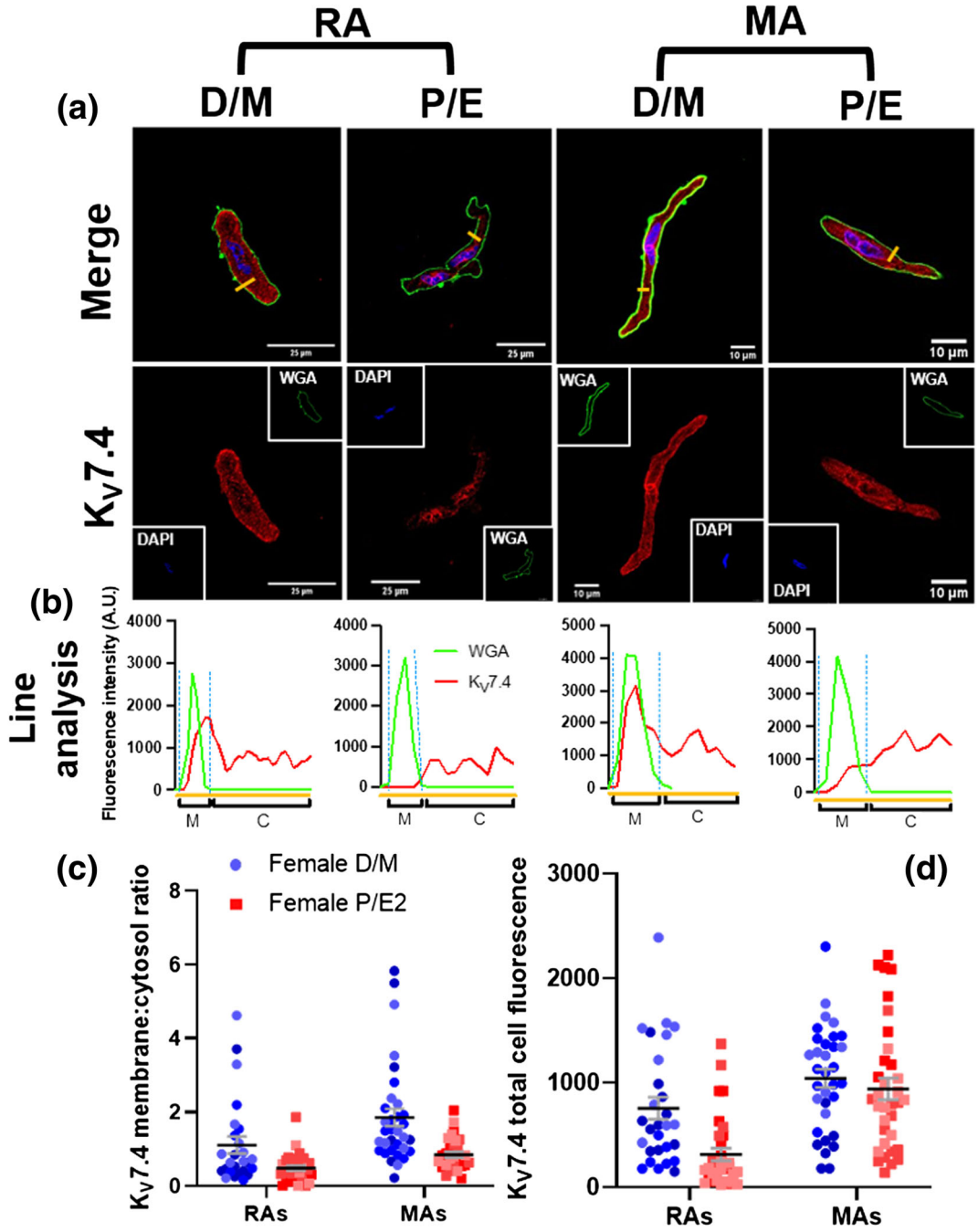


FIGURE 5 Oestrous cycle-dependent reduction in K_V7.4 subcellular distribution in mesenteric and renal artery myocytes. Representativeimages of immunocytochemistry demonstrate K_V7.4 expression (red) within renal (RA)and mesenteric (MA; a) artery vascularsmooth muscle cells from female di-oestrus/met-oestrus (D/M) and female pro-oestrus/oestrus (P/E) Wistar rats. Plasma membraneand nuclear markers, wheat germ agglutinin (WGA; green) and 4′,6-diamidino-2-phenylindole (DAPI; blue), respectively, are alsoshown. Fluorescence intensity profiles were plotted for K_V7.4 and WGA measured in arbitrary units (A.U.) along the yellow line seenin the merged image above (b). Fluorescence intensity ≥ 200 A.U. was considered as the plasma membrane (M), and below the threshold was considered as the cytosol (C; b). The membrane:cytosol ratio for K_V7.4 expression was calculated by measuring thefluorescence intensity of K_V7.4 within the membrane and dividing it by the fluorescence intensity of K_V7.4 within cytosol from threerandomly drawn lines. Data shown are scatterplots for membrane:cytoplasm ratio (c)and total fluorescence (d)from 8-12 individualcells isolated from 3rats. Different colours represent different animals. The mean ± SEM are included in theplot.

observed between renal, but not mesenteric VSMCs between the groups (Figure 5d). Similar experiments failed to reveal comparable oestrous cycle-dependent differences in staining for the other K_V7 subtypes associated with vascular function, K_V7.1 and K_V7.5, or the β-auxiliary subunit protein Kcne4 (Figure S7). Therefore, further experiments focused on K_V7.4 alone. As the number of animals

14765381, 2023, 2, Downloaded from https://bpspubs.onlinelibrary.wiley.com/doi/10.1111/bph.15947 by Test, Wiley Online Library on [10/01/2025]. See the Terms and Conditions (https://onlinelibrary.wiley.com/terms-and-conditions) on Wiley Online Library for rules of use; OA articles are governed by the applicable Creative Commons License

TABLE 2 Plasma hormone concentrations

Hormone	F-P/E plasma concentration ($ng \cdot ml^{-1}$)	SEM (±)	n	F-D/M plasma concentration ($ng \cdot ml^{-1}$)	SEM	n	Student's *t* test
Oestradiol	0.36	0.005	8	0.019	0.005	8	*
Testosterone	0.04	0.018	8	0.023	0.005	8	ns
Androstenedione	0.101	0.42	8	0.063	0.015	8	ns
Progesterone	2.977	0.28	6	5.802	1.217	6	*
Aldosterone	0.018	0.006	8	0.017	0.004	8	ns
Follicular stimulating hormone	0.972	0.174	14	0.958	0.274	14	ns
Luteinising hormone	3.499	0.655	14	3.373	0.368	14	ns

Note: Hormonal plasma concentration was determined using liquid chromatography–tandem mass spectrometry (steroids) and enzyme-linked immunoblot assay (ELISA) (luteinising hormone and follicular stimulating hormone) and expressed as $ng \cdot ml^{-1}$ in female rats during either pro-oestrus/oestrus (F-P/E) or di-oestrus/met-oestrus (F-D/M). Data shown are means, with SEM and number of animals used (n).
*$P \leq 0.05$, significant difference between F-P/E and F-D/M groups; ns, no significant difference; Student's *t* test.

sampled was only 3, we did not apply statistical analysis to these exploratory findings.

3.4 | Cyclical increases in plasma oestradiol mediate a reduction in $K_V7.4$ membrane abundance via GPER1, impairing ML213-mediated relaxation

To identify potential candidates that drive the observed oestrous cycle-dependent fluctuation in $K_V7.4$ membrane abundance and function, sex steroids were extracted from plasma from animals,obtained immediately after killing. Concentrations of circulating steroidal and gonadal hormones were determined via ELISA and LC–MS/MS (Table 2). Plasma E2 was significantly higher in samples from F-P/E rats, compared with that found in F-D/M, whereas levels of progesterone was conversely different (Table 2). No differences between F-D/M and F-P/E values were observed with regard to the other hormones assayed (Table 2).

The onset of a pro-contractile phenotype in arteries from F-P/E occurs within a narrow time frame in the absence of a change in the relative abundance of *Kcnq*/*Kcne* transcripts. In addition, E2-mediated internalisation of $K_V7.1$ channels occurred via a fast-acting, 'non-genomic' signalling cascade (Alzamora et al., 2011; Rapetti-Mauss et al., 2013). We proposed that a rise in plasma E2 during pro-oestrus mediates a reduction in $K_V7.4$ membrane abundance in a 'non-genomic' process, similar to previous reports (Rapetti-Mauss et al., 2013), which does not recover until met-oestrus. The three principal E2 receptors comprise **ERα** and **ERβ**, canonically considered nuclear receptors, and a novel membrane bound receptor, GPER1, that are encoded for by *Ers1*, *Ers2* and *Gper1*, respectively. We ascertained the expression of these receptors in rat arteries using whole uterine lysates as a positive control. Rat mesenteric and renal artery lysates from both groups had an expression profile of *Esr1* > *Gper1* > *Esr2*, whereas the expression profile in uterus was *Esr1* > *Esr2* > *Gper1* (Figure S8A–C).

We then determined whether short-term treatment with exogenous E2 could mimic the oestrous cycle-dependent changes in K_V7 responses. Renal and mesenteric arteries from female Wistar rats were incubated with E2 for a period of 5 or 30 min. In mesenteric and renal arteries from F-D/M rats, 5 min and 30 min of E2 pre-incubation significantly impaired ML213-mediated relaxation (Figure S9A,C). Comparable treatment with exogenous E2 had no effect in arteries from F-P/E animals (Figure S9B,D). Additional experiments were undertaken to determine the long-term and potential genomic effects of incubation with exogenous E2 on ML213-mediated relaxation of pre-contracted mesenteric arteries. 4 h incubation with E2, and vessels that were incubated with E2 for 10 min, then washed and left for 4 h prior to application of ML213 were compared against vessels pre-incubated in solvent control (Figure S9E,F). In both conditions, E2 attenuated ML213-mediated relaxation only in arteries taken from F-D/M rats (Figure S9E,F).

Pre-incubating renal and mesenteric arteries from F-D/M rats with the specific GPER1 agonist G-1 ($1\ \mu mol \cdot L^{-1}$) attenuated ML213-mediated relaxations in a fashion analogous to pre-incubation with E2 (Figure 6a,c). Again, G-1 pre-incubation had no effect on renal (Figure 6b) or mesenteric (Figure 6d) arteries from F-P/E rats. The response to ML213 in mesenteric arteries from F-D/M pre-incubated in E2 ($EC_{50} = 1 \pm 0.17\ \mu mol \cdot L^{-1}$) or G-1 ($EC_{50} = 0.9 \pm 0.17\ \mu mol \cdot L^{-1}$) mirrored the profile for ML213 seen in mesenteric arteries from F-P/E Wistars pre-incubated in solvent controls ($EC_{50} = 0.84 \pm 0.1\ \mu mol \cdot L^{-1}$; Figure 6c,d). Moreover, pre-incubating mesenteric arteries with the selective GPER1 antagonist G-36 ($1\ \mu mol \cdot L^{-1}$; Dennis et al., 2011) prior to application of E2 prevented its inhibitory effects on ML213-mediated relaxation (Figure 6e). In contrast, G-36 had no effect on ML213-mediated relaxation in arteries from F-P/E rats (Figure 6f).

In a subsequent set of exploratory experiments, isolated mesenteric artery VSMCs from F-DM rats were incubated with either E2 ($10\ nmol \cdot L^{-1}$) for 10 min (Figure 7a) or 30 min (Figure 7b). The data suggests an E2-mediated reduction in the overlap of $K_V7.4$ staining

14765381, 2023, 2, Downloaded from https://bpspubs.onlinelibrary.wiley.com/doi/10.1111/bph.15947 by Test, Wiley Online Library on [10/01/2025]. See the Terms and Conditions (https://onlinelibrary.wiley.com/terms-and-conditions) on Wiley Online Library for rules of use; OA articles are governed by the applicable Creative Commons License

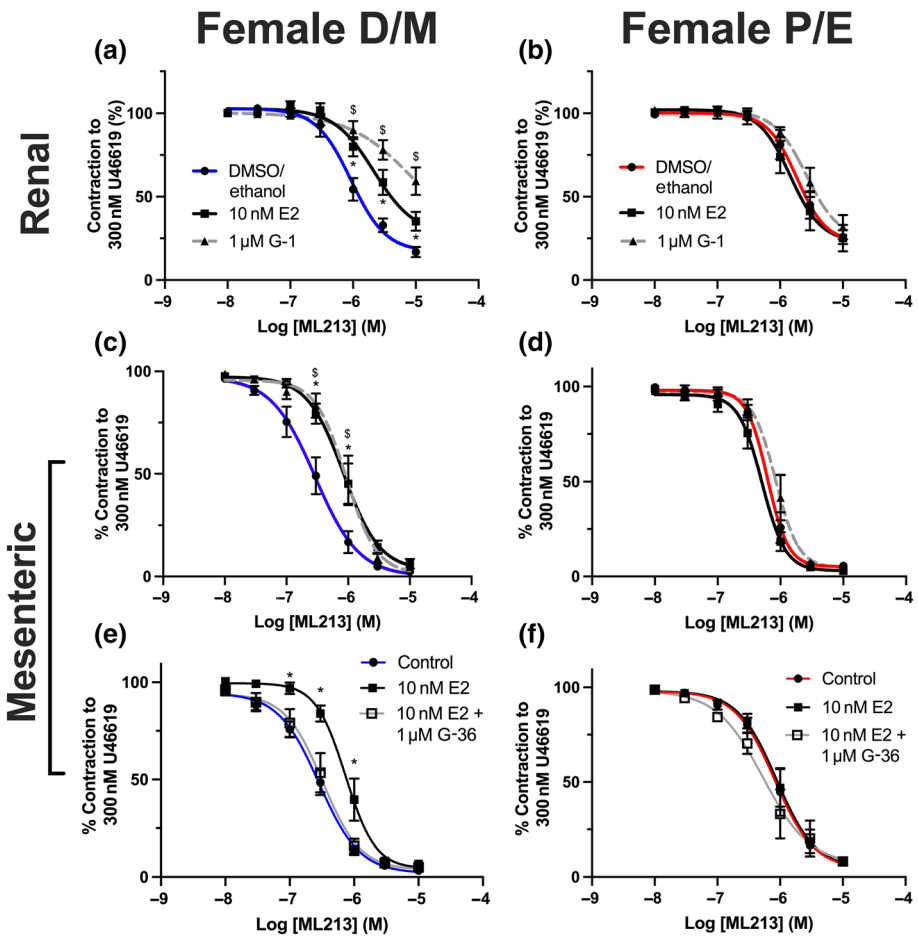


FIGURE 6 Oestradiol attenuation of the effects of ML213 is GPER1-mediated. Mean data for ML213-mediated relaxation of pre-constricted arterial tone (U46619; 300 nmol·L^{-1}) in renal (a, b) and mesenteric (c–f) arteries from female Wistar rats in di-oestrus/met-oestrus (F-D/M; a–c; n = 5–12) or pro-oestrus/oestrus (F-P/E; d–f; n = 6–11) pre-incubated in the DMSO/ethanol solvent control (F-D/M; F-P/E), oestradiol (E2; 10 nmol·L^{-1}) or GPER1 agonist G-1 (1 μmol·L^{-1}, a–d) or GPER1 antagonist G-36 (1 μmol·L^{-1}) in combination with E2 (10 nmol·L^{-1}; e, f). Data shown are means ± SEM; n = number of animals used. */$ $P \leq 0.05$, significantly different from solvent control; two-way ANOVA with post hoc Dunnett's test.

with WGA when compared with the corresponding solvent controls (Figure 7a,b), and a reduction in the membrane:cytosol ratio for K_V7.4 staining (Figure 7b,d), that was analogous to the reduction observed when comparing myocytes from F-D/M and F-P/E (Figure 5). Preliminary data also indicated that pre-incubating isolated VSMCs with the specific GPER1 antagonist G-36 for 10 min prior to the application for E2 prevented a reduction in K_V7.4 membrane abundance (Figure 7c), whereas the GPER1 agonist G-1 replicated E2-mediated K_V7.4 translocation (Figure 7d). Further, that neither E2 nor G-1 had any effect on the predominantly cytosolic staining for K_V7.4 in VSMCs from mesenteric arteries from F-P/E Wistar rats (Figure S10A–C). In summary, raised plasma E2 during the P/E stages of the oestrous cycle correlated with, 1.) a potentially diminished K_V7.4 membrane abundance, and 2.) impaired K_V7.4 function. Both of these effects were reproduced in arteries from F-D/M rats by activation of GPER1.

E2 and G-1 incubation also impaired ML213-mediated relaxations in mesenteric arteries from male rats, whereas relaxations to the BK_{Ca} activator NS11021 were unaffected by E2 pre-incubation (Figure S11).

Compared with E2, little is known of the effect of progesterone on K_V7 channel function. However, as progesterone was significantly raised in the plasma from F-D/M rats, we assayed the effects of pre-incubating mesenteric arteries from F-P/E and F-D/M rats in progesterone (10 nmol·L^{-1}) for 5 and 30 min on ML213-mediated responses (Figure S12). No change in ML213-mediated relaxation was observed in any vessels from either group (Figure S12). Consequently, progesterone was not considered in the following investigations but was helpful in confirming cycle stage.

3.5 | Oestrogenic inhibition of K_V7 activator-mediated relaxation is not endothelium-dependent

A series of experiments were performed to ascertain if the modulatory effects of GPER1 activation were dependent on the presence of functional endothelium. Similar to our previous findings, removing the endothelium significantly attenuated ML213-mediated relaxation in mesenteric arteries from both F-D/M and F-P/E rats (Figure 8a,c). Pre-incubating EC-denuded vessels from F-D/M rats with E2 (10 nmol·L^{-1}) additively attenuated ML213-elicited relaxation (Figure 8a), whereas E2 pre-incubation had no effect in EC-denuded arteries from F-P/E rats (Figure 8c; n = 5–6). The relative fold change in expression of oestrogen receptor and VSMC and EC marker transcripts was compared between EC(+) and EC(−) vessels, using whole lysates ($2^{-\Delta\Delta Cq}$). When comparing relative transcript abundance

14765381, 2023, 2, Downloaded from https://bpspubs.onlinelibrary.wiley.com/doi/10.1111/bph.15947 by Test, Wiley Online Library on [10/01/2025]. See the Terms and Conditions (https://onlinelibrary.wiley.com/terms-and-conditions) on Wiley Online Library for rules of use; OA articles are governed by the applicable Creative Commons License

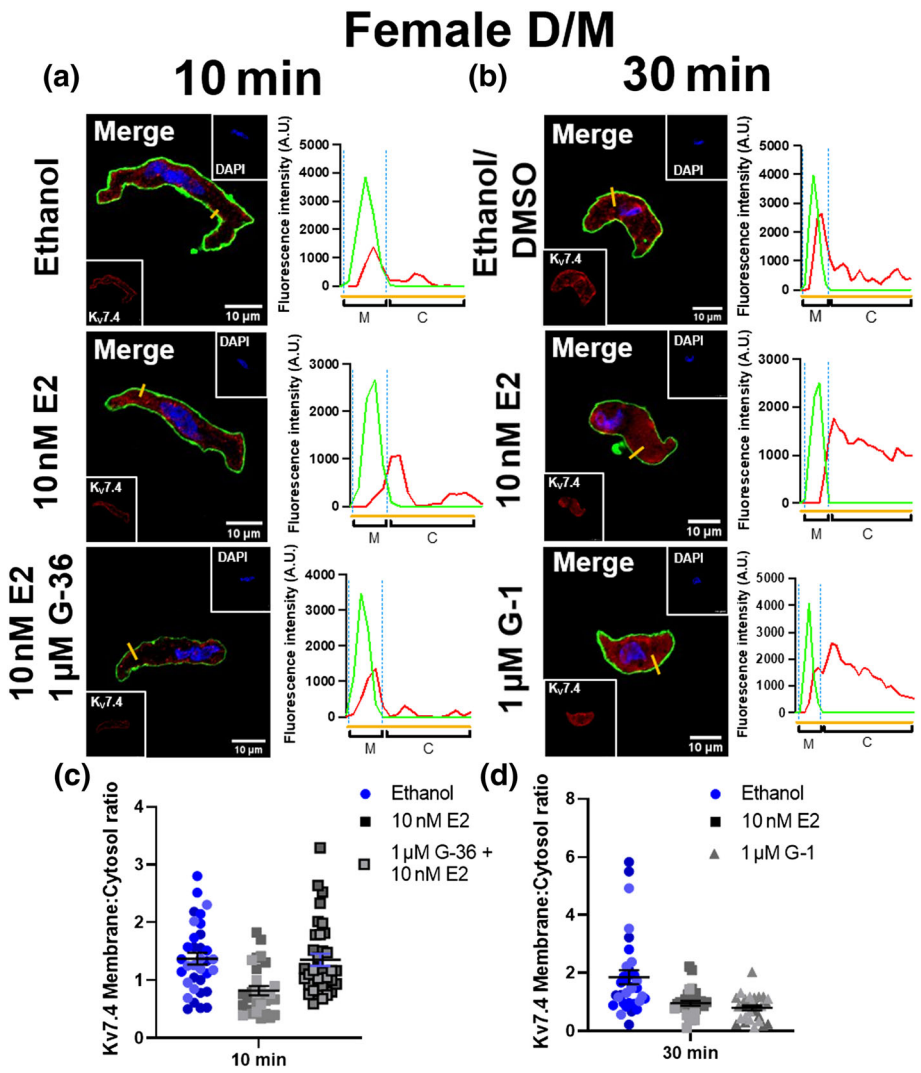


FIGURE 7 Oestradiol E2 incubation diminishes $K_V7.4$ membrane abundance in isolated mesenteric artery vascular smooth muscle cells from female D/M Wistar rats. Representative images of immunocytochemistry demonstrate $K_V7.4$ expression (red) in mesenteric artery vascular smooth muscle cells from females in di-oestrus/met-oestrus (D/M), pre-incubated in either solvent control (ethanol/ DMSO), oestradiol (E2; 10 nmol·L^{-1}) or E2 + GPER1 antagonist G-36 (1 µmol·L^{-1}) for 10 min (a) or ethanol/DMSO, E2 (10 nmol·L^{-1}) or GPER1 agonist G-1 (1 µmol·L^{-1}) for 30 min (b). Plasma membrane and nuclear markers wheat germ agglutinin (WGA; green) and 4′,6-diamidino-2-phenylindole (DAPI; blue) are also shown. Fluorescence intensity profiles were plotted for $K_V7.4$ and WGA measured in arbitrary units (A.U.) along the yellow line seen in the merged image above. Fluorescence intensity ≥ 200 A.U. was considered the plasma membrane (M), and below the threshold was considered the cytosol (C). The membrane:cytosol ratio for $K_V7.4$ expression was calculated by measuring the fluorescence intensity of $K_V7.4$ within the membrane and dividing it by the fluorescence intensity of $K_V7.4$ within cytosol from three randomly drawn lines in individual cells. Data shown are scatterplots for membrane:cytoplasm ratio (c,d) from 10-12 individual cells isolated from 3 rats. Different colours represent different animals. The mean ± SEM are included in the plot.

between EC(−) and EC(+) arteries, a significant reduction in *Cd31* (platelet or endothelial cell marker 1) transcript was observed in conjunction with a significant increase in that of *Acta2* (α-smooth muscle actin; Figure 8e). A small increase in *Ers1* and *Ers2* transcripts and a minor decrease in *Gper1* transcripts were observed in EC(−) lysates when compared with EC(+) lysates (Figure 8e), although this failed to reach significance. In summary, although GPER1 expression was moderately higher within the endothelium, the effect of GPER1 signalling on vascular $K_V7.4$ appears to originate from within the smooth muscle.

3.6 | GPER1 activation reduced $K_V7.4$ currents

Ruptured whole-cell recording from HEK cells expressing $K_V7.4$, was used as a secondary means of determining the effect of GPER1 activation on $K_V7.4$ channel activity. Incubation of HEK-$K_V7.4$ cells with the GPER1 agonist G-1 (1 µmol·L^{-1}) or E2 (10 nmol·L^{-1}) for 30 min produced a considerable reduction in $K_V7.4$ currents only in cells expressing GPER1 receptor (Figure 9). GPER1 stimulation by either G-1 or E2 did not affect voltage of half activation ($V_{1/2}$) of $K_V7.4$ currents (Figure 9d). Currents recorded under solvent control conditions were identical in untransfected and GPER1-expressing HEK cells (Figure 9).

3.7 | E2 reduces $K_V7.4$ interaction with forward trafficking molecular chaperone protein HSP90 in F-D/M, but not F-P/E VSMCs

The molecular chaperone protein HSP90 is critical in the folding and biogenesis of potassium channels including K_{ATP} (Yan et al., 2010), $K_V11.1$ (Ficker, 2003) and $K_V7.4$ (Gao et al., 2013). Additionally, GPER1 activation increases human myometrial contractility by phosphorylation of HSP27 (Maiti et al., 2011), and infusion of angiotensin II decreased the interaction of $K_V7.4$ and HSP90, diminishing $K_V7.4$ membrane abundance (Barrese, Stott, Figueiredo, et al., 2018). Therefore, we proposed that the reduction in membrane:cytosol ratio observed in response to E2/G-1 was mediated by a reduction in the

14765381, 2023, 2, Downloaded from https://bpspubs.onlinelibrary.wiley.com/doi/10.1111/bph.15947 by Test, Wiley Online Library on [10/01/2025]. See the Terms and Conditions (https://onlinelibrary.wiley.com/terms-and-conditions) on Wiley Online Library for rules of use; OA articles are governed by the applicable Creative Commons License

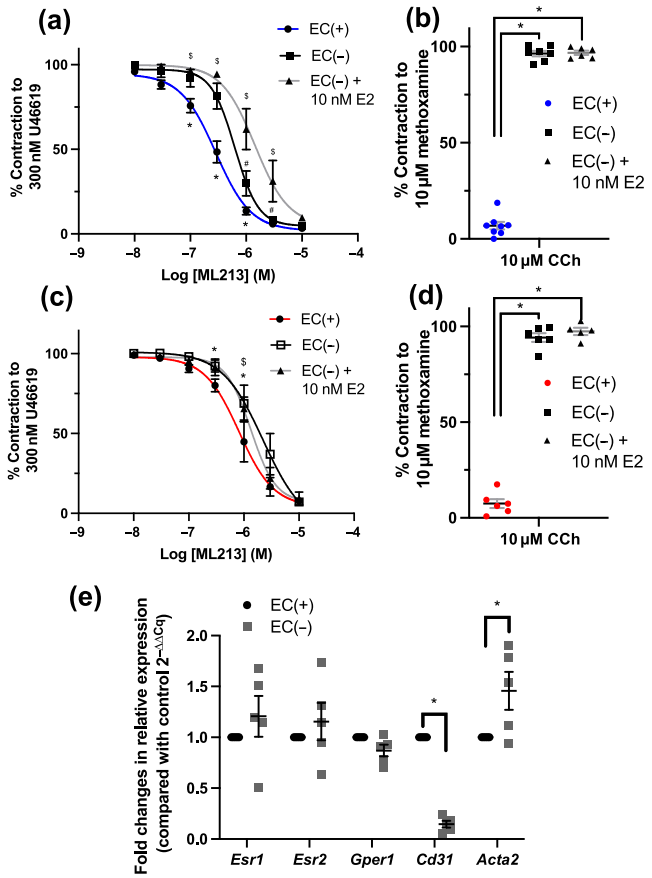


FIGURE 8 Attenuation by oestradiol of ML213-mediated relaxation is not endothelium dependent. Mean data for ML213-mediated relaxation of pre-constricted arterial tone (U46619; 300 nmol·L^{-1}) in arteries from female Wistar rats in di-oestrus/met-oestrus (F-D/M; a, b; n = 6–8) or pro-oestrus/oestrus (F-P/E; c, d; n = 5–6) in the presence and absence of endothelial cells (ECs(+)/(−)) and in the absence of endothelial cells pre-incubated in oestradiol (E2, 10 nmol·L^{-1}; EC(−) + E2). Mean data and scatter plot for carbachol (CCh)-mediated relaxation of pre-contracted arterial tone (10 μmol·L^{-1} methoxamine) generated within the same vessels prior to application of ML213 (b, d). Relative fold expression in oestrogen receptors (*Esr1*, *Esr2* and *Gper1*), EC marker *Cd31* and vascular smooth muscle marker *Acta2* in whole lysates of mesenteric arteries from female Wistar rats in vessels denuded of endothelium (EC(−)) compared with vessels with intact endothelium (EC(+); $2^{-\Delta\Delta Cq}$; n = 5; e). Data shown are means ± SEM; n = number of animals used. * $P \leq 0.05$, significantly different from EC(+); $ $P \leq 0.05$, significant difference between EC(+) and EC(−) + 10 nM E2; # $P \leq 0.05$, significant difference between EC(−) and EC(−) + 10 nM E2: two-way ANOVA with post hoc Bonferroni test.

interaction of K_V7.4 and HSP90, in a process similar to that following infusion of angiotensin II. PLA was used to resolve protein–protein interactions ≤ 40 nm, which are expressed as red puncta within the cell. As the data were derived from less than 5 animals we cannot apply statistical analysis to our findings but the indication is that pre-incubation for 30 min with E2 (10 nmol·L^{-1}) reduced the interaction between K_V7.4 and:HSP90, within mesenteric VSMCs from F-D/M Wistar rats, compared with the solvent control (Figure 10). No change in K_V7.4:HSP90 interactions was observed in similar experiments with VSMCs from F-P/E rats incubated with E2 (Figure 10b). Additionally, the puncta per cell in VSMCs from F-P/E rats was equivalent to that observed in VSMCs from F-D/M pre-incubated in E2.

4 | DISCUSSION

In this study, we demonstrate clear oestrous cycle-dependent changes in vascular reactivity, whereby pro-contractile vessels from F-P/E rats exhibited diminished K_V7.4 channel function and membrane abundance, in conjunction with significantly raised plasma E2. Moreover, a F-P/E pro-contractile phenotype could be replicated in pro-relaxant F-D/M rats by exposure to E2 or the novel GPER1 activator G-1, a change that was prevented by the GPER1-specific inhibitor G-36. In a heterologous overexpression system, both E2 and G-1 diminished human K_V7.4 channel currents only in cells transfected with *GPER1*, independent of a change in the biophysical properties of the current and consistent with a reduction in channel number. Finally, pilot data indicated that exogenous E2 diminished the interaction of K_V7.4 with its forward trafficking molecular chaperone protein HSP90 only in those rats in a 'low plasma E2' stage of the oestrous cycle.

4.1 | Cyclical reduction in K_V7.4 membrane abundance correlates with a pro-contractile phenotype

In spite of the known sexual dimorphisms in cardiovascular physiology and pathophysiology (Pabbidi et al., 2018), little is known about K_V7 channel activity in arteries from females. Of the few studies to consider sex as a factor, K_V7 channels within the female were shown to (1) be differentially regulated by its β-auxiliary subunit protein Kcne4 (Abbott & Jepps, 2016) and (2) to impair **noradrenaline**-induced increases in total peripheral resistance in normotensive and spontaneously hypertensive female rats only (Berg, 2018).

Here, we demonstrate that two K_V7.2–5 channel activators, S-1 and ML213, relaxed pre-contracted arterial tone in a range of arteries and the pan-K_V7 channel inhibitor linopirdine and not the specific inhibitor of K_V7.1 channels, HMR-1556, increased basal tone (Chadha et al., 2012; Mackie et al., 2008; Ng et al., 2011), though significantly more potently and efficaciously in arteries from F-D/M rats. Additionally, K_V7.2–5 channel inhibition enhanced TXA_2-mediated contractions and impaired **β-adrenoceptor**-driven relaxations, though more effectively in arteries from F-D/M rats. Immunocytochemistry revealed a corona-like staining for K_V7.4 in myocytes from F-D/M renal and mesenteric arteries that was absent in myocytes from these arteries from F-P/E rats. However, neither total cell fluorescence nor the relative abundance of the *Kcnq4* transcripts were altered. Thus, our findings indicate a post-transcriptional cycle-based reduction in K_V7.4 membrane abundance, which correlates with diminished contribution of K_V7 channels to both basal tone and receptor-mediated

14765381, 2023, 2, Downloaded from https://bpspubs.onlinelibrary.wiley.com/doi/10.1111/bph.15947 by Test, Wiley Online Library on [10/01/2025]. See the Terms and Conditions (https://onlinelibrary.wiley.com/terms-and-conditions) on Wiley Online Library for rules of use; OA articles are governed by the applicable Creative Commons License

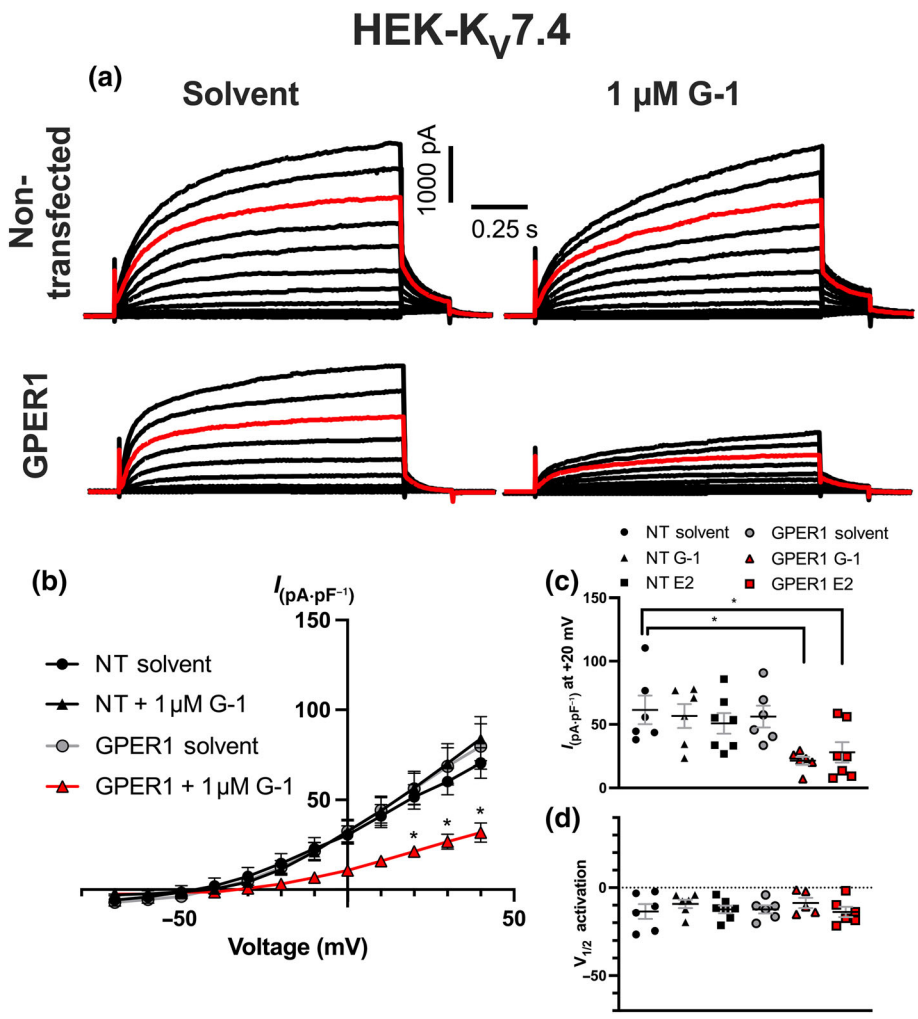


FIGURE 9 Pre-incubation with oestradiol (E2) or G-1 impairs K_V7.4 channel activity in GPER1-transfected cells. Representative current recordings during ruptured whole-cell voltage clamp in non-transfected (NT) HEK-K_V7.4 cells, pre-incubated (30 min) in solvent control (upper left) or G-1 (1 μmol·L^{-1}; upper right) and GPER1-transfected cells pre-incubated in solvent control (lower left) or G-1 (lower right; a). Red line represents current flow in response to +20 mV. Cells were held at a holding potential of −60 mV and then stepped to test voltage for 1.5 s every 15 s ranging from −70 to +40 mV increasing in 10 mV intervals. Before returning to rest potential, voltage was stepped to an inactivation potential of −40 mV. Mean *IV* relationships plotted for HEK-K_V7.4 cells; NT in solvent control (n = 5) or G-1 (n = 6) and GPER1-transfected cells in solvent control (DMSO; n = 6) or G-1 (n = 6; b). Scatter graph demonstrates peak current amplitude at +20 mV in non-transfected cells pre-incubated in solvent control (n = 6), G-1 (n = 6), oestradiol (E2, 10 nmol·L^{-1}, n = 7) and GPER1-transfected cells solvent control (n = 6), G-1 (n = 6) or E2 (n = 7; c). Voltage dependence of activation for K_V7.4 currents (d). Data shown are means ± SEM; n = number of animals used. * $P \leq 0.05$, significantly different as indicated; (b) two-way ANOVA with post hoc Dunnett's correction, (c, d) one-way ANOVA.

responses, contributing to a pro-contractile phenotype. No change in transcript no membrane abundance of the other candidates for vascular K_V7 channel function (K_V7.1, K_V7.5 and KCNE4) was observed, reinforcing the previous suggestioin that K_V7.4 is the critical component of the functional K_V7.4/K_V7.5 heterotetramer (Barrese, Stott, & Greenwood, 2018). However, other ion channels may also be modulated, as the present study showed significant oestrous cycle-dependent differences in relaxations to the K_{ATP} activator pinacidil in mesenteric arteries. Further research will focus on this aspect.

4.2 | E2 may diminish K_V7.4 membrane abundance through reduced interaction with HSP90, via GPER1 signalling

When screening for candidates that drive the oestrous cycle-dependent differences in vascular K_V7 activity, our data revealed an increase in plasma E2 in F-P/E rats. The role for E2 in modulating vascular reactivity is complex. E2 up-regulates the bioavailability of **nitric oxide** and **PGI_2** within ECs and decreases intracellular calcium availability in VSMCs (Mazzuca et al., 2015; Novella et al., 2019). However, there is less consensus in the published reports of ion channel modulation by E2. E2 is known to both increase and decrease the activity of ion channels such as BK_{Ca}, K_{ATP} and K_V (Kow & Pfaff, 2016). With regard to K_V7 channels, E2 rapidly internalises K_V7.1 in crypt cells of the distal colon in female rats, in a fast-acting, non-genomic signalling cascade (O'Mahony et al., 2007; Rapetti-Mauss et al., 2013). E2 also diminished I_{Ks} currents in overexpression models and rabbit cardiac myocytes (Busch et al., 1996; Möller & Netzer, 2006) but increased M-currents (K_V7.2/3) in mouse **NPY** neurons (Roepke et al., 2011). Very little is known of the effect of E2 on vascular K_V7 channels. E2 injection into rats with bilateral ovariectomy significantly increased mean arterial pressure (Takezawa et al., 1994). Here, short incubation with supplemental E2 reduced the extent of ML213-mediated relaxation in arteries from F-D/M rats, in an endothelium-independent process. No additive inhibition of function by E2 was observed in F-P/E rats where plasma E2 was higher, supporting a role for oestrogenic signalling in driving the observed cycle-dependent shifts in vasoreactivity. Our exploratory evidence indicated that K_V7.4 membrane abundance and forward trafficking were

14765381, 2023, 2, Downloaded from https://bpspubs.onlinelibrary.wiley.com/doi/10.1111/bph.15947 by Test, Wiley Online Library on [10/01/2025]. See the Terms and Conditions (https://onlinelibrary.wiley.com/terms-and-conditions) on Wiley Online Library for rules of use; OA articles are governed by the applicable Creative Commons License

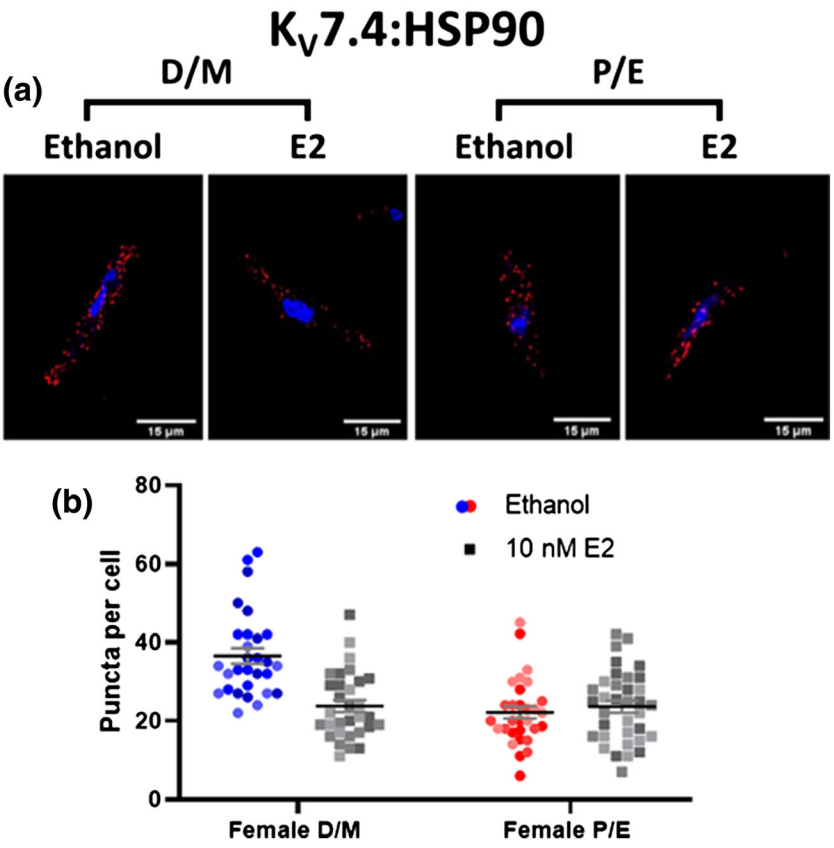


FIGURE 10 Oestradiol reduces K_V7.4–heat shock protein 90 interactions in mesenteric artery myocytes from F-D/M, but not F-P/E rats. Proximity ligation assay (PLA) for K_V7.4 and heat shock protein 90 (HSP90) interaction within female di-oestrus/met-oestrus (D/M) and female pro-oestrus/oestrus (P/E) mesenteric artery myocytes pre-incubated in either solvent control(ethanol) or 10 nmol·L^{-1} oestradiol (E2; 30 min). Representative images of mesenteric artery myocyte mid-cell cross section exhibit fluorescent puncta that illustrate K_V7.4:HSP90 interactions within a distance of <40 nm (red) and the nucleoli via 4′,6-diamidino-2-phenylindole (DAPI; blue; a). Data shown are scatterplots for number of puncta per cell (b) from 10-15 individual cells isolated from 3 rats. Different colours represent different animals. The mean ± SEM are included in the plot.

impaired by exogenous E2, similarly, no effect was observed in F-P/E rats.

As the onset of a pro-contractile phenotype during the oestrous cycle occurs within a narrow time frame, we postulated that the effects of oestrogenic signalling were also non-genomic. The candidates for fast-acting oestrogenic signalling include the membrane-associated GPER1 (Filardo et al., 2000) and ERα following palmitoylation at Cys446 (Simoncini et al., 2000). As mentioned above, E2 rapidly reduced colonic crypt cell conductance via ERα down-regulation of K_V7.1 channels via fast-acting processes that were **PKA–PKCδ** dependent (O'Mahony et al., 2007, 2009). Here, the effects of extraneous E2 on K_V7.4 function and membrane abundance were replicated by a specific agonist of GPER1, G-1 (Bologa et al., 2006) and prevented by the GPER1 antagonist G-36 (Dennis et al., 2011), indicating a role for GPER1 rather than ERα/β. This was supported by single-cell electrophysiology in a heterologous overexpression system, whereby E2/G-1 regulation of K_V7.4 channels was dependent on GPER1 expression. GPER1 activation mediated a reduction in total K_V7.4 current, independent of a change in the conductance of the individual channel, further supporting a role for GPER1. However, as longer-term (4 h) incubation with E2 also inhibited ML213-mediated relaxation in vessels from F-D/M rats, we cannot rule out a contribution from the nuclear oestrogen receptors ERα/β. Further, although aldosterone cannot bind GPER1 (Cheng et al., 2014), aldosterone mediates GPER1-dependent sensitisation to angiotensin II (Batenburg et al., 2012) and phenylephrine-mediated contractions (Ferreira et al., 2015). Current understanding indicates that aldosterone-mediated, GPER1-sensitive, vascular effects may be derived from cross talk between **mineralocorticoid** and oestrogen receptors (Barton & Meyer, 2015). Although we observed no differences in plasma aldosterone levels between F-D/M and F-P/E females, further studies aiming to characterise GPER1 signalling should consider receptor cross talk.

Our data suggest that GPER1 activation alters the forward trafficking of K_V7.4 through altered interaction with the chaperone HSP90. Angiotensin II also alters HSP90:K_V7.4 association, resulting in channel ubiquitination and proteasomal degradation (Barrese, Stott, Figueiredo, et al., 2018). We do not know whether similar signalling occurs during the oestrous cycle and channel protein is created de novo or ultimate degradation is prevented and the existing K_V7.4 can recycle back to the membrane, as shown previously (Rapetti-Mauss et al., 2013). Moreover, we do not know the signals linking GPER1 activation to HSP90 instability. As there is growing appreciation for the importance of ion channel membrane trafficking as the basis for many channelopathies (Curran & Mohler, 2015), the mechanisms linking GPER1 to HSP90 should be the focus of further studies.

4.3 | Perspectives

Diminished K_V7.4 channel function in response to increased plasma E2 has considerable implications for women's health. Mean arterial

14765381, 2023, 2, Downloaded from https://bpspubs.onlinelibrary.wiley.com/doi/10.1111/bph.15947 by Test, Wiley Online Library on [10/01/2025]. See the Terms and Conditions (https://onlinelibrary.wiley.com/terms-and-conditions) on Wiley Online Library for rules of use; OA articles are governed by the applicable Creative Commons License

pressure is reportedly higher in the luteal phase of the menstrual cycle (Danborno et al., 2018), a phase historically associated with progesterone production from the corpus luteum. However, Stricker et al. (2006) demonstrated that E2 levels within mid-luteal phase were greater than in the early follicular phase. Further, hormone replacement therapy (HRT) has become one of the most controversial topics of women's health of the last three decades. Trends in disease outcomes for patients on combined oestrogen/progestin in the Heart and Estrogen/progestin Replacement Study (HERS) I (Hulley et al., 1998) and II (Hulley et al., 2002) were not favourable, as adverse cardiovascular events were increased. However, there is conflict within the literature (Yang & Reckelhoff, 2011), as animal and human studies on HRT, prior to the HERS, had positive outcomes. Although the effect of E2 on the prevalence of cardiovascular disease in humans remains unclear, an extrapolation of the findings detailed here could imply diminished K_V7 channel function in the detrimental attributes of exogenous E2 in rodents and humans, as a reduced K_V7 channel membrane abundance is associated with the hypertensive phenotype. Additionally, aldosterone meditates increased vascular resistance and an increase in blood pressure. Interaction between the mineralocorticoid receptor and GPER1 may diminish K_V7 function, contributing to aldosterone-mediated changes in blood pressure. Although GPER1 is largely viewed as a promising therapeutic target in the treatment of cardiovascular disease, we would argue that its effects are currently incompletely understood, meriting further investigation.

ACKNOWLEDGEMENTS

The authors would like to thank Miss Hericka B. Figueriedo for her contribution to the pilot data that formed the basis for this study and the Image Resource Facility at the St George's University, London. SNB was funded by the British Heart Foundation (Grant #FS/18/41/33762) awarded to IAG. For work conducted in the University of Edinburgh Clinical Research Mass Spectrometry Core Facility (RRID:SCR_021833), we are grateful to Scott Denham, Jo Simpson and Tricia Lee for their technical expertise.

AUTHOR CONTRIBUTIONS

SNB and EAF performed the functional and molecular research. NZMH and RA executed and interpreted the steroid assays. BEI provided essential tools and reagents. SNB and IAG wrote the manuscript. SNB, VB, JBS and IAG designed the research study. All authors contributed to the manuscript and approved the submitted version.

CONFLICT OF INTEREST

The authors declare no conflict of interest.

DECLARATION OF TRANSPARENCY AND SCIENTIFIC RIGOUR

This Declaration acknowledges that this paper adheres to the principles for transparent reporting and scientific rigour of preclinical research as stated in the *BJP* guidelines for Design and Analysis, Immunoblotting and Immunochemistry, and Animal Experimentation, and as recommended by funding agencies, publishers and other organisations engaged with supporting research.

DATA AVAILABILITY STATEMENT

The data generated herein are available upon reasonable request to the corresponding author.

ORCID

Samuel N. Baldwin https://orcid.org/0000-0002-3796-6090
Ruth Andrew https://orcid.org/0000-0002-6916-2994
Brant E. Isakson https://orcid.org/0000-0002-7692-6294
Iain A. Greenwood https://orcid.org/0000-0002-0603-0492

REFERENCES

Abbott, G. W., & Jepps, T. A. (2016). Kcne4 deletion sex-dependently alters vascular reactivity. *Journal of Vascular Research*, *53*, 138–148. https://doi.org/10.1159/000449060

Alexander, S. P., Christopoulos, A., Davenport, A. P., Kelly, E., Mathie, A., Peters, J. A., Veale, E. L., Armstrong, J. F., Faccenda, E., Harding, S. D., Pawson, A. J., Southan, C., Davies, J. A., Abbracchio, M. P., Alexander, W., Al-hosaini, K., Bäck, M., Barnes, N. M., Bathgate, R., … Ye, R. D. (2021). THE CONCISE GUIDE TO PHARMACOLOGY 2021/22: G protein-coupled receptors. *British Journal of Pharmacology*, *178*(S1), S27–S156. https://doi.org/10.1111/bph.15538

Alexander, S. P., Cidlowski, J. A., Kelly, E., Mathie, A., Peters, J. A., Veale, E. L., Armstrong, J. F., Faccenda, E., Harding, S. D., Pawson, A. J., Southan, C., Davies, J. A., Coons, L., Fuller, P. J., Korach, K. S., & Young, M. J. (2021). THE CONCISE GUIDE TO PHARMACOLOGY 2021/22: Nuclear hormone receptors. *British Journal of Pharmacology*, *178*(S1), S246–S263. https://doi.org/10.1111/bph.15540

Alexander, S. P., Fabbro, D., Kelly, E., Mathie, A., Peters, J. A., Veale, E. L., Armstrong, J. F., Faccenda, E., Harding, S. D., Pawson, A. J., Southan, C., Davies, J. A., Boison, D., Burns, K. E., Dessauer, C., Gertsch, J., Helsby, N. A., Izzo, A. A., Koesling, D., … Wong, S. S. (2021). THE CONCISE GUIDE TO PHARMACOLOGY 2021/22: Enzymes. *British Journal of Pharmacology*, *178*(S1), S313–S411. https://doi.org/10.1111/bph.15542

Alexander, S. P., Mathie, A., Peters, J. A., Veale, E. L., Striessnig, J., Kelly, E., Armstrong, J. F., Faccenda, E., Harding, S. D., Pawson, A. J., Southan, C., Davies, J. A., Aldrich, R. W., Attali, B., Baggetta, A. M., Becirovic, E., Biel, M., Bill, R. M., Catterall, W. A., … Zhu, M. (2021). THE CONCISE GUIDE TO PHARMACOLOGY 2021/22: Ion channels. *British Journal of Pharmacology*, *178*(S1), S157–S245. https://doi.org/10.1111/bph.15539

Alexander, S. P. H., Roberts, R. E., Broughton, B. R. S., Sobey, C. G., George, C. H., Stanford, S. C., Cirino, G., Docherty, J. R., Giembycz, M. A., Hoyer, D., Insel, P. A., Izzo, A. A., Ji, Y., MacEwan, D. J., Mangum, J., Wonnacott, S., & Ahluwalia, A. (2018). Goals and practicalities of immunoblotting and immunohistochemistry: A guide for submission to the *British Journal of Pharmacology*. *British Journal of Pharmacology*, *175*(3), 407–411. https://doi.org/10.1111/bph.14112

Alzamora, R., O'Mahony, F., Bustos, V., Rapetti-Mauss, R., Urbach, V., Cid, L. P., Sepúlveda, F. V., & Harvey, B. J. (2011). Sexual dimorphism and oestrogen regulation of KCNE3 expression modulates the functional properties of KCNQ1 K^+ channels. *Journal of Physiology*, *589*, 5091–5107. https://doi.org/10.1113/jphysiol.2011.215772

14765381, 2023, 2, Downloaded from https://bpspubs.onlinelibrary.wiley.com/doi/10.1111/bph.15947 by Test, Wiley Online Library on [10/01/2025]. See the Terms and Conditions (https://onlinelibrary.wiley.com/terms-and-conditions) on Wiley Online Library for rules of use; OA articles are governed by the applicable Creative Commons License

Askew Page, H. R., Dalsgaard, T., Baldwin, S. N., Jepps, T. A., Povstyan, O., Olesen, S. P., & Greenwood, I. A. (2019). TMEM16A is implicated in the regulation of coronary flow and is altered in hypertension. *British Journal of Pharmacology*, *176*, 1635–1648. https://doi.org/10.1111/bph.14598

Baldwin, S. N., Sandow, S. L., Mondéjar-Parreño, G., Stott, J. B., & Greenwood, I. A. (2020). K_V7 channel expression and function within rat mesenteric endothelial cells. *Frontiers in Physiology*, *11*(December), 1–16. https://doi.org/10.3389/fphys.2020.598779

Barrese, V., Stott, J. B., Figueiredo, H. B., Aubdool, A. A., Hobbs, A. J., Jepps, T. A., McNeish, A., & Greenwood, I. A. (2018). Angiotensin II promotes $K_V7.4$ channels degradation through reduced interaction with HSP90 (heat shock protein 90). *Hypertension*, *71*, 1091–1100. https://doi.org/10.1161/HYPERTENSIONAHA.118.11116

Barrese, V., Stott, J. B., & Greenwood, I. A. (2018). KCNQ-encoded potassium channels as therapeutic targets. *Annual Review of Pharmacology and Toxicology*, *58*, 625–648. https://doi.org/10.1146/annurev-pharmtox-010617-052912

Barton, M., & Meyer, M. R. (2015). Nicolaus Copernicus and the rapid vascular responses to aldosterone. *Trends in Endocrinology & Metabolism*, *26*(8), 396–398. https://doi.org/10.1016/j.tem.2015.05.005

Batenburg, W. W., Jansen, P. M., & van den Bogaerdt, A. J. (2012). Angiotensin II-aldosterone interaction in human coronary microarteries involves GPR30, EGFR, and endothelial NO synthase. *Cardiovascular Research*, *94*, 136–143. https://doi.org/10.1093/cvr/cvs016

Berg, T. (2018). Kv7(KCNQ)-K^+-channels influence total peripheral resistance in female but not male rats, and hamper catecholamine release in hypertensive rats of both sexes. *Frontiers in Physiology*, *9*, 117. https://doi.org/10.3389/fphys.2018.00117

Bologa, C. G., Revankar, C. M., Young, S. M., Edwards, B. S., Arterburn, J. B., Kiselyov, A. S., Parker, M. A., Tkachenko, S. E., Savchuck, N. P., Sklar, L. A., & Oprea, T. I. (2006). Virtual and biomolecular screening converge on a selective agonist for GPR30. *Nature Chemical Biology*, *2*(4), 207–212. https://doi.org/10.1038/nchembio775

Boulton, K., Wilson, P. W., Bishop, V. R., Perez, J. H., Wilkinson, T., Hogan, K., Homer, N. Z. M., Robert, C., Smith, J., Meddle, S. L., Dunn, I. C., & Watson, K. (2021). Parental methyl-enhanced diet and in ovo corticosterone affect first generation Japanese quail (*Coturnix japonica*) development, behaviour and stress response. *Scientific Reports*, *11*(1), 21092. https://doi.org/10.1038/s41598-021-99812-w

Brueggemann, L. I., Moran, C. J., Barakat, J. A., Yeh, J. Z., Cribbs, L. L., & Byron, K. L. (2006). Vasopressin stimulates action potential firing by protein kinase C-dependent inhibition of KCNQ5 in A7r5 rat aortic smooth muscle cells. *AJP: Heart and Circulatory Physiology*, *292*(3), H1352–H1363. https://doi.org/10.1152/ajpheart.00065.2006

Busch, A. E., Suessbrich, H., Waldegger, S., Sailer, E., Greger, R., Lang, H. J., Lang, F., Gibson, K. J., & Maylie, J. G. (1996). Inhibition of IKs in guinea pig cardiac myocytes and guinea pig IsK channels by the chromanol 293B. *Pflügers Archiv - European Journal of Physiology*, *432*(6), 1094–1096. https://doi.org/10.1007/s004240050240

Carr, G., Barrese, V., Stott, J. B., Povstyan, O. V., Jepps, T. A., Figueiredo, H. B., Zheng, D., Jamshidi, Y., & Greenwood, I. A. (2016). MicroRNA-153 targeting of KCNQ4 contributes to vascular dysfunction in hypertension. *Cardiovascular Research*, *112*, 581–589. https://doi.org/10.1093/cvr/cvw177

Chadha, P. S., Jepps, T. A., Carr, G., Stott, J. B., Zhu, H. L., Cole, W. C., & Greenwood, I. A. (2014). Contribution of Kv7.4/Kv7.5 heteromers to intrinsic and calcitonin gene-related peptide-induced cerebral reactivity. *Arteriosclerosis, Thrombosis, and Vascular Biology*, *34*(4), 887–893. https://doi.org/10.1161/ATVBAHA.114.303405

Chadha, P. S., Zunke, F., Zhu, H. L., Davis, A. J., Jepps, T. A., Olesen, S. P., Cole, W. C., Moffatt, J. D., & Greenwood, I. A. (2012). Reduced KCNQ4-encoded voltage-dependent potassium channel activity underlies impaired β-adrenoceptor-mediated relaxation of renal arteries in hypertension. *Hypertension*, *59*(4), 877–884. https://doi.org/10.1161/HYPERTENSIONAHA.111.187427

Cheng, S.-B., Dong, J., Pang, Y., LaRocca, J., Hixon, M., Thomas, P., & Filardo, E. J. (2014). Anatomical location and redistribution of G protein-coupled estrogen receptor-1 during the estrus cycle in mouse kidney and specific binding to estrogens but not aldosterone. *Molecular and Cellular Endocrinology*, *382*(2), 950–959. https://doi.org/10.1016/j.mce.2013.11.005

Cora, M. C., Kooistra, L., & Travlos, G. (2015). Vaginal cytology of the laboratory rat and mouse: Review and criteria for the staging of the estrous cycle using stained vaginal smears. *Toxicologic Pathology*, *43*, 776–793. https://doi.org/10.1177/0192623315570339

Curran, J., & Mohler, P. J. (2015). Alternative paradigms for ion channelopathies: Disorders of ion channel membrane trafficking and posttranslational modification. *Annual Review of Physiology*, *77*, 505–524. https://doi.org/10.1146/annurev-physiol-021014-071838

Curtis, M. J., Alexander, S., Cirino, G., Docherty, J. R., George, C. H., Giembycz, M. A., Hoyer, D., Insel, P. A., Izzo, A. A., Ji, Y., MacEwan, D. J., Sobey, C. G., Stanford, S. C., Teixeira, M. M., Wonnacott, S., & Ahluwalia, A. (2018). Experimental design and analysis and their reporting II: Updated and simplified guidance for authors and peer reviewers. *British Journal of Pharmacology*, *175*, 987–993. https://doi.org/10.1111/bph.14153

Danborno, A. M., Nwankwo, M., Kure, J., & Eluwa, C. (2018). Prevalence of premenstrual syndrome and changes in blood pressure with menstrual cycle among university students. *Nigerian Journal of Physiological Sciences: Official Publication of the Physiological Society of Nigeria.*, *33*(2), 117–124.

Dennis, M. K., Burai, R., Ramesh, C., Petrie, W. K., Alcon, S. N., Nayak, T. K., Bologa, C. G., Leitao, A., Brailoiu, E., Deliu, E., Dun, N. J., Sklar, L. A., Hathaway, H. J., Arterburn, J. B., Oprea, T. I., & Prossnitz, E. R. (2009). In vivo effects of a GPR30 antagonist. *Nature Chemical Biology*, *5*(6), 421–427. https://doi.org/10.1038/nchembio.168

Dennis, M. K., Field, A. S., Burai, R., Ramesh, C., Petrie, W. K., Bologa, C. G., Oprea, T. I., Yamaguchi, Y., Hayashi, S., Sklar, L. A., Hathaway, H. J., Arterburn, J. B., & Prossnitz, E. R. (2011). Identification of a GPER/GPR30 antagonist with improved estrogen receptor counterselectivity. *The Journal of Steroid Biochemistry and Molecular Biology*, *127*(3–5), 358–366. https://doi.org/10.1016/j.jsbmb.2011.07.002

Docherty, J. R., Stanford, S. C., Panattieri, R. A., Alexander, S. P. H., Cirino, G., George, C. H., Hoyer, D., Izzo, A. A., Ji, Y., Lilley, E., & Sobey, C. G. (2019). Sex: A change in our guidelines to authors to ensure that this is no longer an ignored experimental variable. *British Journal of Pharmacology*, *176*(21), 4081–4086. https://doi.org/10.1111/bph.14761

Ferreira, N. S., Cau, S. B. A., Silva, M. A. B., Manzato, C. P., Mestriner, F. L. A. C., Matsumoto, T., Carneiro, F. S., & Tostes, R. C. (2015). Diabetes impairs the vascular effects of aldosterone mediated by G protein-coupled estrogen receptor activation. *Frontiers in Pharmacology*, *6*, 34. https://doi.org/10.3389/fphar.2015.00034

Ficker, E. (2003). Role of the cytosolic chaperones Hsp70 and Hsp90 in maturation of the cardiac potassium channel hERG. *Circulation Research*, *92*, e87–e100. https://doi.org/10.1161/01.RES.0000079028.31393.15

Filardo, E. J., Quinn, J. A., Bland, K. I., & Frackelton, A. R. J. (2000). Estrogen-induced activation of Erk-1 and Erk-2 requires the G protein-coupled receptor homolog, GPR30, and occurs via trans-activation of the epidermal growth factor receptor through release of HB-EGF. *Molecular Endocrinology (Baltimore, Md.)*, *14*(10), 1649–1660. https://doi.org/10.1210/mend.14.10.0532

Gao, Y., Yechikov, S., Vazquez, A. E., Chen, D., & Nie, L. (2013). Distinct roles of molecular chaperones HSP90α and HSP90β in the biogenesis

14765381, 2023, 2, Downloaded from https://bpspubs.onlinelibrary.wiley.com/doi/10.1111/bph.15947 by Test, Wiley Online Library on [10/01/2025]. See the Terms and Conditions (https://onlinelibrary.wiley.com/terms-and-conditions) on Wiley Online Library for rules of use; OA articles are governed by the applicable Creative Commons License

of KCNQ4 channels. *PLoS ONE*, *8*, e57282. https://doi.org/10.1371/journal.pone.0057282

Haavisto, A. M., Pettersson, K., Bergendahl, M., Perheentupa, A., Roser, J. F., & Huhtaniemi, I. (1993). A supersensitive immunofluorometric assay for rat luteinizing hormone. *Endocrinology*, *132*, 1687–1691. https://doi.org/10.1210/endo.132.4.8462469

Hulley, S., Furberg, C., Barrett-Connor, E., Cauley, J., Grady, D., Haskell, W., Knopp, R., Lowery, M., Satterfield, S., Schrott, H., Vittinghoff, E., Hunninghake, D., & HERS Research Group. (2002). Noncardiovascular disease outcomes during 6.8 years of hormone therapy: Heart and Estrogen/progestin Replacement Study follow-up (HERS II). *Journal of the American Medical Association*, *288*, 58–66. https://doi.org/10.1001/jama.288.1.58

Hulley, S., Grady, D., Bush, T., Furberg, C., Herrington, D., Riggs, B., & Vittinghoff, E. (1998). Randomized trial of estrogen plus progestin for secondary prevention of coronary heart disease in postmenopausal women. Heart and Estrogen/progestin Replacement Study (HERS) Research Group. *Jama*, *280*(7), 605–613. https://doi.org/10.1001/jama.280.7.605

Jaimes, L., Vinet, R., Knox, M., Morales, B., Benites, J., Laurido, C., & Martínez, J. L. (2019). A review of the actions of endogenous and exogenous vasoactive substances during the estrous cycle and pregnancy in rats. *Animals: An Open Access Journal from MDPI*, *9*(6). https://doi.org/10.3390/ani9060288

Jepps, T. A., Bentzen, B. H., Stott, J. B., Povstyan, O. V., Sivaloganathan, K., Dalby-Brown, W., & Greenwood, I. A. (2014). Vasorelaxant effects of novel Kv7.4 channel enhancers ML213 and NS15370. *British Journal of Pharmacology*, *171*(19), 4413–4424. https://doi.org/10.1111/bph.12805

Jepps, T. A., Chadha, P. S., Davis, A. J., Harhun, M. I., Cockerill, G. W., Olesen, S. P., Hansen, R. S., & Greenwood, I. A. (2011). Downregulation of Kv7.4 channel activity in primary and secondary hypertension. *Circulation*, *124*, 602–611. https://doi.org/10.1161/CIRCULATIONAHA.111.032136

Kow, L.-M., & Pfaff, D. W. (2016). Rapid estrogen actions on ion channels: A survey in search for mechanisms. *Steroids*, *111*, 46–53. https://doi.org/10.1016/j.steroids.2016.02.018

Lilley, E., Stanford, S. C., Kendall, D. E., Alexander, S. P., Cirino, G., Docherty, J. R., George, C. H., Insel, P. A., Izzo, A. A., Ji, Y., Panettieri, R. A., Sobey, C. G., Stefanska, B., Stephens, G., Teixeira, M., & Ahluwalia, A. (2020). ARRIVE 2.0 and the *British Journal of Pharmacology*: Updated guidance for 2020. *British Journal of Pharmacology*, *177*(16), 3611–3616. https://doi.org/10.1111/bph.15178

Mackie, A. R., Brueggemann, L. I., Henderson, K. K., Shiels, A. J., Cribbs, L. L., Scrogin, K. E., & Byron, K. L. (2008). Vascular KCNQ potassium channels as novel targets for the control of mesenteric artery constriction by vasopressin, based on studies in single cells, pressurized arteries, and in vivo measurements of mesenteric vascular resistance. *Journal of Pharmacology and Experimental Therapeutics*, *325*, 475–483. https://doi.org/10.1124/jpet.107.135764

Maiti, K., Paul, J. W., Read, M., Chan, E. C., Riley, S. C., Nahar, P., & Smith, R. (2011). G-1-activated membrane estrogen receptors mediate increased contractility of the human myometrium. *Endocrinology*, *152*(6), 2448–2455. https://doi.org/10.1210/en.2010-0979

Mazzuca, M. Q., Mata, K. M., Li, W., Rangan, S. S., & Khalil, R. A. (2015). Estrogen receptor subtypes mediate distinct microvascular dilation and reduction in $[Ca^{2+}]_i$ in mesenteric microvessels of female rat. *The Journal of Pharmacology and Experimental Therapeutics*, *352*(2), 291–304. https://doi.org/10.1124/jpet.114.219865

Möller, C., & Netzer, R. (2006). Effects of estradiol on cardiac ion channel currents. *European Journal of Pharmacology*, *532*(1–2), 44–49. https://doi.org/10.1016/j.ejphar.2006.01.006

Mondéjar-Parreño, G., Moral-Sanz, J., Barreira, B., De la Cruz, A., Gonzalez, T., Callejo, M., Esquivel-Ruiz, S., Morales-Cano, D., Moreno, L., Valenzuela, C., & Perez-Vizcaino, F. (2019). Activation of Kv7 channels as a novel mechanism for NO/cGMP-induced pulmonary vasodilation. *British Journal of Pharmacology*, *176*, 2131–2145. https://doi.org/10.1111/bph.14662

Mulvany, M. J., & Halpern, W. (1976). Mechanical properties of vascular smooth muscle cells in situ. *Nature*, *260*(5552), 617–619. https://doi.org/10.1038/260617a0

Ng, F. L., Davis, A. J., Jepps, T. A., Harhun, M. I., Yeung, S. Y., Wan, A., Reddy, M., Melville, D., Nardi, A., Khong, T. K., & Greenwood, I. A. (2011). Expression and function of the K^+ channel *KCNQ* genes in human arteries. *British Journal of Pharmacology*, *162*(1), 42–53. https://doi.org/10.1111/j.1476-5381.2010.01027.x

Nilsson, M. E., Vandenput, L., Tivesten, Å., Norlén, A.-K., Lagerquist, M. K., Windahl, S. H., Börjesson, A. E., Farman, H. H., Poutanen, M., Benrick, A., & Maliqueo, M. (2015). Measurement of a comprehensive sex steroid profile in rodent serum by high-sensitive gas chromatography-tandem mass spectrometry. *Endocrinology*, *156*(7), 2492–2502. https://doi.org/10.1210/en.2014-1890

Novella, S., Pérez-Cremades, D., Mompeón, A., & Hermenegildo, C. (2019). Mechanisms underlying the influence of oestrogen on cardiovascular physiology in women. *Journal of Physiology*, *597*(19), 4873–4886. https://doi.org/10.1113/JP278063

Ohya, S., Sergeant, G. P., Greenwood, I. A., & Horowitz, B. (2003). Molecular variants of KCNQ channels expressed in murine portal vein myocytes: A role in delayed rectifier current. *Circulation Research*, *92*, 1016–1023. https://doi.org/10.1161/01.RES.0000070880.20955.F4

O'Mahony, F., Alzamora, R., Betts, V., LaPaix, F., Carter, D., Irnaten, M., & Harvey, B. J. (2007). Female gender-specific inhibition of KCNQ1 channels and chloride secretion by 17β-estradiol in rat distal colonic crypts. *Journal of Biological Chemistry*, *282*, 24563–24573. https://doi.org/10.1074/jbc.M611682200

O'Mahony, F., Alzamora, R., Chung, H.-L., Thomas, W., & Harvey, B. J. (2009). Genomic priming of the antisecretory response to estrogen in rat distal colon throughout the estrous cycle. *Molecular Endocrinology (Baltimore, Md.)*, *23*(11), 1885–1899. https://doi.org/10.1210/me.2008-0248

Pabbidi, M. R., Kuppusamy, M., Didion, S. P., Sanapureddy, P., Reed, J. T., & Sontakke, S. P. (2018). Sex differences in the vascular function and related mechanisms: Role of 17β-estradiol. *American Journal of Physiology. Heart and Circulatory Physiology*, *315*(6), H1499–H1518. https://doi.org/10.1152/ajpheart.00194.2018

Percie du Sert, N., Hurst, V., Ahluwalia, A., Alam, S., Avey, M. T., Baker, M., Browne, W. J., Clark, A., Cuthill, I. C., Dirnagl, U., Emerson, M., Garner, P., Holgate, S. T., Howells, D. W., Karp, N. A., Lazic, S. E., Lidster, K., MacCallum, C. J., Macleod, M., … Würbel, H. (2020). The ARRIVE guidelines 2.0: Updated guidelines for reporting animal research. *PLoS Biology*, *18*(7), e3000410. https://doi.org/10.1371/journal.pbio.3000410

Rapetti-Mauss, R., O'Mahony, F., Sepulveda, F. V., Urbach, V., & Harvey, B. J. (2013). Oestrogen promotes KCNQ1 potassium channel endocytosis and postendocytic trafficking in colonic epithelium. *Journal of Physiology*, *591*, 2813–2831. https://doi.org/10.1113/jphysiol.2013.251678

Roepke, T. A., Qiu, J., Smith, A. W., Ronnekleiv, O. K., & Kelly, M. J. (2011). Fasting and 17β-estradiol differentially modulate the M-current in neuropeptide Y neurons. *Journal of Neuroscience*, *31*(33), 11825–11835. https://doi.org/10.1523/JNEUROSCI.1395-11.2011

Schnee, M. E., & Brown, B. S. (1998). Selectivity of linopirdine (DuP 996), a neurotransmitter release enhancer, in blocking voltage-dependent and calcium-activated potassium currents in hippocampal neurons. *Journal of Pharmacology and Experimental Therapeutics*, *286*, 709–717.

14765381, 2023, 2, Downloaded from https://bpspubs.onlinelibrary.wiley.com/doi/10.1111/bph.15947 by Test, Wiley Online Library on [10/01/2025]. See the Terms and Conditions (https://onlinelibrary.wiley.com/terms-and-conditions) on Wiley Online Library for rules of use; OA articles are governed by the applicable Creative Commons License

Simoncini, T., Hafezi-Moghadam, A., Brazil, D. P., Ley, K., Chin, W. W., & Liao, J. K. (2000). Interaction of oestrogen receptor with the regulatory subunit of phosphatidylinositol-3-OH kinase. *Nature*, *407*(6803), 538–541. https://doi.org/10.1038/35035131

Stott, J. B., Barrese, V., Jepps, T. A., Leighton, E. V., & Greenwood, I. A. (2015). Contribution of Kv7 channels to natriuretic peptide mediated vasodilation in normal and hypertensive rats. *Hypertension*, *65*(3), 676–682. https://doi.org/10.1161/HYPERTENSIONAHA.114.04373

Stricker, R., Eberhart, R., Chevailler, M.-C., Quinn, F. A., Bischof, P., & Stricker, R. (2006). Establishment of detailed reference values for luteinizing hormone, follicle stimulating hormone, estradiol, and progesterone during different phases of the menstrual cycle on the Abbott ARCHITECT analyzer. *Clinical Chemistry and Laboratory Medicine*, *44*(7), 883–887. https://doi.org/10.1515/CCLM.2006.160

Takezawa, H., Hayashi, H., Sano, H., Saito, H., & Ebihara, S. (1994). Circadian and estrous cycle-dependent variations in blood pressure and heart rate in female rats. *The American Journal of Physiology*, *267*(5 Pt 2), R1250–R1256. https://doi.org/10.1152/ajpregu.1994.267.5.R1250

Thomas, G. P., Gerlach, U., & Antzelevitch, C. (2003). HMR 1556, a potent and selective blocker of slowly activating delayed rectifier potassium current. *Journal of Cardiovascular Pharmacology*, *41*, 140–147. https://doi.org/10.1097/00005344-200301000-00018

Yan, F.-F., Pratt, E. B., Chen, P.-C., Wang, F., Skach, W. R., David, L. L., & Shyng, S. L. (2010). Role of Hsp90 in biogenesis of the beta-cell ATP-sensitive potassium channel complex. *Molecular Biology of the Cell*, *21*(12), 1945–1954. https://doi.org/10.1091/mbc.e10-02-0116

Yang, X.-P., & Reckelhoff, J. F. (2011). Estrogen, hormonal replacement therapy and cardiovascular disease. *Current Opinion in Nephrology and Hypertension*, *20*(2), 133–138. https://doi.org/10.1097/MNH.0b013e3283431921

Yeung, S. Y. M., Pucovský, V., Moffatt, J. D., Saldanha, L., Schwake, M., Ohya, S., & Greenwood, I. A. (2007). Molecular expression and pharmacological identification of a role for Kv7 channels in murine vascular reactivity. *British Journal of Pharmacology*, *151*(6), 758–770. https://doi.org/10.1038/sj.bjp.0707284

SUPPORTING INFORMATION

Additional supporting information can be found online in the Supporting Information section at the end of this article.

How to cite this article: Baldwin, S. N., Forrester, E. A., Homer, N. Z. M., Andrew, R., Barrese, V., Stott, J. B., Isakson, B. E., Albert, A. P., & Greenwood, I. A. (2023). Marked oestrous cycle-dependent regulation of rat arterial $K_V7.4$ channels driven by GPER1. *British Journal of Pharmacology*, *180*(2), 174–193. https://doi.org/10.1111/bph.15947

14765381, 2023, 2, Downloaded from https://bpspubs.onlinelibrary.wiley.com/doi/10.1111/bph.15947 by Test, Wiley Online Library on [10/01/2025]. See the Terms and Conditions (https://onlinelibrary.wiley.com/terms-and-conditions) on Wiley Online Library for rules of use; OA articles are governed by the applicable Creative Commons License

Check for updates

Received: 28 June 2021 | Revised: 21 September 2021 | Accepted: 19 October 2021

DOI: 10.1111/bph.15722

RESEARCH ARTICLE

Sexual dimorphism in prostacyclin-mimetic responses within rat mesenteric arteries: A novel role for $K_V7.1$ in shaping IP receptor-mediated relaxation

Samuel N. Baldwin | Elizabeth A. Forrester | Lauren McEwan | Iain A. Greenwood

Molecular and Clinical Sciences Research Institute, St. George's University, London, UK

Correspondence
Samuel N. Baldwin, Molecular and Clinical Sciences Research Institute, St. George's University, Cranmer Terrace, London SW17 0RE, UK.
Email: m1405629@sgul.ac.uk

Funding information
British Heart Foundation, Grant/Award Numbers: #FS/18/41/33762, FS/18/41/33762

Background and Purpose: Prostacyclin mimetics express potent vasoactive effects via prostanoid receptors that are not unequivocally defined, as to date no study has considered sex as a factor. The aim of this study was to determine the contribution of IP and EP_3 prostanoid receptors to prostacyclin mimetic iloprost-mediated responses, whether $K_V7.1$–5 channels represent downstream targets of selective prostacyclin-IP-receptor agonist MRE-269 and the impact of the oestrus cycle on vascular reactivity.

Experimental Approach: Within second-order mesenteric arteries from male and female Wistar rats, we determined (1) relative mRNA transcripts for EP_{1-4} (*Ptger*$_{1-4}$), IP (*Ptgi*) and TXA_2 (*Tbxa*) prostanoid receptors via RT-qPCR; (2) the effect of iloprost, MRE-269, isoprenaline and ML277 on precontracted arterial tone in the presence of inhibitors of prostanoid receptors, potassium channels and the molecular interference of $K_V7.1$ via wire-myograph; (3) oestrus cycle stage via histological changes in cervical cell preparations.

Key Results: Iloprost evoked a biphasic response in male mesenteric arteries, at concentrations ≤100 nmol·L^{-1} relaxing, then contracting the vessel at concentration ≥300 nmol·L^{-1}, a process attributed to IP and EP_3 receptors respectively. Secondary contraction was absent in the females, which was associated with a reduction in *Ptger3*. Pharmacological inhibition and molecular interference of $K_V7.1$ significantly attenuated relaxations produced by the selective IP receptor agonist MRE-269 in male and female Wistar in dioestrus/metoestrus, but not pro-oestrus/oestrus.

Conclusions and Implications: Stark sexual dimorphisms in iloprost-mediated vasoactive responses are present within mesenteric arteries. $K_V7.1$ is implicated in IP receptor-mediated vasorelaxation and is impaired by the oestrus cycle.

KEYWORDS
GPCR, Iloprost, Kv7, MRE-269, Prostacyclin, Sex, Vascular

This is an open access article under the terms of the Creative Commons Attribution License, which permits use, distribution and reproduction in any medium, provided the original work is properly cited.
© 2021 The Authors. *British Journal of Pharmacology* published by John Wiley & Sons Ltd on behalf of British Pharmacological Society.

1 | INTRODUCTION

Prostacyclin (PGI_2), a product **cyclooxygenase-1 (COX-1)** and **cyclooxygenase-2 (COX-2)** metabolism of **arachidonic acid**, has anti-thrombotic, anti-inflammatory and potent vasodilatory properties attributed to the activation of G_s-coupled **prostanoid (IP) receptor** signalling. PGI_2 and stable analogues, including **iloprost**, however bind to a plethora of G-protein coupled receptors (GPCR) including $EP_{1,2,3,4}$, IP, **TP**, **FP** and **DP_1** (Katusic et al., 2012), though with different affinities. For instance, in human and rat pulmonary arteries, iloprost binds to IP/EP_1 with high affinity, FP > $EP_{3/4}$ with moderate affinity and DP_1 > EP_2 > TP with low affinity (Whittle et al., 2012). As such, the potential effect of PGI_2/iloprost within the vasculature includes both $EP_{1/3}$/FP prostanoid receptor-evoked contraction (Kobayashi et al., 2011; Orie & Clapp, 2011; Tang et al., 2008) and EP_4/IP prostanoid receptor-mediated relaxation (e.g. Dumas et al., 1997; Lombard et al., 1999; Schubert et al., 1996, 1997). These diverse responses to prostacyclin mimetics remain largely uncharacterized and, moreover, few studies have considered sex as a factor when characterizing prostacyclin-memetic mediated vascular responses.

Previously, large conductance **calcium activated potassium channels ($K_{Ca}1.1$/BK_{Ca}**; Schubert et al., 1997), **ATP-sensitive potassium channels (K_{ATP}**; Lombard et al., 1999; Schubert et al., 1997) and **inwardly rectifying potassium channels (K_{IR}**; Orie et al., 2006) have been identified as the downstream targets of IP receptor-mediated vasorelaxation. Voltage-gated potassium channels encoded by *KCNQ1-5* genes (termed **K_V7.1-5** channels) are voltage-gated potassium channels with a negative threshold for activation that have well-identified roles in maintaining resting excitability in neurones, cardiac myocytes, epithelia and smooth muscle cells (Barrese et al., 2018). Of the five subtypes genes, ***Kcnq1***, ***4*** and ***5*** are robustly expressed in arterial smooth muscle (Barrese et al., 2020; Mackie et al., 2008; Yeung et al., 2007) and blockers of the expressed channels elicit contraction or enhanced vasoconstrictor response (e.g. Mackie et al., 2008; Yeung et al., 2007). K_V7 channels are also key functional components of vasorelaxations generated by several agonists of G_s-linked receptors including β-**adrenoceptors** (Chadha, Zunke, Zhu, et al., 2012; Stott et al., 2016), **calcitonin gene-related peptide receptors** (Chadha et al., 2014; Stott et al., 2018) and **adenosine receptors** (Khanamiri et al., 2013). Additionally, novel findings implicate sexual dimorphisms in channel physiology (Abbott & Jepps, 2016; Alzamora et al., 2011) and pathophysiology (Berg, 2018).

As the contribution of K_V7 channels to prostanoid receptor-mediated relaxations is unknown, we sought to determine whether K_V7 channels were involved with prostacyclin mimetic-mediated responses in rat mesenteric arteries from aged-matched male and female rats. This artery was chosen because (1), K_V7 expression has been established (Jepps et al., 2011, 2015; Mackie et al., 2008), (2) K_V7 activators are effective relaxants (Jepps et al., 2014), (3) a role for K_V7 channels in $G_{\alpha s}$-linked responses has been identified (e.g. Lindman et al., 2018; Stott et al., 2016, 2018) and (4), endothelium dependent production of PGI_2 mediates concomitant IP receptor-mediated relaxation (Liu et al., 2012) and TP/EP_3-mediated contraction (Liu et al., 2012, 2017). Moreover, in line with Docherty et al. (2019), we investigated possible sex difference as nothing is known about the impact of sex on prostanoid-mediated vascular responses. To circumvent the short half-life of prostacyclin, we characterized the contribution of EP_3 and IP receptors to responses mediated by its stable analogue iloprost and defined the contribution of K_V7 channels to IP receptor-mediated vasorelaxation using a selective IP receptor agonist, **MRE-269**. Our data demonstrate a striking sex-dependent difference in response to iloprost and a role for K_V7.1 channels in shaping IP receptor-evoked vasorelaxation within rat mesenteric arteries, which is oestrus cycle sensitive.

What is already known

- The prostacyclin analogue iloprost evokes vasoactive responses through a myriad of receptors.
- K_V7 channels are targets of endogenous vasoactive signalling cascades.

What does this study add

- Iloprost evoked biphasic relaxant-contrail responses in males, which is absent in females.
- K_V7.1 inhibition impairs MRE-269 mesenteric arteries relaxation which is affected by the oestrus cycle.

What is the clinical significance

- Sex must be considered as a factor when considering prostacyclin mimetics as a therapeutic tool.

2 | METHODS

2.1 | Animal models

Animal studies are reported in compliance with the ARRIVE guidelines (Percie du Sert et al., 2020) and with the recommendations made by the *British Journal of Pharmacology* (Lilley et al., 2020). Experiments were performed on arteries from male and female Wistar rats (RRID: RGD_734476, Charles River, Margate, UK) ages 11–14 weeks (200–350 g) housed at the Biological Research Facility, St George's, London, UK. A maximum of 5 rats were housed in NKP cages with free access to water and food (RM1; Dietex Inter-national, UK) with a 12-h light/dark cycle and constant temperature and humidity (21 ± 1°C; 50% ± 10% humidity) in accordance with the Animal (Scientific Procedures)

14765381, 2022, 7, Downloaded from https://bpspubs.onlinelibrary.wiley.com/doi/10.1111/bph.15722 by Test, Wiley Online Library on [10/01/2025]. See the Terms and Conditions (https://onlinelibrary.wiley.com/terms-and-conditions) on Wiley Online Library for rules of use; OA articles are governed by the applicable Creative Commons License

Act 1986. Animals were kept in LSB Aspen woodchip bedding. Animals were killed by cervical dislocation with secondary confirmation via cessation of the circulation by femoral artery severance in accordance with Schedule 1 of the ASPA 1986.

For the following investigations, second-order mesenteric arteries were used, identified as the second bifurcation of the superior mesenteric artery. Arteries were dissected, cleaned of fat and adherent tissue and stored on ice in physiological salt solution (PSS) of the following composition (mmol·L^{-1}): 119 NaCl, 4.5 KCl, 1.17 $MgSO_4{\cdot}7H_20$, 1.18 NaH_2PO_4, 25 $NaHCO_3$, 5 glucose, 1.25 $CaCl_2$.

2.2 | Oestrus cycle stage determination

After killing, 50 µl of PSS was inserted into the vaginal canal via a 2- to 200-µl pipette tip and flushed four to six times to liberate cells from the surface of the cervix and then stored on ice; 25 µl of the subsequent cell suspension was mounted on a glass slide and examined under light microscopy (×10 to ×20 magnification). Previously described changes in cervical cell histology allowed for the determination of oestrus cycle stage (Cora et al., 2015) as either (in order of the 4–5 day cycle) pro-oestrus, oestrus, metoestrous or dioestrus. Cycle stage determination was performed post-experiment during functional investigation as a means of blinding; this was not possible during molecular techniques.

2.3 | Wire myography

For functional investigations, ~2-mm arterial segments were mounted on a 40-µm tungsten steel wire within a myograph chamber (Danish Myo Technology, Arhus, Denmark) containing 5 ml of PSS (composition described above) oxygenated with 95% O_2 and 5% CO_2 at 37°C. Vessels then underwent a passive force normalization process to achieve an internal luminal circumference at a transmural pressure of 100 mmHg (13.3 kPa) to standardize pre-experimental conditions (Mulvany, 1977). Force generated was first amplified by a PowerLab (ADInstruments, Oxford, UK) and then recorded via LabChart software (RRID:SCR_017551; ADInstruments, Oxford, UK). Vessels were then challenged with isotonic high K^+ physiological salt solution (K^+PSS) of the following composition (mmol·L^{-1}): 63.5 NaCl, 60 KCl, 1.17 $MgSO_4{\cdot}7H_20$, 1.18 NaH_2PO_4, 25 $NaHCO_3$, 5 glucose, 1.25 $CaCl_2$, to determine viability. Vessels were then constricted with 10 µmol·L^{-1} **methoxamine**, an **α_1-adrenoreceptor** agonist, and endothelial cell integrity was determined via vasorelaxation in response to 10 µmol·L^{-1} of the synthetic acetylcholine analogue, **carbachol**, prior to investigation. Subsequently, vessels were preconstricted with 300 nmol·L^{-1} thromboxane A_2 mimetic **U46619**. Following which single dose responses or cumulative concentration effect curve were generated in response to either prostacyclin mimetic iloprost (0.001–3 µmol·L^{-1}), IP receptor agonists **selexipag** (0.03–3 µmol·L^{-1})/MRE-269 (0.01–1/0.01–3 µmol·L^{-1}), β-adrenoreceptor agonist **isoprenaline** (0.03–3 µmol·L^{-1}) or K_V7.1 activator **ML277**. Vessels were pre-incubated in the presence or absence of a combination of solvent control dimethyl sulphoxide (DMSO) or antagonists of the following: - IP prostanoid receptor-**CAY10441 (RO1138452**; 100 nmol·L^{-1}); EP_3 prostanoid receptor-**L-798,106** (300 nmol·L^{-1}); pan-K_V7 channel, **linopirdine** (10 µmol·L^{-1}); K_V7.1, **HMR-1556** (10 µmol·L^{-1}); **adenylate cyclase** ,SQ22,562 (10 µmol·L^{-1}); **PKA**, Rp-8-Br-cAMP/KT5720 (1 µmol·L^{-1}); **EPAC** (100 nmol·L^{-1}); $G_{\beta\gamma}$, M119K (10 µmol·L^{-1}); BK_{Ca}/K_{Ca}1.1, **iberiotoxin** (100 nmol·L^{-1}); K_{ATP}, **glibenclamide** (1 µmol·L^{-1}) for a period of 10 min.

2.4 | Reverse transcription quantitative polymerase chain reaction

mRNA from whole mesenteric arteries was extracted using Monarch Total RNA Miniprep Kit (New England BioLabs, Ipswich, Massachusetts, USA) and reverse transcribed via LunaScript RT SuperMix Kit (New England BioLabs, Ipswich, Massachusetts, USA). Quantitative analysis of relative gene expression was determined via CFX-96 Real-Time PCR Detection System (RRID:SCR_018064, BioRad, Hertfordshire, UK). Samples were run in BrightWhite qPCR plate (Primer Design, Camberley, UK) in combination with PrecisionPLUS qPCR Master Mix (Primer Design, Camberley, UK), 300 nmol·L^{-1} of gene specific target primer (Thermofisher scientific, Waltham, Massachusetts, USA) and 10-ng cDNA as per manufacturers instruction. Quantification cycle (Cq) was determined via Bio-Rad CFX96 Manager 3.0. Cq values are expressed as normalized values to appropriate, stable, housekeeper genes ($2^{-\Delta Cq}$) calnexin (*Canx*) and cytochrome C1 (*Cyc1*) chosen for their stable, and similar Cq values. Housekeeper genes were acquired from Primer Design (Camberley, UK); as such, for proprietary reasons, the sequences are not disclosed. See Table 1 for a list of primers used in the following investigation.

2.5 | Morpholino transfection

Knockdown of K_V7.1 in whole mesenteric arteries was performed by transfection with morpholinos that prohibit protein translation but do not affect transcript levels (see Barrese et al., 2020; Jepps et al., 2015). Either K_V7.1 morpholino nucleotides or mismatch controls (5 µmol·L^{-1}, RRID:SCR_005663, Genetools, USA) were mixed with Lipofectamine 2000 (ThermoFisher, Paisley, UK) and Opti-MEM (Sigma, UK) and left at room temperature for 2 h. Morpholino/Lipofectamine/Opti-MEM mixture was added to Dulbecco's modified Eagle medium (DMEM) F-12 (Sigma, UK) containing 1% penicillin/streptomycin. Arteries were added and left for 48 h at 37°C with 5% CO_2.

2.6 | Immunocytochemistry

The Immuno-related procedures used comply with the recommendations made by the *British Journal of Pharmacology* (Alexander et al., 2018). Vascular smooth muscle cells were isolated from morpholino-transfected mesenteric arteries via incubation in isolation PSS of the following composition (mmol·L^{-1}): 120 NaCl, 6 KCl,

14765381, 2022, 7, Downloaded from https://bpspubs.onlinelibrary.wiley.com/doi/10.1111/bph.15722 by Test, Wiley Online Library on [10/01/2025]. See the Terms and Conditions (https://onlinelibrary.wiley.com/terms-and-conditions) on Wiley Online Library for rules of use; OA articles are governed by the applicable Creative Commons License

TABLE 1 RT-qPCR primer sequences

Gene name	(+) Forward primer sequence 3′-5′ (−) Reverse primer sequence 5′-3′	Gene accession number	Amplicon	Concentration
EP_1 (*Ptger1*)	(+) AGTTCGAACGTTGGTCACGA (−) TAAGGTTGCAGCATTGTGCG	NM_001278475.1	112	300 nmol·L^{-1}
EP_2 (*Ptger2*)	(+) TATGCTCCCTGCCTTTCACAA (−) GGAGGTCCCACTTTTCCTTT	NM_031088.2	72	300 nmol·L^{-1}
EP_3 (*Ptger3*)	(+) GTGCAATTCCTTCCTAATCGCC (−) TCAGGTTGTTCATCATCTGGCA	NM_012704.1	122	300 nmol·L^{-1}
EP_4 (*Ptger4*)	(+) ATGAGCATTGAGCGCTACCT (−) AGATGCATAGACGGCGAAGA	NM_032076.3	102	300 nmol·L^{-1}
IP (*Ptgir*)	(+) TGACACTTTCGCCTTCGCTA (−) TAGATGGCAGGCAAAGCCAA	NP_001071112.1	156	300 nmol·L^{-1}
TXA2 (*Tbxa2r*)	(+) TTGACATTCCCAGGCCCAAA (−) ACGTGATAAGGGGGTCAACA	NM_017054.2	141	300 nmol·L^{-1}
Clnexin (*Canx*)	N/A (Primer design, Camberley, UK)			300 nmol·L^{-1}
Cytochrome C1 (*Cyc1*)	N/A (Primer design, Camberley, UK)			300 nmol·L^{-1}

12 glucose, 10 HEPEs and 1.2 $MgCl_2$ supplemented with 1.75 mg·ml^{-1} Collagenase Type IA, 0.9 mg·ml^{-1} protease, 1 mg·ml^{-1} trypsin inhibitor and 1 mg·ml^{-1} bovine serum albumin (Sigma, UK) at 37°C for 17 min. Vessels then underwent mechanical trituration by wide bore glass pipette to liberate vascular smooth muscle cells. The subsequent cell suspension was plated onto 13-mm coverslips in a 24-well plate, supplemented with an equal volume of Ca^{2+} (2.5 mmol·L^{-1}) containing PSS and left to attach for 1 h.

Vascular smooth muscle cells were fixed in 3% paraformaldehyde for 15 min and then stored at 4°C in PBS prior to staining. Cells were then incubated in the following: 100 mmol·L^{-1} glycine in PBS, 5 min; blocking solution (PBS containing 0.1% Triton X-100 and 10% FBS in PBS), 45 min; primary antibody (K_V7.1, 1:100, Rabbit, Pineda Antikörper-Service, Germany), overnight at 4°C. The following day, cells were incubated in secondary antibody (Goat anti-rabbit IgG [H + L] cross-absorbed secondary antibody, Alexa Fluro™ 568, 1:100, Goat, RRID:AB_143157, ThermoFisher, UK), then mounted in Vectasheild (Sigma, P4170). Cells were imaged via Nikon A1R confocal microscope (inverted) on Ti2 chassis (Image Resource Facility, St George's University, London), and total cell fluorescence was analysed using ImageJ (RRID:SCR_003070) software.

2.7 | Cell culture

The K_V7.1 antibody was validated using Chinese Hamster Ovarian (CHO) cells (RRID:CVCL_0213) overexpressing KCNQ1. CHO cells were grown in DMEM/F-12 (Sigma, UK) supplemented in 1% penicillin/streptomycin in an incubator with 5% CO_2 at 37°C. CHO cells were incubated with either a total of 3 μg of plasmid containing *Kcnq1* (University of Copenhagen, Denmark) in a Lipofectamine 2000/Opti-MEM mixture (*Kcnq1*-transfected CHO), or lipofectamine/Opti-MEM only for 24 h (nontransfected CHO). Cells were mounted onto glass coverslips, fixed and stained for K_V7.1 as above. Antibody specificity demonstrated by positive staining for K_V7.1 (Pineda Antikörper-Service, Germany) in *Kcnq1*-transfected CHO cells (Figure S1A), but not non-transfected CHO cells (Figure S1B).

2.8 | Materials

All drugs for the following investigation were procured from Tocris Bioscience (Oxford, UK). Excluding CAY-10441 and MRE-269, which were acquired from Cayman chemical (Michigan, USA), Rp-8-Br-cAMP which was aquired from Sigma-Aldrich (UK) and M119K which was provided by the National Cancer Institute Drug Development Programme. All drugs were dissolved in DMSO and final vehicle concentrations were always ≤0.01. For materials regarding morpholino transfection, immunodetection or RT-qPCR, see relevant sections above.

2.9 | Data and statistical analysis

All values are expressed as mean ± standard error of the mean (SEM) for no less than five independent data points, excluding measurement of total cell fluorescence during immunocytochemistry, in which 10 cells were measured per cell. For isometric tension recordings, single dose responses to iloprost are expressed as (%) change from stable tone in response to 300 nmol·L^{-1} U46619, contractions from basal tone are expressed as (%) contraction when normalized to vasoconstriction to 10 μmol·L^{-1} methoxamine and all cumulative concentration effect curves are expressed as (%) stable contraction in response to 300 nmol·L^{-1} U46619. This is to account for changes in vessel contractility. For functional experiments involving cumulative concentration effect curves, a transformed data set was generated using; X = Log(X), to reduce representative skew. Following which, either a four parametric linear regression analysis was performed using either (Log(Agonist) vs. response variable slope [four parameters Bottom/Hillslope/top/EC_{50}]) using GraphPad Prism (RRID:SCR_002798, Version 9.0.0) to fit a cumulative concentration effect curve to the figure.

14765381, 2022, 7, Downloaded from https://bpspubs.onlinelibrary.wiley.com/doi/10.1111/bph.15722 by Test, Wiley Online Library on [10/01/2025]. See the Terms and Conditions (https://onlinelibrary.wiley.com/terms-and-conditions) on Wiley Online Library for rules of use; OA articles are governed by the applicable Creative Commons License

When generating data with morpholino-transfected arteries, the investigator was blinded, whereby a second researcher would mount the vessels and then post-investigation reveals which arteries had been transfected with scrambled control or *Kcnq1* targeted morpholino. Blinding for the remaining investigations was impractical because researchers were working in isolation during the COVID-19 pandemic. However, vessel segments were cut prior to mounting during isometric tension recording and invert in an Eppendorf suspended in PSS. In doing so, vessel segments either proximal or distal to the bifurcation from first-order mesenteric arteries were randomly selected for drug treatments. For data comparing multiple groups, a paired Student's t-test or a two-way ANOVA was performed for comparison of mean values. If statistical significance was achieved up two-way ANOVA ($P < 0.5$), a post hoc Bonferonni (for comparing one condition against control) test or Dunnett's (for comparing multiple conditions against control) test was also performed to generate corrected significance values. Significant values are represented as $P < 0.05$ (*/#). Sample sizes subject to statistical analysis contain at least 5 animals per group, where n= number of independent values. Investigations expressing groups. Investigations expressing groups of unequal numbers were gathered due to technical failure or an artefact of cycle stage determination post-experiment during functional investigations. The data and statistical analysis comply with the recommendations of the *British Journal of Pharmacology* on experimental design and analysis in pharmacology in accordance with Curtis et al. (2018).

2.10 | Nomenclature of targets and ligands

Key protein targets and ligands in this article are hyperlinked to corresponding entries in the IUPHAR/BPS Guide to PHARMACOLOGY http://www.guidetopharmacology.org and are permanently archived in the Concise Guide to PHARMACOLOGY 2021/22 (Alexander, Christopoulos, et al., 2021; Alexander, Mathie, et al., 2021).

3 | RESULTS

3.1 | Iloprost-mediated vasoactive responses

In mesenteric arteries from male rats stably contracted by U46619 (300 nmol·L^{-1}), iloprost (0.1–3 μmol·L^{-1}) evoked a biphasic response, producing relaxation at lower concentrations followed by contraction at concentrations >300 nmol·L^{-1} (Figure 1a,b, black). This phenomenon was notably absent in mesenteric arteries from female rats, wherein iloprost only evoked concentration-dependent vasorelaxation (Figure 1a,b, red). See representative traces in Figure 1a. Application of solvent control had negligible effect on established tone in mesenteric arteries from either male or female rats (Figure 1b). For concentration effect curves generated in response to iloprost on precontracted tone, see Figure S2. Prostacyclin-mediated relaxations are conventionally mediated via activation of IP receptors, while EP_3 receptors have been implicated in contractile responses to iloprost in mesenteric arteries from hypertensive rats (Liu et al., 2017). To establish the role of these receptors in the biphasic or monophasic response observed in male and female rats, respectively, vessels were preincubated in either EP_3 receptor antagonist L-798,106 (300 nmol·L^{-1}) or IP receptor antagonist CAY-10441 (100 nmol·L^{-1}).

In the presence of the EP_3 receptor antagonist L-798,106, 1 μmol·L^{-1} iloprost-mediated contraction was converted to a relaxation (Figure 2a). In mesenteric arteries from females, EP_3 receptor blockade had no effect (Figure 2a). In the presence of IP receptor antagonist CAY-10441, 0.3 μmol·L^{-1} iloprost-mediated relaxation was abolished in both groups (Figure 3a,b; $P \geq 0.05$). Similarly, 3 μmol·L^{-1} iloprost evoked significantly greater contraction from

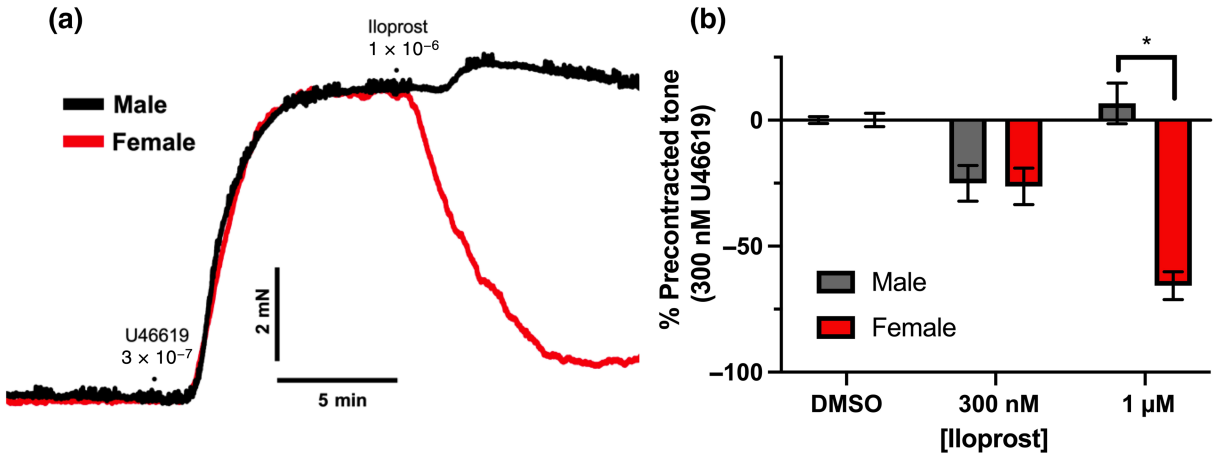


FIGURE 1 Iloprost evokes biphasic vasoactive responses within male, but not female mesenteric arteries. Representative traces of iloprost (0.3–1 μmol·L^{-1}) mediated vasoactive responses on precontracted tone (300 nmol·L^{-1} U46619) within mesenteric arteries from male (a; black) or female (a; red) Wistar rats. Mean data for DMSO solvent control and iloprost-mediated vasoactive responses on precontracted (300 nmol·L^{-1} U46619) mesenteric arteries (a; 0.3–1 μmol·L^{-1}; $n = 6–8$). All values are expressed as mean ± SEM. A two-way statistical ANOVA with a post-hoc Bonferroni test was used to generate significance values ($^*P < 0.05$). n = number of animals used

14765381, 2022, 7, Downloaded from https://bpspubs.onlinelibrary.wiley.com/doi/10.1111/bph.15722 by Test, Wiley Online Library on [10/01/2025]. See the Terms and Conditions (https://onlinelibrary.wiley.com/terms-and-conditions) on Wiley Online Library for rules of use; OA articles are governed by the applicable Creative Commons License

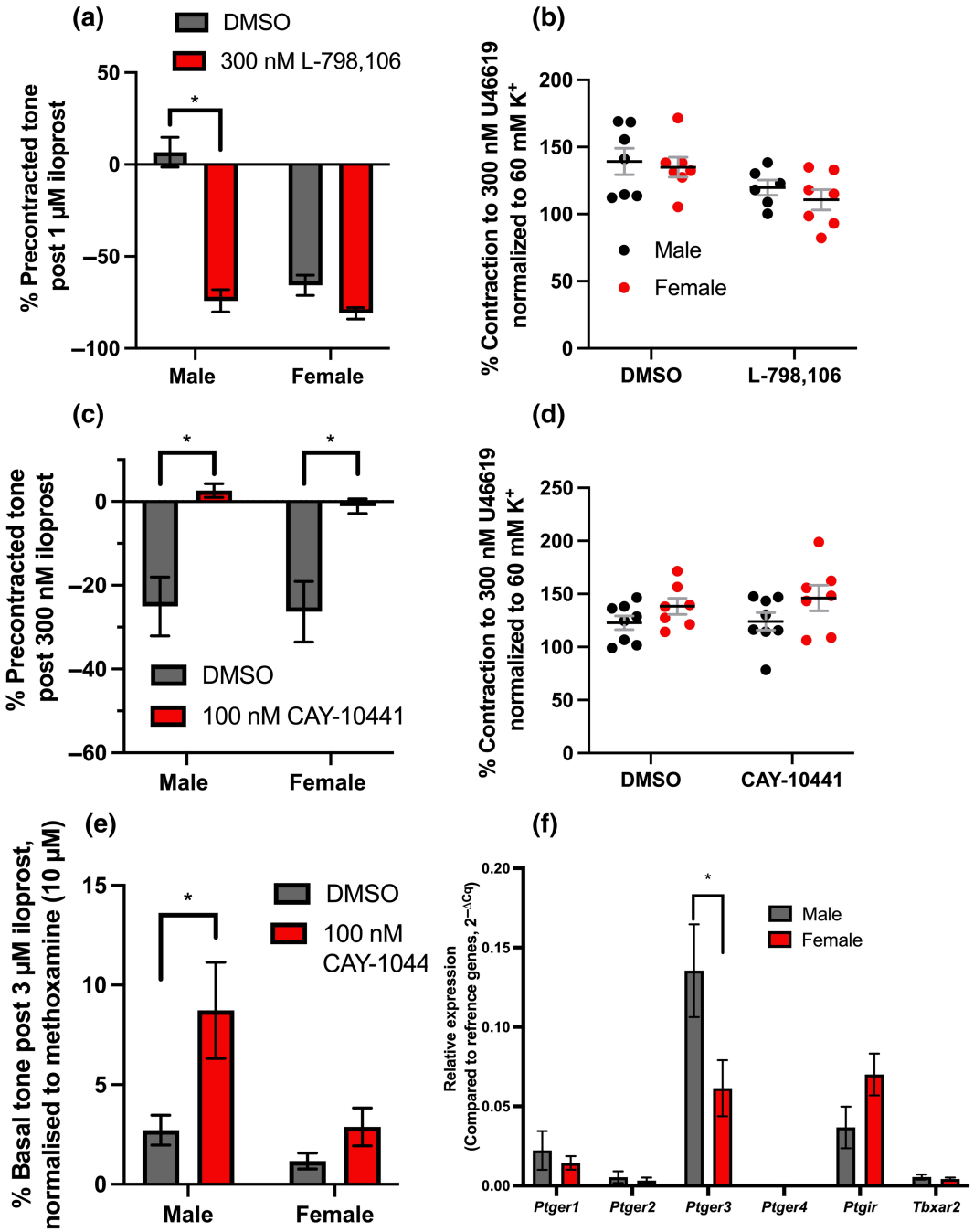


FIGURE 2 Iloprost-mediated contraction and relaxation is blocked by EP_3 and IP receptor-mediated inhibition, respectively. Mean data for iloprost-mediated vasoactive responses (a, 1 µmol·L^{-1}; c, 300 nmol·L^{-1}) within precontracted (300 nmol·L^{-1} U46619) mesenteric arteries from male and female rats preincubated in either solvent control (DMSO; a,c; $n = 6–8$), 300 nmol·L^{-1} L-798,106 (a; $n = 6–8$) or 100 nmol·L^{-1} CAY-10441 (c; $n = 6–8$). Scatter graph showing individual and mean values of stable precontracted tone from male and female arteries prior to adding iloprost to the chamber (b,d). Mean data for vasoconstriction from base line tension in response to 3 µmol·L^{-1} iloprost in male (black; $n = 7$) and female (red; $n = 10$) mesenteric arteries in the presence of DMSO or 100 nmol·L^{-1} CAY-10441 normalized to peak contraction in response to 10 µmol·L^{-1} methoxamine (e). Relative gene expression of prostanoid receptors (*Ptger1–4* = $EP_{1–4}$, *Ptgi* = IP, *Tbxar2* = TXA_2) normalized to stable housekeeper genes (*Canx*, *Cyc1*) expressed as $2^{-\Delta Cq}$ from male (black; $n = 5$) and female (red; $n = 5–10$) whole mesenteric artery lysates (f). A two-way statistical ANOVA with a post-hoc Bonferroni test was used to generate significant values ($^*P < 0.05$). n = number of animals used

base-line tone in mesenteric arteries from male rats preincubated in CAY-10441 when compared to mesenteric arteries from female rats (Figure 3e). No differences were observed in precontracted tone in vessels preincubated in either L-798,106 or CAY-10441 when compared to DMSO solvent control or between the sexes (Figure 2b/d). Subsequently, we performed quantitative PCR to determine the relative expression of prostanoid receptors (Table 1) in the mesenteric arteries from both sexes. Figure 2.F shows that expression of *Ptger2/4*

14765381, 2022, 7, Downloaded from https://bpspubs.onlinelibrary.wiley.com/doi/10.1111/bph.15722 by Test, Wiley Online Library on [10/01/2025]. See the Terms and Conditions (https://onlinelibrary.wiley.com/terms-and-conditions) on Wiley Online Library for rules of use; OA articles are governed by the applicable Creative Commons License

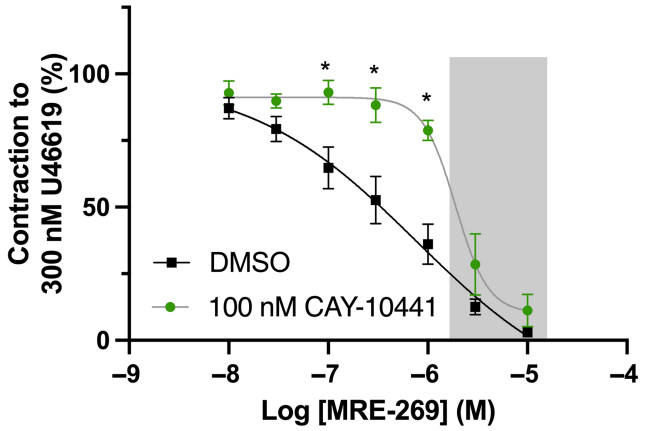


FIGURE 3 MRE-269 relaxation is inhibited by CAY-10441 to a threshold of 1 μmol·L^{-1} in male mesenteric arteries. Mean data of MRE-269 (0.01–10 μmol·L^{-1}) mediated relaxation of precontracted arterial tone (300 nmol·L^{-1}) in vessels preincubated in DMSO solvent control (black; $n = 7$) or 100 nmol·L^{-1} CAY-10441 ($n = 5$) in male mesenteric arteries. Grey box demonstrates non-CAY-10441 sensitive MRE-269-mediated relaxation. All values are expressed as mean ± SEM. A two-way statistical ANOVA with a post-hoc Bonferroni test was used to generate significant values ($^*P < 0.05$). n = number of animals used

($EP_{2/4}$) was negligible in mesenteric arteries from both sexes compared to *Ptger3* > *Ptgir* > *Ptger1* (EP_3; IP; EP_1), which were well expressed (Figure 2f). However, *Ptger3* was expressed at significantly lower level in mesenteric arteries from female rats compared to mesenteric arteries from males (Figure 2f). Thus, our data demonstrate that iloprost-mediated relaxation in rat mesenteric arteries occurs predominantly via IP receptors, while contraction was caused by activation of EP_3 receptors. Additionally, the absence of a biphasic response to iloprost in female mesenteric arteries was associated with a comparably smaller effect of EP_3 receptor inhibition on iloprost-mediated relaxation and a reduction in *Ptger3* expression.

3.2 | Characterizing MRE-269-mediated relaxation

As iloprost has a plethora of potential targets, we used the clinically available IP receptor agonist, selexipag (NS-304), to delineate the mechanisms underlying IP-mediated relaxation. Application of selexipag produced concentration-dependent relaxations of precontracted mesenteric arteries from male rats (Figure S3). However, this effect was insensitive to preincubation with IP receptor antagonist CAY-10441 (Figure S3) thus, selexipag effects are non-IP

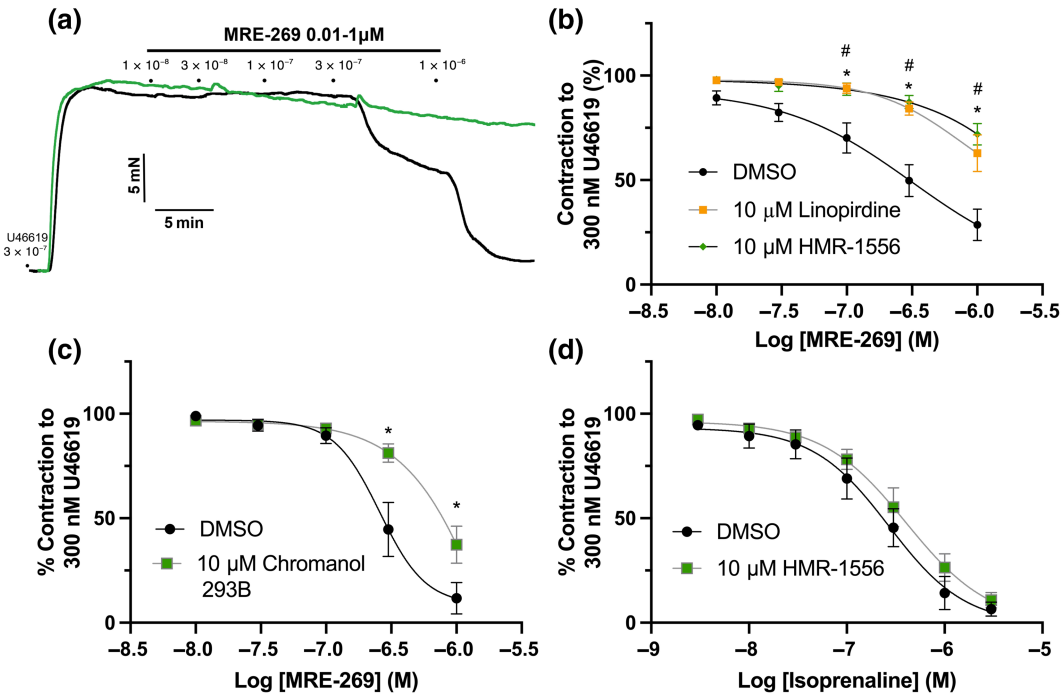


FIGURE 4 Linopirdine and HMR-1556 attenuate MRE-269-mediated vasorelaxation in mesenteric arteries from male and female rats. Representative traces of MRE-269-mediated (0.01–1 μmol·L^{-1}) relaxation of precontracted tone (300 nmol·L^{-1} U46619) within mesenteric arteries preincubated in either DMSO solvent control (a; black) or 10 μmol·L^{-1} K_V7.1 specific blocker HMR-1556 (a; green) from male Wistar rats. Mean data for MRE-269-mediated vasorelaxation (0.01–1 μmol·L^{-1}) of precontracted tone (300 nmol·L^{-1} U46619) within mesenteric arteries preincubated in either DMSO (b; black) solvent control, 10 μmol·L^{-1} pan-K_V7 channel blocker linopirdine (b; yellow) or HMR-1556 (b; green) or 10 μmol·L^{-1} K_V7.1 seelective blocker Chromanol 293B (c; green; $n = 7$–10). Mean data for isoprenaline-mediated relaxation in vessels preincubated in DMSO (black) or 10 μmol·L^{-1} HMR-1556 (green) in male mesenteric arteries (d; $n = 9$). All values are expressed as mean ± SEM (a–f). A two-way statistical ANOVA with a post-hoc Dunnet (b) or Bonferroni (c,d) test was used to generate significant values ($^*P < 0.05$). n = number of animals used

14765381, 2022, 7, Downloaded from https://bpspubs.onlinelibrary.wiley.com/doi/10.1111/bph.15722 by Test, Wiley Online Library on [10/01/2025]. See the Terms and Conditions (https://onlinelibrary.wiley.com/terms-and-conditions) on Wiley Online Library for rules of use; OA articles are governed by the applicable Creative Commons License

receptor dependent. It is now known that in the body, selexipag is metabolized into the active compound, inhibited by CAY-10441 pre-incubation up to threshold of 1 μmol·L^{-1}. At higher concentrations, the MRE-269-mediated relaxation was not sensitive to CAY-10441 and therefore does not involve IP receptor activation. This non-IP receptor-mediated relaxation is highlighted by the grey box in Figure 3 and in the following investigations, MRE-269 was used at concentrations ≤1 μmol·L^{-1} to ensure only IP receptor-mediated effects were investigated.

3.3 | A novel role for K_V7.1 in shaping IP receptor-selective agonists in mesenteric arteries

Kv7 channels, especially Kv7.4 and Kv7.5, are functional endpoints for several G_s-linked receptors (see Barrese et al., 2020; Byron & Brueggemann, 2018). As such, we characterized the potential contribution of K_V7 channels to IP-receptor selective MRE-269-mediated relaxation. In mesenteric arteries from male rats, MRE-269-mediated relaxation was significantly attenuated by preincubation with the pan-K_V7 channel inhibitor linopirdine (10 μmol·L^{-1}; yellow) when compared to DMSO (Figure 4, black). Strikingly, preincubation with the K_V7.1 selective inhibitor HMR-1556 (10 μmol·L^{-1}) also inhibited MRE-269-induced relaxations to the same extent as linopirdine (Figure 4a,b, green;). The structurally dissimilar K_V7.1 inhibitor chromanol 293B (3S,4R-293B) also significantly attenuated MRE-269-mediated relaxation of male mesenteric arteries (Figure 4c). In contrast and consistent with previous reports (Stott et al., 2016), relaxations of mesenteric arteries induced by the mixed β-adrenoceptor agonist isoprenaline were not affected by pre-incubation with 10 μmol·L^{-1} HMR-1556 (Figure 4d).

To corroborate the contribution of K_V7.1 to IP receptor-mediated vasorelaxation, we transfected mesenteric arteries with morpholinos that prevent translation of Kv7.1 or a scrambled control. Immunocytochemistry with an antibody for K_V7.1 validated by overexpression studies (Figure S1) showed a significant reduction in total cell fluorescence (A.U) in *Kcnq1* morpholino-transfected arteries when compared to mismatch control (Figure 5a–c). Functionally, arteries incubated

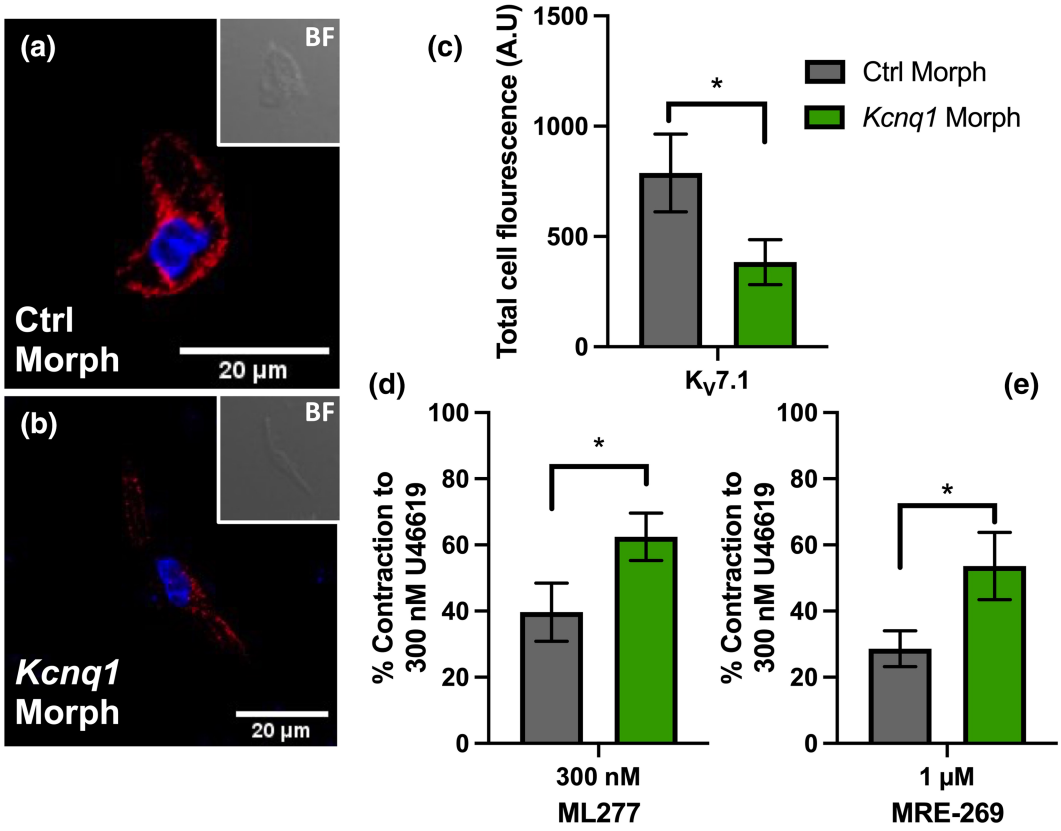


FIGURE 5 Molecular interference of *Kcnq1* via targeted morpholino knockdown impairs MRE-269-mediated relaxation. Representative immunofluorescence showing K_V7.1 in isolated vascular smooth muscle cells from either scrambled control (Ctrl morph; a) or *Kcnq1* (*Kcnq1* morph; b) morpholino-transfected mesenteric arteries. K_V7.1 shown in red, nuclear staining in blue (DAPI [4′,6-diamidino-2-phenylindole, dihydrochloride]). Insets show brightfield (BF) images of the cell. Mean data for total cell fluorescence measured in arbitrary units (A.U) for Ctrl morph (grey; $n = 3$; $N = 10$) and *Kcnq1* morph (green; $n = 3$; $N = 10$; d) transfected cells. Mean data for 300 nmol·L^{-1} ML277-mediated relaxation ($n = 7$; e). Mean data for 1 μmol·L^{-1} MRE-269-mediated relaxation ($n = 7$; f). All values are expressed as mean ± SEM (a–f). A paired Student's *t*-test was used to generate significant values (*$P < 0.05$). n = number of animals used, N = number of cells per biological repeat

14765381, 2022, 7, Downloaded from https://bpspubs.onlinelibrary.wiley.com/doi/10.1111/bph.15722 by Test, Wiley Online Library on [10/01/2025]. See the Terms and Conditions (https://onlinelibrary.wiley.com/terms-and-conditions) on Wiley Online Library for rules of use; OA articles are governed by the applicable Creative Commons License

with mismatch control produced a significantly greater relaxant response to 300 nmol·L^{-1} K_V7.1 activator ML277 (Baldwin et al., 2020; Yu et al., 2013) compared to *Kcnq1* morpholino-transfected arteries (Figure 5d). Similarly, relaxation produced by 1 μmol·L^{-1} MRE-269 was greater in arteries transfected with mismatch control morpholino when compared *Kcnq1* morpholino-transfected arteries (Figure 5e). Thus, a reduction in K_V7.1 protein was observed in conjunction with an attenuated relaxation by MRE-269.

Subsequently, we aimed to determine the signalling cascade activated in response to IP receptor stimulation. Previously, Schubert et al. (1996) demonstrated that iloprost-evoked hyperpolarization of rat tail artery vascular smooth muscle cells is mediated via G_s–cyclic adenosine 3′-5′-monophosphate (cAMP)–protein kinase A (PKA) stimulation of potassium currents (Schubert et al., 1996) in a process attributed to IP receptors, although not fully defined. Here, we similarly demonstrate that adenylate cyclase inhibitor SQ22,562 (10 μmol·L^{-1}) and PKA inhibitors Rp8 (1 μmol·L^{-1}) and KT5720 (1 μmol·L^{-1}) significantly attenuated MRE-269-mediated relaxation (1 μmol·L^{-1}; $P \geq 0.05$; Figure 6a–c). In addition, inhibition of an alternative secondary signalling molecule activated by G_s–cAMP, exchange protein directly activated by cAMP (EPAC), via **ESI-09** had no effect

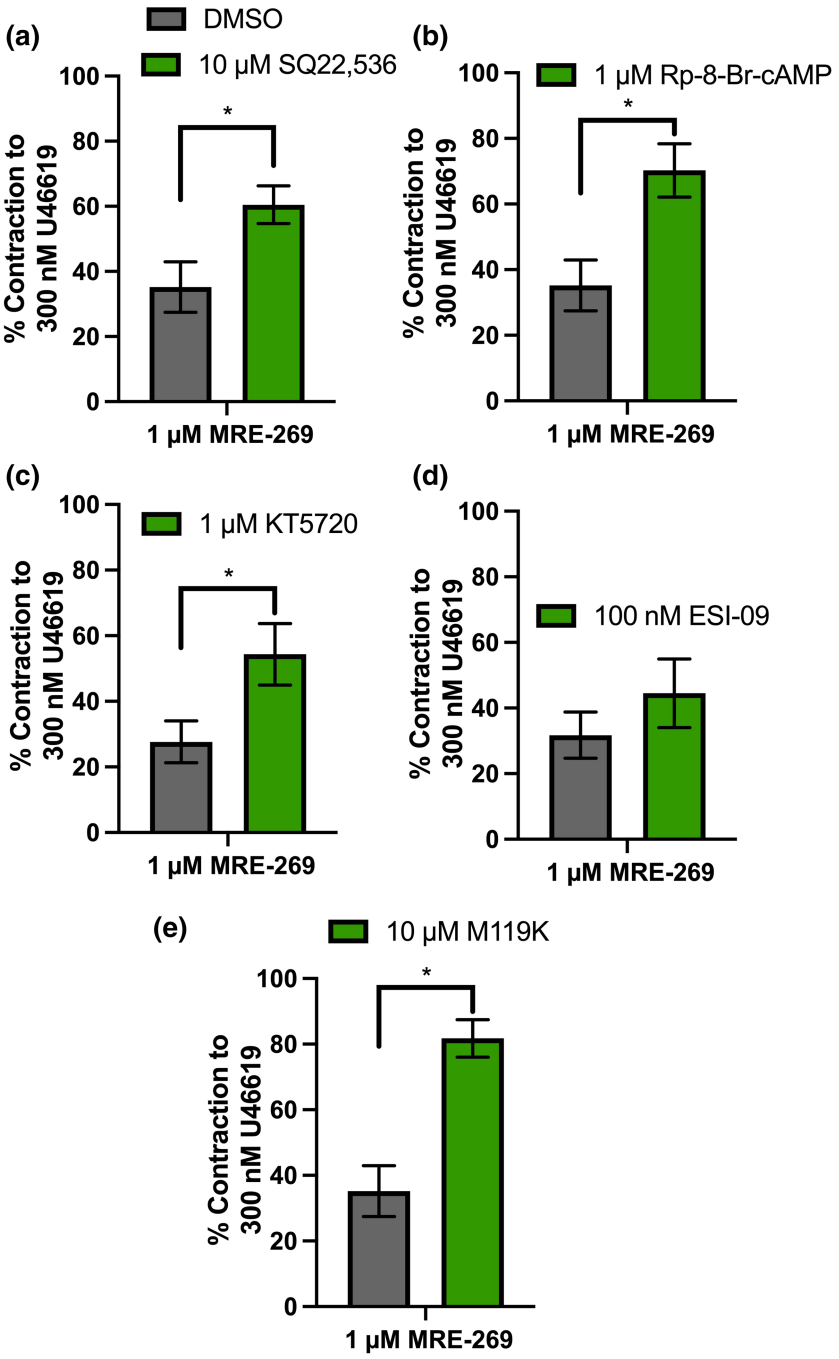


FIGURE 6 MRE-268-mediated relaxation is sensitive to adenylate cyclase, Gβγ and protein kinase A inhibition, but not effector protein activated by cAMP in male rat mesenteric arteries. Mean data for MRE-269-mediated vasorelaxation (1 μmol·L^{-1}) of precontracted tone (300 nmol·L^{-1} U46619) within mesenteric arteries preincubated in either DMSO (a–e; $n = 9$; grey) solvent control or inhibitors of the following (green); adenylate cyclase–SQ22,562 (10 μmol·L^{-1}; $n = 7$; a), protein kinase A–Rp-8-Br-cAMP (1 μmol·L^{-1}; $n = 5$; b)/KT5720 (1 μmol·L^{-1}; $n = 8$; c), effector protein inhibited by cAMP–ES09 (100 nmol·L^{-1}; $n = 8$; d) and Gβγ–ML119K (1 μmol·L^{-1}; $n = 7$; e). All values are expressed as mean ± SEM (a–e). An unpaired Students *t*-test was used to generate significant values ($^*P < 0.05$). n = number of animals used

14765381, 2022, 7, Downloaded from https://bpspubs.onlinelibrary.wiley.com/doi/10.1111/bph.15722 by Test, Wiley Online Library on [10/01/2025]. See the Terms and Conditions (https://onlinelibrary.wiley.com/terms-and-conditions) on Wiley Online Library for rules of use; OA articles are governed by the applicable Creative Commons License

(100 nmol·L^{-1}; Figure 6d). Finally, $G_{\beta\gamma}$ inhibition by M119K (1 μmol·L^{-1}) also significantly attenuated MRE-269-mediated relaxation (Figure 6e).

BK_{Ca} and K_{ATP} channels have also been identified as downstream targets of cAMP-PKA-dependent relaxations evoked by iloprost (Schubert et al., 1997). Here, we demonstrate that BK_{Ca} inhibitor iberiotoxin (100 nmol·L^{-1}) but not K_{ATP} inhibitor glibenclamide (1 μmol·L^{-1}) partially inhibited MRE-269-mediated relaxation in male mesenteric arteries (Figure S4A,B), though this failed to reach statistical significance.

3.4 | Oestrus cycle-dependent shifts in the sensitivity of MRE-269-mediated vasorelaxation to K_V7 channel modulators

The pan K_V7 channel inhibitor linopirdine and $K_V7.1$ channel inhibitor HMR-1556 also significantly attenuated MRE-269-mediated relaxation in mesenteric arteries from female rats when compared to DMSO solvent control (Figure 7a;), though the latter to a smaller degree when compared to linopirdine. However, we observed two-distinct populations of possible responses to MRE-269-mediated relaxation and its subsequent sensitivity to K_V7 channel modulators, categorized into rats in dioestrus/metestrus or proestrus/oestrus (Pro/Est). Oestrus cycle stage was identified by defined histological changes in cells lifted from the cervix after killing (as per methods; Cora et al., 2015). Both the pan-K_V7 channel inhibitor linopirdine and $K_V7.1$ selective inhibitor HMR-1556 impaired MRE-269-mediated relaxation to the same degree in arteries from female in dioestrus/metestrus (Figure 7b) but had no effect in arteries from rats in proestrus/oestrus (Figure 7c). Moreover, MRE-269-mediated relaxation in arteries from female proestrus/oestrus rats was significantly less sensitive to the IP-selective agonist than arteries from rats in dioestrus/metestrus (Figure 7d;). However, we observed no differences in $K_V7.1$ activator ML277 (0.1–0.3 μmol·L^{-1}) mediated relaxation on precontracted tone between the separated groups (Figure 7e). These data reveal an oestrus cycle stage-dependent regulation of the contribution of $K_V7.1$ to IP receptor-mediated relaxation, which underpins diminished sensitivity to MRE-269-mediated relaxation during proestrus/oestrus.

4 | DISCUSSION

To our knowledge, the present study is the first to highlight sex as a factor in the arterial response to prostacyclin mimetics. The study shows that application of iloprost to pre-contacted mesenteric arteries from male rats produced bimodal responses, relaxation at low concentrations, followed by contraction at higher concentrations, whereas mesenteric arteries from female arteries presented with monophasic relaxation only. In arteries from both sexes the relaxant effect of iloprost was enhanced by EP_3 receptor antagonist L-798106 and was blocked by IP receptor antagonist CAY-10441. Our data demonstrated iloprost-mediated contractions in mesenteric arteries from male rats were more efficacious when compared to vessels from females, correlating with a higher level of *Ptger*$_3$ expression. Finally, our data show that the selective IP receptor agonist MRE-269 was a potent relaxant of precontracted mesenteric arteries from both sexes. This relaxation was inhibited by both the pan-K_V7 blocker linopirdine and $K_V7.1$ selective blocker HMR-1556 in arteries from males and dioestrus/metestrus females but strikingly not proestrus/oestrus rats. These findings are the first observation of $K_V7.1$ as a downstream target of an endogenous vasoactive signalling cascade and reveal oestrus cycle-dependent regulation of K_V7 channels within the vasculature.

4.1 | Iloprost-evoked vasoconstriction

While principally regarded as a vasodilator, PGI_2 mediates both relaxation and contraction of smooth muscle (Dusting et al., 1977; Liu et al., 2017; Moncada et al., 1976). PGI_2 has subsequently been identified as an endothelial-derived contracting factor produced in response to acetylcholine within rat aorta (Gluais et al., 2005), mesenteric (Liu et al., 2017), iliac (Zhang et al., 2021) and renal arteries (Zhang et al., 2021) in a process attributed to the activation of both EP and TP prostanoid receptors. Consistent with Liu et al. (2017), we show that high concentrations of iloprost-evoked contractions were blocked by the EP_3 receptor antagonist L-798,106. As iloprost has a low affinity for TP receptors (Whittle et al., 2012), TP receptor knockout has no effect on PGI_2-mediated contraction in mesenteric arteries (Liu et al., 2017) and all vessels in this study were precontracted with U46619, a TP receptor agonist. TP receptors were not considered for the scope of this investigation. Additionally, EP_1 receptor agonists do not elicit contractions in male mesenteric arteries (Kobayashi et al., 2011), and in agreement with previous findings (Kobayashi et al., 2011), a reduced expression of *Ptger1* was observed when compared to *Ptger3*. Furthermore, iloprost had negligible contractile effect in mesenteric arteries from female rats, which was associated with a lower expression level of *Ptger3* in these arteries.

4.2 | $K_V7.1$ underpins IP receptor-mediated relaxation

Our data show that relaxations of mesenteric arteries mediated by low concentrations of iloprost were driven primarily through CAY-10441-sensitive IP receptor activation. We subsequently showed that CAY-10441-sensititve relaxations produced by the selective IP receptor agonist MRE-269 were impaired by the selective K_V7 channel blocker, linopirdine. Within the vasculature, of the five subtypes, *Kcnq4 > Kcqn5 > Kcnq1* are the principally expressed transcripts with little to no expression of *Kcnq2/3* (Chadha, Zunke, Zhu, et al., 2012; Jepps et al., 2011; Yeung et al., 2007). $K_V7.4$/$K_V7.5$ alone however are implicated in the regulation of the resting

14765381, 2022, 7, Downloaded from https://bpspubs.onlinelibrary.wiley.com/doi/10.1111/bph.15722 by Test, Wiley Online Library on [10/01/2025]. See the Terms and Conditions (https://onlinelibrary.wiley.com/terms-and-conditions) on Wiley Online Library for rules of use; OA articles are governed by the applicable Creative Commons License

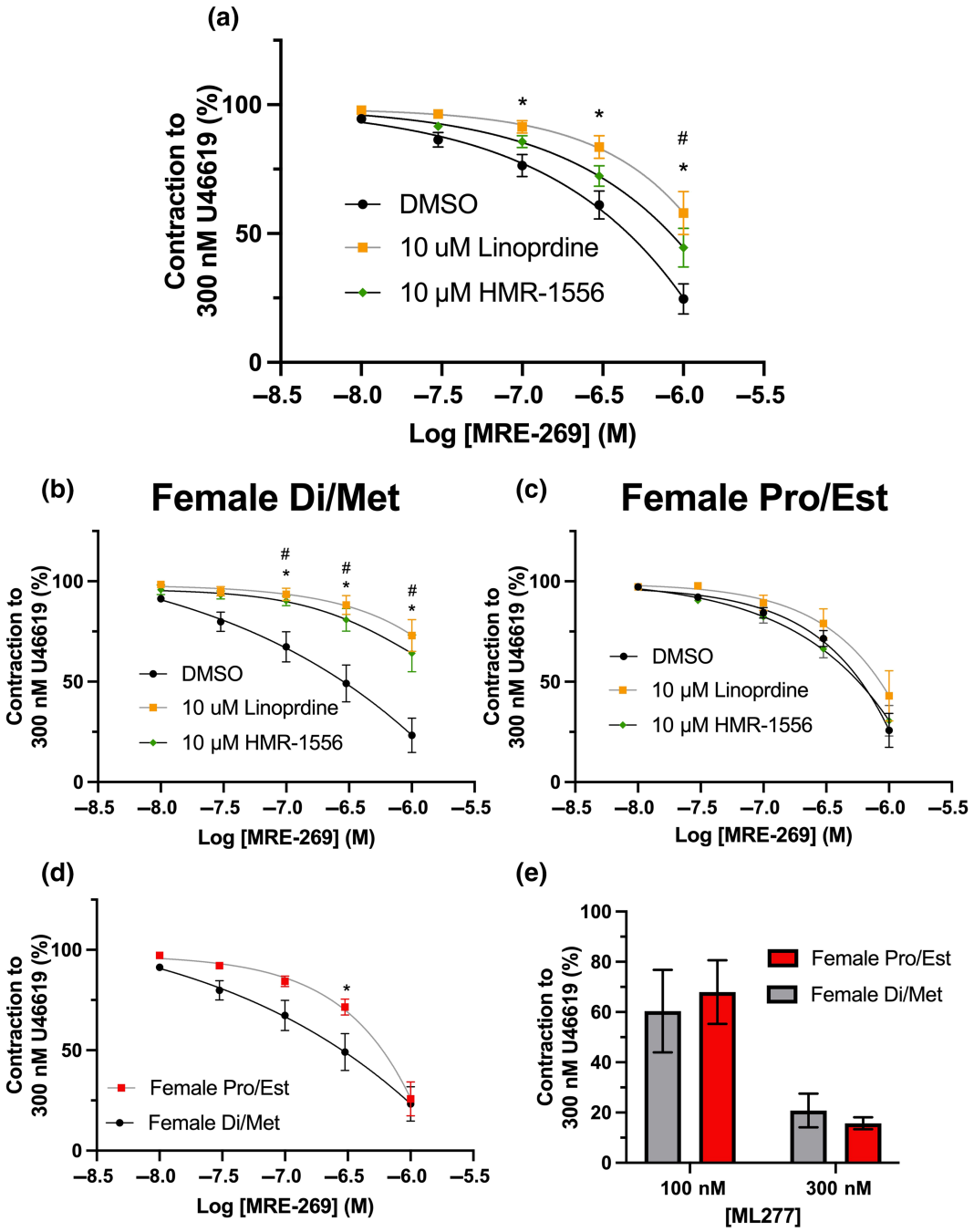


FIGURE 7 K_V7 channel inhibition attenuates MRE-269-mediated vasorelaxation in mesenteric arteries from dioestrus/metestrus (Di/Met), but not proestrus/oestrus (Pro/Est) female rats. Mean data for MRE-269-mediated vasorelaxation (0.01–1 µmol·L^{-1}) within mesenteric arteries preincubated in DMSO solvent control (a–c; black), 10 µmol·L^{-1} pan K_V7 channel inhibitor linopirdine (a–c; yellow) or 10 µmol·L^{-1} $K_V7.1$ specific inhibitor HMR-1556 (a–c; green) from female Wistar rats. Data are expressed as either all female (a), female Di/Met (n = 5–7; b) and female Pro/Est (n = 6–8; c). MRE-269 (0.01–1 µmol·L^{-1}; d) and ML277 (0.01–0.03 µmol·L^{-1}) mediated relaxation in vessels from either female Pro/Est (red; n = 6–8) or female Di/Met (black; n = 5–6). All values are expressed as mean ± SEM (a–e). A two-way statistical ANOVA with a post-hoc Dunnett's test (a–c) or Bonferroni test (d,e) was used to generate significant values ($^*P < 0.05$). n = number of animals used

membrane potential (Mackie et al., 2008) and basal tone (Mackie et al., 2008; Ng et al., 2011). In addition, pharmacological inhibition or molecular knockdown of $K_V7.4/7.5$ impairs relaxations to many different relaxants including isoprenaline, calcitonin gene-related peptide (CGRP), adenosine (G_s linked), atrial natriuretic peptide (ANP; cGMP linked) and adipose derived relaxant factors in several arteries (Byron & Brueggemann, 2018; Chadha et al., 2014; Gollasch, 2017; Khanamiri et al., 2013; Morales-Cano et al., 2015; Stott et al., 2016; Stott, Barrese, et al., 2015). Our data suggest that IP receptor activation in male mesenteric arteries involves another GPCR that also

14765381, 2022, 7, Downloaded from https://bpspubs.onlinelibrary.wiley.com/doi/10.1111/bph.15722 by Test, Wiley Online Library on [10/01/2025]. See the Terms and Conditions (https://onlinelibrary.wiley.com/terms-and-conditions) on Wiley Online Library for rules of use; OA articles are governed by the applicable Creative Commons License

relies on K_V7 channels for functional responses. In contrast to previous reports (Lombard et al., 1999; Schubert et al., 1997) IP receptor-mediated relaxation was not affected by K_{ATP} nor BK_{Ca} blockade. However, this discrepancy is potentially accounted for by a difference in vascular model used, as Lombard et al. (1999) investigated the rat middle cerebral artery and Schubert et al. (1997) used the rat tail artery.

Surprisingly, MRE-269-evoked CAY-10441-sensitive relaxations in mesenteric arteries from male rats were also potently inhibited by two structurally dissimilar $K_V7.1$ selective inhibitors (HMR-1556, chromanol 293B) and molecular knockdown of the channel. In contrast to $K_V7.4/K_V7.5$, the role of $K_V7.1$ within the vasculature remains enigmatic. Though $K_V7.1$ is expressed within vascular smooth muscle cells (Baldwin et al., 2020; Chadha, Zunke, Zhu, et al., 2012; Tsvetkov et al., 2017) and $K_V7.1$ selective activators RL-1 and ML277 are effective relaxants of precontracted arterial tone (Baldwin et al., 2020; Chadha, Zunke, Davis, et al., 2012), $K_V7.1$ has not been identified as the downstream target of any endogenous vasoactive signalling cascades (Chadha et al., 2014; Stott et al., 2016; Stott, Barrese, et al., 2015). Yet in the present study, HMR-1556 produced as full an inhibition as linopirdine, which suggests $K_V7.1$, and not $K_V7.4/7.5$, contributes to MRE-269-mediated relaxations. Under the same conditions, the mixed β-adrenoceptor agonist isoprenaline produced relaxations that were not HMR1556 sensitive. Thus, our findings appear not to be an off-target effect of HMR-1556. Moreover, a role for $K_V7.1$ in MRE-269-mediated relaxation was substantiated by morpholino-induced reduction in $K_V7.1$ protein levels. While further work is required to validate these findings, to our knowledge, the first to describe an effect on vascular reactivity by $K_V7.1$ inhibition is our data. Additionally, our data support the notion that IP receptor-mediated responses are cAMP-PKA mediated. In agreement with previous work done by our lab (Stott et al., 2016, 2018; Stott, Povstyan, et al., 2015), we demonstrate that relaxations that are mediated PKA, but not EPAC, are also sensitive to $G_{\beta\gamma}$ inhibition. The identification of $G_{\beta\gamma}$ contribution to IP receptor-mediated relaxation adds new complexity to the vascular response and gives credence to the novel role of $G_{\beta\gamma}$ in the functional relationship between GPCRs and K_V7s.

To date, comparably little is known as to how K_V7 channels operate within the female. However, K_V7 has been shown to regulate both human and murine myometrium (McCallum et al., 2009) and human chorionic plate artery (Mills et al., 2015) contractility. Intriguingly, while MRE-269-mediated relaxation was attenuated by linopirdine and HMR-1556 in arteries from female rats, the effect of the latter was far smaller than in the male. When separated into oestrus cycle stages, arteries from females in dioestrus/metestrus expressed sensitivities to HMR-1556 and linopirdine equivalent to the male, whereas arteries from females in proestrus/oestrus were entirely insensitive to either. However, $K_V7.1$ activator-ML277-mediated relaxation was insensitive to changes in the oestrus cycle. As the functional output of pharmacological activation of the channel remains the same, the data indicate an oestrus cycle-dependent impairment of $K_V7.1$ channel coupling to IP receptor-mediated relaxation. Oestrus cycle-dependent regulation of vascular reactivity is a known but incompletely understood phenomenon (Jaimes et al., 2019) largely attributed to endogenous sex-hormones, primarily, **17-β oestradiol.** 17-β oestradiol negatively regulates $K_V7.1$ in distal colic crypt cells and cardiac myocytes (Alzamora et al., 2011; O'Mahony et al., 2007; Rapetti-Mauss et al., 2013; Waldegger et al., 1996). As previous work demonstrates that within the Wistar rat, oestradiol peaks within pro-oestrus rats followed by comparably little to none in oestrus, metestrus and dioestrus (Nilsson et al., 2015), we propose that during pro-oestrus, oestradiol levels rise, impairing $K_V7.1$ coupling to IP receptor during proestrus/oestrus phase, thus reducing the potency of MRE-269-mediated relaxation and its HMR-1556/linopirdine sensitivity, which does not recover until dioestrus/metestrus. Our data imply an oestrus cycle.

4.3 | Perspectives

Sexual dimorphisms in cardiovascular physiology and pathophysiology are known (Pabbidi et al., 2018), whereby women express a cardioprotective factor or factors that differentiates the aetiology of vascular disease between age-matched men and women. Chronic **aldosterone** treatment in male Wistar–Kyoto rats induces hypertension through endothelial dysfunction attributed to upregulated COX-2 production of PGI_2 (Blanco-Rivero et al., 2005). Diminished EP_3-mediated contraction/expression in female rats may potentially negate the pathophysiological levels of PGI_2 production observed by Blanco-Rivero et al. (2005), contributing to the known cardioprotective phenotype expressed by females, though further work is required to validate this hypothesis.

5 | CONCLUSION

The data of the present study demonstrate a remarkable sexual dimorphism in the vascular response to synthetic prostacyclin analogues and highlight the importance of considering sex as a determinant in vascular physiology. Strikingly, the potent relaxations to the selective IP receptor agonist MRE-269 were sensitive to the Kv7.1-selective blocker HMR1556 in mesenteric arteries from males and females in dioestrus/metestrus but not at all in proestrus/oestrus. These novel findings demonstrate both a functional role for $K_V7.1$ in receptor mediated vascular reponses and cyclical changes in K_V7 channel activity across the oestrus cycle, and form the basis of future investigations.

ACKNOWLEDGEMENT

S.N.B was funded by the British Heart Foundation (Grant #FS/18/41/33762) awarded to I.A.G.

AUTHOR CONTRIBUTIONS

S.N.B designed and implemented all experiments. S.N.B, E.A.F and L. M performed experiments, generated and analysed data. S.N.B and I.A.G drafted the manuscript. I.A.G oversaw the project and prepared the submission of the paper. I.A.G provided funding.

14765381, 2022, 7, Downloaded from https://bpspubs.onlinelibrary.wiley.com/doi/10.1111/bph.15722 by Test, Wiley Online Library on [10/01/2025]. See the Terms and Conditions (https://onlinelibrary.wiley.com/terms-and-conditions) on Wiley Online Library for rules of use; OA articles are governed by the applicable Creative Commons License

CONFLICT OF INTEREST

The authors declare no conflict of interest.

DECLARATION OF TRANSPARENCY AND SCIENTIFIC RIGOUR

This Declaration acknowledges that this paper adheres to the principles for transparent reporting and scientific rigour of preclinical research as stated in the *BJP* guidelines for Design & Analysis, Immunoblotting and Immunochemistry and Animal Experimentation, and as recommended by funding agencies, publishers and other organizations engaged with supporting research.

DATA AVAILABILITY STATEMENT

The data generated herein are available upon reasonable request to the corresponding author.

ORCID

Samuel N. Baldwin https://orcid.org/0000-0002-3796-6090
Elizabeth A. Forrester https://orcid.org/0000-0002-2164-103X
Lauren McEwan https://orcid.org/0000-0002-1983-2574
Iain A. Greenwood https://orcid.org/0000-0002-0603-0492

REFERENCES

Abbott, G. W., & Jepps, T. A. (2016). Kcne4 deletion sex-dependently alters vascular reactivity. *Journal of Vascular Research*, *53*, 138–148. https://doi.org/10.1159/000449060

Alexander, S. P., Christopoulos, A., Davenport, A. P., Kelly, E., Mathie, A., Peters, J. A., Veale, E. L., Armstrong, J. F., Faccenda, E., Harding, S. D., Pawson, A. J., Southan, C., Davies, J. A., Abbracchio, M. P., Alexander, W., Al-hosaini, K., Bäck, M., Barnes, N. M., Bathgate, R., … Ye, R. D. (2021). THE CONCISE GUIDE TO PHARMACOLOGY 2021/22: G protein-coupled receptors. *British Journal of Pharmacology*, *178*(S1), S27–S156. https://doi.org/10.1111/bph.15538

Alexander, S. P., Mathie, A., Peters, J. A., Veale, E. L., Striessnig, J., Kelly, E., Armstrong, J. F., Faccenda, E., Harding, S. D., Pawson, A. J., Southan, C., Davies, J. A., Aldrich, R. W., Attali, B., Baggetta, A. M., Becirovic, E., Biel, M., Bill, R. M., Catterall, W. A., … Zhu, M. (2021). THE CONCISE GUIDE TO PHARMACOLOGY 2021/22: Ion channels. *British Journal of Pharmacology*, *178*(S1), S157–S245. https://doi.org/10.1111/bph.15539

Alexander, S. P. H., Roberts, R. E., Broughton, B. R. S., Sobey, C. G., George, C. H., Stanford, S. C., … Ahluwalia, A. (2018). Goals and practicalities of immunoblotting and immunohistochemistry: A guide for submission to the *British Journal of Pharmacology*. *British Journal of Pharmacology*, *175*, 407–411. https://doi.org/10.1111/bph.14112

Alzamora, R., O'Mahony, F., Bustos, V., Rapetti-Mauss, R., Urbach, V., Cid, L. P., Sepúlveda, F. V., & Harvey, B. J. (2011). Sexual dimorphism and oestrogen regulation of KCNE3 expression modulates the functional properties of KCNQ1 K^+ channels. *Journal of Physiology*, *589*, 5091–5107. https://doi.org/10.1113/jphysiol.2011.215772

Baldwin, S. N., Sandow, S. L., Mondéjar-Parreño, G., Stott, J. B., & Greenwood, I. A. (2020). KV7 channel expression and function within rat mesenteric endothelial cells. *Frontiers in Physiology*, *11*(December), 1–16. https://doi.org/10.3389/fphys.2020.598779

Barrese, V., Stott, J. B., Baldwin, S. N., Mondejar-Parreño, G., & Greenwood, I. A. (2020). SMIT (sodium-myo-inositol transporter) 1 regulates arterial contractility through the modulation of vascular Kv7 channels. *Arteriosclerosis, Thrombosis, and Vascular Biology*, *40*(10), 2468–2480. https://doi.org/10.1161/ATVBAHA.120.315096

Barrese, V., Stott, J. B., & Greenwood, I. A. (2018). KCNQ-Encoded Potassium Channels as Therapeutic Targets. *Annual review of pharmacology and toxicology*, *58*, 625–648. https://doi.org/10.1146/annurev-pharmtox-010617-052912

Berg, T. (2018). Kv7(KCNQ)-K^+-channels influence total peripheral resistance in female but not male rats, and hamper catecholamine release in hypertensive rats of both sexes. *Frontiers in Physiology*, *9*, 117. https://doi.org/10.3389/fphys.2018.00117

Blanco-Rivero, J., Cachofeiro, V., Lahera, V., Aras-Lopez, R., Márquez-Rodas, I.´., Salaices, M., Xavier, F. E., Ferrer, M., & Balfagón, G. (2005). Participation of prostacyclin in endothelial dysfunction induced by aldosterone in normotensive and hypertensive rats. *Hypertension*, *46*(1), 107–112. https://doi.org/10.1161/01.HYP.0000171479.36880.17

Byron, K. L., & Brueggemann, L. I. (2018). Kv7 potassium channels as signal transduction intermediates in the control of microvascular tone. *Microcirculation*, *25*, e12419. https://doi.org/10.1111/micc.12419

Chadha, P. S., Jepps, T. A., Carr, G., Stott, J. B., Zhu, H. L., Cole, W. C., & Greenwood, I. A. (2014). Contribution of Kv7.4/Kv7.5 heteromers to intrinsic and calcitonin gene-related peptide-induced cerebral reactivity. *Arteriosclerosis, Thrombosis, and Vascular Biology*, *34*(4), 887–893. https://doi.org/10.1161/ATVBAHA.114.303405

Chadha, P. S., Zunke, F., Davis, A. J., Jepps, T. A., Linders, J. T. M., Schwake, M., Towart, R., & Greenwood, I. A. (2012). Pharmacological dissection of Kv7.1 channels in systemic and pulmonary arteries. *British Journal of Pharmacology*, *166*, 1377–1387. https://doi.org/10.1111/j.1476-5381.2012.01863.x

Chadha, P. S., Zunke, F., Zhu, H. L., Davis, A. J., Jepps, T. A., Olesen, S. P., Cole, W. C., Moffatt, J. D., & Greenwood, I. A. (2012). Reduced KCNQ4-encoded voltage-dependent potassium channel activity underlies impaired β-adrenoceptor-mediated relaxation of renal arteries in hypertension. *Hypertension*, *59*, 877–884. https://doi.org/10.1161/HYPERTENSIONAHA.111.187427

Cora, M. C., Kooistra, L., & Travlos, G. (2015). Vaginal cytology of the laboratory rat and mouse: Review and criteria for the staging of the estrous cycle using stained vaginal smears. *Toxicologic Pathology*, *43*, 776–793. https://doi.org/10.1177/0192623315570339

Curtis, M. J., Alexander, S., Cirino, G., Docherty, J. R., George, C. H., Giembycz, M. A., Hoyer, D., Insel, P. A., Izzo, A. A., Ji, Y., MacEwan, D. J., Sobey, C. G., Stanford, S. C., Teixeira, M. M., Wonnacott, S., & Ahluwalia, A. (2018). Experimental design and analysis and their reporting II: Updated and simplified guidance for authors and peer reviewers. *British Journal of Pharmacology*, *175*, 987–993. https://doi.org/10.1111/bph.14153

Docherty, J. R., Stanford, S. C., Panattieri, R. A., Alexander, S. P. H., Cirino, G., George, C. H., Hoyer, D., Izzo, A. A., Ji, Y., Lilley, E., & Sobey, C. G. (2019). Sex: A change in our guidelines to authors to ensure that this is no longer an ignored experimental variable. *British Journal of Pharmacology*, *176*(21), 4081–4086. https://doi.org/10.1111/bph.14761

Dumas, M., Dumas, J. P., Rochette, L., Advenier, C., & Giudicelli, J. F. (1997). Role of potassium channels and nitric oxide in the effects of iloprost and prostaglandin E1 on hypoxic vasoconstriction in the isolated perfused lung of the rat. *British Journal of Pharmacology*, *120*, 405–410. https://doi.org/10.1038/sj.bjp.0700912

Dusting, G. J., Moncada, S., & Vane, J. R. (1977). Prostacyclin (PGI2) is a weak contractor of coronary arteries of the pig. *European Journal of Pharmacology*, *45*, 301–304. https://doi.org/10.1016/0014-2999(77)90014-0

Gluais, P., Lonchampt, M., Morrow, J. D., Vanhoutte, P. M., & Feletou, M. (2005). Acetylcholine-induced endothelium-dependent contractions in the SHR aorta: The Janus face of prostacyclin. *British Journal of Pharmacology*, *146*, 834–845. https://doi.org/10.1038/sj.bjp.0706390

14765381, 2022, 7, Downloaded from https://bpspubs.onlinelibrary.wiley.com/doi/10.1111/bph.15722 by Test, Wiley Online Library on [10/01/2025]. See the Terms and Conditions (https://onlinelibrary.wiley.com/terms-and-conditions) on Wiley Online Library for rules of use; OA articles are governed by the applicable Creative Commons License

Gollasch, M. (2017). Adipose-vascular coupling and potential therapeutics. *Annual Review of Pharmacology and Toxicology*, *57*, 417–436. https://doi.org/10.1146/annurev-pharmtox-010716-104542

Jaimes, L., Vinet, R., Knox, M., Morales, B., Benites, J., Laurido, C., & Martínez, J. (2019). A review of the actions of endogenous and exogenous vasoactive substances during the estrous cycle and pregnancy in rats. *Animals : An Open Access Journal from MDPI*, *9*(6), 288. https://doi.org/10.3390/ani9060288

Jepps, T. A., Bentzen, B. H., Stott, J. B., Povstyan, O. V., Sivaloganathan, K., Dalby-Brown, W., & Greenwood, I. A. (2014). Vasorelaxant effects of novel Kv7.4 channel enhancers ML213 and NS15370. *British Journal of Pharmacology*, *171*(19), 4413–4424. https://doi.org/10.1111/bph.12805

Jepps, T. A., Carr, G., Lundegaard, P. R., Olesen, S. P., & Greenwood, I. A. (2015). Fundamental role for the KCNE4 ancillary subunit in Kv7.4 regulation of arterial tone. *Journal of Physiology*, *593*, 5325–5340. https://doi.org/10.1113/JP271286

Jepps, T. A., Chadha, P. S., Davis, A. J., Harhun, M. I., Cockerill, G. W., Olesen, S. P., Hansen, R. S., & Greenwood, I. A. (2011). Downregulation of Kv7.4 channel activity in primary and secondary hypertension. *Circulation*, *124*, 602–611. https://doi.org/10.1161/CIRCULATIONAHA.111.032136

Katusic, Z. S., Santhanam, A. V., & He, T. (2012). Vascular effects of prostacyclin: Does activation of PPARδ play a role? *Trends in Pharmacological Sciences*, *33*, 559–564. https://doi.org/10.1016/j.tips.2012.05.005

Khanamiri, S., Soltysinska, E., Jepps, T. A., Bentzen, B. H., Chadha, P. S., Schmitt, N., Greenwood, I. A., & Olesen, S. P. (2013). Contribution of KV7 channels to basal coronary flow and active response to ischemia. *Hypertension*, *62*(6), 1090–1097. https://doi.org/10.1161/HYPERTENSIONAHA.113.01244

Kobayashi, K., Murata, T., Hori, M., & Ozaki, H. (2011). Prostaglandin E2-prostanoid EP3 signal induces vascular contraction via nPKC and ROCK activation in rat mesenteric artery. *European Journal of Pharmacology*, *660*, 375–380. https://doi.org/10.1016/j.ejphar.2011.03.032

Lilley, E., Stanford, S. C., Kendall, D. E., Alexander, S. P. H., Cirino, G., Docherty, J. R., George, C. H., Insel, P. A., Izzo, A. A., Ji, Y., Panettieri, R. A., Sobey, C. G., Stefanska, B., Stephens, G., Teixeira, M., & Ahluwalia, A. (2020). ARRIVE 2.0 and the British Journal of Pharmacology: Updated guidance for 2020.

Lindman, J., Khammy, M. M., Lundegaard, P. R., Aalkjær, C., & Jepps, T. A. (2018). Microtubule regulation of Kv7 channels orchestrates cAMP-mediated vasorelaxations in rat arterial smooth muscle. *Hypertension (Dallas, Tex.: 1979)*, *71*, 336–345. https://doi.org/10.1161/HYPERTENSIONAHA.117.10152

Liu, B., Luo, W., Zhang, Y., Li, H., Zhang, J., Tan, X. R., & Zhou, Y. (2012). Concomitant activation of functionally opposing prostacyclin and thromboxane prostanoid receptors by cyclo-oxygenase-1-mediated prostacyclin synthesis in mouse arteries. *Experimental Physiology*, *97*(7), 895–904. https://doi.org/10.1113/expphysiol.2011.063784

Liu, B., Zhan, M., Zhang, Y., Li, H., Wu, X., Zhuang, F., Luo, W., & Zhou, Y. (2017). Increased role of e prostanoid receptor-3 in prostacyclin-evoked contractile activity of spontaneously hypertensive rat mesenteric resistance arteries. *Scientific Reports*, *7*(1), 8927. https://doi.org/10.1038/s41598-017-09288-w

Lombard, J. H., Liu, Y., Fredricks, K. T., Bizub, D. M., Roman, R. J., & Rusch, N. J. (1999). Electrical and mechanical responses of rat middle cerebral arteries to reduced PO2 and prostacyclin. *American Journal of Physiology - Heart and Circulatory Physiology*, *276*, H509–H516. https://doi.org/10.1152/ajpheart.1999.276.2.h509

Mackie, A. R., Brueggemann, L. I., Henderson, K. K., Shiels, A. J., Cribbs, L. L., Scrogin, K. E., & Byron, K. L. (2008). Vascular KCNQ potassium channels as novel targets for the control of mesenteric artery constriction by vasopressin, based on studies in single cells, pressurized arteries, and in vivo measurements of mesenteric vascular resistance. *Journal of Pharmacology and Experimental Therapeutics*, *325*, 475–483. https://doi.org/10.1124/jpet.107.135764

McCallum, L. A., Greenwood, I. A., & Tribe, R. M. (2009). Expression and function of Kv7 channels in murine myometrium throughout oestrous cycle. *Pflügers Archiv / European Journal of Physiology*, *457*, 1111–1120. https://doi.org/10.1007/s00424-008-0567-5

Mills, T. A., Greenwood, S. L., Devlin, G., Shweikh, Y., Robinson, M., Cowley, E., Hayward, C. E., Cottrell, E. C., Tropea, T., Brereton, M. F., Dalby-Brown, W., & Wareing, M. (2015). Activation of K_V7 channels stimulates vasodilatation of human placental chorionic plate arteries. *Placenta*, *36*(6), 638–644. https://doi.org/10.1016/j.placenta.2015.03.007

Moncada, S., Gryglewski, R., Bunting, S., & Vane, J. R. (1976). An enzyme isolated from arteries transforms prostaglandin endoperoxides to an unstable substance that inhibits platelet aggregation. *Nature*, *263*, 663–665. https://doi.org/10.1038/263663a0

Morales-Cano, D., Moreno, L., Barreira, B., Pandolfi, R., Chamorro, V., Jimenez, R., Villamor, E., Duarte, J., Perez-Vizcaino, F., & Cogolludo, A. (2015). Kv7 channels critically determine coronary artery reactivity: Left-right differences and down-regulation by hyperglycaemia. *Cardiovascular Research*, *106*(1), 98–108. https://doi.org/10.1093/cvr/cvv020

Mulvany, M. (1977). Contractile properties of small arterial resistance vessels in spontaneously hypertensive and normotensive rats. *Circulation Research*, *41*, 19–26. https://doi.org/10.1161/01

Ng, F. L., Davis, A. J., Jepps, T. A., Harhun, M. I., Yeung, S. Y., Wan, A., Reddy, M., Melville, D., Nardi, A., Khong, T. K., & Greenwood, I. A. (2011). Expression and function of the K^+ channel KCNQ genes in human arteries. *British Journal of Pharmacology*, *162*(1), 42–53. https://doi.org/10.1111/j.1476-5381.2010.01027.x

Nilsson, M. E., Vandenput, L., Tivesten, Å., Norlén, A.-K., Lagerquist, M. K., Windahl, S. H., Börjesson, A. E., Farman, H. H., Poutanen, M., Benrick, A., Maliqueo, M., Stener-Victorin, E., Ryberg, H., & Ohlsson, C. (2015). Measurement of a comprehensive sex steroid profile in rodent serum by high-sensitive gas chromatography-tandem mass spectrometry. *Endocrinology*, *156*, 2492–2502. https://doi.org/10.1210/en.2014-1890

O'Mahony, F., Alzamora, R., Betts, V., LaPaix, F., Carter, D., Irnaten, M., & Harvey, B. J. (2007). Female gender-specific inhibition of KCNQ1 channels and chloride secretion by 17β-estradiol in rat distal colonic crypts. *Journal of Biological Chemistry*, *282*, 24563–24573. https://doi.org/10.1074/jbc.M611682200

Orie, N. N., & Clapp, L. H. (2011). Role of prostanoid IP and EP receptors in mediating vasorelaxant responses to PGI2 analogues in rat tail artery: Evidence for Gi/o modulation via EP3 receptors. *European Journal of Pharmacology*, *654*, 258–265. https://doi.org/10.1016/j.ejphar.2010.12.005

Orie, N. N., Fry, C. H., & Clapp, L. H. (2006). Evidence that inward rectifier K^+ channels mediate relaxation by the PGI2 receptor agonist cicaprost via a cyclic AMP-independent mechanism. *Cardiovascular Research*, *69*, 107–115. https://doi.org/10.1016/j.cardiores.2005.08.004

Pabbidi, M. R., Kuppusamy, M., Didion, S. P., Sanapureddy, P., Reed, J. T., & Sontakke, S. P. (2018). Sex differences in the vascular function and related mechanisms: Role of 17β-estradiol. *American Journal of Physiology. Heart and Circulatory Physiology*, *315*(6), H1499–H1518. https://doi.org/10.1152/ajpheart.00194.2018

Percie du Sert, N., Hurst, V., Ahluwalia, A., Alam, S., Avey, M. T., Baker, M., Browne, W. J., Clark, A., Cuthill, I. C., Dirnagl, U., Emerson, M., Garner, P., Holgate, S. T., Howells, D. W., Karp, N. A., Lazic, S. E., Lidster, K., MacCallum, C. J., Macleod, M., … Würbel, H. (2020). The ARRIVE guidelines 2.0: Updated guidelines for reporting animal research. *Experimental Physiology*, *105*(9), 1459–1466. https://doi.org/10.1113/EP088870

Rapetti-Mauss, R., O'Mahony, F., Sepulveda, F. V., Urbach, V., & Harvey, B. J. (2013). Oestrogen promotes KCNQ1 potassium channel

14765381, 2022, 7, Downloaded from https://bpspubs.onlinelibrary.wiley.com/doi/10.1111/bph.15722 by Test, Wiley Online Library on [10/01/2025]. See the Terms and Conditions (https://onlinelibrary.wiley.com/terms-and-conditions) on Wiley Online Library for rules of use; OA articles are governed by the applicable Creative Commons License

endocytosis and postendocytic trafficking in colonic epithelium. *Journal of Physiology*, *591*, 2813–2831. https://doi.org/10.1113/jphysiol.2013.251678

Schubert, R., Serebryakov, V. N., Engel, H., & Hopp, H. H. (1996). Iloprost activates K (Ca) channels of vascular smooth muscle cells: Role of cAMP-dependent protein kinase. *American Journal of Physiology - Cell Physiology*, *271*, C1203–C1211. https://doi.org/10.1152/ajpcell.1996.271.4.c1203

Schubert, R., Serebryakov, V. N., Mewes, H., & Hopp, H. H. (1997). Iloprost dilates rat small arteries: Role of K (ATP)- and K (Ca)-channel activation by cAMP-dependent protein kinase. *American Journal of Physiology - Heart and Circulatory Physiology*, *272*, H1147–H1156. https://doi.org/10.1152/ajpheart.1997.272.3.h1147

Stott, J. B., Barrese, V., & Greenwood, I. A. (2016). Kv7 channel activation underpins EPAC-dependent relaxations of rat arteries. *Arteriosclerosis, Thrombosis, and Vascular Biology*, *36*(12), 2404–2411. https://doi.org/10.1161/ATVBAHA.116.308517

Stott, J. B., Barrese, V., Jepps, T. A., Leighton, E. V., & Greenwood, I. A. (2015). Contribution of Kv7 channels to natriuretic peptide mediated vasodilation in normal and hypertensive rats. *Hypertension*, *65*, 676–682. https://doi.org/10.1161/HYPERTENSIONAHA.114.04373

Stott, J. B., Barrese, V., Suresh, M., Masoodi, S., & Greenwood, I. A. (2018). Investigating the role of G protein βγ in Kv7-dependent relaxations of the rat vasculature. *Arteriosclerosis, Thrombosis, and Vascular Biology*, *38*, 2091–2102. https://doi.org/10.1161/ATVBAHA.118.311360

Stott, J. B., Povstyan, O. V., Carr, G., Barrese, V., & Greenwood, I. A. (2015). G-protein βγ subunits are positive regulators of Kv7.4 and native vascular Kv7 channel activity. *Proceedings of the National Academy of Sciences*, *112*, 6497–6502. https://doi.org/10.1073/pnas.1418605112

Tang, E. H. C., Jensen, B. L., Skott, O., Leung, G. P. H., Feletou, M., Man, R. Y. K., & Vanhoutte, P. M. (2008). The role of prostaglandin E and thromboxane-prostanoid receptors in the response to prostaglandin E2 in the aorta of Wistar Kyoto rats and spontaneously hypertensive rats. *Cardiovascular Research*, *78*, 130–138. https://doi.org/10.1093/cvr/cvm112

Tsvetkov, D., Kaßmann, M., Tano, J. Y., Chen, L., Schleifenbaum, J., Voelkl, J., Lang, F., Huang, Y., & Gollasch, M. (2017). Do KV7.1 channels contribute to control of arterial vascular tone? *British Journal of Pharmacology*, *174*, 150–162. https://doi.org/10.1111/bph.13665

Waldegger, S., Lang, U., Herzer, T., Suessbrich, H., et al. (1996). Inhibition of minK protein induced K^+ channels in Xenopus oocytes by estrogens. *Pflügers Archiv / European Journal of Physiology*, *457*, 1111–1120. https://doi.org/10.1007/s00424-008-0567-5

Whittle, B. J., Silverstein, A. M., Mottola, D. M., & Clapp, L. H. (2012). Binding and activity of the prostacyclin receptor (IP) agonists, treprostinil and iloprost, at human prostanoid receptors: Treprostinil is a potent DP 1 and EP 2 agonist. *Biochemical Pharmacology*, *84*, 68–75. https://doi.org/10.1016/j.bcp.2012.03.012

Yeung, S. Y. M., Pucovský, V., Moffatt, J. D., Saldanha, L., Schwake, M., Ohya, S., & Greenwood, I. A. (2007). Molecular expression and pharmacological identification of a role for Kv7 channels in murine vascular reactivity. *British Journal of Pharmacology*, *151*(6), 758–770. https://doi.org/10.1038/sj.bjp.0707284

Yu, H., Lin, Z., Xu, K., Huang, X., Long, S., Wu, M., McManus, O. B., & Le Engers, J, Mattmann, M.E., Engers, D.W., Le, U.M., Lindsley, C. W., Hopkins, C. R., & Li, M. (2013). Identification of a novel, small molecule activator of KCNQ1 channels. In: Probe Reports from the NIH Molecular Libraries Program [Internet].

Zhang, Y., Luo, W., Li, H., Yu, G., Luo, H., Leng, J., Ge, J., Zeng, R., Guo, T., Yin, Y., Zhou, Y., & Liu, B. (2021). Larger endothelium-dependent contractions in iliac arteries of adult SHRs are attributed to differential downregulation of TP and EP3 receptors in the vessels of WKYs and SHRs during the transition from adolescence to adulthood. *European Journal of Pharmacology*, *893*, 173828. https://doi.org/10.1016/j.ejphar.2020.173828

SUPPORTING INFORMATION

Additional supporting information may be found in the online version of the article at the publisher's website.

How to cite this article: Baldwin, S. N., Forrester, E. A., McEwan, L., & Greenwood, I. A. (2022). Sexual dimorphism in prostacyclin-mimetic responses within rat mesenteric arteries: A novel role for $K_V7.1$ in shaping IP receptor-mediated relaxation. *British Journal of Pharmacology*, *179*(7), 1338–1352. https://doi.org/10.1111/bph.15722

14765381, 2022, 7, Downloaded from https://bpspubs.onlinelibrary.wiley.com/doi/10.1111/bph.15722 by Test, Wiley Online Library on [10/01/2025]. See the Terms and Conditions (https://onlinelibrary.wiley.com/terms-and-conditions) on Wiley Online Library for rules of use; OA articles are governed by the applicable Creative Commons License